ISBN 978-82-326-7108-3 (printed ver.)
ISBN 978-82-326-7107-6 (electronic ver.)
ISSN 1503-8181 (printed ver.)
ISSN 2703-8084 (electronic ver.)

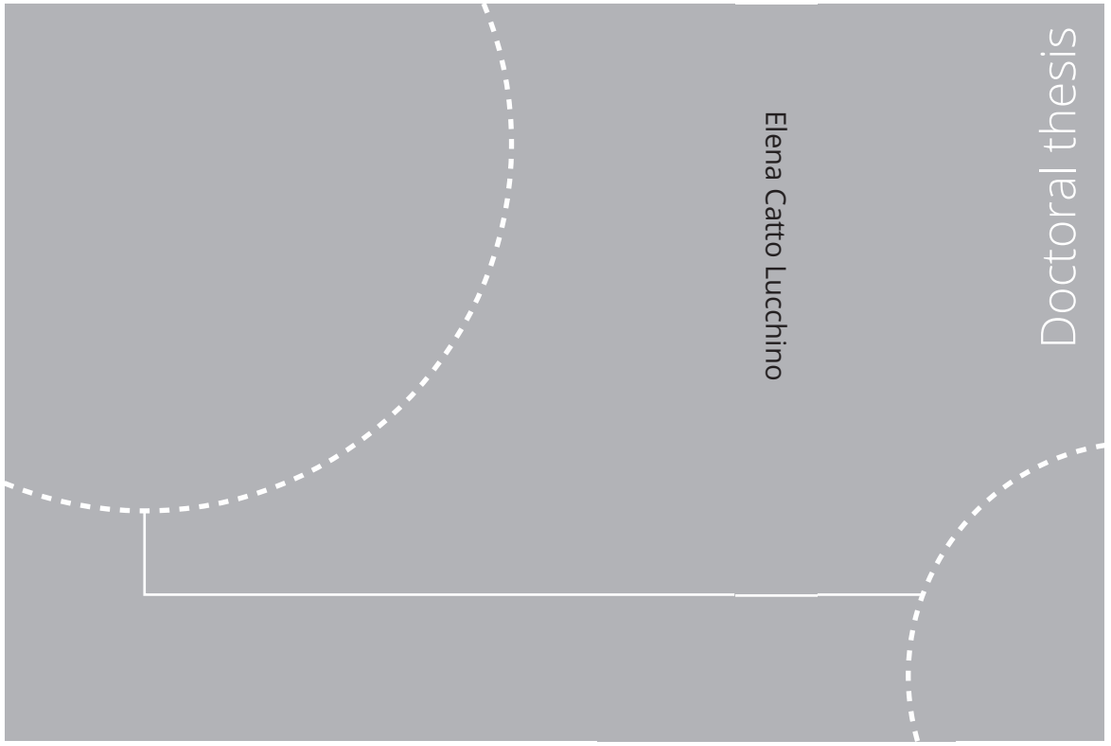

Doctoral theses at NTNU, 2023:203

Elena Catto Lucchino

Modelling, simulation and control of Double Skin Façades

NTNU
Norwegian University of
Science and Technology

Doctoral theses at NTNU, 2023:203

NTNU

NTNU
Norwegian University of
Science and Technology
Thesis for the degree of
Philosophiae Doctor
Faculty of Architecture and Design
Department of Architecture and Technology

NTNU
Norwegian University of
Science and Technology

Elena Catto Lucchino

Modelling, simulation and control of Double Skin Façades

Thesis for the degree of Philosophiae Doctor

Trondheim, June 2023

Norwegian University of Science and Technology
Faculty of Architecture and Design
Department of Architecture and Technology

NTNU
Norwegian University of
Science and Technology

NTNU
Norwegian University of Science and Technology

Thesis for the degree of Philosophiae Doctor

Faculty of Architecture and Design
Department of Architecture and Technology

ISBN 978-82-326-7108-3 (printed ver.)
ISBN 978-82-326-7107-6 (electronic ver.)
ISSN 1503-8181 (printed ver.)
ISSN 2703-8084 (electronic ver.)

Doctoral theses at NTNU, 2023:203

PRINTED IN NORWAY
NO - 1598

NORDIC SWAN ECOLABEL
Printed matter
2041 0731

Printed by Skipnes Kommunikasjon AS

“ The only true wisdom is knowing that you know nothing.”

Socrate

Preface

This thesis is submitted to the Norwegian University of Science and Technology (NTNU), Trondheim, Norway, in partial fulfilment of the requirements for the degree of Philosophiae Doctor.

This doctoral work was carried out at the Department of Architecture and Technology, NTNU, Trondheim, under the supervision of Prof. Francesco Goia as the main supervisor and co-supervision of Ass. Prof. Gabriele Lobaccaro and Ass. Prof. Olena Kalyanova Larsen (Aalborg University).

This work is part of the research project "REsponsive, INtegrated, VENTilated - REINVENT–windows," supported by the Research Council of Norway through the research grant 262198, and the partners SINTEF, Hydro Extruded Solutions, Politecnico di Torino and Aalto University.

Acknowledgements

The path to a PhD is considered a journey by many; mine started a little more than five years ago with a SAS flight that brought me from the foot of the Alps to the middle of Norway. As any traveller knows, the joy of discovery is amplified when shared, and this journey was no exception. To each individual who has contributed to it in their unique way, I express my deepest gratitude. The shared experiences, lessons learned, and connections forged have enriched my journey, and for that, I am eternally grateful.

First and foremost, I'd want to express my gratitude to my supervisor, Francesco Goia, for his guidance and mentoring during this journey. He has taught me vital research skills and given me opportunities to demonstrate my abilities in ways I never imagined possible. His unwavering support, listening ear, and straightforward guidance have been critical to my success. Thank you for raising the bar and never doubting that I will ultimately accomplish it. Thank you for all of your time, the thorough criticism, and the numerous futile attempts to find a decent cup of coffee on campus. I am extremely grateful for your assistance, without which this accomplishment would not have been possible.

I would also like to thank my co-supervisors, Gabriele Lobaccaro and Olena Kalyanova Larsen, for their support during this long process. I met Gabriele during my first time in Norway as an Erasmus student, and since then, you always believed in me way more than I ever did. Thank you for being a great motivator and a friend. Thank you, Olena, for your warm welcome at Aalborg University and your precious advice.

I am grateful to the people I had the opportunity to work with, my co-authors. Thank you for the collaboration and the team effort that led to very good published work, despite the "Reviewer n.2" efforts. Thank you, in particular, to the people from the Politecnico di Torino, my home university, which hosted the experiment facility that was key for this doctorate study. Thank you, Giovanni, for sharing the highs and lows of the experimental activities and the great unknowns of BES tools. Thank you, Fabio, for sharing your knowledgeable insights and useful comments on my research. I would also like to thank Marco Perino, professor at POLITO and my master thesis supervisor; first, for transmitting the passion for building physics and putting NTNU on my radar for the very first time.

I will be eternally grateful to my fellow PhD-ers who went through hard times with me, sharing laughs, discussions and achievements: Eirik, Arian, Steinar, Maria, Ray, David, Filippo, Sassu, Lucy, Ellika, Aleksandr, Mrudhula, Bjørn Inge, Johannes, Matteo, Yunbo, Tanja, David, Ørjan, Tonje, Ali, Samuel, Øystein. You made these long years fly by, and I consider myself very lucky to have crossed paths with all of you. I cherish the memories of all the shared moments inside and outside NTNU. I may have forgotten to mention someone, so I apologise for that.

Thank you to all my friends in Trondheim who have made this place my second home. Thank you to the SpS friends who made Sunday's dinner a fixed routine, which made me feel less alone when I was new in the country. Thank you, Ruben, Martin, Felix, Kam, Vivien, Sandra, Franziska, Marieke, Martjin, and Melina, for being one of the reasons why I have enjoyed this journey so much.

Thank you to the Italian family I have found along the way for making me feel like we never left. I would be lost without your support, advice, and constant reminder that no matter how far you go, with the right friends by your side, home is always within reach. Thank you, Elena, Anna, Francesco, Cesilie, Mattia, Alessandro, Ida, Giovanni, Line, Simone, Marta, and Patrick, for being such a big reason why Trondheim feels like home.

Thank you to my friends of a lifetime back at home, who, even when scattered around the world, were able to make me feel rooted and loved, often in doubt if I was “actually” working on something or just on endless holidays but always supporting me. Growing up means that our lives continue on different lines that tend to be more and more apart, but I hope we will continue to find bridges and be there for each other, just as we have always done, through the sands of time. Grazie Scarpe, Giuly, Ale, Matti, Barbi, Eli, Giulia, Tibo, Teo, Jo, Ely perchè tornare a casa non sarebbe la stesso senza di voi.

My biggest thank you goes to my parents, Poalo e Cristina, and my sister Caterina for their endless love, support and encouragement throughout the years. Grazie Mamma e Papà per avermi sempre supportata in tutte le mie decisioni, anche quando questo voleva dire vedermi andare lontana. Mi avete cresciuta con l’insegnamento di credere sempre in quello che faccio, e che il duro lavoro e la costanza pagano. Se ora posso celebrare questo traguardo lo devo sopratutto a voi.

At last, Kristian, I consider this achievement to be equally yours. You have supported, helped, and listened to me every single step of the way. I cannot express how grateful I am for your presence in my life and your companionship in this adventure. It hasn't always been easy to bear with me while you, yourself, were going through the same challenges. Yet, not once did you refuse to help me, discuss something, or read the piece of text I was struggling with. From the bottom of my heart, thank you. I love you always.

They say that a PhD is often a lonely and solitary pursuit, but I couldn't disagree more. Having you all by my side made it a wonderful ride.

Trondheim, June 2023

Abstract

Adaptive envelopes can reduce energy use in buildings while achieving high levels of comfort. These envelopes dynamically interact with multiple interconnected domains, such as daylight, indoor air quality, thermal comfort, and energy use, which can often conflict with one another. The 'dynamic' and 'adaptive principles imply that such envelopes should dynamically adjust their thermo-optical properties in response to transient boundary conditions (either external, such as climate, or internal, such as occupant requirements) and to changing priorities (i.e., minimising the building energy use, maximising the use of natural light, etc.).

Many different façade systems can be classified as adaptive façades. Double skin façades (DSFs) are highly transparent façades with adaptive capabilities, as they allow the exploitation of solar energy to allow both passive solar thermal gains and daylighting, with the aim of reducing energy use for building climatisation and providing better thermal and visual comfort conditions compared to a traditional single-skin façade. The adaptive principle in a DSF is based on the dynamic management of the ventilation flow in the façade cavity, often in combination with a shading system installed in the cavity to achieve balanced performance under variable conditions. This type of envelope requires the integration of multiple controllable elements with an intelligent control system driven by a suitable strategy to fully exploit their potential and optimise their performance.

This doctoral thesis aims to address the current lack of models for flexible double skin façades (a naturally or mechanically ventilated façade with an integrated shading device DSF able to switch between multiple configurations) and understand the performances of such a system by exploring the capabilities of the tools researchers and practitioners have at their disposal: BES (Building Energy Simulation). The goal is to fully understand the potential of a flexible DSF and identify the most effective control strategies to optimise its performance. To achieve this, BES tools' capabilities to simulate the thermal, fluid mechanics, and optical behaviour of traditional DSFs and the interactions between DSFs and other building systems needed to be accurately investigated. This led to the development of the main research question:

How can an adaptive façade based on a flexible DSF concept be modelled, simulated, and controlled?

The main research question was answered through a set of specific sub-questions (RQs):

RQ1. What are the current possibilities to model a DSF with the existing BES tools?

RQ2. What is the performance of the available models in the BES tools?

RQ3. What improvements are needed to model an adaptive façade based on the concept of a flexible DSF?

RQ4. What is a suitable approach to control adaptive façades to fully exploit their potential?

The research design was structured around seven research activities to answer these questions, and their results were presented in six peer-reviewed papers (P1-P6). The approach necessary to fill the presented knowledge gap included the following activities: conducting a literature review to identify the potential of the current practices in modelling and controlling DSFs, uncovering the existing research gap, and directing the course of the overall research. The core of the work was '**Modelling and Simulation**' since the adoption of models of DSFs is at the base of all the published work, and thus, it was a means to answer all the research questions. '**Sensitivity analyses**' were carried out to identify the most important parameters to focus on in the design and modelling of DSFs. Recurrent and tightly linked elements in the presented research work were '**Experimental Data-Collection and Processing**' and '**Model Validation**', which were used to answer the first three research questions. Finally, '**Co-Simulation**' was necessary to develop an '**Advanced Control**' of the model and to answer the last research question. Figure 3 shows the links between the research questions, the research activities and the papers included in the thesis.

By carrying out these research activities, this thesis investigated the reliability and capabilities of different BES tools in simulating the performance of DSFs and identified the challenges designers may face when using these tools. The comparison of the numerical simulations and experimental data was carried out for different DSF configurations and on a series of significant thermophysical quantities, and the assumptions of each model employed were analysed in depth. The results showed that no tool performs significantly better than others, but some tools offer better predictions when the focus is placed on specific thermophysical quantities, while others should be chosen if the focus is on different ones.

The multi-tool comparison of different DSF configurations highlighted the lack of a model able to fully utilise the operational capability of a fully flexible double-skin façade. The façade's full dynamics were explored by developing, in IDA ICE, a flexible DSF model able to switch between ten different cavity ventilation strategies and change the shading device position in the cavity. Starting from the existing in-built model, an enhanced model was developed and improved to control the connection between the cavity and the indoor or outdoor environment during the simulation runtime. The comparison with experimental data showed that its prediction accuracy was in line with the results obtained by applying a single ventilation strategy one at a time. The key aspect of this enhanced model is its ability to integrate

both natural and mechanical ventilation strategies and allow the possibility of changing operation modes within the same simulation.

The presented model was employed to develop a suitable control strategy that could integrate the adaptive capabilities of the envelope and the other active building systems. Several approaches for their control were evaluated, and a novel multi-domain optimal control was developed. This control approach allows for any type of adaptive façade to be optimally controlled using building energy simulation tools. The proposed control approach can be valuable for optimising the building envelope's performance and achieving the desired thermal, daylighting, and air quality conditions.

This study is aimed at both the R&D and professional communities. The first group could further investigate the performance of this concept and expand knowledge about the challenges and possibilities in modelling (and controlling) advanced façade systems in BES. Furthermore, the work described in this thesis could be useful as a demonstration of how to use existing BES tools to model advanced functionalities for building envelope systems that are not found in the modules embedded in a BES release. This could increase the adoption of more advanced technologies in the building sector, giving the envelope a whole new role.

Sammendrag

Adaptive fasader kan redusere energiforbruket i bygninger uten å gå på bekostning av komfort. Disse fasadene står i interaksjon med flere sammenkoblede domener, som dagslys, innendørs luftkvalitet, termisk komfort og energibruk, som ofte er under gjensidig påvirkning. De "dynamiske" og "adaptive" prinsippene antyder at disse fasadene bør tilpasse sine termo-optiske egenskaper dynamisk som respons på transiente grensebetingelser (enten eksterne, som klima, eller interne, som brukerbehov) samtidig som de tar høyde for skiftende prioriteringer (dvs. å minimere bygningens energiforbruk, maksimere bruken av dagslys, osv.).

Mange ulike fasadesystemer kan klassifiseres som adaptive fasader. Dobbeltfasader (DSF) er fasader med høy transparens og adaptive evner, da de tillater utnyttelse av solenergi for å oppnå både solvarmetilskudd og dagslys, med formål å redusere energiforbruket til bygningsklimatisering og gi bedre termiske og visuelle komfortforhold sammenlignet med en tradisjonell enkeltfasade. Det adaptive prinsippet i en DSF er basert på dynamisk styring av ventilasjonsstrømmen i luftrommet mellom den innvendige fasaden og det ytre skallet, ofte i kombinasjon med et solskjermingssystem installert i luftrommet for å oppnå balansert ytelse under ulike forhold. Denne typen fasade krever integrering av flere kontrollerbare elementer i et intelligent styringssystem drevet av en passende strategi for å utnytte hvert elements potensiale fullt ut og optimalisere ytelsen.

Denne doktoravhandlingen har som mål å adressere den nåværende mangelen på modeller som kan representere fleksible dobbeltfasader (en naturlig eller mekanisk ventilert fasade med integrert solskjerming som er i stand til å skifte mellom flere konfigurasjoner) og å forstå ytelsene til et slikt system ved å utforske mulighetene i verktøyene som forskere og rådgivere har til rådighet: BES (Building Energy Simulation). Målet er å fullt ut forstå potensialet til en fleksibel DSF og identifisere de mest effektive styringsstrategiene for å optimalisere ytelsen. For å oppnå dette måtte BES-verktøyets evner til å simulere den termiske, fluidmekaniske og optiske oppførselen til tradisjonelle DSF-er og interaksjonene mellom DSF-er og andre bygningssystemer undersøkes nøyaktig. Dette leder til hovedspørsmålet:

Hvordan kan en adaptiv fasade basert på et fleksibelt DSF-konsept modelleres, simuleres og styres?

Hovedforskningspørsmålet ble besvart gjennom en rekke spesifikke delspørsmål (RQs):

RQ1. Hva er de nåværende mulighetene til å modellere en DSF med eksisterende BES-verktøy?

RQ2. Hva er ytelsen til de tilgjengelige modellene i BES-verktøyene?

RQ3. Hvilke forbedringer er nødvendig for å modellere en adaptiv fasade basert på konseptet med en fleksibel DSF?

RQ4. Hva er en passende tilnærming for å kontrollere adaptive fasader for å utnytte deres potensial fullt ut?

For å besvare disse spørsmålene var forskningsdesignet strukturert rundt syv forskningsaktiviteter, og resultatene ble presentert i seks fagfellevurderte artikler (P1-P6). Tilnærmingen som var nødvendig for å fylle kunnskapsgapet som ble presentert, inkluderte følgende aktiviteter: å gjennomføre en litteraturgjennomgang for å identifisere potensialet til nåværende praksiser for modellering og styring av DSF, avdekke det eksisterende forskningsgapet og retningen for den overordnede forskningen. Kjernen i arbeidet var "**Modellering og simulering**", siden bruk av modeller av DSF er grunnlaget for alt det publiserte arbeidet, og dermed var det en måte å besvare alle forskningsspørsmålene på. "**Sensitivitetsanalyser**" ble utført for å identifisere de viktigste parameterne å fokusere på i design og modellering av DSF. Gjentakende og tett sammenkoblede elementer i det presenterte forskningsarbeidet var "**Datainnsamling og -behandling**" og "**Modellvalidering**", som ble brukt til å besvare de første tre forskningsspørsmålene. Til slutt var "**Co-Simulering**" nødvendig for å utvikle en "**Avansert Styring**" av modellen og for å besvare det siste forskningsspørsmålet. Figur 3 viser sammenhengen mellom forskningsspørsmålene, forskningsaktivitetene og artiklene som er inkludert i avhandlingen. Ved å utføre disse forskningsaktivitetene, undersøkte denne avhandlingen påliteligheten og evnen ulike BES-verktøy har til å simulere ytelsen til DSF-er og identifiserte utfordringene designere kan møte når de bruker disse verktøyene. Sammenligningen av numeriske simuleringer og eksperimentelle data ble utført for ulike DSF-konfigurasjoner og på en rekke termofysiske størrelser, og antagelsene til hver modell som ble brukt, ble analysert grundig. Resultatene viste at ingen av verktøyene presterer betydelig bedre enn de andre, men noen verktøy gir bedre prediksjoner når fokuset er rettet mot spesifikke termofysiske størrelser, mens andre bør velges hvis fokuset er på andre størrelser.

Sammenligningen av ulike verktøy og DSF-konfigurasjoner avdekket at det mangler modeller i eksisterende verktøy som kan utnytte driftsevnen til en fleksibel dobbeltfasade fullt ut. Fasadens fulle dynamiske egenskaper ble utforsket ved å utvikle en fleksibel DSF-modell i IDA ICE som kunne bytte mellom ti ulike ventilasjonsstrategier og endre posisjonen til den innebygde solskjermingen. Ut fra den eksisterende modellen som kommer med IDA-ICE ble en mer fleksibel modell utviklet og forbedret for å ta kontroll over tilkoblingen mellom hulrommet og innemiljøet eller utemiljøet mens simuleringen kjører. Sammenligningen med eksperimentelle data viste at nøyaktigheten av modellprediksjonene var i tråd med resultatene som ble oppnådd ved å anvende én ventilasjonsstrategi om gangen. Det viktigste aspektet

ved denne forbedrede modellen er dens evne til å integrere både naturlige og mekaniske ventilasjonsstrategier og tillate muligheten for å endre driftsmoduser innenfor samme simulering.

Den presenterte modellen ble brukt til å utvikle en passende styringsstrategi som kunne integrere de adaptive egenskapene til fasaden og de andre aktive bygningssystemene. Flere tilnærminger ble evaluert, og en ny flerdomeneregulering ble utviklet. Denne styringstilnærmingen gjør det mulig å optimalt styre enhver type adaptiv fasade ved hjelp av bygningsenergisimuleringsverktøy. Den foreslåtte styringslogikken kan være verdifull for å optimalisere bygningens ytelse og oppnå ønskede luftkvalitet, dagslys og termiske forhold.

Denne studien er rettet mot både FoU- og fagmiljøer i arkitekt og rådgiverbransjen. Den første gruppen kunne videre undersøke ytelsen til dette konseptet og utvide kunnskapen om utfordringer og muligheter ved modellering (og styring) av avanserte fasadesystemer i BES. Videre kan arbeidet beskrevet i denne avhandlingen være nyttig som en demonstrasjon av hvordan man bruker eksisterende BES-verktøy til å modellere fasadekomponenter med avanserte funksjoner for klimatisering som ikke finnes i modulene som er innebygd i en BES-utgivelse. Dette kan bidra til å øke utbredelsen av mer avanserte klimatiseringsteknologier i byggesektoren, og gi klimaskallet en helt ny rolle.

Table of Contents

Preface v

Acknowledgements vii

Abstract ix

Sammendrag xiii

List of Figures xix

List of Tables xxv

List of Acronyms and Abbreviations xxix

1. Introduction 1

1.1 Context 1

1.2 Aim, audience, and structure of the thesis 2

1.3 Background and knowledge gap 4

1.4 Research questions and research design 9

1.5 Research methods 12

1.6 Research articles 22

2 A review of current practices and possibilities for future developments 25

3 A sensitivity analysis with building energy simulation tools 55

4 Validation and inter-software comparison of a mechanically ventilated single-story DSF 83

5 Validation and inter-software comparison of a naturally ventilated single-story DSF 111

6 Modelling and validation of a single-storey flexible double-skin façade system 135

7 Multi-domain model-based control of a flexible double skin façade system 159

8 Conclusions 179
8.1 Research Outputs 179
8.2 Discussion and limitations 185
8.3 Original contribution and impact of the work 188
8.4 Future outlook 190
Bibliography 193

List of Figures

Chapter 1

Figure 1 Ventilation strategies applicable in a DSF..... 6

Figure 2 Integration between the room systems and a DSF..... 7

Figure 3 Overview of the thesis structure, the addressed research questions and the research methods employed..... 11

Figure 4 Modelling approach of a DSF in BES tool: a) zonal approach and b) in-built model..... 13

Figure 5 Test-cell facilities used in the experimental campaign. a) Mechanically ventilated exhaust DSF used in P2 and P3; b) flexible DSF used in P4 and P5..... 16

Figure 6 Multi-objective optimal control algorithm used in P6..... 21

Chapter 2

Figure 1 Possible airflows in double skin facades..... 29

Figure 2 Overview of numerical modelling approaches..... 30

Chapter 3

Figure 1 Sections of exhaust-air façades a) air exhaust façade b) climate facade..... 59

Figure 2 Schematic of parameters defined in Table 2, view, axonometric view and section: a) IDA ICE b) EnergyPlus..... 60

Figure 3 $S_{i,d}$, Internal glazing temperature, Torino, all orientations, IDA ICE a) shading off b) shading on..... 64

Figure 4 $S_{i,d}$, Internal glazing temperature, Torino, all orientations, EnergyPlus a) shading off b) shading on..... 65

Figure 5 $S_{i,d}$, Internal glazing temperature, all locations, EnergyPlus a) South, shading on b) North, shading on, c) North, shading off..... 66

Figure 6 $S_{i,d}$, Daily energy gain, Torino, all orientations, IDA ICE a) shading off b) shading on..... 67

Figure 7 $S_{i,d}$, Daily energy gain, Torino, all orientations, EnergyPlus a) shading off b) shading on 67

Figure 8 $S_{i,d}$, Energy gain, all locations, EnergyPlus, a) South, shading on b) North, shading off..... 68

Figure 9 $S_{i,d}$, Daily heat loss, Torino, all orientations, IDA ICE a) shading off b) shading on..... 68

Figure 10 $S_{i,d}$, Daily heat loss, Torino, all orientations, EnergyPlus a) shading off b) shading on..... 69

Figure 11 $S_{i,d}$, Energy loss, all locations, EnergyPlus, a) South, shading on b) North, shading off..... 69

Figure 12 Intersoftware comparison of $S_{i,d}$ for IDA ICE and EnergyPlus: a) Internal glazing temperature b) Daily energy gain e^{+}_{24h} c) Daily energy loss e^{-}_{24h}..... 70

Chapter 4

Figure 1 Schematic section and glazing configuration of the DSF..... 87

Figure 2 Zonal modelling of the DSF..... 87

Figure 3 Sensor a) scheme and b) instalment on the experiment facility..... 88

Figure 4 Time profile of the outdoor and indoor air temperature [°C] and horizontal global solar irradiance [W/m²] for the four modelling periods: a) Winter with shading down, b) Winter with shading up, c) Summer with shading down and d) Summer with shading up..... 91

Figure 5 Comparison between predicted and experimental data for the two models carried out in Energy Plus. a) Air Gap Temperature b) Inner glass surface temperature c) Heat flux d) Transmitted solar irradiance. The four simulated periods are combined..... 92

Figure 6 Time distributions of the two Energy Plus models predictions in the four configurations. Air gap temperature. Surface temperature. Heat flux. Transmitted solar irradiance. a) Winter shading down, b)Winter shading up, c) Summer shading down, d) Summer shading up. A single, representative day was selected from the simulated periods..... 93

Figure 7 Comparison between predicted and experimental data for the two models carried out in IDA ICE. a) Air Gap Temperature b) Inner glass surface temperature c) Heat flux d) Transmitted solar irradiance. The four simulated periods are combined..... 94

Figure 8 Time distributions of the two IDA ICE models predictions in the four configurations. Air gap temperature. Surface temperature. Heat flux. Transmitted solar irradiance. a) Winter shading down, b)Winter shading up, c) Summer shading down, d) Summer shading up. A single, representative day was selected from the simulated periods..... 95

Figure 9 Comparison between predicted and experimental data for the two models carried out in Trnsys. a) Air Gap Temperature b) Inner glass surface temperature c) Heat flux d) Transmitted solar irradiance. The four simulated periods are combined..... 96

Figure 10 Time distributions of the two Trnsys models predictions in the four configurations. Air gap temperature. Surface temperature. Heat flux. Transmitted solar irradiance. a) Winter shading down, b)Winter shading up, c) Summer shading down, d) Summer shading up. A single, representative day was selected from the simulated periods..... 97

Figure 11 Comparison between measured data and predicted air gap temperature values. The four simulated periods are combined..... 98

Figure 12 Time profiles of the air gap temperature prediction in the four configurations. A single, representative day was selected from the simulated periods..... 98

Figure 13 Time profiles of the vertical distribution of the air gap temperature. Winter period with the shading in the cavity. The graph shows the results of the model with the zonal approach of Energy Plus and IDA ICE..... 98

Figure 14 Comparison between measured data and predicted values of the surface temperature. The four simulated periods are combined..... 99

Figure 15 Time profiles of the surface temperature prediction in the four configurations. A single, representative day was selected from the simulated periods..... 100

Figure 16 Comparison between measured data and predicted values of the heat flux. The four simulated periods are combined..... 100

Figure 17 Time profiles of the heat flux prediction in the four configurations. A single, representative day was selected from the simulated periods..... 100

Figure 18 Comparison between measured data and predicted values of the transmitted solar irradiance..... 101

Figure 19 Time profiles of the transmitted solar irradiance prediction in the four configurations A single, representative day was selected from the simulated periods. 101

Chapter 5

Figure 1 Zonal (a) versus in-built component (b) approach. Shading device is not drawn for clarity..... 115

Figure 2 Schematic section and physical properties of the double skin façade prototype..... 117

Figure 3 Sensors scheme (a) and picture of flexible DSF prototype in OAC mode and shading up (b)..... 118

Figure 4 Time profile of indoor air temperature, outdoor air temperature and horizontal solar irradiance during the six periods. The representative day for each dataset is highlighted in grey..... 119

Figure 5 Comparison between experimental data and predicted outcomes carried out with Energy Plus. From top to bottom: Cavity air temperature, Surface Temperature, Transmitted Solar Irradiance. From left to right: Thermal Buffer, Outdoor Air Curtain and Supply Air... 121

Figure 6 Comparison between experimental data and predicted outcomes carried out with TRNSYS. From top to bottom: Cavity air temperature, Surface Temperature, Transmitted Solar Irradiance. From left to right: Thermal Buffer, Outdoor Air Curtain and Supply Air. The shading configurations are combined..... 122

Figure 7 Comparison between experimental data and predicted outcomes carried out with IDA-ICE. From top to bottom: Cavity air gap temperature, Surface Temperature, Transmitted Solar Irradiance. From left to right: Thermal Buffer, Outdoor Air Curtain and Supply Air. The shading configurations are combined..... 123

Figure 8 Comparison between experimental data and predicted outcomes carried out with IES-VE. From top to bottom: Cavity air temperature, Surface Temperature, Transmitted Solar Irradiance. From left to right: Thermal Buffer, Outdoor Air Curtain and Supply Air. The shading configurations are combined..... 124

Figure 9 Comparison between measured data and predicted outcomes of the cavity air temperature (up) – the six façade configurations are combined. Time profile of the cavity air temperature prediction and experimental data during the representative day of the datasets (down)..... 125

Figure 10 Comparison between measured data and predicted surface temperature (up) outcomes – the six façade configurations are combined. Time profile of the surface temperature prediction and experimental data during the representative day of the datasets (down)... 125

Figure 11 Comparison between measured data and predicted outcomes of the transmitted solar irradiance (up) – the six façade configurations are combined. Time profile of the transmitted solar irradiance prediction and experimental data during the representative day of the datasets (down)..... 126

Figure 12 Sensitivity analysis for zoning optimisation (a), pressure loss distribution (b), wind pressure coefficients (c), inlet and outlet modelling (d), air tightness of the inlet/outlet openings (e), convective heat transfer coefficient (f), capacitive node (g). Different tools and DSF modes have been used, as indicated in the graphs..... 128

Chapter 6

Figure 1	Ventilation strategies implementable in a fully flexible DSF module	138
Figure 2	Integration between the room systems and a DSF	139
Figure 3	a) Schematic view of the 'Double Glass Façade' component as implemented in IDA ICE with the different air links available (only one ventilation strategy at a time is implementable in a model) – b) Ventilation strategies that can be modelled using the component: 1) OAC_N, 2) OAC_M, 3) IAC_N, 4) IAC_M, 5) SA_N, 6) SA_M, and 7) TB	141
Figure 4	Schematic view of the adaptive façade model implemented in IDA ICE based on the fully flexible DSF architecture (the model can switch among all the configurations presented in Fig. 1 within the same simulation) – in red, the newly added elements	143
Figure 5	Schematic section and glazing configuration of the DSF	144
Figure 6	Sensor a) scheme and b) instalment on the experiment facility	145
Figure 7	Control strategies applied in the two analysed periods a) Hourly Control – applied for every day of the week and b) Daily Control	146
Figure 8	Time profile of the outdoor and indoor air temperature [◦C] and horizontal global solar irradiance [W/m2] for the two modelling periods: a) Hourly Control and b) Daily Control	147
Figure 9	Statistical indicators a) MBE and b) RMSE distribution for each configuration tested during the Daily Control	150
Figure 10	a) Time profile of the transmitted solar irradiance for the hourly controlled days; b) detailed view of Day 4 and 5. The error is expressed in [W/m²]. The uncertainty band is calculated as ±5% of the measured values	151
Figure 11	Time profile of the transmitted solar irradiance for the daily controlled days. The error is expressed in [W/m²]. The uncertainty band is calculated as ±5% of the measured values.	151
Figure 12	a) Time profile of the air gap temperature for the hourly controlled days; b) detailed view of Day 4 and 5. The error is expressed in [◦C]. The uncertainty band shows the experimental values measured by the sensors in the cavity placed at two different heights in the cavity	152
Figure 13	Time profile of the air gap temperature for the daily controlled days. The error is expressed in [◦C]. The uncertainty band shows the experimental values measured by the sensors in the cavity placed at two different heights in the cavity	153

Figure 14 a) Time profile of the surface temperature for the hourly controlled days; b) detailed view of Day 4 and 5. The error is expressed in [◦C]. The uncertainty band shows the two experimental values measured by the sensors on the surface..... 154

Figure 15 Time profile of the surface temperature for the daily controlled days. The error is expressed in [◦C]. The uncertainty band shows the two experimental values measured by the sensors on the surface..... 155

Figure 16 a) Time profile of the transmitted heat flux for the hourly controlled days; b) detailed view of Day 4 and 5. The error is expressed in [W/m²]. The uncertainty band shows the two experimental values measured by the heat flux meters..... 156

Figure 17 Time profile of the transmitted heat flux for the daily controlled days. The error is expressed in [W/m²]. The uncertainty band shows the two experimental values measured by the sensors on the surface..... 157

Chapter 7

Figure 1 A) Ventilation strategies implementable in a fully flexible DSF module; b) Schematic view of the fully flexible DSF model implemented in IDA ICE..... 165

Figure 2 MBC scheme: the simulated cases are filtered by the multi-domain trade-off algorithm to obtain the optimised solution for the i^{th} timestep..... 167

Figure 3 RBC strategy for the thermal and air quality domain. TMR–Running medium temperature [°C]; T_GAP–Temperature inside of the DSF airgap [°C]; Q_SOL–Solar radiation hitting the façade on which the DFS is installed [W/m²]; CO2-Amount of CO2 in the occupied room [PPM]..... 169

Figure 4 RBC strategy for the visual domain; Q_SOL–Solar radiation hitting the façade on which the DFS is installed [W/m2]; H_SOL–Solar altitude [°]..... 169

Figure 5 Workflow of the automated process to adopt the MBC. The interaction between IDA ICE and Python is carried out by the API's functions called directly via Python..... 170

Figure 6 MBC results for the winter period..... 171

Figure 7 MBC results for the summer period..... 172

Figure 8 MBC results for the mid-season..... 173

Figure 9 Energy uses from the different control strategies in the three simulated periods. SBC, RBC and MBC control..... 174

Figure 10 Comparison of the energy requirements for cooling and heating between the DSF and SK models..... 175

List of Tables

Chapter 2

Table 1 Overview of different features of BES tools concerning modelling phenomena of DSFs.... 33

Table 2 Overview of papers analysing the performances of double skin facades..... 38

Table 3 Correlation between BES tool adopted and the analysis conducted..... 45

Chapter 3

Table 1 Parameters considered in the sensitivity analysis..... 63

Table 2 Definition of variants of solar properties, example..... 63

Chapter 4

Table 1 Thermal model of the DSF in the zonal approach..... 89

Table 2 Airflow network connection in the zonal approach of the DSF..... 89

Table 3 Calculation methods for establishing the exterior (outdoor) and interior (indoor) convective surface coefficients..... 89

Table 4 Convective heat transfer correlations adopted for the ventilated cavity's vertical surfaces..... 90

Table 5 MBE and RMSE values calculated for the two EnergyPlus models..... 92

Table 6 MBE and RMSE values calculated for the two IDA ICE models..... 94

Table 7 MBE and RMSE values calculated for the two Trnsys models..... 96

Table 8 MBE and RMSE values calculated for the model in Energy Plus 'Airflow Window', TRNSYS, IDA ICE 'Ventilated Window' and IES<VE>..... 101

Table 9 Performance overview of the tools in the four different periods. Comparison with the experiment results in the two seasons, Winter and Summer, with the shading ON or OFF..... 101

Table 10 Energy performance of the different tools in the four analysed periods..... 102

Table 11 NMBE and CV(RMSE) values calculated for the energy performance of each tool..... 103

Chapter 5

Table 1 Settings of simulation condition and DSF modelling approach used for each BES tool.... 120

Table 2 MBE and RMSE values of the cavity air temperature calculated for the six DSF configurations..... 122

Table 3 MBE and RMSE values of the surface temperature calculated for the six DSF configurations 126

Table 4 MBE and RMSE values of the transmitted solar irradiance calculated for the six DSF configurations..... 126

Table 5 Performance overview of the tools in the three different ventilation modes. The performance of the two shading modes is combined..... 127

Table 6 Summary of findings from the sensitivity analysis..... 130

Chapter 6

Table 1 Performances of the 'Double Glass Façade' model in modelling a single-story DSF: mechanically and naturally ventilated..... 143

Table 2 MBE and RMSE values calculated for the model run adopting the Hourly Control and the Daily Control..... 149

Table 3 Detail of the MBE and RMSE calculated for each ventilation strategy adopted in the Daily Control..... 150

Table 4 Daily total transmitted energy performances and statistical values (NMBE and CV (RMSE)) calculated for the Hourly Control and Daily Control (7 days period) and for each day of the Daily Control (24H period)..... 150

Chapter 7

Table 1 A) indoor temperatures range as a function of the running mean temperature [58]; b) Internal Loads; c) Airflows values for fans (for each window) calculated according to the conditions of Class II..... 166

Table 2 Possible combinations of all the controlled parameters in the model-based controlled DSF..... 168

Table 3 KPI selected for each set of simulations and their thresholds values..... 168

Table 4 Schedule definition for the SBC of the DSF flow path and shading position..... 170

Table 5 List of API functions used in the Python workflow..... 171

Table 6 Ventilation strategies adopted during the different simulated periods..... 172

Table 7 Fulfilment criteria for the different control strategies adopted during the combined three simulation periods. The KPIs E_{plane} ; ΔCO_2 and T_{op} are calculated only during the occupied hours. Q is calculated for the whole simulation hours..... 174

Table 8 KPIs of the MBC applied to the flexible DSF and to a simpler single skin (SK). E_{plane}; ΔCO_2 and T_{op} were calculated only during the occupied hours. Q was calculated for the whole simulation hours..... 175

List of Acronyms and Abbreviations

API	Application Programming Interface
BES	Building Energy Simulation
CFD	Computational Fluid Dynamics
DSF	Double Skin facade
EA	Exhaust Air
IAC	Indoor Air Curtain
MBC	Model-based control
MPC	Model-Predictive control
OAC	Outdoor Air Curtain
RBC	Rule-based control
RBE	Responsive Building Elements
SA	Supply Air
SBC	Schedule-based control
SK	Single skin facade
RQ	Research Question
TB	Thermal Buffer
TB_v	Ventilated Thermal Buffer

1. Introduction

1.1 Context

Reducing emissions from the building sector has been and is the focus of both the building industry and researchers to respond to climate change and increasingly stricter environmental policies. The traditional building design has had to be revised to reduce the energy demand and increase energy exploitation from renewable resources. In this context, all building elements have been subject to extensive research and development to improve the match between energy production and build loads. A significant result of this work is the identification of so-called Responsive Building Elements (RBE) as an important technology. IEA-ECBS Annex 44 defined an RBE as a 'building component that assists in maintaining an appropriate balance between optimum interior conditions and environmental performance by reacting in a controlled and holistic manner to changes in external or internal conditions and to occupant intervention' (Heiselberg 2012).

RBEs are centred around their ability to respond to changes in their environment and user needs. This includes exhibiting dynamic behaviour, adapting to different environmental conditions, performing various functions, and being controlled intelligently. Since the building envelope is a direct filter between the indoor and outdoor environment and it interacts with one of the main renewable resources - solar radiation - it is one element where adaptive strategies have been investigated to transform a rather static element into an active player of the building system able to adapt to the external environment or the users' needs. Due to these characterises, this type of façade is often referred to in literature as "responsive", "adaptive", "dynamic", "flexible", etc.

The 'dynamic' and 'adaptable' principles imply that such a type of envelope should dynamically adjust its thermo-optical properties in response to transient boundary conditions (either external, such as climate, or internal, such as occupants' requirements) and to changing priorities (i.e., minimising the building energy use, maximising the use of natural light, etc.). Adaptive building envelopes can exploit many

possibilities enabled by different technologies, ranging from material up to system levels, to control properties that impact energy transmission, reflection, absorption, and conversion (Perino M. et al. 2008).

Many different façade systems can be classified as adaptive façade s. Double skin façades (DSFs) are highly transparent façades with adaptive capabilities as they allow the exploitation of solar energy to allow both passive solar thermal gains and daylighting, with the aim of reducing energy use for building climatisation (Huckemann et al. 2010) and providing better thermal and visual comfort conditions compared to a traditional single-skin façade (Pomponi et al. 2016). The adaptive principle in a DSF is based on the dynamic management of the ventilation flow in the façade cavity (Haase, Marques da Silva, and Amato 2009), which is often combined with a shading system installed in the cavity to achieve variable performance goals; manipulating the airflow in the cavity impacts the ventilative heating/cooling load and the indoor air quality.

Designing an adaptive façade is not a trivial task. The temperatures and airflows of the DSFs are influenced simultaneously by thermal, optical, and fluid-dynamic processes. The complexity of the phenomena occurring in the DSF's cavity makes it challenging to make reliable predictions supporting design choices. Moreover, the dynamic integration between a ventilated façade and the HVAC system could also play a significant role in enhancing the adaptive behaviour of a façade. This feature requires the use of suitable tools capable of providing an integrated analysis of the adaptive element and the whole building system.

In addition to their physical complexity, adaptive façades such as DSFs require intelligent control to exploit their flexibility; without smart control, the potential flexibility is lost, and the advantage of this concept remains untapped. Traditional control strategies may not be sufficient to effectively manage the dynamic nature of adaptive façades, and as a result, their performance in real-world applications may not live up to expectations. The integration of an intelligent control system driven by a suitable strategy into adaptive envelopes makes it possible to exploit their potential and fully optimise their performance. This requires careful consideration of the control strategy and the interactions between the façade and other building systems, such as the HVAC system. Moreover, since the envelope interacts with several domains, a suitable control for this type of technology will likely require multiple domains to be included.

1.2 Aim, audience, and structure of the thesis

This thesis presents a comprehensive overview of the research that has been conducted on the topic of DSFs. This includes an examination of the research questions, results, and conclusions of previous studies in this field. The aim of this work is to contribute to developing new knowledge on using novel approaches and methods that utilise building performance simulation to investigate and enhance the potential this type of envelope can offer.

One of the first objectives of the research activities presented in this thesis is to investigate the reliability and capabilities of building energy simulation (BES) tools in simulating the performance of adaptive

façades, focusing in particular on DSFs, and the possibilities that these tools offer for implementing advanced control strategies. To be more specific, this work's objectives are:

- to identify the challenges users may face when using these tools for modelling DSFs;
- to evaluate the reliability of DSF models available in multiple software by comparing simulation results with experimental data collected on a full-scale mock-up;
- to research the potential of these tools in modelling a more advanced concept of a DSF where the various ventilation options are integrated as a controllable aspect of the adaptive façade.
- to highlight the complexity and the challenges required for the control of such an adaptive concept;
- to research the possibilities of implementing high-performance control routines in BES tools.

This thesis is aimed at a wide range of professionals in the field of building design as it addresses topics of relevance to multiple disciplines. The methods and findings presented in the thesis are likely to be of interest to the professional community (architects and engineers) using BES tools as an aid for building design, as well as to researchers and developers of the specific building technology. In this thesis, the professional community can find an overview of the reliability of several tools in modelling DSFs and a demonstration of how to exploit existing BES tools to model advanced functionalities for building envelope systems that are not native in the modules embedded in the release of a BES. The experimental data collected for model validation will be useful for researchers for model validation or performance analysis purposes. Additionally, some more general investigations, such as those related to co-simulation for control purposes, are likely to interest a broad audience as the knowledge developed applies to all simulations requiring advanced control. The numerical model developed in this work for the flexible DSF and the script used for its control are also available in a public repository for the professional (and R&D) community.

The thesis is organised as follows to fulfil the objectives previously described. Chapter 1 – Introduction provides a short introduction to the problem - *Chapter 1.1* details the research motivations and aims - *Chapter 1.2* presents the background and highlights current knowledge gaps in *Chapter 1.3*. In *Chapter 1.4 - Research questions and research* design, the research questions formulated to cover the gaps in the knowledge are presented, and the research design is outlined. In this section, the different research activities carried out during the research are linked to the formulated research questions, and how the outputs of these activities are gathered and presented in the next chapters of this work is outlined. *Chapter 1.5 - Research methods* describes the methods used in each activity previously outlined. Finally, in *Chapter 1.6,* the published journal papers representing this work's core are introduced, and each of them is a chapter of this thesis from Chapter 2 to Chapter 7. *Chapter 2 - A review of current practices and possibilities for future developments* contains *Paper 1,* which provides the state of the art of current DSFs modelling

approaches and presents the specific modelling challenges associated with these tools. Furthermore, the chapter provides a foundation for outlining the main challenges associated with these types of tools, which helps guide the next step of the research. *Chapter 3 - A sensitivity analysis with building energy simulation tools* contains *Paper 2*, which presents a sensitivity study that helps to identify the parameters that the designer should pay the most attention to during the design of the DSF. By employing a mechanically ventilated exhaust façade, using two different BES tools, and performing this analysis on multiple climates and orientations, the work aims at highlighting the most sensitive characteristics of a DSF. *Chapter 4 - Validation and inter-software comparison of a mechanically ventilated single-story DSF* contains *Paper 3,* in which the capabilities in modelling DSFs of four different tools are tested by using experimental data collected for a mechanically ventilated DSF. The modelling approaches of each tool are presented and compared in order to understand the impact of certain assumptions on the accuracy of the results. Similarly, *Chapter 5 4 - Validation and inter-software comparison of a naturally ventilated single-story DSF* contains *Paper*, which presents the evaluation of the performances of the same tools but for a naturally ventilated DSF. Moreover, this chapter discusses the results of a sensitivity analysis on some of the modelling assumptions for the different tools and highlights the key aspects that most affect the results. *Chapter 6 - Modelling and validation of a single-storey flexible double-skin façade system* contains *Paper 5,* which details how the DSF model of the tool that was evaluated as the most suitable for modelling the concept of a flexible DSF was enhanced, and compares its performance with experimental data from a prototype flexible DSF operating with different airflow paths/regimes tested in outdoor conditions. *Chapter 7– Multi-domain model-based control of a flexible double skin façade system* contains *Paper 6,* in which the model presented in *Chapter 6* was used to develop an advanced control that accounted for a multi-domain optimisation. This approach was enabled by establishing a co-simulation workflow between the used BES tool and the optimisation algorithm. The results of this control are compared with more traditional control strategies, and the same advanced control is applied to a building with standard windows. Finally, *Chapter 8 - Conclusions*, presents the conclusive summary of this work. In the first section, *8.1 - Research* Outputs, the answers to the research questions are outlined, and the outputs of each research activity are summarised. In the discussion section, *8.2 - Discussion and limitations*, the strengths and limitations of this work are addressed. The main research contributions of the thesis are presented in section 8.3 - *Original contribution and impact of the work*, and finally, the future work and development possibilities are presented in 8.4 - *Future outlook*.

1.3 Background and knowledge gap

Background

Adaptive façades are envelope systems that dynamically adjust their physical properties in response to transient boundary conditions (either external, such as climate, or internal, such as occupants' requirements) (R. Loonen et al. 2013). The strength of this type of façade lies in its ability to ensure high building performance across a wide range of physical domains. Adaptive façades aim to successfully

balance competing performance aspects using a combination of advanced material properties, components, and integrated control strategies (Taveres-Cachat et al. 2021).

In this rather wide category, “double skin façade” (DSF) is an example of an adaptive envelope where control over solar radiation and heat transmission is obtained by regulating the airflow mechanism. The name refers to a rather large spectrum of façade solutions, but a DSF can be generally described as a “system made of an external glazed skin and the actual building façade, which constitutes the inner skin, [where] the two layers are separated by an air cavity, which has fixed or controllable inlets and outlets and may or may not incorporate fixed or controllable shading devices.”(Pomponi et al. 2016). The adoption of a DSF aims primarily at realising a building with a “fully glazed” appearance, while still preserving high energy and indoor environmental performance by using the air zone between the two skins as an integrated element of the building energy concept.

One of the main benefits of a DSF is its ability to improve the energy efficiency of a building. By providing a layer of insulation between the exterior and interior of the building, a ventilated façade can help to reduce heat loss in the winter and heat gain in the summer. This can result in lower heating and cooling costs, as well as a more comfortable indoor environment for occupants. In addition to improving energy efficiency, a ventilated façade can positively impact the overall performance of the building. By regulating the airflow through the façade, it is possible to improve indoor air quality and reduce the risk of condensation and mold growth.

A DSF cavity can be either naturally or mechanically ventilated, and different airpaths can be adopted, depending on the cavity opening configurations and operations (Figure 1): in thermal buffer (TB) mode, it is only operated as a buffer space between the indoor and outdoor hosting the shading device; in supply air (SA) and indoor air curtain (IAC) mode, the DSF cavity is used to pre-heat air from either the outdoor or indoor environment, respectively, before supplying it to the indoor environment; in outdoor air curtain (OAC) and exhaust air (EA) mode, the DSF is used to reduce the cooling energy needs by exhausting to the outdoor environment the cavity air that entered the cavity from either the outdoor or indoor environment, respectively, thereby removing unwanted solar gains. Moreover, the control of the shading device affects the room's thermal and visual comfort (daylight and glare), greatly impacting the cavity’s conditions.

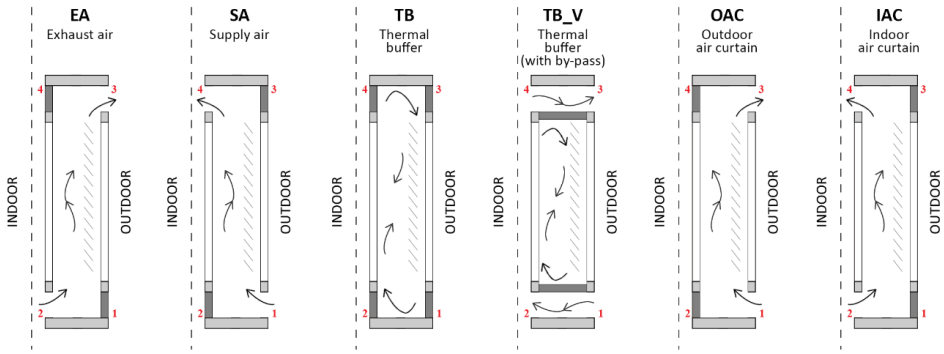

Figure 1 Ventilation strategies applicable in a DSF (Catto Lucchino et al. 2022)

The ventilation in a DSF cavity is a complex process that involves the simultaneous interaction of thermal, optical, and fluid-dynamic phenomena. In mechanically ventilated DSFs, the airflow is driven by fans, while in naturally ventilated DSFs, the airflow is influenced by wind and buoyancy-driven air movement. These factors are impacted by the geometry of the cavity and openings, the glazing that encloses the cavity, and the shading device's properties, geometry, and operation (Jankovic and Goia 2021). The fluid-dynamic phenomena within the DSF cavity significantly affect the heat exchange within the cavity which subsequently influences the cavity air and exhaust temperature, as well as the indoor surface temperatures and transmitted long-wave solar radiation entering the indoor environment through the DSF. The design of the DSF itself, including the size and shape of the openings, the position of the shading device, and the material properties of the glazing and shading device, can also impact the ventilation within the cavity. Overall, the complexity of the physical processes at play in a DSF makes it a challenging but potentially rewarding design element for buildings.

Unfortunately, adaptive capabilities in a building envelope do not guarantee its successful operation. In order to function properly, an adaptive façade must simultaneously meet multiple interdependent performance requirements, which can often be conflicting. Therefore, it is not only important to have the right materials and technologies in place to enable dynamic behaviour, but it is also crucial to have a proper control system in place to ensure that the adaptive façade operates correctly.

Often, DSFs are controlled using simple, rule-based systems that focus on a single performance and are often based on threshold values derived from educated guesses or expert knowledge. These control systems can be limiting as they are pre-set, cannot adapt, and are generally limited to a small number of output states. As a result, it is not uncommon for the full potential of DSFs to go unfulfilled, leading to suboptimal performance (Y. Kim, Park, and Suh 2011). This is the cause of the long-standing debate on the efficacy of DSFs (Oesterle et al. 2001); some studies have shown that DSFs can increase the indoor environmental quality and reduce energy use in operation compared to traditional single skins (Singh,

Garg, and Jha 2008; Chan 2011; D. Kim et al. 2018), while other studies have unveiled some controversial aspects of DSF performance (Gratia and Herde 2004).

To overcome these limitations and maximise the performance of DSFs, it is necessary to have a tool that considers not only the performance of a DSF alone but also the combined effect of a DSF and other building services. This can involve coupling mechanically ventilated façades to the building's HVAC system or regulating the airflow path through operable openings in naturally ventilated façades. The dynamic interaction between a ventilated façade and the HVAC system can significantly improve the façade's adaptive behaviour, although this feature has rarely been investigated (Park and Augenbroe 2013). By doing so, it may be possible to reduce the demand for mechanical ventilation if the façade can provide sufficient fresh air while reducing the heating demand since the supply air is pre-heated in the cavity. By exploring various possibilities for the airflow path, type of airflow (mechanical or natural), solar shading system, and overall integration with the building's HVAC elements, it is possible to achieve a wide range of variability in the façade design.

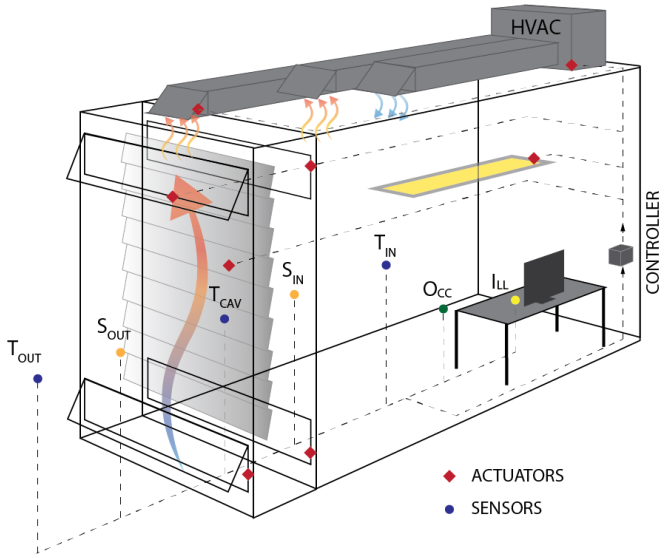

Figure 2 Integration between the room systems and a DSF (Catto Lucchino et al. 2022)

To accurately analyse the performance, optimise the design, and determine suitable control strategies for a flexible DSF system, it is necessary to have a reliable numerical representation of the DSF. This can be achieved through the use of on-purpose built models (Park, Augenbroe, Messadi, et al. 2004; Park, Augenbroe, Sadegh, et al. 2004; Wang, Chen, and Zhou 2016) or dedicated CFD simulations (Li, Darkwa, and Kokogiannakis 2017; Dama, Angeli, and Kalianova Larsen 2017). However, given the dynamic nature of the DSF, the model must allow for easy connectivity with other models that simulate the heat and light balance within a closed space and representations of other HVAC components that may be integrated into the dynamic façade concept. Coupling the simulation of the entire building with specific building

components is essential for accurately assessing the overall energy and comfort performance and understanding the complex interactions between the airflow in the façade, the HVAC system, and the building energy management system. It is also the best way to study how a local control strategy for the façade can be integrated into the overall building control strategy to ensure that both the envelope and the environmental system for building climate control are working towards the same goal.

In this context, despite their limitations, BES tools can be useful for studying adaptive envelope systems in connection with the space behind them. While BES tools are primarily designed to simulate the overall performance of a building, where the envelope is just one component of a larger system (R. C. G. M. Loonen et al. 2016), it is possible to modify existing modules to model adaptive façade systems or explore more advanced strategies such as a co-simulation approach. Some BES tools (Energy Plus, IDA ICE and TRNSYS) even include dedicated modules for simulating DSFs (Catto Lucchino et al. 2019), but it is more common that the modelling of these systems requires the use of relatively advanced simulation strategies or workarounds.

Knowledge gap

When using BES, their limitations in evaluating DSFs must be considered as the results they produce may not be fully accurate or reliable. There have been several studies in which various BES tools have been used to assess the behaviour of DSFs (Saelens, Roels, and Hens 2008; Mateus, Pinto, and Da Graça 2014; Pomponi, Barbosa, and Piroozfar 2017; Gelesz, Bognár, and Reith 2018; Eskinja, Miljanic, and Kuljaca 2018; D. Kim et al. 2018). However, dedicated validation and verification activities targeting their reliability in replicating DSF system performance are rare, and more than ten years have passed since the only major inter-comparison of software tools (Kalyanova et al. 2009) in modelling DSFs was performed. It is important to ensure that the tools used to evaluate DSFs are consistent and accurate, as the performance of these systems has a significant impact on the overall energy efficiency and comfort of a building. By conducting more thorough validation and verification activities, we can improve the reliability and trustworthiness of the results obtained using BES tools in evaluating DSFs. This will allow for more accurate design and optimisation of DSFs, leading to better-performing building envelope systems and, ultimately, to more energy-efficient and comfortable buildings.

Moreover, these tools may not natively include the capabilities needed to fully model the flexible DSF concept proposed in this research as the available modules often have limitations regarding fully flexible cavity ventilation paths, alternating ventilation mechanisms, and integration with HVAC systems (Catto Lucchino et al. 2021). This limits the possibility of simulating a flexible DSF system to apply co-simulation approaches, a process that presents advantages and a series of limitations and challenges (Taveres-Cachat et al. 2021).

In addition, more advanced forms of control are necessary to optimise the performance of adaptive envelopes to allow them to adapt to changing conditions and simultaneously consider multiple performance requirements to achieve a more balanced performance across different domains. These

control strategies can be based on the use of real-time simulation to identify the most effective state for the façade at each timestep without the need for rigid rules. Developing an effective control system for a highly flexible DSF requires a deep understanding of the interactions between the DSF and the rest of the building system, which can only be achieved if the DSF control system is integrated into BES tools. This integration is essential for developing an effective control strategy that can optimise the performance of the DSF and the building as a whole.

1.4 Research questions and research design

This work aims to address the current lack of knowledge on modelling flexible double-skin façades by exploring the capabilities of BES tools and developing a suitable modelling approach. The goal is to fully understand the potential of a flexible DSF and identify the most effective control strategies for optimising its performance. To do this, the work focuses on the use of BES tools to simulate the thermal, fluid mechanics, and optical behaviour of the DSF, as well as the interactions between the DSF and other building systems. This focus led to the development of the main research question:

How can an adaptive façade based on a flexible DSF concept be modelled, simulated, and controlled?

The main research question is answered through a set of specific sub-questions (RQ):

RQ1. *What are the current possibilities to model a DSF with the existing BES tools?*

In order to address this question, the research was structured with the following set of objectives:

- to survey how BES tools have been used to simulate DSFs;
- to map the methods and approaches available in BES to simulate DSFs;
- to assess the impact of design choices on the model performances;
- to identify the critical aspects of modelling DSFs.

RQ2. *What is the performance of the available models in the BES tools?*

In order to address this question, the research was structured with the following set of objectives:

- to model different types of DSFs with multiple tools, using the models' approach available;
- to record experimental data of different types of DSFs from a full-scale mock-up;
- to identify the most suitable metrics for evaluating the DSF performances.

RQ3. *What improvements are needed to model an adaptive façade based on the concept of a flexible DSF in BES tools?*

In order to address this question, the research was structured with the following set of objectives:

- to highlight the potential of the available BES tools in modelling a more advanced concept of DSF;
- to map the changes needed to obtain a model able to vary the ventilation options as a controllable aspect of the adaptive façade;

- to record experimental data of such a DSFs from a full-scale mock-up;
- to evaluate the improved model's performances and compare them with experimental data.

RQ4. *What is a suitable approach to control adaptive façades to fully exploit their potential?*

In order to address this question, the research was structured with the following set of objectives:

- to map the current approaches available for controlling adaptive façades;
- to highlight the complexity and the challenges required for the control of such an adaptive concept;
- to research the possibilities of implementing high-performance control routines in BES tools.

In order to answer these research questions, and with the related objectives in mind, the research design was structured around seven research activities, and their results are presented in six peer-reviewed papers. The approach necessary to fulfil the presented knowledge gap included the following activities:

Literature Review | Modelling and Simulation | Sensitivity Analysis | Experimental Data-Collection and Processing | Model Validation | Co-Simulation | Advanced Control

The first activity, **Literature Review**, laid the basis for the other activities by identifying the potential of the current practices in modelling and controlling DSFs. Moreover, it was necessary to uncover the existing research gap and direct the course of the overall research. It was employed to achieve some objectives of RQ1 and RQ4. Once the research focus was identified, the core of the work was the activity called '**Modelling and Simulation**'. Indeed, the adoption of models of DSFs was at the base of almost all the published work and, thus, a means to answer RQ1, RQ2, RQ3 and RQ4. To be able to assess the goodness of the developed models, the design and the realisation of experimental activities were necessary. '**Sensitivity analyses**' were carried out to identify the most important parameters to focus on in the design and modelling of DSFs, which played a key role in responding to RQ2. The activities '**Experimental Data-Collection and Processing**' and '**Model Validation**' were tightly linked and a recurrent element in the presented research work to answer RQ1, RQ2 and RQ3. Finally, a '**Co-Simulation**' activity was necessary to develop an '**Advanced Control**' of the model and answer RQ4.

The connection between the research questions, the activities carried out, and the output of this work is given in **Figure 3**. The outputs of these activities have been gathered in six peer-reviewed papers (Chapter 1.6) .

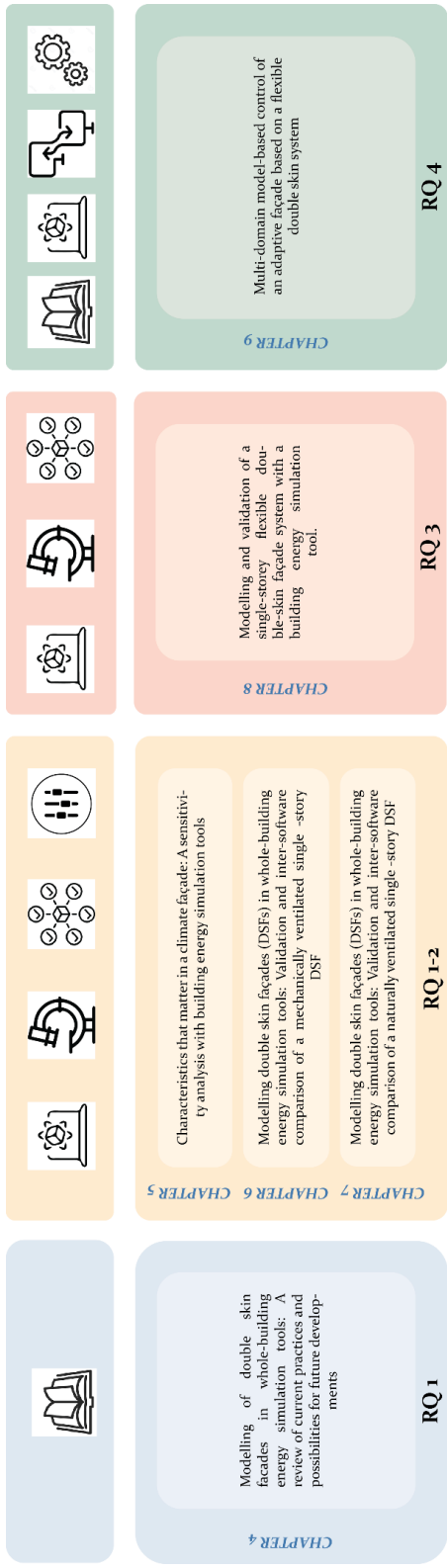

Figure 3 Overview of the thesis structure, the addressed research questions and the research methods employed

1.5 Research methods

Literature Review

The first paper (**P1**) adopted a systematic review method to examine peer-reviewed journals that used BES tools to study the behaviour of double skin façades. One of the goals of this activity was to provide an overview of the different approaches used to model DSFs, including lumped models, airflow network models, intermediate models, and computational fluid dynamics (CFD) simulations. After considering the pros and cons of each approach, it was concluded that the airflow network model, which is commonly employed by BES tools, was the most suitable approach for further developing the concept of a flexible DSF. The studies analysed in this work were selected based on a set of criteria, including the use of thermal-airflow network coupling or dedicated subroutines to model DSFs and the inclusion of analysis of parameters related to the thermal and airflow domain, preferably with validation studies. The choice of BES tools was limited to five specific tools (Energy Plus, IDA ICE, IES VE and TRNSYS), chosen based on evidence from the literature and first-hand expertise. The snowball sampling method was used to identify relevant papers in online scientific publication databases. Studies that focused solely on the energy use of the DSF system were not included. This selection process ensured that the analysed studies were relevant to the research goals and provided a comprehensive overview of the current state of knowledge on modelling DSFs using BES tools. This review served as the foundation for this thesis's subsequent work and guided the research direction by identifying the main knowledge gaps in the existing literature.

Similarly, a review of scientific publications is presented in the final chapter of this thesis (**P6**) to provide an overview of the current control possibilities for adaptive façades. This review analysed the control approaches available in BES tools and more advanced control strategies applied to simplified models. This analysis identified the challenges and limitations of these approaches and made a case for a more sophisticated approach when dealing with a façade system with many degrees of freedom, such as a DSF. By considering the current control possibilities and the limitations of traditional approaches, this contribution helps to guide the development of a more effective control strategy for adaptive façades.

Modelling and simulation

The modelling of DSFs was the core of the research work, and this activity recurred in most of the presented work and helped to answer all the research questions (Figure 3). The research review stirred the decision to focus solely on modelling using BES tools, particularly adopting some of the most commonly employed tools by researchers and practitioners (Energy Plus (Energy Plus 2019), IDA ICE (EQUA AB 2009), IES VE (IES VE 2014) and TRNSYS (TRNSYS 17 2013)). The author's previous experience with some of these tools made it possible to carry out such a multi-tool analysis. The need for verification

of the available performance of the existing models led to the production of three papers, **P2**, **P3** and **P4,** where different types of façade were modelled using the thermal-airflow network either with the zonal approach or, where available, the in-built DSF model. In the first case, the ventilated cavity was modelled as multiple thermal zones stacked vertically. The number of zones was chosen to equal the number of measuring sensors used in the experimental activity. This decision was supported (or at least not confuted) by the literature study, in which the effect of the number of stacked thermal zones on the quality and reliability of the simulation (Leal et al. 2004; Mateus, Pinto, and Da Graça 2014) was explored. However, no consensus was found on the number of zones into which the cavity should be divided (from a minimum of one to a maximum of six (Catto Lucchino et al. 2019)). Surely, increasing the number of zones does not significantly affect the results (Gelesz 2019).

Conversely, while using the dedicated module to model the DSF, the cavity was modelled within the in-built model, so no workarounds were necessary. The approach adopted in the inter-software comparison was to ensure that, regardless of the actual way to implement certain information, the core of the modelling was kept identical in all the tools. Moreover, during activity linked to the model validation, in order to minimise the influence of other factors on the final results, the outdoor conditions and boundary conditions of the room (surface temperatures and indoor air conditions) to which the DSF belonged were set to be the same as the experimental conditions. This removed possible errors linked to the room modelling and restricted the uncertainty of the model to only the DSF element.

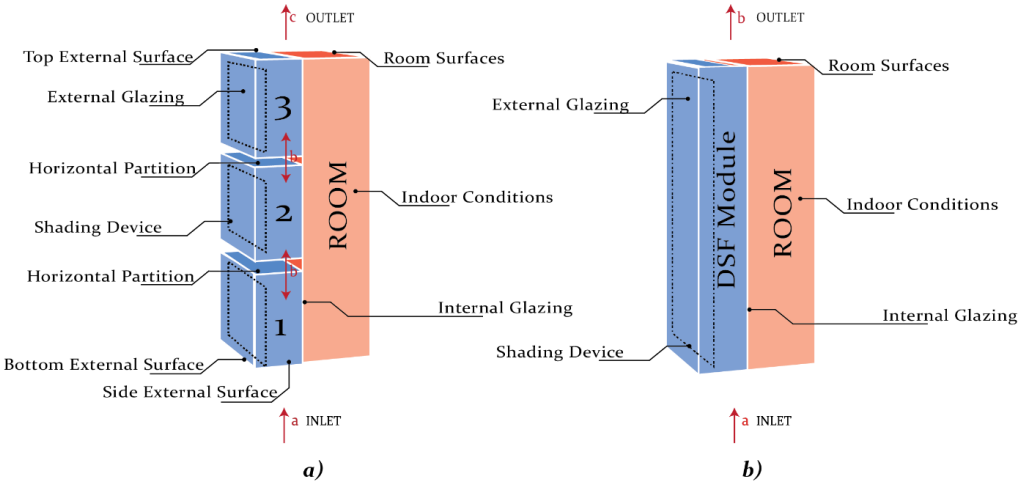

Figure 4 Modelling approach of a DSF in BES tool: a) zonal approach and b) in-built model (Gennaro et al. 2023)

One factor that influenced the choice of the BES tools to develop further was the ability to model different types of ventilation paths in a DSF. Many BES tools offer a dedicated module for simulating DSFs, but these modules are often limited to mechanically ventilated façades, and thus the use of a zonal approach to model other configurations is required. To overcome this limitation, the authors chose the IDA ICE

BES tool since it could be modified to model a flexible DSF. This tool allowed for some modifications to the in-built model and was used to simulate the flexible DSF concept presented in **P5.**

Sensitivity analysis

In order to determine the key parameters that have the greatest impact on the performance of DSFs, sensitivity analysis was employed in two different studies, **P2** and **P4**. In **P2**, sensitivity analysis was used to examine the performance of a mechanically ventilated façade, while in **P4**, it was applied to evaluate the performance of a naturally ventilated façade. By using this research method in both cases, it was possible to identify which parameters were most critical in determining the overall performance of each type of DSF.

Sensitivity analysis is a method used to investigate how variations in the inputs of a model affect the outputs of the model. Various techniques for performing sensitivity analysis exist, each of which yields a ranking of the input parameters according to their influence on the output (Kristensen and Petersen 2016). A local sensitivity analysis is a useful tool for assessing the impact of individual parameters in a model with a relatively small number of simulations. However, it does not take into account the non-linear effect that can occur from variations in multiple input parameters. In these cases, a global sensitivity analysis may be more appropriate as it can assess the effect of multiple combinations of input variations. This type of analysis is particularly useful in models with many factors as it allows for a more comprehensive understanding of how variations in multiple inputs can affect the model output. It is important to note that while the actual ranking may vary depending on the method used, the key parameters that consistently appear near the top of the list are considered to be the most sensitive and require the most attention (D. M. Hamby 1994).

The research aimed to adopt a method that practitioners can easily replicate during the design phase when computational costs must be kept to a minimum. Given this requirement, it was determined that a method based on local sensitivity analysis would be the most appropriate for the analysis, as it is able, to a large extent, to identify the same cluster of most sensitive input parameters. In this research, a local sensitivity analysis is implemented using the so-called "One-At-A-Time" (OAT) technique, which consists of changing each parameter individually (Gelesz et al. 2020).

The sensitivity analysis conducted in **P2** evaluated 18 parameters, including variations in cavity geometry, materials used, ventilation settings, façade orientation, and different climates. This analysis focused on how design choices impact the performance of DSFs. The in-built DSF models of Energy Plus and IDA ICE were employed for this work, and the case of an exhaust façade was used. The results were analysed for three different KPIs (temperature of the indoor glass surface and positive and negative daily energy crossing the façade). A ranking of the most influential parameters was identified for each KPI.

In the study of the naturally ventilated cavity in **P4**, the sensitivity analysis focused more on the modelling approach of the DSF and how certain assumptions or tools used in the modelling process can affect the

performance results. Different tools (Energy Plus, IDA ICE, IES VE and TRNSYS) and different ventilation strategies were employed for this analysis. The focus of this analysis was mainly on the capabilities of the BES tools and how the selection of certain modelling assumptions or parameters can impact the results. Given that applying the same variations to each tool is not feasible, only one tool and one configuration were used for each evaluated parameter. Accordingly, the results of this study were not compared against each other but against experimental data to demonstrate the influence of different assumptions.

Experimental Data Collection and Processing

The experimental data were derived from long-term monitoring in two test cells using a single-story box window DSF. Two outdoor test-cell facilities (Figure 5) - that replicated a full-scale office room - were employed for this activity, and they were located in a temperate sub-continental climate in northern Italy (Torino - 45 ° N latitude). These campaigns took place over an extended period of time, during which the DSF was exposed to a variety of weather conditions. The DSF was operated with either the shading device deployed or retracted, and with different ventilation strategies. The performances were investigated in winter, summer, and mid-season for an extended period of time to test a broad spectrum of boundary conditions (sunny days and cloudy days, warm days and cold days). The goal of these campaigns was to gather data on the performance of the DSF under different seasons and configurations. This data was used in the validation procedures to evaluate the accuracy of the developed models.

In both experimental campaigns, the setup to record data was similar. The indoor air temperature of the test room was carefully controlled to minimise inaccuracies resulting from changes in the indoor environment and to ensure stable testing conditions. The test cell and the DSF module were equipped with a variety of sensors to record the thermophysical and optical processes occurring in the DSF, including pyranometers, thermocouples, heat flux sensors, air velocity sensors, and more. Temperature sensors were placed on the different glass surfaces of the DSF, on the shading device, and inside the cavity to measure the air temperature within the gap. Thermocouples and heat flux meters exposed to solar radiation were shielded with highly reflective aluminium foil to reduce the influence of solar irradiance on the measured physical quantities. The outdoor solar irradiance was measured on both the horizontal and vertical planes using two pyranometers. The solar irradiance transmitted through the DSF was measured on the vertical plane, with an additional pyranometer installed next to the inner skin of the DSF. In addition, the wind velocity and wind direction were recorded. The room was also equipped with contact sensors to record surface temperature values for all cell surfaces, as well as sensors for indoor air temperature measurements. On the occasion that some data was not measured in the field, the weather station of the nearby Politecnico di Torino was used to make up for the missing data.

a) b)

Figure 5 Test-cell facilities used in the experimental campaign. a) Mechanically ventilated exhaust DSF used in P2 and P3; b) flexible DSF used in P4 and P5.

Once the raw data was collected, it was then processed and converted into a time-series format. The multipurpose programming language, Python, was used to process and convert the raw data into a time-series format. This language was chosen due to its versatility and wide range of libraries and modules available for data manipulation and analysis. Python's easy-to-read syntax and large developer community also made it an ideal choice for this process. By using Python, the data could be manipulated and processed in an efficient and accurate manner.

This data was used in different ways, depending on the stage of the process. In some cases, the data were used to set the boundary conditions for the control system. In other cases, the data were compared with the outputs of the control model during the validation process. Some of the data required minimal manipulation, such as reducing the frequency of the timestep to 10-minute or hourly intervals. Sometimes, the experimental data had a high resolution (1-minute) timestamp, but in other cases, the data had a lower level of detail and needed to be used with a higher timestamp, which introduced some inaccuracies, particularly in the treatment of solar radiation data and its effect on the final results. However, other data required more complex manipulation, such as combining the output from multiple sensors or using mathematical models to obtain the desired variable.

An example of this is the treatment of solar data, where a decomposition model was implemented to provide separate values for direct and diffuse radiation for the control models. This was done by

calculating the beam and diffuse components of the solar radiation using the ENGERER2 (Bright and Engerer 2019) separation model. Besides the solar data, the measurements used to create the custom weather data files included outdoor air temperature and wind direction and velocity in addition to outdoor dry bulb temperature, the fraction of the sky covered by clouds, and the relative humidity of the air. The relative humidity data were obtained from the official weather station of Politecnico di Torino, located near the testing site. The total cloud cover was sourced from the widely used ERA5 climate reanalysis (Hersbach, H., Bell, B., Berrisford, P., Biavati, G., Horányi, A., Muñoz Sabater, J., Nicolas, J., Peubey, C., Radu, R., Rozum, I., Schepers, D., Simmons, A., Soci, C., Dee, D., Thépaut 2018).

Model Validation

The model validation activity has an important role in establishing the capabilities of the tools employed and assessing their performances. The validation process aimed to determine how well the DSF models could replicate the thermophysical and optical characteristics of the façade mock-up. In order to do this, the focus was placed on the DSF model alone rather than on the combination of the DSF and the virtual room. To ensure that the virtual room accurately reflected the physical test cell, the same dimensions were used, and the temperature of each surface and the indoor air node were set using schedules based on the available experimental data. This approach allowed the validation to be focused on the DSF model as all uncertainties related to the surrounding environment were removed. If a different approach had been taken, such as validating using quantities at the room level (e.g. indoor air temperature or energy required to regulate the temperature in the test cell), it would have been more difficult to identify the source of any discrepancies as there would be more variables and simulation routines involved, and it would be harder to determine whether the discrepancies were due to the routine under test or to other routines used to model other components in the room or to unknown factors in the modelling of other components of the room.

In addition to focusing only on the DSF model alone, it is also worth noting that no model calibration was carried out prior to the model validation. This approach was chosen to ensure that the model assumptions were replicable even in the absence of measured data to confront the results, which is often the case during the design phase. This approach allows the model to be more easily applied to other projects and situations where measured data may not be available. It can also help reduce the potential for bias in the model as its assumptions are not influenced by the specific data set it is being calibrated with. Overall, this approach can help improve the proposed models' reliability and applicability, making them more robust and generalisable.

The models were run using the different tested configurations, and for each of them, a period of approximately a week was used for the model validation. A warm-up period of the same length was used before the evaluated week. The validation of the models was carried out by identifying the main thermophysical parameters that play a role in the performance of DSF: the indoor surface temperature, the airgap temperature, heat flux exchanged by the inner skin with the indoor environment and the

transmitted solar irradiance. Moreover, the total energy crossing the façade was used to evaluate the influence of installing a DSF on the energy balance of the whole building. This parameter was not directly measured in the experimental campaign, but it had to be derived by two other measured quantities: the heat flux exchanged at the indoor-facing surface of the DSF and the transmitted solar radiation. In some cases, not all the parameters were available for the validations, either because the experimental data lacked a certain measured quantity for the analysed period or because not all the tools provided the same outputs. For example, due to some equipment issues during the experimental campaign, the heat flux data for the validation of the natural ventilation case could not be included in the results.

The different software tools were validated through quantitative analyses using both performance metrics and qualitative analysis of time profiles. This approach allows for the quantification of the performance and a deeper understanding of the different observed behaviours. The mismatch between the experimental data and the numerical data was quantified by calculating commonly used statistical indicators such as the Root Mean Square Error (RMSE) and the Mean Bias Error (MBE) (Hyndman and Koehler 2006).

The RSME indicator is used to quantify the degree to which the simulated data series differs from the experimental data series by calculating the average mean deviation (error) and the degree of data variation. Unlike the mean square error (MSE), the RMSE uses the same unit of measurement as the parameter of interest. Root means square error (RMSE) highlights the presence of larger errors better than other indicators like Mean Absolute Error (MAE), which is more sensible to outliers. However, this indicator does not indicate whether the model underestimates or overestimates the experimental data. To overcome this limitation, the MBE is used, which returns the average bias in the prediction of the simulated data. The MBE is a good indicator of the overall behaviour of the simulated data but should not be used as a measure of the model error since high individual errors in the prediction can still lead to a low MBE value due to cancellation effects (Ruiz and Bandera 2017). Nonetheless, since it has a sign, it can be used to quickly assess whether the overall prediction overestimates or underestimates the experimental data.

To evaluate the fitness of the models in predicting the total energy crossing the DSF over a given period, the normalised values of these indicators were also calculated. These indicators are the Coefficient of Variation of the Root Mean Square Error (CV(RMSE)) and the Normalised Mean Bias Error (NMBE). The NMBE measures how closely the energy use predicted by the model corresponds to the experimental data. CV(RMSE) allows one to determine how well a model fits the data; the lower the CV(RMSE), the better the simulated data. The choice of not using normalised indicators for assessing the thermophysical quantities was linked to the challenge of expressing the percentage error. Adopting this procedure for temperature, for example, would require calculating an average value of certain quantities that can be close to zero, resulting in very high errors even if the variation between the prediction and the measured value would be considered within the uncertainty of the instrument. This consideration led to using normalised indicators only when referring to predicting energy performances (ASHRAE 2014).

In addition to the numerical analysis using statistical indicators, graphical representations of the time profiles of the thermophysical quantities, both measured and simulated, were used to provide a qualitative and explanatory assessment of the models' performance. This approach was supported by the use of scatterplot and error distribution box-plot representations. The use of graphical representations helped to gain a better understanding of some phenomena that the statistical indicators were not able to depict. For example, the time shift of the surface temperature can be more clearly visualised through a graph of the temperature data over time rather than through a single numerical value. This approach allowed for a more comprehensive understanding of the DSF's performance and helped identify improvement areas.

Co-simulation

In building simulation, the term co-simulation is usually used to describe approaches allowing the coupling of different models, each describing only one part of the governing physical relationships in the overall system (e.g., thermal, airflow, daylighting, etc.). Each model is run in a separate simulation tool or unit so they can exchange simulation data during runtime and replicate the system's behaviour as a whole. Applying co-simulation techniques to an adaptive façade has been beneficial in taking advantage of the adaptive façade's intrinsic characteristic of adapting to trigger events (Taveres-Cachat et al. 2019). Co-simulation allows for dynamic creation and input of control sequences during the same simulation loop by exchanging information between tools at different time steps. This enables control responses for an adaptive façade to be defined during the simulation run based on a boundary condition, the current building state, and a pre-set control algorithm, resulting in a wider range of control options than offered by traditional BPS tools. Co-simulation approaches are also the only possibility to evaluate trade-offs in multi-domain controls that combine different sources of information for the control logic. For example, they are useful when energy performance requirements must interplay with user requirements and indoor environmental quality performance. (Taveres-Cachat et al. 2021).

The need for control of the modelled fully flexible DSF, particularly for investigating the performances of applying a model-based control (MBC) within a building energy simulation tool, led to the development of a co-simulation approach between IDA ICE and the controlling algorithm. As mentioned before and as shown in **P5** and **P6**, the tool chosen for developing a flexible model of DSF was IDA ICE, and the control algorithm was implemented into a Python script. Therefore, a routine was created to access the simulation results from IDA ICE and process them within the developed algorithm.

To achieve this, the model in IDA ICE was run through the IDA ICE Application Programming Interface (API). IDA ICE provides API functions in C programming language through a dynamic-link library called *idaapi2.dll*. By making direct calls to the API functions, it is possible to load a previously developed model into IDA ICE and perform operations using Python scripts. The IDA Message Broker Service communicates with IDA ICE and the external program. The API's functions allowed for connecting the model to IDA ICE (such as opening the model and saving the model) and managing the model objects.

The version of Python used was 3.8 64bit. The Python library *win32process* and *ctypes* enabled the IDA ICE process in Windows environment and interacted with the API, calling API functions.

To reduce computational time, the state of the actuators was communicated to IDA ICE through a text file, specifically a *.prn* file. IDA ICE uses these formatted text files, which are space delimited, to read external data such as weather files and to write the simulation results. The simulation was run using the "*Advanced level*" simulation, and the results of the simulation at the end of each parametric run were accessed directly from the model by reading the node value of the analysed element (room temperature, CO_2 level, etc.). These data were then passed to the optimisation algorithm, which chose the configuration for the following timestep. This operation was done for each hour of the analysed period. The use of hourly timesteps is connected to the computational time, and the timestep can be adjusted depending on the computational resources available and the desired level of precision.

Advanced Control

When developing an advanced form of control, it is important to define the objective that needs to be optimised to achieve the desired performance. In the case of an adaptive façade, its behaviour can impact numerous areas. As a result, optimal control for this type of façade must be able to satisfy multiple objectives simultaneously. This can include energy efficiency, thermal comfort, lighting quality, and other factors. Defining these objectives and understanding how they are interrelated will help guide the design and implementation of the control system and ensure that it can effectively manage the complex behaviour of the adaptive façade.

The control applied in the model-based control proposed in this work covers four different domains. To set priorities among these different domains, an overarching control tree was developed. Instead of formulating the optimisation problem as a single objective by weighting the different domains, the control tree allows for a more nuanced approach. Considering how the adaptive façade works and its potential interactions with the surrounding environment, the following priorities were established: indoor lighting, indoor air quality, thermal comfort, and minimum energy consumption (Figure 6). The multi-domain filters were applied with two fulfilment levels: for the indoor lighting, the thresholds were set according to the ISO 8995 (ISO 8995 2002) for office space; for the indoor air quality and thermal comfort, the thresholds were set according to the EN 16798-1 (EN 16798 -1 2019); finally, the energy consumption for cooling and heating was minimised.

The presence of occupants in the room affected which domains were further analysed using the control tree. In the case of an occupied room, the first domain that filtered the results was the 'natural light domain'; all the configurations that fulfilled the minimum requirements set for the values on the illuminance plane were used to check the following domain requirements 'air quality domain'. In case none of the simulated cases gave results within the criteria, the filter was disregarded, and all the configurations were used for the next step. This is done because there is no minimisation (or maximisation) in any of the filtering domains (except for the last one) to avoid the risk of selecting a

solution at the beginning that only satisfies (or partially satisfies) the requirements of one domain. After the 'air quality domain', the 'thermal domain' filtered the results; here, the operative temperature in the room was checked with the tolerance levels. Finally, the configurations that respected all these domains were filtered by the last condition: "minimum energy consumption". This last condition imposed a minimisation function to end up with a unique set of configurations to apply to the analysed timestep.

The described algorithm can be applied to any envelope systems used to tackle these four performance domains (a window, HVAC system, heating and cooling device, etc.), and in this work, it is applied to a flexible DSF integrated with the HVAC system. This approach allows the control system to make decisions that are in line with the goals and objectives of the building and help to optimise the performance of the adaptive façade.

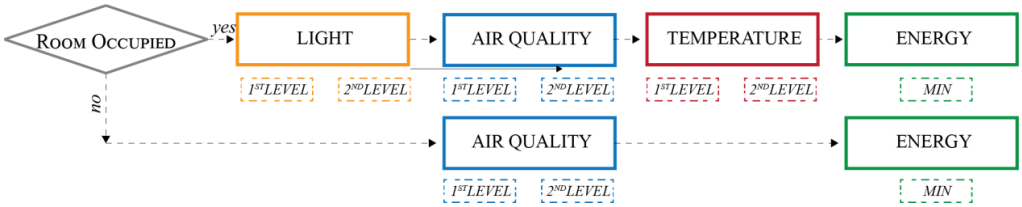

Figure 6 Multi-objective optimal control algorithm used in P6 (Catto Lucchino and Goia 2023)

1.6 Research articles

This work includes research articles that answer the identified research questions. Each of them includes a detailed description of the aims, objectives and methods. Therefore, rather than repeating those descriptions, the previous section served as a general overview of the methods employed in this thesis that will be detailed in the next chapters. Figure 3 shows the link between each paper and the research activities carried out in them.

The contribution of the author of this thesis in each scientific paper is listed below.

P1 E. Catto Lucchino, F. Goia, G. Lobaccaro, G. Chaudhary. Modelling of double skin façades in whole-building energy simulation tools: a review of current practices and possibilities for future developments. *Building Simulation, 12 (2019).* https://doi.org/10.101 7/s12273-019-0511-y

Contribution: Writing – original draft, Visualisation, Validation, Software, Methodology, Investigation, Formal analysis, Data curation, Conceptualisation.

P2 A. Gelesz, E. Catto Lucchino, F. Goia, V. Serra, A. Reith. Characteristics that matter in a climate façade: A sensitivity analysis with building energy simulation tools. *Energy and Buildings 229 (2020), 110467.* https://doi.org/10.1016/j.enbuild.2020.110467

Contribution: Writing – original draft, Visualisation, Validation, Software, Methodology, Investigation, Formal analysis, Data curation, Conceptualisation.

P3 E. Catto Lucchino, A. Gelesz, K. Skeie, G. Gennaro, A. Reith, V. Serra, F. Goia. Modelling double skin façades (DSFs) in whole-building energy simulation tools: validation and inter-software comparison of a mechanically ventilated single-story DSF. *Building and Environment 199 (2021), 107906.* https://doi.org/10.1016/j.buildenv.2021.107906

Contribution: Writing – original draft, Visualisation, Validation, Software, Methodology, Investigation, Formal analysis, Data curation, Conceptualisation.

P4 G. Gennaro, E. Catto Lucchino, F. Goia, F. Favoino. Modelling double skin façades (DSFs) in whole-building energy simulation tools: validation and inter-software comparison of naturally ventilated single-story DSFs. *Building and Environment (2023), https://doi.org/10.1016/j.buildenv.2023.110002.*

Contribution: Writing – original draft, Validation, Software, Methodology, Formal analysis, Data curation, Conceptualisation.

P5 E. Catto Lucchino, G. Gennaro, F. Favoino, F. Goia. Modelling and validation of a single-storey flexible double-skin façade system with a building energy simulation tool. *Building and Environment 226 (2022), 109704*. https://doi.org/10.1016/j.buildenv.2022.109704

Contribution: Writing – original draft, Visualisation, Validation, Software, Methodology, Investigation, Formal analysis, Data curation, Conceptualisation.

P6 E. Catto Lucchino, F. Goia. Multi-domain model-based control of an adaptive façade based on a flexible double skin system. *Energy & Buildings 285 (2023), 112881. https://doi.org/10.1016/j.enbuild.2023.112881*

Contribution: Writing – original draft, Visualisation, Validation, Software, Methodology, Investigation, Formal analysis, Data curation, Conceptualisation.

2 A review of current practices and possibilities for future developments

P1 *E. Catto Lucchino, F. Goia, G. Lobaccaro, G. Chaudhary. Modelling of double skin façades in whole-building energy simulation tools: a review of current practices and possibilities for future developments. Building Simulation, 12 (2019). https://doi.org/10.101 7/s12273-019-0511-y*[1]

Advanced building envelope systems can contribute to the reduction of greenhouse gas emissions and improve the energy flexibility of buildings while maintaining high levels of indoor environmental quality. Among different transparent envelope technologies, the so-called double skin façades (DSFs) have been proposed as an effective, responsive building system. The implementation of DSF systems in a real building is highly dependent on the capabilities of the prediction of their performance, which is not a trivial task. The possibility to use whole-building energy simulation (BES) tools to replicate the behaviour of these systems when integrated into a building is, therefore, a crucial step in the effective and conscious spread of these systems. However, the simulation of DSFs with BES tools can be far more complex than that of more conventional façade systems and represents a current barrier. This article is based on evidence from the scientific literature on the use of BES tools to simulate DSFs and provides: (i) an overview of the implementation of DSFs systems in BES tools, with the current capabilities of some selected BES tools; (ii) a comprehensive review of recent, relevant simulation studies, where different approaches to modelling and simulating DSFs are reported; and (iii) the identification of current gaps and limitations in simulation tools which should be overcome to increase the possibilities to correctly predict the performance of DSFs when integrated into a building.

[1] *Reproduced with permission from Springer Nature*

BUILD SIMUL (2019) 12: 3–27
https://doi.org/10.1007/s12273-019-0511-y

Modelling of double skin facades in whole-building energy simulation tools: A review of current practices and possibilities for future developments

Elena Catto Lucchino, Francesco Goia (✉), Gabriele Lobaccaro, Gaurav Chaudhary

Department of Architecture and Technology, Faculty of Architecture and Design, NTNU, Norwegian University of Science and Technology, Trondheim, Norway

Abstract

Advanced building envelope systems can contribute to the reduction of greenhouse gas emissions and improve the energy flexibility of buildings while maintaining high levels of indoor environmental quality. Among different transparent envelope technologies, the so-called double skin facades (DSFs) have been since long time proposed as an effective, responsive building system. The implementation of DSF systems in a real building is highly dependent on the capabilities of the prediction of their performance, which is not a trivial task. The possibility to use whole-building energy simulation (BES) tools to replicate the behaviour of these systems when integrated into a building is, therefore, a crucial step in the effective and conscious spread of these systems. However, the simulation of DSFs with BES tools can be far more complex than that of more conventional facade systems and represents a current barrier. This article is based on evidence from the scientific literature on the use of BES tools to simulate DSF, and provides: (i) an overview of the implementation of DSFs systems in BES tools, with the current capabilities of some selected BES tools; (ii) a comprehensive review of recent, relevant simulation studies, where different approaches to modelling and simulating DSFs are reported; and (iii) the identification of current gaps and limitations in simulation tools which should be overcome to increase the possibilities to correctly predict the performance of DSFs when integrated into a building.

Keywords

whole-building energy simulation (BES),
double skin facade (DSF),
EnergyPlus,
ESP-r,
IDA-ICE,
IES Virtual Environment,
TRNSYS

Article History

Received: 31 August 2018
Revised: 18 December 2018
Accepted: 24 December 2018

1 Introduction

1.1 Background

The name "double skin facade" (DSF) refers to a rather large spectrum of facade solutions that can be generally described as a *"system made of an external glazed skin and the actual building facade, which constitutes the inner skin, [where] the two layers are separated by an air cavity, which has fixed or controllable inlets and outlets and may or may not incorporate fixed or controllable shading devices."* (Pomponi et al. 2016). The adoption of a DSF aims primarily at realising a building with a "fully-glazed" appearance, while still preserving high energy and indoor environmental performance by using the air zone between the two skins as an integrated element of the building energy concept.

Efficacy of DSFs is a long-time debate (Oesterle et al. 2001), with studies showing that DSF can increase the indoor environmental quality and reduce the energy use in operation compared to traditional single skins (Singh et al. 2008; Chan 2011), as well as other studies which unveiled some controversial aspects of DSFs performance (Gratia and De Herde 2004).

A conclusive answer to the debate whether DSFs are more or less efficient than high-performing single skin facade is far from being found, and it cannot probably be reached in absolute terms. This is due to the fact the effectiveness of one solution or the other depends to a great extent on the detailed conditions of each specific situation, and the assessment needs to be carried out case by case.

The impossibility to define general rules in the design of DSFs and the need to optimize these systems in relation

E-mail: francesco.goia@ntnu.no

to the entire building energy concept, thus calls for suitable design tools, such as whole-building energy simulation (BES) tools, which can address the performance of such systems in combination with that of the entire building, thus supporting architects and engineers in the design process towards energy efficient buildings.

In this context, the successful design of DSFs remains a challenging task. The untapped potentials given by a carefully design DSF, suitably integrated in a high-performance building energy concept, and properly controlled while in operation, can be partly attributed due to a lack of thorough understanding of the benefits and possible risks, and the inability to measure them reliably during the design (and preliminary design) phases.

1.2 Challenge in the use of BES tools for the simulation of DSFs

BES tools have the potential to provide information to several stakeholders (Clarke and Hensen 2015), and in particular to facade engineers when it comes to DSFs. However, the historical development of BES tools has always followed the development of new technologies with a certain delay. While current tools are reliable when it comes to the modelling and simulation of conventional building envelope systems (Loutzenhiser et al. 2007), the modelling and simulation of DSFs through BES tools is still a challenging task even if DSF is nowadays considered an "established" technology, and it is still questionable whether such tools can accurately or not describe the transient heat and mass transfer phenomena that occur in these facade systems.

The reason for this is that the detailed description of the physical behaviour behind each building component is not the primary consideration in BES tools, which instead focus on the evaluation of the energy loads of an entire building (Oh and Haberl 2016), and on the interaction between the various parts. Moreover, even in the case of very advanced or flexible engines, some limitations in the implementation of more sophisticated models might be related to the graphical user interface of the tools, rather than to the calculation engine, or to the possibility to implement more advanced control strategies and to run multi-domain analyses within the same software (Loonen et al. 2017).

BES tools have since years considered a necessary element to move forward with the real uptake of advanced building systems, and among them DSFs, and the reliability of these tools was tested in a series of research activities. For example, the first systematic approach to the evaluation of the performance of BES tools in replicating the behaviour of DSFs was presented ten years ago in the final report of IEA ECBCS Annex 43 and SHC Task 34 "Testing and Validation of Building Energy Simulation Tools" (Kalyanova and Heiselberg 2008). However, since this activity, no significant follow up on this topic was carried out. New, custom-made models for DSFs were developed, but minimal upgrades have occurred in BES tools in the last decades when it comes to the possibility of simulating DSF systems.

1.3 Aims and structure of the paper

This paper intends to provide those researchers and designers who are approaching the simulation of DSFs through BES tools, with an overview of existing information and practices in this domain, in order to enable them to make an informed decision on the tools and approaches, given the current panorama of possibilities implemented in BES tools.

The paper presents, in Section 2, a brief re-cap on few selected background topics related to DSF technologies and their physical-mathematical models. This information can be useful for the readers, especially those less familiar with DSF systems before the following sections are read. The overview of the current capabilities of some selected BES tools for the modelling and simulation of DSFs is then presented in Section 3, followed by a review of recent selected simulation studies appeared in the scientific literature, where different approaches for modelling DSFs are seen, together with their effects (Section 4).

Furthermore, the article presents a comprehensive identification of gaps and limitations in present-day simulation tools, which should be overcome to increase the possibilities to correctly predict the performance of DSFs when integrated into a building (Section 5).

In order to frame the information to be elaborated and conveyed through the paper, and to base the paper on a clear set of records, the analysis has been limited to five of the most popular BES tools – EnergyPlus, IDA–ICE, IES Virtual Environment, ESP-r, and TRNSYS (Crawley et al. 2000, 2008; Aschaber et al. 2009; Hand 2011) – and to a relatively recent time range (after year 2000).

The planned audience for this paper is composed by both, researchers and practitioners who want to use, evaluate, and develop BES tools for the simulation of DSFs. It is not the intention of this paper to provide a comprehensive and comparative evaluation of the performance of the different BES tools in replicating one or another specific DSF (i.e. the paper does not report a quantitative estimation of each software's reliability, nor an inter-software comparison). However, the paper has the ambition to gather the most recent trends and report evidence of modelling of DSFs through BES in order to become a reference document for those who approach this topic and are willing to contribute to the development of the field of simulation of advanced window technologies. This is, in fact, a clear gap in the current scientific literature, where information on the simulation of

DSFs though BES tools is not gathered in an easy to use way.

2 Briefs of double skin facade systems and their modelling

Comprehensive reviews and focused studies can be found in the literature on a wide range of different elements related to DSFs, including:

- the analysis of the performance of DSF systems (Shameri et al. 2011; Barbosa and Ip 2014; Pomponi et al. 2016);
- the typology of glass that is usually used for the different layers of the facade (Roth et al. 2007; Baldinelli 2009);
- the shading systems that are usually hosted in the ventilated cavity between the two layers of the facade (Jiru and Haghighat 2008; Barbosa and Ip 2014);
- the cavity depth of the DSFs, which may vary, usually, in the range from 200 mm to more than 2 m (Chan et al. 2009);
- the different overall typology of DSFs according to the geometrical features of the facade (Kim and Song 2007; Wong 2008).

While DSFs have been primarily investigated as solutions to allow thermal loads to be reduced, both in winter and in summer (Chan et al. 2009), acoustics, daylighting and fire protection behaviour (Ding et al. 2005) are also among the analysed aspects of the performance of these systems.

2.1 Typologies and classification of DSF

DSFs are usually classified according to specific characteristics such as the type of construction, the geometry, the ventilation mechanisms in the cavity, and the different flow paths. The classification of DSF according to the structure of the cavity (Oesterle et al. 2001) (i.e. as box-window, shaft-box, corridor type and multi-storey facade) is among the most used ones. Barbosa and Ip (2014) and Poirazis (2004), have classified DSF between a narrow cavity and a wide cavity, with narrow being cavity width up to 40 cm and wide being cavity width more than 40 cm. This limit was determined by the minimum width required for maintenance purposes in the cavity, and not based on considerations on the thermofluid behaviour within the cavity. Other studies (Saelens et al. 2003; Jiru and Haghighat 2008; De Gracia et al. 2013) have categorised DSF cavity based on ventilation, which can be either mechanical or natural. Mechanically ventilated facades are usually strongly integrated with the HVAC system of the building (where the airflow is an imposed quantity set by the HVAC plant). In a naturally ventilated facade, the driving force for natural ventilation is either thermal buoyancy or wind pressure, or both. Therefore, the airflow is in this latter case not easy to control nor to predict, as it continuously changes depending on the weather conditions.

Other classifying dimensions of a DSF involve the origin of the airflow and its destination (Saelens et al. 2003), which eventually define the airflow concepts as summarised by Haase et al. (2009). The possible flow paths, illustrated in Fig. 1, are:

- Supply air: the DSF supplies air to the indoor environment.
- Exhaust air: the DSF removes indoor air.
- Static air buffer: the DSF acts as a buffer with convective air movement only within the cavity.
- External air curtain: the DSF cavity is ventilated by outdoor air with no connection to the indoor air.
- Internal air curtain: the DSF cavity is ventilated by indoor air with no connection to the outdoor air.

2.2 Numerical modelling of DSF

Numerical simulation of DSF systems consists in the modelling of both heat transfer phenomena inside solid components, and between solid components and air, as well as the mass transfer (airflow) within the (ventilated) cavity and the indoor/outdoor environment. All these phenomena can be modelled with different degree of accuracy/detail, following established methods for building physics modelling in buildings (Underwood and Yik 2008). A survey in the scientific literature (De Gracia et al. 2013) shows indeed that there is a very broad spectrum of approaches that have been adopted in this context. These approaches can be grouped into four categories, as illustrated in Fig. 2, ordered by the level of complexity (and associated computational time):

i) empirical correlations and simple analytical models;
ii) combined thermal and airflow networks models;
iii) intermediate explicit models;
iv) computational fluid dynamics (CFD) models.

2.2.1 Empirical correlations and simple analytical models

This modelling approach focuses on the overall performance

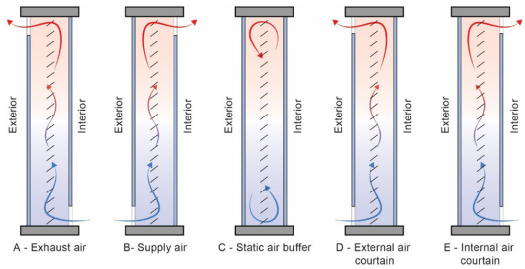

Fig. 1 Possible airflows in double skin facades (redrawn from: Haase et al. 2009)

Modelling approach	Short description	Features (possibilities vs. limitations)
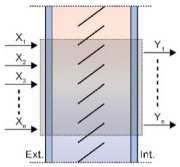 i) empirical correlations and simple analytical models	• Empirical correlations or simplified analytical relationships. • The overall performance of the DSF as a single component. • Simple performance parameters.	✓ Very scalable and computationally efficient. ✓ Easily integrated into larger models. ✖ Outputs not useful for the optimisation of the DSF. ✖ Lack of sensitiveness to small variation in the configuration. ✖ Correlations obtained from experiments or simulations.
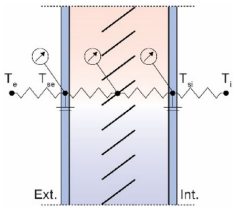 ii) combined thermal and airflow networks models	• Directly derived from the architecture of BES tools. • Based on the integration of two equivalent networks: the thermal and the airflow network. • Different degree of complexity of R-C networks of the components of the DSFs. • Pressure-driven network to account for air movement.	✓ Not too high computational demanding. ✓ Implemented in most BES tools. ✓ It can be used for both mechanically and naturally ventilated DSF. ✓ It provides data on the thermophysical behaviour of the DSF as a function of its geometrical and material properties. ✖ The reliability of the fluid-dynamic phenomena might be improved. ✖ Mass and heat convective transport based on empirical correlations. ✖ Calibration of the model often needed. ✖ Lack of comprehensive, freely available data set for the calibration of the models.
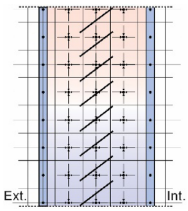 iii) intermediate explicit models	• It is used when the level of explicit description of the phenomena is greater than the combined thermal and airflow networks models. • More comprehensive formulations of conservation equations are adopted. • The cavity is divided into control volumes that are coupled due to the presence of the air channel.	✓ Different levels of complexities in modelling the fluid dynamics processes. ✓ Suitable for integration (through co-simulation) in BES tools. ✓ Provides a higher level of detailed analyses of the thermofluid dynamic behaviour of the DSFs. ✖ High(er) computational time. ✖ Currently, the co-simulation approach is not fully developed. ✖ Models may be readjusted to take into account different flow regimes.
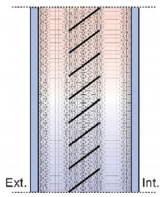 iv) computational fluid dynamics (CFD) models	• Based on the solution of the conventional set of conservation equations in computation fluid dynamics, in combination with turbulence models. • Detailed volume division of the cavity and coupling with detailed masse/energy transport equations.	✓ Provide different levels of analysis (from a complete system to sub-system/components). ✓ Very detailed information on the thermofluid phenomena. ✓ Fluid-dynamics, turbulence, thermal and radiation accounted into one model. ✖ Very high computational time. ✖ Only steady state conditions, or very short-time transient state phenomena. ✖ Not integrated with the entire building. ✖ Complexity in choosing the turbulence model.

Fig. 2 Overview of Numerical modelling approaches

of the DSF as a single component, and therefore without defining the performance of its subsystems. This strategy is based on either empirical correlations or simplified analytical relationships (usually derived by solving a simple version of the energy balance conservation equation).

An interesting sub-group in this category is represented b models based on a non-dimensional analysis (application of Buckingham theorem) of the thermofluid-dynamic behaviour of a DSF. For example, in a study 14 non-dimensional number have been proposed to model a DSF (Balocco 2004; Balocco and Colombari 2006).

Other examples of this type of models are those based on simple lumped-parameters representation of the 1D (or sometimes 2D) structure of the DSF (e.g., Park et al. 2004;

Oliveira Panão et al. 2016)), which require relatively few input data.

One of the main strengths of these approaches is that they are very scalable and computationally efficient, and can, therefore, be easily integrated into larger models (for example in whole-energy building simulation tools). This method can provide some useful information in the early stage of the design process; however the information that can be extracted is usually limited to the overall behaviour of the system, and cannot be used for the optimisation of the design of the DSF (the approach is too little sensitive to small variation in the configuration). The main drawback of these methods is the need to rely on correlations, which are obtained through either experimental analysis or higher-order simulations.

2.2.2 Combined thermal and airflow networks models

This approach is directly derived from the architecture of BES tools and is based on the integration of two equivalent networks: the thermal and the airflow network. This approach has a rather long history, dating more than 20 years (Tanimoto and Kimura 1997), and is still at the basis of most of the simulation of DSFs carried out with BES tools, and can be used for both mechanically (Stec and van Paassen 2005) and naturally ventilated DSF (Fallahi et al. 2010). Given its relevance and uptake in many BES tools, more information on this approach will be given in the following Section 3. In short, these models are based on lumped-parameter descriptions (with different degree of complexity of R-C networks) of the components of the DSFs coupled with a (primarily) pressure-driven network to account for air movement between the different nodes of the model, which represent a certain domain of the DSF cavity.

These models still rely, in some aspects, on empirical correlations to solve some of the transport equations (especially the mass transport and convective heat transfer), and on a rather detailed information of the thermophysical properties and geometrical feature of the components constituting the DSFs (glazing systems, shading devices, openings, etc.).

The combined thermal and airflow networks approach has its main strength in providing fast, useful information about bulk flows still without consuming high computational resources. These models can, up to some extent, be used to select and optimise different configurations of DSFs and to carry out sensitivity analyses which can be useful not only at the preliminary stage of the design but also at a later phase when the configuration of the DSF need to be investigated further. Furthermore, because of their intrinsic architecture, they still can be easily integrated into BES tools.

However, the reliability, when it comes to the description of the fluid-dynamic phenomena (and, where these are strongly linked to the thermal phenomena, the reliability of the thermal performance too) might not be too high, and much is left to the sensitivity of the modeller when it comes to the selection of the empirical correlations to be used in different domains. In this context, the calibration of the models is often a necessary activity to assure robustness of the results, but the lack of comprehensive, freely available dataset for this activity is one of the main obstacles in the implementation of more accurate models based on this approach.

2.2.3 Explicit intermediate models

This group gather different approaches where the level of explicit description of the (especially fluid-dynamic) phenomena is greater than the combined thermal and airflow networks models, but less than more complex modelling approaches (computational fluid dynamics, CFD). In these cases, the simulation of the fluid motion in the cavity is not obtained only by pressure-driven equations, but more comprehensive formulations of conservation equations are adopted. Because of this, the computational time increases, together with the level of detail of the described phenomena, which therefore allows deeper analyses to be carried out.

Examples of explicit intermediates models are the so-called zonal approach (Jiru and Haghighat 2008; Wang et al. 2016), and the so-called control volume approach (Faggembauu et al. 2003a,b; Saelens et al. 2003, 2008). In both these cases, the cavity of the DSF system is divided into control volumes (in a number greatly smaller than that typical of CDF) that are coupled due to the presence of the air channel. In this class of methods, different levels of complexity can be adopted in order to model the fluid dynamics processes, ranging from rather advanced empirical correlations up to the explicit formulation of the momentum conservation equation, in combination with conventional approximations of the physics of the fluid flow (e.g. Boussinesq approximation). These modelling are used to determine, in combination with the thermal flows through the DSFs, the airflow in the cavity.

Because of their architectures, these approaches are still suitable for integration (through co-simulation) in BES tools, even if as revealed by the research presented in this paper, such a combination is not really seen in the current panorama. Explicit intermediate models can allow, when compared to combine thermal and airflow networks, more detailed analyses on the thermofluid dynamic behaviour of the DSFs to be carried out, and probably represents the most detailed model that can support the study of transient states without requiring too extensive computational resources. This means that such a modelling level can work well both regarding preliminary design and optimisation. However, as much as for the combined thermal and airflow networks, a large number of correlations and approximations are necessary to

assure a short-time calculation time, and this calls for the need of validation and/or calibration of models, as well as high competence of the modeller to select the most suitable correlations and auxiliary equations, which can have a large impact on the results of the simulations.

2.2.4 Computational fluid dynamics analysis (CFD)

This method, based on the solution of the conventional set of conservation equations in computation fluid dynamics, usually in combination with turbulence models, cannot only accurately describe the flow regime, velocity, and turbulence of the airflow in the cavity, but also can determine the heat transfer coefficient of the DSF system (Bhamjee et al. 2013; Darkwa et al. 2014; Iyi et al. 2014; Dama and Angeli 2016).

If from the one hand this method has its main strength in the possibility of obtaining very detailed information on the thermofluid phenomena in the skins and cavities, on the other hand, this comes at the cost of the very long time necessary to carry out the calculation. This means that such an approach is only suitable to analyse steady state conditions, or very short-time transient state phenomena, but are instead not suitable to investigate transient states. This limitation clearly reveals that CFD is usually reserved for a very detailed analysis of phenomena in DSFs, which are usually accounted for at the stage of optimisation of the system, or system development. CFD has proven to be a useful tool on the study and optimisation of DSF due to its ability to conjoint fluid dynamics, turbulence, thermal and radiation models into a single computer simulation, allowing to parameterise such complex multi-physics problem numerically (Pasut and De Carli 2012), but only when the focus is placed on the building envelope system alone – i.e. not integrated with the entire building. Because of the discontinuity in terms of time-scale, space-scale, and computational time between CDF and BES tools (Srebric et al. 2000), the coupling of these two approaches is, for the time being, not an exploited solution, as this leads to an exponential increase in the computational time in the BES tool (Tian et al. 2018).

3 Numerical modelling approaches in five selected BES tools

3.1 Overview and methodology

In the following sections, two alternative ways of modelling DSFs in five selected BES tools are presented. The first one (combined thermal and airflow networks) is the most general one and can be implemented, though in different ways, in all the selected BES tools. This modelling approach is capable of handling very different configurations of DSF, thus allowing researchers and designers to evaluate solutions that are fully custom-made.

The second one (a dedicated sub-routine that simulates specifically a DSF component, and that can be based either on simplified models, or on combined thermal and airflow networks, or on explicit intermediate models), is only seen in some of the five tools, and can be adopted only if an ad-hoc module has been developed (either by researchers or by a software house) to explicitly model a DSF system in a specific simulation environment. The key features of these BES tools are summarised in Table 1, as shown in Catto Lucchino and Goia (2019).

The choice of the BES tools to limit the investigation presented in this paper is based on both evidence from the literature about the most used BES tools in research and consulting engineering practice (Loonen et al. 2017), as well as, on the first-hand expertise of the authors. The analysis presented in this section focuses on how each software deals with the thermal and airflow analysis of DSFs and is based on the analysis of both the available technical information on the tools (e.g. manual, engineering references), relevant information found through the scientific publications, and on the experience of the authors.

3.2 Combined thermal and airflow networks

In general, an airflow network in combination with a thermal network is based on the discretisation of the temperature and pressure field of a thermodynamic system (i.e. of a volume of air, or of a building element, or a combination of the two) through the identification of a suitable number of representative nodes where the energy (thermal network) and mass (airflow network) conservation equation is computed. Each node is linked to the adjacent nodes by relevant transport equations for both the thermal network (different heat transfer equations depending on the nature of the heat exchange) and airflow network (Bernoulli equation), and can including the source or sink for both heat and pressure. Airflow, which is primarily attributed to pressure differences between two nodes, can also take into account the air motion due to the wind – and not only the temperature difference across two nodes resulting in a buoyancy-driven flow (Zhai et al. 2015). Elements capable of storing internal energy are associated with thermal capacity.

The two networks can be coupled in two different ways, following the classification proposed by Hensen (1995): through a "ping-pong" method, in which the thermal and flow model run in sequence (i.e. each use the results of the other model in the previous time step); and through the "onion" method, in which the thermal and flow model iterate within one-time step until satisfactory small error estimates are achieved. Even if the second way is more accurate than the first one (but less computationally expensive), both techniques are suitable to realise an overall algorithm that

Table 1 Overview of different features of BES tools concerning modelling phenomena of DSFs (table derived from Catto Lucchino and Goia (2019))

		EnergyPlus	ESP-r	IES–VE	TRNSYS	IDA–ICE
Airflow–thermal coupling		Airflow network "AIRNET"	Airflow network	Airflow network "MACROFLO"	Airflow network model "CONTAM" or "COMIS" -TRNFLOW	Airflow network model
DSF component		"Airflow Windows"	—	—	—	"Double-Glass Facade"
Conduction solution method		CTF, finite difference[1]	Finite volume	Finite difference	CTF, finite difference [2]	Finite difference
Convection	External	6 empirical models[3]	12 empirical models[3]	Single empirical model: McAdams (1954)	Fixed value	Single empirical model McAdams (1954)
	Internal	Several models[4]	Alamdari and Hammond (1983)	5 different models[5]	2 models[6]	DNCA (Brown and Isfält 1974)
Radiation		n-surfaces interaction, infinite reflections (exact solution)	2- and 3-surfaces interaction, infinite reflections	Fresnel Equations applied to 2 surfaces interaction, 10 angles of incidence, infinite reflections	n-surfaces interaction by using (Gebhart 1961) factors	n-surfaces interaction, infinite reflections (exact solution)
Influencing parameters in the flow model	Wind force	X	X	X	X	X
	Wind fluctuations	—	—	—	—	—
	Buoyancy	X	X	X	X	X
Leakage area		Crack method or Effective Leakage Area (ELA) method	Crack method	Crack Flow Coefficient AIVC (1994)[7]	Crack method	Crack method or Effective Leakage Area (ELA) method

[1] By default, EnergyPlus uses the CTF method, but it was recently extended with a new finite difference scheme for conduction, to allow for modelling temperature- or time-dependent material properties (Pedersen 2007; Tabares-Velasco and Griffith 2012). The usage of this new approach has been largely unexplored in the literature.

[2] Simulation users can also choose to bypass the CTF approach by coupling TRNSYS Type 56 with finite element or finite difference schemes such as Type 260 or Type 399 (Kośny 2015).

[3] The work of Mirsadeghi et al. (2013) identify 17 different models used in BPS tools.

[4] There are different settings to set the calculation routine: TARP Algorithm, Simple natural convection, Trombe Wall, Adaptive, Adaptive Convection Algorithm (US Department of Energy 2010). In the last one, there are 29 different settings of hc equations. For vertical surfaces, according to room airflow conditions and heat flow direction different correlations are available. For simple buoyancy: Fohanno and Polidori (2006), Alamdari and Hammond (1983), ASHRAE Vertical Wall. Mechanical ventilation: Khalifa (1989). Mixed: Beausoleil-Morrison (2000).

[5] Fixed coefficients specified by CIBSE; variable coefficients calculated according to CIBSE methods; variable coefficients calculated from the relations proposed by Alamdari and Hammond (1983); user-specified fixed convection coefficients (IES 2014).

[6] The routine used by Type 80 applies two different correlations. No reference to existing models has been found (TRNSYS 17 2009).

[7] The equation used represents the best fit to a large range of experimental data analysed by the Air Infiltration and Ventilation Centre.

keeps together the two aspects of the thermal fluid model of the DSF (Stec and van Paassen 2003).

Integrated thermal and airflow networks are implemented differently in each software tools, as illustrated in the next five sub-sections. The modelling of a DSF through this approach consists in realising a combined thermal and airflow network that represents the DSF's cavity and its boundary layers, and to connect this with the overall thermal and airflow network representing the building. In this approach, a DSF becomes an "integrated" part of the building, and is not a building envelope component, with the advantage of (usually) high flexibility in the way the airflow can be connected to the different parts of the building, including the integration with HVAC systems.

3.2.1 EnergyPlus

In *EnergyPlus* the pressure and airflow model is based on AIRNET (Walton 1989). A detailed description of the airflow network model may be found in the work of Waldon and Dols (2013). This model can be used to accurately simulate the sophisticated relationship between the airflow and the transient heat transfer phenomena, including multi-zone airflows driven by outdoor wind, buoyancy, and forced air (US Department of Energy 2010).

In order to model a DSF using the thermal and airflow network model in *EnergyPlus*, the zones of the ventilated cavity and room are divided into several stacked zones, where each zone is an airflow network node. These nodes are linked by using different airflow network objects in *EnergyPlus,* which calculates the pressure at every node, and airflow through each linkage, which then calculates (in an iterative way) the node temperatures and humidity ratios with the given zone air temperatures and zone humidity ratios. These multizone airflow calculations combined with heat transfer calculations are performed at each HVAC system time step which determines the final zone air temperatures, pressures, and humidity ratios (Le et al. 2014; Peng et al. 2016).

In order to predict the leakage phenomena, two ways are available in *EnergyPlus*: (i) the crack method and (ii) the Effective Leakage Area (ELA) method. For the use of the crack method, the following inputs such as air mass flow coefficient, reference condition temperature correction factor and air flow exponent (dimensionless) are required. Their values are not easily found in literature, while leakage area values are available for different building component types (ASHRAE 1993).

When it comes to the thermal network, *EnergyPlus* offers a wide selection of different methods for calculating both exterior and interior heat transfer coefficient (ranging from the so-called TARP (Sparrow et al. 1979; Walton 1981), to the MoWiTT correlation (Yazdanian and Klems 1994), and to more basic, simple ASHRAE models (ASHRAE 1993)), as well as, different algorithms for the solution of conduction in building assembly.

3.2.2 *ESP-r*

ESP-r's building thermal model is based upon a finite-volume heat balance discretisation method. A nodal network is also incorporated into *ESP-r* for airflow modelling and is integrated with the thermal model network in the "onion" form.

Following the same approach adopted in *EnergyPlus*, the ventilated cavity of a DSF can be studied through *ESP-r* by virtually dividing this environment in a stack of a certain amount of thermal zones, which are separated one from the other by fictitious transparent surfaces with high conductivity, negligible thermal mass, and high emissivity. These zones are interconnected to the adjacent one or the external nodes by air ducts and inlet/outlet air openings (network components).

Different convection regimes can be used in *ESP-r* to model the operations of a DSF. For example, the cavity can be enclosed and have only internal circulation, or it can be open with air flowing through the cavity from outside which can be both stack effect driven and wind-driven. When the DSF is ventilated, the Bar-Cohen and Rohsenow (1984) correlation can be used to predict the convective heat transfer for the surfaces facing the cavity; when the cavity is closed, the default Alamdari and Hammond (1983) correlation is instead adopted. For calculating the external convection heat transfer, several methods are implemented in the tool (McAdams, CIBS, MoWiTT, etc. (Mirsadeghi et al. 2013)).

3.2.3 *IES–Virtual Environment*

In opposition to *EnergyPlus* and *ESP-r*, two simulation environments developed and maintained with a strong focus on research, and characterised by being open-source tools, *IES* Virtual Environment is a commercial program whose code is not accessible, and the user cannot add any additional simulation modules to enhance either application-oriented or general-purpose modelling capabilities. This limits the application of *IES* Virtual Environment to "application oriented" models already included in the software.

The airflow network approach integrated into the software is called *MacroFlo* and is based on (macroscopic) zone mass balance and inter-zone flow–pressure relationships (MacroFlo 2012; Hensen and Djunaedy 2005). The flow through each opening is calculated as a function of imposed pressure difference and the characteristics of the opening. These characteristics differ for cracks and larger openings. For a given set of room conditions (temperature and humidity), *MacroFlo* solves the air flow problem by balancing net air mass flows into and out of each zone by considering the net air inflow for each of the room's openings, and any net room airflow imbalance imposed by the system simulation program *ApacheHVAC* (the sub-routine that models the HVAC of the building).

The main driving forces of natural airflow are the pressure field generated by the wind and the buoyancy effect. Wind pressures on the building exterior are calculated at each simulation time step from the weather data file. Wind speed and direction data is combined with information on opening orientations and wind exposures to generate wind pressures on each external opening. The calculation involves wind pressure coefficients derived from wind tunnel experiments, combined with an adjustment for wind turbulence.

MacroFlo calculates buoyancy-related pressures, which vary with height in accordance to air density, on the assumption of a uniform air density in each room.

For the outside air mass, both wind and buoyancy-induced pressure must be included. At the start of a flow calculation the wind pressures are known (from the weather file), but then a buoyancy component of pressure in each room is only determined up to an additive constant. This constant is established from the opening flow characteristics and the requirement for flow balancing in each room.

ApacheSim is the name of the sub-routine dedicated to the dynamic thermal simulation program (IES 2004), based on a finite difference approach for the solution of the heat transfer in solid components. When it comes to convective heat transfer coefficient, the external surfaces of the building, where wind-driven forced convection is dominant, are modelled using McAdams' empirical equations (McAdams 1954). Five options are available for modelling the convective heat exchange between air masses inside the building and the adjacent building elements, ranging from CISBE fixed and variable coefficient to the "Alamdari and Hammond" (1983) calculation method, from the European standard BS EN 15265 to user-specified fixed convection coefficients that can be set directly in the construction database (IES

2004). Air temperature and humidity values are assumed to be uniform within the room.

IES couples the airflow and the thermal network by using the "onion" approach. *MacroFlo* and *ApacheHVAC* run in tandem with *ApacheSim*, and the calculations of the programs are interdependent. In the course of an iterative procedure, zone temperature and humidity conditions (together with any net supply or extract from *ApacheHVAC* supply or extract rates) are repeatedly passed to *MacroFlo*, which calculates the resulting natural ventilation flows. These flows are then used by *ApacheSim* to update the zone conditions, and so on. Upon convergence, this procedure balances both air flows, and heat flows for each zone.

The theory applied in *MacroFlo* is based on the flow characteristics of openings that are small if compared with the volumes they connect. While this is a good approximation for most windows, doors and louvres, it is a poor approximation in some other modelling situations, notably, flow in facade cavities and flues. For this type of situation, where the openings have a diameter similar or equal to the diameter of the adjacent spaces, adjustments to the opening parameters are necessary in order to achieve a good model. For this reason, it is possible in a ventilated cavity to adopt different types of resistance for the airflow. These can be: the resistance associated with the exchange of air between the cavity, the outside environment, and the adjacent building spaces; the resistance due to the obstructions in the cavity (internal blinds, constrictions, obstructions protruding from the sides, walkways etc.); the frictional resistance with the walls of the cavity.

3.2.4 TRNSYS

TRNSYS is a simulation code originally developed by solar thermal systems (TRNSYS 17 2013), which also offers the possibility to model and simulate multi-zone buildings through the so-called "Type 56", a sub-routine of the software specifically developed for the solution of the energy balance in a building. Since the release of version 17, a thermal zone can have more than one air node. Each node represents a volume of air perfectly mixed, characterised by one temperature. It is possible to define the thermal capacity of the air enclosure and additional heat capacity (i.e. blinds) within the air node itself. Moreover, the exchange of the heat flow is not automatically defined as "mutual" among adjacent air nodes. The reason for this is to allow the user to describe cross ventilation or a ventilation circle within three or more air nodes.

The treatment of long-wave radiation exchange with the outside (sky, ground, external obstructions and shading devices), as well as long-wave radiation resulting from multiple reflections on interior surfaces within the cavity, applies the so-called "Gebhart" factor (Gebhart 1961). The view factors are the key tools of this method; in contrast to the purely geometric view factor, the factor by Gebhart includes optical properties, and it is defined as the part of the emission of a surface that is absorbed by another surface including all alternative paths within reach. The implementation of this detailed approach has been applied to a highly-glazed atrium with good outcomes (Aschaber et al. 2009). At the same time, a detailed model of the beam and diffuse solar radiation is available to model a DSF cavity. Standard treatment of solar radiation, beam and diffuse separately is now applied when passing the second layer of fenestration (the inner skin of the DSF). The specification of solar properties of the glazed facades is performed using the LBNL tool "Window" that generates the glazing description data to be added to the standard TRNSYS windows library.

To perform combined heat transfer and airflow simulations, TRNSYS provide two different approaches, through two different sub-routines/software: CONTAM and TRNFLOW. CONTAM is the bulk airflow modelling program developed by NIST (Walton and Dols 2002, 2013). In TRNFLOW the multi-zone airflow model COMIS has been integrated into the thermal building model Type 56 (Weber et al. 2002). CONTAM uses the so-called "ping-pong" approach, while TRNFLOW applies the "onion" method.

- CONTAM

The process of creating a link between CONTAM and Type56 involves three steps. The utility link to do this is called "Type 97".

As the first step, the building's thermal model with appropriate inputs and outputs is created using TRNBuild. The second step concerns the creation of an airflow model of the same building in CONTAM. Thirdly, the CONTAM building model and the TRNBuild building model are linked together using either the TRNSYS Simulation Studio or TRNSHELL (TRNSYS 17 2009). The process of creating a model in CONTAM involves defining zones and defining air links that connect the zones to one another and that connect the zones to ambient conditions. By using the utility link Type 97, the thermal model takes infiltration and interzonal air flows and calculates zone temperatures in return. Then Type 97 takes these zone temperatures and recalculates the interzonal airflows based on the updated information. Iteration continues until both the zone temperatures and the interzonal air flows converge upon a solution.

- TRNFLOW

TRNFLOW is the integration of the multizone airflow model COMIS (Conjunction of Multizone Infiltration Specialists) into the thermal building module of TRNSYS (Type 56). The data for both models can be input with the enhanced user interface TRNBUILD.

Using air mass conservation in each node, a system of nonlinear equations is built and solved to determine the node pressures, and the mass flows. Four classes of nodes are used to define the airflow network: constant pressure nodes, thermal air nodes, auxiliary nodes, and external nodes. It is important to notice that TRNSYS distinguishes between zones and air nodes. TRNFLOW interacts with the air nodes, not zones. Cracks, window joints and openings, shafts as well as ventilation components like inlets and outlets, ducts and fans represent the links among nodes (University of Wisconsin 2005). For each type of connection, there exists a relationship between the flow through the component and the pressure difference across it. The driving forces of the flow are, as always, wind pressure and buoyancy (resulting from temperature and air composition differences). On the latter, specifying the height of each air node and air-link to each other is important in order to account the pressure distribution correctly.

3.2.5 IDA–ICE

In IDA–ICE the thermal model is fully integrated with the airflow network. As the other BES tools, each thermal zone is schematized as an air-node, which represent the conditions of the room. The information available is not only the temperature but also the humidity and the CO_2 ratio for each thermal zone. Wind and buoyancy driven airflows through leaks and openings are taken into account via a fully integrated airflow network model (Kalamees 2004).

IDA–ICE handles a wide range of simulation problems by using equation-based modelling adopting a variable time-step differential-algebraic (DAE) solver. The model library of IDA–ICE is written in Neutral Model Format (NMF), a common format of model expression that allows users to interconnect different modules, as well as develop sub-routines directly in the programming interface. The link concept also allows a user of a simulation environment to connect sub-models at the interface level rather than variable by variable (Sahlin et al. 1996). IDA–ICE provides three different user interface levels; at the most advanced one, the "Mathematical" level, the models can be changed and own models can be written by using the NMF language. Among the different components available, there is a specific component for modelling DSF, called "Double-Glass Facade". This component, which will be discussed in Section 3.3.3, is in practice a node (representing the indoor air of the cavity) connected to the thermal–airflow network of the entire building, as well as to all the other objects (surfaces, blinds) that constitutes the DSF. This air-node can be linked to other nodes of the thermal-airflow network according to the need of the user, and can, therefore, represent in a relatively easy way different configurations of DSF. Because of this feature, the simulation of a DSF in IDA–ICE through the establishment of an ad-hoc, thermal–airflow network (as seen in all the previous software tools) is, to some extent, not very different than the use of the dedicated sub-component.

3.3 DSF component

In addition to the modelling strategy where an airflow network is combined with a thermal network to represent the cavity of the DSF, and to connect the component to the outdoor and indoor environment of the building, some software directly integrate a sub-routine dedicated to the modelling of DSF systems. These sub-models follow in the category of building envelope systems and are object linked to the other components of the simulated environment according to the requirements and possibilities set by each of the simulation environment. While on the one hand this approach should lead to more accurate simulation (as the models for DSF are on-purpose developed to replicate the thermal-fluid behaviour of these systems), on the other hand, this approach is usually less flexible than the one where an ad-hoc, combined thermal and airflow network is created by the modeller.

3.3.1 EnergyPlus

A dedicated component is available in *EnergyPlus* to simulate ventilated glazed cavities, under the name "Airflow Windows". The component models only forced airflow between glass panes. It can run in five different modes, i.e. supply, exhaust, indoor air curtain, outdoor air curtain, and dual airflow window (US Department of Energy 2018). In this simplified configuration, the convective heat transfer coefficient from the glass pane to the air gap is calculated as the combination of the glass-to-glass heat transfer coefficient for non-vented (closed) cavity and the effect of the mean air velocity in the gap. The mean temperature of the gap air is calculated as a function of the inner glass surfaces' temperature and the inlet and outlet air temperature, and the change in the temperature across the height of the window is calculated using a logarithmic correlation between the height of the cavity and the air temperature. The modelling approach implemented through this model is, therefore, a simple analytical model when it comes to the airflow calculation algorithm, coupled with a quite detailed modelling when it comes to heat transfer in the window assembly. The entire module is then linked to a larger BES tool (*EnergyPlus*) based on combined thermal and airflow networks. One of the major limitations of the current module is that only mechanically ventilated cavities can be modelled, and therefore the airflow rate needs to be given as input (either as a fixed value or as a variable value through a schedule).

In the case of a shading device installed in the cavity, the software allows to couple this component with a detail

thermal model, which accounts for the thermal interactions between the shading layer (shade, screen or blind) and the adjacent glass. It is assumed that the shading device is centred between the two panes of glass so that the airflow is divided equally between the two gaps.

3.3.2 TRNSYS

The official releases of TRNSYS do not contain any dedicated DSF component model. However, due to the architecture of the software, which allows add-on sub-routines to be realized (primarily in Fortran, C, C++, or more in general, any other language provided a DLL can be created), some researchers have developed on-purpose Types, which perform as a plug-play codes, that model DSF systems (Safer et al. 2005, 2006; Gavan et al. 2007).

In these studies, a DSF was modelled with single glazing as the external facade and internal double-glazing with internal venetian blinds as solar protection. The whole model was divided into a series of temperature nodes with balance equations to calculate convection exchanges between the air of the channel and glazing; short/long wave exchanges and enthalpy exchanges between the air of each band are also considered.

However, while the descriptions of the models can, up to some extent, be found in the published article, the codes are often not released together with the publications, and therefore not easily accessible.

3.3.3 IDA–ICE

A separate component called "Double-Glass Facade" exists in IDA–ICE (Equa 2013). The integrated double facade model is based on specified leakage areas at the top and bottom of a window system. The leakages represent the systems openings and the airflow through them is based on air pressure differences between the facade cavity and the external environment. It should be noted that the program accounts both for thermally driven airflow through the cavity and wind effects. The model can however also be run to represent a mechanically ventilated system, by imposing a known airflow rate, which then overwrites the automatically calculated airflow based on natural mechanisms.

The window detailed calculation method makes a layer by layer computation of multiple reflections. Entering direct and diffuse short-wave radiation is absorbed first by the outer window plus possible curtain, and then by the inner window. The external convective heat transfer coefficient is calculated using the equations given by (Clarke 1985).

The component has been investigated with comparative and empirical tests under the IEA SHC Task 34 (Kalyanova and Heiselberg 2008). It is fully integrated with the thermal and airflow network of the rest of the building. Natural airflow through the air gap is driven by the density difference between the gap and ambient air and the wind. All airflows can have arbitrary directions, and through the connection to other components (e.g. HVAC), it is possible to apply an induced flow into the cavity. The component creates a wall adjacent thermal zone in which the air mass, the moisture and CO_2 balance are conducted.

The software also conducts a heat balance at the level of the inner wall, in which is accounted the convection between the interior glass and the air node of the cavity. Accordingly to which is the dominant flow (natural or forced convection), the software chooses the appropriate convective heat transfer coefficient. Convection from surfaces is treated non-linearly using a standard IDA–ICE function called *u_film* for natural convection. The forced convection is calculated as a function of the airspeed and dominated one from natural and forced convection is selected with a maximum function.

4 Capabilities and limitations of BPS tools in modelling DSFs

4.1 Methodology

In this section, a collection of selected simulation studies focusing on the modelling of DSFs through a BES tool is presented. The systematic review was conducted by mean of the scientific literature databases (i.e. SCOPUS and Google Scholar), coupled with a chain-sampling technique. The following keywords were used to identify the primary documents in the search: "Double skin facade", "DSFs", "Simulation", "BPS" and "name of the software". Identified papers investigating only the energy use of the system, without taking into account in the analysis of any parameters related to the thermal/airflow domain (e.g. temperature, mass flow, air velocity, etc.) (Leigh et al. 2004; Sala and Romano 2011; Marinosci et al. 2011; Seferis et al. 2011; Cheong et al. 2014; Shan 2014; Barecka et al. 2016; Fantucci et al. 2017) were also included in the review, as well as few, selected studies where interesting modelling approached for opaque ventilated cavities were investigated, to provide the readers with a wider overview of the possibilities and challenges of these systems.

At first, the analysis was restricted only to a time period ranging from 2011 to 2018, in order to catch the latest development in the field. However, by applying this criterion, it was noticed that the reference collected did not fully cover the five software tools previously identified. For this reason, the search was later extended to publications dating back until 2000. This decision has probably reduced the degree of novelty of the studies analysed, but it also allowed to track the evolution of some tools (for example, *EnergyPlus* and *TRNSYS*), as well as to unveil trends in the use of one software or another. Notably, it is possible to see that *ESP-r*,

very used in the early years of the Millennium, when it was one of the very few codes available, has been in the latest years is less and less used compared to the other simulation environments.

4.2 Overview

The focus of the review of the selected simulation studies presented in the section is primarily placed on the analysis of the choices of the modelling strategy and the different parameters in the simulation environment. The studies reported in this review are listed in Table 2, and discussed in the following section, by grouping them according to the BES tool used for the simulation instead of using other categories (such as the type of DSF with respect to the geometry or the airflow type), and by placing them in chronological order. The selection of studies does not aim to comprehend all the analysis appeared in the literature, as

Table 2 Overview of papers analysing the performances of double skin facades

BPS	Reference	Year	Climate (Koppen-Geiger)	Transparent Opaque (T, O)	Type of DSF	Cavity width	Shading devices in the cavity	Cavity Ventilation (N, M)	Type of analysis (Thermal/ Visual/ Airflow)	Method of modelling (DSF component vs T+A network)	Airflow rate or airspeed	No. of thermal zones	Validation of results
EnergyPlus	(Kim and Park 2011b)	2011	Dfa	T	Box Window	50 cm	X	N	T, A	T+A network	max 0.16 m/s	3	Yes
EnergyPlus	(Choi et al. 2012)	2012	Dfa	T	Multi Storey	N/A	—	N	T	T+A network	N/A	1[1]	Yes[2]
EnergyPlus	(Soto Francés et al. 2013)	2013	Bsk	T	Box Window	N/A	—	N	T	DSF component	N/A	N/A	Yes
EnergyPlus	(Papadaki et al. 2013)	2013	Csa	T	Corridor-type	100 cm or more	X	N	T	T+A network	Buffer zone or 6 ACH	N/A	Yes
EnergyPlus	(Le et al. 2014)	2014	Cfa	T	Box Window	50 cm	X	N	T, A	T+A network	N/A	3	No
EnergyPlus	(Mateus et al. 2014)	2014	Csb	T	Box Window	20 cm	X	N and M	T	T+A network	0.11 m^3/s [3]	3	Yes
EnergyPlus	(Anđelković et al. 2016)	2016	Cfa	T	Multi Storey	N/A	—	N	T, A	T+A network	N/A	3[4]	Yes
EnergyPlus	(Peng et al. 2016)	2016	Cwa	Semi-T	Box Window[5]	40 cm	X	N	T, A	T+A network	N/A	3	Yes
EnergyPlus	(Alberto et al. 2017)	2017	Csb	T	Different configurations	25 cm, 50 cm, 100 cm	—	N	T, A	T+A network	N/A	N/A	No
EnergyPlus	(Abazari and Mahdavinejad 2017)	2017	Bsk	T	Box Window	N/A	X	N	T	DSF component	N/A	N/A	No
EnergyPlus	(Kim et al. 2018)	2018	Cwa	T	Box Window	44 cm	X	N	T, V	T+A network	N/A	4	Yes
ESP-r	(Barták et al. 2001)	2001	Cfb	T	Multi Storey	N/A	X	N	T,A	T+A network	0.7 m/s	1[1]	No
ESP-r	(Leal et al. 2003, 2004a)[7]	2003	Csb	T	Box Window	N/A	—	N	T,A	T+A network	0.4 m/s	1, 2, 4 or 8[6]	Yes
ESP-r	(Kokogiannakis and Strachan 2007)	2007	Cfb, Csa	T	Multi Storey	10 cm	—	M	T,A	T+A network	N/A	N/A	No
ESP-r	(Leal and Maldonado 2008)[7]	2008	Csb	T	Box Window	N/A	—	N	T,A	T+A network	0.4 m/s	4	Yes
ESP-r	(Høseggen et al. 2008)	2008	Cfb	T	Multi Storey	N/A	—	M	T	T+A network	N/A	3	No
ESP-r	(Qiu et al. 2009)	2009	Cwa	T	Box Window[5]	60 cm	—	N	T,A	T+A network	min 0.08 m/s max 0.7 m/s	4	Yes
ESP-r	(Marinosci et al. 2011)	2011	Cfb	O	Multi Storey	24 cm	—	N	T,A	T+A network	0.12 m/s	3	Yes
ESP-r	(Seferis et al. 2011)	2011	Csa	O	One Storey	4 cm	—	N	T,A	T+A network	N/A	3	Yes
ESP-r	(Fantucci et al. 2017)	2017	Cfa	O	One Storey	5 cm	—	N	T,A	T+A network	N/A	3	Yes[8]

Table 2 Overview of papers analysing the performances of double skin facades (Continued)

BPS	Reference	Year	Climate (Koppen-Geiger)	Transparent Opaque (T, O)	Type of DSF	Cavity width	Shading devices in the cavity	Cavity Ventilation (N, M)	Type of analysis (Thermal/ Visual/ Airflow)	Method of modelling (DSF component vs T+A network)	Airflow rate or airspeed	No. of thermal zones	Validation of results
IES–VE	(Pekdemir and Muehleisen 2012)	2012	17 climates	T	Different configurations	2 ft–3 ft–4 ft	—	N	T, A	T+A network	N/A	N/A	No
IES–VE	(Pomponi et al. 2017)	2017	Am, Cfb	T	Multi Storey	1 m	X	N	T, A	T+A network	Max 1.7 m/s	1[1]	Yes[10]
TRNSYS	(Saelens et al. 2004)	2004	Cfb	T	Box Window	N/A	X	N and M	T,A	DSF component	N/A	N/A	Yes
TRNSYS	(Eicker et al. 2008)	2008	Cfb	T	Box Window	50 cm	X	N	T,A	DSF component	Max 0.6 m/s	N/A	Yes[2]
TRNSYS	(López et al. 2012)	2012	Dfb	O	One Storey	5 cm	—	N	T,A	T+A network	0.15 m/s	5	Yes[2]
TRNSYS	(Aparicio-Fernández et al. 2014)	2014	BSk	O	Multi Storey	10 cm	—	N	T, A	T+A network	N/A	2–3[1]	Yes
TRNSYS	(Elarga et al. 2016)	2015	Bwh, Cfa, Cfb	T	Multi Storey[5]	14 cm	X	M in Summer, N in Winter	T, A	T+A network	N/A	2[1]	Yes
TRNSYS	(Khalifa et al. 2015)	2015	Csb	T	Box Window	30 cm	X	N	T, A	T+A network	20–60 m^3/h	6	Yes[11]
TRNSYS	(Khalifa et al. 2017)	2017	Csa	T	Box Window	30 cm	X	N	T, A	T+A network	N/A	6	No
TRNSYS	(Yu et al. 2017)	2017	Dfa	T/O	Multi Storey[5]	50 cm	—	N	T,A	T+A network	N/A	N/A	No
TRNSYS	(Shahrestani et al. 2017)	2017	Cfb	O	—	15 cm	—	N	T,A	T+A network	N/A	1	Yes
IDA–ICE	(Gelesz and Reith 2015)	2015	Cfb	T	Box Window	80 cm	X[9]	M	T	DSF Component	N/A	N/A	No
IDA–ICE	(Colombo et al. 2017)	2017	Cfb	T	Multi Storey	75 cm	X	N	T, A	T+A network[12]	1.6–1.7 m/s	N/A	No
IDA–ICE	(Eskinja et al. 2018)	2018	N/A3	T	Box Window	N/A	—	M	T	T+A network	N/A	1	Yes

[1] For each floor.

[2] Calibration of the model.

[3] The value is referred to the mechanically ventilated DSF.

[4] The facade is divided into three zones (lower (1st and 2nd floor), middle (2nd and 3rd floor) and upper (4th and 5th floor) zone).

[5] The DSF has integrated PV panels.

[6] In Leal et al. (2004a), the authors test the accuracy of a 16-zones and 4 × 2-zones model. While the 16-zones model performs as or better than the 8-zones model, the 4 × 2 ones perform worse.

[7] The SOLVENT window has been studied in different test cells, Leal et al. (2003, 2004a) in PASSYS test cell and Leal and Maldonado (2008) in PASLINK test cell, both in Porto, Portugal.

[8] In all performed tests, simulations were carried out with artificial weather conditions, adopting constant temperature for some time and then applying a temperature gap from 0 to 35 °C. The tests were performed without solar radiation or any other disturbance with the intention to isolate only one single event. Authors consider solar influence, regarding HVAC control, to be only disturbance.

[9] The shading devices are modelled only in the summer configuration.

[10] Proper validation of the results has not been carried out; nevertheless, a calibration of the model with the results of a CFD analysis has been conducted.

[11] The airflow rates, since no data were available, come from the measurements presented in Saelens (2002).

[12] The results obtained by the thermal network are coupled with a CFD analysis.

it is almost impossible to assure full coverage of available studies, but rather to be fully representative of the different adopted modelling strategies, the variety of DSF configurations analysed, and the large spectrum of study's objectives (the reason of the study). In particular, this last aspect, which can give some insights into the use of one or another type of BES tool, will be deepened further in Section 4.9 with the information provided in Table 3.

The review also reports if validation of the simulation study results through comparison with experimental data has been done. It is herewith important to highlight that calibration and validation of the model, which are two distinct

procedures, aiming at two different scopes, are sometimes blurred into a single activity. This makes it complicated to understand what is the actual performance of the simulation tools when predicting the behaviour of a DSF system without a calibration process – something that it is not always possible.

However, it is important to remember that it is not the aim of this paper to compare the software tools in terms of performance, nor in terms of usability. The scope of the review is instead to obtain an overview of the different possibilities and challenges (as identified by the modellers and by the authors) of different implementations of DSF modelling in BES tools, as well as to review current practices in the use of different BES tools in the simulation of DSF systems.

4.3 Key elements searched in the simulation studies

When it comes to the key elements of the review of the selected studies, it is evident that the modelling of a naturally ventilated cavity is most difficult one (Kalyanova and Heiselberg 2008), as the uncertainty in the modelling regards not only some simulation's assumptions, like the number of thermal zones in which the cavity needs to be divided but also other issues related to the heat transfer phenomena and the airflow modelling. These aspects still need a more detailed study as only a few studies deepened them (Charron and Athienitis 2006; Eicker et al. 2008; Kim and Park 2011b; López et al. 2012; Mateus et al. 2014; Khalifa et al. 2015).

The heat transfer phenomena is a complex problem that has to take into account the simultaneous action of conduction, convection and radiation heat exchange. One of its most challenging aspects is the determination of the convective heat transfer coefficients, both internal and external. The choice of the internal convective heat transfer coefficient is fundamental for the estimation of the air velocity, and greatly affects the overall performance of the DSF, in particular when a shading device is present in the cavity.

On the side of the airflow modelling, the main challenge is probably to set or estimate the appropriate discharge coefficients and pressure loss coefficients for each part of the DSFs, and to estimate the correct relation between pressure loss and airflow rate through the opening, especially when the DSFs is connected with the outdoor air. It is challenging to find alternative values to the default ones offered by the software, which are not always suitable to model the pressure drops in a DSF.

4.4 EnergyPlus

Kim and Park (2011b) simulated different flow paths in a naturally ventilated box window DSF by using *EnergyPlus 6.0*. The major errors between the simulation results and actual measurements were addressed to the uncertainty of measurement and simulation input parameters, the assumptions and simplifications of the reality needed during the modelling process and the limitations of the tool. The limitations pointed out are mainly connected to the several calculation methods available for estimating the interior convective heat transfer coefficient, which does not consider the cavity airflow pattern for the calculation of the convective heat transfer. In this case, the ASHRAE Vertical Wall algorithm has been chosen. As for the exterior convective heat transfer coefficient, the authors choose the "MoWiTT" method, which is known to be suitable for very smooth vertical surfaces (e.g., windows) in low-rise buildings. It is important to underline that *EnergyPlus* also gives the possibility to calculate the convective heat transfer of the air-gap between each blind opening. However, the software simplifies the complex geometry and features of the blinds: for example, the blind opening is assimilated to equivalent hole area which leads to an inaccurate air gap velocity and the effect of the cavity air velocity on the interior convective heat transfer coefficient is ignored. The effect of the uncertainty in simulation inputs relevant to the airflow (heat transfer coefficients, leakage area, and wind pressure coefficient) in and around buildings is a potential cause of inconsistency between the simulation and measurement.

For this reason, the authors run a calibration of these parameters on the model, showing a better agreement, with the measured values. Successively Kim and Park (2011a), the authors compared these results with the ones of an in-house DSF component (written in MATLAB language) and co-coupled with *EnergyPlus*. In terms of temperature prediction, the results are more accurate because the model includes an airflow velocity term in the heat transfer coefficients expression. Nevertheless, the simulated cavity air velocity of both models does not precisely mimic the actual physical phenomena.

Similar conclusions are reached by Le et al. (2014) while studying a box-window DSF modelled under a typical hot summer and cold winter climate in Changsha via *EnergyPlus 7.0*. The paper presents a simulation method, which is suitable for designers to establish some optimal configurations of DSF. The modelled cavity has been divided into three stacked zones. The authors, as already stated by Kim and Park (2011b), identify the calculation method of the interior convective heat transfer coefficient as one of the main liability of the software.

In a similar study, Mateus et al. (2014) carried out the validation of a DSF box-window model, both naturally and mechanically ventilated, developed using *EnergyPlus 7.1*. The developed model uses, as internal and external convection coefficients, the TARP algorithm, based on ASHRAE

correlations. In the natural ventilation mode, DSF ventilation was modelled using the effective leakage area (ELA). In both cases, the authors opted to consider only buoyancy-driven natural ventilation, without accounting the wind effects. The errors, from the measured temperature, result smaller in the mechanically ventilated configuration; yet the difference in the prediction of internal temperatures in a free running DSF is considered acceptable. In their study, they conduct a sensitivity analysis on the number of thermal zones to adopt in the modelling; the use of a single vertical thermal zone for the DSF (as opposed to three vertical zones) lead to significant increase in error in radiant temperatures. Moreover, the authors investigate the impact of solar radiation measurement accuracy on the simulations; the standard single horizontal global radiation sensor technique is proved inadequate.

In the process of establishing the best control strategy during the heating operation phase, Choi et al. (2012) carried out a calibration of the model, developed using *EnergyPlus 6.0*, of a multi-storey DSF of a building located in South Korea. Although the airflow network method is adopted, the wind pressure coefficient was calculated by using CFD, which can lead to more accurate results than by using data from wind tunnel experiments or analytic models. The whole facade was modelled as four discretised thermal zones (one per floor) with virtual horizontal openings set as always open, while the temperature measurements were referred to four vertical points. Since the software cannot account for temperature stratification in one node, the average value of the temperature recorded during the experiment was adopted in the validations process. The limitations of this tool, as well as the absence of the cavity's air velocity validation, affect the reliability of the model. In a follow-up study (Joe et al. 2013), the calibrated model is furtherly enhanced to take into account the effect of the BIPV and the catwalks present in the facade. Moreover, each storey is divided into two thermal zones rather than one. In this paper, the authors provide more information regarding which parameters adopted in developing the model (opening discharge coefficients, crack flow and air mass coefficient, interior and exterior convection algorithm, etc.).

Anđelković et al. (2016) modelled a multi-storey DSF of an office building in Serbia using *EnergyPlus 8.2*. The choice of some model parameters is based on the previously mentioned studies (Kim and Park 2011b; Choi et al. 2012; Joe et al. 2013; Mateus et al. 2014). The major obstacles identified in this study is the time step-resolution of the software, which is not low enough to predict the airflow correctly in the cavity. Whereas, the authors consider *EnergyPlus* to be a reliable choice when it came to the relation between simulation accuracy and the time required for the simulation.

Peng et al. (2016) developed a PV-DSF model representative in *EnergyPlus*. The interactions among thermal, power and daylighting performances were reasonably well modelled by coupling the heat-transfer model, airflow network model, PV power model and daylighting model in *EnergyPlus*. The limitation of the software in representing the inlet and outlet louvres of the real PV-DSF was overcome by adopting four openable windows with interior venetian blinds in the PV-DSF model. This approximation was proved to be a reasonable solution by comparing the results with experimental data.

Other studies analyse the performance of double skin facades by mean of *EnergyPlus* without mentioning the challenges of the modelling process. Papadaki et al. (2013) carried out a parametric analysis to evaluate the DSFs' configuration in hot climatic condition; the outcomes show the importance of an adequate ventilation rate in the cavity. Alberto et al. (2017) conducted a parametric study performed for a DSF, applied in a building with indoor gains corresponding to office type occupation and located in Porto. The reduction of the cooling load is directly connected to reducing air temperature inside the air gap.

The possibility to implement a different numerical model was studied in the work conducted by Soto Francés et al. (2013). An opaque-facade model was integrated into the simulation code of *EnergyPlus* by using a non-dimensional approach (Balocco 2004). The model was then compared with experimental data; the significant discrepancies are found in the air velocity prediction, mainly due to the difficulties to predict the wind direction correctly. Among the simplifications adopted by the authors, the model ignores the thermal inertia of the outer layer of the facade.

4.5 ESP-r

One of the first examples of using ESP-r in analysing a DSF can be found in Barták et al. (2001). The authors compared the results of different configurations of a multi-storey DSF during summer: naturally ventilated and as a buffer zone. In this case, the influence of the wind is not relevant; the buoyancy forces are the dominant driving force for the airflow. The results of their analysis show the strict correlation between the airflow in the cavity and the temperatures both in the cavity and on the panes' surfaces.

Leal et al. (2003, 2004a) studied the SOLVENT prototype, a box window in which absorptive glazing with a low shading coefficient is adopted as a shading device. In summer, it is applied on the exterior side while in winter it is applied inside. A parametric study is carried out about the number of thermal zones into which the window air channel should be divided (1, 2, 4 or 8). Results show that there is the dependence of the simulation outputs upon the number of zones into which

the window is divided. The air gap velocity and cooling needs are predicted noticeably better by the 4-zone and 8-zone models, while none of the models correctly predict the air gap temperature. It should be noted that the models do not take in consideration the effect of wind. Moreover, they investigated which heat transfer and localised loss coefficients should be adopted in order to obtain satisfying simulations results. The results show that these parameters have little effect on the accuracy of the predictions for the air temperature and the velocity in the air gap. There is, also, a perceptible overestimation of thermal inertia in ESP-r simulation, which may have a substantial impact if there is a dynamic HVAC control of the zone. In a later study, Leal and Maldonado (2008), conducted another analysis of the SOLVENT window, adopting slightly different assumptions (4 stack thermal zones, "MoWiTT" method for external convection). The developed model is then calibrated with the results of a more detailed study on the nature and quantification of the heat convection at the open air channel (Leal et al. 2004b). This improved model shows a good agreement between the measured and the calculated air velocity.

Høseggen et al. (2008) studied the performances of a multi-storey DSF on an office building in Nordic climate. The simulations predict a reduction of 20% in heating demand when a DSF alternative was used instead of a single skin facade. In order to guarantee a tolerably accurate prediction of the facade performance, the cavity convection regimes and the connection between the cavity fiction divisions were assessed. The zones are divided by fictitious transparent surfaces with high conductivity, negligible thermal mass and high emissivity, and coupled by an airflow-network, which also includes the inlet opening at the bottom and the top outlet opening at the top of the facade. The Bar-Cohen & Rohsenow correlation is used to predict the convective heat transfer for the surfaces facing the cavity when it is open. When the cavity is closed, the default Alamdari and Hammond (1983) correlation is adopted. The paper also details on how a DSF with controllable windows and hatches for natural ventilation can be implemented in the simulation program. The operation of the window was set to depend on both the temperature in the office and the cavity of the DSF, but since in ESP-r there is no option to control two parameters at the same time, a dummy air node was introduced. This made it possible to have two openings between the indoor air node and the node in the DSF, where one represented the actual window, and other represented the negligible fluid resistance when open.

Kokogiannakis and Strachan (2007) used the EN ISO 13790 standard to set the boundary conditions for modelling and simulating a multi-storey DSF. The authors discuss the differences that might occur when the DSF is modelled using inputs mentioned in standard (e.g. fixed values of inside and outside convective and radiative heat transfer coefficients) instead of adopting values generated by a transient simulation program, such as ESP-r. For both annual heating and cooling demand, the results are lower than those obtained by the simplified ones. During the cooling season, the results between the two calculation methods differ on a larger scale (more than 50%) than of those obtained for the heating cases. Moreover, the analysis investigates the behaviour of the facade cavity works as a supply duct or an external curtain. In both cases, regarding heating and cooling demand, the external air curtain settings performs worse than the external supply.

Qiu et al. (2009) developed a model of a box window DSF with PV panels integrated. The authors divided the air cavity into four stack zones and the "MoWitt" method has been adopted to calculate the external convection coefficient. The outcomes show that the simulated temperatures of the glass and the solar electricity output are in good agreement with the measured data. The outward ventilation of the ventilated photovoltaic double skin facade could reduce the cooling load in summer and, in contrast, increase the heating load in winter. The results show a higher chimney effect, with airflow rates sensitively more significant, in winter rather than in summer.

Some studies (Marinosci et al. 2011; Seferis et al. 2011; Fantucci et al. 2017) where an opaque ventilated facade was modelled and simulated also used the approach of multiple vertically stacked thermal zones which represented the air gap in the ventilated facade. The number of these vertical zones depends upon the total height of the gap to give a reasonable representation of the stratified air. Each zone is interconnected to the adjacent one or the external nodes by air ducts and inlet/outlet air openings. In their works, the authors carry on a thorough analysis of the convective coefficients, even though in the different correlations are adopted in the different studies. Fantucci et al. (2017) run a calibration process of the model, in which among other parameters, different convective heat transfer correlations are. MoWiTT (external surfaces), Halcrow (low vert.) correlation (Halcrow 1987) (internal surfaces) and Bar-Cohen – Rosenhow (air cavity) produce the closest results to experimental data.

4.6 IES–VE

As in the *IDA–ICE* case, not many results matched the research keywords; a reason could be the prevalent commercial use of this tool. Not many details on how the model was developed are given if not only the material and geometric properties. Nevertheless, some application of the software highlights the speed in implement models and processing

information. Pekdemir and Muehleisen (2012) compared various types of naturally ventilated DSFs in all seventeen ASHRAE climate zones, obtaining results from 187 models. The different types of DSFs are created following a set of parameters such as stratification type, the permissibility of airflow, and width of interstitial space. The depth of the DSF cavity was shown to influence the performance significantly with the narrowest cavities showing higher overheating occurrences. Pomponi et al. (2017) carried on a comparative thermal comfort analysis of a whole building model with DSF in both tropical and temperate climates (London and Rio de Janeiro). *IES–VE* has been used as the main software tool, but at the same time, the accuracy and reliability of the results were also cross-checked against a computational fluid dynamic (CFD) software package. *IES–VE* seems to underestimate induced airflow rates in comparison to CFD. Trying to reduce this difference, the authors performed other simulation changing the interior heat transfer coefficient (the commonly used 'Alamdari & Hammond' calculation method is not suited for narrow cavities (Dickson 2004)), the discharge coefficients (the default value 0.62 is adopted by the software) and the number of zones in which the cavity is divided. On this matter, *IES–VE* itself warns not to adopt too many divisions, as it would introduce an artificial resistance to the flow field because the software algorithm does not model stratification explicitly. Nonetheless, none of the tests conducted led to significant changes in the airflow prediction. The study shows that wind force plays a dominant role in driving airstreams in and through the DSF, which highly impacts the overall thermal performance of the buildings.

4.7 TRNSYS

Some authors developed external components to couple with *TRNSYS*. Saelens et al. (2004) highlighted the significance of the inlet temperature as a boundary condition for numerical DSF models. Especially when the air flowing through the cavity is to be reused, a correct inlet temperature modelling is of significant importance to come to reliable energy assessments. A numerical model, of both mechanical and natural ventilation, based on a finite volume method, is developed externally and then coupled with the BPS tool *TRNSYS*. Eicker et al. (2008) implemented their model, with a new experimentally derived empirical Nusselt correlation, in Type 111. Experiments on a box window were done both in the laboratory and in a real office-building project in Germany. From the experiment results, the authors were able to calculate the heat transfer coefficient to use in the building simulation. The simulation results show that the air gap velocity, calculated using this coefficient, is a good approximation to the measured value.

In the other papers found in literature, the thermal model is coupled with the airflow network. Khalifa et al. (2015) coupled CONTAM with *TRNSYS* to evaluate the thermal/ventilation performance of a single-storey naturally ventilated DSF (provided with a shading device). The modelled temperature distribution was validated against experimental results, showing a maximum error of 3%. The differences occurring can be contributed to the combined effects of error propagation due to simplification in geometry and lack of accuracy in some boundary conditions. The enhanced radiation modelling, provided by *TRNSYS* version 17, plays a key role and shows very good results in estimating transmitted solar irradiance, both in winter and summer. As for the airflow rates, since no data were available, the results were compared with the measurements presented in another study (Saelens 2002), an experiment on which the whole paper is based on. Some limitations were found in estimating the blind influence by using the shading factor defined in TYPE 56; it may not be so appropriate in the case of venetian blinds where the complexity expected in airflow and shading modelling imposes further requirements. By using the same validated model, Khalifa et al. (2017) assessed the impact of the inner layer composition in a double-skin facade system on the energy requirements of conditioned office buildings. The results show that using a high thermal mass is beneficial in both winter and summer.

Elarga et al. (2016) run a comparative analysis of the cooling energy performance of a DSF integrated with semi-transparent PV cells inside the facade cavity. Both naturally and mechanical ventilation has been modelled using TRNFLOW, in different climate conditions. In developing the transient model, the authors adopt characteristic flow parameters commonly found in the literature (Charron and Athienitis 2006) and international standards (ASHRAE 2007). The comparison of the measured values of the exhaust air temperature from the cavity and *TRNSYS* calculated results shows a good approximation. The integration of PV system shows positively effect on the building sensible cooling energy demands and in increasing the peak production power. Yu et al. (2017) conducted a similar study on a double skin facade with integrated PV panels in R.O. Korea. The model uses both TRNFLOW and a specific DSF-PV component, Type 568 (TESS 2014) to calculate no convective and radiative losses at the back of the PV collector. This module allows to calculate the PV production and to model the heat through the rear of the PV. As in the other study, in terms of heating load, a PV-DSF is a better solution regarding using a double skin to prevent an increase in the cooling load. The positive influence on PV production of coupling a PV system with a ventilated opaque facade is also showed in Shahrestani et al. (2017). In order to obtain a more accurate simulation, the

air cavity on the back of each PV module is defined as a single zone with thermal interaction with each other as well as the PV modules. The airflow network was modelled in TRNFLOW and it was coupled with the multi-zone model in *TRNSYS*.

In assessing the energy performances of an opaque facade, López et al. (2012) carried out an in-depth analysis of the parameters that mostly affect the thermal model coupled with TRNFLOW. Starting from the data collected from the experiment conducted in the Indoor Environmental Engineering Laboratory of the Department of Civil Engineering of the Aalborg University, the authors carefully calibrate the model. The experimental results showed that the flow rates induced in the facade cavity were due to mixed driving forces: wind and buoyancy. In order to replicate these effects in the model, the pressure coefficient (Cp), the discharge coefficient (Cd), the convective heat transfer (interior and exterior), are evaluated from the measured data. Comparing the results of the modelling, the air and surface temperatures were predicted with better accuracy than flow and energy rates, even if the cavity airflow conditions were predicted correctly. If these precautions are not taken, not always the results are satisfying. The study conducted by Aparicio-Fernández et al. (2014), which used a TRNFLOW to model a multi-storey opaque naturally ventilated facade, shows the difference from the experimental data. The deviation from the mean distribution of the measured air temperature in the cavity is between 15% and 20%.

4.8 IDA–ICE

In the three studies of *IDA–ICE* found in literature, there is no deep description of how the DSF models have been built, neither of whose parameters have been chosen; yet for the thoroughness of the review, they have been reported. Gelesz and Reith (2015) used *IDA–ICE* model for DSF to compare the energy effects of choosing a DSF over a traditional double glazed pane. They used the "double facade" component to model two configurations of DSF, one set as a buffer zone in winter conditions and the other one as a ventilated cavity with shading devices for summer analysis. Eskinja et al. (2018) investigated the air temperature in the cavity using the airflow network approach. In their analysis, the authors compared the results with the experimental results of a scaled system, showing a great disagreement about the results. In another study (Colombo et al. 2017), the thermal network was coupled with an external CFD simulator. In the iterative process, the results from the BES tool, at first performed with approximate values, are used as boundary conditions for the first CFD simulation that yields the flow field, the temperatures of the air and the heat fluxes to and from the facade components. The second iteration uses these heat fluxes instead of the initial approximate values to improve the BES tool estimation, yielding increasingly accurate values for the surface temperatures as input for the following CFD computation and so on until convergence is reached.

4.9 Summary of use of BES tools for DSF simulations

The review of the selected studies reveals that there is not a clear dependence between the type of DSF investigated and the selected BES tool. This information shows that BESTs are relatively flexible tools for the analysis of DSF systems, as different configurations can be modelled and simulated within the same environment. The only exception to this is represented by the dedicated DSF models implemented in EnergyPlus and in IDA–ICE. Both these systems are only possible for single-storey heigh DSFs; however, in IDA–ICE it is possible to connect in stack more DSF modules to create a multi-storey system – though the suitability and correctness of this modelling approach need to be further investigated. When it comes to EnergyPlus, it is also important to highlight that the use of the airflow window module is only possible in case of mechanically ventilated facades.

The use of an on-purpose modelled airflow-thermal network is the most common approach, and the most general one, which guarantees good flexibility in terms of characteristics of DSF. In this approach, one of the biggest challenges for the modeller is to decide the numbers of thermal zones to represent the cavity. The collection of studies shows that there is not a standard approach when it comes to this issue, and the number of zones usually ranges from a minimum of one thermal zone up to a maximum of six (referred to one storey DSF). The number of thermal zones adopted is usually driven by the limitation of the software and by the long computational time connected to a large number of divisions.

Moreover, analysing the data collected from these studies is not possible to identify a clear pattern between the tool chosen and the scope of the conducted analysis, as highlighted by the overview given in Table 3. The choice of the BES tool to be used is frequently the first step in the planning of the simulation task. This choice is, very often, not due the possibilities and limitations of one simulation environment in comparison to the others, especially in a panorama where all the tools are still under development and are pointing towards very similar goals. On the contrary, the decision to adopt one tool or another is more likely to be linked, as in the professional sector as in the research sector, to the previous expertise of the modeller, the availability of the tool (in terms of licence, if not open-source), as well as the possibility to have easy access to information (such as reference materials, technical documentation, and first-hand experience on the use of the tool).

Table 3 Correlation between BES tool adopted and the analysis conducted

	EnergyPlus	ESP-r	IDA–ICE	IES–VE	TRNSYS
Thermal, airflow or daylight analysis of DSF	(Choi et al. 2012) (Le et al. 2014) (Mateus et al. 2014) (Andelković et al. 2016) (Peng et al. 2016) (Abazari and Mahdavinejad 2017) (Kim et al. 2018)	(Høseggen et al. 2008) (Qiu et al. 2009) (Marinosci et al. 2011) (Seferis et al. 2011)	(Colombo et al. 2017) (Eskinja et al. 2018)	(Pekdemir and Muehleisen 2012) (Pomponi et al. 2017)	(Saelens et al. 2004) (Eicker et al. 2008) (Khalifa et al. 2015) (Elarga et al. 2016) (Yu et al. 2017) (Shahrestani et al. 2017)
Energy performance of DSF	(Choi et al. 2012) (Le et al. 2014) (Peng et al. 2016)	(Kokogiannakis and Strachan 2007) (Høseggen et al. 2008) (Qiu et al. 2009) (Seferis et al. 2011)	(Gelesz and Reith 2015)		(Elarga et al. 2016) (Yu et al. 2017) (Shahrestani et al. 2017)
Parametric study	(Kim and Park 2011b) (Papadaki et al. 2013) (Alberto et al. 2017)			(Pekdemir and Muehleisen 2012)	
Sensitivity analysis	(Kim and Park 2011b) (Papadaki et al. 2013) (Alberto et al. 2017)	(Fantucci et al. 2017)			(Saelens et al. 2004) (Khalifa et al. 2017)
Design or operation support of DSF	(Choi et al. 2012)	(Barták et al. 2001) (Høseggen et al. 2008)			(López et al. 2012) (Elarga et al. 2016)
Study of modelling approaches		(Leal et al. 2003, 2004a) (Kokogiannakis and Strachan 2007) (Leal and Maldonado 2008)			(Khalifa et al. 2015) (Shahrestani et al. 2017)

5 Current gaps, limitations, and possibilities for future developments

The previous section of the paper has demonstrated that BES tools can be used to simulate DSFs, even if a series of limitations remains. The list of current gaps in the modelling of these facade systems with BES tools spans over a relatively large domain, which is briefly summarised in the following paragraphs.

Presently, none of the BES analysed natively implement a capacitor node to model a glazed layer. This is due to the historical development of BES tools, which were created when a single glazed unit where standard solutions. In that case, and in the case of conventional double glazed units, the influence of a capacitor node in the simulation is relatively small (Freire et al. 2011), and may, therefore, be neglected. However, in the case of a multi-layered facade, which can be characterized by three to four glass panes, and where some of them might have a thickness in the order of 1 cm (safety glass), the effect of the thermal inertia of the entire glazed package can become significant (in the order of 1 to 2 hours of delay in the peak of the heat flux). The development of more refined models for BES should, therefore, take into account this aspect, or at least deepen what is the effect of considering (or not) the inertial effect under these conditions.

A well-known effect in DSFs is that the air (either coming from the outside or the inside) can be heated up during the path in the inlet section at the bottom of the cavity, because of an overheated (due to solar irradiation) frame (Saelens and Hens 2001). The increase in the temperature of the inlet air depends, of course, on many variables, but can be in the order of few degrees, and therefore should not be neglected. While this effect can be modelled, in the case of the approach based on a combined airflow and thermal network, by injecting a certain heat gain in the thermal zone representing the inlet section of the paper (this an additional heat can be, for example, automatically calculated base on the solar irradiance), such a correction cannot be carried out in the two existing native modules for DSF modelling in EnergyPlus and in IDA–ICE.

One of the main potentials of DSFs is the possibility to dynamically change the airflow path in order to obtain the best possible behaviour by these systems, depending on the different boundary conditions. The modelling (and control) of a variable airflow path is not an easy task when the DSF is implemented in BES tools in the form of a combined thermal and airflow network. Moreover, when it comes to the existing stand-alone module in EnergyPlus and IDA–ICE, these capabilities become even more challenging to be implemented – in EnergyPlus, for example, only the adoption of a dedicated script for the EMS module can be suitable, yet the not trivial solution to overcome this limitation. The analysis and development of DSFs characterised by high performance can only be carried out in conjunction of

advanced control systems, and the enabling of more user-friendly solutions that allow the airflow paths to be dynamically modified is, at the present, a relevant gap in BES tools that should be addressed.

Solar shading systems play a major role in the thermo-fluid behaviour of a DSF, and the type and placement of these devices in the cavity can improve or worsen the overall performance of the facade (Gratia and De Herde 2007). The placement of the shading device at the desired distance from the external/internal skin is not always an easy task, nor in the case of the dedicated modules for DSF simulations implemented in some BES environment, nor in the case of an integrated thermal and airflow network to replicate the facade cavity. Furthermore, while modelling of naturally ventilated cavities necessarily rely on the heat released by the shading devices to determine, together with other variables, the airflow rate, when mechanically ventilated cavities are modelled, the influence of the heat released to the airflow on the determination of the actual air mass rate is neglected. If this assumption can be valid for wide cavities with high airflow rate, in the case of narrow cavities characterised by relatively slow (forced) airflows such an effect might be not negligible. Improved models and modelling approaches for DSF in BES tools should, therefore, include the possibility to better specify the position of the in-cavity shading device and account for its influence on the airflow rates not only when under a natural convection regime.

For naturally ventilated facades and, to some extent, for mechanically ventilated facades too, realistic discharge coefficients (Heiselberg and Sandberg 2006) need to be used to model the inlet, outlet, and in general every section of the facade where a pressure drop can occur. The identification through a search in the literature, or experimental analysis, or more sophisticated simulations (e.g. CFD) is one of the most complex tasks that a modeller need to face when developing the DSF model. The development of more accurate and user-friendly models for DSF simulation need therefore to focus on these quantities and possibly provide the modeller with a series of "robust-enough" coefficients, capable of addressing the most common situations that can be met regarding the geometrical relationship between the openings and the cavity.

Finally, the complexity of the airflow can be far higher than what can be realistically expected as a simulation output from BES tools. Flow reversal and recirculation phenomena (Dama et al. 2017) are not uncommon in a DSF's cavity, and especially for those naturally ventilated and characterised by being high and deep. While on the one hand it appears unrealistic to develop dedicated models directly integrated into a BES capable of fully accounting for these phenomena, on the other hands there is an almost untapped potential in the possible link (co-simulation) between models with different level of complexity (Kim and Park 2011a; Elarga et al. 2016). Future modules for DSF simulation should be constructed with having in mind the possibility to link them, through a middleware program (e.g. Wetter 2011) that allow data to be exchanged between the two software tools.

6 Conclusion and recommendations

In this paper, an extensive overview of different topics related to the DSF systems through whole-building energy simulation (BES) tools have been reported. The need to carry out reliable simulations to design a DSF lies in the higher complexity of these systems, which can represent an effective solution only when optimised and well integrated into the overall energy concept of a building. The stand-alone simulation of DSFs is of limited use when the focus is placed on the interaction between this technology and the entire building, and the simulation of DSF with BES tools represents the most comprehensive approach to support the design of highly efficient ventilated facades in the context of the building where they need to operate.

Even if the simulation of DSF in BES tools is an activity with a history of more than 20 years, there is an untapped potential in the development of dedicated sub-routines, integrated into a BES environment, to simulate these systems. While the most conventional approach to this simulation (through an integrated thermal and airflow network) presents some advantages in terms of flexibility, the resources necessary to set-up such a simulation, and the assumptions to be made over a long series of variables, especially affecting the airflow network, and in particular in the case of naturally ventilated cavities, are often a major barrier that limits the possibility of simulating with enough accuracy a DSF in a BES environment. On the contrary, the few examples of dedicated modules, natively integrated into some BES tools, are still at a young stage, and rather limited in the possibilities that they offer.

When it comes to the physical phenomena modelled in these environments, and especially in the case of the dedicated modules, it is seen that well-known gaps have not been yet implemented into the available tools. Furthermore, it is also evident from the review that a common agreement on detailed parameters to be implanted in the modelling a DSF has not been reached yet. In general, it is possible to say that modelling a natural ventilated cavity is far more challenging than when the ventilation is mechanical, due to loop generated between thermal domain and the fluid domain, and to a large number of (often unknown) parameters that affect the airflow rate, mostly driven by buoyancy forces. Among the parameters that play a role in determining the outcome of the simulation, the following ones can be listed as the most relevant: the number of thermal zones into which

divide the cavity; the correlations adopted to determine the convective heat exchange coefficient; the discharge coefficient to apply to the inlet, outlet and fictitious openings of the DSF; the wind pressure effect on the airflow in the case of DSFs that are connected to the outdoor air; the shading systems' positioning, and its interaction with the airflow.

The validation of models is also a crucial aspect of the simulation of DSF in BES tools. While users of BES are very familiar with the concept of calibration and can make use of this procedure to obtain more reliable simulation output under specific conditions, it is also important to stress that the validation of models should become the best practice also when simulations are carried out with BES environments.

The future development of BES tools for the simulation of DSF systems should, therefore, focus on the following two activities. Firstly, systematic validation of existing models and approaches, by inter-software comparison between simulations of some selected representative configurations of DSFs, and reliable experimental data. Secondly, the definition, for different BES environments, of ad-hoc sub-routines, based on the extensive literature on physical-mathematical models for DSFs, in order to create specific integrated modules that are: easy to use by modeller with different degree of expertise; flexible enough to cover a wide range of configurations of DSFs, as well as, different integration with the building and building heating, ventilation, and air condition plan; planned for dynamic operations (i.e. changing the airflow path according to the need) in order to allow the study and design of DSFs as far as one of the most important aspects is concerned – i.e. dynamic control of the double skin to enhance its performance.

Finally, co-simulation may represent a large area of untapped potentials for the development of a more accurate simulation, in those cases where the BES tool alone is not enough to catch the desired level of detail because of its intrinsic nature of simulation environment aiming at the assessment of the whole building energy performance, and not at the particular thermofluid behaviour of just one component of the entire building.

Acknowledgements

This research is supported by the Research Council of Norway research grant 262198 and by the industrial partners SINTEF and Hydro Extruded Solutions through the project "REsponsive, INtegrated, VENTilated - REINVENT – windows". The authors would like to gratefully acknowledge the COST Action TU1403 "Adaptive Facades Network" for providing excellent research networking. This facilitated fruitful scientific discussions with several participants in the network, which led to increasing the quality of the paper.

References

Abazari T, Mahdavinejad M (2017). Integrated model for shading and airflow window in BSk. *Energy Procedia*, 122: 571–576.

AIVC (1994). An analysis and data summary of the AIVC's numerical database—Technical Note 44.

Alamdari F, Hammond GP (1983). Improved data correlations for buoyancy-driven convection in rooms. *Building Services Engineering Research and Technology*, 4: 106–112.

Alberto A, Ramos NMM, Almeida RMSF (2017). Parametric study of double-skin facades performance in mild climate countries. *Journal of Building Engineering*, 12: 87–98.

ASHRAE (1993). ASHRAE Handbook: Fundamentals. Atlanta: American Society of Heating Refrigerating and Air Conditioning Engineers.

ASHRAE (2007). ANSI/ASHRAE Standard 62.1-2004: Ventilation for Acceptable Indoor Air Quality. Health Care (Don Mills). Atlanta: American Society of Heating Refrigerating and Air Conditioning Engineers.

Anđelković AS, Mujan I, Dakić S (2016). Experimental validation of a EnergyPlus model: Application of a multi-storey naturally ventilated double skin facade. *Energy and Buildings*, 118: 27–36.

Aparicio-Fernández C, Vivancos JL, Ferrer-Gisbert P, Royo-Pastor R (2014). Energy performance of a ventilated facade by simulation with experimental validation. *Applied Thermal Engineering*, 66: 563–570.

Aschaber J, Hiller M, Weber R (2009). TRNSYS17: New features of the multizone building model. In: Proceedings of the 11th International IBPSA Building Simulation Conference, Glasgow, UK, pp. 1983–1988.

Baldinelli G (2009). Double skin facades for warm climate regions: Analysis of a solution with an integrated movable shading system. *Building and Environment*, 44: 1107–1118.

Balocco C (2004). A non-dimensional analysis of a ventilated double facade energy performance. *Energy and Buildings*, 36: 35–40.

Balocco C, Colombari M (2006). Thermal behaviour of interactive mechanically ventilated double glazed facade: Non-dimensional analysis. *Energy and Buildings*, 38: 1–7.

Bar-Cohen A, Rohsenow WM (1984). Thermally optimum spacing of vertical, natural convection cooled, parallel plates. *Journal of Heat Transfer*, 106: 116–123.

Barbosa S, Ip K (2014). Perspectives of double skin facades for naturally ventilated buildings: A review. *Renewable and Sustainable Energy Reviews*, 40: 1019–1029.

Barecka MH, Zbicinski I, Heim D (2016). Environmental, energy and economic aspects in a zero-emission facade system design. *Management of Environmental Quality: An International Journal*, 27: 708–721.

Barták M, Dunovská T, Hensen J (2001). Design support simulations for a double-skin facade. In: Proceedings of the 1st International Conference on Renewable Energy in Buildings "Sustainable Buildings and Solar Energy", Prague, Czech Republic, pp. 126–129.

Beausoleil-Morrison I (2000). The adaptive coupling of heat and air flow modelling within dynamic whole-building simulation. PhD Thesis, University of Strathclyde, Glasgow, UK.

Bhamjee M, Nurick A, Madyira DM (2013). An experimentally validated mathematical and CFD model of a supply air window: Forced and natural flow. *Energy and Buildings*, 57: 289–301.

Brown G, Isfält E (1974). Solinstrålning och solavskärmning (Solar Irradiation and Sun Shading Devices)—Report 19. Stockholm, Sweden.

Catto Lucchino E, Goia F (2019). Reliability and performance gap of whole-building energy software tools in modelling double skin facades. In: Proceedings of PowerSkin Conference 2019, Munich, Germany, pp. 249–262.

Chan ALS, Chow TT, Fong KF, Lin Z (2009). Investigation on energy performance of double skin facade in Hong Kong. *Energy and Buildings*, 41: 1135–1142.

Chan ALS (2011). Energy and environmental performance of building facades integrated with phase change material in subtropical Hong Kong. *Energy and Buildings*, 43: 2947–2955.

Charron R, Athienitis AK (2006). Optimization of the performance of double-facades with integrated photovoltaic panels and motorized blinds. *Solar Energy*, 80: 482–491.

Cheong CH, Kim T, Leigh SB (2014). Thermal and daylighting performance of energy-efficient windows in highly glazed residential buildings: Case study in Korea. *Sustainability*, 6: 7311–7333.

Choi W, Joe J, Kwak Y, Huh JH (2012). Operation and control strategies for multi-storey double skin facades during the heating season. *Energy and Buildings*, 49: 454–465.

Clarke JA (1985). Energy Simulation in Building Design. Bristol and Boston, MA, USA: Adam Hilger.

Clarke JA, Hensen JLM (2015). Integrated building performance simulation: Progress, prospects and requirements. *Building and Environment*, 91: 294–306.

Colombo E, Zwahlen M, Frey M, Loux J (2017). Design of a glazed double-facade by means of coupled CFD and building performance simulation. *Energy Procedia*, 122: 355–360.

Crawley DB, Lawrie LK, Pedersen OC, Winkelmann FC (2000). EnergyPlus: Energy Simulation Program. *ASHRAE Journal*, 42(4): 49–56.

Crawley DB, Hand JW, Kummert M, Griffith BT (2008). Contrasting the capabilities of building energy performance simulation programs. *Building and Environment*, 43: 661–673.

Dama A, Angeli D (2016). Wind and buoyancy driven natural ventilation in double skin facades. *International Journal of Ventilation*, 15: 288–301.

Dama A, Angeli D, Kalianova Larsen O (2017). Naturally ventilated double-skin facade in modeling and experiments. *Energy and Buildings*, 144: 17–29.

Darkwa J, Li Y, Chow DHC (2014). Heat transfer and air movement behaviour in a double-skin facade. *Sustainable Cities and Society*, 10: 130–139.

De Gracia A, Castell A, Navarro L, Oró E, Cabeza LF (2013). Numerical modelling of ventilated facades: A review. *Renewable and Sustainable Energy Reviews*, 22: 539–549.

Dickson A (2004). Modelling double-skin facades. Master Thesis, University of Strathclyde, UK.

Ding W, Hasemi Y, Yamada T (2005). Natural ventilation performance of a double-skin facade with a solar chimney. *Energy and Buildings*, 37: 411–418.

Eicker U, Fux V, Bauer U, Mei L, Infield D (2008). Facades and summer performance of buildings. *Energy and Buildings*, 40: 600–611.

Elarga H, Zarrella A, De Carli M (2016). Dynamic energy evaluation and glazing layers optimization of facade building with innovative integration of PV modules. *Energy and Buildings*, 111: 468–478.

Equa (2013). EQUA Simulation AB User Manual IDA Indoor Climate and Energy.

Eskinja Z, Miljanic L, Kuljaca O (2018). Modelling thermal transients in controlled double skin facade building by using renowned energy simulation engines. In: Proceedings of the 41st International Convention on Information and Communication Technology, Electronics and Microelectronics, pp. 897–901.

Faggembauu D, Costa M, Soria M, Oliva A (2003a). Numerical analysis of the thermal behaviour of ventilated glazed facades in Mediterranean climates. Part I: Development and validation of a numerical model. *Solar Energy*, 75: 217–228.

Faggembauu D, Costa M, Soria M, Oliva A (2003b). Numerical analysis of the thermal behaviour of glazed ventilated facades in Mediterranean climates. Part II: Applications and analysis of results. *Solar Energy*, 75: 229–239.

Fallahi A, Haghighat F, Elsadi H (2010). Energy performance assessment of double-skin facade with thermal mass. *Energy and Buildings*, 42: 1499–1509.

Fantucci S, Marinosci C, Serra V, Carbonaro C (2017). Thermal performance assessment of an opaque ventilated facade in the summer period: Calibration of a simulation model through in-field measurements. *Energy Procedia*, 111: 619–628.

Fohanno S, Polidori G (2006). Modelling of natural convective heat transfer at an internal surface. *Energy and Buildings*, 38: 548–553.

Freire RZ, Mazuroski W, Abadie MO, Mendes N (2011). Capacitive effect on the heat transfer through building glazing systems. *Applied Energy*, 88: 4310–4319.

Gavan V, Woloszyn M, Roux JJ, Muresan C, Safer N (2007). An investigation into the effect of ventilated double-skin facade with venetian blinds: Global simulation and assessment of energy performance. In: Proceedings of the 10th International IBPSA Building Simulation Conference, Beijing, China, pp. 127–133.

Gebhart B (1961). Surface temperature calculations in radiant surroundings of arbitrary complexity-for gray, diffuse radiation. *International Journal of Heat and Mass Transfer*, 3: 341–346.

Gelesz A, Reith A (2015). Climate-based performance evaluation of double skin facades by building energy modelling in Central Europe. *Energy Procedia*, 78: 555–560.

Gratia E, De Herde A (2004). Optimal operation of a south double-skin facade. *Energy and Buildings*, 36: 41–60.

Gratia E, De Herde A (2007). The most efficient position of shading devices in a double-skin facade. *Energy and Buildings*, 39: 364–373.

Haase M, Marques da Silva F, Amato A (2009). Simulation of ventilated facades in hot and humid climates. *Energy and Buildings*, 41: 361–373.

Halcrow W (1987). Report on heat transfer at internal building surfaces Project report to the Energy Technology Support Unit. No. ETSU S 1993-P1.

Hand JW (2011). The ESP-r Cookbook: Strategies for Deploying Virtual Representations of the Built Environment. University of Strathclyde, UK.

Heiselberg P, Sandberg M (2006). Evaluation of discharge coefficients for window openings in wind driven natural ventilation. *International Journal of Ventilation*, 5: 43–52.

Hensen JLM (1995). Modelling coupled heat and airflow: ping pong vs. onions. In: Proceedings of the 16th Conference Implementing the Results of Ventilation Research, pp. 253–262.

Hensen J, Djunaedy E (2005). Building simulation for making the invisible visible-air flow in particular. In: Proceedings of the International Conference on Energy Efficient Technologies in Indoor Environment, Delft, Netherlands.

Høseggen R, Wachenfeldt BJ, Hanssen SO (2008). Building simulation as an assisting tool in decision making. Case study: With or without a double-skin facade? *Energy and Buildings*, 40: 821–827.

IES (2004). ApacheSim Calculation Methods, Virtual Environment 5.0. IESVE Therm Ref 25.

IES (2014). ApacheSim User Guide. IES VE User Guide.

Iyi D, Hasan R, Penlington R, Underwood C (2014). Double skin facade: Modelling technique and influence of venetian blinds on the airflow and heat transfer. *Applied Thermal Engineering*, 71: 219–229.

Jiru TE, Haghighat F (2008). Modeling ventilated double skin facade—A zonal approach. *Energy and Buildings*, 40: 1567–1576.

Joe J, Choi W, Kwon H, Huh JH (2013). Load characteristics and operation strategies of building integrated with multi-story double skin facade. *Energy and Buildings*, 60: 185–198.

Kalamees T (2004). IDA ICE: the simulation tool for making the whole building energy- and HAM analysis. IEA-Annex 41 MOIST-ENG, Working Meeting, Zürich, Switzerland.

Kalyanova O, Heiselberg P (2008). Empirical validation of building simulation software: Modeling of double facades. Department of Civil Engineering, Aalborg University. DCE Technical reports, No. 30.

Khalifa A-JN (1989). Heat transfer processes in buildings. PhD Thesis, University of Wales College of Cardiff, UK.

Khalifa I, Ernez LG, Znouda E, Bouden C (2015). Coupling TRNSYS 17 and CONTAM: Simulation of a naturally ventilated double-skin facade. *Advances in Building Energy Research*, 9: 293–304.

Khalifa I, Gharbi-Ernez L, Znouda E, Bouden C (2017). Assessment of the inner skin composition impact on the double-skin facade energy performance in the Mediterranean climate. *Energy Procedia*, 111: 195–204.

Kim D, Cox SJ, Cho H, Yoon J (2018). Comparative investigation on building energy performance of double skin facade (DSF) with interior or exterior slat blinds. *Journal of Building Engineering*, 20: 411–423.

Kim D, Park C-S (2011a). A heterogeneous system simulation of a double-skin facade. In: Proceedings of the 12th International IBPSA Building Simulation Conference, Sydney, Australia.

Kim DW, Park CS (2011b). Difficulties and limitations in performance simulation of a double skin facade with EnergyPlus. *Energy and Buildings*, 43: 3635–3645.

Kim SY, Song KD (2007). Determining photosensor conditions of a daylight dimming control system using different double-skin envelope configurations. *Indoor and Built Environment*, 16: 411–425.

Kokogiannakis G, Strachan P (2007). Modelling of double ventilated facades according to the CEN Standard 13790 method and detailed simulation. In: Proceedings of the 2nd PALENC Conference and 28th AIVC International Conference, Crete, Greece, pp. 547–551.

Kośny J (2015). PCM-Enhanced Building Components. Cham, Switzerland: Springer.

Le S, Chen Y, Bi Y, Lu X (2014). Modeling and simulation of ventilated double-skin facade using EnergyPlus. In: Proceedings of the 8th International Symposium on Heating, Ventilation and Air Conditioning, pp. 241–252.

Leal VMS, Maldonado E, Erell E, Etzion Y (2003). Modelling a reversible ventilated window for simulation within Esp-r—The SOLVENT case. In: Proceedings of the 8th International IBPSA Building Simulation Conference, Eindhoven, Netherlands, pp. 713–720.

Leal V, Erell E, Maldonado E, Etzion Y (2004a). Modelling the SOLVENT ventilated window for whole building simulation. *Building Services Engineering Research and Technology*, 25: 183–195.

Leal V, Sandberg M, Maldonado E, Erell E (2004b). An analytical model for the airflow in a ventilated window with known surface temperatures. In: Proceedings of ROOMVENT 2004, Coimbra, Portugal.

Leal V, Maldonado E (2008). The role of the PASLINK test cell in the modelling and integrated simulation of an innovative window. *Building and Environment*, 43: 217–227.

Leigh S-B, Bae J-I, Ryu Y-H (2004). A study on cooling energy savings potential in high-rise residential complex using cross ventilated double skin facade. *Journal of Asian Architecture and Building Engineering*, 3: 275–282.

Loonen RCGM, Favoino F, Hensen JLM, Overend M (2017). Review of current status, requirements and opportunities for building performance simulation of adaptive facades. *Journal of Building Performance Simulation*, 10: 205–223.

López FP, Jensen RL, Heiselberg P, de Adana Santiago MR (2012). Experimental analysis and model validation of an opaque ventilated facade. *Building and Environment*, 56: 265–275.

Loutzenhiser PG, Manz H, Felsmann C, Strachan PA, Maxwell GM (2007). An empirical validation of modeling solar gain through a glazing unit with external and internal shading screens. *Applied Thermal Engineering*, 27: 528–538.

MacroFlo (2012). MacroFlo Calculation Methods. Techniques 1–25.

Marinosci C, Strachan PA, Semprini G, Morini GL (2011). Empirical validation and modelling of a naturally ventilated rainscreen facade building. *Energy and Buildings*, 43: 853–863.

Mateus NM, Pinto A, Da Graça GC (2014). Validation of EnergyPlus thermal simulation of a double skin naturally and mechanically ventilated test cell. *Energy and Buildings*, 75: 511–522.

McAdams WH (1954). Heat Transmission. Tokyo: McGraw-Hill Kogakusha.

Mirsadeghi M, Cóstola D, Blocken B, Hensen JLM (2013). Review of external convective heat transfer coefficient models in building energy simulation programs. *Implementation and Uncertainty*, 56: 134–151.

Oesterle E, Leib RD, Lutz G, Heusler B (2001). Double Skin Facades: Integrated Planning: Building Physics. Munich: Prestel.

Oh S, Haberl JS (2016). Origins of analysis methods used to design high-performance commercial buildings: Whole-building energy

simulation. *Science and Technology for the Built Environment*, 22: 118–137.

Oliveira Panão MJN, Santos CAP, Mateus NM, Carrilho da Graça G (2016). Validation of a lumped RC model for thermal simulation of a double skin natural and mechanical ventilated test cell. *Energy and Buildings*, 121: 92–103.

Papadaki N, Papantoniou S, Kolokotsa D (2013). A parametric study of the energy performance of double-skin facades in climatic conditions of Crete, Greece. *International Journal of Low-Carbon Technologies*, 9: 296–304.

Park CS, Augenbroe G, Messadi T, Thitisawat M, Sadegh N (2004). Calibration of a lumped simulation model for double-skin facade systems. *Energy and Buildings*, 36: 1117–1130.

Pasut W, De Carli M (2012). Evaluation of various CFD modelling strategies in predicting airflow and temperature in a naturally ventilated double skin facde. *Applied Thermal Engineering*, 37: 267–274.

Pedersen CO (2007). Advanced zone simulation in EnergyPlus: Incorporation of variable properties and phase change material (PCM) capability. In: Proceedings of the 10th International IBPSA Building Simulation Conference, Beijing, China, pp. 1341–1345.

Pekdemir EA, Muehleisen RT (2012). A parametric study of the thermal performance of double skin facades at different climates using annual energy simulation. In: Proceedings of the 5th National Conference of IBPSA-USA, Madison, USA, pp. 211–218.

Peng J, Curcija DC, Lu L, Selkowitz SE, Yang H, Mitchell R (2016). Developing a method and simulation model for evaluating the overall energy performance of a ventilated semi-transparent photovoltaic double-skin facade. *Progress in Photovoltaics: Research and Applications*, 24: 781–799.

Poirazis H (2004). Double skin facades for office buildings—Literature review report. Report EBD-R--04/3. Department of Construction and Architecture, Lund University, Sweden.

Pomponi F, Barbosa S, Piroozfar PAE (2017). On the intrinsic flexibility of the double skin facade: A comparative thermal comfort investigation in tropical and temperate climates. *Energy Procedia*, 111: 530–539.

Pomponi F, Piroozfar PAE, Southall R, Ashton P, Farr ERP (2016). Energy performance of Double-Skin Facades in temperate climates: A systematic review and meta-analysis. *Renewable and Sustainable Energy Reviews*, 54: 1525–1536.

Qiu Z, Chow T, Li P, Li C, Ren J, Wang W (2009). Performance evaluation of the photovoltaic double skin facade. In: Proceedings of the 11th International IBPSA Building Simulation Conference, Glasgow, UK, pp. 2251–2257.

Roth K, Lawrence T, Brodrick J (2007). Double-skin facades. *ASHRAE Journal*, 49(10): 70–73.

Saelens D, Hens H (2001). Experimental evaluation of airflow in naturally ventilated active envelopes. *Journal of Thermal Envelope and Building Science*, 25: 101–127.

Saelens D (2002). Energy performance assessment of single storey multiple-skin facades. PhD Thesis, Catholic University of Leuven, Belguim.

Saelens D, Carmeliet J, Hens H (2003). Energy performance assessment of multiple-skin facades. *HVAC&R Research*, 9: 167–185.

Saelens D, Roels S, Hens H (2004). The inlet temperature as a boundary condition for multiple-skin facade modelling. *Energy and Buildings*, 36: 825–835.

Saelens D, Roels S, Hens H (2008). Strategies to improve the energy performance of multiple-skin facades. *Building and Environment*, 43: 638–650.

Safer N, Gavan V, Woloszyn M, Roux J (2006). Double-skin facade with venetian blind: Global modelling and assessment of energy performance. In: Proceedings of EPIC Conference.

Safer N, Woloszyn M, Roux J-J, Kuznik F (2005). Modeling of the double-skin facades for building energy simulations: radiative and convective heat transfer. In: Proceedings of the 9th International IBPSA Building Simulation Conference, Montréal, Canada, pp. 1067–1074.

Sahlin P, Bring A, Sowell EF (1996). The neutral model format for building simulation (V.3.02). Technical Report, Department of Building Sciences, The Royal Institute of Technology, Stockholm, Sweden.

Sala M, Romano R (2011). Building envelope innovation: smart facades for non residential buildings. *TECHNE Journal of Technology for Architecture and Environment*, 2: 158–169.

Seferis P, Strachan P, Dimoudi A, Androutsopoulos A (2011). Investigation of the performance of a ventilated wall. *Energy and Buildings*, 43: 2167–2178.

Shahrestani M, Yao R, Essah E, Shao L, Oliveira AC, Hepbasli A, Biyik E, del Caño T, Rico E, Lechón JL (2017). Experimental and numerical studies to assess the energy performance of naturally ventilated PV facade systems. *Solar Energy*, 147: 37–51.

Shameri MA, Alghoul MA, Sopian K, Zain MFM, Elayeb O (2011). Perspectives of double skin facade systems in buildings and energy saving. *Renewable and Sustainable Energy Reviews*, 15: 1468–1475.

Shan R (2014). Optimization for heating, cooling and lighting load in building facade design. *Energy Procedia*, 57: 1716–1725.

Singh MC, Garg SN, Jha R (2008). Different glazing systems and their impact on human thermal comfort—Indian scenario. *Building and Environment*, 43: 1596–1602.

Soto Francés VM, Sarabia Escriva EJ, Pinazo Ojer JM, Bannier E, Cantavella Soler V, Silva Moreno G (2013). Modeling of ventilated facades for energy building simulation software. *Energy and Buildings*, 65: 419–428.

Sparrow EM, Ramsey JW, Mass EA (1979). Effect of finite width on heat transfer and fluid flow about an inclined rectangular plate. *Journal of Heat Transfer*, 101: 199–204.

Srebric J, Chen Q, Glicksman LR (2000). A coupled airflow and energy simulation program for indoor thermal environmental studies. *ASHRAE Transactions*, 106(1): 465–476.

Stec W, van Paassen D (2003). Defining the performance of the double skin facade with the use of the simulation model. In: Proceedings of the 8th International IBPSA Building Simulation Conference, Eindhoven, Netherlands, pp. 1243–1250.

Stec WJ, van Paassen AHC (2005). Symbiosis of the double skin facade with the HVAC system. *Energy and Buildings*, 37: 461–469.

Tabares-Velasco PC, Griffith B (2012). Diagnostic test cases for verifying surface heat transfer algorithms and boundary conditions in building energy simulation programs. *Journal of Building Performance Simulation*, 5: 329–346.

Tanimoto J, Kimura KI (1997). Simulation study on an air flow window system with an integrated roll screen. *Energy and Buildings*, 26: 317–325.

TESS (2014). Libraries version 17.0. Volume 3: The Electrical Component Library. TRNSYS17 Doc.

Tian W, Han X, Zuo W, Sohn MD (2018). Building energy simulation coupled with CFD for indoor environment: A critical review and recent applications. *Energy and Buildings*, 165: 184–199.

TRNSYS 17 (2009). Mathematical Reference. TRNSYS Doc.

TRNSYS 17 (2013). Multizone Building modeling with Type56 and TRNBuild.

US Department of Energy (2010). EnergyPlus Engineering Reference: The Reference to EnergyPlus Calculations.

US Department of Energy (2018). EnergyPlus Version 8.9.0: Engineering Reference.

Underwood CP, Yik FWH (2008). Modelling Methods for Energy in Buildings. Oxford, UK: John Wiley & Sons.

University of Wisconsin (2005). TRNFlow: A module of an air flow network for coupled simulation with TYPE 56.

Walton GN (1981). Passive solar extension of the building loads analysis and system thermodynamics (BLAST) program. Technical Report. United States Army Construction Engineering Research Laboratory.

Walton GN (1989). AIRNET: A Computer program for building airflow network modeling. Technical Report, DE-AI01-36CE2101-3. US Department of Commerce, National Institute of Standards and Technology, National Engineering Laborary.

Walton GN, Dols WS (2002). CONTAMW 2.0 User Manual. NISTIR 7251. US Department of Commerce, National Institute of Standards and Technology.

Walton GN, Dols WS (2013). CONTAM User Guide and Program Documentation. US Department of Commerce, Technology Administration, National Institute of Standards and Technology.

Wang Y, Chen Y, Zhou J (2016). Dynamic modeling of the ventilated double skin facade in hot summer and cold winter zone in China. *Building and Environment*, 106: 365–377.

Weber A, Koschenz M, Holst S, Hiller M, Welfonder T (2002). TRNFLOW: Integration of COMIS into TRNSYS TYPE 56.

Wetter M (2011). Co-simulation of building energy and control systems with the Building Controls Virtual Test Bed. *Journal of Building Performance Simulation*, 4: 185–203.

Wong PC (2008). Natural ventilation in double-skin facade design for office buildings in hot and humid climate. PhD Thesis, University of New South Wales, Australia.

Yazdanian M, Klems JH (1994). Measurement of the exterior convective film coefficient for windows in low-rise buildings. *ASHRAE Transactions*, 100(1): 1087–1096.

Yu J-S, Kim J-H, Kim S-M, Kim J-T (2017). Thermal and energy performance of a building with PV-applied double-skin facade. *Proceedings of the Institution of Civil Engineers - Engineering Sustainability*, 170: 345–353.

Zhai Z, El Mankibi M, Zoubir A (2015). Review of natural ventilation models. *Energy Procedia*, 78: 2700–2705.

BUILD SIMUL (2019) 12: 547–547
https://doi.org/10.1007/s12273-019-0523-7

Erratum to: Modelling of double skin facades in whole-building energy simulation tools: A review of current practices and possibilities for future developments

Elena Catto Lucchino, Francesco Goia (✉), Gabriele Lobaccaro, Gaurav Chaudhary

Department of Architecture and Technology, Faculty of Architecture and Design, NTNU, Norwegian University of Science and Technology, Trondheim, Norway

Erratum to
BUILD SIMUL (2019) 12: 3–27
DOI: 10.1007/s12273-019-0511-y

The original version of this article unfortunately contained an error in the second paragraph of Section 5 on page 19. Instead of

Presently, none of the BES analysed natively implement a capacitor node to model a glazed layer.

It should read

Presently, not all of the BES analysed natively implement a capacitor node to model a glazed layer.

The online version of the original article can be found at
https://doi.org/10.1007/s12273-019-0511-y

E-mail: francesco.goia@ntnu.no

3 A sensitivity analysis with building energy simulation tools

P2 *A. Gelesz, E. Catto Lucchino, F. Goia, V. Serra, A. Reith. Characteristics that matter in a climate façade: A sensitivity analysis with building energy simulation tools. Energy and Buildings 229 (2020), 110467. https://doi.org/10.1016/j.enbuild.2020.110467*

Double skin façades (DSFs) are considered façade technologies that can reduce energy use and improve occupant comfort due to their advanced features. Their design requires reliable simulations due to their complex thermophysical behaviour, which are often carried out by practitioners using building energy software (BES) tools. Using an exhaust-air façade (also called climate façade) case study, the paper analyses the sensitivity of in-built DSF models in two popular BES tools (EnergyPlus and IDA ICE) for different orientations and climates. Small variations in input variables were considered to identify the parameters that the designer should pay the most attention to during the design of the DSF according to different performance indicators. The results show that, regardless of the climate or orientation, the optical properties of the system (glazing and shading) were the most important in determining its performance, followed by the thermal properties of the glazing, while the geometrical, airflow and frame characteristics were less relevant. The model validation process also showed how differences in the in-built models (i.e., the use of a capacitance node for the glazed layers) lead to a difference in the reliability of the two BES tools.

Energy & Buildings 229 (2020) 110467

Contents lists available at ScienceDirect

Energy & Buildings

journal homepage: www.elsevier.com/locate/enb

Characteristics that matter in a climate façade: A sensitivity analysis with building energy simulation tools

Adrienn Gelesz [a,b], Elena Catto Lucchino [c], Francesco Goia [c,*], Valentina Serra [d], András Reith [a,e]

[a] Advanced Building and Urban Design Ltd, Budapest, Hungary
[b] Budapest University of Technology and Economics, Faculty of Architecture, Budapest, Hungary
[c] Department of Architecture and Technology, Norwegian University of Science and Technology, NTNU, Trondheim, Norway
[d] Department of Energy, Politecnico di Torino, Italy
[e] University of Pécs, Faculty of Engineering and Information Technology, Hungary

ARTICLE INFO

Article history:
Received 10 March 2020
Revised 2 September 2020
Accepted 6 September 2020
Available online xxxx

Keywords:
Exhaust-air double skin façade (climate façade)
Sensitivity analysis
Different climates
Model validation
EnergyPlus
IDA ICE

ABSTRACT

Double skin façades (DSFs) are considered façade technologies that can reduce energy use and improve occupant comfort due to their advanced features. Their design requires reliable simulations due to their complex thermophysical behaviour, which are often carried out by practitioners using building energy software (BES) tools. Using an exhaust-air façade (also called climate façade) case study, the paper analyses the sensitivity of in-built DSF models in two popular BES tools (EnergyPlus and IDA ICE) for different orientations and climates. Small variations in input variables were considered to identify the parameters that the designer should pay most attention to during the design of the DSF according to different performance indicators. The results show that, regardless of the climate or orientation, the optical properties of the system (glazing and shading) were the most important in determining its performance, followed by the thermal properties of the glazing, while the geometrical, airflow and frame characteristics were less relevant. The model validation process also showed how differences in the in-built models (i.e. the use of a capacitance node for the glazed layers) lead to a difference in the reliability of the two BES tools.

1. Introduction

Double skin façades (DSFs) are building envelope systems that can reduce energy use and improve occupant comfort due to their advanced characteristics. A recent *meta*-analysis showed that the advantages given by these solutions can be up to 90% energy reduction potential, but when not properly designed or managed, an increase in energy use of up to more than 30% can be seen [1]. The large variation in performance is linked to the high complexity of these systems, which can often introduce non-optimal designs. This highlights the need to support the development, detailed design, and management of DSFs through advanced numerical tools.

Whole-Building Energy Software (BES) tools are meant for modelling and predicting the performance of an entire building including the interactions between its sub-systems. They are therefore particularly suitable to investigate how a DSF is integrated into the larger building energy concept, and how it can be dynamically controlled [2]. BES tools can be used at different stages of the design process to support the integrated performance design of both the building and single subcomponents and can provide informed support in detailing the characteristics of DSFs.

The research activity presented in this paper investigates the sensitivity of selected energy and comfort performance indicators to the DSF design parameters in two BES tools. The goal of the research is two-fold: i) to understand which are the most relevant construction parameters of this class of DSF that affect the energy and comfort performance of the façade using as case-study a climate façade; ii) to verify the extent to which the two selected BES tools produce coherent results concerning the importance of these parameters.

The target audience for the first part of this study is designers and researchers interested in the characteristics of climate façades and the factors that most affect their performance. This fills a current knowledge gap in the literature and can help practitioners to focus on the most relevant aspects of a DSF during the design phase when the exact design parameters of the system need to be set according to specific requirements like climate and orientation.

The second part of the study is aimed at helping consultants and developers working with BES tools to define reasonable expectations of the performance in two simulations tools, and assess the

* Corresponding author.
E-mail address: francesco.goia@ntnu.no (F. Goia).

https://doi.org/10.1016/j.enbuild.2020.110467

Nomenclature

A_{inlet}	Area of the inlet [m^2]
α_{sh}	Solar absorptance of shading [–]
BES	Building Energy Simulation
DSF	Double Skin Facades
d_{cav}	Depth of the cavity [m]
d_{recess}	Recess depth of window (distance of interior window and building external plane) [m]
d_{sh}	Position of the shading measured from the external skin [m]
$d_{sh,gap}$	Ventilation gap around the shading [m]
e^{+}_{24h}	Area-specific daily heat gain [Wh/m^2]
e^{-}_{24h}	Area-specific daily heat loss [Wh/m^2]
f_{ext}	External frame fraction [%]
f_{int}	Internal frame fraction [%]
I_{tr}	Transmitted solar irradiance (on the vertical plan) [W/m^2]
h_{inlet}	Position of inlet measured from the floor level [m]
$\dot{q}_{LW,conv}$	Surface heat flux (includes long-wave radiative and convective heat flux) [W/m^2]
$\dot{q}^{+}_{tot}$	Total heat gain rate (includes short and long-wave radiative and convective heat flux) [W/m^2]
$\dot{q}^{-}_{tot}$	Total heat loss rate (includes short and long-wave radiative and convective heat flux) [W/m^2]
RMSE	Root Mean Squared Equivalent
ρ_{sh}	Solar reflectance of shading [–]
$S_i(t)$	Sensitivity index
$S_{i,d}$	Distance of sensitivity index
T_{glass}	Indoor surface temperature of the glass pane (inner skin, indoor-facing glass pane) [°C]
τ_{e,g_ext}	Solar transmittance of external glazing [–]
τ_{e,g_int}	Solar transmittance of interior glazing [–]
$\tau_{e,sh}$	Solar transmittance of shading [–]
U_{f_ext}	Heat transfer coefficient of the frame of the exterior skin including linear heat transfer coefficients of the glazing edge (Ψ_g) [W/(m^2K)]
U_{f_int}	Heat transfer coefficient of the frame of the interior skin including linear heat transfer coefficients of glazing edge (Ψ_g) [W/(m^2K)]
U_{g_int}	Center of glass heat transfer coefficient of interior glazing calculated at reference conditions (ISO 15099) [W/(m^2K)]
U_{g_ext}	Center of glass heat transfer coefficient of exterior glazing calculated at reference conditions (ISO 15099) [W/(m^2K)]
V_{cav}	Volumetric airflow rate in the cavity [L/s]

relevance of using these tools for the prediction of advanced façade systems. Readers interested in these aspects will find details about the validation work carried out through comparison with experimental data of two in-built modules for DSF simulations available in EnergyPlus and IDA ICE [3] in the Appendix. A critical analysis of the discrepancies between the results obtained in different tools is also provided, aiming to contribute to further developments of simulation models for advanced façade systems.

The paper is organised around four sections described hereafter.

In the Background section, we provide an overview of the current knowledge available in the literature, including previous activities where DSF systems have been modelled with BES tools and a sensitivity analysis to determine their key design parameters. We introduce the case study selected for the analysis, a so-called climate façade, with a description of its general features and its detailed characteristics (i.e. the actual façade chosen for the analysis). Finally, we provide the reader with a short introduction on the concept of sensitivity analysis and on the considerations used to select an appropriate method for this specific activity.

In the Materials and Methods section, we briefly report how the DSF has been modelled in two BES tools and the parameter settings necessary to run the simulations. We present the implementation of the local sensitivity analysis with details on the variables investigated and the three Performance Indicators (PIs) used in this phase namely the indoor surface glass temperature, the area-specific daily positive energy, and the area-specific daily negative energy crossing the façade.

In the Results and discussion section, we present the detailed outcomes of the sensitivity analysis in the BES tools. We reflect on how the resulting variability seen in the sensitivity analyses is linked to the differences in the two software tools.

The main findings of the study are summarised in the Conclusions section, which also highlights some limitations of the current study and the potential for future developments.

The paper also has two Appendix sections. In Appendix A, the main equations and explanation of the physico-mathematical models implemented in the two BES tools are described. In Appendix B, we present the validation of the modelling approaches and modules in the two software tools, including information on the experimental data collection and validation methodology. The reason for addressing these two topics in the Appendix is to keep the focus of the main body of the article on the key aspects of the study which are the role and the impact of the constructional and material properties of the climate façade on its performance.

2. Background

2.1. Simulations of DSF with BES tools

Many models exist for studying numerically the thermal performance of the DSF systems: analytical and lumped models, non-dimensional analysis, network models, control volume models, zonal approach, and computational fluid dynamics (CFD) [4]. DSF models in BES tools incorporate airflow network models integrated with a thermal network and a building energy model. These tools are particularly suitable as performance simulation tools to investigate the behaviour of DSFs in the framework of the overall building energy concept [2]. Different approaches can be adopted to study DSFs [5–7] and detailed analysis of the thermal and optical behaviour of DSFs can be carried out with more detailed simulation approaches (such as, for example, FEM and CFD [8–11]). BES tools have been widely used to simulate different types of DSFs primarily for the following two reasons: first to obtain a good balance between computational load associated with simulating a long period (usually one year) and the required accuracy to predict the overall performance of the façade; and second, the possibilities given by BES tools to test, in a quick way, different configurations and control possibilities for DSFs [12]. Examples of previous activities using BES tools to replicate the thermal behaviour of these façade systems includes simulations of almost the large spectrum of construction possibilities (e.g. [13,14]), as well as analysis of the advantages of DSF against single-skin façades [15,16]. In some cases [13,14,17,18], BES tools have been used to investigate the impact of the DSF's configuration on the thermal performance of the building. More parametric studies can be found in the litera-

ture if the search is not limited to simulations carried out with BES tools. In these studies, the parametric analysis is most typically focused on just one or a small number of parameters (e.g. cavity depth [13,19,20]; glazing U-values [13,20–24], glazing solar properties [13,21,23–26], the position of the shading [19,27] etc.), and in the majority of the cases, they only investigate a short period, e.g. single-day analysis with representative environmental conditions (either only winter or summer). The parametric analyses typically cover input parameters that illustrate different design choices and make also use of different methodologies (2D analysis [21,28], energy modelling [12,13,24,27,29], CFD [19,26], experiments [19], etc.) and boundary conditions. This variation of features, methods, and techniques makes it difficult to come to a general conclusion on the importance of one parameter over another. Some sensitivity analysis investigating the effect of small changes of a baseline [13,30] have also been performed but these studies are also characterised by a limited number of parameters. Studies that analyse different orientations are also rare, even though to reach a uniform architectural expression, fully glazed – especially high rise – buildings are in many cases constructed with the same type of façade on all orientations while allowing some flexibility in the actual specifications. While it is typical to limit the scope of the analyses to the South orientation, it has been seen previously that the summer overheating risk in the cavity is the highest on the West orientation [27].

The modelling of DSF systems in BES has some intrinsic limitations due to simplifications in the geometry and heat flow characteristics of components (inlet and outlet regions, enclosures around the cavity, shading) and the use of empirical correlations to solve some of the transport equations (especially the mass transport and convective heat transfer). This allows quickly obtaining useful information about bulk energy and mass flows without requiring high computational resources [2,7], although this might come at the cost of accuracy in prediction.

The reliability and precision of BES tools in replicating the thermal behaviour of DSFs have been addressed in a handful of previous activities, with sometimes contradictory results. EnergyPlus is among the most used BES tools for the simulation of DSFs, and consequently, it has been tested against experimental data in several studies. While some found a good agreement between the quantities calculated by the tool and the measured ones [31,32], for both single-storey and multiple-storey height DSFs, there are also studies showing a rather large discrepancy between simulations and experiments [17,33]. Such differences might be linked to the use of a calibration procedure. The adoption of this procedure, which can be legitimately used to reduce the uncertainty in the inputs of the models, may, however, lead to an overestimation of the performance of the BES tool in terms of validation. In most cases, the validation with experimental data only concerned the comparison of the simulated indoor glazing surface temperature and/or the temperature of the air gap and left out the tool's capability to replicate other relevant quantities that affect the total performance of the system. The literature available on the modelling possibilities given by EnergyPlus also reflects the two possible approaches of modelling a DSF, i.e. as a series of stacked thermal zones [17,31,32] or a dedicated "airflow-window" module embedded in the tool [33].

Both possibilities of modelling DSFs are also given in IDA ICE [34]. Examples for the use of the in-built module can be found in the literature [12,35], but only a couple of experimental validations are available. This software tool has been assessed approximately ten years ago, in an extensive inter-software comparison [36], and more recently by the same author of this paper [3]. The latter validation activity forms the basis of the extended validation presented in this paper, where the reliability of the software tools has been assessed not on the single thermo-physical quantities (temperature, heat fluxes, solar irradiance values), but on the aggregated, daily values of total transmitted energy through the façade, as more comprehensively described in Appendix B.

2.2. Climate façade (mechanically ventilated exhaust-air façade)

Several types of DSFs [29] present different characteristics in geometry, materials, ventilation mode, and air-flow modes. The case study façade selected for this investigation is an exhaust-air façade, which consists of one storey-high, mechanically ventilated elements that are juxtaposed on the façade. In these façades, the air typically enters from the indoor environment in the lower region of the façade through an opening in the frame and leaves the cavity at the upper part of the façade, either expelled to the outdoor environment (Fig. 1 a) or extracted through a duct as part of the HVAC system (Fig. 1 b) – and in the latter case, it takes the name of "climate façade".

Because the façade can be considered a part of the ventilation plant of the building, the operation in terms of airflow rate is rather constant, both in winter and summer conditions. This means that the possibilities to play with the airflow rate to remove a greater or smaller amount of heat from the cavity is usually not adopted as the airflow rate is linked to the volume of air supplied to the room for ventilation purpose.

A screen or venetian blinds in the climate façade is an important element to promote the exploitation of the solar heat gain through the ventilation airflow, to prevent indoor discomfort due to the excess of luminous gain, and to avoid excessive cooling loads due to direct solar gains to the room. In practice, the use of the shading element is necessary most of the time to ensure that the direct solar gain and the luminous flux on the user is not creating uncomfortable conditions.

2.3. Local sensitivity analysis

Sensitivity analysis is the study of how uncertainty in the model outputs can be allocated to the uncertainty in the model inputs [37]. It is a technique widely used across different fields such as ecology, chemistry, material science, economics, and energy modelling [38–41].

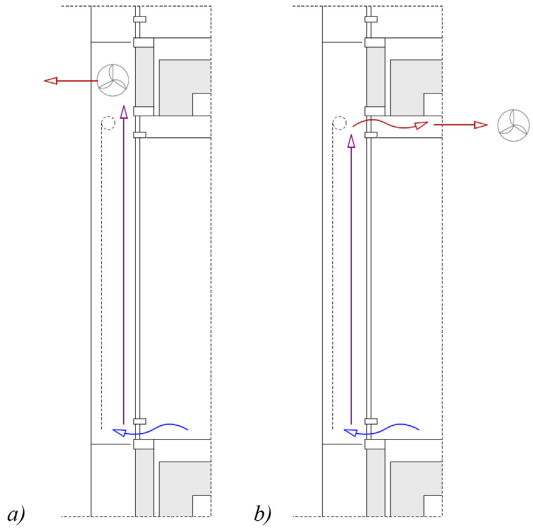

Fig. 1. Sections of exhaust-air façades a) air exhaust façade b) climate facade.

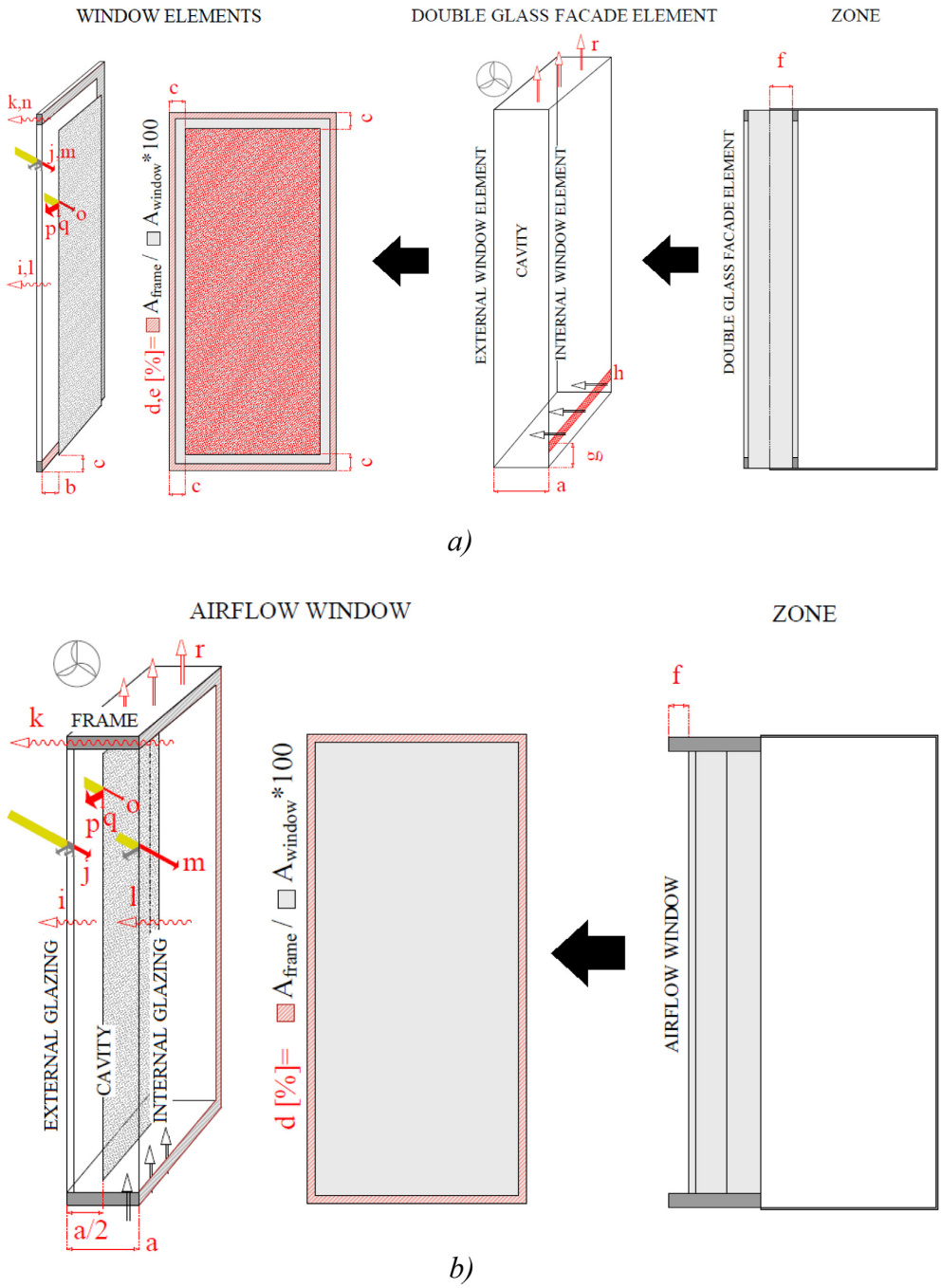

Fig. 2. Schematic of parameters defined in Table 2, view, axonometric view and section: a) IDA ICE b) EnergyPlus.

Many types of sensitivity analysis techniques exist but all return a list or a "sensitivity ranking" of the input parameters according to their influence on the outputs of the model. As each sensitivity analysis technique results in a slightly different sensitivity ranking, the actual ranking is not as important as much as is the determination of the key parameters to which the model is most sensitive [42]. From a practical point of view, the parameters consistently appearing near the top of the list will be the ones which are the most sensitive and require the most attention.

In this paper, a local sensitivity analysis is implemented using the so-called "One-At-A-Time" (OAT) technique, which consists in changing each parameter individually. This approach is useful to assess the impact of parameters in a model that contains *n* factors with a relatively small number of simulations, equal to *n + 1*. However, the non-linear effect in the output variation due to a combination of two or more variations in the inputs, cannot be studied with this method. One must then use a global sensitivity analysis that can assess the effect of multiple combinations of input variations [43].

Global sensitivity analysis techniques return a more comprehensive understanding of the general picture compared to local sensitivity analyses but require a much higher computational cost. The choice of the method to be adopted in a sensitivity analysis study heavily relies on considerations of computational time versus aims [44]. Local sensitivity analysis is a computationally efficient screening method proven to be a reliable strategy if the purpose of the analysis is to identify a cluster of input parameters most sensitive to the model output variability [43]. Because part of the scope of the research presented in this paper is to adopt a method that can be replicated by practitioners during the design phase when computational cost must be minimal, a method based on local sensitivity analysis was deemed more appropriate and selected for the analysis. This choice is also supported by indications in the literature showing that different sensitivity analysis methods can, to a large extent, identify the same cluster of most sensitive input parameters [37] as a global sensitivity analysis, and is still a very useful technique because of its simple implementation, low computational costs, and easy interpretation [40].

While, technically, the local sensitivity analysis must satisfy the condition of linearity to be applicable, the relationship between the outputs and the inputs in the case of the thermal simulation of DSF may be strongly non-linear. However, by making use of relatively small variations around the baseline input values, the linearity requirement around the point of investigation is, based on our experience on modelling approaches implemented in BPS tools, satisfied and the technique can be used with a high degree of confidence. The correctness of the approach is also justified by its popularity in the scientific literature and wide adoption for local sensitivity analysis using BES tools [37,44]. The remaining challenge associated with adopting this technique is the identification of the largest magnitude of the perturbation that can be used and satisfies the condition of linearity. This topic alone would require a comprehensive discussion that goes beyond the scope of this paper. However, as explained more in the following section, different perturbations have been tested in this analysis to ensure the robustness of the outcome of the analysis.

A final remark concerns the conceptual comparison between a parametric analysis and a sensitivity analysis. While a local sensitivity analysis is suitable to give information on the relative order of importance of different parameters, a parametric analysis, e.g. [14,18], is more suitable to investigate the optimal design choices within a given domain of possibilities. In an ideal design or research process, the sensitivity analysis is developed prior to the parametric analysis to initially reduce the numbers of parameters that later need to be investigated by identifying those that have a larger impact on the selected simulation output.

3. Materials and methods

3.1. Building energy simulation tools

BES tools either include dedicated models for DSF elements or allow the modeller to define DSFs as thermal-airflow networks. Two widely popular BES tools, EnergyPlus (version 9.1) and IDA Indoor Climate and Energy (IDA ICE) (version 4.8) incorporate in-built models for DSFs and have been selected for this investigation as the models most likely to be selected by practitioners during the design phase. In-built models are specific models that allow the user to directly enter specific input information that is then used to modify the heat balance of the window following the consideration that a ventilation flow is provided between the glass panes without requiring any additional modelling effort from the user.

The in-built models also allow sometimes users to pick between different levels of complexity for the description of the thermal and optical properties of the glass panes and frame constructions, and in this study, the more complex approach was selected as far as allowed by the BES tool.

A more detailed description of the dedicated sub-routines and the physical–mathematical models implemented in the two BPS tools is reported in Appendix A.

3.2. Experimental validation of the modelling approach in the two software tools

Experimental data collected during a long-term measurement campaign on a test cell facility was used to validate the two in-built models of DSFs available in the two BES tools considered for this study. More information about this procedure is given in Appendix B. The results shown in this paper are an extension of the ones previously reported in [3] and aggregate simple measured physical quantities into Performance Indicators (PIs). The measured values of solar radiation, indoor and ambient temperatures and indoor surface temperatures were used to recreate the real boundary conditions in the simulations by modifying the weather data file used by the simulation tools. The solar radiation was calculated from the values of outdoor solar irradiance measured on the horizontal and vertical plane. The outdoor air temperature was used in the custom weather files, while indoor temperatures were given as setpoints within the models. Indoor surface temperature measurements were also imposed in the models using schedules and applied to the corresponding surfaces within the models. In EnergyPlus, this was given directly as a set value for the surface temperature node. This approach was not possible in IDA ICE and instead, the same result was achieved by creating an additional conditioned zone around the volume of the cell delimited by fictitious surfaces. The air temperature inside this new zone surrounding zone was controlled using setpoints that matched the measured temperatures and recreated the experimental boundary conditions, as described in [3].

Summarising the results presented in Appendix B, the validation of the modules in IDA ICE and EnergyPlus revealed a series of mismatches in the prediction of internal glass surface temperatures and daily heat gains and losses. Despite these disparities, the tools could predict the main features of the time profiles in terms of peaks, valleys, and intensities, as well as the trends in surface temperatures, and energy loss and gain for double skin façades. The software tools also provided a more convincing performance in terms of matching the experimental data when the shading device in the DSF was lowered compared to when the DSF was simulated without the shading device, where much greater deviations between simulation and experiments can be seen. This suggests that the results of the sensitivity analysis were robust for configurations with the shading devices activated; but for configurations without the shading device, the reliability of the analysis cannot be fully ensured because of the discrepancies seen between simulations and experimental data. The validity of the analysis is, however, maintained by the fact that for optimal DSF operation, the shading device should be activated frequently both to ensure thermal comfort and to ensure a suitable visual performance for the

highly glazed façade which is subject to a risk of glare in most orientations.

Finally, the model in IDA ICE generally captured the time profiles more accurately, while EnergyPlus showed a shift in the profiles due to the lack of a heat capacity node for the glazing. This difference in the features of the two in-built models also has implications for the general reliability of EnergyPlus versus IDA ICE.

3.3. Settings of the sensitivity analysis

After checking the reliability of the simulation tools with the experimental data, a general model for the room and the façade was defined for the sensitivity analysis. Except for the walls incorporating the DSFs, all other surfaces were modelled as adiabatic and not interacting with the surroundings. The indoor air temperature setpoint value was changed for the different seasons and equal to 20 °C in Winter (January-February; November-December), 23 °C in Spring and Autumn (March-April; September-October), and 26 °C in Summer (May-August). This choice was done to minimise the impact of the differences that can occur within the two simulations at the whole building/room level on the sensitivity analysis at façade scale. By keeping constant the indoor air temperature, the discrepancies seen in the sensitivity analysis between the two software tools were then only due to the differences in the modelling of the façade.

The orientation of the office room was set so that the DSFs were exactly aligned with one of the four cardinal directions each time. The simulations were run in three different climates to assess whether the different outdoor boundary condition influenced the results of the analysis. The three climates were selected to be representative of different boundary conditions: Torino, located in a humid subtropical climate (Cfa according to the Köppen-Geiger climate classification), which is where the validation case study was located; Oslo located in the warm summer continental climate typical of Northern Europe (Dfb); and Hong Kong, located in a dry-winter humid subtropical climate (Cwa).

In total, 18 parameters likely to be considered by the designers or consultants planning the DSF's configuration during the design phase were selected for the sensitivity analysis (Table 1). Although the cavity height is considered to affect the results, this was not assessed, as this parameter is dependent on the floor height, which is usually a basic input given to the façade consultant by the design team.

The perturbation (variation) was set to ±10% for each parameter around the baseline case (Table 2) after testing different perturbation intervals (±5% and ±25%) on a few selected orientations and one climate to verify the robustness of the selected approach. This analysis yielded similar values to those obtained with the selected ±10% variation, thus confirming the relevance of the selected approach.

The effect of the perturbation was assessed using three PIs:

- the indoor surface glass temperature (T_{glass} [°C]);
- the area-specific daily positive energy (e^{+}_{24h} [Wh/m^2], daily heat gain) crossing the façade;
- the area-specific daily negative energy (e^{-}_{24h} [Wh/m^2], daily heat loss) crossing the façade.

These PIs aim at understanding the impact of the design choice on the thermal domain. The equations for calculation of e^{+}_{24h} [Wh/m^2] and e^{-}_{24h} [Wh/m^2] can be found in Appendix B of the paper.

The choice to focus the sensitivity analysis on PIs that address the thermal and comfort performance of the façade was done to limit the scope of the research, and to ensure that the results obtained could be as general and as interesting as possible. A sensitivity analysis focused on the impact on the visual environment of the different DSF's configuration would have lacked both in generality and real scientific interest. Indeed, the visual environment depends not only on the DSF's characteristics but also on the configuration of the indoor space (geometry, optical properties) and the exact position of the user. Furthermore, it is understood that the characteristics of the DSF impacting on the visual environment are those related to the optical properties of the system, such as the visual transmittance of the glass panes and roller screen. While it is trivial to demonstrate that several other quantities potentially affecting the thermal behaviour have no role in the determination of the visual environment.

3.4. Index for the sensitivity analysis

The method adopted in this study follows the technique outlined in [45,46] and explores a limited input space around a baseline case following a method where all parameters are modified by the same order of magnitude, i.e. by the same perturbation. Local sensitivity indices are defined as follows: consider a model with n independent inputs $X_i = 1, \ldots, n$. For a given value of X , the local sensitivity indices are proportional to the partial derivatives of the output y with respect to the chosen ith input parameter x_i (first-order sensitivity index):

$$S_i(t) = X_i \frac{\partial y_k(t)}{\partial X_i} \quad (1)$$

The sensitivity index is calculated for each hour of the annual simulation. To get a single value of each parameter, the impact of each parameter is then determined by using the distance of the sensitivity index, $S_{i,d}$, following Spitz et al. [45], and is calculated using the mean ($S_{i,m}$) and the standard deviation ($S_{i,std}$) of S_i over the considered (annual) period according to the following equation:

$$S_{i,d} = \sqrt{{S_{i,m}}^2 + {S_{i,std}}^2} \quad (2)$$

3.5. Challenges in modelling and simulation for sensitivity analysis in different BES tools

While comparing the possibilities for sensitivity analysis with the two selected BES tools, it was revealed that EnergyPlus has limited flexibility in defining input parameters. The shading device is EnergyPlus by a hardcoded default placed in the middle of the cavity when the airflow window module is used. The frame properties (ratio, U_f values) cannot be defined for each one of the two skins, but as one parameter for the whole element. Moreover, the inlet area, the inlet height, and the ventilation gap around the shading are not used in the model (Table 1).

When it comes to the sensitivity analysis, most parameters can be directly defined in the software tools except for the changes in the U-values and spectral properties which are calculated inputs. The U-value cannot directly be adjusted by ±10% in either software when using an advanced window modelling approach, as this performance value is calculated from the given spectral properties and conductivity values of the glazing panes. In IDA ICE, a layer-by-layer calculation is used, while in EnergyPlus an equivalent glazing is used for the internal pane. The variations for the U-value were implemented by adjusting either the emissivity values of the glazed layers and/or the gas in the cavity without changing the thickness or other features so that the reference value reaches the targeted value and the optical properties of the glazed system were not modified.

For the solar transmission (τ), reflectance (ρ) and absorption (α) values of the shading or glazing, no single value can be modified without adjusting the two others since $\tau + \rho + \alpha = 1$ in all cases.

Table 1
Parameters considered in the sensitivity analysis.

Parameter		Parameter Values			Unit of measurement	Parameter availability		ID in Fig. 2
		Baseline X_i	+10% $X_i + \Delta X_i$	−10% $X_i - \Delta X_i$		IDA ICE	EnergyPlus	
Geometrical parameters								
Depth of the cavity measured from glass to glass	d_{cav}	0.22	0.242	0.198	(m)	+	+	(a)
Position of the shading measured from the internal surface of the external skin glazing system	d_{sh}	0.073	0.0803	0.0657	(m)	+	d_{cav}*0.5 by default	(b)
Ventilation gap around the shading, all directions (Distance of shading edge from the edge of the window element)	$d_{sh,gap}$	0.03	0.033	0.027	(m)	+	N/A	(c)
Frame fraction of external window element	f_{ext}	10%	0.11	0.09	(%)	+	$F_{f\_combined}$: Single frame is defined for	(d)
Frame fraction of internal window element	f_{int}	10%	0.11	0.09	(%)	+	the whole element	(e)
Recess depth of window (distance of window external surface to building face)	d_{recess}	0.22	0.242	0.198	(m)	+	+	(f)
Area of the inlet	A_{inlet}	0.015	0.0165	0.0135	(m^2)	+	N/A	(g)
Position of inlet measured from the floor level	h_{inlet}	0.05	0.055	0.045	(m)	+	N/A	(h)
Thermal and optical parameters								
Centre of glass heat transfer coefficient of exterior glazing calculated at reference conditions (ISO 15099)	U_{g_ext}	1.357	1.4927	1.2213	(W/m^2K)	+	+	*(i)*
Total energy (shortwave) transmittance of external glazing system	τ_{e,g_ext}	0.324	0.3564	0.2916	(−)	+	+	*(j)*
Centre of glass heat transfer coefficient of interior glazing system calculated at reference conditions (ISO 15099)	U_{g_int}	1.507	1.6577	1.3563	(W/m^2K)	+	+	*(l)*
Total energy (shortwave) transmittance of interior glazing system	τ_{e,g_int}	0.492	0.5412	0.4428	(−)	+	+	*(m)*
Total energy (shortwave) transmittance of shading	$\tau_{e,sh}$	0.2	0.22	0.18	(−)	+	+	*(o)*
Total energy (shortwave) reflection of shading	ρ_{sh}	0.7	0.77	0.63	(−)	+	+	*(p)*
Total energy (shortwave) absorption of shading	α_{sh}	0.1	0.11	0.09	(−)	+	+	*(q)*
Heat transfer coefficient of the frame of the exterior skin including linear heat transfer coefficients of the glazing edge (Ψ_g)	U_{f_ext}	2	2.2	1.8	(W/m^2K)	+	$U_{f\_combined}$: Single frame is defined for the whole element. Equivalent value of 1 W/m2K is used.	*(k)*
Heat transfer coefficient of the frame of the interior skin including linear heat transfer coefficients of glazing edge (Ψ_g)	U_{f_int}	2	2.2	1.8	(W/m^2K)	+		*(n)*
Airflow parameters								
Volumetric airflow rate in the cavity	V_{cav}	5.556	6.1116	5.0004	(L/s/unit)	+	+	*(r)*

Table 2
Definition of variants of solar properties, example.

	τ	ρ	α
$\tau_{e,sh}$	0.2	0.7	0.1
$\tau_{e,sh}$ - 10%	0.18	0.718	0.102

Hence, all three values were modified for each variant with the following method: e.g. in case τ is the assessed parameter, the difference in τ is added to ρ and α with the same proportion as their original value (Table 2).

IDA ICE uses a variable timestep to solve the equations, in which the timestep is adapted to the frequency content of the solution to optimize simulation time [47]. Using the default setting with a maximum of a 1.5 h timestep is acceptable for annual energy simulations, as the small differences in the hourly values due to the different timesteps of the different models will not cause bias in the results. However, for the sensitivity analysis, where the input values of the models have only small differences, the small inaccuracies of the hourly values will affect the overall results. Hence, the maximum timestep is set to 6 min for both tools.

4. Results and discussion

The results are presented analysing one PI (see Section 3.3 and Appendix B) at a time (Section 4.1 for T_{glass}, Section 4.2 for e^{+}_{24h}, and Section 4.3 for e^{-}_{24h}), with comparisons for different climates and orientations. Section 4.4 focuses on the inter-software comparison.

4.1. Internal glass temperature

Both optical and thermal properties of the glazing and the shading (when present) were sensitive parameters, although the order of the parameters slightly differed for the two software tools and case assessed. In IDA ICE (Fig. 3), when the shading was not activated, the solar transmittance of the external skin was the most sensitive parameter, followed by the U-value of the internal and external glazing, and then by the solar properties of the internal skin. When the shading system was activated, the shading reflectance became the most sensitive parameter, resulting in the solar transmission the external pane becoming less significant. Additionally, the U-values of the external and the internal glazing were also ranked as sensitive parameters.

Comparison of the orientations shows that the ranking of the parameters was the same for South, East and West orientations, while on the North orientation, the optical properties of the glazing and the shading (when present) had a relatively lower effect than the thermal properties of the glazing. U_{g_ext} then ranked up among the most sensitive parameter, both with (2^{nd} place) and without (1st place) the shading device activated. It is also worth mentioning that while $V_{cav,}$ the ventilation airflow rate in the cavity, was only moderately sensitive for the former three orientations and ranked at the 7^{th} place when the shading is activated, the relative lower sensitivity of the optical properties of the glazing and shad-

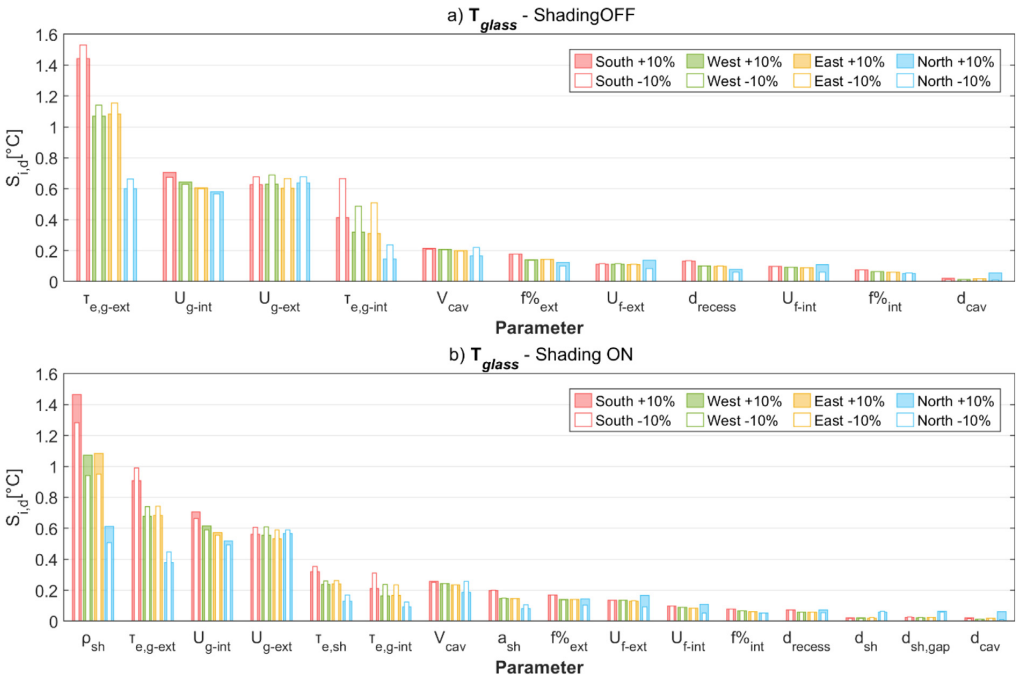

Fig. 3. $S_{i,d}$, Internal glazing temperature, Torino, all orientations, IDA ICE a) shading off b) shading on.

ing on the North orientation resulted in V_{cav} becoming the 5th most sensitive parameter, which was higher than the solar transmission of the shading and internal glazing.

In EnergyPlus (Fig. 4), the solar transmission of the internal glass was the most sensitive parameter when shading was not activated, followed by the solar transmission of the external glazing, and the U-values of both glazings and the cavity ventilation rate. With shading activated, the shading reflectance became the most sensitive parameter just like in IDA ICE, followed by the U-values of the internal glazing and the solar transmission of both glazings.

The comparison of the orientations shows that the ranking of the parameters was the same for most of the orientations. Like in IDA ICE, on the North orientation, the optical properties of the glazing and the shading had a relatively lower effect than the thermal properties of the glazing, thus resulting in U_{g_ext} as the second most sensitive parameter, both with and without the shading device activated.

The climate analysis showed that the most sensitive parameter was the same for all three locations for the South orientation with the only exception of U_{g_ext} becoming more sensitive in Oslo, and less sensitive in Hong Kong in the + 10% configuration (Fig. 5). On the North orientation, the most sensitive parameters showed a different behaviour in the various locations. The thermal properties of both glass panes and V_{cav} became significantly more sensitive in Oslo, and less sensitive for Hong Kong, both with and without the shading device activated. By contrast, the optical properties of the glazings and the shading device showed an opposite trend.

It is possible to conclude that in general terms, the indoor-side surface temperature of the DSF, which can play a role in terms of thermal comfort, is primarily affected by the optical properties of the glazed and shading layers, as well as by the thermal transmittance of the internal and external skin. Other parameters had a minimal impact on this variable, especially compared to the impact of the above-mentioned parameters.

4.2. Daily energy gain

$e^{+}_{24h}$was most sensitive to solar properties. As expected, when the shading was not activated in the cavity, the solar transmission of the external glazing was the most sensitive parameter, while when shading was activated, the shading solar reflection became the most sensitive parameter, as seen for T_{glass}. When the shading is off, in EnergyPlus, τ_{e,g_ext} was the only parameter with an outstandingly high $S_{i,d}$, and was more than three times higher than the $S_{i,d}$ of any other parameter which had a similarly low sensitivity (Fig. 7); IDA ICE (Fig. 6) also returned that the solar transmission of the external glazing was a parameter with high impact, closely followed by τ_{e,g_int}. With shading on, the difference between $\rho_{sh,}$ and the former parameters are lower for both tools.

For the daily energy gain, the comparison of the orientations showed that there were no notable differences in the ranking of the parameters.

The results of the climate analysis showed similarities results to those seen in the T_{glass} analysis (Fig. 8). The shading reflectance (when shading was activated) and the external glazing transmission were the most sensitive parameter for all three locations and all orientations, while the ranking of the parameters was only slightly affected by the change of the relative significance of U_{g_ext} on the South façade and both glazing U_g on the North façade.

In conclusion, the total daily heat gain, which affects the energy performance of the DSF in terms of cooling and heating loads, was driven by the optical properties of the external glazing such as the transmittance, and of the shading when present. Only one of the thermal properties, the thermal transmittance of the internal glazing, was significant but still had a somewhat limited impact. Over-

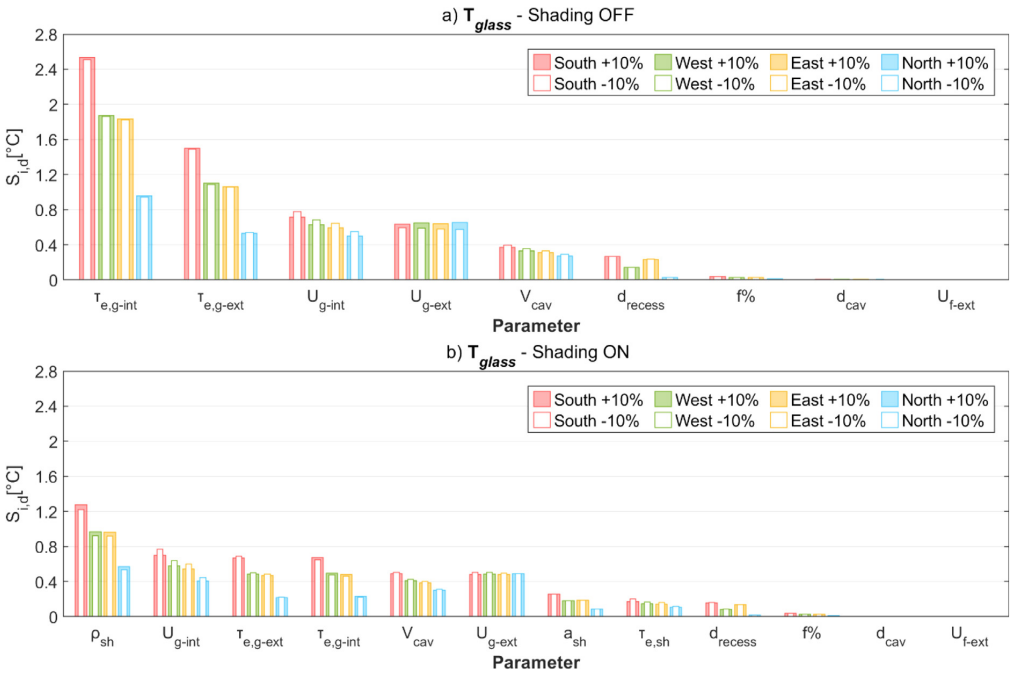

Fig. 4. S_{id}, Internal glazing temperature, Torino, all orientations, EnergyPlus a) shading off b) shading on.

all, the parameters with the highest impact were the same ones as those observed in the analysis of T_{glass} with the exception that when the shading was not activated, the role of the frame had more impact than the thermal properties of the glazing.

4.3. Daily energy loss

In the case of e^{-}_{24h} the most sensitive parameters were easily distinguished. In IDA ICE, the U-values of both glazings were significantly more sensitive than any other parameter, regardless of the presence of shading in the cavity or not (Fig. 9). In EnergyPlus, V_{cav} also appeared as one of the most sensitive parameters along with the U-values of the glazing (Fig. 10).

As previously seen for the energy gain, the most sensitive parameters for energy loss analysis were the same for all orientations.

Some minor changes can be seen in the ranking of this PI in different climates (Fig. 11), e.g. in Hong Kong, the frame fraction received a higher ranking than shading reflection; or in Oslo, τ_{e,g_ext} was ranked higher than in other climates for a North orientation when the shading device was deactivated. However, the list of the most sensitive parameters was not affected in any of the cases.

In conclusion, when it comes to the daily heat losses, which impact the DSF's energy performance through the heating load (i.e. primarily due to the behaviour during the night time and or in cold, cloudy winter days), the only relevant parameters were the thermal transmittance of the two skins and the airflow rate in the façade cavity.

4.4. Intersoftware comparison

As previously mentioned, the in-built model for the airflow window available in EnergyPlus requires a smaller amount of input than IDA ICE's but includes all of the parameters that were determined as the most sensitive in IDA ICE. These parameters are visible in Fig. 12 which also shows the results for a south-oriented façade in Turin.

For most parameters, the two tools have sensitivity indices in the same order of magnitude for T_{glass} and e^{+}_{24h}, with the only exception being the internal glass solar transmission. EnergyPlus shows a much higher sensitivity index for the T_{glass} while in IDA ICE, it is comparable in magnitude to the thermal properties of the glazing. In the case of e^{+}_{24h}, the behaviour of the tools was the opposite, with IDA ICE showing an almost four times bigger value then EnergyPlus.

For e^{-}_{24h} IDA ICE had higher $S_{i,d}$ values for most parameters, except for V_{cav}, where instead EnergyPlus returned higher variations compared to IDA ICE.

There is a significant difference in the weight of the solar transmission of the internal glazing, shading solar properties and airflow rate on the selected PIs. The solar transmission of the internal glazing had a significantly greater role in EnergyPlus than in IDA ICE for the glass temperature. This is anticipated to be due to the missing heat capacity node of the glass, as changing glazing solar properties will have an instantaneous effect on the glass pane temperature.

In EnergyPlus, V_{cav} is among the most sensitive parameters (3rd position) for e^{-}_{24h} and moderately sensitive for the other two PIs. However, in IDA ICE, it is only moderately sensitive for T_{glass} and e^{-}_{24h}, and even insensitive for e^{+}_{24h}. This indicates that the two tools calculate convective heat transfer coefficients differently, which also explains why there is a notable difference in the impact of the absorption of the shading.

It is particularly interesting that the cavity depth, d_{cav}, was found insensitive in both software tools and with all three PIs. Yet it is a reasonable outcome, as the analysed case is mechanically ventilated with fixed airflow rates, where the airflow rate is not dependent on this characteristic. The analysis reveals therefore

Fig. 5. S_{id}, Internal glazing temperature, all locations, EnergyPlus, a) South, shading on b) North, shading on, c) North, shading off.

that the cavity aspect ratio (cavity height over cavity depth) plays a marginal role when single-storey climate façade is assessed using the selected PI. The cavity depth affects the average velocity of the fluid given a fix airflow rate, and the average velocity of the fluid is a quantity used in the calculation of the convective heat exchange coefficient. This result shows that the models are not sensitive, at least in the explored range, to a small change in the convective heat exchange coefficient. In order to see a more relevant change in the fluid-dynamic characteristic of the cavity (at least as much as this domain is replicated by the models embedded in the BES tools), the airflow rate needs to change by at least of one order of magnitude. The insensitivity of the models is also seen when it comes to the inlet position and height (which is possible to implement in IDA ICE), which are instead parameters expected to be important in case of natural ventilation.

Regardless of the used software tools, some parameters had notable differences in the $S_{i,d}$ values resulting from the + 10% and −10% variations. This might indicate that the relationship between the parameter and the PI is non-linear in the evaluated input data region. These can be a subject for further analysis exploring the whole range of input space (e.g. the Morris method).

On a final note, even if not reported in this analysis, the height of the DSF can play a relevant role in the façade performance, both in terms of T_{glass} and in terms of e^{+}_{24h} and e^{-}_{24h}. However, this parameter is often not free to be decided by the designer or consultant, as it is often set due to other considerations than energy or environmental optimisation.

5. Conclusion

The comparison of the sensitivity of the results in IDA ICE and EnergyPlus showed that the ranking and magnitude of sensitivity indices were similar for most of the assessed parameters in the

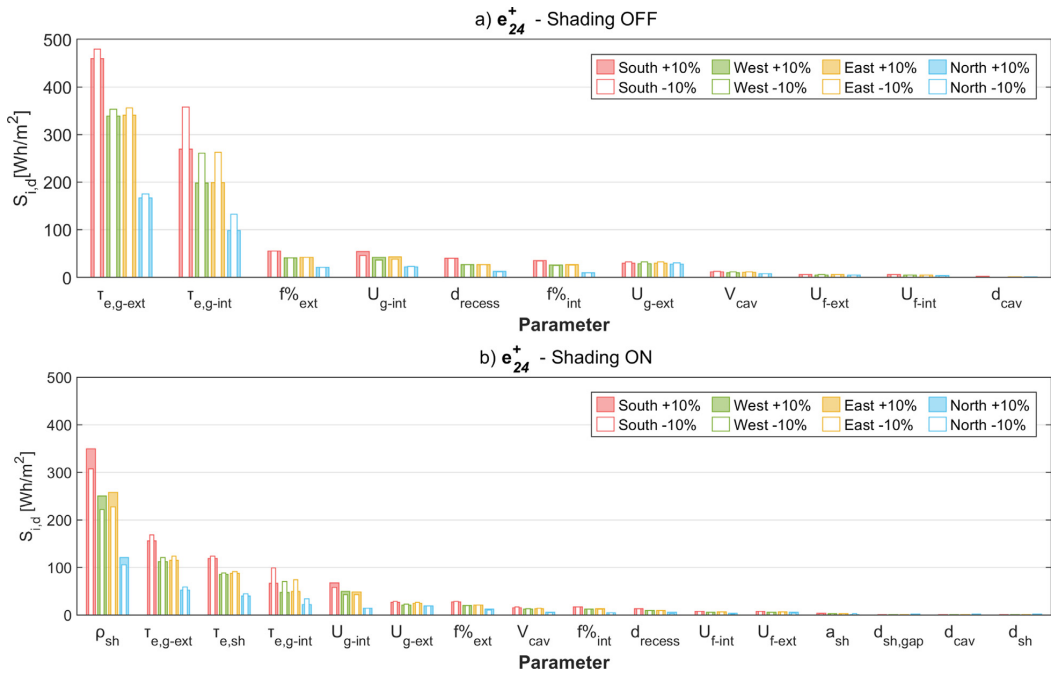

Fig. 6. S_{id}, Daily heat gain, Torino, all orientations, IDA ICE a) shading off b) shading on.

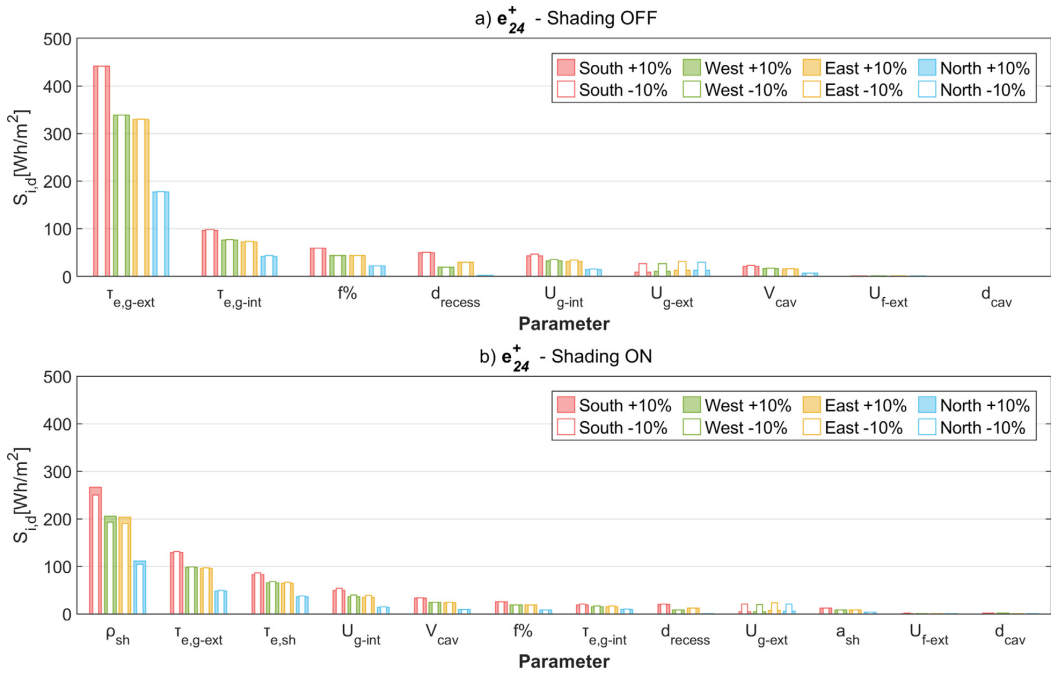

Fig. 7. S_{id}, Daily energy gain, Torino, all orientations, EnergyPlus a) shading off b) shading on.

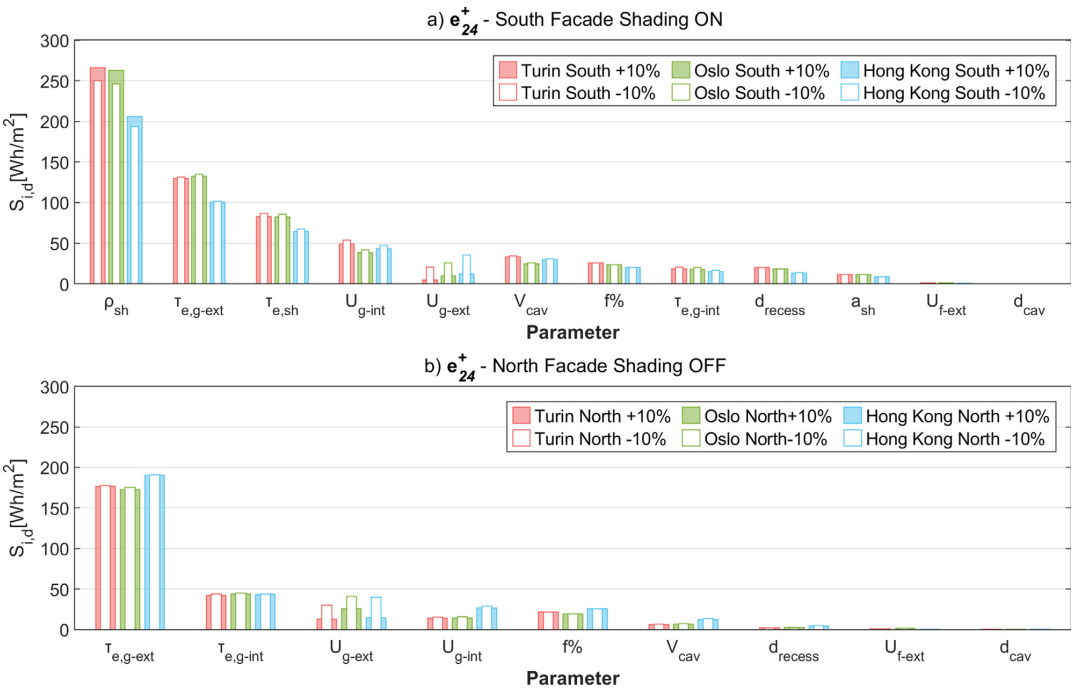

Fig. 8. S_{id}, Energy gain, all locations, EnergyPlus, a) South, shading on b) North, shading off.

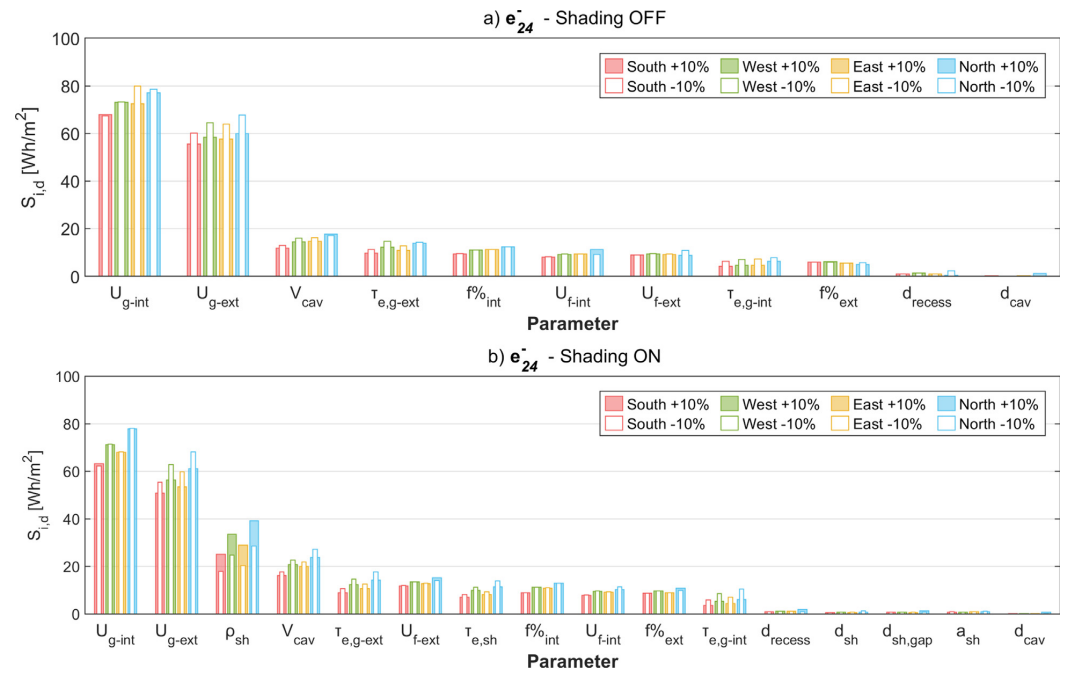

Fig. 9. S_{id}, Daily heat loss, Torino, all orientations, IDA ICE a) shading off b) shading on.

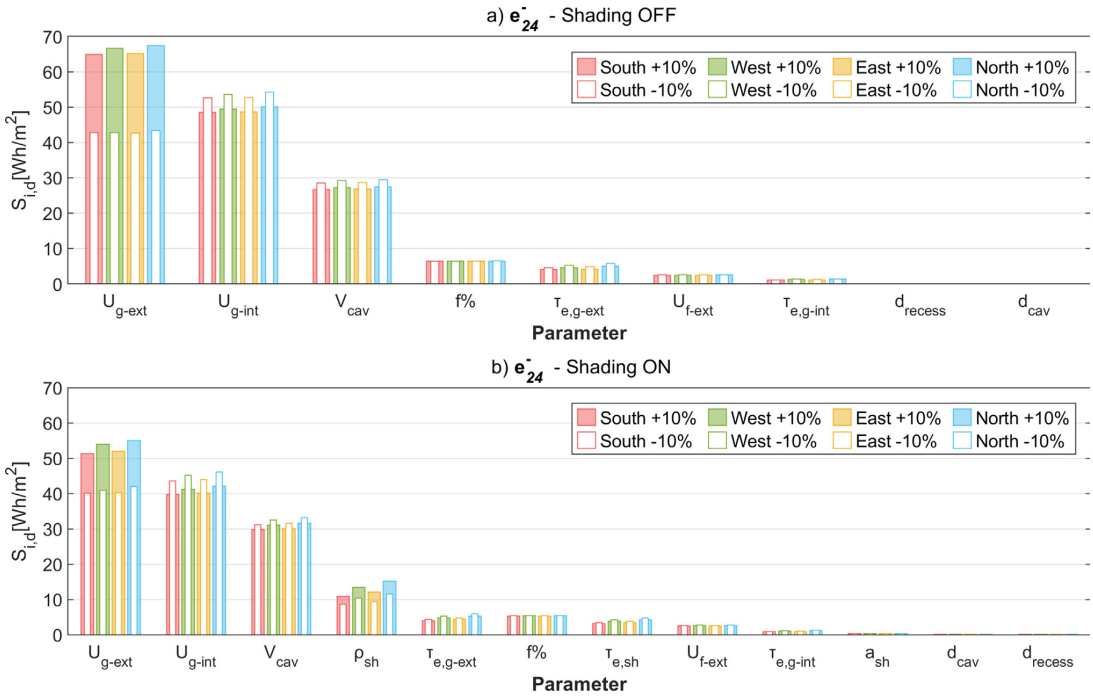

Fig. 10. S_{id}, Daily heat loss, Torino, all orientations, EnergyPlus a) shading off b) shading on.

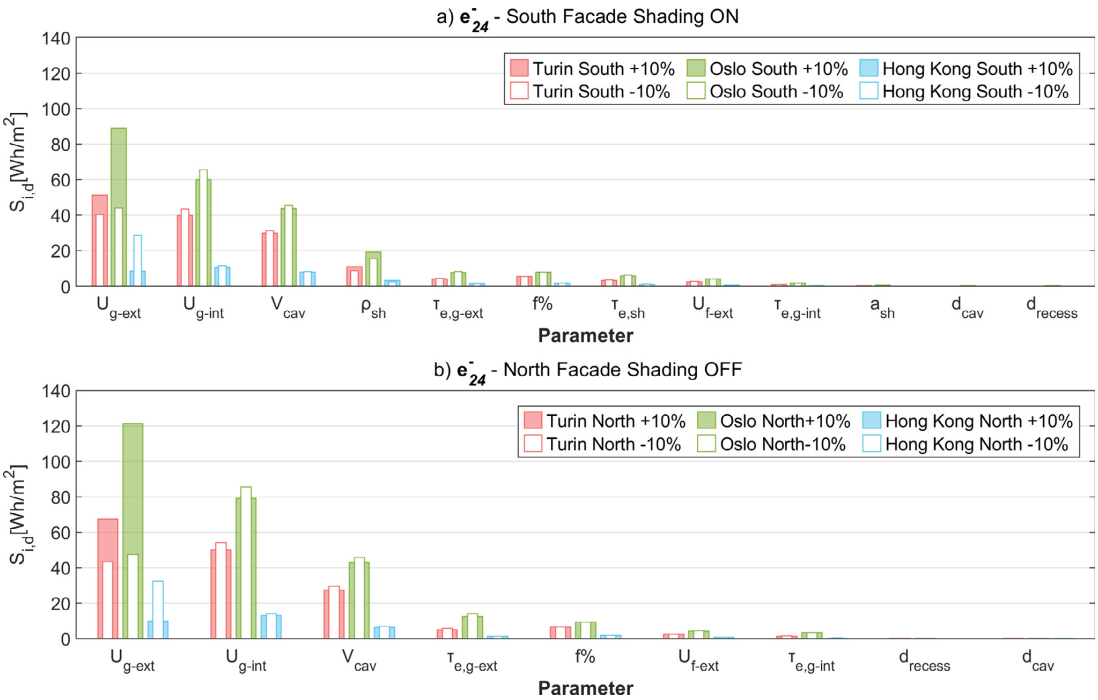

Fig. 11. Sid, Energy loss, all locations, EnergyPlus a) South, shading on b) North, shading off.

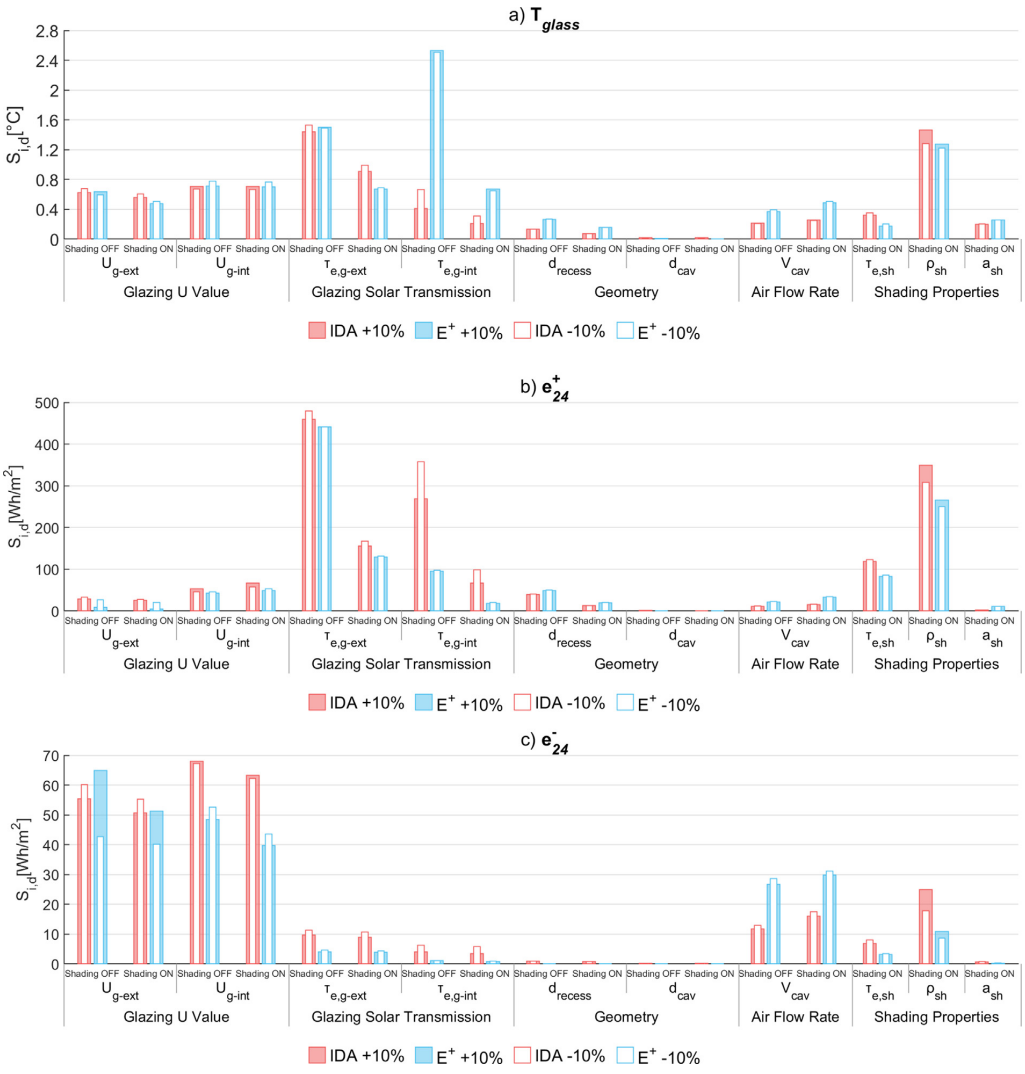

Fig. 12. Intersoftware comparison of $S_{i,ds}$ for IDA ICE and EnergyPlus: a) Internal glazing temperature b) Daily energy gain e^{+}_{24h} c) Daily energy loss e^{-}_{24h}.

two tools, with few exceptions. The general trend was that models were more sensitive to the parameters describing the glazing thermal and optical properties, and shading optical properties, when activated, than to the geometrical and frame properties. The effect of the airflow rate was, however, different in the two tools, as this parameter had a higher effect on the PIs in EnergyPlus. Additionally, the internal glazing temperature in EnergyPlus showed a higher sensitivity to the solar properties of the internal glazing than it did in IDA ICE. This can probably be explained by the missing heat capacity node in EnergyPlus. The models also showed moderate sensitivity to a variation in the air flow rate, which means that the convective heat exchange coefficients only had small variations within the investigated range. The airflow rate through a climate façade (that acts as an exhaust in the HVAC plant) is often determined by the necessary ventilation airflow rate due to the presence of occupants and a baseload. This value can to some extent be controlled (for example in combination with variable air volume systems) by reducing the air flow rate as a function of the actual environmental loads. However, for most of the applications, the allowed variation in the airflow to be explored in the design phase is usually small, as based on the design value assessed though standardised calculations, while the variation in the operation is normally not implemented. Within the possible small range of variation of the airflow rate, the performance of the climate façade is rather insensitive to this parameter. A different picture can be obtained when and if the climate façade is operated in a completely different way outside the occupancy time (e.g. during the night or the weekends) when the façade operates without forced airflow since the mechanical ventilation can be turned off – a strategy that is more likely to be adopted in highly efficient buildings.

The analysis showed that the ranking of the sensitivity indexes ($S_{i,d}$), is significantly different for each PI. However, the list of the most sensitive parameters for each PI remained the same for every

orientation and each climate, while minor differences occurred in the order of the moderately sensitive parameters.

In conclusion, the optical (solar transmittance) and thermal properties (thermal transmittance) of the glazing, and the optical properties (solar reflectance) of the shading systems adopted generated a larger variation on the selected performance parameters than those generated by other characteristics related to the geometrical features of the façade. This take-home lesson is important because it shows that the main constructional (size and airflow rate) characteristics of the climate façade can be fixed at the preliminary stage, when both the overall envelope vision and energy concept of the building is designed, without hindering the possibility to significantly modify the behaviour of the system at a later stage (by a careful selection of the glazed and shading layers). In a software tool perspective, the use of one or another tool should return the same results when it comes to selecting the optimal solution within a sensitivity analysis. While IDA ICE allows more inputs than EnergyPlus to be tested, the sensitivity analysis showed that this had little value since the most sensitive parameters are available in both tools.

CRediT authorship contribution statement

Adrienn Gelesz: Methodology, Formal analysis, Data curation, Software, Validation, Writing - original draft, Visualization, Funding acquisition. **Elena Catto Lucchino:** Methodology, Formal analysis, Data curation, Software, Validation, Writing - original draft, Visualization. **Francesco Goia:** Conceptualization, Methodology, Investigation, Validation, Writing - original draft, Funding acquisition, Project administration. **Valentina Serra:** Investigation, Writing - review & editing, Supervision. **András Reith:** Writing - review & editing, Supervision, Funding acquisition.

Declaration of Competing Interest

The authors declare that they have no known competing financial interests or personal relationships that could have appeared to influence the work reported in this paper.

Acknowledgements

The authors would like to thank the researchers and technical staff from Politecnico di Torino (Italy) involved in the experimental activity which provided the data used for model validation in this study.

Part of the activities presented in this paper were carried out within the research project "REsponsive, INtegrated, VENTilated - REINVENT – windows", led by the Norwegian University of Science and Technology (NTNU), supported by the Research Council of Norway through the research grant 262198, and research and industrial partners SINTEF, Hydro Extruded Solutions, Politecnico di Torino, and Aalto University.

The validation activity has been supported by the ÚNKP-18-3 New National Excellence Program of the Ministry of Human Capacities of Hungary.

The authors would like to thank Ellika Taveres-Cachat for proofreading the manuscript and improving its readability.

Appendix A

Airflow window – EnergyPlus model description

The built-in model adopted in Energy Plus is called 'Airflow Window'. This component allows the modelling of only mechanical ventilated façades. The model allows five different configurations for the airflow path, depending on which is the source and the destination of the forced air:

- Inside Air – Outside Air
- Inside Air – Inside Air
- Inside Air – Return Air
- Outside Air – Inside Air
- Outside Air – Outside Air

The configuration implemented in this study was the 'Inside Air-Outside Air' path because the return air was not used to climatize the indoor air.

This model adopts the calculation method described in the ISO Standard 15099 [48] for the ventilated gap. The following information is derived from the Engineering Reference of EnergyPlus [49].

Heat balance calculation

The window glass face temperatures are determined by solving the heat balance equations on each face of the glass at every time step.

The following assumptions are made in deriving the heat balance equations:

(1) The glass layers are thin enough (a few millimetres) that heat storage in the glass can be neglected; therefore, there are no heat capacity terms in the equations.
(2) The heat flow is perpendicular to the glass faces and is one dimensional.
(3) The glass layers are opaque to IR.
(4) The glass faces are isothermal. This is assumpted since the glass conductivity is usually very high.
(5) The short wave radiation absorbed in a glass layer can be distributed equally to the two faces of the layer.

The heat balance equations for the surfaces take into account the conductive, radiative and convection heat transfer of all the layers.

The heat balance equation for the external surface of 'Glass 1' in Fig. A1 is:

$$E_o\varepsilon_1 - \varepsilon_1\sigma\theta_1^4 + k_1(\theta_2 - \theta_1) + h_o(T_o - \theta_1) + S_1 = 0 \quad (A.1)$$

For the internal surface of 'Glass 1' is:

$$k_1(\theta_1 - \theta_2) + h_{cv}(T_{gap} - \theta_2) + \sigma\frac{\varepsilon_2\varepsilon_3}{1-(1-\varepsilon_2)(1-\varepsilon_3)}(\theta_3^4 - \theta_2^4) + S_2 = 0 \quad (A.2)$$

While for the internal surface of 'Glass 2':

$$k_2(\theta_4 - \theta_3) + h_{cv}(T_{gap} - \theta_3) + \sigma\frac{\varepsilon_2\varepsilon_3}{1-(1-\varepsilon_2)(1-\varepsilon_3)}(\theta_2^4 - \theta_3^4) + S_3 = 0 \quad (A.3)$$

And for the external surface of 'Glass 2':

$$E_i\varepsilon_4 - \varepsilon_4\sigma\theta_4^4 + k_2(\theta_3 - \theta_4) + h_i(T_i - \theta_4) + S_4 = 0 \quad (A.4)$$

where

ε = Emissivity of face i [–]
E_o, E_i = Exterior, interior long-wave radiation incident on window [W/m^2]
k_i = Conductance of glass layer i [W/ m^{2}K]
h_o, h_i = Outside, inside air film convective conductance [W/m^{2}K]

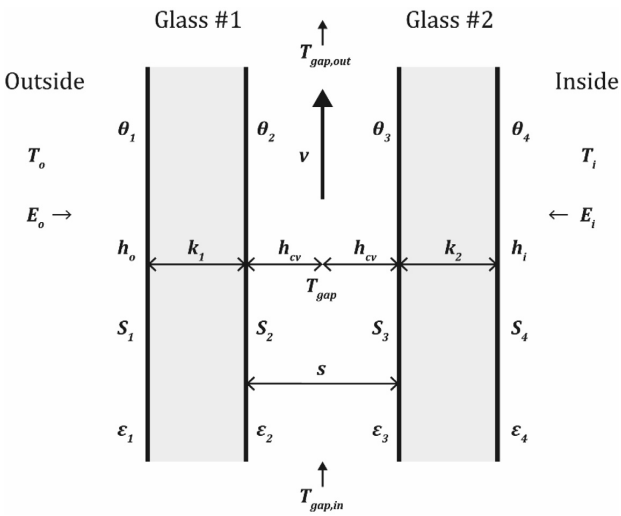

Fig. A1. Glazing system with forced airflow between two glass layers showing variables used in the heat balance equations [49].

h_{cv} = convective heat transfer coefficient from glass to gap air [W/m^{2}K]
θ_i = temperature of face i [K]
T_o, T_i = Outdoor and indoor air temperatures [K]
T_{gap} = effective mean temperature of the gap air [K]
σ = Stefan-Boltzmann constant [W/m^{2}K^4]
S_i = Radiation (short-wave, and longwave) absorbed by the ith glazing layer [W/m^2]

The convective heat transfer coefficient of both surfaces facing the same cavity is considered to be equal and given by:

$$h_{cv} = 2h_c + 4v \tag{A.5}$$

where

h_c = glass-to-glass heat transfer coefficient for non-vented (closed) cavity [W/m^{2}K] and calculated according to the ISO Standard 15099
v = air velocity in the gap (m/s) and it is calculated as

$$v = \frac{F}{A_{gap}} \tag{A.6}$$

where

F = airflow rate (m^3/s) which is assumed to be uniform across the width of the window.
A_{gap} = gap cross-sectional area in direction of flow (m^2)

The mean temperature of the gap air is given by the following expression:

$$T_{gap} = T_{ave} - \frac{H}{H_0}\left(T_{gap,out} - T_{gap,in}\right) \tag{A.7}$$

where

$$T_{ave} = \frac{\theta_2 + \theta_3}{2} \tag{A.8}$$

$$H_0 = \frac{\rho C_p S}{2h_{cv}} v \tag{A.9}$$

H = glazing height (m)
$T_{gap,in}$ = gap air inlet temperature (T_i if the airflow source is indoor air, T_o if the airflow source is outside air) (K).

The outlet air temperature is given by:

$$T_{gap,out} = T_{ave} - \left(T_{ave} - T_{gap,in}\right)e^{-H/H_0} \tag{A.10}$$

In the overall balance, the fan energy used to move air through the gap is ignored since is very.

In case of a shading device in the cavity (Fig. A2), the heat balance equations are the same as those for the between-glass shading device with natural convection. For each layer (glass or shading) the heat balance equations take also into account the energy reflected, absorbed and transmitted by the shading device.

For the internal surface of 'Glass 1' is:

$$\begin{aligned} &k_1(\theta_1 - \theta_2) + h_{cv,1}\left(T_{gap,1} - \theta_2\right) \\ &+ \frac{\sigma\varepsilon_2}{1-\rho_2 R_1}\left[\frac{\tau_{sh}}{1-\rho_6\rho_3}\left(\varepsilon_3\theta_3^4 + \varepsilon_6\theta_6^4\rho_3\right) + \varepsilon_5\theta_5^4 + \varepsilon_2\theta_2^4 R_1\right] \\ &- \sigma\varepsilon_2\theta_2^4 + S_2 \\ &= 0 \end{aligned} \tag{A.11}$$

For the shading layer surface facing 'Gap 1':

$$\begin{aligned} &k_{sh}(\theta_6 - \theta_5) + h_{cv,1}\left(T_{gap,1} - \theta_5\right) \\ &+ \frac{\sigma\varepsilon_5}{1-\rho_2 R_1}\left[\frac{\tau_{sh}\rho_2}{1-\rho_5\rho_3}\left(\varepsilon_3\theta_3^4 + \varepsilon_6\theta_6^4\rho_3\right) + \varepsilon_2\theta_2^4 + \varepsilon_5\theta_5^4\rho_2\right] \\ &- \sigma\varepsilon_5\theta_5^4 + S_5 \\ &= 0 \end{aligned} \tag{A.12}$$

with

$$R_1 = \rho_5 + \frac{\tau_{sh}^2\rho_3}{1-\rho_6\rho_3} \tag{A.13}$$

where

k_{sh} = Conductance of shading layer [W/ m^{2}K]

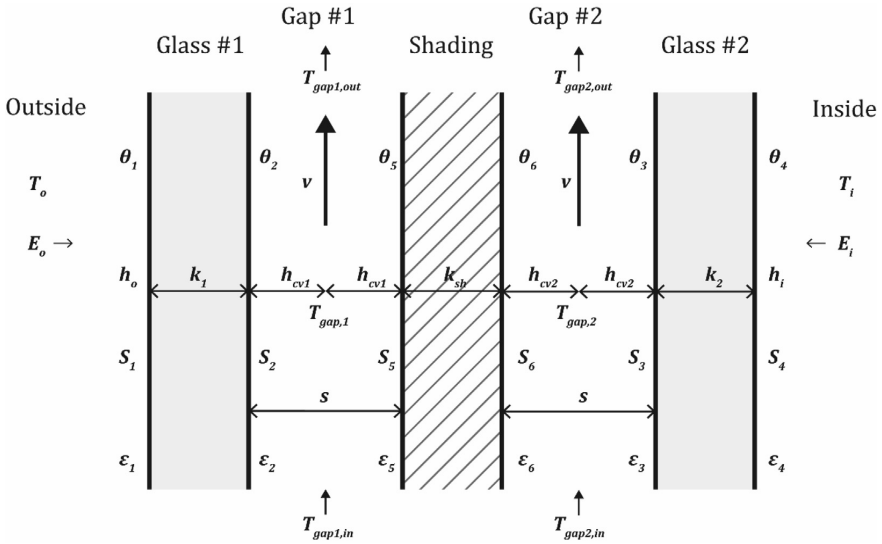

Fig. A2. Airflow window with between-glass shading device showing variables used in the heat balance equations [49].

τ_{sh} = IR diffuse transmittance of shading device
$\varepsilon_{sh(5,6)}$ = diffuse emissivity of shading device
$\rho_{sh(5,6)}$ = IR diffuse reflectance of shading device (=1 - (τ_{sh} + ε_{sh}))
$\theta_{sh(5,6)}$ = temperature of the surface of the shading layer that faces the gap (K).

The term 1 - $\rho_{sh}\rho_{glass}$ accounts for the inter-reflection of IR radiation between glass and shading layer.

To determine the gap air velocity, gap air mean-equivalent temperature and gap outlet air temperature a pressure-balance set of equations is used. The pressure balance equals the buoyancy pressure acting on the gap air to the pressure losses associated with gap airflow between gap inlet and outlet. The balance equations account for the two air gaps generated by the presence of the shading device in the cavity [48].

The heat convective coefficient of each gap is:

$$h_{cv,1} = 2h_{c,1} + 4v$$

$$h_{cv,2} = 2h_{c,2} + 4v \quad (A.14)$$

where

$h_{c,1}$, $h_{c,2}$ = surface-to-surface heat transfer coefficients for gap #1 and #2, respectively, when these gaps are non-vented (closed).
v = air velocity in the gap (m/s) and it is calculated as

$$v = \frac{F/2}{A_{gap}} \quad (A.15)$$

where

A_{gap} = sW is the cross-sectional area of the gap on either side of the shading device. It is assumed that the shading device is centred between the two panes of glass so that the airflow, F, is divided equally between the two gaps.

The average temperature of the two outlet air streams is:

$$T_{gap,ave,out} = (T_{gap,1,out} + T_{gap,2,out})/2 \quad (A.16)$$

Glazing system optical properties

In EnergyPlus, the optical properties of individual glass layers are given by the following quantities at normal incidence as a function of wavelength:

- Transmittance, T
- Front reflectance, R_f
- Back reflectance, R_b

The optical properties of a glazing system consisting of N glass layers separated by nonabsorbing gas layers are determined by solving the following recursion relations for $T_{i;j}$, the transmittance through layers i to j; $R^f_{i;j}$ and $R^b_{i;j}$, the front and back reflectance, respectively, from layers i to j; and A_j , the absorption in layer j.

For the case of double glazing (Fig. A3) this mean:

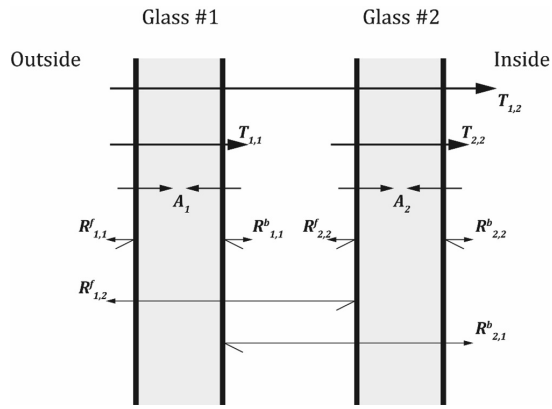

Fig. A3. Schematic of transmission, reflection and absorption of solar radiation within a multilayerglazing system [49].

$$T_{1,2} = \frac{T_{1,1}T_{2,2}}{1 - R^f_{2,2}R^b_{1,1}} \tag{A.17}$$

$$R^f_{1,2} = R^f_{1,1} + \frac{T^2_{1,1}R^f_{2,2}}{1 - R^f_{2,2}R^b_{1,1}} \tag{A.18}$$

$$R^b_{2,1} = R^b_{2,2} + \frac{T^2_{2,2}R^f_{1,1}}{1 - R^b_{1,1}R^f_{2,2}} \tag{A.19}$$

$$A_1 = (1 - T_{1,1} - R^f_{1,1}) + \frac{T_{1,1}R^f_{2,2}(1 - T_{1,1} - R^b_{1,1})}{1 - R^f_{2,2}R^b_{1,1}} \tag{A.20}$$

$$A_2 = \frac{T_{1,1}(1 - T_{2,2} - R^b_{2,2})}{1 - R^f_{2,2}R^b_{1,1}} \tag{A.21}$$

These relations account for multiple internal reflections within the glazing system. If the above transmittance and reflectance properties are input as a function of wavelength, EnergyPlus calculates "spectral average" values of the above glazing system properties by integrating over wavelength.es is a function of wavelength. The angular properties are calculated as a function of the angle of incidence. Two different methods apply if the glass is coated or uncoated.

Shading device optical properties

Shading devices affect the system transmittance and glass layer absorptance for short-wave radiation and long-wave (thermal) radiation. The effect depends on the shade position (interior, exterior or between-glass), its transmittance, and the amount of interreflection between the shading device and the glazing. Also of interest, it is the amount of radiation absorbed by the shading device. The shading device implemented in the model used for this study is the type "shades". "Shades" are assumed to be perfect diffusers. This means that direct radiation incident on the shade is reflected and transmitted as hemispherically uniform diffuse radiation: there is no direct component of transmitted radiation. It is also assumed that the transmittance, τ_{sh}, reflectance, ρ_{sh}, and absorptance, α_{sh}, are the same for the front and back of the shade and are independent of angle of incidence.

The optical properties, both shortwave and longwave, of the glazing system (with the shading device) are calculated as a function of the isolated shade properties (i.e., shade properties in the absence of the glazing) and the isolated glazing properties (i.e., glazing properties in the absence of the shade).

Double glass façade (DgFacade) – IDA ICE model description

The double skin façade was modelled as a Detailed Window model and a custom component called Double Glass Facade (DgFacade) attached to it (Fig. A4). These modules can model the connection of the air inlet and outlet both towards the indoor environment and to the outside. A forced flow rate can be assigned to it if the façade is connected to the HVAC system.

The façade cavity is partitioned vertically and horizontally, surrounded in all directions by air spaces with identical conditions. Both horizontal and vertical partitions are transparent to the incoming solar radiation, and heat flux through them is neglected [50]. The shading device, if present, can be assigned to both glazings. In the presented work, the shading has been assigned to the external glazing, as interior shade. The inner façade can also include opaque parts as well, which are considered in the heat balance equations.

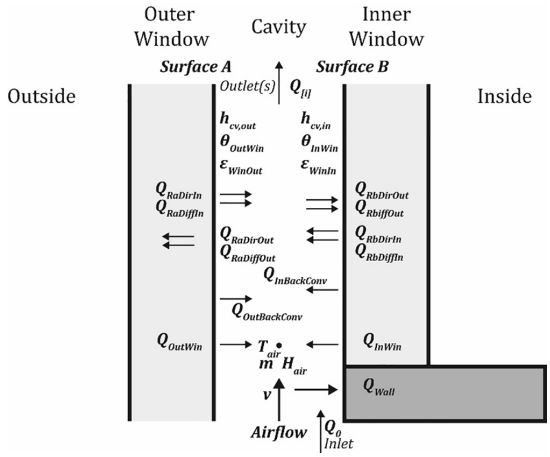

Fig. A4. Model of the DbFacade.

The Detailed Window Model follows the ISO 15099 [48] calculation method described above.

Energy balance at the window surfaces

The heat flux to the windows from the double façade is the sum of the convective heat flux and the longwave heat flux at the window surfaces.

For inner window:

$$Q_{InWin} = Q_{conv,InWin} + Q_{LW,InWin} \tag{A.22}$$

For outer window:

$$Q_{OutWin} = Q_{conv,OutWin} - \Sigma Q_{LW,wall} - Q_{LW,InWin} \tag{A.23}$$

where

Q_{InWin} = heat flux into the inner window from double façade [W]
$Q_{conv,InWin}$ = convective heat flux from the inner window [W]
$Q_{LW,InWin}$ = Longwave heat flux from the inner window [W]
Q_{OutWin} = heat flux to the outer window from the double façade [W]
$Q_{conv,OutWin}$ = convective heat flux from the outer window [W]
$\Sigma Q_{LW,Wall}$ = Longwave heat flux from the wall (currently 0) [W]

Energy balance of the cavity air

The air enthalpy gain is calculated as a combination of the convective heat gain from the windows and the wall, the back convection from the shaded window(s) and the heat flow from the terminals. Moisture balance and CO_2 balance is calculated in each timestep as well, and the mass of the air is calculated with "RhoMois" – function from the air temperature and humidity.

$$m\frac{\partial H_{air}}{\partial t} = Q_{ConvOutWin} + Q_{ConvInWin} + Q_{ConvWallTot} + Q_{OutBackConv} + Q_{InBackConv} + Q_0 + \sum_{i=1}^{nTerminals} Q[i] \tag{A.24}$$

$$m = \rho V \tag{A.25}$$

where

m = mass of air [kg]

ρ = density [kg/m^3]
V = volume of cavity air [m^3]
H_{air} = air enthalpy [J/kg]
$Q_{OutBackCv}$ = heat flow from outside curtain back convection [W]
$Q_{InBackCv}$ = heat flow from inside curtain back convection [W]
$Q_{ConvWallTot}$ = convective heat flux from wall [W]
Q_0 = heat flux from term_0 [W]
Q_i = heat flux from term_i [W]

The vertical temperature gradient of the air space is neglected as the air is considered well mixed.

Convection

Convective heat gain is calculated as follows:

$$Q_{conv,InWin} = h_{cv,InWin} A_{InWin} (\theta_{InWin} - T_{air}) \quad (A.26)$$

Where

θ_{InWin} = temperature of the inner window surface [K]
T_{air} = air temperature in the gap [K]
h_{cv} = surface convective heat transfer coefficient [W/m^{2}K]
A_{InWin} = surface of the inner window [m^2]

Convection from surfaces is treated as non-linearly using standard ICE natural convection function called *u_film*. The convective heat transfer coefficients in the DBfacade model follow equation (A.27). The value is chosen for each window surface (external glazing and the cavity, when no shading is present/between the shading and cavity when present, and the internal glazing and the cavity) from the greater of the convective heat transfer coefficient from natural and forced airflow:

$$h_{cv} = \max\left(h_{cv,forced}; h_{cv,nat}\right) \quad (A.27)$$

where

$h_{cv,forced}$ = surface convective heat transfer coefficient calculated for forced convection [W/m^{2}K]
$h_{cv,nat}$ = surface convective heat transfer coefficient for natural convection [W/m^{2}K]

The forced convection heat transfer function is taken from the VDI Heat Atlas [51]. First, the Reynold's number is calculated, that is used then to calculate the Nusselt number. Both laminar flow and turbulent flow can be considered, depending on the cavity geometry and airspeed. The calculation method for the natural convection follows the Detailed Natural Convection Algorithm (DNCA), depending on the temperature difference of the surface and the air, and also the inclination of the surface (surface slope = 0 for floor and 180 for ceiling) (Table A1).
where

v = airspeed [m/s]
l = *height of the cavity [m]*
$\cdot$ = dynamic viscosity of the air [N s/m^2]
Re = Reynolds number
λ = thermal conductivity of the air [W/m^2]
Pr = Prandtl-number

The convection in the enclosed gaps of the glazing and between the shading and the external glazing is defined in the Detailed Window Model, that follows ISO 15099 [48]. The convection heat gain between the back surface of the shading and the shaded window(s) is considered in the ventilated cavity air heat balance.

Table A1
Equations used for calculating convective heat transfer coefficients within the ventilated window model.

Natural flow (DNCA)		Forced flow	
If $\Delta T < 0$ K and surface	slope < 90 °Or $\Delta T > 0$ K and surface slope > 90°	$h_{nat,conv} = \frac{9.482\cdot\lvert\Delta T\rvert^{1/3}}{7.823-\lvert\cos\left(\pi\frac{\varphi}{180}\right)\rvert}$	$h_{conv,forced} = Nu * \frac{\lambda}{l}$ $Re = lv\frac{\rho}{\eta}$
Else	$h_{nat,conv} = \frac{1.81\cdot\lvert\Delta T\rvert^{1/3}}{1.382+\lvert\cos\left(\pi\frac{\varphi}{180}\right)\rvert}$	if, Re < 10^4 (laminar flow)	$Nu = 0.664\cdot\sqrt{Re}\cdot Pr^{\frac{1}{3}}$
		if Re > 10^4: (turbulent flow)	$Nu = \frac{0.037\cdot Re^{0.8}\cdot Pr}{1+2.443\cdot Re^{-0.1}\cdot\left(Pr^{\frac{2}{3}}-1\right)}$

Long-wave radiation

Long-wave radiation is treated with the full non-linear Stefan-Boltzmann relations and view factors between the surfaces.

$$Q_{LW,InWin} = \frac{1}{\frac{1}{\varepsilon_{WinIn}} + \frac{1}{\varepsilon_{WinOut}} - 1} A\sigma \cdot \lvert((\theta_{InWin} - 273K)^2 + (\theta_{OutWin} - 273K)^2) \cdot ((\theta_{InWin} - 273K) + (\theta_{OutWin} - 273K)) \cdot (\theta_{InWin} - \theta_{OutWin})\rvert \quad (A.28)$$

where

ε = Emissivity of face i [–]
θ_i = temperature of face i [K]
σ = Stefan-Boltzmann constant [W/m^{2}K^4]

Solar radiation

Entering direct and diffuse short-wave radiation is absorbed first by the outer window, then by the eventual shading and then by the inner window (Calculations based on ISO 15099 [48]). The inner window is shaded first by any surrounding buildings (standard ICE function), then by the shading device.

At the beginning of the calculation, the actual shading factors are precomputed for all (plausible) solar locations and stored as parameters in the shading model connected to each window/opening [47]. The fraction of radiation (k) reaching each window and surface is calculated, both for diffuse and direct radiation, with the help of the *Shading, Winlight, Lightfract models*. The first reflection is captured by the model.

Once the radiation hits a window, the whole surface of the window is considered as the diffuse or direct radiation source, not just the lit portion of this surface, that is not shaded by external objects. The exact target location of the transmitted direct light beam is computed, the reflected portion spread diffusely. Reflected short wave radiation is assumed to be diffusely distributed according to surface view factors, the window is radiating with equal intensity, not considering the position of the direct radiation falling on the surface. [47]

Radiation heat balance of cavity surfaces:

$$Q_{ra,dir,out} = Q_{rb,dir,in} \quad (A.29)$$

$$Q_{ra,diff,out} = Q_{rb,diff,in} + Q_{SW,ref,tot} \quad (A.30)$$

Calculation of the radiation from the external window:

$$Q_{rb,dir,out} = k_{dir} \cdot Q_{ra,dir,in} \quad (A.31)$$

$$Q_{rb,diff,out} = k_{diff} \cdot Q_{ra,diff,in} \quad (A.32)$$

where

k_{diff} = Fraction of diffuse radiation to the inner window
k_{dir} = Fraction of direct radiation to the inner window
$Q_{ra,dir,out}$ = leaving direct solar radiation through surface A (outer window)
$Q_{rb,dir,in}$ = entering solar radiation from surface B (inner window)
$Q_{ra,diff,out}$ = leaving diffuse solar radiation through surface A (outer window)
$Q_{rb,diff,in}$ = entering diffuse solar radiation from surface B (outer window)
$Q_{SW,ref,tot}$ = radion reflected backwards from the outer window

Airflow

The airflow through the air space is driven by the density difference between space and ambient air. Intake and exhaust air grilles are assumed to be at the floor and ceiling level respectively. A leakage path between the room and the air space is also provided (in a separate model). All airflows can have arbitrary directions, bidirectional transport of energy, humidity and mass fraction is possible through the openings. Pressure drop in the intake and exhaust grilles is modelled in separate leak models (which may be controlled by specific signals)

$$\dot{m}_0 + \sum_{i=1}^{nTerminals} m[i] = 0 \tag{A.33}$$

where

$\dot{m}_0$ = mass flow from terminal 0

Since the shading device is assigned to the external window, the airflow between the external glass and the shading is calculated within the Detailed Window Model.

Appendix B

Experimental analysis for software tools validation

A full-scale office room with two exhaust-air façade modules located in a temperate sub-continental climate location in northern Italy (45° N latitude) was continuously monitored for around two years, as more extensively described in [3,52]. The test cell consisted of one zone representing an office space (H × W × D = 3.4 m × 3.2 m × 6.5 m) and two DSF modules (1.60 m wide, 3.40 m high) on the (almost exactly) south-exposed façade. Each DSF had a mechanically ventilated cavity, where the indoor air flowed into the cavity from a bottom opening and was extracted through a duct, placed at the top of the ventilated gap. The Climate façade configuration under investigation in this paper had a double glazed unit in both the internal and external skin, and a controllable, highly reflective roller blind placed at approximately one-third of the cavity, measured from the exterior glazing unit (Fig. B1).

During the long-term measurements, the indoor temperature was maintained at the desired setpoint of 20 °C in winter and 26 °C in summer by means of a combined air system and ceiling radiant panel. The test cell and the modules were equipped with a wide range of sensors: thermocouples for surface and air temperature measurements, heat flux meter sensors, pyranometers both inside and outside. Sensors were placed in several heights (+1,00, +2,00, +3,00 m) both inside and outside of the façade. The procedures adopted for data acquisition, sensors positions and considerations on the influence of sensors on the acquired values are not here detailed for the sake of brevity but follows the same methods and analyses presented in [53]. The measurement accuracies of the sensors and the measurement chain were: ±0.3 °C, ±5% and ±5%, for thermocouples, heat flux meters (hourly values) and pyranometers (hourly values), respectively (Table B1).

This accuracy led to the estimation of the uncertainty on the daily energy flows through the façade to be around 30% due to error propagation in data postprocessing (data aggregation to obtain daily energy flows through the façade, as described more in details in Section 3.3. More details on the experimental analysis can be found in [52] and are not herewith given for the sake of brevity.

Software tools validation procedures and key performance indicators

The validation through comparison with experimental data was carried out over four different weeks. The selected periods included two weeks (one in summer and one in winter) with shading up (OFF) and two weeks (one in summer and one in winter) with shading down (ON). These weeks had temperature peaks (low/high) and solar irradiation peaks representative for the corresponding season. Moreover, each period included both sunny and warm days, and sunny and cold days, as well as overcast sky conditions.

The validation of the two BES tools was performed at the façade level, and not at room level. Interest was placed on the reliability of the DSF model and not on the entire BES tool. Thus, the measured and simulated quantities that are compared are related to the DSF alone and not to the system "façade-plus-room". Since the BES tools were already validated in all the other parts against several standards –e.g. EN 15255-2007, Envelope BESTEST, etc–, only the performances of the sub-models representing the DSF were assessed.

The validation was carried out by comparing the measured data with the results of the simulations. Using the recorded experimental data, a weather data file (based on the original EnergyPlus Weather Data for the location of the experiment) was created to replicate the boundary conditions occurred during the experiments. Outdoor air temperature, global and beam solar irradiation were changed in the weather data file to allow the simulations to be done with input data derived from the measurement.

The validation procedure was based on the comparison of two types of PIs, which were later used in the sensitivity analysis. The PIs were selected to be representative of the thermal and comfort performance of the façade. The daily energy across the façade, specified as daily heat gain e^{+}_{24h} [Wh/m^2] and daily heat loss e^{-}_{24h} [Wh/m^2] were used to assess the sensitivity of the parameters when considering the energy performance of the DSF. The surface temperature of the indoor-facing surface of the inner skin, T_{glass} [°C], was instead used to assess the sensitivity of the parameters that affect the indoor thermal comfort.

While the surface temperature is a rather straightforward quantity, the daily heat gain and loss were obtained as described in Eqs. (B.1)–(B.3), where $I_{tr}(t)$ was the transmitted solar radiation, and $\dot{q}_{LW,conv}(t)$ was the sum of the longwave radiation and convective heat flux at the surface of the innermost glass pane, facing the indoors.

Hourly heat transfer:

$$\dot{q}_{tot}(t) = I_{tr}(t) + \dot{q}_{LW,conv}(t) \tag{B.1}$$

Daily heat gain:

$$e^{+}_{24h} = \int_{00:00}^{00:00+1day} \dot{q}^{+}_{tot}(t)dt \tag{B.2}$$

Daily heat loss:

$$e^{-}_{24h} = \int_{00:00}^{00:00+1day} \dot{q}^{-}_{tot}(t)dt \tag{B.3}$$

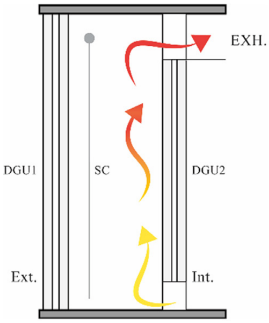

ID	Layers from exterior to interior	
DGU1	20 mm	Laminated, low-iron glass with selective coating, pos.2, 10.10.4
	16 mm	Air
	10 mm	Low-iron clear glass
SC		High reflectance roller blind
DGU2	10 mm	Low-e clear glass pos.2
	16 mm	Air
	10 mm	Laminated clear glass 5.5.4

Fig. B1. Schematic section and glazing configuration of the DSFs.

Table B1
Experimental periods.

		WINTER		SUMMER	
	Week	1	2	3	4
Outdoor temperature [°C]	max	7	7	34	26
	min	−1	−1	17	12
	average	3	2	25	18
Shading device	ON	OFF	ON	OFF	
Max vertical outdoor irradiance [W/m^2]	866	880	641	797	
Daily horizontal irradiation [kWh/m^2]	max	2.34	1.75	6.92	5.33
	average	1.67	1.3	5.5	3.79
Daily vertical irradiation [kWh/m^2]	max	4.98	4.47	6.7	5.44
	average	2.72	2.6	3.75	3.58

Table B2
RMSE values for interior glazing surface temperature [°C]

	Winter		Summer	
	Shading down	Shading up	Shading down	Shading up
IDA ICE [°C]	0.7 °C	1.1 °C	0.6 °C	0.9 °C
EnergyPlus	2.0 °C	3.0 °C	1.6 °C	2.0 °C

From the measured experimental data, the PIs were calculated as described here below:

- The surface temperature of the indoor glass was calculated by area-weighted averaging the values measured at three heights.
- The daily energies were calculated using:
- The surface heat flux (combining the convective heat exchange and the long-wave radiative heat exchange) measured at the indoor surface of the interior glazing pane, calculated by area-weighted averaging the values measured at three heights.
- The vertical transmitted solar irradiance, measured at the middle of the DSF's height.

As for the outputs of the simulations, T_{glass} values were directly logged in both simulation tools, while the daily heat loss and gain were calculated as the following:

- In IDA ICE daily energy gain/loss were calculated from hourly values of the transmitted solar radiation through the glazing and heat flux (radiative long-wave and convective) exchanged at the internal surface of the glazing, as described above (Eqs. (B.1)– (B.3)):
- In EnergyPlus the following output variables were logged for daily energy values:
  - Daily heat gain is directly obtained from Surface Window Heat Gain Energy [J]
  - Daily heat loss is directly obtained from Surface Window Heat Loss Energy [J]

The validation was carried out qualitatively by comparing time evolution of the quantities, and also quantitatively, by means of the Root Mean Square Error (RMSE) as an indicator of fitness of the models with the experiments, as described in Eq. (B.4),

$$RMSE = \sqrt{\frac{1}{n}\sum_{i=1}^{n}(X_{sim} - X_{exp})^2} \quad \text{(B.4)}$$

where n is the number of measurements,X is the hourly value, the subscript *sim* is for the simulated value, *exp* is for the experimental value.

Results of the software tools validation

Indoor surface temperature

The time evolution of the quantities simulated by IDA ICE matched well the experimental values, while simulations in EnergyPlus returned a time shift in the peaks up to 3 h, compared to the experiments. IDA ICE underestimated peaks in summer and overestimated them in winter with an error in the range −2 °C to + 3

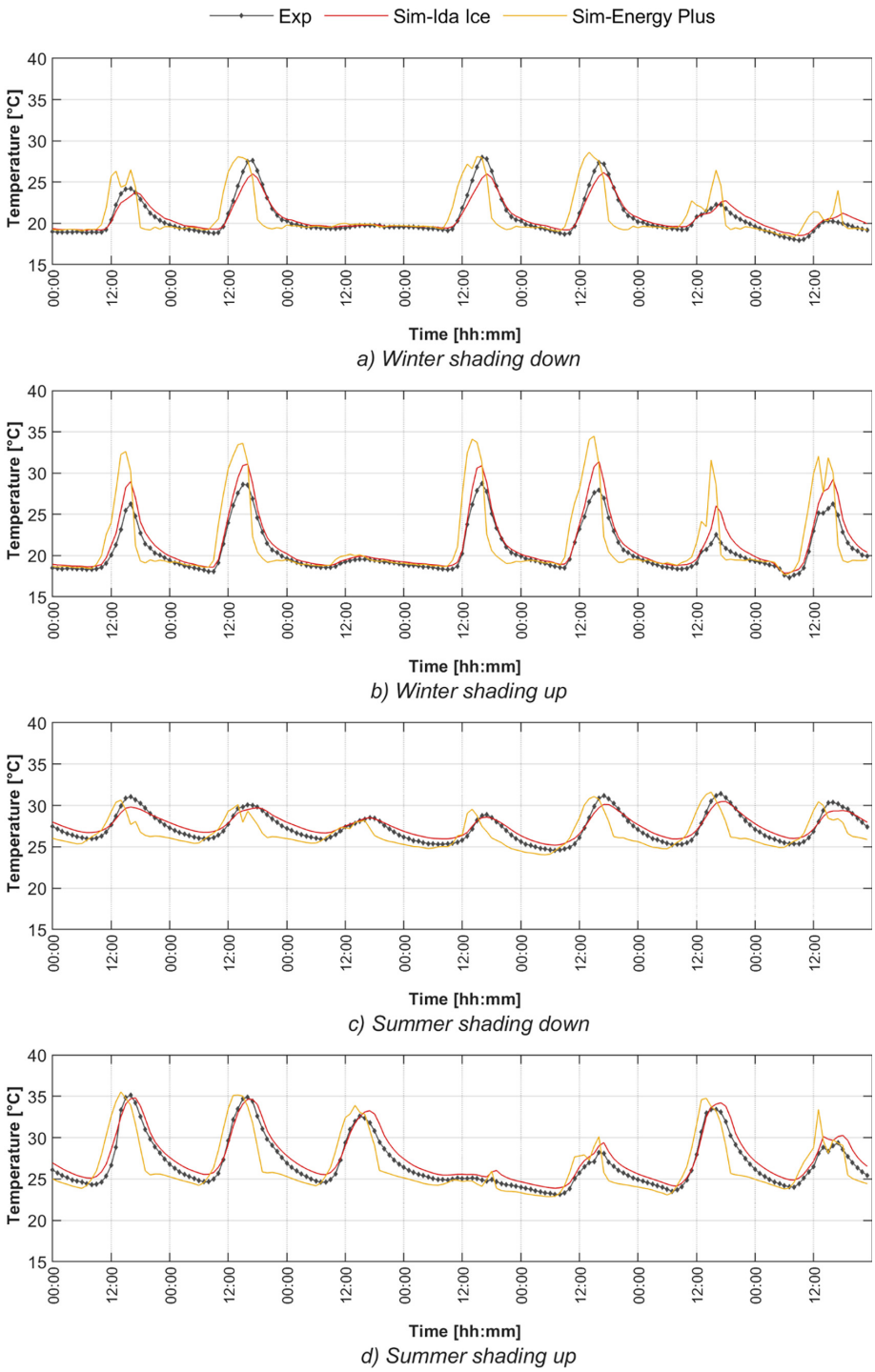

Fig. B2. Interior glazing surface temperature.

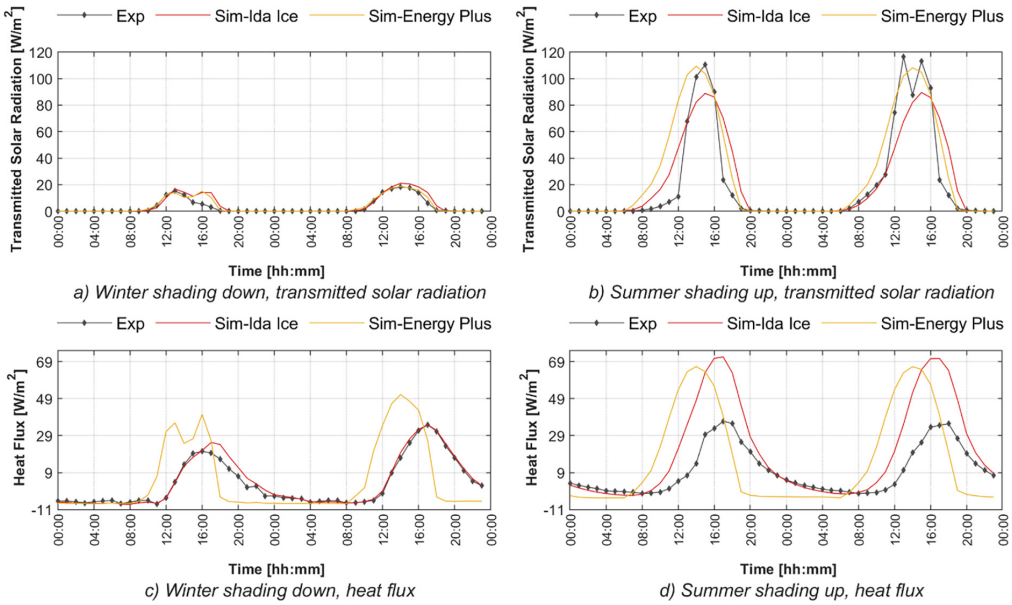

Fig. B3. Time profiles of transmitted solar radiation and heat flux for the first two days of two selected periods.

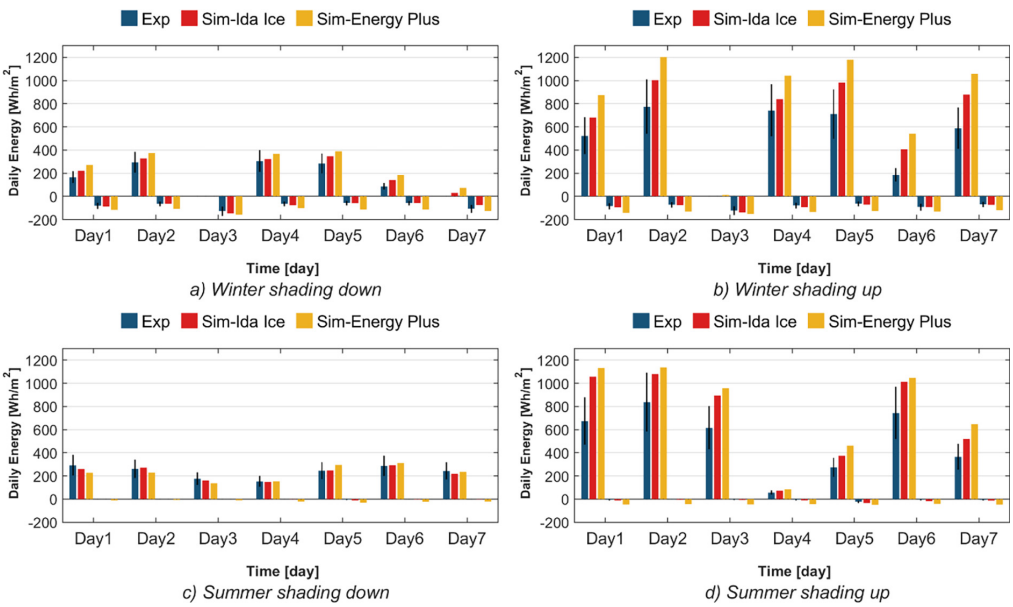

Fig. B4. Daily transmitted energy.

.5 °C. Minimum values were close to the experiments, with small overestimation, showing a maximum difference of nearly 0.9 °C. RMSE values were lower for IDA ICE in all periods compared to EnergyPlus. The latter often overestimated the values of the peaks, exceeding 10 °C when shading was disabled. Conversely, as for IDA ICE, the minimum values were close to the experiments, with a maximum difference of approximately 1 °C. In general, the errors in EnergyPlus were circa 1.5 °C greater than in IDA ICE (Table B2).

The main reason for the higher errors in EnergyPlus is due to the model of the glass panes. While IDA ICE includes a heat capacity

Table B3
RMSE values for Daily transmitted energy.

	Winter				Summer			
	Shading down		Shading up		Shading down		Shading up	
	IDA ICE	EnergyPlus	IDA ICE	EnergyPlus	IDA ICE	EnergyPlus	IDA ICE	EnergyPlus
e^{+}_{24h} [Wh/m^2]	43	83	205	371	17	37	237	299
e^{-}_{24h} [Wh/m^2]	15	42	11	53	3	18	8	38

node for the glazing, the thermal inertia of the glazing is not implemented in the EnergyPlus model. Hence, any heat absorbed by the glass surface shows an instantaneous effect on the glass temperature, causing a higher temperature rise than in reality. While one can be surprised to imagine such a large effect of the heat capacity of the glass panes, it is important to remember that the simulated system has a rather thick glass structure (50 mm of glass when both the exterior and the interior skin are considered). A conventional, single skin, glazing system is usually composed of a total thickness of glass in the range around 1 cm. Therefore, its inertial characteristics are relatively low, and the impact of this feature on the dynamics of the heat transfer rather limited – if not negligible. Conversely, in a double skin façade (with safety glass panes), the accounting of the heat absorbed and released because of the specific heat capacity of the material is no longer imperceptible. To highlight this effect, a simulation comparison was carried out by repeating a simulation in IDA ICE using the real value of the specific heat capacity of the glass and by setting a zero value. This investigation showed that when the specific heat capacity is neglected in IDA ICE, the simulation results in IDA ICE were extremely close to those obtained by EnergyPlus. On the contrary, when the specific heat capacity of the glass was used (and hence the system simulates correctly the effect of the heat capacity of the glazed system), the time evolution simulated by IDA ICE was much closer to the experimental data (as already shown Fig. B2 and B3c-3d), and different from the one calculated by EnergyPlus.

Daily transmitted energy

The transmitted energy was calculated from the transmitted solar radiation component and the long-wave and convective heat flux at the internal glass surface. The time profiles of these two components are shown to understand the causes of the deviations if present (Fig. B3).

While the time profiles and values of the solar radiation followed the experimental values generally well, with some differences in case of the shading being absent, the heat flux showed higher differences for the same periods (Fig. B4).

Despite the differences in the values and time profiles of solar transmission and heat flux, the general trend of the area-specific energy gain e^{+}_{24h} and heat loss e^{-}_{24h} was captured in a rather similarly by both software tools. However, the accuracy of the simulation tools seems to be strongly related to the simulated configuration: when the shading was in use (and hence all the heat gain and loss reduced), both tools returned results that are within the experimental uncertainty range; conversely, when the DSF was simulated without the roller screen, the inaccuracy increased considerably. In wintertime, the two tools had rather similar performances. Their results were mostly within the experimental error range. In the summer, there was a clearer difference between the two tools, with IDA ICE performing better then EnergyPlus which constantly overestimated the heat gain, surpassing the maximum values of the experimental errors. In general, e^{-}_{24h} had much lower RMSE values (Table B3), but this is also due to the much less intense values for this variable when compared to e^{+}_{24h}. In periods with shading up, e^{+}_{24h} was often highly overestimated in both tools, and up to almost twice the measured values when the simulation was carried out with EnergyPlus in the summer season. This latter discrepancy can be inferred to be primarily due to the lack of the capacitive node in EnergyPlus's model. While such a simplification is usually of little relevance in traditional windows characterised by few and thin glass layers, the effects of multiple and rather thick glass layers usually seen in DSF systems are not properly replicated by the available model.

Errors were higher for heat gains, and especially during days with high solar radiation. Apart from the model simplifications (as described in the article main body), the high deviation of heat flux values was, to some extent, caused by procedures and practices adopted in the measurements. When solar radiation is present, the measurement devices for temperature and heat flux could heat up, affecting the measured values. For this reason, dedicated shielding solutions [54] were implemented in the experimental campaign [52]. However, these solutions determine a local change of the thermophysical behaviour near the measurement points. While for temperature sensors such an approach usually leads to rather accurate results, when applied to heat flux sensors, it can result in an excessive influence on the thermophysical phenomena under assessment.

References

[1] F. Pomponi, P.A.E. Piroozfar, R. Southall, P. Ashton, E.R.P. Farr, Energy performance of Double-Skin Façades in temperate climates: A systematic review and meta-analysis, Renew. Sustain. Energy Rev. 54 (2016) 1525–1536, https://doi.org/10.1016/j.rser.2015.10.075.
[2] E. Catto Lucchino, F. Goia, G. Lobaccaro, G. Chaudhary, Modelling of double skin facades in whole-building energy simulation tools: A review of current practices and possibilities for future developments, Build. Simul. 12 (2019) 3–27, https://doi.org/10.1007/s12273-019-0511-y.
[3] A. Gelesz, E. Catto Lucchino, F. Goia, A. Reith, V. Serra, Reliability And Sensitivity Of Building Performance Simulation Tools In Simulating Mechanically Ventilated Double Skin Facades, in: V. Corrado, A. Gasparella (Eds.), Proc. Build. Simul. 2019 16th Conf. IBPSA, Rome, 2019.
[4] A. De Gracia, A. Castell, L. Navarro, E. Oró, L.F. Cabeza, Numerical modelling of ventilated facades: a review, Renew. Sustain. Energy Rev. 22 (2013) 539–549, https://doi.org/10.1016/j.rser.2013.02.029.
[5] C. Underwood, F. Yik, Modelling Methods for Energy in Buildings, John Wiley & Sons, 2008.
[6] B. Bueno, M. Street, T. Pflug, C. Braesch, A co-simulation modelling approach for the assessment of a ventilated double-skin complex fenestration system coupled with a compact fan-coil unit, Energy Build. 151 (2017) 18–27, https://doi.org/10.1016/j.enbuild.2017.04.029.
[7] A. De Gracia, L. Navarro, A. Castell, L.F. Cabeza, Numerical study on the thermal performance of a ventilated facade with PCM, Appl. Therm. Eng. 61 (2013) 372–380, https://doi.org/10.1016/j.applthermaleng.2013.07.035.
[8] A. Hazem, M. Ameghchouche, C. Bougriou, A numerical analysis of the air ventilation management and assessment of the behavior of double skin facades, Energy Build. (2015), https://doi.org/10.1016/j.enbuild.2015.05.057.
[9] N. Safer, M. Woloszyn, J.J. Roux, Three-dimensional simulation with a CFD tool of the airflow phenomena in single floor double-skin facade equipped with a venetian blind, Sol. Energy. 79 (2005) 193–203, https://doi.org/10.1016/j.solener.2004.09.016.
[10] D. Angeli, A. Dama, Modelling natural ventilation in double skin facade, Energy Procedia. 78 (2015) 1537–1542, https://doi.org/10.1016/j.egypro.2015.11.186.
[11] A. Dama, D. Angeli, O. Kalyanova Larsen, Naturally ventilated double-skin façade in modeling and experiments, Energy Build. 114 (2017) 17–29.
[12] A. Gelesz, Á. Bognár, A. Reith, Effect of shading control on the energy savings of an adaptable ventilation mode double skin facade, in: 13th Conf. Adv. Build. Ski. 1-2 Oct. 2018, Bern, Switz. - Prog., 2018.
[13] A. Alberto, N.M.M. Ramos, R.M.S.F. Almeida, Parametric study of double-skin facades performance in mild climate countries, J. Build. Eng. 12 (2017) 87–98, https://doi.org/10.1016/j.jobe.2017.05.013.

[14] T. Saroglou, T. Theodosiou, B. Givoni, I.A. Meir, Studies on the optimum double-skin curtain wall design for high-rise buildings in the Mediterranean climate, Energy Build. 208 (2020), https://doi.org/10.1016/j.enbuild.2019.109641.
[15] R. Høseggen, B.J. Wachenfeldt, S.O. Hanssen, R. Hoseggen, B.J. Wachenfeldt, S. O. Hanssen, Building simulation as an assisting tool in decision making. Case study: With or without a double-skin facade?, Energy Build 40 (2008) 821–827, https://doi.org/10.1016/j.enbuild.2007.05.015.
[16] N. Hamza, Double versus single skin facades in hot arid areas, Energy Build. 40 (2008) 240–248, https://doi.org/10.1016/j.enbuild.2007.02.025.
[17] A.L.S. Chan, T.T. Chow, K.F. Fong, Z. Lin, Investigation on energy performance of double skin façade in Hong Kong, Energy Build. 41 (2009) 1135–1142, https://doi.org/10.1016/j.enbuild.2009.05.012.
[18] M. Ghadimi, H. Ghadamian, A.A. Hamidi, M. Shakouri, S. Ghahremanian, Numerical analysis and parametric study of the thermal behavior in multiple-skin façades, Energy Build. 67 (2013) 44–55.
[19] M.H. Tascon, Experimental and computational evaluation of thermal performance and overheating in double skin façades, (2008) 370.
[20] A. Malkawi, Y.K. Yi, A Method for Evaluating the Efficiency of Double-skin Facades, (n.d.) 1–8.
[21] H. Poirazis, Double skin façade glazed office buildings ; A parametric study for optimized energy and thermal comfort performance, 2 (2007) 797–801.
[22] M.H.H. Tascon, Experimental and Computational Evaluation of Thermal Performance and Overheating in Double Skin Facades, University of Nottingham, 2008.
[23] J. Joe, W. Choi, Y. Kwak, J.H. Huh, Optimal design of a multi-story double skin facade, Energy Build. 76 (2014) 143–150, https://doi.org/10.1016/j.enbuild.2014.03.002.
[24] D. Saelens, Energy performance assessment of single storey multiple-skin facades, 2002. https://doi.org/Ph. D. thesis.
[25] M.H. Tascon, CFD SIMULATION OF A DOUBLE SKIN FAÇADE MODEL, (2006).
[26] I. Pérez-Grande, J. Meseguer, G. Alonso, Influence of glass properties on the performance of double-glazed facades, Appl. Therm. Eng. 25 (2005) 3163–3175, https://doi.org/10.1016/j.applthermaleng.2005.04.004.
[27] E. Gratia, A. De Herde, The most efficient position of shading devices in a double-skin facade, Energy Build. 39 (2007) 364–373, https://doi.org/10.1016/j.enbuild.2006.09.001.
[28] H. Poirazis, Double skin façade cavities; a parametric study, in: Glas. Perform. Days 2007, 2007: pp. 271–275.
[29] A. Gelesz, A. Reith, Classification and re-evaluation of double-skin facades, Int. Rev. Appl. Sci. Eng. 2 (2011) 129–136, https://doi.org/10.1556/IRASE.2.2011.2.9.
[30] W.J. Stec, Symbiosis of double skin facade and indoor climate installation, Technische Universiteit Delft (2006).
[31] A.S. Anđelković, I. Mujan, S. Dakić, Experimental validation of a EnergyPlus model: Application of a multi-storey naturally ventilated double skin façade, Energy Build. 118 (2016) 27–36, https://doi.org/10.1016/j.enbuild.2016.02.045.
[32] N.M. Mateus, A. Pinto, G.C. Da Graça, Validation of EnergyPlus thermal simulation of a double skin naturally and mechanically ventilated test cell, Energy Build. 75 (2014) 511–522, https://doi.org/10.1016/j.enbuild.2014.02.043.
[33] D.W. Kim, C.S. Park, Difficulties and limitations in performance simulation of a double skin façade with EnergyPlus, Energy Build. 43 (2011) 3635–3645, https://doi.org/10.1016/j.enbuild.2011.09.038.
[34] A. Gelesz, Sensitivity of exhaust-air façade performance prediction to modelling approaches in IDA ICE, Int. Rev. Appl. Sci. Eng. 10 (2019) 241–252.
[35] A. Gelesz, A. Reith, Climate-based performance evaluation of double skin facades by building energy modelling in Central Europe, in, Energy Procedia (2015) 555–560, https://doi.org/10.1016/j.egypro.2015.11.735.
[36] O. Kalyanova, P. Heiselberg, Empirical Validation of Building Simulation Software, Modeling of Double Facades (2008).
[37] M.H. Kristensen, S. Petersen, Choosing the appropriate sensitivity analysis method for building energy model-based investigations, Energy Build. 130 (2016) 166–176, https://doi.org/10.1016/j.enbuild.2016.08.038.
[38] J.C. Lam, S.C.M. Hui, Sensitivity analysis of energy performance of office buildings, Build. Environ. 31 (1996) 27–39, https://doi.org/10.1016/0360-1323(95)00031-3.
[39] K. Petr, J. Filip, K. Karel, H. Jan, Technique of uncertainty and sensitivity analysis for sustainable building energy systems performance calculations, IBPSA 2007 - Int, Build. Perform. Simul. Assoc. 2007 (2007) 629–636.
[40] W. Tian, A review of sensitivity analysis methods in building energy analysis, Renew. Sustain. Energy Rev. 20 (2013) 411–419, https://doi.org/10.1016/j.rser.2012.12.014.
[41] C.J. Hopfe, J.L.M. Hensen, Uncertainty analysis in building performance simulation for design support, Energy Build. 43 (2011) 2798–2805, https://doi.org/10.1016/j.enbuild.2011.06.034.
[42] D.M. Hamby, A Review of Techniques for Parameter Sensitivity Analysis of Environmental Models, Environ. Monit. Assess. 32 (1994) 135–154.
[43] S. Petersen, M.H. Kristensen, M.D. Knudsen, Prerequisites for reliable sensitivity analysis of a high fidelity building energy model, Energy Build. 183 (2019) 1–16, https://doi.org/10.1016/j.enbuild.2018.10.035.
[44] K. Menberg, Y. Heo, R. Choudhary, Sensitivity analysis methods for building energy models: Comparing computational costs and extractable information, Energy Build. 133 (2016) 433–445, https://doi.org/10.1016/j.enbuild.2016.10.005.
[45] C. Spitz, L. Mora, E. Wurtz, A. Jay, Practical application of uncertainty analysis and sensitivity analysis on an experimental house, Energy Build. 55 (2012) 459–470, https://doi.org/10.1016/j.enbuild.2012.08.013.
[46] G. Cattarin, L. Pagliano, F. Causone, A. Kindinis, F. Goia, S. Carlucci, C. Schlemminger, Empirical validation and local sensitivity analysis of a lumped-parameter thermal model of an outdoor test cell, Build. Environ. (2018), https://doi.org/10.1016/j.buildenv.2017.12.029.
[47] Equa AB, EQUA Simulation AB User Manual IDA Indoor Climate and Energy, (2013).
[48] International Organisation for Standardisation, ISO 15099:2003 Thermal performance of windows, doors and shading devices - detailed calculations, 2003.
[49] U.S. Department of Energy, Engineering Reference 8.8, (2017).
[50] Equa AB, IDA – Indoor Climate and Energy ver 3.0 NMF-model documentation, (n.d.).
[51] VDI Heat Atlas, 2010. https://doi.org/10.1007/978-3-540-77877-6.
[52] F. Goia, L. Bianco, M. Perino, V. Serra, Energy performance assessment of and advanced integrated facade through experimental data analysis, Energy Procedia. 48 (2014) 1262–1271, https://doi.org/10.1016/j.egypro.2014.02.143.
[53] F. Goia, V. Serra, Analysis of a non-calorimetric method for assessment of in-situ thermal transmittance and solar factor of glazed systems, Sol. Energy. (2018), https://doi.org/10.1016/j.solener.2018.03.058.
[54] O. Kalyanova, F. Zanghirella, P. Heiselberg, M. Perino, R. Jensen, Measuring air temperature in glazed ventilated façades in the presence of direct solar irradiation, in: Proc. Roomvent 2007 - 10th 7th Int. Conf. Air Distrib. Rooms, Helsinki, 2007: pp. 209–218.

4 Validation and inter-software comparison of a mechanically ventilated single-story DSF

P3 *E. Catto Lucchino, A. Gelesz, K. Skeie, G. Gennaro, A. Reith, V. Serra, F. Goia. Modelling double skin façades (DSFs) in whole-building energy simulation tools: validation and inter-software comparison of a mechanically ventilated single-story DSF. Building and Environment 199 (2021), 107906. https://doi.org/10.1016/j.buildenv.2021.107906*

Double skin façades (DSFs) have been proposed as responsive building systems to improve the building envelope's performance. Reliable simulation of DSF performance is a prerequisite to support the design and implementation of these systems in real buildings. Building energy simulation (BES) tools are commonly used by practitioners to predict the whole building energy performance, but the simulation of the thermophysical behaviour of DSFs may be challenging when carried out through BES tools. Using an exhaust-air façade case study, we analyse and assess the reliability of four popular BES tools when these are used to simulate a DSF, either through available in-built models or through custom-built representations based on zonal models. We carry out this study by comparing numerical simulations and experimental data for a series of significant thermophysical quantities, and we reflect on the performance and limitations of the different tools. The results show that no tool is performs significantly better than the others, but some tools offer better predictions when the focus is placed on certain thermophysical quantities, while others should be chosen if the focus is on different ones. After comparing the different models' limitations and challenges, we conclude that BES tools can simulate the performance of DSF systems over long periods. However, their use alone is not recommended when the simulation's scope is to replicate and study short-term phenomena and dynamic aspects, such as sizing the building's HVAC system.

Building and Environment 199 (2021) 107906

Contents lists available at ScienceDirect

Building and Environment

journal homepage: www.elsevier.com/locate/buildenv

Modelling double skin façades (DSFs) in whole-building energy simulation tools: Validation and inter-software comparison of a mechanically ventilated single-story DSF

Elena Catto Lucchino [a], Adrienn Gelesz [b,c], Kristian Skeie [a], Giovanni Gennaro [d,e], András Reith [b,f], Valentina Serra [d], Francesco Goia [a,*]

[a] Department of Architecture and Technology, Norwegian University of Science and Technology, NTNU, Trondheim, Norway
[b] Advanced Building and Urban Design Ltd, Budapest, Hungary
[c] Faculty of Architecture, Budapest University of Technology and Economics, Budapest, Hungary
[d] Department of Energy, Politecnico di Torino, Torino, Italy
[e] Institute for Renewable Energy, EURAC Research, Bolzano, Italy
[f] Faculty of Engineering and Information Technology, University of Pécs, Pécs, Hungary

ARTICLE INFO

Keywords:
Inter-software comparison
Model validation
EnergyPlus
TRNSYS
IDA ICE
IES VE

ABSTRACT

Double skin façades (DSFs) have been proposed as responsive building systems to improve the building envelope's performance. Reliable simulation of DSF performance is a prerequisite to support the design and implementation of these systems in real buildings. Building energy simulation (BES) tools are commonly used by practitioners to predict the whole building energy performance, but the simulation of the thermophysical behaviour of DSFs may be challenging when carried out through BES tools. Using an exhaust-air façade case study, we analyse and assess the reliability of four popular BES tools when these are used to simulate a DSF, either through available in-built models or through custom-built representations based on zonal models. We carry out this study by comparing numerical simulations and experimental data for a series of significant thermophysical quantities, and we reflect on the performance and limitations of the different tools. The results show that no tool is outstandingly better performing over the others, but some tools offer better predictions when the focus is placed on certain thermophysical quantities, while others should be chosen if the focus is on different ones. After comparing the different models' limitations and challenges, we conclude that BES tools can simulate the performance of DSF systems over long periods. However, their use alone is not recommended when the simulation's scope is to replicate and study short-term phenomena and dynamic aspects, such as sizing the building's HVAC system.

1. Introduction

Double skin façades (DSFs) are a typology of solar façades which are often adopted to reduce energy use [1] and to provide better thermal and visual comfort conditions compared to traditional single-skin façades [2]. Because of the more complicated behaviour than conventional building envelope solutions, the design and optimisation of a DSF cannot be based on rules-of-thumb or simple performance parameters. However, they should be based on results derived from dynamic energy performance simulation. A detailed simulation of the thermal, fluid mechanics and optical behaviour of a DSF can be obtained using different approaches, such as on-purpose built models [3–5] or dedicated CFD simulations [6,7]. However, the simulation of the DSF alone, without the integration into the building. limits to a great extent the possibility to study the DSF's performance under real operation. Building Energy Software (BES) tools are, on the other side, meant for modelling an entire building and predicting the whole building energy performance, and when a DSF is modelled in a BES tool, it is, therefore, possible to link the DSF's performance with that of the entire building. The coupled simulation of the whole building and the specific building components is essential for correctly assessing the overall energy and comfort performance. It is the only way to replicate the complex interaction between airflow in the façade, the HVAC system, and the building energy management system. There are indeed a series of studies where different BES tools have been used to evaluate the behaviour of DSFs

* Corresponding author.
E-mail address: francesco.goia@ntnu.no (F. Goia).

https://doi.org/10.1016/j.buildenv.2021.107906
Received 2 November 2020; Received in revised form 14 April 2021; Accepted 15 April 2021
Available online 23 April 2021

Nomenclature

ACH	ventilation rate (air changes per hour, 1/h)
ΔT	temperature difference (K)
g	solar factor (−)
h_c	convective heat transfer coefficient (W/(m^{2}K))
H	height of the window (m)
k	thermal conductivity of the fluid (W/(mK))
L	cavity width (m)
λ	thermal conductivity of air (W/mK)
M_i	measured value at one point
n	total number of measurements
Nu	Nusselt number (−)
P_i	simulated predicted value
Pr	Prandtl number (−)
Ra_H	Rayleigh number based on the height (−)
Re	Reynolds number (−)
ρ_{in}	glazing solar reflectance, inner face (−)
ρ_{out}	glazing solar reflectance, outer face (−)
τ	glazing solar transmittance (−)
U	thermal transmittance (W/(m^{2}K))
$\dot{V}$	airflow rate (m^3/s)
v	velocity (m/s)
$\bar{y}$	mean value of the measured values

[8–13]. BES tools have not been developed with the precise requirement to simulate an advanced building envelope system such as a DSF. Only a few BES tools include dedicated modules for DSFs' simulation, while it is more common that the modelling of these systems might require some workarounds or the use of relatively advanced simulation strategies [14].

The main aim of the research activity presented in this paper is to evaluate the capabilities and accuracy of some of the most commonly adopted BES tools in modelling a relatively common mechanically ventilated DSF type, called *climate façade*. In these façades, which can be single-storey or multiple-storey high, the air typically enters the façade cavity from the indoor environment in the lower region of the façade and leaves the cavity at the upper part of the façade extracted through a duct as part of the HVAC system [15]. This research's secondary aim is to highlight how current shortcomings in BES software programs regarding modelling and simulation of DSF systems should be addressed to improve the simulation tools' reliability.

Robust and comprehensive comparison and experimental validation of building performance simulation tools are common practices and have been carried out for commercially available BES tools. Often, standardised geometries and configurations, such as the IEA Building Energy Simulation Test and Diagnostic Method (IEA BESTEST) or the ANSI/ASHRAE Standard 140, are used to validate and verify different functions of BES tools, ranging from building systems and wall assemblies (e.g. Refs. [16,17]) to environmental systems (e.g. Refs. [18,19]). These procedures' objectives are to increase confidence in using BES tools and improve simulation engines' current generation. However, dedicated validation and verification activities targeting such tools' reliability in replicating DSF systems' performance are rare, even though DSFs are building envelope systems nowadays rather largely employed and frequently designed through BES tools [20]. More than ten years have passed since the only major inter-comparison of software tools [21] in modelling DSFs was performed. In that study, the empirical validation of a naturally ventilated DSF, when operated as an outdoor air curtain and when in "thermal buffer", was presented, while mechanically ventilated configurations were not addressed. The results showed that none of the models found in the software tools at that time produced consistent results if compared to the experimental data, especially in periods of higher solar intensity.

In this paper, we extend the preliminary work on the experimental validation of an exhaust-air façade model through comparison with experimental data from a test cell experiment [22], assessing and comparing the performance of different modelling approaches and models implemented in four different BES tools: EnergyPlus, IDA Indoor Climate and Energy (IDA ICE), IES Virtual Environment (IES VE), and TRNSYS. EnergyPlus [23] is a whole building energy simulation program used to model energy consumption—heating, cooling, ventilation, lighting and plug and process loads—and water use in buildings. It is a freeware software tool with a publicly available source code, which the user can modify to create an ad-hoc version to add simulation functions – which is not a trivial task. When it comes to possibilities to model DSF systems, Energy Plus has an in-built model called "Airflow Window", which has been used in a few studies for modelling a DSF [22,24]. Most of the studies adopt instead the so-called zonal approach [13,25–28], which also allows naturally ventilated cavities to be modelled (a possibility not allowed by the "Airflow Window" model). IDA ICE [29] is a licensed equation-based multi-zone simulation building program whose library is written in Neutral Model Format (NMF), a common format of model expression that allows users to interconnect different modules and develop sub-routines directly in the programming interface. The structure of IDA ICE allows easier on-demand modifications of the different models already implemented. IDA ICE, as EnergyPlus, includes an in-built component specifically developed to model DSFs called "Ventilated Window" [22]. Adopting multiple zone modelling based on the typical stacked thermal zones approach is always possible and seen in the literature, especially when modelling multi-storeys [30]. IES VE Virtual Environment [31] is a commercial software tool whose code is not accessible, limiting its application to models already included in the software's distributed version. Few examples of DSFs modelled as stacked thermal zones are available in the literature [10,32]. TRNSYS [33] is a commercial simulation code initially developed for solar thermal systems, which offers the possibility to model and simulate multi-zone buildings through a combined thermal and airflow network model. The use of this tool among researchers is well established, as it also allows the development of dedicated sub-routines in a relatively easy way. Multiple studies on DSFs are available in the literature, where the majority of them has covered naturally ventilated façades [34–41]. In a recent release of Trnsys 18, an inbuilt model called "Complex Fenestration System" was made available. Besides implementing an optical model based on the so-called "Bidirectional Scattering Distribution Function" (BSDF) to provide high-quality daylighting simulation for fenestrations equipped with slat systems or honeycomb structures, this component allows modelling mechanically ventilated gaps [42].

The investigation results of this study are meant for both the research and the practitioners' community and for building performance software developers, as they both unveil the reliability and challenges of modelling and simulating mechanically ventilated DSFs with current BES tools.

The article is organised as follows. In Section 2 – Methodology, we present the research activity's overall objectives, together with the different methods employed: ranging from the presentation of the case-study façade to the modelling implementation in BES tools, from experimental data collection and processing to the validation procedure. For the sake of readability, more details on the data for validation and the DSF's implementation for each BES tool are reported in Appendix A and Appendix B, respectively. In Section 3 – Results, we provide an extensive report of the validation and performance assessment outcomes for the different tools, based on several validation variables and periods/

conditions. We analyse the results in terms of individual thermophysical quantities and software performance under different boundary conditions. In Section 4 – Discussions, we reflect on our analysis results and highlight current limitations in the different tools that lead to inaccuracy in the performance prediction, while the conclusive summary of the paper is presented in Section 5 – Conclusions.

2. Methodology

The methodological approach to the research has been broken down in a series of steps that are described by the following objectives: i) to model, with different BES tools, a case study façade that can be representative of a relatively large number of mechanically ventilated façades; ii) to process data from a previous experimental analysis on the same type of DSF and prepare them for the use in the validation process, identifying a series of thermophysical quantities available in both the experimental dataset and the simulation outputs, and identifying a series of suitable periods characterised by different boundary conditions and operational modes; iii) to run the different BES tools' models for the DSF for a relatively long-time simulation run (two weeks for each period), using as input data the boundary conditions registered during the experiments; iv) to establish a suitable set of methods and performance metrics to compare the simulated and measured values, for the selected thermophysical quantities, through both a qualitative and quantitative approach; v) to analyse and quantify the performance of each simulation tool against the experimental data; vi) to understand the possible reasons for discrepancies between different software tools and between numerical and experimental data. The objectives i to iv are detailed in the next sections 2.1, 2.2, 2.3, and 2.4, respectively, while the last two objectives are presented in Section 3 and Section 4, respectively.

2.1. Numerical modelling in four BES tools

2.1.1. Case study façade

The DSF used in this investigation is a mechanically ventilated, single-story high DSF operated as a so-called *climate façade*. In climate façades, the air from the room enters the cavity at the bottom, flows through the cavity and is extracted at the top and directed to the HVAC system's air handling unit as a part of the ventilation network of the building. Therefore, the flow rate is usually linked to fresh air supply requirements rather than optimised to achieve a specific performance when it comes to the façade. A climate façade can guarantee a stable glass surface temperature (thus reducing the risk of thermal discomfort), remove a large share of the (potential) cooling loads due to the solar gains through the ventilation air, especially when a shading device is installed in the cavity, and reduce to a great extent the transmission heat loss due to the double glazed layer. Climate façades are among the most popular DSFs, and single-storey climate façades are solutions that assure a (relatively) simple construction, safety, and simpler operation – compared to multi-storey double-skin facades.

The specific façade in this study, as schematised in Fig. 1, was modelled to represent in the DSF that was experimentally tested (Fig. 3): dimensions 1.60 m (width) and 3.40 m (height), and a ventilated cavity of 0.24 m (depth), with a volumetric airflow of 20 m^3/h and hosting a highly reflective roller blind as a shading device, located 0.07 m from the external skin. The airflow enters the ventilated cavity from small openings in the frame at the bottom of the façade and a fan extracts the air from the cavity top through a duct. The shading installed in the cavity is placed at 7 cm from the external glazing, and while the airflow is not constrained in one of the two half-cavities created by the roller blind, there is no particular measure to assure that the airflow is evenly distributed between the two sides of the shading device.

The external skin of the DSF was made of an insulated glazed unit with two glass panes with a selective coating, and the internal skin was made of a single, clear glass pane. Most of the façades' thermal and optical properties were available from technical documentation. Simultaneously, a few data (related to the shading device) that was not wholly documented was assumed based on our experience and realistic

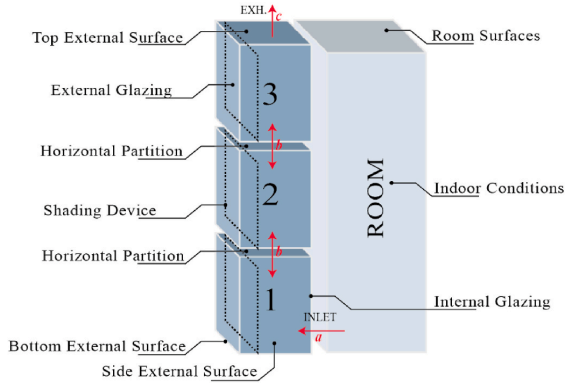

Fig. 2. Zonal modelling of the DSF.

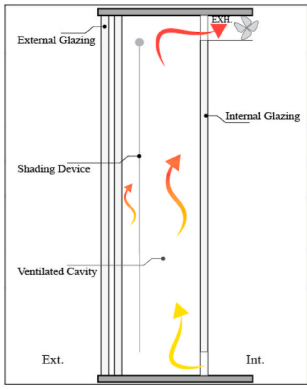

Layers from exterior to interior		Thickness [mm]	τ_{sol} [-]	ρ_{out} [-]	ρ_{in} [-]	U * [W/m²K]	g* [-]
External glazing	Laminated glass - selective coating, pos.2, 10.10.4	20	0.32	0.31	0.45	1.36	0.38
	Air	16					
	Clear glass	10					
Shading Device	High reflectance roller blind	1	0.10	0.80	0.80	-	-
Ventilated Cavity	Air	240	-	-	-	-	-
Internal glazing	Laminated clear glass 5.5.4	10	0.7	0.07	0.07	5.59	0.79

**At reference conditions defined by ISO 15099:2003.*

Fig. 1. Schematic section and glazing configuration of the DSF
*At reference conditions defined by ISO 15099:2003.

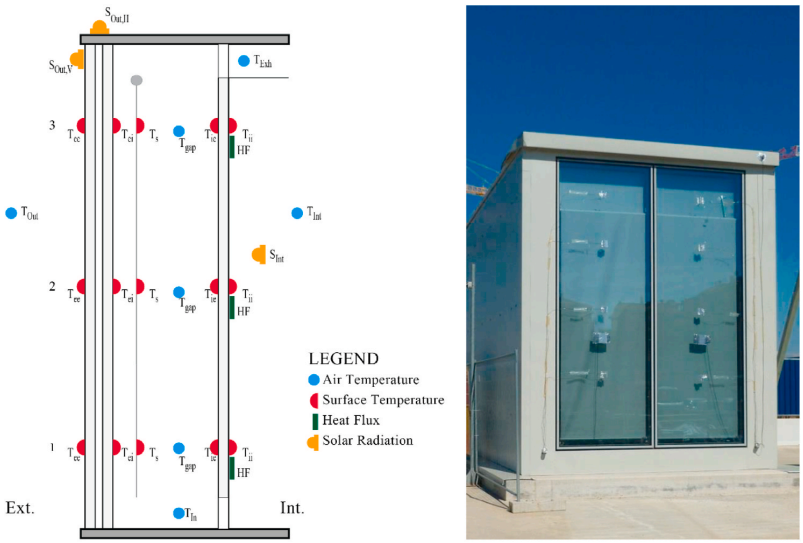

Fig. 3. Sensor a) scheme and b) instalment on the experiment facility.

hypothesis based on similar designs. The global solar optical and thermal properties of the glazing and shading have been calculated, based on the available information, using LBNL Window 7.7 and Optics 6 using the IGDB v29, and are reported in Fig. 1.

The geometrical, thermal, optical, and operational (airflow rate) features of the DSF have been implemented in different BES tools, according to the possibilities given by each software environment, as described in the next section.

2.2. DSF model implementation in BES tools

This study's primary goal is to compare the different modelling approaches and embedded modules available in some BES tools and evaluate their abilities to replicate the thermophysical and optical behaviour of mechanically ventilated DSFs. For this reason, the entire modelling and validation task focused on the case-study façade and the façade-related quantities (e.g. the thermophysical quantities linked to the façade alone, such as the air gap temperature, the surface temperatures, heat flux exchanged at the façade interface) and not on the environment and environment-related quantities (indoor air temperature, or energy for heating or cooling of the building behind the façade). The façade was modelled as belonging to one of the surfaces of a simple box-shaped thermal zone, whose constructional features—except for the DSF—were not of interest in this study. The other surfaces of the box's envelope were modelled as non-exposed surfaces (nor sun, nor wind exposure). Implementing the input data in the different simulation environments might require different strategies or methods, but we paid attention to be sure that, regardless of the actual way to implement certain information, the core of the modelling was kept identical in all the tools.

However, some differences can arise from each tool's processor engines outside the set of equations that describe the façade's optical and thermophysical behaviour. For example, the input data read from an hourly value and used to run a sub-hourly simulation, and then reported as hourly output. Moreover, each tool has different routines to treat solar data. During the daytime, the way solar radiation is treated in the different models may generate inaccuracy in the predictions that cannot be accounted to the modelling approach or the physical-mathematical description of the DSF, but rather to the overall simulation environment.

As described in full details in Appendix B, different approaches were used in the four selected tools to model the case-study façade. In general, it was possible to model the DSF either through available in-built modules (in EnergyPlus, IDA ICE, and Trnsys) or using the so-called zonal approach. In the latter modelling strategy, the cavity is divided into several thermal zones stacked one over the other. The zones are connected through an airflow network representation that allows one to describe the airflow through the different zones. Several authors explored the role of the number of stacked thermal zones on the quality and reliability of the simulation [9,43], but there is no consensus nor a standardised approach when it comes to this setting, which usually ranges (when referred to single-storey DSFs) from a minimum of one to a maximum of six [20]. A dedicated comparative analysis on models with one to six zones stacked upon each other showed that, in the case of a mechanically ventilated exhaust-air façade, an increase in the zones' number does not significantly affect the results [44]. For these reasons, we decided to model the DSF, when the zonal approach was used, with three stacked thermal zones (Fig. 2), which also corresponded to the experimental setup adopted for the measurement campaign that provided data for the validation – sensors were installed at three different levels of the façade's cavity, as explained more in details in Section 2.3. Table 1 and Table 2 describe the thermal and the airflow network models in the different BES tools.

We used our best knowledge as modellers of the different simulation environments and as building physicists about the thermophysical behaviour of the case study façade to provide the four BES tools with the same level of information about the DSF. We consciously decided not to calibrate the models on available experimental data. This approach is motivated by the fact that only through un-calibrated models it is possible to assess the simulation performance of the different tools during a hypothetical design phase – when experimental data on the solution under design are not available. Furthermore, only with un-calibrated models the reasons for mispredictions can potentially be unveiled. The choice to avoid any calibration to assess the "true" performance of the different BES might lead to inaccuracy in the simulation workflow due to a user error in place of a program error, as a calibration process can somehow "fix" a user error. In order to reduce the risk of a

Table 1
Thermal model of the DSF in the zonal approach.

	EnergyPlus	TRNSYS	IDA ICE	IES-VE
Horizontal Partition	Infrared material	Virtual surface	Adiabatic surface[a]	Hole
Top/Side/ Bottom External Surfaces	Adiabatic surface	Adiabatic surface	Adiabatic surface	Adiabatic surface
Room surfaces	Highly conductive surface with temperature on the other side assigned by a schedule	Temperature assigned by a schedule	Highly conductive surface with temperature on the other side assigned by a schedule	Highly conductive surface with temperature on the other side assigned by a schedule
Shading Device	Internal - Shade	Internal – Shading	Internal - Shade	Internal - Blind
Temperature Set-point	Ideal load	Ideal load	HVAC	HVAC

[a] See Appendix B, Modelling of DSF in IDA ICE.

Table 2
Airflow network connection in the zonal approach of the DSF.

		EnergyPlus	TRNSYS	IDA ICE	IES VE
a)	**Inlet**	Leak	Circular duct	Leak	Simple Opening
b)	**Horizontal Partition**	Horizontal Opening	Horizontal Opening	Horizontal Opening	Horizontal Opening
c)	**Exhaust**	Exhaust Fan	Circular duct	Exhaust Fan	Exhaust Fan

user error occurring, all the models implemented in the different tools have been revised multiple times by different modellers, thus assuring a redundant and independent check of the models' quality. Moreover, simulations have been run for more extended periods, using the typical meteorological year, and the simulation outputs from different tools screened in search of significant differences that are usually proof of user errors. However, as we know that user error can in practice be very difficult to avoid completely, we made available on an open-access repository the models used for this simulation study to allow easy replication and, potentially, a quality check of our results by the scientific community – see Appendix B.

We used, as far as possible, homogenous settings for the different general settings of the four simulation engines, and we did not implement particular changes in the different models that might derive by knowing in advance the performance of the façade used for this study. For example, we did not implement modifications in the algorithms for the calculation of the convective heat transfer coefficient in the cavity (which is a factor that might have an impact on the results of the simulation), and we relied on the implemented solutions available in the four simulation tools, selecting (where possible) the best option among those available. In some of the tools, the calculation method is an algorithm that chooses among different correlations as a function of the flow regime (Energy Plus) or the maximum value between two different correlations (IDA ICE); in some other, the choice that the user can make is only between using a constant value or a specific function implemented in the tool (IES-VE and Trnsys). The calculation methods to derive the convective coefficient for the internal (indoor) and external (outdoor) surfaces of the room have been set as displayed in Table 3. In the zonal approach, the same correlations are adopted for the surfaces of the DSF; when using the in-built models, specific correlations within those models are adopted. The convective correlations adopted for the ventilated cavity's vertical surfaces, as implemented in the different tools, are listed in Table 4.

Table 3
Calculation methods for establishing the exterior (outdoor) and interior (indoor) convective surface coefficients.

	External Surfaces	Internal Surfaces
EnergyPlus	*SimpleCombined* [23]	*AdaptiveConvectionAlgorithm* [23]
IDA ICE	*Clarks* [45]	max*(Table, CDA)* [46]
IES VE	*McAdams* [47]	*Alamdari & Hammond* [48]
TRNSYS	*Constant Value* [49]	*Constant Value*[a] [49]

[a] For the surfaces of the cavity, the Internal Calculation Method is selected (see Table 4).

2.3. Experimental data collection and validation of data processing

Two modules of the case-study DSF were continuously monitored for around two years using an outdoor test-cell facility (that replicated a full-scale office room) located in a temperate sub-continental climate location in northern Italy (45° N latitude). The DSF was installed on the 15° southwest exposed façade.

The room's indoor air temperature was set at 20 °C in winter and 26 °C in summer to minimise inaccuracies due to transient states in the indoor environment and ensure stable testing conditions. The test-cell and the DSF modules (Fig. 3) were equipped with a wide range of sensors (thermocouples for surface and air temperature measurements, heat flux meter sensors, pyranometers both inside and outside) to record the thermophysical and optical processes occurring in the DSF. Temperature and heat flux sensors were placed at three height levels, both inside and outside of the façade, measuring: the surface temperature of the interior glazing and the exterior glazing (both towards the indoor and the cavity); the surface temperature of the roller screen (towards the indoor glazing); the temperature of the air in the cavity behind the shading (when present); the inlet and outlet cavity-air temperature; the frame temperature; the heat flux exchanged at the indoor surface of the glazing. Thermocouples and heat flux meters directly exposed to solar radiation were shielded with highly reflecting aluminium foils to reduce solar irradiance's influence on the measured physical quantity, following best practices established in the literature [54]. Furthermore, the outdoor solar irradiance was measured both on the horizontal and vertical plane, employing two pyranometers. The solar irradiance transmitted through the DSF was measured, on the vertical plane, with an additional pyranometer installed right next to the inner skin of the DSF. The test-cell was also equipped with contact sensors to record the surface temperature values for all the cell's surface, as well as with sensors for indoor air temperature measurements.

The measurement accuracies for the entire measurement chain, after calibration and verification, were: ±0.3 °C, ±5% and ±5%, for thermocouples, heat flux meters, and pyranometers, respectively. More detailed information on the experimental campaign can be found in Refs. [22,55].

From the entire dataset of nearly two years of measurements, we selected for this validation study a series of weeks that could represent different operational conditions, different periods of the year, and different boundary conditions. DSF was operated with either the shading device deployed or retracted, with considerably different performance. For a validation purpose, it is interesting to investigate the performance at least in winter and in summer, and different conditions should be included in each of the seasons (sunny days and cloudy days, warm days and cold days) to test a broad spectrum of boundary conditions. Based on these considerations, four periods of two weeks each were selected, characterised by different weather conditions, so that two operational modes (with and without the shading device) can be combined with the two seasons. For each period, the first week was only used for modelling warm-up, while the second week was used for the actual validation process. Fig. 4 shows the main boundary conditions (outdoor and indoor air temperature and global irradiance on the horizontal plane) for the second week of each of the four periods. Due to limitations in the

Table 4
Convective heat transfer correlations adopted for the ventilated cavity's vertical surfaces.

Software	Calculation Method	Reference	Convective heat transfer coefficient model
EnergyPlus	Adaptive Convection Algorithm - Windows	ISO 15099 [50]	$h_{c,nat} = Nu*\frac{\lambda}{H}$ $Nu = f(Ra_H)$
		Goldstein -Novoselac [51]	$h_{c,forced} = 0.103\left(\frac{\dot{V}}{L}\right)^{0.8}$
EnergyPlus AW	Airflow window model	ISO 15099 [50]	$h_c = 2h_{c,\ enclosed\ gap} + 4v$
IDA ICE	max (Table, CDA)	$h_c = \max(h_{c,table}; h_{c,CDA})$	
		Table (U_vert) [52]	ΔT [K] $h_{c,table}$ [W/m2K] −1020 0.58 0 0.58 0.5 1.63 2 2.44 7 3.60 30 5.70 50 6.40 1020 10
		CDA – Ceiling Diffuser Algorithm [46]	$h_{c,CDA} = 1.208$*red $+ 1.012$ * $\max(0.0, ACH)^{0.604}$ $red = min(5.0, ACH)/5.0$ red – reduction in case of ACH<5
IDA ICE VW	Ventilated window model	$h_c = \max(h_{c,forced}; h_{c,nat})$	
		DNCA - Detailed Natural Convection Algorithm [46]	$h_{c,nat} = \frac{1,81*\lvert\Delta T\rvert^{1/3}}{1,382}$
		VDI Heat Atlas [53]	$h_{c,forced} = Nu*\frac{\lambda}{H}$ $Nu_l = 0.664*\sqrt{Re}*Pr^{\frac{1}{3}}$ $Nu_t = \frac{0.037*Re^{0.8}*Pr}{1+2.443*Re^{-0.1}*\left(Pr^{\frac{2}{3}}-1\right)}$
IES VE	Alamdari & Hammond	[48]	$h_c = \left(\left(1.5\left(\frac{\lvert\Delta T\rvert}{H}\right)^{\frac{1}{4}}\right)^6 + \left(1.23\lvert\Delta T\rvert^{\frac{1}{3}}\right)^6\right)^{\frac{1}{6}}$
TRNSYS	Internal Calculation Method	[33]	$h_c = 1.5*(\Delta T)^{0.25}$
TRNSYS CFS	Complex Fenestration System (CFS)	ISO 15099 [50]	$h_c = 2h_{c,\ enclosed\ gap} + 4v$

experimental monitoring system, wind data was not recorded; hence the effect of the wind condition on the performance of the DSF is not accounted for. However, due to the location of the measurement site and its surroundings, and the type of tested DSF (which does not exchange air mass with the outdoor environment), it is possible to assess that the impact of such missing information is negligible compared to other aspects in the numerical modelling procedure.

2.4. Simulation runs and output processing

The experimental data were used to construct customised weather data files (according to the formats required by the different simulation environments) for the periods to be simulated. The measurements available to create the customised weather data files included the global solar irradiance data on the horizontal plane and the outdoor air temperature. The required weather data are, in addition to the outdoor dry bulb temperature, the direct beam and diffuse horizontal solar irradiance, the cloud cover fraction of the sky, and horizontal infrared radiation intensity from the sky. These quantities related to the solar and infra-red radiative heat exchange have been numerically derived for each time step (hourly) from the experimental data available using the following correlations: Reindl et al. [56] and Perez et al. [57] for the calculation of the beam and diffuse component of the solar radiation; Kasten et al. [58] for the cloudiness factor and Martin et al. [59] for the sky temperature used in the calculation of the infrared radiation from the sky. Sensitivity analysis has been carried out to verify that the uncertainty in the decomposition of the solar irradiance in the direct and diffuse components (which were not directly measured) has little impact on the validation process results. Furthermore, since the measurement of the global irradiance on the vertical (façade) plane was available from the experimental dataset, the goodness of the decomposition procedure adopted was verified by comparing the numerically calculated global solar irradiance on the vertical (façade) plane with the measured value for the same quantity.

The measured indoor air temperature and the test cell's opaque surfaces temperatures were adopted in the simulation to assure identical boundary conditions in all the tools and identical to the experiments. This equivalency was achieved by giving each surface, and the indoor air node (measured) temperature values through schedules created using the available experimental data. This strategy allowed us to replicate the entire set of indoor and outdoor boundary conditions surrounding the DSF. In this way, the validation procedure can focus on the DSF models' performance only because all the other possible uncertainties linked to the different processes in the simulation tools linked to the environments surrounding the DSF were eliminated.

In each tool, the simulation time-step was set to 10 min, and then the numerical outputs were extracted, with a time-step of 1 h, so that the following (simulated) physical quantities could be obtained (See Appendix A, Fig. A.1 and Fig. A.2):

- the (average) air temperature of the cavity [°C];
- the (average) surface temperature of the interior surface of the interior glazing [°C];
- the (average) specific heat flux (i.e. the sum of the convective heat flux exchanged between the surface of the inner skin and the indoor air and the radiative heat flux in the longwave infrared region exchanged between the surface of the inner skin and the surfaces of the room behind the DSF) [W/m^2];
- the transmitted solar irradiance through the entire DSF structure, measured on the vertical plane [W/m^2].

More in details, depending on the exact modelling approach

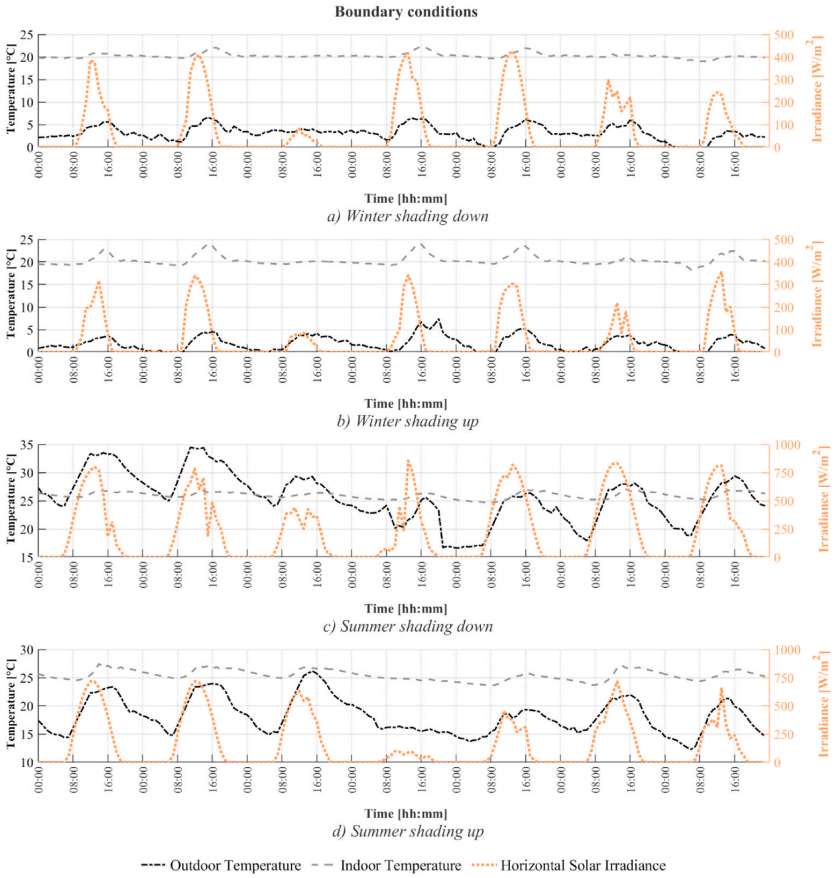

Fig. 4. Time profile of the outdoor and indoor air temperature [°C] and horizontal global solar irradiance [W/m^2] for the four modelling periods: a) Winter with shading down, b) Winter with shading up, c) Summer with shading down and d) Summer with shading up.

adopted, more values for the temperature, the heat flux, and the transmitted irradiance can be obtained – this is typical, for example, for the models with stacked zones, while in the case of models with an in-built component, only one value per façade element is calculated. In order to obtain homogenous information regardless of the adopted modelling approach, area-weighted averages were calculated when more than one value for the same physical quantities was obtained from the simulation.

Furthermore, not all the BES tools allow one to obtain the entire set of quantities used in this validation study: IES VE does not provide the heat flux exchanged by the inner skin with the indoor environment. In some other cases, not all the desired variables are directly available among the output from the software: in the zonal approach in EnergyPlus and TRNSYS, the transmitted solar irradiance can only be obtained by combining different outputs; in the "*Airflow Window*" of EnergyPlus, it is not possible to directly obtain the temperature of the air in the ventilated cavity. In all the cases where the desired quantities could only be derived through intermediate calculations or combinations of different outputs, dedicated data postprocessing was carried out to obtain these parameters.

2.5. Validation procedure

The validation of the different software tools was carried out through combined qualitative and quantitative analyses. This approach provides the possibility to quantify the performance and deepen the understanding of the different observed behaviours. Time profiles of the thermophysical quantities identified in the previous section were useful to support the qualitative (and explanatory) assessment in combination with scatter-plot and error distribution box-plot representations. The quantification of the mismatch between the experimental data and the numerical data was assessed through the calculation of two commonly used statistical indicators, as described in the following equations: the Root Mean Square Error (RMSE) (Eq. (1)) and the Mean Bias Error MBE) (Eq. (3)). The normalised values of these indicators were calculated for evaluating the fitness of the models in predicting the total energy crossing the DSF in one week: Coefficient of Variation of the Root Mean Square Error [CV(RMSE)] (Eq. (2)) and the Normalised Mean Bias Error (NMBE) (Eq. (4)).

$$RMSE = \sqrt{\frac{\sum_{i=1}^{n}(P_i - M_i)^2}{n}} \quad \text{Eq. 1}$$

$$CV(RMSE) = \frac{RMSE}{\bar{y}} * 100 \quad \text{Eq. 2}$$

$$MBE = \frac{\sum_{i=1}^{n}(P_i - M_i)}{n} \quad \text{Eq. 3}$$

$$NMBE = \frac{MBE}{\bar{y}} * 100 \quad \text{Eq. 4}$$

where.

P_i – predicted value by the simulation; Mi – measured value at one point; n – total number of measurements;

$\bar{y}$ – mean value of the measured values.

The RSME indicator quantifies how much the simulated data series differs from other experimental data series by returning the average mean deviation (error) and the degree of data variation. However, this indicator does not provide the error information on whether the misprediction underestimates or overestimates the experimental data. The MBE, instead, returns the average bias in the prediction of the simulated data. The MBE should not be used as a measure of the model error since high individual errors in the prediction can still lead to a low MBE value, but since the MBE value has a sign, it can be used to assess whether the overall prediction over-or under-estimates the experimental data. These indicators' normalised values facilitate comparing the tools' performance between the four periods when it comes to the total energy crossing the façade in one week. The NMBE measures how closely the energy use predicted by the model corresponds to the experimental data. CV(RMSE) allows one to determine how well a model fits the data; the lower the CV(RMSE), the better the simulated data. NMBE and CV (RMSE) are performance metrics adopted, among other functions, to assess the match between a calibrated model and experimental data (e.g. ASHRAE Guideline 14 [60]).

3. Results

3.1. Zonal approach versus component modelling

In the first part of the presentation of the results, for each software tool that implements a dedicated in-build model for DSFs, we compared the performance of such a dedicated routine and the zonal modelling approach. This is done for EnergyPlus, IDA ICE and Trnsys. For each of these tools, only the best performance approach is later compared with the other tools in Section 3.2.

3.3.1. Energy Plus

The comparison between the simulations carried out with the zonal approach and the Airflow Window model is shown below in Fig. 5 (as previously described, all the values for the given physical quantity in the stacked multi-zone model have been averaged to one single value for each variable). The scatter plots show the results of all the four analysed periods combined.

Among the two models, the zonal approach shows the worse fit to the experimental data for all the different parameters selected for the validation procedure (Table 5). The two models show different behaviour in predicting the air gap temperature; this behaviour also depends on the shading device's presence in the cavity. Compared to observations (see results of the zonal model in Fig. 5), the zonal approach overestimates the air temperature in the ventilated cavity, especially in the upper range at high airgap and surface temperatures, and over a wide range of heat flux values. The Airflow window model highly underestimates the peaks when the shading system is inside the cavity (Fig. 6a and c), while the zonal model has relatively good results while still underestimating the predictions.

Conversely, when the shading system is not deployed (i.e. rolled up), the zonal model highly overestimates the air gap temperature (Fig. 6b and d). The time distribution of the surface temperature and the heat flux shows that the two models have good predictions, and they are more or less equivalent when the shading system inside the cavity is activated. For both models and seasons, the RMSE value of the heat flux is around 10 W/m^2. This behaviour changes dramatically when the shade is not used: the errors in the predictions of the heat flux of the zonal approach reach up to four times the measurement data ($RMSE_{Winter,\ ShOFF} = 40$ W/m^2, $RMSE_{Summer,\ ShOFF} = 32$ W/m^2).

Moreover, the EnergyPlus' zonal approach leads to a great underprediction of the solar irradiance transmitted to the room behind the DSF. The algorithm implemented for the processing of diffuse irradiance through thermal zones in this tool distributes the diffuse incoming irradiance evenly on all the surfaces of the thermal zone [23]. In the zonal approach, the ventilated cavity is modelled as a series of thermal zones, and therefore, the diffuse component of the solar irradiance

Table 5
MBE and RMSE values calculated for the two EnergyPlus models.

	EnergyPlus Zone Model		EnergyPlus Airflow Window	
	MBE	RMSE	MBE	RMSE
Air gap temperature [°C]	0.9	4.5	−0.9	3.9
Surface temperature [°C]	0.6	3.1	−0.2	2.4
Heat flux [W/m^2]	7.5	27	0.2	14
Solar irradiance [W/m^2]	−7.9	22	0.9	13

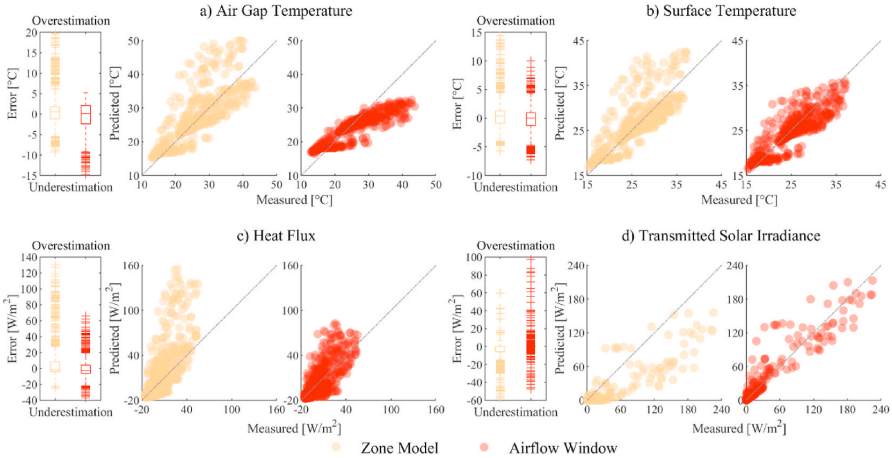

Fig. 5. Comparison between predicted and experimental data for the two models carried out in Energy Plus. a) Air Gap Temperature b) Inner glass surface temperature c) Heat flux d) Transmitted solar irradiance. The four simulated periods are combined.

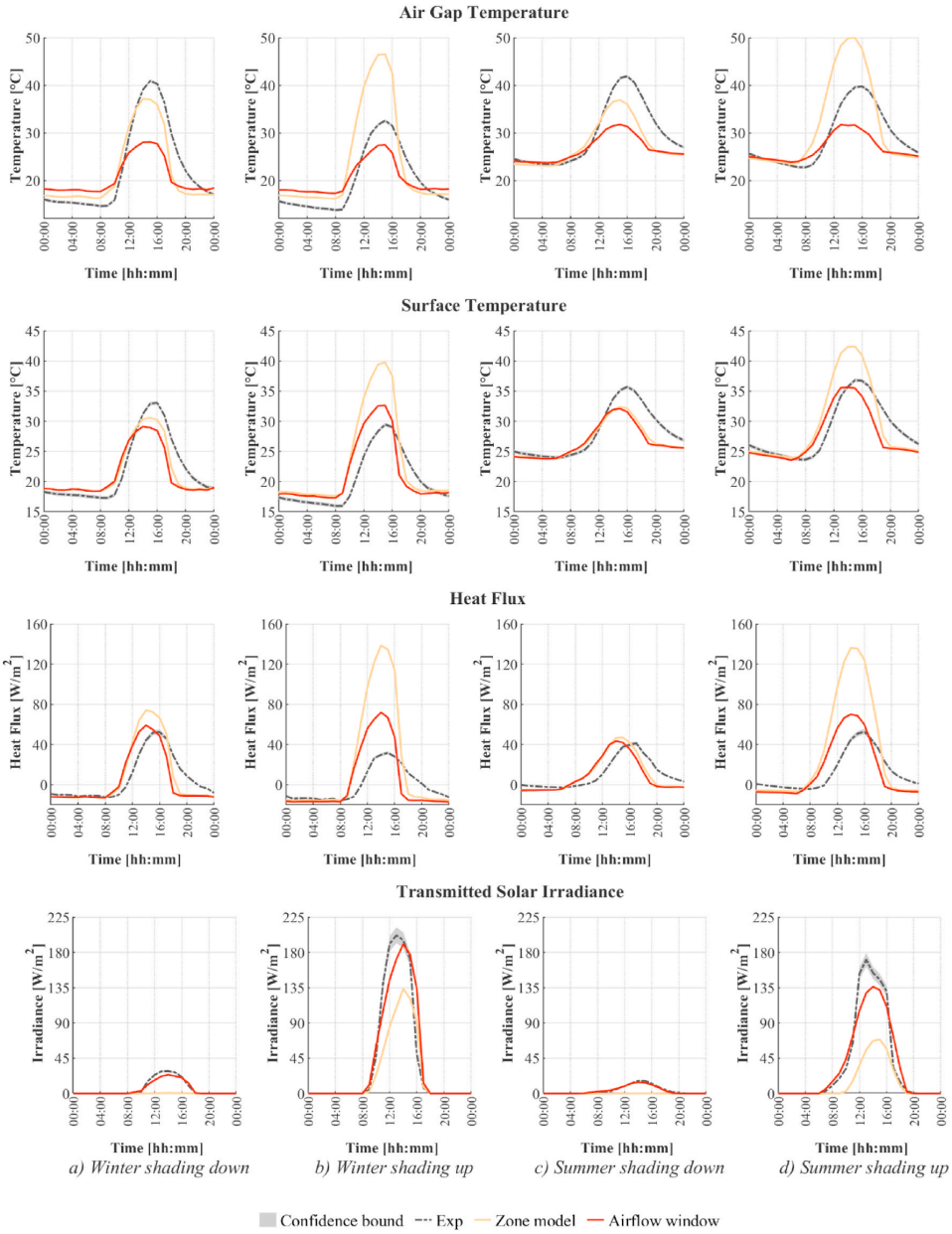

Fig. 6. Time distributions of the two Energy Plus models predictions in the four configurations. Air gap temperature. Surface temperature. Heat flux. Transmitted solar irradiance. a) Winter shading down, b)Winter shading up, c) Summer shading down, d) Summer shading up. A single, representative day was selected from the simulated periods.

transmitted through the external skin of the DSF is evenly distributed on all the surfaces that delimit the ventilated cavity – hence the outer skin, the inner skin, the virtual surfaces at the top and bottom of each volume in which the cavity is divided, and the sides of the cavity. When the roller screen is deployed, because of EnergyPlus treating the shade as a perfect diffuser, the total irradiance transmitted through the shading (both the direct and the diffuse component) is considered diffuse and thus evenly distributed on every surface of the thermal zone. These procedures lead to the fact that the solar irradiance is not treated correctly when this modelling approach is adopted, and a substantial underestimation of the direct solar gain in the room behind the DSF is revealed.

In light of these results, it was chosen to use the 'Airflow Window' model to continue with the other software comparison.

3.1.2. IDA ICE

The comparison between the performances of the two models of IDA ICE is shown in Fig. 7, where we adopted the same procedure as for the illustrations related to EnergyPlus (i.e. the results of the zonal model have been averaged to one single value, and the charts include the results of all the four analysed periods).

The two models give quite similar results for all the evaluated parameters. The ventilated window model shows a slightly better fit in replicating the heat flux and the transmitted solar irradiance while showing a slightly worse fit in predicting the air gap temperature. As shown in Table 6, the two models predict the surface temperature of the inner glazing with the same accuracy.

Observing the time profiles (Fig. 8), it is possible to notice that the models' predictions changes if the shades are present in the cavity or not. It appears that the prediction of the air gap temperature is more accurate if the shading is not activated (with a better prediction of the ventilated window model in winter – $RMSE_{Winter,\ ShOFF} = 1.5\ °C$ (Fig. 8 b) and a better prediction of the zonal approach in summer – $RMSE_{Summer,\ ShOFF} = 1.4\ °C$ (Fig. 8 Time distributions of the two IDA ICE models predictions in the four configurations. Air gap temperature. Surface temperature. Heat flux. Transmitted solar irradiance. a) Winter shading down, b)Winter shading up, c) Summer shading down, d) Summer shading up. A single, representative day was selected from the simulated periods. d)). When the shading system is on (Fig. 8 a and c) both models underpredict the results. Similar behaviour is seen for the surface temperature, except that both models predict this variable very well during the summer without the shading in the cavity (Fig. 8 d)).

The heat flux exchanged at the indoor interface of the DSF is overpredicted by both models, especially when the shades are rolled up (off); during summer, the predicted peaks are more than three times higher compared to the measured ones ($RMSE_{Summer,\ ShOFF} = 22\ W/m^2$ for the zonal model and 20 W/m^2 for the inbuilt model - Fig. 8 d)). Instead, the two models underpredict the transmitted solar irradiance during the same periods. There is also a significant difference between the two predictions, which is most likely due to the zonal approach's modelling limitations, where the horizontal partitions need to be opaque components, and thus, this feature may impact the overall optical losses within the system.

Because the 'Ventilated window' model offers slightly better results, and to make use of such an in-built model in IDA ICE is faster than implementing a model based on the zonal strategy, this approach has been chosen for the multi-tool comparison that follows in the next section.

Table 6
MBE and RMSE values calculated for the two IDA ICE models.

	IDA ICE Zone Model		IDA ICE Ventilated Window	
	MBE	RMSE	MBE	RMSE
Air gap temperature [°C]	−0.1	2.5	−0.3	2.6
Surface temperature [°C]	0	1.6	0.4	1.5
Heat flux [W/m^2]	3.5	17	2.6	15
Solar irradiance [W/m^2]	−3.7	22	0.2	21

3.1.3. TRNSYS

The comparison between the performances of the two models of Trnsys is shown in Fig. 9, where we adopted the same procedure as for the illustrations related to EnergyPlus and IDA ICE (i.e. the results of the zonal model have been averaged to one single value, and the charts include the results of all the four analysed periods). The module for implementing a 'Complex Fenestration System – CFS' is only available in a version of Trnsys18 released in 2020, while the zonal approach was implemented in a prior version of this tool (Trnsys17), which can be also used in the newer version Trnsys18.

Among the two models, the zonal approach shows a better fit to the experimental data for most of the parameters selected for the validation procedure (Table 7). The two models show similar behaviour in predicting the air gap temperature when the shading device is not in the cavity. Compared to observations (see the zonal model results in Fig. 9), the zonal approach underestimates the air temperature in the ventilated cavity, especially in the upper range at high airgap and surface temperatures. Conversely, the CFS model shows an overestimation over a wide range of heat flux values and solar irradiance.

When observing the time profiles (Fig. 10), it is possible to notice that the models' predictions change if the shades are present in the cavity or not. It appears that the prediction of the air gap temperature is more accurate if the shading is not activated, with a very similar prediction of the peaks from both models in winter and summer (Fig. 10 b and d). Nevertheless, the statistical values show a better agreement of the zonal approach to the experimental data ($RMSE_{Winter,\ ShOFF,\ Zonal} = 2.8\ °C$ *vs.* $RMSE_{Winter,\ ShOFF,CFS} = 3.5\ °C$ and $RMSE_{Summer,\ ShOFF,\ Zonal} = 2.6\ °C$ *vs.* $RMSE_{Summer,\ ShOFF,CFS} = 2.8\ °C$). When the shading system is on (Fig. 10 a and c) both models underpredict the results. Different behaviour is shown in the surface temperature: both models

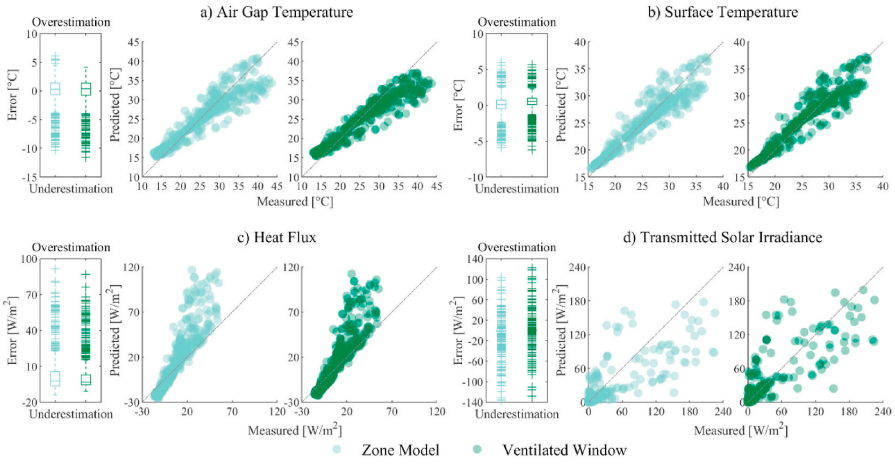

Fig. 7. Comparison between predicted and experimental data for the two models carried out in IDA ICE. a) Air Gap Temperature b) Inner glass surface temperature c) Heat flux d) Transmitted solar irradiance. The four simulated periods are combined.

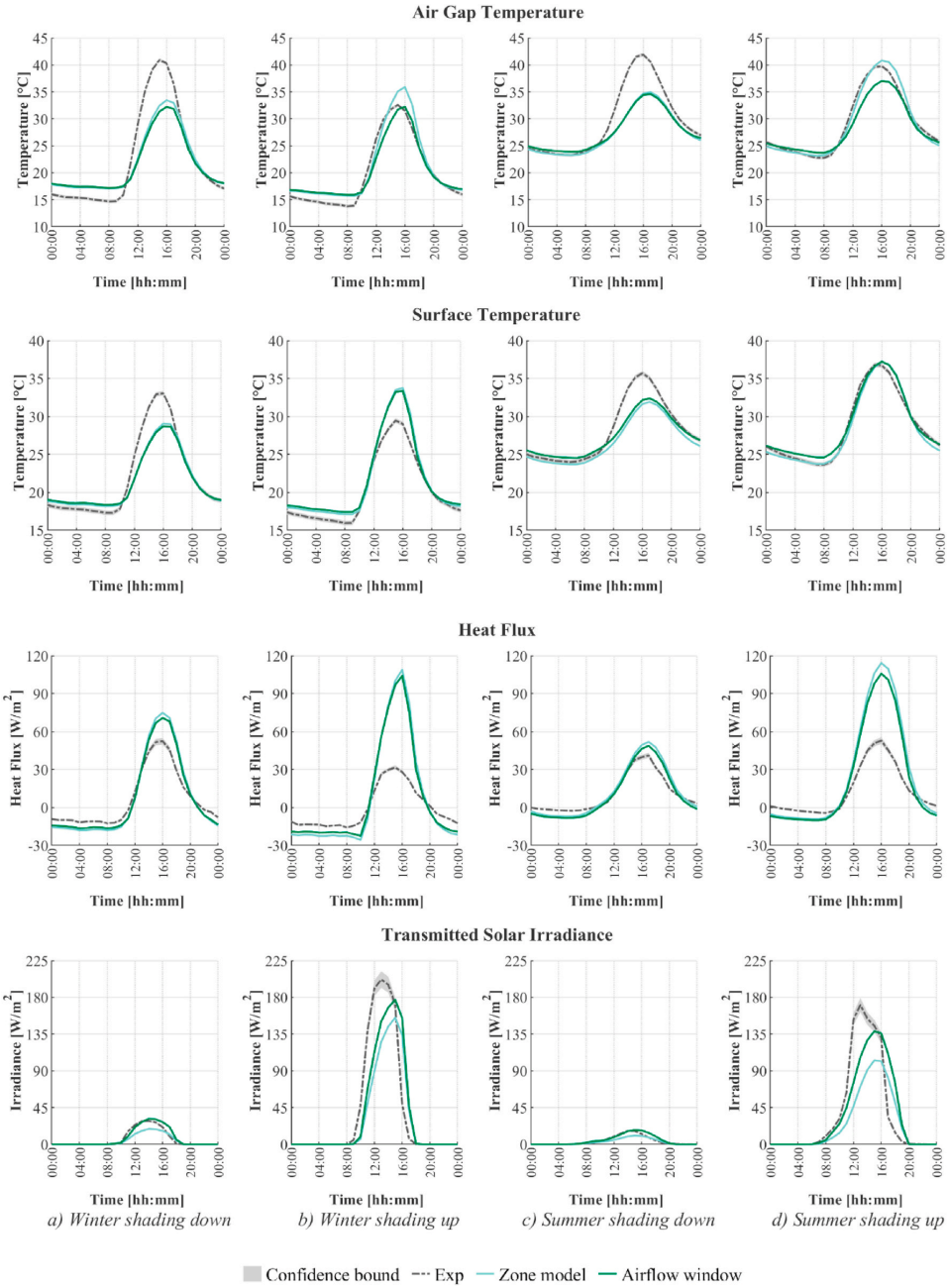

Fig. 8. Time distributions of the two IDA ICE models predictions in the four configurations. Air gap temperature. Surface temperature. Heat flux. Transmitted solar irradiance. a) Winter shading down, b)Winter shading up, c) Summer shading down, d) Summer shading up. A single, representative day was selected from the simulated periods.

underpredict this variable with the shading in the cavity (Fig. 10 a and c), the zonal model offers a better prediction in winter without the shading device ($RMSE_{Winter,\ ShOFF} = 1.8$ °C - Fig. 10 b) while the CFS model performs better in summer ($RMSE_{Summer,\ ShOFF} = 2$ °C - Fig. 10 d).

The heat flux exchanged at the indoor interface of the DSF is overpredicted by both models at night in all four periods. When the shades are rolled up (off), the CFS model's predicted peaks are highly overpredicted. The zonal approach performs better in summer than in winter ($RMSE_{Summer,\ ShOFF} = 11$ W/m^2 $RMSE_{Winter,\ ShOFF} = 13$ W/m^2 - Fig. 10 b and d). There is a significant difference in predicting the

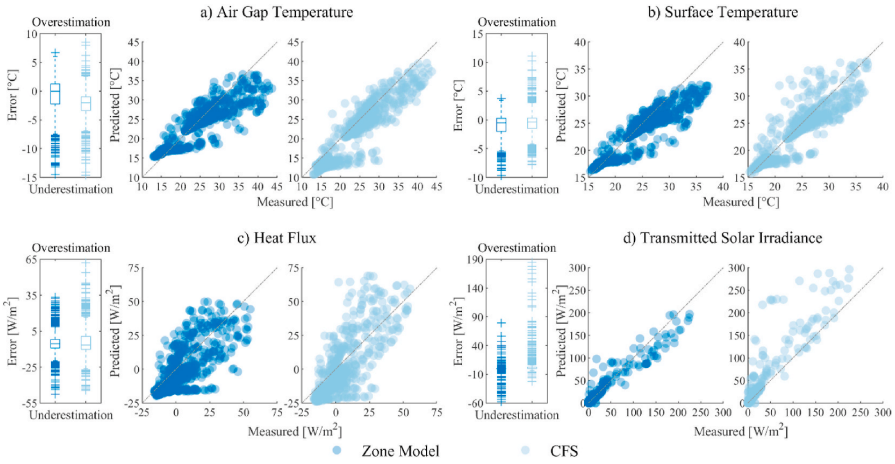

Fig. 9. Comparison between predicted and experimental data for the two models carried out in Trnsys. a) Air Gap Temperature b) Inner glass surface temperature c) Heat flux d) Transmitted solar irradiance. The four simulated periods are combined.

Table 7
MBE and RMSE values calculated for the two Trnsys models.

	Trnsys Zone Model		Trnsys CFS model	
	MBE	RMSE	MBE	RMSE
Air gap temperature [°C]	−0.9	3.5	−2.3	3.7
Surface temperature [°C]	−1.1	2.4	−0.6	2.5
Heat flux [W/m^2]	−4.9	12	−3.8	14
Solar irradiance [W/m^2]	−1	10	7.5	25

transmitted solar irradiance between the models; the CFS model overpredicts the results while the zonal approach underpredicts them. This behaviour is more accentuated in the winter periods. This difference is most likely connected to the changes made to the solar radiation routines in version 18 of Trnsys, and the model adopted to decompose the global solar radiation [61]: the zonal model was implemented in Trnsys17 while the CFS model is only available in the last release of Trnsys18.

Because the 'Complex Fenestration System' model does not offer significantly better results, and to make use of such an in-built model in Trnsys, BDSF data for the glazing and the shading device are needed making it more complicated than implementing a model based on the zonal strategy, this approach was not chosen for the multi-tool comparison. Moreover, one of the model's features is that it is impossible to connect the indoor zone's temperature node to the inlet of the façade since the inlet's temperature has to be set (or fixed or a schedule). This limits the applicability to a real case, where the inlet temperature is not known, or the indoor temperature does not correspond to the set input of the HVAC system. Thus, the zonal approach model will be used in the next section.

3.2. Intersoftware comparison for thermophysical quantities

This section gives an overview of the four analysed tools' overall performance for the chosen physical quantities. As previously described, for the tools providing an in-built model of DSF, the in-built model approach has been generally selected to perform the comprehensive comparison with all the BES tools, as these showed slightly more reliable results. When, due to different reasons, the comparison has been carried out using, for each tool, the results from the zonal modelling approach, this is specified in the text.

3.2.1. Air gap temperature

Fig. 11 shows the errors in predicting each model's air gap temperature in the four BES tools. IDA ICE is the software that returns the most accurate prediction of this variable when all the four periods used in the validation procedure are considered together. Similarly, the magnitude of Energy Plus, Trnsys and IES-VE error is similar. In general, the tools underestimate the temperature during the day and overestimate the lower values, particularly during the winter nights. Particularly, Energy Plus performs poorly, significantly underestimating the peaks all the time.

In general, it is possible to say that all the tools underpredict the intensity of the peaks (Fig. 12). The prediction of EnergyPlus, Trnsys and IES VE is very similar when the shadings are deployed (Fig. 12 a and c): all of them highly underpredict the peaks during the day. IDA ICE performs slightly better than the tools mentioned above whilst still underpredicting the values to a great extent. IDA ICE tends to underestimate the peaks except during the winter period when there is no shading device in the cavity ($RMSE_{Winter,\ ShOFF} = 1.5$ °C - Fig. 12 b). In this period, Trnsys gives very similar results to IES VE, slightly underpredicting the peaks, while EnergyPlus is the worst performing tool. In the summer case where the shading is not in the cavity (Fig. 12 c), Trnsys, IDA ICE and IES VE give almost the same prediction of the peaks. EnergyPlus, as previously said, is the worst-performing software tool by always underpredicting the temperature in the warmest hours of the day.

We can see a tendency in IDA ICE of a small delay in predicting the peaks compared to the experiments and of one to 2 h compared to the other tools. When it comes to Energy Plus, TRNSYS, and IES-VE, these tools anticipate the peak values compared to the experimental data. These time shifts become even more evident in predicting the surface temperature and heat flux. We can assume that they are due to a series of modelling simplifications in some simulation environments (lack of the glazing capacity node in all tools except IDA ICE), the processing of solar irradiance and other input variables related to the outdoor environment (e.g. how the solar irradiance is decomposed from the hourly weather data file in intermediate, sub-hourly values), and how simulation results with sub-hourly time-steps are post-processed to obtain hourly values.

The four tools produce all consistently high errors in predicting the air temperature at night-time during the winter season, while this effect is not as evident during the summer. The inability to reproduce air gap temperatures as low as the observations at night may come from the different inlet temperature used in the model (which corresponds to the

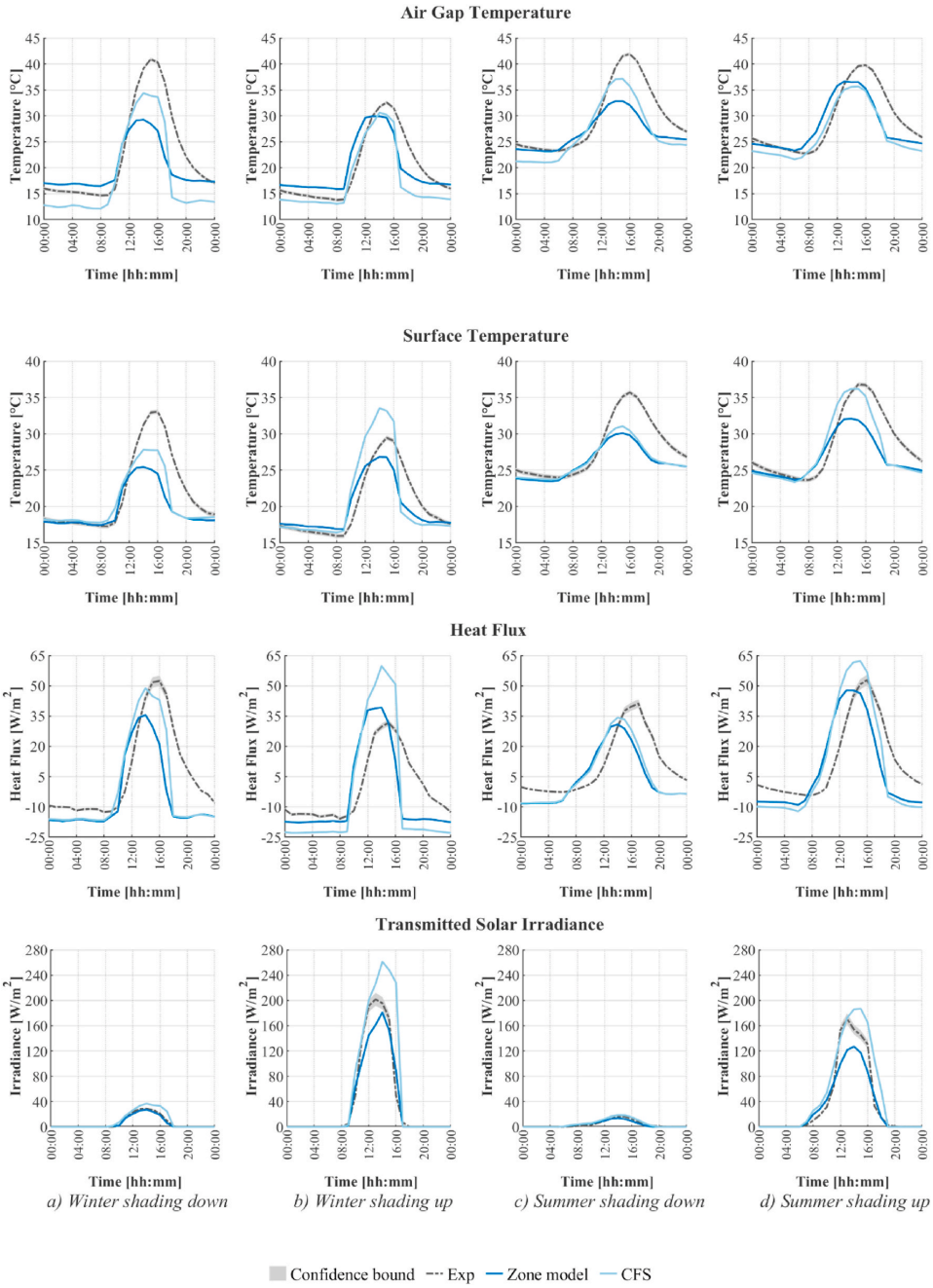

Fig. 10. Time distributions of the two Trnsys models predictions in the four configurations. Air gap temperature. Surface temperature. Heat flux. Transmitted solar irradiance. a) Winter shading down, b)Winter shading up, c) Summer shading down, d) Summer shading up. A single, representative day was selected from the simulated periods.

indoor air temperature) and the experiments' actual conditions. We hypothesise that, as the air enters the DSF's cavity after crossing the aluminium frame at the bottom of the DSF, the airflow undergoes some heat loss due to the heat exchange with the bottom cavity surface. This effect can be visualised by looking at the detailed results obtained from each stacked zone in the simulations using the zonal approach (Fig. 13). Only for this specific comparison, the results of the zonal approach of all the tools are used (instead of the in-built models of Energy Plus and IDA

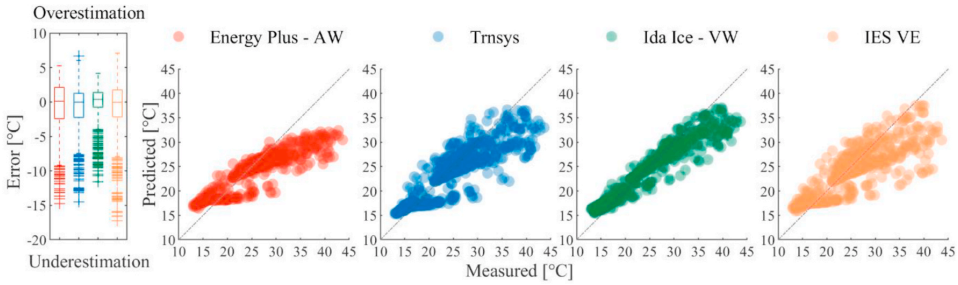

Fig. 11. Comparison between measured data and predicted air gap temperature values. The four simulated periods are combined.

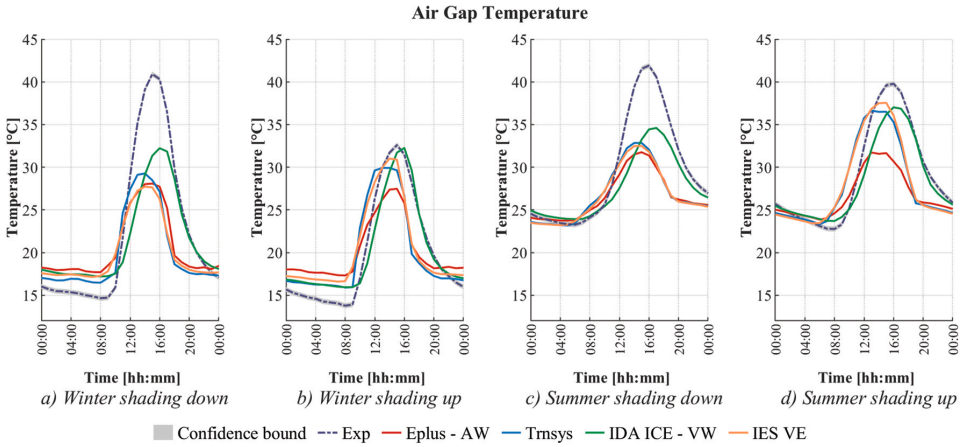

Fig. 12. Time profiles of the air gap temperature prediction in the four configurations. A single, representative day was selected from the simulated periods.

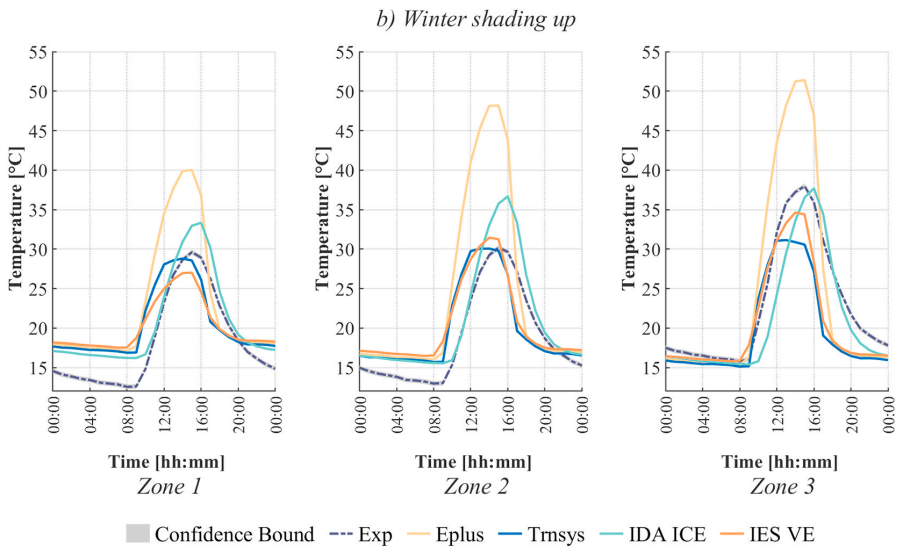

Fig. 13. Time profiles of the vertical distribution of the air gap temperature. Winter period with the shading in the cavity. The graph shows the results of the model with the zonal approach of Energy Plus and IDA ICE.

ICE). The vertical temperature profile shows different errors in the daytime and the night-time. In all the tools, the first (lowest) thermal zone has the lowest temperature, and the cavity air temperature rises with the zone's vertical position. At night time, the temperature values are similar in all tools with an overprediction of the air gap temperature in the first thermal zone, while the predicted temperatures in the third thermal zone overlap the measurements. During the daytime, the results of the tools show a higher spread. The results show a moderate vertical temperature rise in TRNSYS and IDA ICE: the former shows a good agreement with the experiments in the lower two zones, the latter in the third zone. Energy Plus results show a high overprediction of the peaks in all the three zones, while IES VE shows differences of moderate intensity, with the overprediction of the air gap temperature seen only in the middle zone – an effect that is difficult to find an explanation for.

3.2.2. Surface temperature (of the inner skin)

IDA ICE is the best performing tool (Fig. 14) in predicting the surface temperature, as quantified by the statistical indicators and observed in the scatter plot graphs, which consider all four periods together. Conversely, by observing the time profile distribution, it is possible to notice that IDA ICE predicts the peaks significantly more correctly than the other tools in only one period (summer, shading not deployed) out of four ($RMSE_{Summer,\ ShOFF} = 1\ °C$ Fig. 15 d). During the other periods, the peak prediction is very much in line with the results of EnergyPlus. As in predicting the air gap temperature, EnergyPlus, TRNSYS, and IES VE predict the values one or 2 h ahead of the measurement and IDA ICE's predictions. This latter discrepancy is not highlighted in the statistical indicator, so even if IDA ICE has a more significant error in terms of magnitude, it appears to be the one with better performance in predicting this quantity. As previously explained, we believe that this effect can be to a great extent explained by the fact that IDA ICE implements a capacitive node in the glass calculation model – a feature that is missing in the other three BES tools.

It is impossible to define a clear and robust trend on how the tools perform depending on the season, as the overestimation and underestimation are seen within the same period. In general, the time profiles and values have the smallest errors in summer without the shading in the cavity (Fig. 15 d). All the tools tend to underpredict the peak values with shading on, both summer and winter, and overpredict night time values in winter (with the only exception being TRNSYS). In winter, without the shading deployed, almost all the tools (except for Trnsys) overestimate the peaks (Fig. 15 b).

3.2.3. Heat flux (exchanged at the indoor-facing interface of the inner skin)

As it is not possible to extract this information from IES VE, the comparison of the heat flux values' prediction is carried out for the three other tools. The general trend is an overprediction of the peaks and an underestimation of the lower values by EnergyPlus and IDA ICE, and a more accurate prediction by TRNSYS (Fig. 16). In particular, IDA ICE has the highest errors in predicting the high peaks in three of the four periods, while the values show a good match in summer when the shading is activated.

The time distribution charts also show a common trend towards overestimation for EnergyPlus and IDA ICE, with the worse outputs from all the tools with the shading rolled up (not deployed) (Fig. 17 b and d). When the shading system is present in the cavity, TRNSYS underpredicts the peaks. IDA ICE represents quite accurately the peaks in summer when the shading is deployed in the cavity but becomes far less accurate when the shading is retracted. Once again, EnergyPlus and TRNSYS are ahead of the measured data while IDA ICE predicts at the right time, the values of the heat flux exchanged at the indoor-facing surface of the inner skin. The measurement of the heat flux exchanged at the indoor glazing surface is affected by both the sensor's presence and the shielding installed to avoid overheating due to the solar radiation, as explained more in details in Ref. [54]. However, as previously mentioned, the procedure adopted for monitoring the surface heat flux is, to our best knowledge, the best practice for such a measurement that minimises the experimental uncertainty.

3.2.4. Transmitted solar irradiance

The prediction of the solar irradiance transmitted through the entire double-skin façade, and sampled right at the inner skin's indoor interface is shown in Fig. 18. In this case, EnergyPlus (when the Airflow window model is used) is the software tool that offers the most accurate prediction yet underestimating the high peaks during sunny days (Fig. 19). The tools show similar results when the shading is deployed in the cavity. IES VE tends to overpredict the transmitted solar irradiance values when the shading is not present, while IDA ICE underestimates them. The measurement of the transmitted solar irradiance is also affected by some limitations due to the experimental setting. It includes a component (though almost negligible) of diffuse solar irradiance in the indoor environment which is retro-reflected towards the sensor by the glazing surface, as explained more in details in Ref. [54]. This may result in a measured transmitted irradiance that is slightly higher than the "real" one, though such an error may be considered included in the measurement chain's total accuracy for transmitted solar irradiance.

4. Discussion and possibilities for future developments of BES tools

The time distribution of the predicted values (Figs. 12, Figure 15, Figure 17, Figure 19) shows that there is no single tool that outperforms the others in all the different configurations tested. In most cases, the software representing the daytime peak of a particular physical quantity in winter with the shading down is committing a significant error in predicting another physical quantity in the same period. Therefore, it is not straightforward to rank the tools in an absolute way. We believe it is somehow more appropriate to define the simulation environment that provides the best result for each of the analysed physical quantities. Similarly, it is impossible to say which configuration or period is the

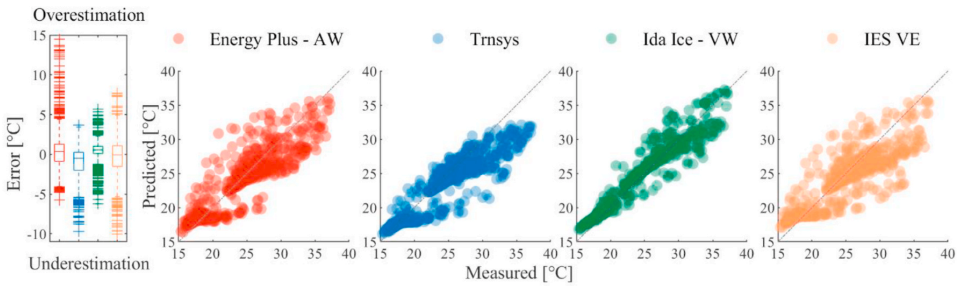

Fig. 14. Comparison between measured data and predicted values of the surface temperature. The four simulated periods are combined.

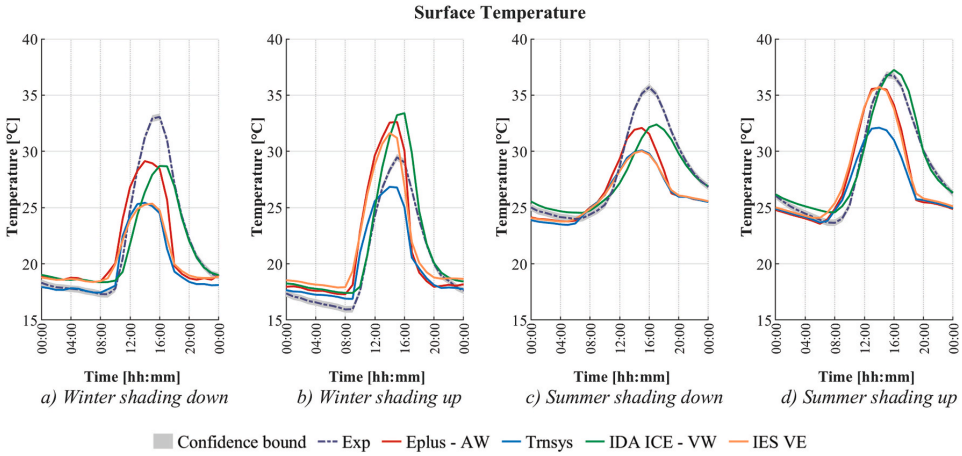

Fig. 15. Time profiles of the surface temperature prediction in the four configurations. A single, representative day was selected from the simulated periods.

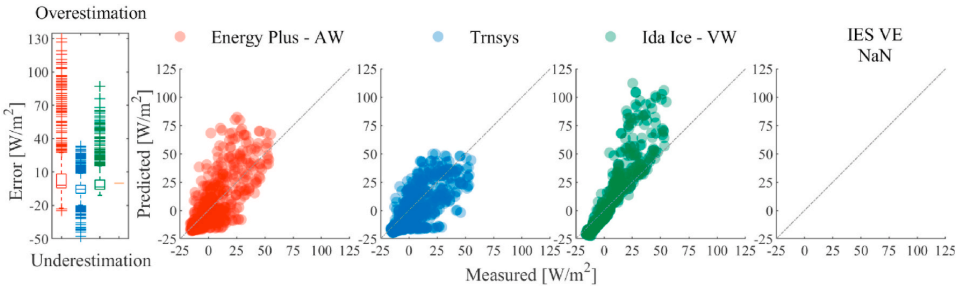

Fig. 16. Comparison between measured data and predicted values of the heat flux. The four simulated periods are combined.

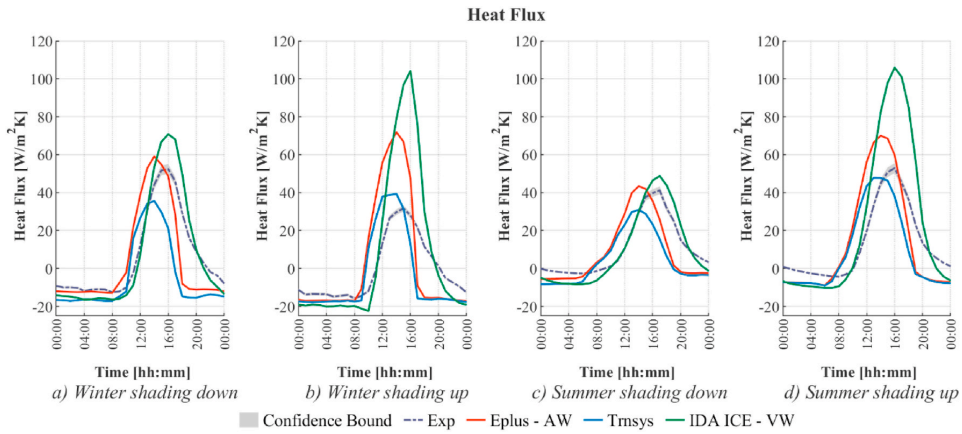

Fig. 17. Time profiles of the heat flux prediction in the four configurations. A single, representative day was selected from the simulated periods.

easiest to be predicted correctly by all the tools.

The statistical indicators for all the analysed physical quantities of the four periods combined are shown in Table 8. According to these values, IDA ICE is the best tool, in terms of fitness of the prediction, when predicting the air gap temperature and the interior glazing surface temperature. EnergyPlus provides the best results for predicting the heat flux and the solar irradiance transmitted through the component. However, these pictures are based on the tools' overall performance, while if the focus is placed on a particular configuration (shading up or down) and a particular season (cold season or warm season), the reliability of the different tools varies to a greater extent.

IDA ICE is very accurate in predicting the surface temperature only

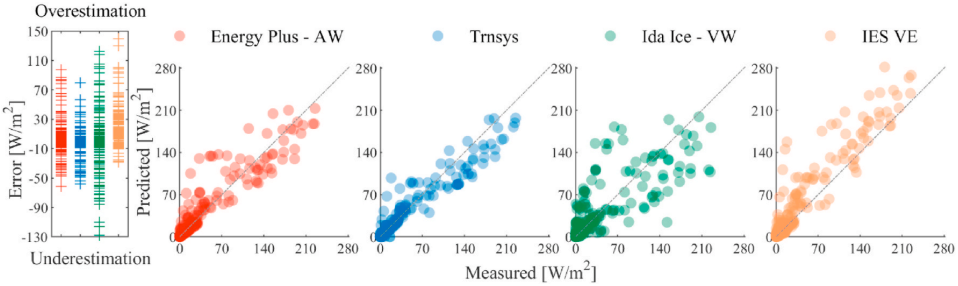

Fig. 18. Comparison between measured data and predicted values of the transmitted solar irradiance.

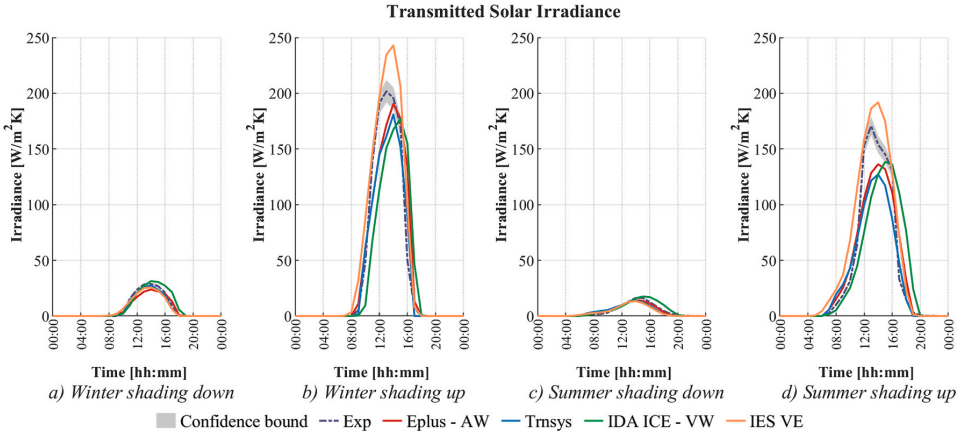

Fig. 19. Time profiles of the transmitted solar irradiance prediction in the four configurations A single, representative day was selected from the simulated periods.

Table 8
MBE and RMSE values calculated for the model in Energy Plus 'Airflow Window', TRNSYS, IDA ICE 'Ventilated Window' and IES<VE>.

	EnergyPlus AW		TRNSYS		IDA ICE VW		IES VE	
	MBE	RMSE	MBE	RMSE	MBE	RMSE	MBE	RMSE
Air gap temperature [°C]	−0.9	3.9	−0.9	3.5	−0.3	2.6	−0.9	3.9
Surface temperature [°C]	−0.2	2.4	−1.1	2.4	0.4	1.5	−0.5	2.6
Heat flux [W/m²]	0.2	14	−4.9	12	2.6	15	N/A	N/A
Solar irradiance [W/m²]	0.9	13	−1	10	0.2	21	4.6	17

when the shading is up but commits considerably high errors in the other periods, even if the statistical indicators seem to show a different behaviour. Energy Plus is the worst tool in predicting the air gap and surface temperature but is accurate in predicting the transmitted solar irradiance.

The presence of the shading device in the cavity cannot be identified

Table 9
Performance overview of the tools in the four different periods. Comparison with the experiment results in the two seasons, Winter and Summer, with the shading ON or OFF. - - - Very high underestimation; - - High underestimation; - Underestimation; = Good Agreement; + Overestimation; ++ High Overestimation; +++ Very High Overestimation; N.A. Data Not Available. Colour code: Red: large error; Orange: moderate error; Yellow: small error; Green: accurate prediction.

Tool	***EnergyPlus AW***				***TRNSYS***				***IDA ICE VW***				***IES VE***			
Season	**Winter**		**Summer**		**Winter**		**Summer**		**Winter**		**Summer**		**Winter**		**Summer**	
Shading	**ON**	**OFF**	**ON**	**OFF**	**ON**	**OFF**	**ON**	**OFF**	**ON**	**OFF**	**ON**	**OFF**	**ON**	**OFF**	**ON**	**OFF**
Air gap temperature [°C]	- -	-	- -	-	- -	-	- -	-	- -	+	- -	-	- -	+	- -	-
Surface temperature [°C]	-	+	-	+	-	-	-	-	-	+	-	+	-	+	- -	=
Heat flux [W/m²]	+	+ + +	=	++	-	+ +	=	+ +	++	+ + +	=	+ + +	*N.A.*	*N.A.*	*N.A.*	*N.A.*
Solar irradiance [W/m²]	=	- -	=	- -	=	- -	=	- -	=	- -	=	- - -	=	+ + +	=	+ +

as a condition that increases the DSF model's complexity, so that it leads to an increase in inaccuracy and prediction errors. Except for EnergyPlus, all the tools are quite reliable in predicting the air gap temperature when the shading is up, but its presence does not affect the accuracy of the better performing tool (IES VE) in predicting the air gap temperature (Table 9). Conversely, it has a more significant impact on EnergyPlus, TRNSYS and IDA ICE results, where the air gap temperature is highly underpredicted. EnergyPlus and TRNSYS offer an even better prediction of the heat flux when the shading is in the cavity rather than when it is not deployed. However, having the shading device activated leads to an underprediction of the surface temperature by all the tools.

The user can set the simulation's time-step and the output results, but there is no control over how this data is aggregated on an hourly basis. The tools' different approach may lead to a discordance over the final results if dynamic variables are considered. These discrepancies are not visible if daily or periodic data are compared. The use of periodic data is interesting, for example, when the focus is not on the DSF itself but on the influence of installing a DSF has on the energy balance. When comparing the energy gained and lost by the DSF over seven days (Table 10), the performance of the tools is very similar, particularly in those periods when the shading is present in the cavity. All tools tend to over predict the total transmitted energy, but TRNSYS has the overall best performance (Table 11). Using this metric, the tools' behaviour appears to be more in line with the experimental data, and the daily variations seen analysing the dynamic parameters are no longer distinguishable.

In most of the tools, the absence of a capacitive node of the glazing system is reflected in a considerate lagging of the predictions compared to the experimental data. While IDA ICE includes a heat capacity node for the glazing and the shading, the glazing's thermal inertia is not implemented in any of the other models. Hence, any heat absorbed by the glass surface shows an instantaneous effect on the glass temperature, causing a higher temperature rise than in reality. This can have a limited effect when considering a conventional single skin glazing system, usually composed of a total thickness of glass in the range of around 1 cm. In that case, the inertial characteristics of the glazing are relatively low, and the impact of this feature on the dynamics of the heat transfer is somewhat limited – if not negligible. However, when modelling a DSF, the simulated system has a relatively thick glass structure (up to 4–5 cm when considering both skins), and a more precise accounting of the heat absorbed and released because of the specific heat capacity of the material is no longer a negligible aspect. Showing the capacitance node's role is an exemplification, in this paper, of the challenges that modellers may face when using legacy software tools in simulating a system that was not originally meant to be simulated with those tools. We do not claim that this particular instance is the only, nor maybe the single most influential source that explains discrepancies between simulations and experiments. However, this example was relatively easy to demonstrate through IDA ICE (that allows users to input the value of the glass-pane material's specific heat capacity while the other tools do not allow this parameter to be modified) by comparing a simulation with and without glass's specific heat capacity. Many other possible causes cannot be so easily tested with BES tools, as there are intrinsic limitations to do so in the tools' structures.

Table 10
Energy performance of the different tools in the four analysed periods.

	Total Energy [kWh/m^2]			
Season	Winter		Summer	
Shading	ON	OFF	ON	OFF
Measured	2.8	6.3	2.4	5.4
EnergyPlus AW	3.1	8.4	2.2	6.9
TRNSYS	3.2	7	2.1	5.8
IDA ICE VW	3.8	8.1	2.8	7.8
IES-VE	N.A.	N.A.	N.A.	N.A.

The shading device's presence does not dramatically affect the tools' performance. This may be because when mechanically ventilated cavities are modelled, the influence of the heat released to the airflow on the determination of the actual air mass rate is neglected. If this assumption can be valid for wide cavities with high airflow rate, in the case of narrow cavities characterised by relatively slow (forced) airflows, such an effect might be not negligible. Improved models and modelling approaches for DSF in BES tools should, therefore, include the possibility better to specify the position of the in-cavity shading device and account for its influence on the airflow rates. So far, only IDA ICE allows specifying the shading position with respect of the cavity, while in the other tools, the shading device is assigned to the window or in a fixed position (Energy Plus) or just specifying if it is an internal or external shading. TRNSYS does not permit defining the shading position but accounts for an additional convection fraction to the zone's air node.

The tools' convection algorithms seem to have a minimal effect on the prediction of the DSF's thermophysical quantities that we used to assess the tools' reliability. It was noticed that, in IDA ICE, when modelling the façade with the zonal approach, the convection heat transfer coefficients for the cavity surfaces can assume values up to ten times higher than those obtained when modelling the same façade with the in-built model. This is because the CDA method used in the zonal approach is a function of the air change rate, which increases due to partitioning the cavity into many stacked zones. The higher the number of zones, the higher this value is [44]. Conversely, Energy Plus (zonal approach) and Trnsys use values of the same magnitude as the in-built model of IDA ICE. Moreover, it is interesting to highlight that both in IDA ICE and in Energy Plus, when the algorithm had to choose between the natural or forced convection calculation method, the natural convection coefficient was chosen. In IDA ICE, this choice was done by choosing the highest value between the two (see Table 4). In Energy Plus, the algorithm runs a series of "if … else" checks to select the calculation method. One of the conditions to use the forced convection coefficient is to have an active HVAC system present in the zone, and this led to the natural convection coefficient being adopted for all the cavity zones. Unfortunately, extracting this information for all the models was impossible (for example, the in-built model of Energy Plus and the IES VE zone-model do not output these quantities), and this limits the possibility to perform a more systematic investigation on the role of these quantities in relation to the tool's performance.

5. Conclusion

Modelling a double-skin façade is not a trivial task, and the reliability of the modelling approaches adopted in building energy simulation (BES) tools need to be verified and validated to build trust in the use of BES programs to simulate DSFs. Four different building energy simulation (BES) tools were tested against experimental data. The accuracy in predicting four physical quantities was evaluated, namely the air gap temperature, the inner glazing surface temperature, the heat flux, and the transmitted solar irradiance.

Three of these tools (EnergyPlus, IDA ICE and Trnsys) offer the modellers the possibility to approach a DSF in two ways: to use the in-built model for the DSF or develop a so-called 'zonal approach'. The two approaches were compared against experiment data, and in two out of three tools, the in-built model was the most accurate in predicting the chosen parameters. In TRNSYS the zonal approach gave better results, whilst in IES VE, it was the only model available. Therefore, the multi-software comparison was carried out by comparing two in-built models ("Airflow window" in EnergyPlus and "Ventilated window" in IDA ICE) and two zones models (TRNSYS and IES VE).

It is not straightforward to identify a tool that is able to predict all the variables in all the conditions with the same accuracy. TRNSYS appeared to be the better performing software when studying the heat flux through the component; thus, it is a more reliable tool if the simulation's goal is the energy balance over a certain amount of time. There is no

Table 11
NMBE and CV(RMSE) values calculated for the energy performance of each tool.

Season	Winter				Summer			
Shading	ON		OFF		ON		OFF	
	NMBE [%]	*CV(RMSE) [%]*	*NMBE [%]*	*CV(RMSE) [%]*	*NMBE [%]*	*CV(RMSE) [%]*	*NMBE [%]*	*CV(RMSE) [%]*
EnergyPlus AW	*14*	*52*	*32*	*77*	*−9*	*66*	*27*	*60*
TRNSYS	*15*	*72*	*11*	*35*	*−13*	*75*	*6*	*55*
IDA ICE VW	*38*	*68*	*29*	*125*	*16*	*38*	*43*	*110*
IES-VE	*N.A.*	*N.A.*	*N.A.*	*N.A.*	*N.A.*	*N.A.*	*N.A.*	*N.A.*

consistency of accurate or inferior predictions related to a specific period, and as a general trend, the winter conditions are not predicted more accurately than the summer ones. The same type of conclusion is valid for the presence of the shading device in the cavity.

BES tools may be acceptable for predicting the overall performance of a façade in terms of energy gain and loss over a certain, rather long period (e.g. a week), and the expected accuracy of the prediction is in line with the general one for BES tools. The capability of the analysed tools to predict the short-term dynamic of a DSF accurately is instead questionable due to the complex behaviour of a DSF system and the limited representation of these systems in the BES tools. Relatively large errors are observed on individual thermophysical quantities that might be used to take important decisions in the design process. The use of BES tools in sizing the systems based on typical or design days might also lead to substantial inaccuracies and should be therefore carried out in combination with other, more detailed simulation approaches. Therefore such predictions should always be either verified through experimental data or carried out with more accurate modelling strategies (e.g. on-purpose codes, CFD codes). Ad-hoc developed simulation codes or detailed CFD models can also make it possible to systematically test, verify, and quantify the impact of the different simplifications, including, for example, more in-depth analysis on the effects of the empirical correlations for calculating the convective heat transfer coefficient – something that is difficult to be done with BES tools because of intrinsic limitations that these simulation environments present.

Declaration of competing interest

None.

Acknowledgements

The authors would like to thank the researchers and technical staff from Politecnico di Torino in Italy involved in the experimental activity, which provided the data used for model validation in this study.

Part of the activities presented in this paper were carried out within the research project “REsponsive, INtegrated, VENTilated - REINVENT – windows”, supported by the Research Council of Norway through the research grant 262198, and partners SINTEF, Hydro Extruded Solutions, Politecnico di Torino, Aalto University.

The activities presented in this paper have also been supported by the ÚNKP-18-3 New National Excellence Program of the Ministry of Human Capacities of Hungary.

Appendix A

Measured quantities

In this section, the measured quantities used for the validation process are shown. The airgap and surface temperature are plotted against the transmitted solar radiation (Fig. A.1). In Fig. A.2 , heat flux is plotted against the transmitted solar radiation.

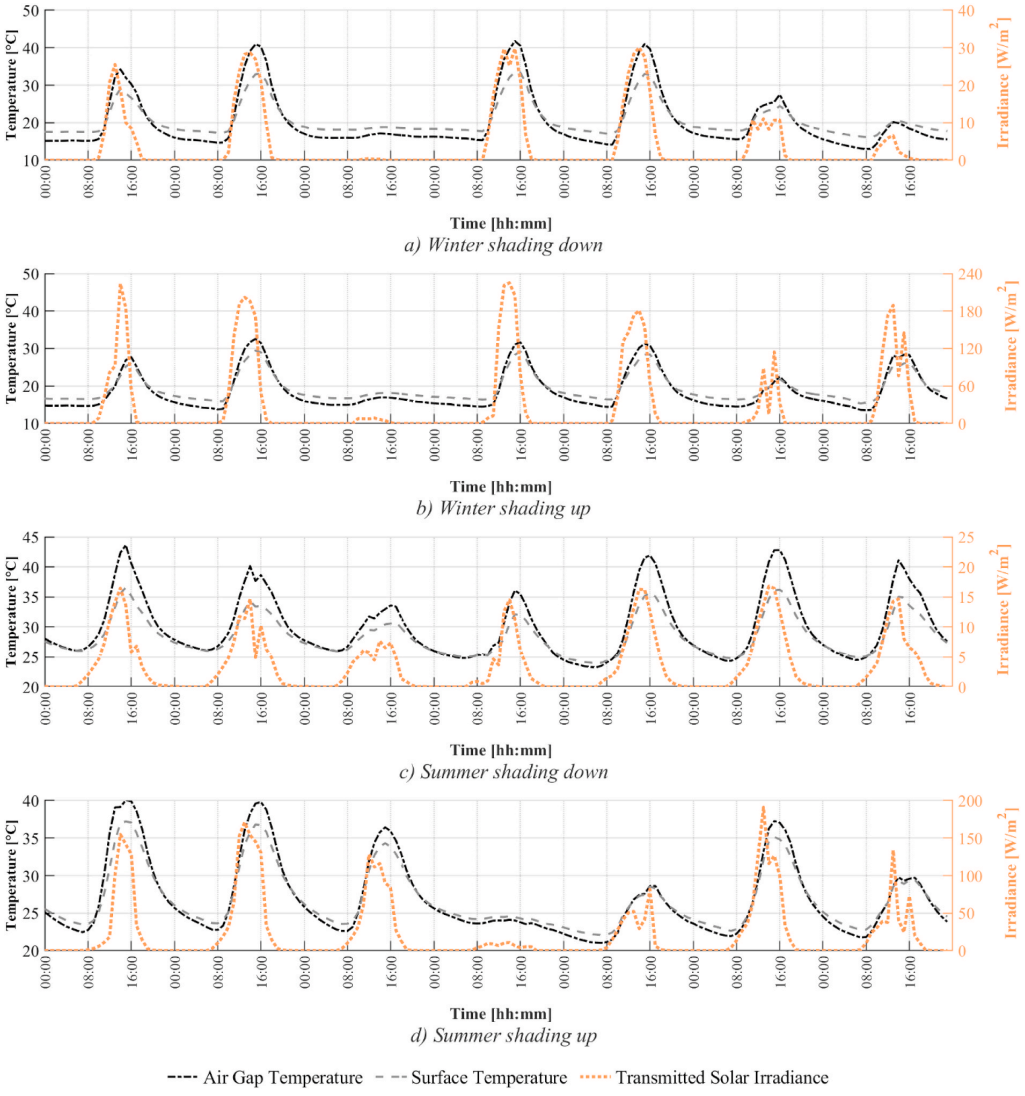

Fig. A1. Time profile of the air gap and the indoor surface temperature [°C] and the transmitted solar irradiance [W/m^2] for the four modelling periods: a) Winter with shading down, b) Winter with shading up, c) Summer with shading down and d) Summer with shading up.

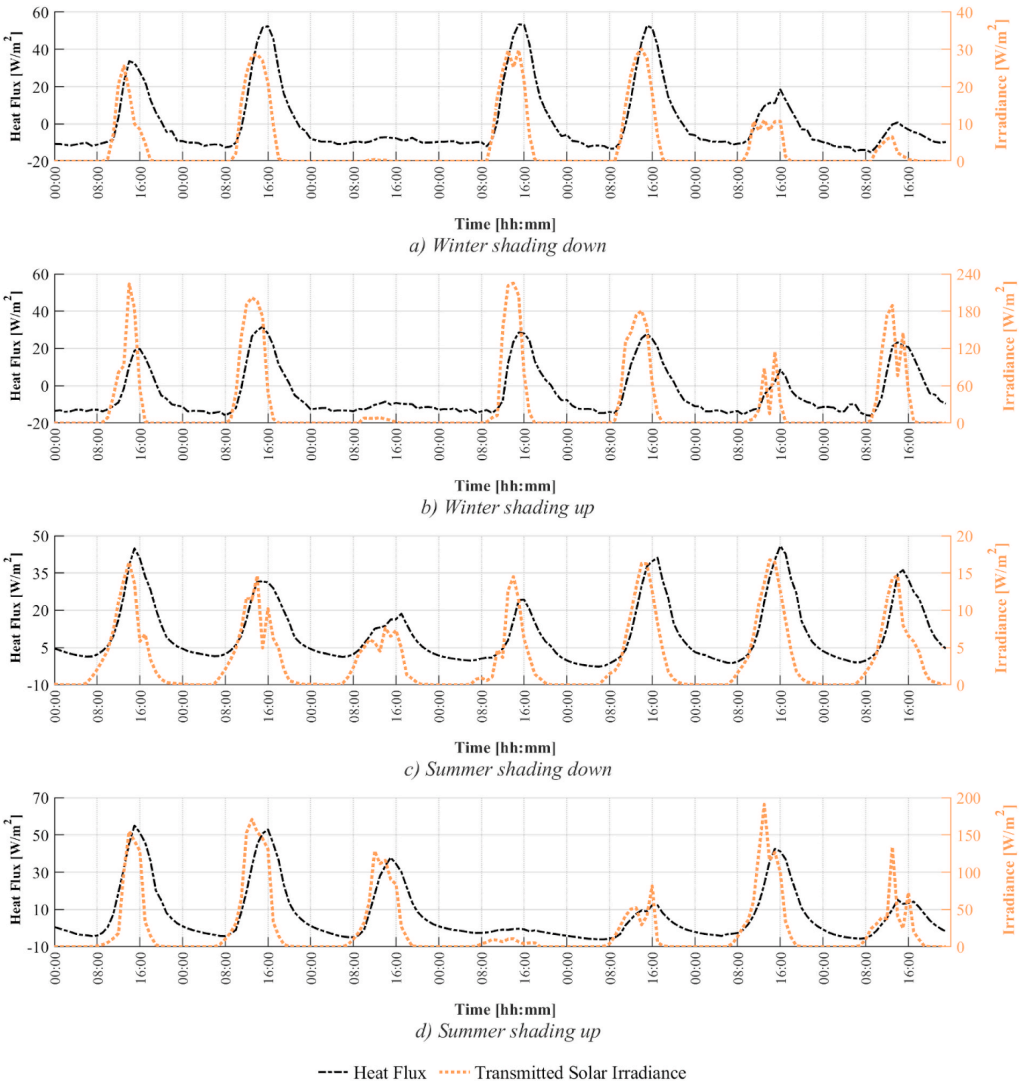

Fig. A2. Time profile of the heat flux and the transmitted solar irradiance [W/m^2] for the four modelling periods: a) Winter with shading down, b) Winter with shading up, c) Summer with shading down and d) Summer with shading up.

Appendix B

Modelling of DSF in EnergyPlus

EnergyPlus allows the modelling a DSF by using an in-built component, called *"Airflow Window"*, or through the implementation of the modelling strategies based on stacked thermal zones, and both methods were tested in this investigation.

In-built model: "Airflow window"

One of the two models of the DSF has been carried out by using the in-built component "*Airflow Window*" (as implemented in EnergyPlus 9.1). This component only allows to model mechanically ventilated windows, and it can run in five different configurations, among which the "Air exhaust" mode [62], which is the one we selected to replicate the climate façade configuration. In this modelling approach, the inlet air to the façade is taken from the indoor air node of the thermal zone to which the DSF is associated, while the exhausted air is linked directly to the outdoor air node.

In general, the software allows the modeller to specify the characteristics of a window construction pane by pane, with a limitation of maximum eight layers in the construction (including glass panes, cavities, and shading) by making use of the conventional features available in EnergyPlus for the modelling of glazing systems. The shading device was modelled as "Between glass shade". The shading device's position cannot be specified, and by default, it is set in the middle of the cavity. It can be controlled through a schedule – following the usual control possibilities for shading devices for

any other conventional window systems in EnergyPlus. When the shading device is deployed, the ventilated cavity results divided into two equal sub-cavities that are crossed by the same airflow rate, which is half of the value provided for the entire cavity. The modeller inputs the nominal (maximum) airflow rate that crosses the ventilated window and the airflow rate can be controlled through a dedicated schedule in the range 0–100%. When set to 0%, the airflow window is operated as a non-ventilated window. No information is required on the fans to mechanically extract the air from the ventilated cavity as these are, in practice, not modelled, and the airflow rate occurring in the cavity is always equivalent to that given through the schedule. The correlation of the heat convection coefficient for the ventilated cavity cannot be chosen or overrode. The in-built model adopts the calculation method detailed in ISO 15099 [50]. It is a function of the air velocity and the convective coefficient calculated for an enclosed gap (Table 4).

Zonal model

The other model implemented in EnergyPlus was obtained by modelling the façade as three stacked thermal zones. Each zone was modelled with an exterior double glazing, an interior single glazing and the opaque surfaces facing the exterior set as adiabatic. The surface between each stack zone is modelled as a window made of infrared transparent material.

The airflow between the occupied zone and the façade zones was modelled utilising the 'Airflow Network'. It consists of a set of nodes corresponding to each zone and the outdoor environment which are linked by airflow components. An effective leakage area (ELA) corresponding to the window opening was used for connecting the occupied zone to the façade bottom zone. The stacked zones of the façade are linked, employing a horizontal opening always open. An exhaust fan was used to connect the top zone of the façade to the exterior. The nodes' variable is the pressure, and the linkage's variable is the airflow rate. Newton's method is used to solve for node air pressures. The pressure difference across each linked component is assumed to be governed by Bernoulli's equation. Internal solar radiation distribution was calculated using the "full interior and exterior" mode. This calculation mode tracks the amount of radiation that reaches each zone's surface by projecting direct solar radiation through the exterior window into the internal surfaces. Wind data were not available from the experimental data, and being the façade running in a mechanical configuration, the influence of the wind can be disregarded. Therefore, the model did not account for wind pressure.

The convection coefficients for the cavity surfaces are chosen by the 'adaptive algorithm'. The adaptive convection algorithm is based on classifying surfaces by flow regime and orientation so that the correct h_c equation can be chosen at a particular point in time during the simulation. The correlations available for the window's surfaces are shown in Table 4. If the flow regime is 'natural' the h_c is calculated according to the ISO 15099 [50]; if the flow regime is forced, the Goldstein Novoselac Ceiling Diffuser Window correlation is adopted [51]. Selecting the flow regime is done according to the HVAC (element type, operating status and ACH). Though, in the thermal zones of the DSF, no HVAC element is present in the zone itself; therefore, the algorithm always chooses the natural convection correlation.

Modelling of DSF in IDA ICE

The models were developed by using IDA ICE 4.8 (SP1). There are two main approaches for modelling DSFs within the tool:

- the in-built component (ventilated window model, *vw*)
- or the façade can be constructed tailor-made consisting of one or more connected thermal zones.

In-built model: "ventilated window model"

The *vw model* consists of two detailed window models representing the two transparent skins, with the possibility to model the shading on either side of the two windows. The detailed window model makes a layer by layer computation of multiple reflections, and each layer temperature is computed, following the modelling procedure presented in the ISO 15099 [50]. The detailed window model also includes a capacity node for the glazing and the shading [63].

The ventilated window model allows implementing the cavity's inlets and outlets both towards the internal and external environment, as well as connection to the HVAC system. A window opening toward the cavity can also be defined. No enclosing elements around the cavity are considered in the calculation, except for the façade elements (glazing, frames, shading) parallel to the façade [64]. Averaged cavity-air temperatures are calculated based on the inlet temperature, mass flow and solar energy and heat transferred through the surfaces. Wind and buoyancy-driven airflows through leaks and openings can be calculated via a fully integrated airflow network model [65].

The shading layer was modelled as part of the exterior window, and it was modelled as an interior shade. Its distance was defined as measured from the external skin and set as in the experimental setup. A schedule controlled the shading's presence inside the cavity. The inlet from the indoor environment was modelled as a leak while the exhaust fan was modelled as an idealised exhaust terminal, which works as ON/OFF fan controlled by a schedule. The modeller inputs the nominal minimum and maximum airflow rate that crosses the façade, and the mass flow is controlled within that range. If the fan is ON, the airflow is the nominal maximum airflow rate. If the fan is set to OFF, the fan behaves as a leak and adopts the nominal minimum airflow rate. This value cannot be set to zero.

The convection coefficients for the indoor surfaces of the DSF are calculated choosing the greater of two methods (natural and forced airflow) calculated for each skin, regardless of the actual main driving force in the model (Table 4).

Zonal model

The DSF can also be modelled by constructing an airflow network across a series of thermal zones. The zonal model was done using three stacked zones, defining the geometry, material and openings towards the cavity through the graphical interface. The inlet to the façade was modelled as a large vertical opening with two-way flows, set as always open by mean of a schedule. The stacked zones' connection was then developed by using the advanced modelling approach.

The zones' horizontal partitions could not be modelled as transparent openings in the graphic model. The reason for this was that the surface of these partitions (0.352 m^2) was too small for the software tool to recognise them as a partitioning element (walls, ceilings, and floors that are smaller than 0.5 m^2 will be ignored in the model) which, on the one hand, caused that the partition surfaces were modelled as adiabatic surfaces, not connected with each other; on the other hand, made it impossible to add windows or openings within these partitions using the graphical interface [65]. To account for the solar radiation through horizontal openings, an element for the light distribution calculation between the surfaces in the zone is

needed (called RAY). Each surface that collaborates in the light distribution (window or opening) undergoes several coordinate transformations in order to be used in the RAY element, hence modifying and extending this set of data was a too complex task, not viable during a standard design project. Therefore each opening that was not automatically created through the graphic interface was modelled as only including the airflow connections, as a large horizontal rectangular opening with two-way flows. The solar radiation transmitted through the façade partitions was hence discarded, but the radiation was absorbed and reflected back to the zone in an equal portion (r = 0.5).

The exhaust from the façade was modelled connecting an exhaust fan to the cavity's top zone. As in the inbuilt model, the element used was an idealised exhaust terminal. Moreover, similarly to the in-built model, the shading layer was modelled as part of the external window. Hence the external cavity was not part of the airflow network. This approach simplifies the airflow patterns seen in reality (e.g. Ref. [66]), where both cavities are ventilated to some extent.

The default settings were used for the convection calculation method of the cavity thermal zone inner surfaces; the zone model uses the greater between the CDA (Ceiling Diffuser Algorithm - a function of air change rate), and the method of Brown & Isfält [52], which between predefined table values as a function of the temperature difference of the surface and the air (Table 4).

Modelling of DSF in IES VE

The model was created employing IES VE 2019. The modelling of the double-skin façade was obtained using different stacked thermal zones. The module *'Apache'* was used to assign the building's thermal properties; *'ApacheHVAC'* was used to model the AHU and the extraction fans; the *'MacroFlo'* module was used to model the openings (inlet and horizontal partitions) and the airflow through them. The occupied zone was created with five surfaces with adjacent surface temperature assigned by a schedule. The temperature inside the zone was also controlled to reach the experiment measured temperature, which was achieved utilising an AHU equipped with electric cooling and heating coils. In order to assign values from a schedule, an external module '*Ergon'* was adopted to couple the IES model. The façade was modelled as three equal stacked zones, as explained in the previous paragraphs. The horizontal partitions were modelled as horizontal windows and then set as 'holes'. Holes are entirely transparent to solar radiation, and MacroFlo treats them as open to the passage of air. The inlet opening area was set as a percentage of the bottom zone's internal glazing. An exhaust fan was applied to the top zone of the DSF to provide the requested airflow through the façade. The connection between the HVAC system's thermal zones was done by defining each stacked zone as a 'Room Component' in the ApacheHVAC module. The airflow extracted by the fan was controlled by a time switch that allowed controlling the nominal airflow and if the fan was ON or OFF. The airflow was set to a constant value and always ON. The shading device (blind) is assigned to the internal side of the external glazing system; it is not possible to define the distance from the glass.

The simulation engine 'ApacheSim' determines the building's thermal conditions by balancing sensible and latent heat flows, entering and leaving each air mass and each building surface. ApacheSim uses a stirred tank model of the air in a room. Since ApacheHVAC and MacroFlo are included, the calculations also include the mechanical and natural ventilation airflow rates calculated by these tools and the inter-dependence between these variables and those calculated within ApacheSim.

The building's inner surfaces' convection coefficient, including the DSF ones, is calculated using the Alamdari and Hammond's correlation [48].

Modelling of DSF in TRNSYS

The models were developed by using Trnsys17 and Trnsys18. There are two main approaches for modelling DSFs within the tool:

- the in-built component (complex fenestration system, *CFS – only available in version 18*)
- or the façade can be constructed tailor-made consisting of one or more connected thermal zones (it is possible to implement this approach in any version of the tool, in this paper, version 17 was used).

In-built model: "complex fenestration system"

In this work, TRNSYS (version 18) was used. The new version of the multi-zone building model Type 56 enables a detailed CFS simulation, which among other features, allows modelling mechanically ventilated gaps. Data for both models were defined through the interface TRNBuild. A single thermal zone with two windows was modelled in TRNSYS 3D Building plug-in for SketchUp. This plug-in allows defining the geometry and the boundary conditions. The glazing's thermal and optical properties were prior defined in Window 7.7. For every glazing/shading configuration, the BSDF matrixes (transmission front/back, reflection front/back and absorption per layer) was generated beforehand for the whole system in the solar and visual band. The BSDF matrixes were combined into one external file, which was imported by Type 56 during the initializing step. A specific standard created by Transso-lar is necessary to create a readable file by Type 56.

The position of the shading in the cavity is also defined in Window. It can be controlled through a schedule – following the usual control possibilities for shading devices.

The component allows to model only mechanically ventilated cavities. It is necessary to define the airflow in two cavities; during the export phase, the cavity is automatically divided into two equally wide cavities in order to model the configuration without the shading. When the shading is deployed, the two cavities have the dimensions defined in the Window 7 model. Thus, the mass flow was distributed 50/50 in the case of no shading and proportionally to the cavity width when there is the blind. The component requires setting the inlet air temperature (fixed value or a schedule), which in this case it is assumed to be equal to the zone air temperature. The model does not require any modelling of the inlet or outlet opening. The façade is modelled as an exhaust façade by choosing to transfer the convective heat flow extracted from the cavity to the outside node's cavity.

No information is required on the fans to mechanically extract the air from the ventilated cavity as these are, in practice, not modelled, and the airflow rate occurring in the cavity is always equivalent to that given value. The correlation of the heat convection coefficient for the ventilated cavity cannot be chosen or overrode. The in-built model adopts the calculation method detailed in ISO 15099 [50,67]. It is a function of the air velocity and the convective coefficient calculated for an enclosed gap (Table 4).

Zonal model

In this work, TRNSYS (version 17) was used with TNRFLOW (version 1.4), a modified version of the multi-zone building model Type 56, which

integrates the multi-zone airflow model COMIS. Data for both models were defined through the interface TRNBuild. The model geometry was defined in the TRNSYS 3D Building plug-in for SketchUp. This plug-in allows defining three zones stacked on top of each other and the adjoining room, to define boundary conditions and perform surface matching between zones. The horizontal openings were modelled as 'virtual surface', and this allowed to maintain three coupled air nodes once that the model is imported into the TRNBuild interface; in fact, the three stacked zones were merged into one thermal (radiative) zone with three air nodes at different heights. The airflow network interacts with air nodes, whereas the radiation balance is solved for thermal zones [68].

Both the air inlet and outlet to the cavity were modelled as a circular duct set to equal the experiment's opening size, and the extraction fan (connected to the outlet node) was modelled as a constant flow fan with a constant pressure curve. To connect the cavity air nodes, horizontal openings (large openings with zero height) matching the cavity dimensions were used.

By using 3D-geometry, models of short-wave direct and diffuse solar irradiance are made available to distribute solar gains entering zones through external glazing [69]. These features allowed for a detailed distribution of direct and diffuse radiation, including multiple reflections in the merged cavity zone. In the zone representing the office space, where solar radiation is only entering through adjacent windows, surface shading and solar gains distribution are simplified. In this case, the default surface distribution factors (for walls, floor and ceiling) were left unchanged. According to the software documentation, the detailed models for direct and diffuse radiation are recommended for highly glazed zones like atriums and DSFs where the distribution of solar radiation is critical but will have a lower impact on the results when shading devices are activated [33].

The shading was assigned to the external glazing layer as an interior shading device. Its position cannot be defined, but a simple fraction of additional convection to the air node can be specified instead. The amount of solar radiation absorbed by the internal shading device that is transferred to the air node by additional convection (between the inner layer pane and the internal shading device) will depend not only on the distance to the shading device but the type and height of the shading device, the geometry of the air volume between the shading device and the glazing and the actual surface and air temperatures. According to the software documentation, a value of zero represents an internal shading device located very close to the pane without any airflow in between. Typical values range between 0.3 and 0.6, and the default value of 0.5 was therefore used.

The convective coefficient of the inner surfaces of the DSF is calculated adopting the internal calculation method (Table 4), while for all the other surfaces, a default fixed value is assigned.

Public availability of models for the different software tools

In an effort to make our research freely accessible and to allow easy replication of our results, we make available, on an open-access repository, the models developed with the different simulation environments for this study. These can be found at, and referenced using, the following https://doi.org/10.5281/zenodo.4573644 [70].

References

[1] V. Huckemann, E. Kuchen, M. Leão, É.F.T.B. Leão, Empirical thermal comfort evaluation of single and double skin façades, Build. Environ. 45 (2010) 976–982, https://doi.org/10.1016/j.buildenv.2009.10.006.

[2] F. Pomponi, P.A.E. Piroozfar, R. Southall, P. Ashton, E.R.P. Farr, Energy performance of Double-Skin Façades in temperate climates: a systematic review and meta-analysis, Renew. Sustain. Energy Rev. 54 (2016) 1525–1536, https://doi.org/10.1016/j.rser.2015.10.075.

[3] C.S. Park, G. Augenbroe, T. Messadi, M. Thitisawat, N. Sadegh, Calibration of a lumped simulation model for double-skin façade systems, Energy Build. 36 (2004) 1117–1130, https://doi.org/10.1016/j.enbuild.2004.04.003.

[4] C.S. Park, G. Augenbroe, N. Sadegh, M. Thitisawat, T. Messadi, Real-time optimization of a double-skin façade based on lumped modeling and occupant preference, Build. Environ. 39 (2004) 939–948, https://doi.org/10.1016/j.buildenv.2004.01.018.

[5] Y. Wang, Y. Chen, J. Zhou, Dynamic modeling of the ventilated double skin façade in hot summer and cold winter zone in China, Build, Environ. Times 106 (2016) 365–377, https://doi.org/10.1016/j.buildenv.2016.07.012.

[6] Y. Li, J. Darkwa, G. Kokogiannakis, Heat transfer analysis of an integrated double skin façade and phase change material blind system, Build. Environ. 125 (2017) 111–121, https://doi.org/10.1016/j.buildenv.2017.08.034.

[7] A. Dama, D. Angeli, O. Kalyanova Larsen, Naturally ventilated double-skin façade in modeling and experiments, Energy Build. 114 (2017) 17–29.

[8] D. Saelens, S. Roels, H. Hens, Strategies to improve the energy performance of multiple-skin facades, Build. Environ. 43 (2008) 638–650, https://doi.org/10.1016/j.buildenv.2006.06.024.

[9] N.M. Mateus, A. Pinto, G.C. Da Graça, Validation of EnergyPlus thermal simulation of a double skin naturally and mechanically ventilated test cell, Energy Build. 75 (2014) 511–522, https://doi.org/10.1016/j.enbuild.2014.02.043.

[10] F. Pomponi, S. Barbosa, P.A.E. Piroozfar, On the intrinsic flexibility of the double skin façade: a comparative thermal comfort investigation in tropical and temperate climates, Energy Procedia 111 (2017) 530–539, https://doi.org/10.1016/j.egypro.2017.03.215.

[11] A. Gelesz, Á. Bognár, A. Reith, Effect of shading control on the energy savings of an adaptable ventilation mode double skin facade, in: 13th Conf. Adv. Build. Ski. 1-2 Oct. 2018, Bern, Switz. - Prog., 2018.

[12] Z. Eskinja, L. Miljanic, O. Kuljaca, Modelling thermal transients in controlled double skin Façade building by using renowned energy simulation engines, in: 2018 41st Int. Conv. Inf. Commun. Technol. Electron. Microelectron. MIPRO 2018 - Proc., 2018, pp. 897–901, https://doi.org/10.23919/MIPRO.2018.8400166.

[13] D. Kim, S.J. Cox, H. Cho, J. Yoon, Comparative investigation on building energy performance of double skin façade (DSF) with interior or exterior slat blinds, J. Build. Eng. 20 (2018) 411–423, https://doi.org/10.1016/j.jobe.2018.08.012.

[14] E. Taveres-Cachat, F. Favoino, R. Loonen, F. Goia, Ten questions concerning co-simulation for performance prediction of advanced building envelopes, Build. Environ. (2021), 107570, https://doi.org/10.1016/j.buildenv.2020.107570.

[15] M. Haase, F. Marques da Silva, A. Amato, Simulation of ventilated facades in hot and humid climates, Energy Build. 41 (2009) 361–373, https://doi.org/10.1016/j.enbuild.2008.11.008.

[16] C. Tabares-Velasco, P.C. Christensen, M. Bianchi, Verification and validation of EnergyPlus phase change material model for opaque wall assemblies, Build. Environ. 54 (2012) 186–196, https://doi.org/10.1016/j.buildenv.2012.02.019.

[17] M. Barclay, N. Holcroft, A.D. Shea, Methods to determine whole building hygrothermal performance of hemp-lime buildings, Build. Environ. 80 (2014) 204–212, https://doi.org/10.1016/j.buildenv.2014.06.003.

[18] R.H. Henninger, M.J. Witte, D.B. Crawley, Analytical and comparative testing of EnergyPlus using IEA HVAC BESTEST E100-E200 test suite, Energy Build. 36 (2004) 855–863, https://doi.org/10.1016/j.enbuild.2004.01.025.

[19] J. Neymark, R. Judkoff, G. Knabe, H.-T. Le, M. Dürig, A. Glass, G. Zweifel, Applying the building energy simulation test (BESTEST) diagnostic method to verification of space conditioning equipment models used in whole-building energy simulation programs, Energy Build. 34 (2002) 917–931, https://doi.org/10.1016/S0378-7788(02)00072-5.

[20] E. Catto Lucchino, F. Goia, G. Lobaccaro, G. Chaudhary, Modelling of double skin facades in whole-building energy simulation tools: a review of current practices and possibilities for future developments, Build. Simul. 12 (2019) 3–27, https://doi.org/10.1007/s12273-019-0511-y.

[21] O. Kalyanova, P. Heiselberg, C. Felsmann, H. Poirazis, P. Strachan, A. Wijsman, An empirical validation of building simulation software for modelling of doubleskin facade (DSF), in: Elev. Int. IBPSA Conf., Glasgow, Scotland, 2009.

[22] A. Gelesz, E. Catto Lucchino, F. Goia, A. Reith, V. Serra, Reliability and sensitivity of building performance simulation tools in simulating mechanically ventilated double skin facades, in: V. Corrado, A. Gasparella (Eds.), Proc. Build. Simul. 2019 16th Conf, IBPSA, Rome, 2019.

[23] Energy Plus, EnergyPlus 9.1 Engineering Reference: the Reference to EnergyPlus Calculations, 2019, pp. 1–847, doi.org/citeulike-article-id:10579266.

[24] V.M. Soto Francés, E.J. Sarabia Escriva, J.M. Pinazo Ojer, E. Bannier, V. Cantavella Soler, G. Silva Moreno, Modeling of ventilated façades for energy building simulation software, Energy Build. 65 (2013) 419–428, https://doi.org/10.1016/j.enbuild.2013.06.015.

[25] D.-W. Kim, C.-S. Park, Difficulties and limitations in performance simulation of a double skin façade with EnergyPlus, Energy Build. 43 (2011) 3635–3645, https://doi.org/10.1016/j.enbuild.2011.09.038.

[26] W. Choi, J. Joe, Y. Kwak, J.H. Huh, Operation and control strategies for multi-storey double skin facades during the heating season, Energy Build. 49 (2012) 454–465, https://doi.org/10.1016/j.enbuild.2012.02.047.

[27] N. Papadaki, S. Papantoniou, D. Kolokotsa, A parametric study of the energy performance of double-skin façades in climatic conditions of Crete, Greece, Int. J. Low Carbon Technol. 9 (2013) 296–304, https://doi.org/10.1093/ijlct/cts078.
[28] A.S. Anđelković, I. Mujan, S. Dakić, A.S. Andelković, I. Mujan, S. Dakić, Experimental validation of a EnergyPlus model: application of a multi-storey naturally ventilated double skin façade, Energy Build. 118 (2016) 27–36, https://doi.org/10.1016/j.enbuild.2016.02.045.
[29] A.B. Equa, IDA Indoor Climate and Energy 4.0 EQUA Simulation AB, 2009.
[30] E. Colombo, M. Zwahlen, M. Frey, J. Loux, Design of a glazed double-façade by means of coupled CFD and building performance simulation, Energy Procedia 122 (2017) 355–360, https://doi.org/10.1016/j.egypro.2017.07.337.
[31] V.E. Ies, ApacheSim User Guide, IES VE User Guid, 2014.
[32] E.A. Pekdemir, R.T. Muehleisen, A parametric study of the thermal performance of double skin façades at different climates using annual energy simulation, Fifth Natl. Conf. IBPSA, 2012, pp. 211–218, https://doi.org/10.1016/j.ijrobp.2008.07.056.
[33] Trnsys 17, Multizone Building modeling with Type56 and TRNBuild 5 (2013) 1–79.
[34] D. Saelens, S. Roels, H. Hens, The inlet temperature as a boundary condition for multiple-skin facade modelling, Energy Build. 36 (2004) 825–835, https://doi.org/10.1016/j.enbuild.2004.01.005.
[35] U. Eicker, V. Fux, U. Bauer, L. Mei, D. Infield, Facades and summer performance of buildings, Energy Build. 40 (2008) 600–611, https://doi.org/10.1016/j.enbuild.2007.04.018.
[36] F.P. López, R.L. Jensen, P. Heiselberg, M. Ruiz de Adana Santiago, Experimental analysis and model validation of an opaque ventilated facade, Build. Environ. 56 (2012) 265–275, https://doi.org/10.1016/j.buildenv.2012.03.017.
[37] C. Aparicio-Fernández, J.L. Vivancos, P. Ferrer-Gisbert, R. Royo-Pastor, Energy performance of a ventilated façade by simulation with experimental validation, Appl. Therm. Eng. 66 (2014) 563–570, https://doi.org/10.1016/j.applthermaleng.2014.02.041.
[38] H. Elarga, A. Zarrella, M. De Carli, Dynamic energy evaluation and glazing layers optimization of façade building with innovative integration of PV modules, Energy Build. 111 (2016) 468–478, https://doi.org/10.1016/j.enbuild.2015.11.060.
[39] I. Khalifa, L.G. Ernez, E. Znouda, C. Bouden, Coupling TRNSYS 17 and CONTAM: simulation of a naturally ventilated double-skin facade, Adv. Build. Energy Res. 9 (2015) 293–304, https://doi.org/10.1080/17512549.2015.1050694.
[40] I. Khalifa, L. Gharbi-Ernez, E. Znouda, C. Bouden, Assessment of the inner skin composition impact on the double-skin façade energy performance in the mediterranean climate, Energy Procedia 111 (2017) 195–204, https://doi.org/10.1016/j.egypro.2017.03.021.
[41] M. Shahrestani, R. Yao, E. Essah, L. Shao, A.C. Oliveira, A. Hepbasli, E. Biyik, T. del Cano, E. Rico, J.L. Lechòn, Experimental and numerical studies to assess the energy performance of naturally ventilated PV facade systems, Sol. Energy 147 (2017) 37–51, https://doi.org/10.1016/j.solener.2017.02.034.
[42] M. Hiller, J. Merk, P. Schöttl, Complex Fenestration Systems Tutorial, 2017, pp. 1–22.
[43] V. Leal, E. Erell, E. Maldonado, Y. Etzion, Modelling the SOLVENT ventilated window for whole building simulation, Build. Serv. Eng. Technol. 25 (2004) 183–195, https://doi.org/10.1191/0143624404bt103oa.
[44] A. Gelesz, Sensitivity of exhaust-air façade performance prediction to modelling approaches in IDA ICE, Int. Rev. Appl. Sci. Eng. 10 (2019) 241–252.
[45] J.A. Clarke, Energy Simulation in Building Design, Adam Hilger Ltd., Bristol & Boston, 1985.
[46] A.B. Equa Simulation, IDA Indoor Climate and Energy [Computer Software] Version: 4.8 SP1, 2018.
[47] W.H. McAdams, Heat Transmission, McGraw-Hill, Kogakusha, Tokyo, Japan, 1954.
[48] F. Alamdari, G. Hammond, Improved data correlation for buoyancy-driven convection in rooms, Build. Serv. Eng. Technol. 4 (1983) 106–112.
[49] TRNSYS 17, mathematical reference, TRNSYS Doc 4 (2009) 1–486.
[50] International Organisation for Standardisation, ISO 15099:2003 Thermal Performance of Windows, Doors and Shading Devices - Detailed Calculations, 2003.
[51] K. Goldstein, A. Novoselac, Convective heat transfer in rooms with ceiling slot diffusers (rp-1416), HVAC R Res. 16 (2010) 629–655, https://doi.org/10.1080/10789669.2010.10390925.
[52] G. Brown, E. Isfält, Solinstrålning Och Solavskärmning (Solar Irradiation and Sun Shading Devices) - Report 19, 1974. Stockholm.
[53] VDI Heat Atlas, 2010, https://doi.org/10.1007/978-3-540-77877-6.
[54] F. Goia, V. Serra, Analysis of a non-calorimetric method for assessment of in-situ thermal transmittance and solar factor of glazed systems, Sol. Energy 166 (2018) 458–471, https://doi.org/10.1016/j.solener.2018.03.058.
[55] F. Goia, L. Bianco, M. Perino, V. Serra, Energy performance assessment of and advanced integrated facade through experimental data analysis, Energy Procedia 48 (2014) 1262–1271, https://doi.org/10.1016/j.egypro.2014.02.143.
[56] D.T. Reindl, W.A. Beckman, J.A. Duffie, Diffuse fraction correlations, Sol. Energy 45 (1990) 1–7, https://doi.org/10.1016/0038-092X(91)90123-E.
[57] R. Perez, R. Stewart, R. Seals, T. Guertin, The development and verification of the Perez diffuse radiation model, Sandia National Laboratories Albuquerque, New Mexico (USA), Report nr. SAND88-7030 (1988), https://doi.org/10.2172/7024029.
[58] F. Kasten, G. Czeplak, Solar and terrestrial radiation dependent on the amount and type of cloud, Sol. Energy 24 (1980) 177–189, https://doi.org/10.1016/0038-092X(80)90391-6.
[59] M. Martin, P. Berdahl, Characteristics of infrared sky radiation in the United States, Sol. Energy 33 (1984) 321–336.
[60] ASHRAE, ASHRAE Guideline 14 - Measurement of Energy, Demand, and Water Savings, 2014.
[61] T.P. Mcdowell, D.E. Bradley, M. Hiller, J. Lam, J. Merk, Trnsys 18 : the continued evolution of the software. IBPSA 2017- Proc, 15th IBPSA Conf., 2017, pp. 1922–1930.
[62] U.S. Department of Energy, Engineering Reference, 8.8, 2017.
[63] J. Hensen, M. Barták, F. Drkal, Modeling and simulation of a double-skin façade system, Build. Eng. 108 (2002) 461–471, https://doi.org/10.1197/jamia.M1103.
[64] Equa Simulation AB, IDA –Indoor Climate and Energy Ver 3.0 NMF-Model Documentation, ((n.d.)).
[65] A.B. Equa, EQUA Simulation AB User Manual IDA Indoor Climate and Energy, 2013.
[66] D. Saelens, Energy Performance Assessment of Single Storey Multiple-Skin Facades, 2002 doi.org/Ph. D. thesis.
[67] M. Hiller, P. Schöttl, MODELLIERUNG KOMPLEXER VERGLASUNGSSYSTEME IN TRNSYS, BauSIM, 2014.
[68] M. Hiller, S. Holst, T. Welfonder, A. Weber, M. Koschenz, TRNFLOW: Integration of the Airflow Model COMIS into the Multizone Building Model of TRNSYS, TRANSSOLAR Energietechnik Gmbh, 2002.
[69] J. Aschaber, M. Hiller, R. Weber, Trnsys 17: New Features of the Multizone Building Model, vol. 2009, Ipbsa, 2009, pp. 1983–1988.
[70] E. Catto Lucchino, A. Gelesz, K. Skeie, G. Gennaro, A. Reith, V. Serra, F. Goia, Models for Mechanically Ventilated Single-Story Double Skin Façade, 2021, https://doi.org/10.5281/zenodo.4573644.

5 Validation and inter-software comparison of a naturally ventilated single-story DSF

P4 *G. Gennaro, E. Catto Lucchino, F. Goia, F. Favoino. Modelling double skin façades (DSFs) in whole-building energy simulation tools: validation and inter-software comparison of naturally ventilated single-story DSFs. Building and Environment – under revision*

Building energy simulation (BES) tools offer the possibility to integrate double skin façade (DSF) technologies into whole building simulation through dedicated modules or possible workarounds. However, the reliability of such tools in predicting the dynamic heat and mass transfer processes within the DSFs is still to be determined. Therefore, this paper aims to assess the performance of four popular BES tools (i.e., EnergyPlus, TRNSYS, IDA-ICE and IES-VE) in predicting the thermal behaviour of a one-storey naturally ventilated DSF in three different ventilation modes. To evaluate their capability to predict thermophysical quantities, we compared the simulation results with experimental data. The results show that it is not possible to identify a tool that outperforms the others for all the analysed quantities, especially for the cavity air temperature, which is the least accurate parameter in all software due to underestimation of the daytime peak. IES-VE seems to be most accurate for Supply Air and Thermal Buffer modes when shading is deployed, while EnergyPlus appears most accurate for Outdoor Air Curtain mode. When it comes to surface temperatures and transmitted solar radiation, TRNSYS appears to be the best-performing software. In addition, this study investigated the challenges that designers may face when modelling a naturally ventilated DSF using whole-building simulation tools. Moreover, the investigation elucidates the challenges that have a more significant effect on the performance of the BES tools in order to reinforce their reliability

Building and Environment 231 (2023) 110002

Contents lists available at ScienceDirect

Building and Environment

journal homepage: www.elsevier.com/locate/buildenv

Modelling double skin façades (DSFs) in whole-building energy simulation tools: Validation and inter-software comparison of naturally ventilated single-story DSFs

Giovanni Gennaro [a,b], Elena Catto Lucchino [c], Francesco Goia [c], Fabio Favoino [a,*]

[a] Department of Energy, Technology Energy Building Environment Research Group, Politecnico di Torino, Torino, Italy
[b] Institute for Renewable Energy, EURAC Research, Bolzano, Italy
[c] Department of Architecture and Technology, Norwegian University of Science and Technology, NTNU, Trondheim, Norway

ARTICLE INFO

Keywords:
Inter-software comparison
Empirical validation
Double skin façade
Naturally ventilated cavities
EnergyPlus
TRNSYS
IDA-ICE
IES-VE

ABSTRACT

Building energy simulation (BES) tools offer the possibility to integrate double skin façade (DSF) technologies into whole building simulation through dedicated modules or possible workarounds. However, the reliability of such tools in predicting the dynamic heat and mass transfer processes within the DSFs is still to be determined. Therefore, this paper aims to assess the performance of four popular BES tools (i.e. EnergyPlus, TRNSYS, IDA-ICE and IES-VE) in predicting the thermal behaviour of one-storey naturally ventilated DSF in three different ventilation modes. To evaluate their capability to predict thermophysical quantities, we compared the simulation results with experimental data. The results show that it is not possible to identify a tool that outperforms the others for all the analysed quantities, especially for the cavity air temperature, which is the least accurate parameter in all software due to underestimation of the daytime peak. IES-VE seems to be most accurate for Supply Air and Thermal Buffer modes when shading is deployed, while EnergyPlus appears most accurate for Outdoor Air Curtain mode. When it comes to surface temperatures and transmitted solar radiation, TRNSYS appears to be the best-performing software. In addition, this study investigated the challenges that designers may face when modelling a naturally ventilated DSF using whole-building simulation tools. Moreover, the investigation elucidates the challenges that have a more significant effect on the performance of the BES tools in order to reinforce their reliability.

1. Introduction

Double skin façades (DSFs) are complex fenestration systems that are designed to actively pursue different building performance objectives, such as thermal and acoustic insulation, ventilation, energy-saving and daylighting. They consist of two parallel transparent façade layers, of single or multiple glazing units, delimiting an air cavity which can offer different ventilation modes between the outdoor and indoor environment, depending on the available openings, while integrating operable solar shading devices. A DSF cavity can be either naturally or mechanically ventilated, and different airpaths can be adopted, depending on the cavity opening configurations and operations: in thermal buffer (TB) mode, it is only operated as a buffer space between the indoor and outdoor; in supply air (SA) and indoor air curtain (IAC) mode, the DSF cavity is used to pre-heat air from the outdoor and indoor environment, respectively, before supplying it to the indoor environment; in outdoor air curtain (OAC) and exhaust air (EA) mode, the DSF is used to reduce the cooling energy needs by exhausting to the outdoor environment the cavity air that entered the cavity from either the outdoor or indoor environment, respectively, thereby removing unwanted solar gains. As far as visual comfort is concerned, the cavity integrated shading device, interacting with the cavity ventilation, can be operated to increase daylight distribution while avoiding glare and overheating. The operational performance of a DSF depends, therefore, on how the different elements are integrated and operated through dedicated control strategies [1,2].

The ventilation in the DSF's cavity is a complex phenomenon, particularly for naturally ventilated cavities, as the temperatures and velocity fields are influenced simultaneously by thermal, optical and fluid-dynamic processes. The airflow in the cavity depends on both wind and buoyancy-driven air movement, which is largely affected by the

* Corresponding author.
E-mail address: fabio.favoino@polito.it (F. Favoino).

https://doi.org/10.1016/j.buildenv.2023.110002
Received 19 September 2022; Received in revised form 16 December 2022; Accepted 9 January 2023
Available online 18 January 2023

Acronym list

BES	building energy simulation
DAQ	data acquisition
DSF	double skin facade
E+	EnergyPlus
EA	exhaust air
ELA	effective leakage area
EMS	energy management system
IAC	indoor air curtain
OAC	outdoor air curtain
MBE	mean bias error
RMSE	root mean squared error
SA	supply air
shOFF	shading is off (up)
shON	shading is on (down)
TB	thermal buffer
TRN	TRNSYS

Nomenclature

ee	External surface of external glazing
ei	Internal surface of external glazing
exh	exhaust
g	solar factor (−)
gap	cavity
ie	External surface of internal glazing
ii	Internal surface of internal glazing
in	Inlet
int	Internal
λ	thermal conductivity of air (W/(m·K))
n	Total number of measurements
out,V	Outdoor vertical
out,H	Outdoor horizontal
ρ_{in}	glazing solar reflectance, inner face (−)
ρ_{out}	glazing solar reflectance, outer face (−)
s	thickness (mm)
S	Irradiance (W/m^2)
τ_{sol}	glazing solar transmittance (−)
T	Temperature (°C)
U	glass thermal transmittance (W/(m^2·K))
U_f	frame thermal transmittance (W/(m^2·K))
X_m	Measured value
X_p	Predicted value

cavity and vent geometries, by the properties of the glazing confining the cavity, and by the properties, geometry, and operations of the shading device. Furthermore, such complex fluid-dynamic phenomena greatly affect the heat exchange within the cavity, thus influencing cavity air and exhaust temperature, cavity and indoor surface temperatures, and long-wave transmitted solar radiation through the DSF towards the indoor environment.

Building Energy Simulation (BES) tools offer the possibility to integrate component-level advanced façade modelling into whole building simulation [3] to study the performance of DSFs under building operation conditions. Nevertheless, just a few of these tools include dedicated modules to model DSF technologies. Thus, modelling workarounds are often necessary. For example, Choi et al. [4] used EnergyPlus to model the operation of a multi-storey natural DSF in TB or SA mode during the heating season. The model was calibrated using experimental data related to the façade temperatures (cavity air, surface temperature of the glazing skins), and the validation results showed good agreement between the predicted and measured values, especially for the inside surface temperature of the inner glazing skin. Khalifa et [5]. investigated the impact of the inner layer composition in a double-skin façade system on the energy loads for conditioning office buildings. The parametric simulation was performed with TRNSYS by varying the glazing type and the glazing area of the inner surface of the naturally ventilated DSF installed on an office building in Tunis (Mediterranean climate). The authors observed that the implications of the various inner skin compositions differ according to the season. For example, double-glazing units reduce the cooling requirements in the hot period by 10%, while single-glazing units perform well in winter.

A series of studies evaluated BES tools' performance [6–9] in simulating DSFs using different methodologies and approaches. However, the accuracy of the different models implemented in the different software tools in describing the dynamic heat and mass transfer processes within DSFs remains largely unknown [10]. This uncertainty is also due to the lack of a homogeneous assessment of the performance of the different software. Notably, there are differences in the use of experimental datasets, façade systems, operational modes, and simulation settings. This greatly reduces the generalisation of the analyses and makes it nearly impossible to compare the performance of the different simulation environments.

This study builds upon previous research [11], where the reliability of four popular BES tools (EnergyPlus, TRNSYS, IDA-ICE and IES-VE, which together cover the vast majority of BES users [12]) in modelling an exhaust-air façade in mechanical ventilation mode (climate façade) was analysed. The present work aims to investigate the performance of the same BES tools in describing the thermal behaviour of a one-storey naturally ventilated DSF, in different airpath modes, by means of experimental validation at façade level. In addition, this work seeks to discuss the challenges that researchers and designers may face when modelling a naturally ventilated DSF using BES tools to reinforce confidence in the performance analysis of buildings integrating such façade systems and highlight directions for model development.

Section 2 presents the main modelling approaches and challenges for naturally ventilated DSFs. Section 3 describes the methodology adopted for the experimental validation and inter-software comparison. Section 4 presents the validation results by comparing main DSF physical quantities from uncalibrated BES models with experimental data. Finally, in Section 5, we reflect on the modelling challenges presented in Section 2 and discuss the impact of specific model parameters.

2. Practices and challenges in modelling naturally ventilated DSFs in BES tools

2.1. Modelling processes

Multiple airflow paths could be adopted in a DSF, and the airflow characteristics depend on the interplay between the outdoor and indoor environmental conditions and the various operational modes. The airflow influences the cavity air temperature profile and the cavity surface temperatures (glass pane temperatures adjacent to the cavity) and is responsible for the convective heat exchange between the cavity and the cavity air. In turn, these variables influence the airflow characteristics, making the problem of simulating the naturally-driven airflow more complex than for DSFs where the airflow is mechanically induced.

Two different approaches exist for modelling DSFs in BES tools (Fig. 1): (i) the "zonal approach", in which thermal and airflow networks are combined to discretise the ventilated cavity in one or more nodes, each corresponding to one zone of the model; (ii) the "in-built component" approach, which consists of a dedicated sub-routine model developed for transparent ventilated façades. In the case of natural

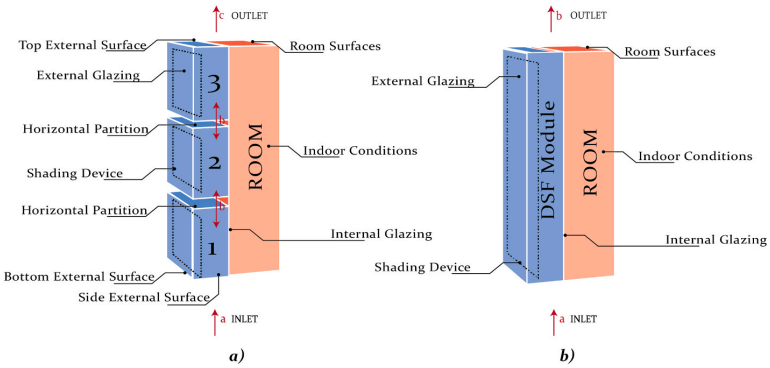

Fig. 1. Zonal (a) versus in-built component (b) approach. Shading device is not drawn for clarity.

ventilation, the zonal approach is the most adopted, especially for multi-storey double-skin façades [13], and it can be implemented in all BES tools by dividing the DSF into several stacked zones linked together to create the airflow network. On the other hand, the in-built component approach can only be implemented in IDA-ICE [14] (among the analysed BES tools) for naturally ventilated DSFs by means of the sub-routine *"Double Glass Façade"*. Similarly, the in-built component models available in EnergyPlus [15] and TRNSYS [16] (*"Airflow Window"* and *"Complex Fenestration System"* module, respectively) can only be used to model mechanically ventilated cavities.

The airflow networks of EnergyPlus and IES-VE [17] are based on the AIRNET model [18], while TRNSYS [19] and IDA-ICE use the COMIS-based model [20]. In all the models, the driving force of the air movement through the airflow network is the pressure difference that occurs due to the combined action of wind pressure and the balance between buoyancy and gravitational forces. While all the models use a general power-law equation to predict flow through cracks and openings, there are differences in the way they deal with the air temperature. In fact, this may change due to heat transfer with the surrounding building fabric (inner and outer skin of the DSF) as the air moves through the cavity. This physical phenomenon affects both the density and viscosity of the air and, consequently, the magnitude of the flow and how this is estimated. Generally speaking, analyses carried out in the past [20] have shown that COMIS and AIRNET lead to similar results in modelling multizone air flows. Thus, there is no ground to assume that one of the two architectures is superior. Different air link components (e.g. cracks, leakage areas, or openings) can be used to link the nodes, each with its mass flow equation as a function of pressure difference, governed by Bernoulli's equation. Based on the relationship between airflow rate and pressure drop for each component, Newton's method is used to solve for the air pressure at each node iteratively until the convergence criteria based on the conservation of air mass flow rate is reached.

The biggest uncertainty in modelling a naturally ventilated DSF in the context of BES tools lies in whether or not the physical-mathematical models adopted to represent airflow and thermal network at the level of the entire building are suitable to represent the physical phenomena occurring in the DSF. In some situations, co-simulation could be technically expedient to solve this problem as it provides an integrated approach to combine different levels and approaches in building simulation by coupling BES tools with component-level models that are based on more detailed physical-mathematical representations [21]. For example, CONTAM [22], a successor of the AIRNET model (as the Airflow Network Model), provides some advantages over EnergyPlus when modelling airflows as it includes a more extensive set of air leakage component models and the ability to define multiple airflow leakage points within a given surface [23]. In the literature, a number of simulation studies of DSF demonstrate the coupling of CONTAM with EnergyPlus [23,24] and TRNSYS [25]. For example, Khalifa et al. [25] applied the co-simulation between TRNSYS and CONTAM to assess the performance in predicting the temperature evolution and the airflow rates into naturally ventilated DSFs, and obtained good agreement between simulation and experimental data using a six nodes airflow network.

When modelling DSFs in BES tools, different modelling assumptions are required, linked both to how to model the façade (i.e., cavity zoning, airflow network design, inlet-outlet opening modelling) and to the type of physical mechanisms occurring inside the ventilated cavity (i.e., wind pressure coefficients, convective heat transfer coefficients, specific heat capacity of glazed systems). Thus, the modelling assumptions are not straightforward, and they became challenges for modellers of naturally ventilated DSFs.

2.2. Modelling assumptions and limitations

Different challenges and intrinsic limitations exist for both approaches (airflow network and in-built component modelling). For the in-built component approach, ad-hoc equations are implemented in the tools able to describe physical phenomena occurring in the ventilated façade. The related parameters and algorithms (e.g., convective heat transfer, solar distribution inside the cavity and pressure drops) are (usually) implemented for a specific type of facade. On the contrary, the zonal approach is more general, as it is meant to model natural air movement throughout the whole building. Nevertheless, DSF parameters for the latter approach are derived and validated at the room (or zone) level, making it more challenging to adopt, as introduced in this section and discussed further in Section 5.

In the zonal approach, the DSF is usually divided into several stacked thermal zones (consisting of the network nodes) linked to the overall thermal and airflow network of the whole building by means of the outlet and/or inlet zones. There is no standardised approach in discretising the number of staked zones, usually ranging from one to six stacked zones for a single-story DSF [12]. In most published studies, the DSF cavity is modelled as three stacked zones per floor [12,26], consisting of the inlet, main cavity and outlet zones. Setting more or less thermal zones to represent the air conditions in the cavity is a choice that usually depends on the complexity of the façade and the desired detail of the outcomes (e.g., the study of the air stratification inside the DSF cavity).

In the zonal approach, the proper design of the airflow network is essential when it comes to modelling a cavity airflow path which connects the cavity to an adjacent zone of the building (e.g. SA, IAC and EA modes) in order to balance the pressure distribution throughout the whole network, as it determines the airflow direction affecting the

facade thermal behaviour. Nevertheless, one of the governing hypotheses of the airflow network in BES tools is that the apertures connecting the airflow nodes are small compared to the space connected (e.g., doors, windows and louvres), which poorly approximates the conditions of a DSF, where the characteristic size of the opening is of the same magnitude as the cavity section, and thus distributed pressure losses along the cavity cannot be considered as negligible. Therefore, in order to achieve a good model formulation, it is necessary to make appropriate adjustments, such as adding narrowings along the cavity in order to distribute pressure losses throughout the cavity or adopting a fictitious airflow resistance due to the obstruction in the cavity, such as shading devices.

The driving forces of the airflow network are the natural stack effect and wind pressure. All BES tools allow the user to define the different surface averaged pressure coefficients to calculate the wind pressure on the different external surfaces by implementing Bernoulli's formulation described in the ASHRAE Fundamentals (2001) [27]. The wind pressure coefficients may be obtained by various means (measurements, CFD studies and wind tunnel experiments), though the modeller does not have access to these data in most cases. Thus, generally, the coefficients employed in the calculations are the ones available in the tool adopted: Energy Plus and TRNSYS refer to ASHRAE Fundamentals values, while IDA-ICE and IES-VE refer to the results of the wind tunnel experiment from the AIVC publication [28]. Except for IES-VE, the tools differentiate the coefficients according to the exposure type (exposed, semi-exposed and sheltered), while IES-VE also takes into account the geometry of the building (low-rise, high rise) and the building surface (short or long wall).

The inlet and outlet openings of the DSF are considered an obstacle to the free movement of the air, and are therefore seen as creating a pressure drop. Additionally, in large openings, the airflow has a vertical velocity profile, which depends on the different air densities as a function of the height. It is best practice in BES tools to use non-linear equations to calculate the flow as a function of the pressure difference through the openings, depending on the opening geometry. Small openings are modelled by the Effective Leakage Area (ELA) or the crack method. The ELA method is implemented in EnergyPlus and IDA-ICE (where both approaches are available), and the complexity of using this method is the estimation of the ELA value to employ. The leakage area values available in the ASHRAE Fundamental for different building component types [29] refer only to a few standard window typologies and do not fit the openings usually installed in a DSF. The latter is also used to model the air infiltration due to the airtightness of the openings; thus, the modeller is required to insert the mass flow and exponent coefficient, which are usually unknown and are not easily found in the literature [10]. More complex formulations considering the airflow in both directions are used for large openings. In all tools, they are treated as sharp-edged orifices, where the mass flow is a function of the equivalent orifice area of the opening and its discharge coefficient. In most tools, the responsibility to define this correlation is left to the modeller, while TRNSYS and IES-VE implement correlations for several opening typologies (sliding doors, side, top and bottom hinged windows). Conversely, most tools allow the definition of the discharge coefficient freely, while in IES-VE, this is fixed to 0.62. Nevertheless, these models were developed to evaluate natural ventilation in buildings and are therefore validated for standard components (e.g., doors and windows) and not for specific ones such as ventilation openings of DSFs.

In the cavity, different heat flow patterns will occur with changing temperatures and varying positions of the ventilation openings and solar shading (e.g., blind slats angle). From the thermal network point of view, the convective heat exchange process between airflow and glass panes enclosing the cavity and between airflow and solar shading surface (if any) is exceedingly difficult to model correctly [10]. EnergyPlus offers a selection of different methods to calculate the interior heat transfer coefficient. The most widely used method is the "adaptive algorithm", which chooses the correct correlation for the convective coefficients based on the classification of surfaces and the flow regime. In the natural regime, the coefficient is calculated according to the Standard ISO 15099 [30]. In TRNSYS, it is possible to choose between variable coefficients derived from empirical equations (provided by the user) or the internal calculation method, which uses the ASHRAE Vertical Wall algorithm, whereas IES-VE adopts Alamdari and Hammond's correlation [31]. As for previous parameters (concentrated and distributed pressure losses), these correlations were developed and validated for room conditions, where the effects of the other surfaces' temperature are negligible and do not impact the flow of the analysed surface. In DSFs, however, the aspect ratio of the cavity section is orders of magnitude different than room geometries (even more so when the shading is present in the cavity). Therefore, replicating the physical behaviour of DSF cavities may require different empirical correlations than those used to model convective heat and mass transfer for conventional rooms.

Cavity shading is usually assigned to one of the two glazing systems of the DSF, as an internal or external shading device, and only the part of the cavity between the shading and the corresponding glazing layer is considered ventilated. Convective heat exchange coefficients for shading devices are also usually derived from configurations with geometrical features and thermal gradient fields far from those seen in a DSF (i.e., internal blinds), potentially leading to inaccuracy in predicting how heat is released to the cavity airflow from the shading device.

Finally, the thermal mass of the materials is usually considered when modelling opaque envelopes but not when modelling glazed ones. This legacy originated when glazed surfaces were often limited in size and weight (e.g., with single-glass panes). However, DSFs are multi-layered glazed structures that usually cover large façade areas and adopt rather thick glass panes for safety and structural reasons. The combination of these two conditions leads to the fact that the inertial features of DSFs might not be negligible, especially when it comes to the prediction of the temperature of the indoor-facing surface of the inner skin. With the exception of IDA-ICE, the analysed tools do not consider the thermal mass of the glazing system [12].

3. Methodology

In this section, the characteristics of the DSF mock-up used for the validation are presented together with the related experimental campaign, and the methodology followed for the model validation. In addition, how the DSF was modelled in the different BES tools is briefly discussed, leaving the details of each DSF model for a specific BES tool in Appendix A, for the sake of readability.

3.1. Case study DSF and experimental campaign

The DSF mock-up is a single-story facade developed to modulate to the maximum extent the overall heat transfer between the indoor and outdoor environment. It consists of two parallel transparent skins with an aluminium framing system as schematised in Fig. 2. Both inner and outer skins present an equally sized (1.22 m width and 2.00 m high) double glazing unit made of a 6 mm outer clear glass pane, a 16 mm cavity filled with a gas mixture of air and Argon at 90% and a 6 mm inner clear glass plane, with low-E coating on surface 3 and 2, the inner and outer surface of the cavity respectively (cf. Fig. 2 for details of the thermal and optical properties of the DSF components). The parallel skins form a 250 mm thick ventilated air cavity containing a controllable light grey roller curtain located at the centre of the cavity. Four pivoted opaque ventilation openings (1.5 m × 0.5 m) are placed on the inner (bottom and top) and outer (bottom and top) skin, controlled by its linear actuator (openable up to 45°). Thus, this prototype can adopt all the possible airpath configurations achievable by a DSF (cf. Fig. 2): Thermal Buffer (TB, all vents closed), Outdoor Air Curtain (OAC, vent 1 and 2 open), Supply Air (SA, vent 1 and 3 open), Exhaust Air (EA, vent 4 and 2 open), and Indoor Air Curtain (IAC, vent 4 and 3 open).

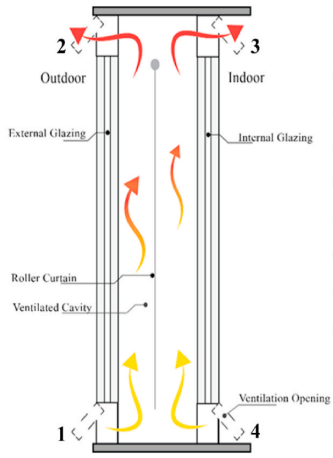

	Ext.Glazing	Shading	Cavity	Int. Glazing
Type	Double glazing – lowE inner glass	Roller curtain	Ventilated	Double glazing – lowE inner glass
s [mm]	29	1	250	29
τ_{sol} [-]	0.55	0.03	-	0.55
ρ_{out} [-]	0.20	0.30	-	0.20
ρ_{in} [-]	0.07	0.30	-	0.07
U [W/m²K]	1.21	-	-	1.21
g [-]	0.58	-	-	0.58
U_f [W/m²K]	1.50	-	-	1.50

1 Outdoor inlet **2** Outdoor outlet **3** Indoor outlet **4** Indoor inlet

1→2	Outdoor Air Curtain - **OAC**	**1→3**	Supply Air - **SA**
4→3	Indoor Air Curtain - **IAC**	**4→2**	Exhaust Air - **EA**
All openings closed		Thermal Buffer - **TB**	

Fig. 2. Schematic section and physical properties of the double skin façade prototype.

The DSF prototype was installed in the south-exposed facade of the TWINS (Testing Window INnovative Systems) outdoor test cell facility of the Polytechnic University of Turin (45 N° latitude 7.4° E longitude), where the monitoring campaign was carried out for several months to fully characterise the performance of the DSF in different airpath configurations and under different boundary condition. The monitoring system acquired the following quantities (Fig. 3): temperatures inside the DSF cavity (one at the inlet, one at the outlet and four at different heights inside the cavity); indoor and outdoor air temperatures; inner and outer surface temperature values for each glazing (2 for each side); test cell average surface temperatures; air speed inside the cavity (at different heights); total vertical solar radiation incident on and transmitted through the facade. Weather data were recorded by integrating the campus weather station (nearby the outdoor test facility) and the local one logging outdoor dry-bulb air temperature and relative humidity, atmospheric pressure, global horizontal solar irradiance, wind velocity and direction.

Measuring air speed in naturally ventilated cavities for continuous monitoring is still challenging [32], and within this campaign, the measuring range was, most of the time, of the same order of magnitude as the accuracy of the hot-wire anemometers; therefore, we decided to exclude this variable in the validation study. Moreover, best practices established in the literature were adopted to reduce the influence of solar irradiance on the measurement of temperature physical quantities [33,34]. Due to the cones adopted to shield the pyranometers from internal reflections, which may reduce the accuracy of the measurements in the early morning and late afternoon, it was decided to filter the irradiances to calculate model performance indicators for this variable by considering only the central hours of the day (from 11:00 to 15:00).

After calibration and verification, the accuracy of the entire measurement chain linked to façade-level physical quantities was: ±0.5 °C for thermocouples, ±0.3 °C for thermal resistances and ±5% for pyranometers.

During the monitoring campaign, the DSF mock-up was operated with different air paths and shading device configurations (positions and types). For validation purposes, it is interesting to investigate the performance of software prediction in the most heterogeneous conditions – in terms of boundary conditions (seasonality, sunny and cloudy days, warm and cold days) and façade configurations. Based on these considerations, three ventilation paths – thermal buffer (TB), outdoor air curtain (OAC), and supply air (SA) – were selected and combined with two shading states; roller screen in position up and down. TB refers to the façade configuration where all the ventilation openings are closed, and there is no mass exchange between the cavity and the surrounding environments. In both OAC and SA, outdoor air enters the cavity but is released towards the outside (OAC) or the inside of the test cell (SA). Fig. 4 displays the boundary conditions (outdoor and indoor air temperatures and global horizontal irradiance) for each configuration; the chosen representative day for the analysis of each dataset is highlighted with a grey background. The cell's indoor air temperature setpoint was set to 20 °C in winter (for SA and TB modes) and 26 °C in summer (OAC mode).

3.2. DSF model implementation and simulation in BES tools

The primary purpose of this investigation was to compare the performance of the different BES tools to replicate the thermophysical behaviour of a single-story naturally ventilated cavity. For this reason, the evaluation was focused on the physical quantities related to the DSF and not on the room-level physical quantities (e.g., indoor air temperature). The internal zone of the test cell was modelled as a simple box whose construction features and equipment quantities (indoor air temperature, walls' stratigraphy and energy needed for heating or cooling) were not of interest to the analysis and therefore were provided as boundary conditions for each software. For this reason, in all the BES tools, the indoor air temperature and surface temperature of zone opaque components were imposed through schedules created using the available experimental data to eliminate the uncertainty due to the internal zone and focus the validation procedure solely on the thermal and airflow network representing the DSF. For this validation study, it was decided to use un-calibrated models. Thus, all available information about the mock-up was inserted into the models and the default values were used for unknown information. In this study, priority was given to the in-built component module over the zonal approach, if available in the tool, as a modeller would use the dedicated module (if any) compared to a more complex modelling task required for the zonal approach. Therefore, the in-built component approach was chosen for IDA-ICE, while the zonal approach was used for the other tools.

In the zonal approach, the DSF cavity was modelled as three stacked thermal zones corresponding to the inlet, the cavity, and the outlet zone.

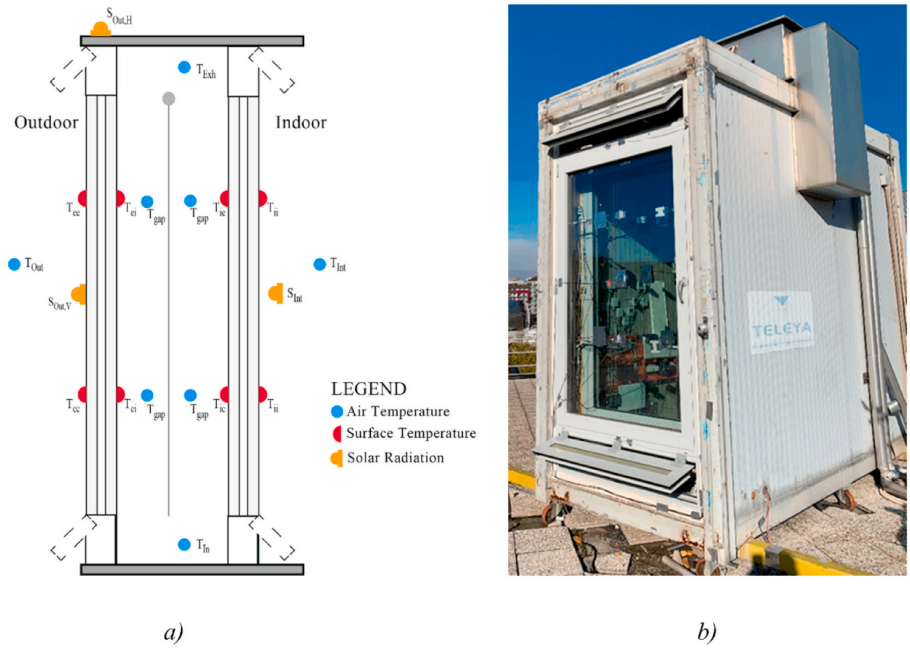

Fig. 3. Sensors scheme (a) and picture of flexible DSF prototype in OAC mode and shading up (b).

Only the cavity zone contains the glazing systems, and its volume is four times the volume of the adjacent stacked zones, while the openings towards indoor and outdoor are placed on the inlet and outlet zones. This allowed us to have model outputs in line with the physical quantities available in the experimental dataset. When modelling the SA mode for the zonal approach, to ensure an overall airflow amount and direction (from the outside, to the DSF cavity, and finally to the adjacent zone) in line with the experimental data, it was necessary to extend the DSF airflow network to the internal zone and to add a fictitious duct connecting the volume of the test cell to the outdoor representing the test cell leaks to the outdoor (1 m high, cross-section of 0.1 m^2).

A customised weather data file with a standard time resolution of 1 h was generated based on the data gathered from the outdoor weather station[1] for the six periods (cf. Fig. 4). The simulation time-step in each tool was set to 10 min, and the numerical output was extracted with a resolution time of 1 h. The variety of the outcomes related to the façade – in terms of the cavity air, surface temperatures, and solar irradiance - depends on the modelling approach adopted by each software. Usually, the component model provides less output information than the zonal model. For example, the "*Double Glass Façade*" component of IDA-ICE calculates a unique temperature for the whole cavity, and it is not possible to extract the cavity outlet air temperature. On the other hand, it is possible to obtain more information and outputs, such as the air temperature stratification along the cavity through the zonal approach. Moreover, dedicated postprocessing of the simulation outputs was carried out to obtain the total transmitted solar radiation by the DSF in EnergyPlus and IES-VE, as detailed in Appendix A. Table 1 summarises the settings of the simulation condition and DSF modelling approach used for each BES tool. Detailed information on DSF model implementation for each BES tool is reported in Appendix A.

3.3. *Validation* ***procedure***

The validation of the different BES tools is based on the comparison of the three physical quantities[2] reflecting the influence of the DSF on the heat balance of the thermal zone adjacent to the facade:

- the temperature of the air in the DSF cavity [°C];
- the temperature of the interior surface of the inner skin [°C];
- the transmitted solar irradiance through the façade [W/m^2];

The performance of each software was analysed qualitatively through a scatter plot that compares the experimental data with the predicted outcomes of the software. In addition, the time profile of one representative day for each configuration was compared with the experimental data to better understand the aggregated results and detect any particular deviations of trends during the day.

Two statistical indicators were used to compare the fitness of the prediction with the experimental data quantitatively: the Mean Bias Error (MBE) and the Root Mean Square Error (RMSE):

$$MBE = \frac{1}{n}\sum_{i=1}^{n}\left(X_p - X_m\right)_i \quad (1)$$

$$RMSE = \sqrt{\frac{1}{n}\bullet\sum_{i=1}^{n}\left(X_p - X_m\right)_i^2} \quad (2)$$

[1] the quantities directly utilised to customise the weather file were outdoor dry bulb air temperature, relative humidity, atmospheric pressure and global solar irradiance. The latter was decomposed in the normal beam and diffuse global solar irradiance, calculated using the ENGERER2 separation model [39], and the cloudiness factor was taken from the climate reanalysis ERA5 [40]. This solar decomposition was validated by comparing the calculated vertical global solar irradiance on the South façade with the measured value.

[2] Since all the tested BES tools provide a unique output value, volume and area weighted average were calculated for the experimental temperature of the air in the cavity and the temperature of the inner skin's surface, respectively.

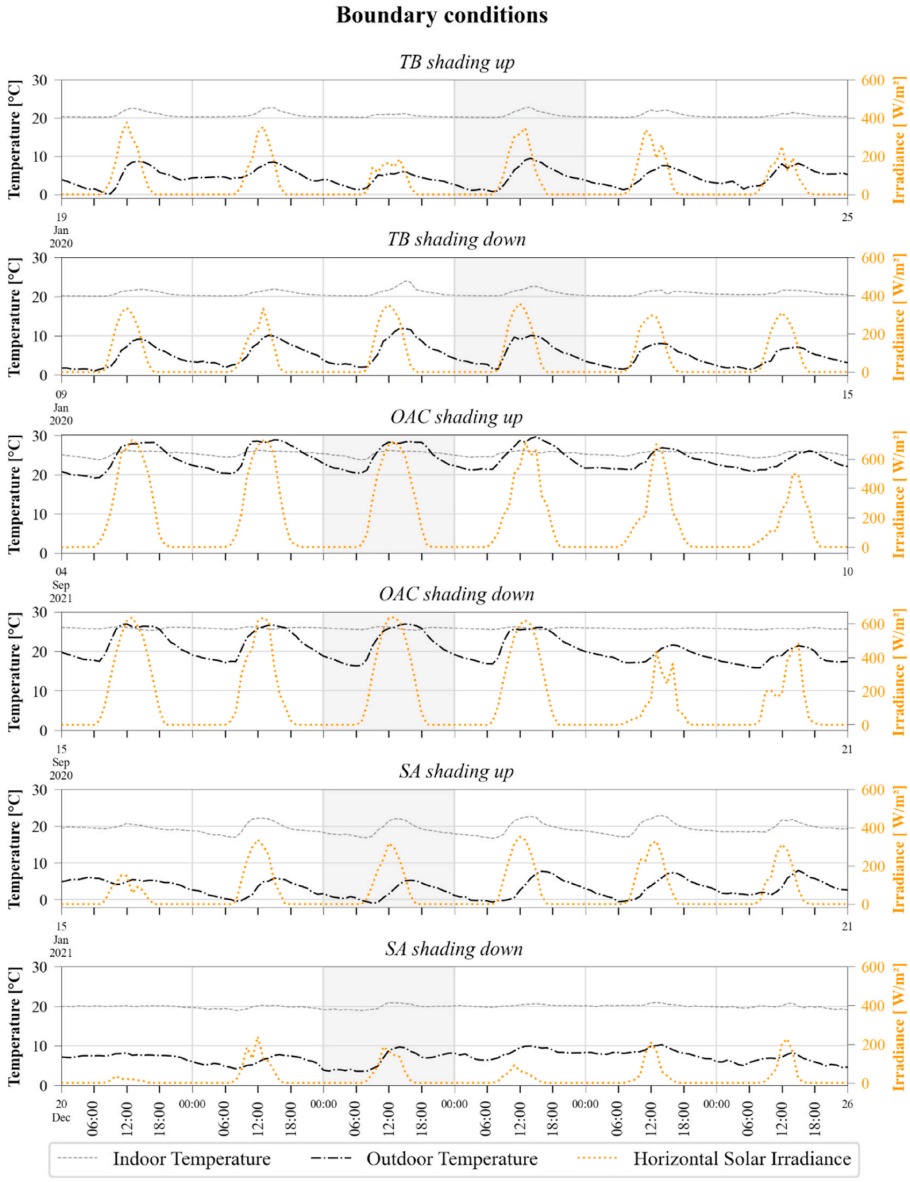

Fig. 4. Time profile of indoor air temperature, outdoor air temperature and horizontal solar irradiance during the six periods. The representative day for each dataset is highlighted in grey.

The MBE provides the average bias of the prediction, and positive values indicate an overall overestimation of the prediction; in contrast, negative values indicate model under-prediction. However, the main drawback of this indicator is that it is subject to error compensation due to the sum of positive and negative values. For this reason, the RMSE index was calculated; it returns the standard deviation of the prediction errors but loses the information on the sign (under- or over-estimation).

It is important to highlight that while threshold values for MBE or RMSE to consider a model validated can be found for whole building models [35], for component-level validation, there are no established maximum values not to be exceeded for any quantitative indicators to consider the model "validated". In the context of the study, we, therefore, use values of the statistical indicators in combination with a qualitative analysis of the results (e.g., time and intensity match between the simulated and experimental hourly profile) to assess the validity of the predictions of each BES tool.

4. Results

The results of the validation study are presented in two main sections.

Firstly, the performance of each BES tool is presented (Section 4.1 to

Table 1
Settings of simulation condition and DSF modelling approach used for each BES tool.

		EnergyPlus	TRNSYS	IDA ICE	IES-VE
Simulation conditions	Exterior convective surface algoritm	SimpleCombined [15]	Vertical window's internal algorithm [19]	Clarks [12]	McAdams [12]
	Interior convective surface algorithm	AdaptiveConvectionAlgorithm [15]	Vertical window's internal algorithm [19]	*Default*[a] max(Table, CDA) [12]	Alamdari & Hammond [31]
	Solar distribution	FullInteriorAndExteriorWithReflections [15]	Detailed radiation model [19]	*Default*[a]	*Default*[a]
	Temperature set-point	Ideal load	Ideal load	Ideal load	HVAC
	Timestep for heat balance	10 min	10 min	*Default*[a] Adaptive	10 min
DSF Modelling approach	Cavity modelling	Zonal approach	Zonal approach	Component model	Zonal approach
	Horizontal partition	Horizontal opening - infrared transparent material	Always-opened large windows	n.a.	Always-opened large windows
	Ventilation openings	Pivoted window	Large pivoted window	Default[a] Leaks (ELA)	Large openings ('*Top - Hung*' category) [17]
	Shading device	Interior shading of the exterior window	Interior shading of the exterior window	Interior shading of the exterior window	Interior shading of the exterior window
	Wind exposure	City	*Default*[a]	Semi-exposed	Semi-exposed low-rise
	Specific heat capacity	n.a.	n.a	Present	n.a.
	Air Mass Flow Coefficient C_{MF} (for closed vents)[b]	0.002 kg/(s·m· $Pa^{0.7}$)	0.002 kg/(s·m· $Pa^{0.7}$)	0.0001 m^2[c]	0.015 l/(s·m· $Pa^{0.6}$)
	Air Mass Flow Exponent n (for vents closed)[b]	0.7	0.7	0.5	*Default*[a] 0.6

[a] Default settings.
[b] When vents are closed, the following power law form (crack flow) is used $Q = C_{MF} \cdot (\Delta P)^n$
[c] ELA method applied [equivalent leakage area at $\Delta P = 4$ Pa ($C_d = 1$)].

4.4) for the prediction of the three physical quantities (cavity air temperature, internal surface temperature, and transmitted solar radiation) in the three air-path configurations (TB, SA and OAC) using scatter plots of simulation output vs experimental data for six days of continuous monitoring (cf. Fig. 4). In each scatterplot summarising the results, from top to bottom, the cavity air temperature (Figs. 5, 6, 7 and 8a), the surface temperature (Figs. 5, 6, 7 and 8b) and the transmitted solar irradiance (Figs. 5, 6, 7 and 8c) are represented for the three air-path configurations (from left to right) in TB, OAC and SA mode. The different curtain shading modes are combined in the same scatterplot.

Then, the time profile of each specific physical quantity of interest (Figs. 9–11) for the different software tools was compared in an inter-software comparison and against experimental data (Section 4.5) for typical days (cf. Fig. 4, grey background), in addition to the scatterplot distribution and error boxplot (including all DSF operational modes and blind configurations together).

4.1. Energy Plus

EnergyPlus showed different performance in the prediction of the cavity air temperature for the different air paths, and this was likely due to the challenges of the Airflow Network to predict the direction of the airflow accurately (Fig. 5): when there is no interaction with the indoor zone (OAC and TB modes), the software exhibited satisfactory performance in the prediction of the cavity air temperature, whereas this quantity was systematically overestimated with an average $RMSE_{E+,SA} = 10.3$ °C for the SA mode (Table 2). To improve the performance of the tool in predicting the cavity air temperature in SA mode, a co-simulation strategy with CONTAM was explored. This approach achieved a significant improvement (Fig. 5.a, right) as all the data points were well distributed among the scatter plot's bisector, albeit with some underestimation outliers (peak values of the cavity air temperature when the shading is raised). Conversely, for OAC mode (Fig. 5, middle), the points were well distributed among the bisector even without the need to implement a co-simulation scheme with CONTAM, showing an elevated performance level in the prediction of the cavity air temperature. For TB mode, a slight underestimation for high temperature and an overestimation for low temperature was seen (Fig. 5, left). The surface temperature exhibited the same trend as the cavity air temperature: the prediction was highly accurate at night, while the magnitude of the peaks was generally underestimated – and this became especially relevant when the curtain was raised. Moreover, for the SA mode, the use of CONTAM resulted in an improved surface temperature prediction, showing that the airflow significantly influenced the temperature distribution in the glazing system (Fig. 5b, right).

Finally, the tool significantly underestimated the total transmitted solar irradiance, as visible from Fig. 5c (cf. Table 4, $RMSE_{OAC} = 81.3$ W/m^2, $RMSE_{SA} = 82.5$ W/m^2).

4.2. TRNSYS

The cavity air and surface temperature predictions (Fig. 6a and Fig. 6b) exhibit a good fit with experimental data, especially for the outdoor air curtain and supply air modes. It is possible to notice that the fitness of the model is better in the low-temperature range, and the points begin to diverge from the bisector for temperatures greater than 30 °C. For the thermal buffer mode, the points were still well distributed along the bisector (with low MBE), but with a wide distribution (high RMSE), especially for the high-temperature range (Fig. 6a and Fig. 6.b, left). As for EnergyPlus, not considering the thermal mass of the glazing systems affected the prediction of the surface temperatures in TB ($RMSE_{TB,\ shON} = 2.2$ °C, Table 2) compared to when the cavity was ventilated, as visible in the SA mode (Fig. 6b) even though some outliers are present in the low-temperature range; in OAC mode the points followed an irregular trend due to an underestimation of surface temperature in the mid-range. Finally, TRNSYS exhibited excellent performance predicting the solar irradiance transmitted through the double skin façade (Fig. 6c), both in configurations with the solar shading raised and deployed (cf. Table 4, $RMSE_{max} = 38.7$ W/m^2).

4.3. IDA-ICE

Unlike with the other BES tools, the in-built DSF component model was used within IDA-ICE. In general, the tool was able to predict the dynamics of thermal behaviour, but the accuracy in the prediction of the magnitudes was lower, especially for high temperatures. Even though it is the only software to include the capacitive node in the window models and provides the dedicated module with the ventilated cavities, the

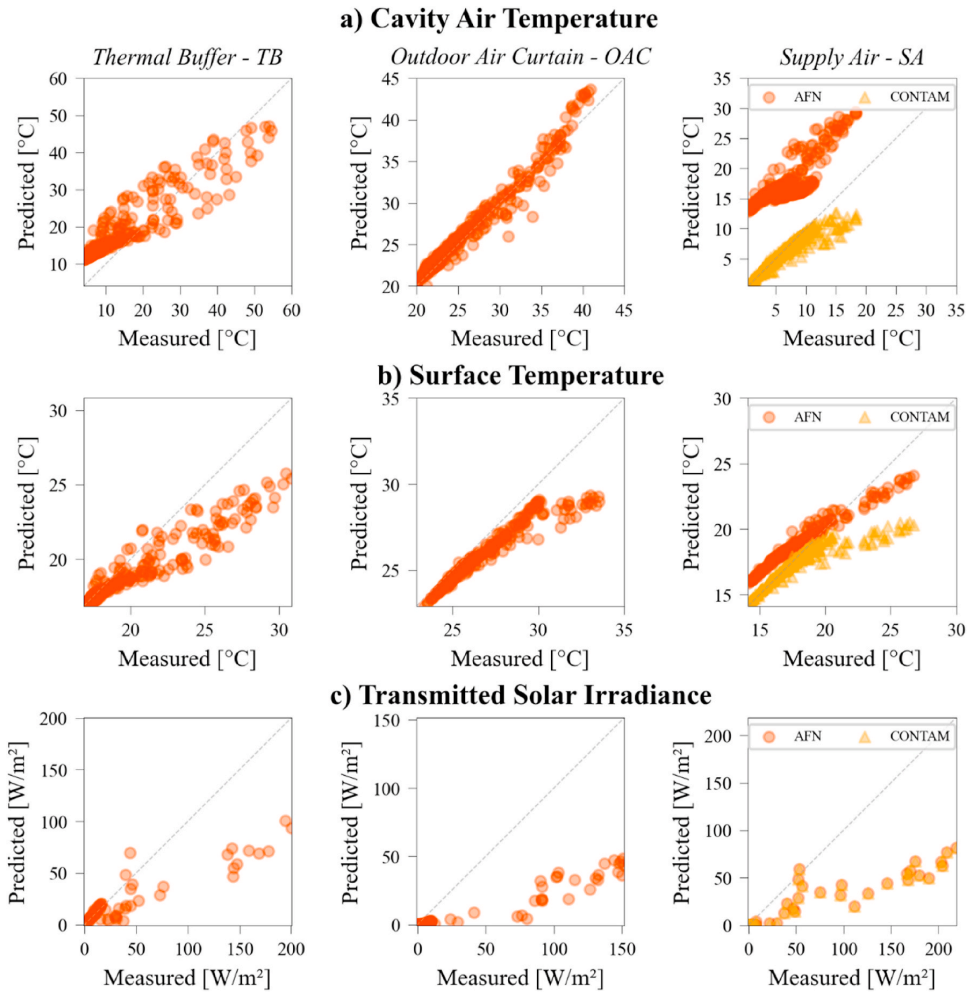

Fig. 5. Comparison between experimental data and predicted outcomes carried out with Energy Plus. From top to bottom: Cavity air temperature, Surface Temperature, Transmitted Solar Irradiance. From left to right: Thermal Buffer, Outdoor Air Curtain and Supply Air.

comparison of the outcomes with the experimental data of the cavity air temperature (Fig. 7a) and surface temperature (Fig. 7b) was not very satisfactory. In the case of the configurations with ventilation in the cavity (OAC and SA modes), the software underestimated the peak with an average error of 10 °C, although the prediction error was drastically reduced at night-time. Conversely, in TB mode the trend of the cavity air temperature was in phase with the measured data and the peak was accurately predicted, whilst higher errors were measured for the cavity air temperature at night time, thereby reducing the performance of the statistical indices ($RMSE_{TB,\ shOFF} = 3.16$ °C, $RMSE_{TB,\ shON} = 4.1$ °C). As far as the time profile of surface temperatures (Fig. 7b) is concerned, for OAC and SA mode, with and without shading, the peak was consistently underestimated, but the prediction error drastically reduced at night time. Additionally, the transmitted solar radiation was accurately predicted (Fig. 7c), with a certain underestimation of the peak when the shading was not present in the cavity, which, nevertheless, did not impair the overall prediction of the shortwave radiative heat transfer across the DSF.

4.4. IES-VE

As far as the prediction of the cavity air temperature is concerned, IES-VE exhibited a varying performance for different ventilation modes: in TB configuration (Fig. 8.a, left), the software tended to overestimate the peak (especially in the absence of the shading) and to anticipate it with respect to the measured data; when the cavity was ventilated in OAC mode (Fig. 8.a, center), the tool underestimated the peak, reducing such difference in the absence of solar radiation; in SA mode the performance of the prediction of the cavity air was improved, especially when the roller shade was deployed (Fig. 8.a, right). The surface temperature prediction (Fig. 8b) followed the trend of the cavity air temperature. As for EnergyPlus and TRNSYS, this is due to the model neglecting the thermal mass of the glazing. Therefore, the peak value was always underestimated and anticipated, especially for the TB mode. The prediction of the solar radiation transmitted by the façade was under-estimated when the shading was raised, and it had an excellent fit in the presence of roller shading in the cavity (Fig. 8c), which could be due to inaccurate distribution of the solar beam radiation between two

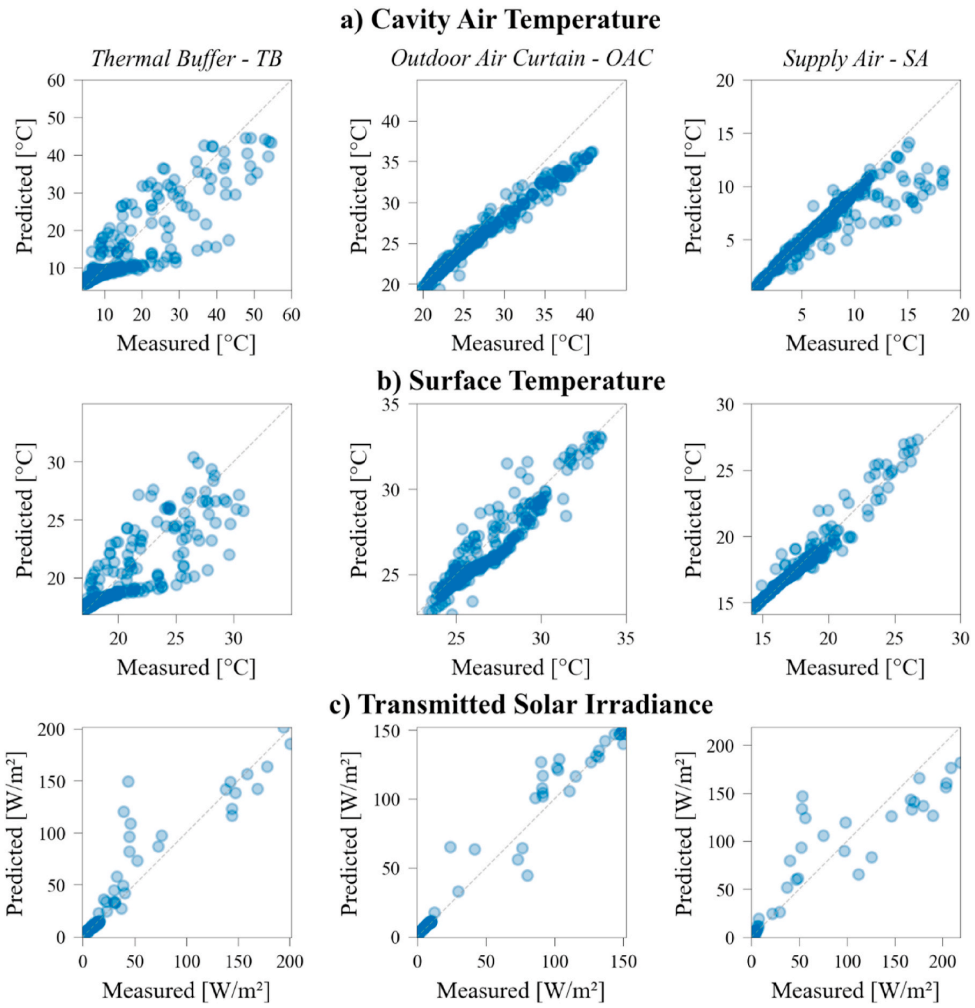

Fig. 6. Comparison between experimental data and predicted outcomes carried out with TRNSYS. From top to bottom: Cavity air temperature, Surface Temperature, Transmitted Solar Irradiance. From left to right: Thermal Buffer, Outdoor Air Curtain and Supply Air. The shading configurations are combined.

Table 2
MBE and RMSE values of the cavity air temperature calculated for the six DSF configurations.

	Cavity air Temperature [°C]											
	Thermal Buffer				Outdoor Air Curtain				Supply Air			
	MBE		RMSE		MBE		RMSE		MBE		RMSE	
Shading	down	up	down	up	down	up	down	up	down	up	down	up
EnergyPlus	3.3	5.8	7.0	6.5	0.6	0.3	1.4	0.9	−0.6	−1.0	0.9	2.4
TRNSYS	−2.1	0.7	7.3	3.9	−1.4	−1.2	2.0	1.8	−0.5	−1.5	0.7	2.7
IDA ICE	0.0	2.4	4.1	3.2	−1.9	−1.6	3.2	2.4	0.5	−0.1	0.7	2.1
IES VE	2.8	4.0	6.8	5.2	−2.3	−1.6	3.7	2.5	0.9	0.5	1.0	1.7

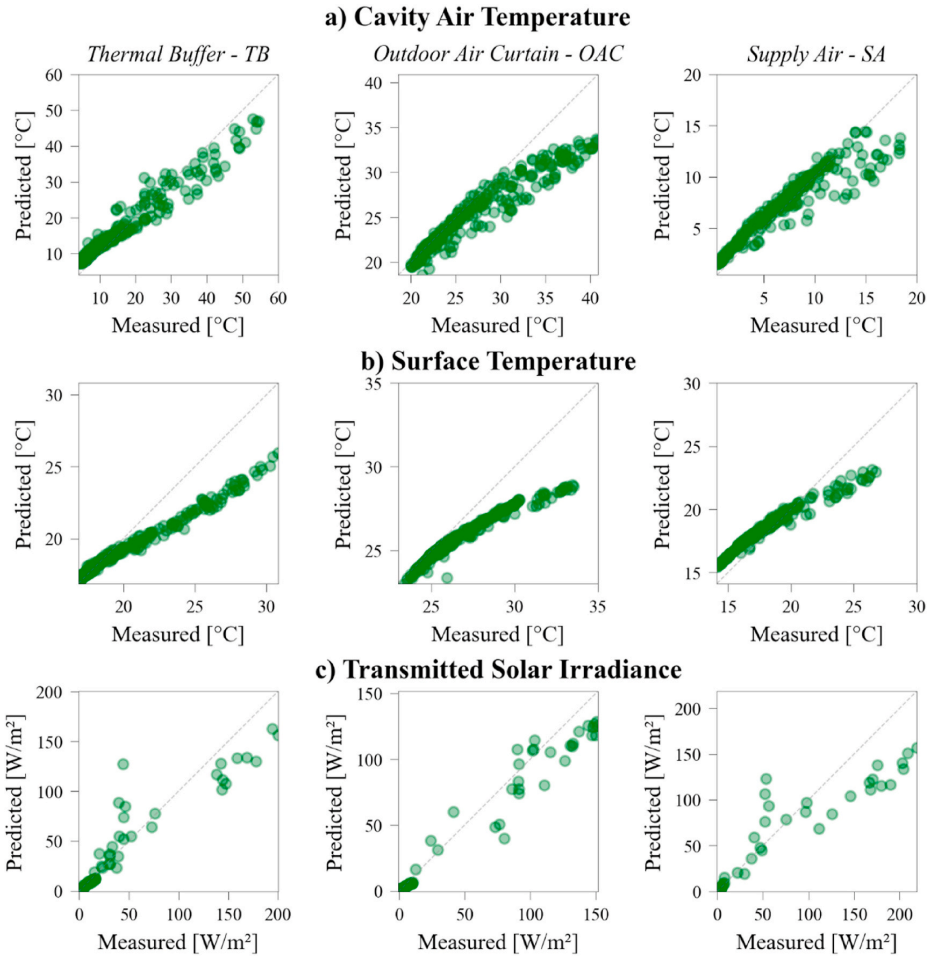

Fig. 7. Comparison between experimental data and predicted outcomes carried out with IDA-ICE. From top to bottom: Cavity air gap temperature, Surface Temperature, Transmitted Solar Irradiance. From left to right: Thermal Buffer, Outdoor Air Curtain and Supply Air. The shading configurations are combined.

internal zones.

4.5. Inter-software comparison

The errors in the prediction of the cavity air temperature for each BES tool are shown in Fig. 9. Under the OAC mode, the prediction of the four tools was quite similar in both states of shading: with the exception of EnergyPlus, the peak values during the day were significantly underpredicted, whereas all trends overlapped very well with the experimental data during the night. The statistical indicators reported in Table 2 reveal that EnergyPlus was the most accurate software for predicting the cavity air temperature for modelling the OAC mode ($RMSE_{E+,shOFF} = 0.9$ °C, $RMSE_{E+,shON} = 1.4$ °C), whereas all other tools were significantly more inaccurate, especially for IES-VE and IDA-ICE when the shading is raised. The overestimation of the mass flow rate in the cavity in TRNSYS, IES-VE and IDA-ICE was greater compared to EnergyPlus (which was the best tool in this case, as mentioned before), reducing the peak of temperature during the daytime. Unfortunately, we cannot use experimental air velocity data to support this assumption.

IES-VE is the tool that best predicted the cavity air temperature for SA mode, as quantified by the statistical indicators of Table 2 and the time series in Fig. 9. Moreover, the performance of the four BES tools was quite similar when the shading is deployed. It is noteworthy that the SA mode requires the integration of the DSF airflow network into the whole building network to balance the pressure distribution properly. However, EnergyPlus failed to predict the cavity air temperature. Comparing the outcomes of EnergyPlus in terms of the cavity air and indoor air temperatures, it appears that the predominant airflow direction was clearly from the room zone to DSF and not vice versa. Using any available connectors among the possible AirflowNetwork components (e.g. cracks, leakage areas, or large openings), it was not possible in EnergyPlus to ensure a flowrate that proceeded smoothly from the outdoor to the DSF cavity and then further to the test cell zone. The co-simulation with CONTAM fixed this issue, as visible from the statistical errors, comparable with the other software (cf. Table 2).

In TB mode, it is possible to observe that TRNSYS, EnergyPlus and IES-VE predicted the cavity air peak values approximately 1 h beforehand compared to experimental data for both shading configurations. This time shift was less evident from IDA-ICE simulation outputs. Since the boundary condition profiles (solar irradiance and outdoor air temperature) were in phase, the time lag was likely due to the absence of information about the heat capacity of the glazed layers in the models of

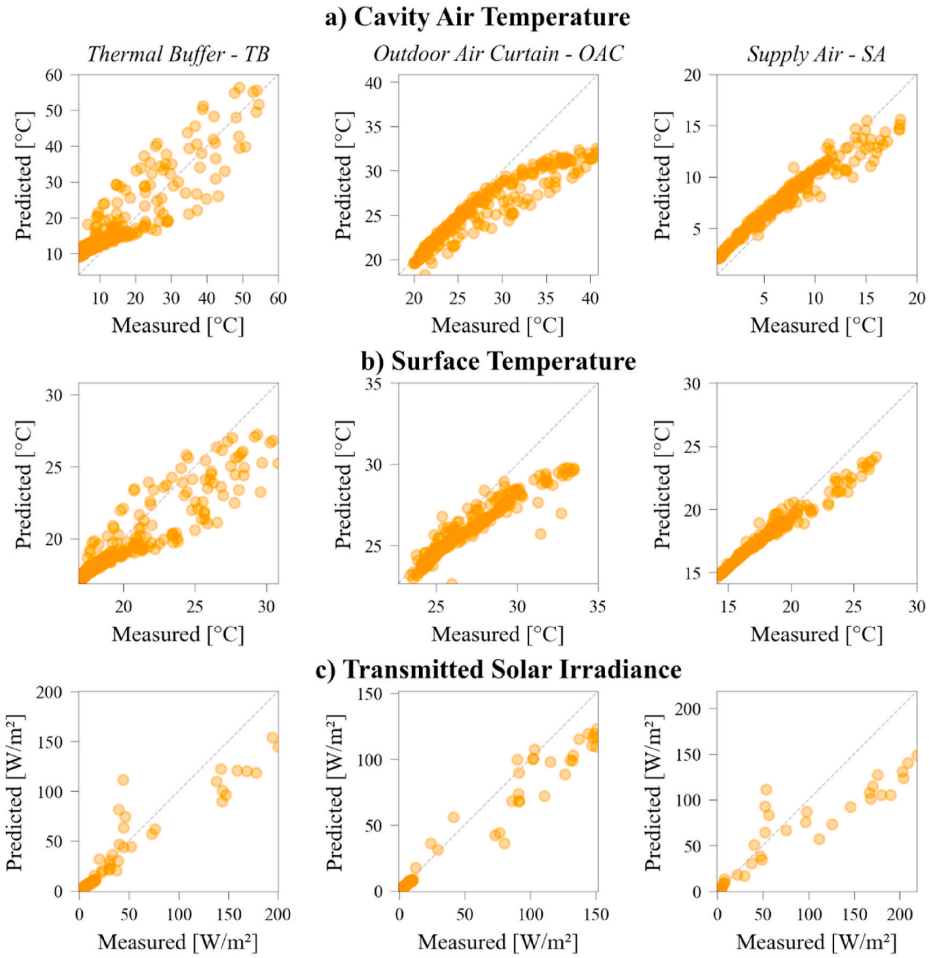

Fig. 8. Comparison between experimental data and predicted outcomes carried out with IES-VE. From top to bottom: Cavity air temperature, Surface Temperature, Transmitted Solar Irradiance. From left to right: Thermal Buffer, Outdoor Air Curtain and Supply Air. The shading configurations are combined.

the transparent components for the three BES tools. With this simplification, the software tools do not correctly model the dynamics of the absorption and reemission by the glazing systems of the solar irradiance, resulting in a delay of the temperature peaks. In TB mode, these effects are more pronounced since mass exchange between the DSF cavity and surrounding zones is minimal - hence the heat transfer from the envelope system to the air in the cavity is the driving force that determines the cavity air temperature. This effect was pronounced when the roller shade is deployed, as the peak underestimation was increased by absorbed solar radiation transferred from the shading to the air cavity by means of convection. For the other ventilation modes, TRNSYS, EnergyPlus and IDA-ICE tended to underpredict the peak cavity temperature when the shading is deployed, whilst the performance of IES-VE was unaltered.

The prediction of the indoor surface temperature of the inner skin of the DSF is shown in Fig. 10. Overall, TRNSYS and IES-VE were the best-performing tools in predicting inner glazing surface temperatures, depending on the ventilation mode. As shown in Table 3, IES-VE was the best-performing tool in predicting the surface temperature in TB mode and both shading modes. TRNSYS, in contrast, had the lowest statistical errors in OAC and SA modes. In particular, in SA mode with shading deployed, the performance of all software was quite similar (cf. Table 3).

EnergyPlus TRNSYS and IES-VE predicted the peaks about 1 h ahead of the measurement data, following a similar trend as for the cavity air temperature. In contrast, IDA-ICE provided a better time match between simulation and experiments due to the inertial features of the glazing

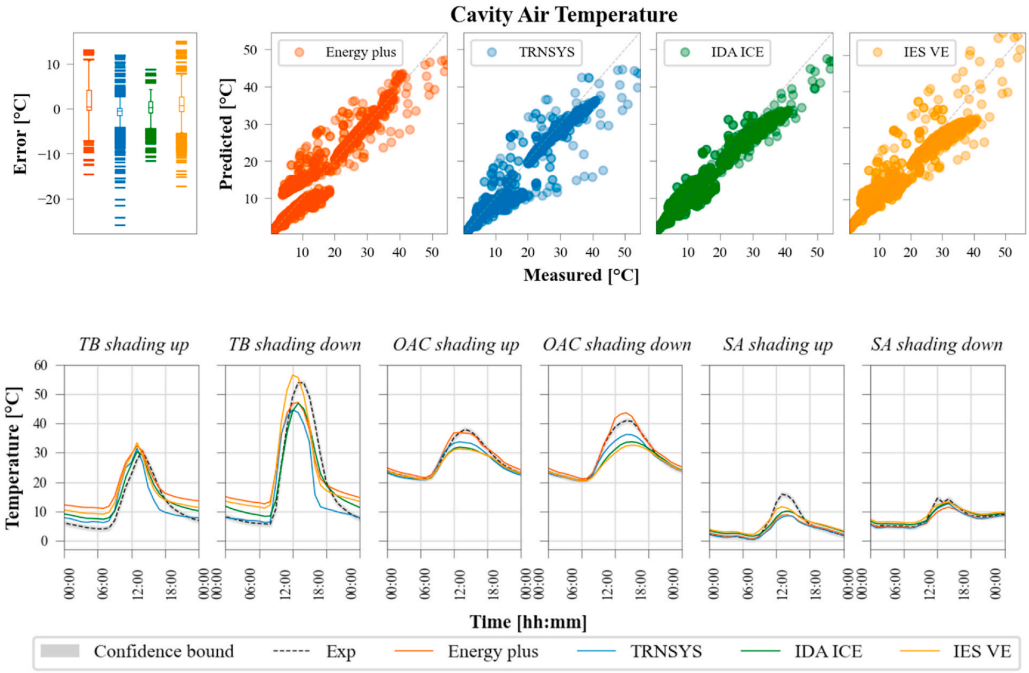

Fig. 9. Comparison between measured data and predicted outcomes of the cavity air temperature (up) – the six façade configurations are combined. Time profile of the cavity air temperature prediction and experimental data during the representative day of the datasets (down).

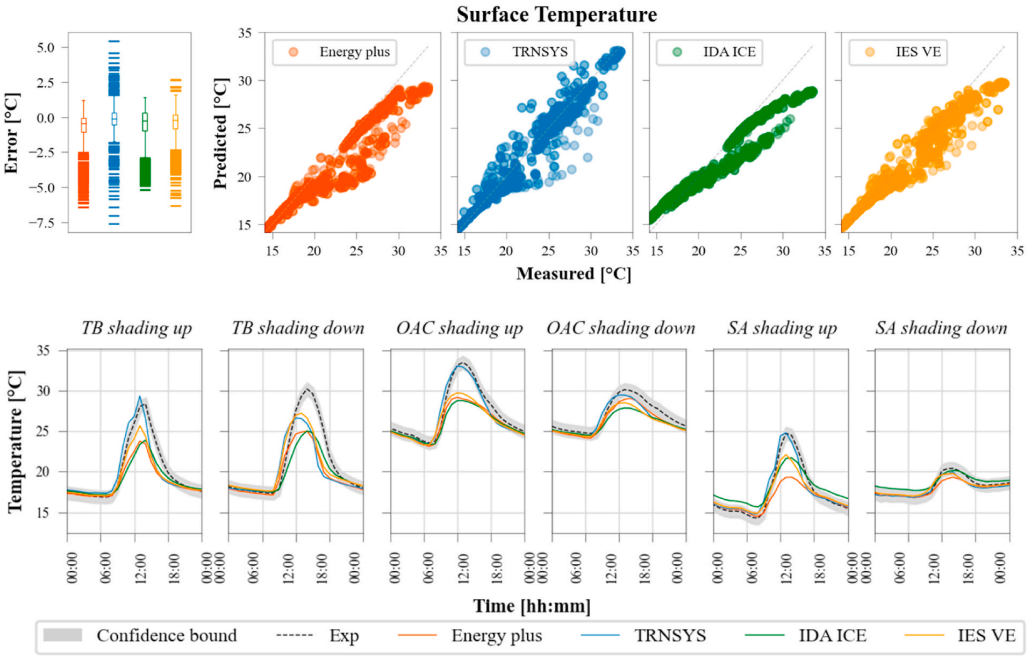

Fig. 10. Comparison between measured data and predicted surface temperature (up) outcomes – the six façade configurations are combined. Time profile of the surface temperature prediction and experimental data during the representative day of the datasets (down).

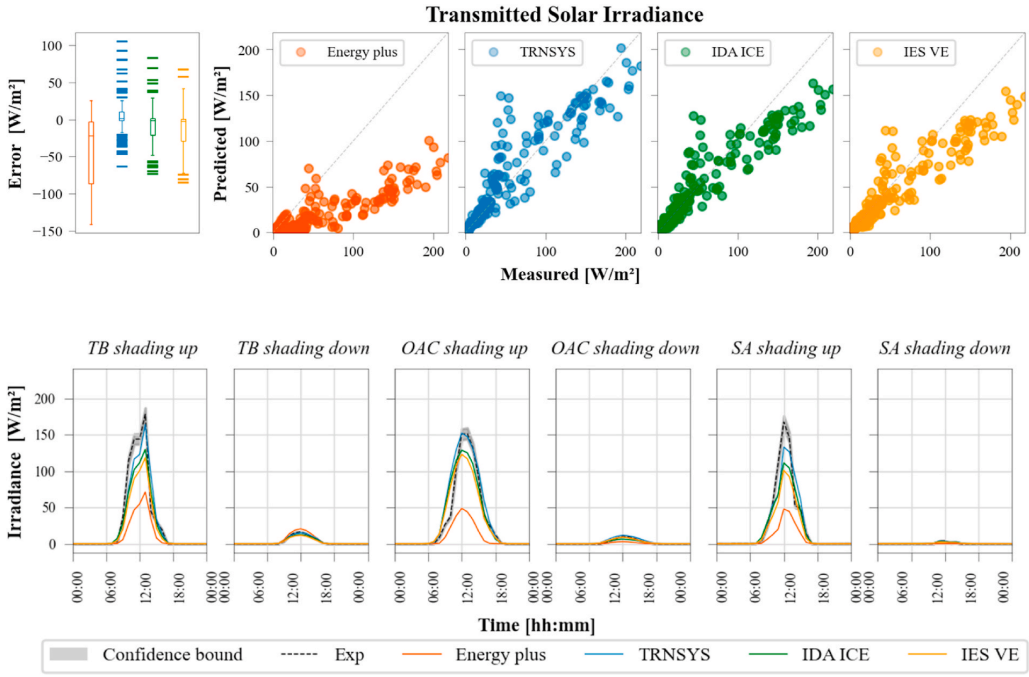

Fig. 11. Comparison between measured data and predicted outcomes of the transmitted solar irradiance (up) – the six façade configurations are combined. Time profile of the transmitted solar irradiance prediction and experimental data during the representative day of the datasets (down).

Table 3
MBE and RMSE values of the surface temperature calculated for the six DSF configurations.

	Surface Temperature [°C]											
	Thermal Buffer				Outdoor Air Curtain				Supply Air			
	MBE		RMSE		MBE		RMSE		MBE		RMSE	
Shading	down	up	down	Up	down	up	down	up	down	up	down	up
EnergyPlus	−1.3	−0.9	2.2	1.6	−0.7	−1.1	0.8	1.6	−0.3	−1.0	0.4	2.1
TRNSYS	−0.7	0.2	2.2	1.4	−0.5	−0.3	0.8	0.9	−0.2	0.1	0.4	0.7
IDA ICE	−1.0	−0.7	2.0	1.5	−0.9	−1.2	1.1	1.8	0.5	0.3	0.5	1.5
IES VE	−0.6	−0.4	1.9	1.2	−0.8	−1.0	1.0	1.6	−0.1	−0.3	0.3	1.1

Table 4
MBE and RMSE values of the transmitted solar irradiance calculated for the six DSF configurations.

	Transmitted solar irradiance [W/m^2]											
	Thermal Buffer				Outdoor Air Curtain				Supply Air			
	MBE		RMSE		MBE		RMSE		MBE		RMSE	
Shading	down	up	down	up	down	up	down	up	down	up	down	up
EnergyPlus	1.9	−42.4	2.5	56.5	−4.4	−76.9	5.1	81.3	−0.7	−64.4	1.7	82.5
TRNSYS	0.3	12.7	1.3	32.0	1.6	−6.1	1.7	16.7	1.3	−1.2	1.6	38.7
IDA ICE	−1.5	−3.2	2.1	28.9	−1.9	−12.6	2.5	20.3	0.9	−17.1	1.2	41.0
IES VE	−2.5	−11.7	2.9	31.3	−0.5	−19.4	1.2	26.0	0.6	−25.6	1.0	45.8

model, but this is not reflected in the statistical indicator (Table 3) as it shows a systematic underestimation of the temperature peaks during the daytime, whereas the quality of the prediction is drastically improved at night-time, as demonstrated by a much lower error during these periods.

The prediction of the solar irradiance transmitted through the double skin façade is shown in Fig. 11 and related statistical indicators in Table 4. The analysis is limited to the central hours of the day (11:00 and 15:00) to increase measurement accuracy, as explained in Section 3.1. TRNSYS offered the most accurate prediction of the transmitted solar irradiance in both solar shading configurations. A more accurate algorithm for solar distribution could be a contributing factor to this satisfactory result, as evidenced by the improvement in solar radiation modelling brought about by version 17 of TRNSYS, where a detailed beam and diffuse solar radiation model is available within the DSF cavity. On the other hand, IDA-ICE and IES-VE underestimated the high peaks during sunny days when the shading was retracted in a

comparable way. In contrast, EnergyPlus led to a great underprediction of the solar irradiance transmitted through the façade. In fact, although the most complex solar distribution model was adopted, among the options proposed by EnergyPlus, this direct and diffuse solar radiation distribution method does not allow description of the complex shortwave radiative heat transfer through the cavity for the zonal approach. Previous work has already assessed unsatisfactory performance [11], where it was highlighted that EnergyPlus offers the most accurate prediction of transmitted solar irradiance, but only when the in-built component approach is adopted (*Airflow window model*). Nevertheless, such a model can only be adopted to model mechanically ventilated DSFs.

In conclusion, it is not possible to identify a tool that outperforms the others for all the analysed quantities and DSF ventilation modes. The comparison with experimental data has revealed that cavity air temperature is the least accurate variable in all software on the basis of underestimation of the daytime peaks. Analysing the time profiles in Fig. 9, EnergyPlus is the most accurate software for cavity air temperatures in OAC mode, while IES-VE seems the most accurate for SA and TB mode (only when the shading is deployed). Regarding surface temperatures and transmitted solar radiation, TRNSYS appears to be the best-performing software, providing satisfactory results in line with experimental data regarding peak magnitude and dynamics.

Although IDA-ICE is the only software which provides the in-built module and considers the thermal inertia of the fenestration elements, this is not evident from the results due to the underestimation of peak temperatures during daytime in all the DSF configurations analysed.

Regarding SA mode, EnergyPlus completely fails to predict cavity air and surface temperature. This is due to the inability of the software to properly consider the airflow direction between the DSF cavity and the adjacent thermal zone (and not vice-versa). Although it was shown that CONTAM could enable a more accurate prediction, the simulation results were not entirely satisfactory. Moreover, the limitation of EnergyPlus in estimating the transmitted solar radiation in the zonal approach, due to the high impact of solar radiation over the other variables, is a potential cause of inconsistency between the measurements and the simulation outputs for the inner glazing surface temperature, and indirectly for the cavity air temperature.

Table 5 provides an overview of the findings of this investigation for the four BES tools analysed. The colour of the cell indicates how accurate the prediction was, while the sign indicates whether the tool underestimated or overestimated the experimental results. For performance detection, we have defined four error ranges: *good agreement* (green) if the temperature error is less than 1 °C (15W/m^2 for solar irradiance), *small error* (yellow) if the temperature error is less than 5 °C (25W/m^2 for solar irradiance), *moderate error* (orange) if the temperature error is less than 10 °C (50W/m^2 for solar irradiance), *large error* (red) otherwise. As for previous work [11], the error between the simulated and measured peaks was considered for judging the overall BES performance in Table 5.

5. Discussion

In this section, the challenges modellers may face when simulating a naturally ventilated DSF (cf. Section 2.2) are discussed and investigated using our modelling and building physics knowledge. Given that no BES tools performed significantly better than the others for all the DSF configurations, we chose the most appropriate DSF airpath configuration and BES tool to address each modelling challenge by means of a one-factor-at-the-time sensitivity analysis. The variable considered for this discussion is primarily the cavity air temperature, as it is the most challenging value to predict accurately and the one most affected by modelling assumptions for the elements that interact with the cavity.

In the zonal approach, there is not a standardised approach when discretising the number of stacked zones for a single-storey DSF cavity (a minimum of one up to a maximum of six zones are adopted in the literature). A sensitivity analysis was carried out on the OAC model in EnergyPlus using one zone, three zones and six zones. Fig. 12.a shows that using a single zone to model the entire cavity is not enough to produce satisfactory results. Conversely, subdividing the cavity into six zones is not rewarded by an improvement in performance compared to the model with three stacked zones in determining the cavity outlet temperature. However, this can be useful to study the stratification of the air along with the cavity.

The influence of the cavity distributed *pressure losses* was investigated using the IES-VE model in OAC mode. The frictional losses along the cavity surfaces were accounted for in the model by considering a concentrated pressure loss, reducing the opening area of virtual surfaces along the cavity. Thereby reducing the free area separating the three stacked zones (perpendicular to the airflow) from 100%, to 25% and 50% of the cavity section. However, these fictitious elements did not significantly impact the prediction of the cavity air temperature (Fig. 12b), which was reduced by a maximum of 1 °C in the case of a free area to the airflow of 25% of the original section.

Similarly, *wind pressure coefficients* did not affect the BES tools' prediction to a great extent. IES-VE was used again to model the supply air mode with the shading up, as this is the configuration where it is reasonable to expect the greatest influence of the wind pressure field on the naturally-driven airflow across the cavity. IES-VE is the tool that provides the modeller with the most detailed choice of pre-set wind pressure coefficients among those employed in the study (according to the exposure and the building geometry). The effect of the *wind pressure coefficient* was explored by varying the exposure type from exposed, to semi-exposed and sheltered. The results in Fig. 12.c show that its impact on the cavity air temperature is negligible. However, it must be highlighted that the wind speed values recorded during the experiment were up to 2 m/s, hence the negligible impact might reflect the small range of wind speed boundary conditions measured.

In order to verify the influence of *inlet and outlet opening characteristics* on the cavity air temperature, the model implemented in TRNSYS in OAC mode was employed, and the opening factor of the ventilation

Table 5
Performance overview of the tools in the three different ventilation modes. The performance of the two shading modes is combined. - - - Very high underestimation; - - High underestimation; - Underestimation;; = Good Agreement; + Overestimation; ++ High Overestimation; +++ Very High Overestimation; Colour code: Red: large error; Orange: moderate error; Yellow: small error; Green: accurate prediction. [ ]* refers to the performance of EnergyPlus using the AirflowNetwork.

Tool	***EnergyPlus***			***TRNSYS***			***IDA ICE***			***IES VE***		
Ventilation mode	**TB**	**OAC**	**SA**	**TB**	**OAC**	**SA**	**TB**	**OAC**	**SA**	**TB**	**OAC**	**SA**
Air gap temperature [°C]	=	=	- [---]*	-	-	-	-	--	-	-	--	-
Surface temperature [°C]	-	-	- [---]*	=	=	=	-	-	-	-	-	-
Solar irradiance [W/m^2]	---	---	---	=	=	=	-	-	-	-	-	--

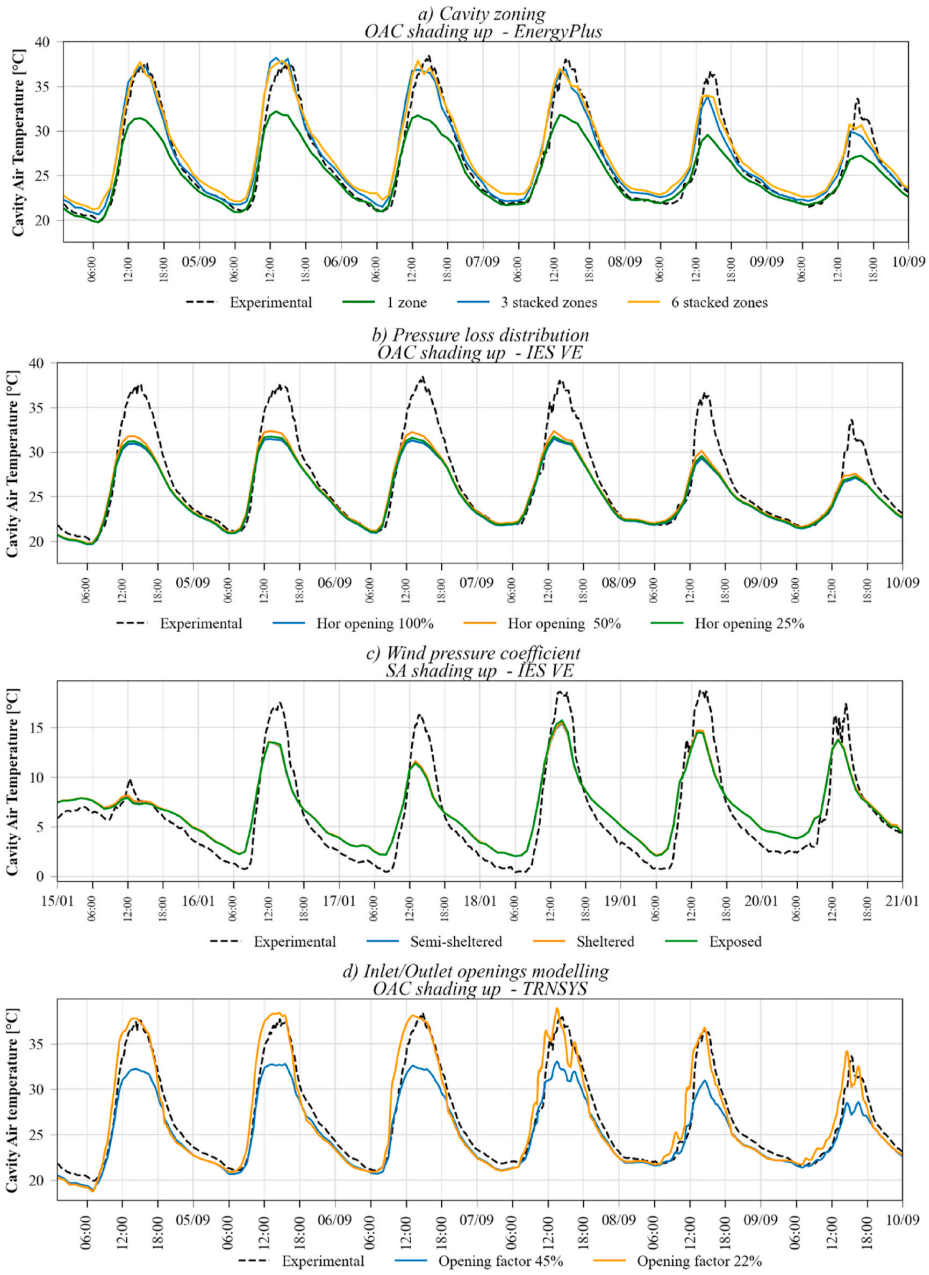

Fig. 12. Sensitivity analysis for zoning optimisation (a), pressure loss distribution (b), wind pressure coefficients (c), inlet and outlet modelling (d), air tightness of the inlet/outlet openings (e), convective heat transfer coefficient (f), capacitive node (g). Different tools and DSF modes have been used, as indicated in the graphs.

openings was varied by ±50% compared to the baseline value used for the investigation. The results shown in Fig. 12.d reveal that by decreasing the window opening, the error in predicting the cavity air temperature is reduced considerably. As explained in Section 4.5, TRNSYS, IES-VE and IDA-ICE tended to underestimate the peak of the cavity air temperature when the cavity was ventilated, especially in OAC mode. This is due to the complexity of estimating the free area of inlet and outlet apertures and related concentrated pressure losses, causing overestimation of the mass flow rate in the cavity within TRNSYS, IES-VE and IDA-ICE. Thus, it is evident that detailed studies on particular opening types should be carried out to model more accurately the flow through DSF cavities.

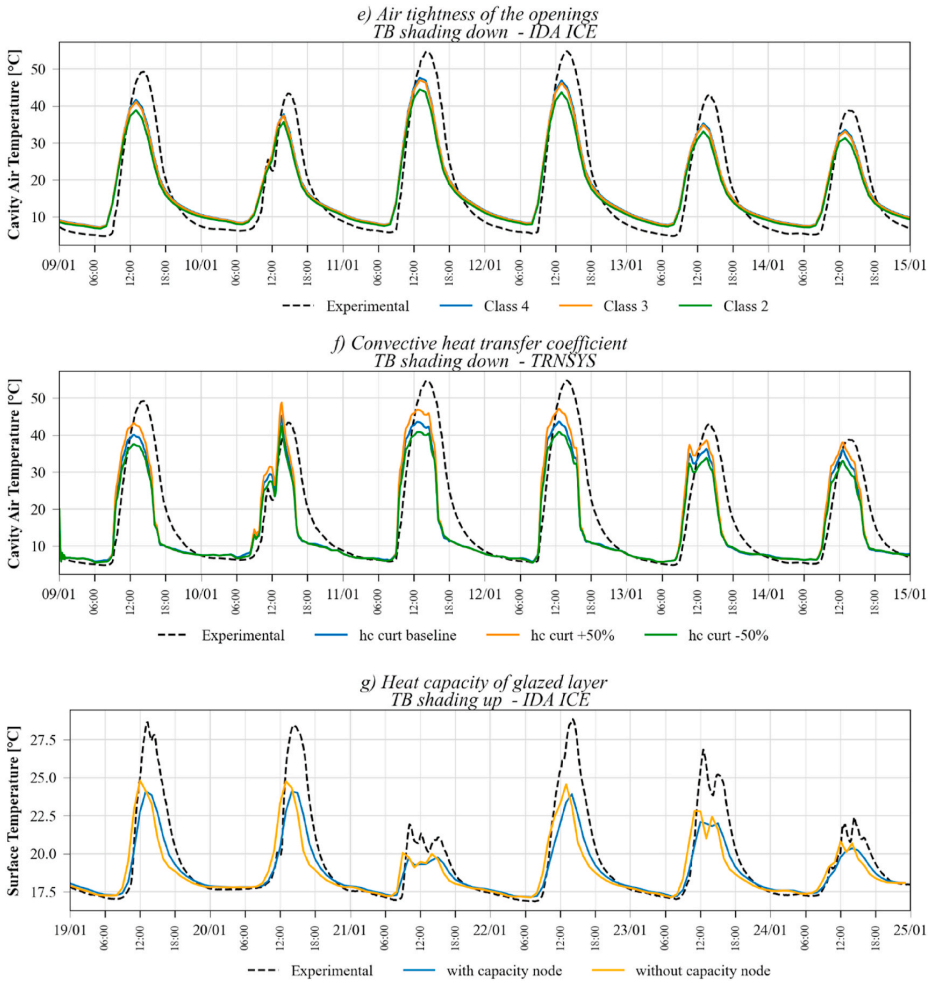

Fig. 12. (*continued*).

The impact of the *air tightness of the openings* was investigated using the model of IDA-ICE. The default leakage settings (0.5 ACH at 50 Pa) are applied only to the external surface corresponding to a window with a permeability of class 4 (3 $m^3/(h\ m^2)$) according to the EN12207:2016 [36]. In order to test the sensitivity of this parameter, the model was run adopting infiltration rates corresponding to class 3 (9 $m^3/(h\ m^2)$) and class 2 (27 $m^3/(h\ m^2)$). The results shown in Fig. 12.e reveal a minimal difference between classes 4 and 3, while higher infiltration rates corresponding to class 2 had a greater impact on the peak values of the cavity air temperatures for the analysed case (TB with shading device), with a reduction in the order of up to 2 °C.

One of the most challenging aspects of the heat transfer phenomena is the determination of the DSF cavity *convective heat transfer coefficients*. The cavity convective coefficient may significantly impact cavity air and surface temperatures. When a shading device is present, the convective heat exchange coefficient between the shading and the cavity air is probably even more relevant compared to that of the glazed surface, given the higher amount of solar irradiance absorbed (and released) by the shading device. For these reasons, a sensitivity analysis was carried out on the TB mode in TRNSYS by varying the convective heat transfer coefficient of the cavity-facing surface of the inner skin, and the convective heat transfer coefficient of the shading device separately. In the first analysis, the convective heat transfer coefficient was modified ±50%. The analysis shows that this variation of the convective coefficient has a minimal effect on the prediction of the DSF's thermophysical quantities, with a maximum improvement of 0.2 °C of the air cavity temperature. In the second analysis, the heat released by the shading device was modelled in simple terms in TRNSYS by varying the ratio between the radiative and the convective heat transferred from the shading. By varying the convective fraction by 50%, it was shown that the peak underestimation error is reduced by approximately 5 °C (Fig. 12f). Therefore, a change in the convective heat exchange is more relevant when applied to shading device than to the other surfaces facing the cavity.

Finally, neglecting the *glazing thermal inertia* by the window model of EnergyPlus, TRNSYS, and IES-VE caused a time-shift of the cavity dynamics (surface and air temperatures) compared to the experimental data as any heat absorbed by the glazed layer is instantaneously transferred to the air window cavity by convection and to the other surfaces by radiation. In the physical system, instead, the heat capacity of the glazed layers causes a delay between the solar radiation absorption and its re-emission via long-wave radiative heat transfer. This effect is

Table 6
Summary of findings from the sensitivity analysis.

Challenges	DSF mode	BES tool	Output Variable	Outcomes
Cavity zoning optimisation	OAC shading up	EnergyPlus	Cavity air temperature	Three stacked zones to divide the cavity may be sufficient
Pressure loss distribution in the cavity	OAC shading up	IES VE	Cavity air temperature	Minimal effect on the prediction
Wind pressure coefficient	SA shading up	IES VE	Cavity air temperature	Minimal effect on the prediction
Inlet/Outlet modelling	OAC shading up	TRNSYS	Cavity air temperature	Inlet/outlet opening factor reduced by half significantly improved results
Opening air tightness	TB shading down	IDA ICE	Cavity air temperature	Minimal effect on the prediction
Convective heat transfer coefficients	TB shading down	TRNSYS	Cavity air temperature	Increasing the convective coefficient of the shading device by 50% improved the estimation of peaks by 5 °C
Heat capacity of glazed layer	TB shading up	IDA ICE	Glazing Surface temperature	The absence of the capacitive node anticipates temperature peaks by 1 h

amplified in DSFs, where there might be a higher thermal mass due to the number and thickness of glass layers. This is particularly evident in Thermal Buffer mode since, apart from the infiltration, there is no mass exchange between the cavity and the boundary zones (indoor and outdoor). IDA-ICE allows the modeller to input values for the heat capacity of the glazed layers. In Fig. 12.g the hourly profiles of the simulated inner surface temperature with and without the glass's specific heat capacity are presented. The temperature profile in the case without the thermal mass of the glazing resembles the temperature outcomes of the other BES tools. In this case, indeed, the temperature peak was predicted approximately 1 h ahead of the measurement data. This limitation could be overcome by increasing the thermal capacity of the (cavity) air node, a feature controlled in both TRNSYS and EnergyPlus. However, such technical expedients are more of an art in nature than based on robust practices, which can work in case of calibration (with available experimental data to compare with), but it is difficult to employ them in a simulation task for system design. A summary of the results of the sensitivity analysis is reported in Table 6.

6. Conclusion

DSF design, due to its more complex behaviour compared to conventional building envelopes, cannot be based on simple performance parameters. It requires more detailed building performance simulation. The accuracy of BES tools in predicting the thermal behaviour of naturally ventilated double-skin façades is crucial in proving their performance and could boost their adoption in real buildings. Furthermore, BES could be used as virtual test beds to design and compare control strategies for DSFs, which are of utmost importance for increasing the whole building operational performance.

The findings of this comprehensive investigation indicate that no single BES tool outperforms the others for different DSF configurations. The cavity air temperature was the most difficult variable to predict: IES-VE provided good predictions in thermal buffer mode and EnergyPlus in outdoor air curtain mode, while the performance of all tools was quite similar for supply air mode– with the exception of EnergyPlus. The use of CONTAM in a co-simulation scheme was necessary to reduce the gap in the performance prediction. In most of the tools, the absence of heat capacity of the glazing system is reflected in a considerate lagging of the prediction of the peak compared to the experimental data. This effect was more pronounced in thermal buffer mode since the thermal behaviour is governed by the heat transfer between the façade system and the cavity air (the mass exchange is minimal in this configuration). The effect is particularly noticeable when the roller shade is deployed. For the other ventilation modes, TRNSYS, EnergyPlus and IDA-ICE tended to underpredict the peak cavity temperature when the shading was deployed, whilst the performance of IES-VE was unaltered. TRNSYS, instead, performed better in predicting the surface temperature and the transmitted solar irradiance, providing satisfactory results in line with experimental data.

With the exception of IDA-ICE, in most BES tools, the zonal approach is the only alternative to model naturally a ventilated DSF. This requires expert knowledge of physical phenomena to understand the simulated results' reliability, going beyond the default parameters, as demonstrated by the modelling, experimental validation and sensitivity analysis carried out. Moreover, building energy simulations often require input data that is not easily accessible from technical drawings, so modellers must devise abstractions and workarounds based on their experience.

Therefore, sensitivity analyses were conducted to discuss the influence of unknowns and challenges modellers may face when simulating a naturally ventilated DSF. The investigation proved that the aspects impacting most the thermal behaviour of the DSF are the ones directly affecting the mass flow in the cavity for ventilated configurations (outdoor air curtain and supply air) and the ability of the model to represent the thermal inertia of the glazing system for thermal buffer mode. The biggest challenge is probably the accurate estimation of inlet/outlet opening areas and related ventilation opening models implemented in the BES tools. In addition, when the shading was present, current correlations employed to calculate the convective heat exchange between the shading and the cavity air led to the underestimation of air temperature in the cavity. Moreover, the ability to account for the heat capacity of the glass layers results in a better estimation of the temperature dynamics within the DSF models. These aspects can represent directions for future work and model development to improve the performance prediction of DSF in BES tools. Finally, providing the modellers with an increased number of BES output variables, especially when it comes to the zonal approach, could contribute to improving the confidence in the results by offering more opportunities for validation and model debugging (i.e. variables such as cavity air velocity and transmitted solar radiation between adjacent internal zones). In light of the above, both the models and the experimental data generated for the present study are publicly and freely available on an open-access repository:

- the models developed with the different simulation environments for this study can be found at, and referenced using, the following https://doi.org/10.5281/zenodo.7437314 [37];
- the experimental data generated for this study, for the validation of the models, can be found at, and referenced using, the following https://doi.org/10.5281/zenodo.7436983 [38].

CRediT authorship contribution statement

Giovanni Gennaro: Writing – original draft, Visualization, Validation, Methodology, Investigation, Formal analysis, Data curation, Conceptualization, Software, Writing – review & editing. **Elena Catto Lucchino:** Writing – original draft, Validation, Formal analysis, Data curation, Conceptualization, Investigation, Methodology, Software, Writing – review & editing. **Francesco Goia:** Writing – review & editing, Supervision, Resources, Project administration, Methodology, Funding

acquisition, Conceptualization, Visualization. **Fabio Favoino:** Writing – review & editing, Visualization, Supervision, Resources, Methodology, Funding acquisition, Conceptualization.

Declaration of competing interest

The authors declare that they have no known competing financial interests or personal relationships that could have appeared to influence the work reported in this paper.

Data availability

We make available on ZENODO, an open-access repository, the models developed with the different simulation environments and the experimental data generated.

Acknowledgements

The authors would like to acknowledge the Research Council of Norway for sponsoring the research project "REsponsive, INtegrated, VENTilated - REINVENT – windows" (research grant no. 262198) and Hydro Extruded Solutions for the realisation and installation of the DSF prototype.

The authors thank the Department of Innovation, Research and University of the Autonomous Province of Bozen/Bolzano for covering the Open Access publication costs.

Appendix A

A description of the physical-mathematical models for energy and mass balance, and for heat transfer processes relevant for the simulation of DSF systems have been presented in a previous study – [11], see Appendix B – for the four BES tools employed in the study. For the sake of brevity, the focus in this Appendix will be placed on the distinctive aspects that play a role in the modelling of natural ventilation and on how the models have been set up to represent the particular test case adopted in this study. The reader might therefore find useful to first go through the description of the physical-mathematical models in Ref. [11] to have a complete overview of how DSFs can be modelled in the different BES tools.

A.1 - EnergyPlus

The model geometry of the case study was first defined in SketchUp through the Euclide plug-in. SketchUp allows the user to define the three stacked zones for the façade and one zone for the indoor environment and automatically matches surfaces between zones. The cavity zone was modelled with exterior and interior double glazing, whilst the inlet and outlet were provided with the ventilation opening modelled as opaque doors. The surface between each stacked zone was modelled as a fictitious window made of infrared transparent material. The other surface of the zones, which corresponds to the frame of the façade, was modelled as massive construction with defined stratigraphy.

The airflow between the stacked zone and the adjacent internal zone was modelled and managed through the Airflow Network, in which each zone corresponds to a single air node linked by airflow components. The fictitious surface zone divider was modelled as an always-open horizontal opening, while pivoted windows were used as ventilation openings to link the façade nodes with the outdoor and indoor nodes. In the pivoted windows, the opening angle is linearly proportional to the window opening factor (an opening factor of 1 equals an opening angle of 90°), and by varying this factor it was possible to open and close the ventilation openings, which were managed by the EMS tool through input schedules, in order to indicate the DSF airpath configuration to simulate.

"*Full interior and exterior with reflections*" was used as the solar distribution algorithm to calculate the interior solar radiation distribution. As a result, transmitted beam solar radiation is divided into each surface in the zone by projecting the sun's rays through the exterior windows, taking into account the effect of the window shading devices. The shading was modelled as a window shade material and assigned to the exterior window as an interior shading device 12.25 cm from the glass surface (middle of the air cavity). The convection coefficient for the cavity surfaces was calculated according to the ISO 15099 [30], chosen automatically by the "*adaptive algorithm*".

Co-simulation between EnergyPlus and CONTAM

The CONTAM user interface, ContamW, was used to create the CONTAM project file containing a scaled representation of the test cell. The cavity and the indoor room were divided into three stacked zones belonging to three different levels. The fictitious zone dividers were modelled as "*Shaft*" elements always opened, while the ventilation openings were modelled as "*Two-way Flow Opening*" elements. Each of these elements requires the geometry of the openings (in terms of cross-sectional area and perimeter for the Shaft elements and height and width for the ventilation openings), the flow exponent (set to 0.5 – default value) and the distance between the floor's level. In addition, for the ventilation openings the discharge coefficient is also required, which was set to 0.65. Finally, the fictitious duct connecting the volume of the test cell to the outdoor was modelled as an "*Orifice area*" with a 0.1 m^2 cross-sectional area.

Starting from the CONTAM project file, the CONTAM3Dexporter was used to generate an IDF file containing building geometry with the construction and the zone infiltration objects. At each simulation time step EnergyPlus gets interzone and infiltration airflows from CONTAM, while CONTAM successively receives indoor air temperature from EnergyPlus and performs airflow simulation. The co-simulation is performed using the Functional Mock-up Unit (FMU), in which EnergyPlus implements a co-simulation master algorithm and CONTAM is a slave process.

A.2 - TRNSYS

The model geometry of the case study was defined in the 3D Building plug-in for SketchUp, which allows the user to define the three stacked zones for the façade and one zone for the indoor environment and to match surfaces between zones automatically. The openings between each stacked zone were modelled as virtual surfaces in order to merge the three air nodes into a single thermal zone. Indeed, TRNSYS distinguishes between zones and air nodes: TRNFLOW interacts with the air nodes, whilst the radiation balance is solved for thermal zones. Thus, the DSF was modelled as one thermal zone containing several stacked air nodes linked with large virtual openings. The DSF air nodes network was linked with the whole building air nodes network so that the DSF became an integrated part of the building.

TRNSYS uses TRNFLOW [19] to integrate the multizone airflow model COMIS into the thermal building module (Type 56). All the ventilation openings were modelled as large pivoted windows whose dimensions replicate the size of the opening size of the case study (1.4 m width and 0.3

height) and the fictitious openings between cavity air nodes were modelled as always-opened large windows, corresponding to the cavity dimensions. In order to make the DSF model flexible, the opening factor of the window (0 for closed and 0.45 for open) was given to TRNFlow as input through Type 9.

The "*detailed radiation model*" was used for shortwave direct and diffuse radiation distribution and long-wave radiation exchange within a zone, as recommended in Ref. [19] for simulating a double-skin façade and atrium. Using the 3D geometry, the model allows for detailed solar distribution, including reflections in the zone cavity. In particular, for the distribution of the beam radiation, matrices based on the 3D dimensional data of the building are used to distribute the primary solar direct radiation entering the zone; for diffuse and long-wave radiation, the radiation model applies the so-called Gebhart factor [19] to generate the view factor matrix.

The shading was assigned to the exterior window as an interior shading device. Therefore, it is not possible to define the position of the shading, and the model allows only to define the fraction of the solar radiation absorbed by the internal device that is transferred by convection to the cavity air between the inner window pane and the internal shading device (this value was set to 0.5 as default).

The internal convective heat transfer coefficient was calculated using the vertical window's internal algorithm.

A.3 - IES VE

The model was created employing IES VE 2021. The modelling of the double-skin façade was obtained using different stacked thermal zones. The '*Apache*' module was used to assign the building's thermal properties and solve the thermal network. The '*MacroFlo*' module was used to define the openings and model the airflow network. The '*ApacheSim*' simulation engine determines the building's thermal conditions by balancing sensible and latent heat flows entering and leaving each air mass and building surface. ApacheSim uses a stirred tank model of the air in a room. Since *ApacheHVAC* and *MacroFlo* are included, the calculations also include the mechanical and natural ventilation airflow rates calculated by these tools and the inter-dependence between these variables and those calculated within ApacheSim.

The DSF was modelled as three stacked zones delimited by two horizontal windows modelled as holes (always open and transparent to solar radiation). The inlet and outlet openings were modelled as large openings using the window category '*Top- Hung*'. The default coefficients were adopted to model the closed opening (Crack Flow 0.015 l/(s*m*Paˆ0.6)).

The shading device was assigned to the internal side of the external glazing system, and it is not possible to define the distance from the glass. It was modelled as an internal curtain and the values of shading coefficient (SC) and shortwave radiant fraction coefficient (SWRF) were calculated starting from the absorption and transmission values of the shading device [17]:

$$SC = \tau + 0.87\alpha;\ SWRF = \frac{\tau}{SC}$$

The inner surface's convection coefficient of the DSF was calculated using Alamdari and Hammond's correlation [30].

A.4 - IDA ICE

The model was developed using IDA ICE 4.8, and the in-built component '*Double-Glass Façade*' was used to model the ventilated cavity. The façade was modelled as a '*Ventilated wall*', which means that the entire façade is modelled as ventilated. The glazing, both internal and external, was modelled using the detail window component that models the window panes and shading layer according to the ISO 15099 [14].

Due to the geometry of the experimental set-up, some adjustments concerning the frame ratio were necessary; the interior window was modelled as a window with dimensions corresponding to the glazed area and 1% frame. The wall on which this window is installed was modelled with a U-value corresponding to the one of the window frames. The exterior window was instead modelled as the real one (full height and 60% of the frame). This workaround was necessary to overcome the tool limitations when distributing the solar radiation from the exterior window to the inner glazing. The calculation methods applied in the '*detailed window model*' assume a geometrical distribution between the glazing and the frame, not as a function of the incident angle. This leads to a sub-optimal distribution of the solar radiation on the inner glazing, thereby significantly underestimating the solar radiation transmitted by the whole component (only 40% of the radiation would be hitting the inner glass). Since the two glazing panes are very close, it can be assumed that a higher percentage of radiation that penetrates the first skin also crosses the second. This distribution cannot be modified if the inner facade is modelled as a whole façade window since the distribution between glazing and frame is done within the "*detail window component*", while the amount of solar distributed to the inner walls of the cavity can be modified instead. Therefore, by assigning the thermal properties of the frame to the wall and modelling the window as almost 100% glazed, it was possible to redistribute the solar radiation with a more realistic ratio (70% to the glazing and 30% to the frame).

The shading device was modelled as part of the exterior glazing and placed 12.5 cm from the inner pane. For both glazing systems, the capacity of each glass pane was set to 750 J/kg K.

The indoor and outdoor openings (according to which configuration was modelled) were modelled as leaks. Therefore, the default effective leakage area (ELA) method was adopted. The ELA values used were calculated using the method described in the TRNSYS manual for hinged windows [19]. To model the infiltration, the tool default assumption was adopted when the windows were closed (0.5 ACH at 50 Pa). This means that, if applied to a single exposed façade, the total ELA was $2x10^{-4}$ m^2, if distributed to the two openings, it corresponds to 10^{-4} m^2 each.

References

[1] A. GhaffarianHoseini, A. GhaffarianHoseini, U. Berardi, J. Tookey, D.H.W. Li, S. Kariminia, Exploring the advantages and challenges of double-skin façades (DSFs), Renew. Sustain. Energy Rev. 60 (2016) 1052–1065, https://doi.org/10.1016/j.rser.2016.01.130.

[2] F. Favoino, M. Baracani, L. Giovannini, G. Gennaro, F. Goia (2022). 6 - Embedding Intelligence to Control Adaptive Building Envelopes, Editor(s): Eugenia Gasparri, Arianna Brambilla, Gabriele Lobaccaro, Francesco Goia, Annalisa Andaloro, Alberto Sangiorgio, In Woodhead Publishing Series in Civil and Structural Engineering, Rethinking Building Skins, Woodhead Publishing, 2022, Pages 155-179, ISBN 9780128224779, https://doi.org/10.1016/B978-0-12-822477-9.00007-3.

[3] R.C.G.M. Loonen, F. Favoino, J.L.M. Hensen, M. Overend, Review of current status, requirements and opportunities for building performance simulation of adaptive facades, J. Build. Perform. Simul. 10 (2) (2017) 205–223, https://doi.org/10.1080/19401493.2016.1152303.

[4] W. Choi, J. Joe, Y. Kwak, J.H. Huh, Operation and control strategies for multi-storey double skin facades during the heating season, Energy Build. 49 (2012) 454–465, https://doi.org/10.1016/j.enbuild.2012.02.047.

[5] I. Khalifa, L. Gharbi-Ernez, E. Znouda, C. Bouden, Assessment of the inner skin composition impact on the double-skin façade energy performance in the

mediterranean climate, Energy Proc. 111 (2017) 195–204, https://doi.org/10.1016/j.egypro.2017.03.021. September 2016.
[6] N.M. Mateus, A. Pinto, G.C. Da Graça, Validation of EnergyPlus thermal simulation of a double skin naturally and mechanically ventilated test cell, Energy Build. 75 (2014) 511–522, https://doi.org/10.1016/j.enbuild.2014.02.043.
[7] A.S. Ancrossed D Signelković, I. Mujan, S. Dakić, Experimental Validation of a EnergyPlus Model: Application of a Multi-Storey Naturally Ventilated Double Skin Façade, vol. 118, Energy Build, 2016, pp. 27–36, https://doi.org/10.1016/j.enbuild.2016.02.045.
[8] M. Shahrestani, et al., Experimental and numerical studies to assess the energy performance of naturally ventilated PV façade systems, Sol. Energy 147 (2017) 37–51, https://doi.org/10.1016/j.solener.2017.02.034.
[9] D. Kim, S.J. Cox, H. Cho, J. Yoon, Comparative investigation on building energy performance of double skin façade (DSF) with interior or exterior slat blinds, J. Build. Eng. 20 (2018) 411–423, https://doi.org/10.1016/j.jobe.2018.08.012. January.
[10] D.W. Kim, C.S. Park, Difficulties and limitations in performance simulation of a double skin façade with EnergyPlus, Energy Build. 43 (12) (2011) 3635–3645, https://doi.org/10.1016/j.enbuild.2011.09.038.
[11] E. Catto Lucchino, et al., Modelling double skin façades (DSFs) in whole-building energy simulation tools: validation and inter-software comparison of a mechanically ventilated single-story DSF, Build. Environ. 199 (2021), https://doi.org/10.1016/j.buildenv.2021.107906. November 2020.
[12] E. Catto Lucchino, F. Goia, G. Lobaccaro, G. Chaudhary, Modelling of double skin facades in whole-building energy simulation tools: a review of current practices and possibilities for future developments, Build. Simulat. 12 (1) (2019) 3–27, https://doi.org/10.1007/s12273-019-0523-7, 10.1007/s12273-019-0511-y)," Build. Simul., pp. 3–27, 2019.
[13] J. Hensen, M. Bartak, F. Drkal, Modeling and simulation of a double-skin façade system, Build. Eng. 108 (2002). January.
[14] A.B. Equa Simulation, IDA ICE 4, 8 User Manual," No, 2018. January,.
[15] U. S. DOE, Engineering Reference, 2014.
[16] M. Hiller, J. Merk, P. Schöttl, TRNSYS 18 - Type 56: Complex Fenestration Systems Tutorial, 2017, pp. 1–22. January.
[17] V.E. Ies, ApacheSim User Guide," *IES VE User Guide*, 2014.
[18] G.N. Walton, Airnet - a computer program for building airflow network modelling, Nistir 89-4072 77 (1989) no. April.
[19] Solar Energy Laboratory, Trnsys 18, Vol. 5 Multizone Build. Model. with Type 56 TRNBuild 3 (2018) 7–36.
[20] P. Warren, Multizone air flow modelling (COMIS, Int. Energy Agency 48 (2000).
[21] E. Taveres-Cachat, F. Favoino, R. Loonen, F. Goia, Ten questions concerning co-simulation for performance prediction of advanced building envelopes, Build. Environ. 191 (2021), 107570, https://doi.org/10.1016/j.buildenv.2020.107570. January.
[22] W.S. Dols, B.J. Polidoro, CONTAM User Guide and Program Documentation, 2020, p. 330, https://doi.org/10.6028/NIST.TN.1887r1. https://nvlpubs.nist.gov/nistpubs/TechnicalNotes/NIST.TN.1887r1.pdf [Online]. Available:, Version 3.4.
[23] W.S. Dols, S.J. Emmerich, B.J. Polidoro, Coupling the multizone airflow and contaminant transport software CONTAM with EnergyPlus using co-simulation, Build. Simulat. 9 (4) (2016) 469–479, https://doi.org/10.1007/s12273-016-0279-2.
[24] M. Justo Alonso, W.S. Dols, H.M. Mathisen, Using Co-simulation between EnergyPlus and CONTAM to evaluate recirculation-based, demand-controlled ventilation strategies in an office building, Build. Environ. 211 (2022), 108737, https://doi.org/10.1016/j.buildenv.2021.108737.
[25] I. Khalifa, L.G. Ernez, E. Znouda, C. Bouden, Coupling TRNSYS 17 and CONTAM: simulation of a naturally ventilated double-skin façade, Adv. Build. Energy Res. 9 (2) (2015) 293–304, https://doi.org/10.1080/17512549.2015.1050694.
[26] N. Yoon, D. Min, Y. Heo, Dynamic compartmentalization of double-skin façade for an office building with single-sided ventilation, Build. Environ. 208 (September 2021) (2022), 108624, https://doi.org/10.1016/j.buildenv.2021.108624.
[27] ASHRAE, 2001 Fundamental Handbook 30 (2001).
[28] M.W. Liddament, Air Infiltration Calculation Techniques - an Application Guide, Air Infiltration and Ventilation Centre, 1986.
[29] ASHRAE, ASHRAE fundamental handbook, Atlanta 30 (2001).
[30] ISO 15099, "International Standard ISO 15099:2003., Thermal Performance of Windows, Doors and Shading Devices — Detailed Calculations, 2003.
[31] F. Alamdari, G.P. Hammond, Improved data correlation for buoyancy-driven convection in rooms, Build. Serv. Eng. Technol. 4 (3) (1983) 106–112.
[32] A. Jankovic, G. Gennaro, G. Chaudhary, F. Goia, F. Favoino, Tracer gas techniques for airflow characterization in double skin facades, Build. Environ. 212 (2022), 108803, https://doi.org/10.1016/j.buildenv.2022.108803. January.
[33] F. Favoino, F. Goia, M. Perino, V. Serra, Experimental analysis of the energy performance of an ACTive, RESponsive and Solar (ACTRESS) façade module, Sol. Energy 133 (2016) 226–248, https://doi.org/10.1016/j.solener.2016.03.044, 2016.
[34] F. Goia, V. Serra, Analysis of a non-calorimetric method for assessment of in-situ thermal transmittance and solar factor of glazed systems, Sol. Energy 166 (2018) 458–471, https://doi.org/10.1016/j.solener.2018.03.058. November 2017.
[35] ASHRAE, Guideline 14-2014, Measurement of Energy and Demand Savings, Atlanta, 2014.
[36] EN 12207 Windows and Door Air Permeability Classification, 2016.
[37] G. Gennaro, E. Catto Lucchino, F. Goia, F. Favoino, Models for Validation of a Naturally Ventilated Single-Story Double Skin Facade in Whole-Building Energy Simulation Tools, 2022, https://doi.org/10.5281/zenodo.7437314.
[38] G. Gennaro, E. Catto Lucchino, F. Goia, F. Favoino, Experimental Data for Validation of a Naturally Ventilated Single-Story Double Skin Facade in Whole-Building Energy Simulation Tools, 2022, https://doi.org/10.5281/zenodo.7436983.
[39] J.M. Bright, N.A. Engerer, Engerer2: global re-parameterisation, update, and validation of an irradiance separation model at different temporal resolutions, J. Renew. Sustain. Energy 11 (3) (2019), https://doi.org/10.1063/1.5097014.
[40] J.-N. Hersbach, H, B. Bell, P. Berrisford, G. Biavati, A. Horányi, J. Muñoz Sabater, J. Nicolas, C. Peubey, R. Radu, I. Rozum, D. Schepers, A. Simmons, C. Soci, D. Dee, Thépaut, ERA5 hourly data on single levels from 1979 to present. Copernicus Climate Change Service (C3S) Climate Data Store (CDS) (2018), https://doi.org/10.24381/cds.adbb2d47. Accessed on < 26-APR-2021 >).

6 Modelling and validation of a single-storey flexible double-skin façade system

P5 *E. Catto Lucchino, G. Gennaro, F. Favoino, F. Goia. Modelling and validation of a single-storey flexible double-skin façade system with a building energy simulation tool. Building and Environment 226 (2022), 109704. https://doi.org/10.1016/j.buildenv.2022.109704*

Double skin façades are adaptive envelopes designed to improve building energy use and comfort performance. Their adaptive principle relies on the dynamic management of the cavity's ventilation flow and, when available, of the shading device. They can also be integrated with the environmental systems for heating, cooling, and ventilation. However, in most cases, the possible exploitation of the ventilation airflow is not fully enabled as the adoption of only one or two possible airpaths limits the possibility that this façade architecture offers, meaning that flexible interaction with the environmental systems cannot be planned. Using an existing software tool for building energy simulation, this work aims to develop a numerical model of a flexible double-skin façade module capable of fully exploiting the adaptive features of such an envelope concept by switching between different cavity ventilation strategies. Leveraging the "Double Glass Façade " component available in IDA ICE, a new model for a flexible double-skin façade module was developed, and its performance in replicating the thermophysical behaviours of such a dynamic system was assessed by comparison with experimental data collected through a dedicated experimental activity using the outdoor test cells of the TWINS facility in Torino (Italy). The accuracy of the predictions of the new model for a flexible double-skin façade was in line with that obtained by the conventional "Double Glass Façade" component to simulate traditional double-skin façades. The mean bias errors obtained were lower than 1.5 ◦C and 4 W/m² for air and surface temperature values and for transmitted long-wave or short-wave heat flux values, respectively. By establishing a new archetype model to study the performance and optimal integration of a large class of double-skin façade modules, including

fully flexible ones, this work demonstrates the possibility of modifying existing models in building energy simulation tools to study unconventional building envelope model solutions such as adaptive façade systems.

Building and Environment 226 (2022) 109704

Contents lists available at ScienceDirect

Building and Environment

journal homepage: www.elsevier.com/locate/buildenv

Modelling and validation of a single-storey flexible double-skin façade system with a building energy simulation tool

Elena Catto Lucchino [a], Giovanni Gennaro [b,c], Fabio Favoino [b], Francesco Goia [a,*]

[a] Department of Architecture and Technology, Norwegian University of Science and Technology, NTNU, Trondheim, Norway
[b] Department of Energy, Politecnico di Torino, Torino, Italy
[c] Institute for Renewable Energy, EURAC Research, Bolzano, Italy

ARTICLE INFO

Keywords:
Adaptive façades
Double-skin facades (DSF)
Model validation
Building energy simulation
IDA ICE

ABSTRACT

Double skin façades are adaptive envelopes designed to improve building energy use and comfort performance. Their adaptive principle relies on the dynamic management of the cavity's ventilation flow and, when available, of the shading device. They can also be integrated with the environmental systems for heating, cooling, and ventilation. However, in most cases, the possible exploitation of the ventilation airflow is not fully enabled, as the adoption of only one or two possible airpath limits the possibility that this façade architecture offers, meaning that flexible interaction with the environmental systems cannot be planned. This work aims to develop, using an existing software tool for building energy simulation, a numerical model of a flexible double-skin façade module capable of fully exploiting the adaptive features of such an envelope concept by switching between different cavity ventilation strategies. Leveraging the "Double Glass Facade" component available in IDA ICE, a new model for a flexible double-skin façade module was developed, and its performance in replicating the thermophysical behaviours of such a dynamic system was assessed by comparison with experimental data collected through a dedicated experimental activity using one the outdoor test cells of the TWINS facility in Torino (Italy). The accuracy of the predictions of the new model for a flexible double-skin façade was in line with that obtained by the conventional "Double Glass Facade" component to simulate traditional double-skin facades. The mean bias errors obtained were lower than 1.5 °C and 4 W/m^2, for air and surface temperature values and for transmitted long-wave or short-wave heat flux values, respectively. By establishing a new archetype model to study the performance and optimal integration of a large class of double-skin façade modules, including fully flexible ones, this work demonstrates the possibility of modifying existing models in building energy simulation tools to study unconventional building envelope model solutions such as adaptive façade systems.

1. Introduction

1.1. Background and research relevance

Double skin façades (DSFs) are highly transparent envelope technologies that can dynamically adjust their thermo-optical properties in response to transient boundary conditions (either external, such as climate, or internal, such as occupants' requirements). Such adaptive behaviour can allow the exploitation of solar energy for both passive solar thermal gains and daylighting, which can reduce energy use for building climatisation [1] and provide better thermal and visual comfort conditions compared to a traditional single-skin façade [2]. An important adaptive principle in a DSF is the dynamic management of the ventilation flow in the façade cavity [3], often in combination with a shading system installed in the cavity to achieve variable performance goals. In most cases, however, the possible exploitation of the ventilation airflow is limited to just one or two options: only *outdoor air curtain* (OAC) ([4–9]); only *supply air* (SA) [10]; OAC and e*xhaust air* (EA) [11]; *indoor air curtain* IAC and OAC [12]; *thermal buffer* TB and OAC [13,14]; or TB and SA [15]. This conventional approach significantly reduces the possibility of fully exploiting the conceptual flexibility offered by this façade architecture as, in theory, both the inlet side (either outdoor air or indoor air) and the outlet side (again, towards the inside or the outside) can be combined to obtain a significant variation in the performance of the façade.

Moreover, the dynamic integration between a ventilated façade and the HVAC system could also play a significant role in enhancing the

* Corresponding author.
E-mail address: francesco.goia@ntnu.no (F. Goia).

https://doi.org/10.1016/j.buildenv.2022.109704
Received 28 June 2022; Received in revised form 20 September 2022; Accepted 11 October 2022
Available online 14 October 2022

Acronym list

BES	building energy simulation
***CV*(*RMSE*)**	coefficient of variation of the root mean square error
DSF	double skin facade
EA	exhaust air
IAC	indoor air curtain
OAC	indoor air curtain
SA	supply air
TB	thermal buffer
MBE	mean bias error
NMBE	normalised mean bias error
RMSE	root mean squared error

Nomenclature

g	solar factor (−)
λ	thermal conductivity of air (W/mK)
M_i	Measured value at one point
n	Total number of measurements
P_i	Simulated predicted value
ρ_{in}	glazing solar reflectance, inner face (−)
ρ_{out}	glazing solar reflectance, outer face (−)
s	thickness (mm)
τ_{sol}	glazing solar transmittance (−)
U	glass thermal transmittance (W/(m^{2}K))
U_f	frame thermal transmittance (W/(m^{2}K))

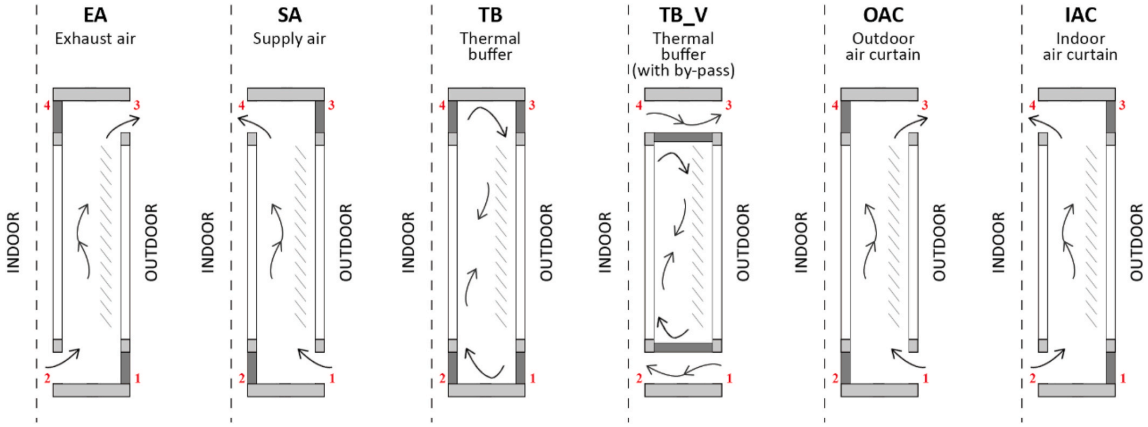

Fig. 1. Ventilation strategies implementable in a fully flexible DSF module.

adaptive behaviour of a façade, yet this feature has been rarely investigated so far [16]. Doing so could open new possibilities to further improve the overall performance of the building, e.g., by reducing the demand for mechanical ventilation if the conditions for supplying fresh air through the façade are met. By stretching the borders of the existing concept of DSFs, playing with the airflow path, the airflow type (mechanically or naturally driven), the interplay with the solar shading system, and the overall integration with the HVAC elements in the buildings, one could thus, in theory, enable a vast range of variability in the façade.

The advantages and performance linked to the dynamic exploitation of different airflow paths and a variable integration with the HVAC system have been rarely explored in real cases and also at the research level. Park and co-authors [17,18] developed a lumped model of a flexible DSF with calibration with in-situ measurements and tested it with an optimised control strategy; the developed model allowed for ten different natural ventilation strategies, together with varying positions of shading and opening degrees. Later studies by the same authors adopted a co-simulation approach between an improved version of the previously developed lumped model [19] and a building energy simulation (BES) tool [20], achieving better results than using a zonal method.

As demonstrated by the previous studies, a detailed simulation of the thermal, fluid mechanic, and optical behaviour of a DSF is necessary to test and optimise the behaviour of such a façade concept. The coupling between such an envelope model and a whole building energy simulation (BES) tool is essential for correctly assessing the interplay between the envelope system and the overall building environmental systems and, consequently, the overall performance of this concept. Only a few BES tools include dedicated modules for DSFs' simulation [21], but none allow the façade to adopt different ventilation strategies within the same simulation run, which is one of the gaps in existing models of DSF systems for BES tools [22]. Currently, the simulation of a flexible DSF system with a BES tool can only be carried out by co-simulation, a process that presents advantages and a series of limitations and challenges - such as the need to develop a dedicated model for the flexible DSF and to couple it with a BES tool.

The scope of the research presented in this paper covers the possibilities and challenges of simulating a flexible double-skin façade system using existing software tools for building energy simulation without the need to resort to co-simulation. The research showcases how existing structures in established software environments can be modified to meet the modelling requirements for building envelope systems that go beyond the current possibilities in the specific tool. The elements of innovation of this research can be summarised in the list below:

- a new DSF model archetype, based on the calculation routines for DSFs available in the tool IDA ICE, where ventilation air path and driving force can be continuously changed during the simulation runtime, as well as the interaction between the façade and the HVAC of the building;
- a comprehensive validation of the DSF model archetype using experimental data, covering different airflow paths, and driving forces, which demonstrates the reliability of the numerical model,

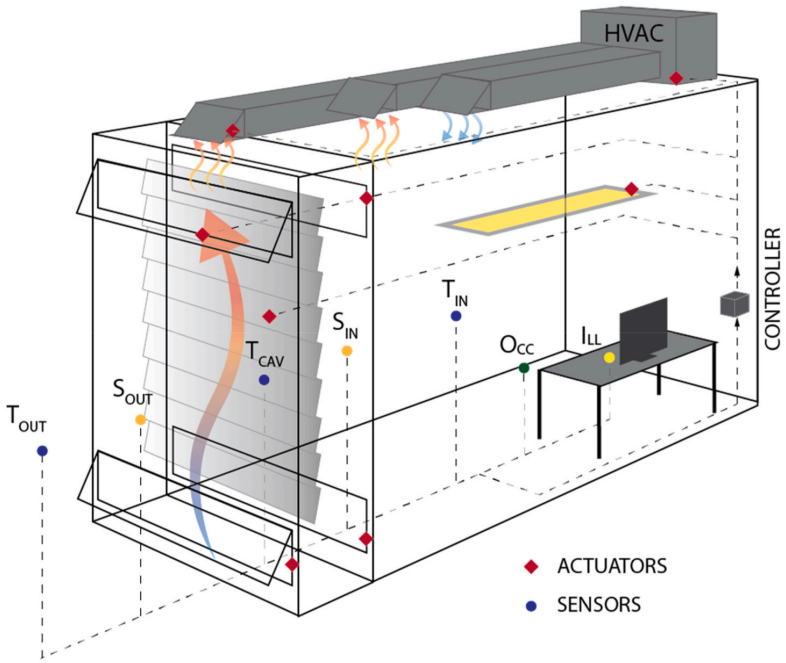

Fig. 2. Integration between the room systems and a DSF.

using data collected through a dedicated experimental activity where a façade prototype was installed on one outdoor test cell of the TWINS facility in Torino (Italy)
- the flexible DSF system model is made publicly available through a repository [23].

1.2. Research aims and objectives, manuscript structure and target audience

The primary aim of the research activity was to develop and validate a numerical model of a flexible double-skin façade system with a building energy simulation (BES) tool. Beyond showcasing how BES tools can be modified to simulate more advanced façade systems, the need for a flexible DSF module arose from a dedicated research project on this façade concept. As explained in more detail in the following sections, the core of the dynamic facade concept explored in this research is a flexible DSF module capable of switching between different cavity ventilation strategies (Fig. 1): exhaust air (EA), supply air (SA), outdoor air curtain (OAC), indoor air curtain (IAC) and thermal buffer (TB), and ventilated thermal buffer (TB_V)), coupled with different airflow-inducing mechanisms (i.e., either a natural (N) or a mechanical (M) airflow (a feature that increases the complexity of the operations of the façade element drastically), and therefore interplay with the HVAC plant of the building.

The secondary aim of this activity was to provide the building simulation community and the design community with a single-storey DSF model archetype that could be used not only in its most extreme configuration (with full flexibility in the ventilation airflow path) but also as a standard model to explore better operations for more conventional single-storey DSF modules. Such a model overcomes the current limitations of conventional DSF models in BES tools. Furthermore, given the validation procedure carried out in this study, the reliability of this flexible numerical model has been checked over a large range of operational modes.

The choice of the BES tool employed in this activity builds on a previous study [21], which showed that only a few tools embed routines for modelling a DSF: IDA ICE, EnergyPlus, and TRNSYS. In the latter two tools, these in-built components only model mechanically ventilated facades. Conversely, IDA ICE's component allows the modelling of DSFs with both natural and mechanical cavity ventilation through the in-built component called *"Double Glass Facade"*. This in-built module, presented in the next section, is already integrated into the thermal and airflow network of the BES tool and allows the combined simulation between the façade component and the indoor space.

IDA ICE (IDA Indoor Climate and Energy) is a BES software that supports the simulation of multi-zonal indoor climate phenomena and energy use in buildings when subjected to transient state boundary conditions. It implements state-of-the-art models, and it has been validated according to the relevant international standards (e.g., ISO 13791, now ISO 52016–1:2017 [24]; EN 15255 and 15,265 [25], ASHRAE 140 [26]). IDA ICE is a differential-algebraic equation (DAE) based tool with a library written in neutral model format (NMF) [27,28]. This allows editing the components' connections in a relatively free way (at least compared to the other tools), leading to the possibility of implementing a more flexible model without resorting to establishing co-simulation routines – a frequently necessity in many BES tools when modelling advanced building envelope concepts which structures are not available in numerical representations embedded in these tools, or when multiple physical (and performance) domains need to be simultaneously represented, sometimes with different levels of model complexity [29]. The already available openness of the DSF routine in IDA ICE, together with the overall performance in replicating the thermophysical and optical behaviour of DSF, was the reason for selecting this tool for this research. The *"Double Glass Facade"* option is used in a basic simulation model, and it is then further developed and modified to meet the functionality requirement identified for the flexible DSF module concept.

The overall research design was broken down into a series of steps that are described by the following objectives: i) to identify a suitable

BES tool and, by leveraging its functionalities, to define a numerical representation of the flexible DSF concept (model development); ii) to collect a series of experimental data on a physical mock-up of a flexible DSF system under outdoor boundary conditions and dynamic control sequences; iii) to replicatethe experiments using measured boundary conditions in BES environment; iv) to analyse and compare (both qualitatively and quantitatively) the simulation output of some selected physical quantities at façade level with the correspondent experimental values (model validation) in order to verify the reliability of the newly developed flexible DSF model.

To present the different objectives of the research design, the article is organised as follows. In *Section 2 – DSF-based adaptive façade concept and numerical model in a BES tool*, we provide the reader with a brief overview of the current possibilities and performance of DSF's simulation with different BES tools, and we present the first objective of the research activity, i.e., we describe how the enhanced model that allows the façade to be operated with different airflow paths/regimes was developed in the selected BES tool (IDA ICE). *In Section 3 – Experimental set-up and data collection for model validation*– we present information about a case-study façade prototype used to collect experimental data. In *Section 4 – Numerical model validation: methods, results, and discussion*, we describe how the experiments were replicated in a simulation environment by using the flexible DSF model, and we show the comparison between experimental data and numerical data to assess the reliability of the newly developed model. The conclusive summary of the paper is presented in *Section 5 – Conclusions*.

The research presented in this paper targets both the R&D community and the professional community. The concept of the highly flexible adaptive facade and its numerical model can be relevant for the first group, which can further investigate the performance of this concept and expande the knowledge about the challenges and possibilities in modelling (and controlling) advanced façade systems in BES. Furthermore, the experimental dataset used in this process is also openly shared in a repository for any researcher to use for model validation or performance analysis purposes. In this article, the professional community can find a demonstration of how to exploit existing BES tools to model advanced functionalities for building envelope systems that are not found in the modules embedded in the release of a BES. The flexible DSF model is also made available to stimulate the design and assessment of more advanced DSF systems that can exploit a broader range of operational modes.

2. DSF-based adaptive façade concept and its numerical model in a BES tool

2.1. Enabling adaptive behaviour through a flexible double-skin façade concept

The motivation that drives this study's development is to evolve the double skin façade/window architecture and to combine it with an integrated embedded control system in interaction with different elements of the building HVAC system to realise a flexible envelope component. This adaptive façade concept exploits different cavity ventilation paths with both mechanically and naturally driven airflows, allows the by-pass of the ventilated cavity if desired, and manages the direct solar and luminous gain through an integrated shading system (Fig. 2) in coordination with the building energy management system. One of the core elements of this façade system is the inlet and outlet section, which contains an actuator that makes it possible to easily switch between different ventilation paths. For reasons linked to IPR (Intellectual Property Rights), full details of this component cannot be provided here. Another core aspect of this façade system is that it integrates an embedded controller that manages the different actuators in the façade module (not only the inlet/outlet sections but also the integrated shading device and fans) and interacts with a supervisory level controller to ensure that the optimal control of the façade-level is jointly managed with the other types of equipment in the building.

This façade module is thus a dynamic element that, under the coordination of the room-level controller, becomes a part of an integrated envelope-HVAC system and actively contributes to balancing energy and indoor environmental quality requirements. In fact, to truly exploit the potential of such a fully flexible DSF vision, total variability across different aspects and components is the key to exploiting this highly dynamic element. As such, the performance of this adaptive building envelope system depends not only on the possibility of adapting its performance through changing its functioning modes but also on how such shift between the multiple operational modes is continuously controlled during operation (i.e., the control strategy) [30].

2.2. Modelling requirements, possible approaches and available in-built modules

A reliable numerical representation of the above-described adaptive façade concept based on a flexible DSF system is necessary to analyse the performance of the innovation idea, optimise its design, and define suitable control strategies for its operation. Detailed simulation of the thermal, fluid mechanics and optical behaviour of double skin facades/windows can be obtained using different approaches, such as custom-built models [17,18,31] or dedicated CFD (Computational Fluid Dynamics) simulations [32,33]. However, in terms of modelling requirements, a very dynamic envelope system must allow easy connectivity with other models that reproduce the heat and luminous balance of a closed space, as well as representations of other HVAC components that may become integrated players in the integration of a dynamic façade concept into a room. The coupled simulation of the whole building and the specific building components is essential to correctly assess the overall energy and comfort performance and replicate the complex interaction between airflow in the façade, the HVAC system, and the building energy management system. Finally, it is also the best way to study how a local strategy to control the façade is integrated into the overall building control strategy to ensure that both the envelope and environmental system for building climatisation act towards the same goal.

In this context, Building Energy Simulation (BES) tools are a good trade-off simulation environment to enable the complete study of adaptive envelope systems in connection with the rest of the building, even considering their limitations. BES tools have generally been developed to simulate the variation of physical conditions in the indoor space and calculate the necessary energy use to maintain the indoor space within a given range of conditions. Since they derive from the need to simulate the overall building performance, BES environments have not been designed to easily model and simulate adaptive facades, as the envelope is just a component of a broader system [34]. However, some possibilities exist to model adaptive façade systems by modifying the existing embedded modules suitably without exploring more advanced strategies such as co-simulation [29]. For example, the implementation of DSFs in BES is possible and has been widely explored in the past. A few BES tools include dedicated modules for DSFs' simulation [35]. However, no BES tool natively consists of the features that would allow one to model the highly flexible facade concept put forward in this research, as the few modules available present limitations regarding fully flexible cavity ventilation paths, alternation of ventilation mechanisms, different integration with the HVAC, etc. [21].

Different approaches are available to model the DSF, either through in-built modules or the so-called zonal approach [36]. The zonal approach divides the cavity into several thermal zones stacked vertically. The zones are connected through an airflow network representation that allows one to describe the airflow through the different zones. The effecet of the number of stacked thermal zones on the quality and reliability of the simulation has been previously explored [7,12], but there is no consensus nor a standardised approach when it comes to this setting, which usually ranges (when referred to as single-storey DSFs)

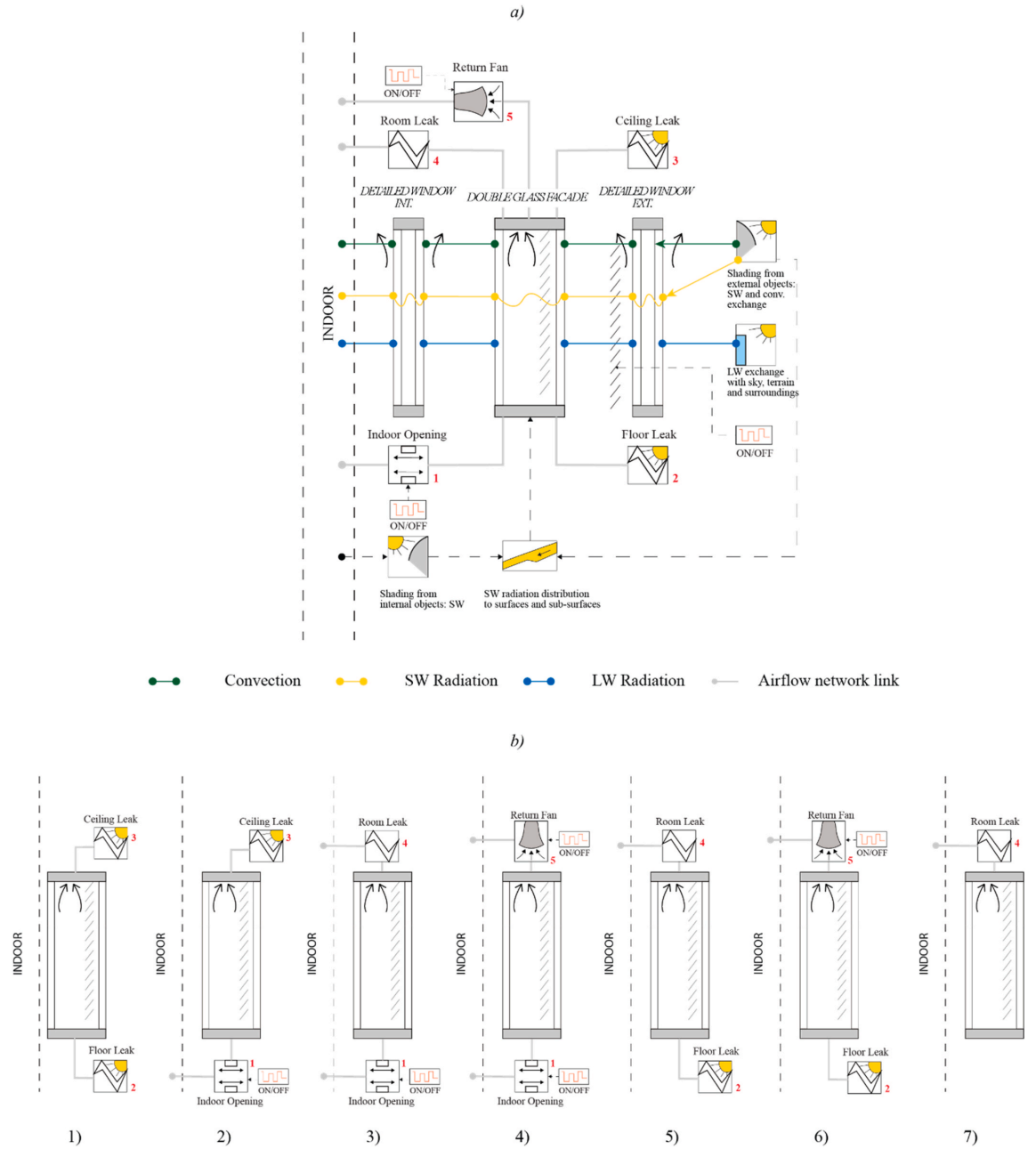

Fig. 3. a) Schematic view of the 'Double Glass Façade' component as implemented in IDA ICE with the different air links available (only one ventilation strategy at a time is implementable in a model) – b) Ventilation strategies that can be modelled using the component: 1) OAC_N, 2) OAC_M, 3) IAC_N, 4) IAC_M, 5) SA_N, 6) SA_M, and 7) TB.

from a minimum of one to a maximum of six.

The other modelling possibility available in some tools is to use an in-built module; a sub-routine dedicated to modelling DSF systems. These sub-models belong to the building envelope systems category and are objects linked to the other components of the simulated environment according to the requirements and possibilities set by each tool. While, on the one hand, this approach should lead to more accurate simulation (as the models for DSF are purposefully developed to replicate the thermal-fluid behaviour of these systems), on the other hand, this approach is usually less flexible than the approach where the modeller creates an ad-hoc, combined thermal and airflow network.

In a previous analysis covering several tools [21], we identified

different modelling approaches and possibilities to simulate DSFs in BES environments. A few simulation environments (EnergyPlus, IDA ICE and TRNSYS) offer dedicated in-built modules to simulate DSFs. In particular, IDA ICE's module for DSF simulation, called *"Double Glass Facade"*, allows the modelling of both naturally driven and mechanically driven DSFs and their dynamic interaction with the indoor space and the environmental systems. This model is suitable for transient state simulations and even includes the effect of the glazed layers' thermal inertia features–a feature not available in any of the other in-built modules embedded in different BES tools.

Another significant feature addressed by IDA ICE is the relatively easy definition of ad-hoc-developed decision trees that can control both façade and HVAC components. From the perspective of a flexible DSF system that can change the flow path and interact with the environmental systems (e.g., supply fresh air for ventilation in place of the mechanical ventilation plant, or act as an exhaust terminal for the ventilation plant), the smooth shift between the multiple, HVAC-integrated operational modes via combined control strategies is an important asset.

However, the in-built module does not present the level of flexibility necessary to meet the goals set for this research activity and will be modified, as explained more in detail in section 2.3.2, to satisfy the performance requirements set for the simulation model of a fully flexible DSF system.

2.3. Model implementation in IDA-ICE environment

In general, IDA ICE allows modelling with three different user interface levels [28]. At the most superficial level, called *Wizard*, the scope is limited to a specific type of study and level of approximation. The user can perform a simulation directly or transfer the data entered to the next level, called the *Standard* level. The user is given greater freedom to design a building model at the standard level. At this level, geometry, materials, controller settings, loads, etc., are defined, and some of them (geometry, external shadings, etc.) are not modifiable further at the next level, called the *Advanced* level. Here the simulation model is no longer defined in physical terms, but as connected component models defined by equations. All equations, parameters and variables can be examined, and the time evolution of variables can be studied.

Moreover, new connections between components can be created using the advanced modelling level, and a more comprehensive range of modelling strategies can be adopted. Furthermore, more advanced control strategies can be implemented, too, i.e., the controllable components can be connected to a schedule, or a control logic defined within the software with a relatively flexible and user-friendly interface. The advanced level was therefore employed in this work. In the first of the following sub-sections, we will describe how a DSF can be modelled at the standard level and which limitations this model presents (2.3.1); in the second sub-section (2.3.2), the modifications necessary to model a fully flexible DSF are presented.

2.3.1. Double Glass Facade component

DSFs can be modelled in IDA ICE at the standard level, using a 'Detail Window Model' component and enabling the possibility of adding a ventilated cavity: a window (which models the DSF as a box window) or wall (which models it as a ventilated wall of the same height as the external wall).

The ventilated cavity component is called *"Double Glass Façade"*-Fig. 3-a), and in it, the averaged cavity-air temperature is calculated based on the inlet temperature, mass flow and solar gains and heat transferred through the surfaces. The component calculates only one temperature for the whole façade, so the effects of the air stratification are not represented in an explicit way. The model geometry is two-dimensional; consequently, heat transferred through the sidewalls of the cavity is excluded from the energy balance calculation.

The *"Detail Window Model"*, both for the interior and exterior skin, adopts a layer-by-layer computation of multiple reflections, and each layer's temperature is computed according to ISO 15099 [37]. The shading layer, if present, needs to be modelled as part of one of the two detailed windows – as such, its properties are calculated according to the ISO 15099 (in case of spectral data being provided, both for the shading device and the glass layers, the calculation method adopted is the one of the ISO 52022–3 [38]). It is recommended to model it as an internal shade of the outer pane [39]. Two different calculation methods (e.g., convection coefficients, airflow, etc.) are adopted on each side of the shading device. One side is modelled as part of the *"Detail Window Model"* element, and the other is part of the *"Double Glass Façade"*. This is the one used in the air mass balance calculation.

From the standard level, as summarised in Fig. 3 a, the *"Double Glass Façade"* component allows five possible air-links to the cavity: *1* - an operable opening towards the zone; *2* - a leakage area at the floor and *3* - ceiling level of the cavity, connecting the cavity with the outdoor air; *4* - a leakage area between the room and the air space at a given height; *5* - a given flow from the cavity to the return air duct. The first three connections are defined as equivalent leakage area (ELA) calculated with a discharge coefficient, Cd = 1 and with the flow depending on the square root of the pressure difference; therefore, they are always open and not controllable. Only the opening towards the inside can be controlled (via schedule or PI control). The AHU fan schedule controls the mechanical air flow extracted from the facade. It is also important to mention that the mechanical ventilation of the cavity only works if coupled with the HVAC system, so the air cannot be exhausted directly to the outdoors.

The ventilation strategies natively available (Fig. 3 b) in this component can cover all the needs in terms of flow path: 1) OAC naturally ventilated; 2) EA naturally ventilated; 3) IAC naturally and 4) mechanically ventilated; 5) SA naturally and 6) mechanically ventilated; 7) TB. In order to model the thermal buffer mode, at least one small leak (either toward the inside or outside) has to be modelled. However, as anticipated, the fixed-configuration feature of the component limits the model's flexibility because of two main constraints: the impossibility of controlling some opening/connection types and the impossibility of modelling all the connections at the same time (i.e., within a single simulation run it is not possible to alternate flow paths and ventilation strategies).

The solar radiation modelling through the facade is carried out in the two complex window components. The solar radiation hitting the façade is calculated from the weather file according to the solar position in the sky and the orientation of each façade. The distribution of diffuse sky radiation is computed by default using the Perez model. Afterwards, the solar radiation on an individual object, such as a window, is computed. A shading calculation model (*"Shade"*) calculates the amount of both direct and diffuse light on the receiving surface as a function of the sun's position and the presence of obstructions, including the building self-shading and the shading of neighbouring buildings. Once in the first window model, the solar radiation is geometrically distributed between the glazed and frame area. The diffused and direct radiation is computed with a layer-by-layer calculation of the multiple reflections. The transmitted solar from the first window is then distributed to the interior window with the same geometrical approach – no angular calculations are performed to calculate the solar distributions on the inner window. The whole surface of the external window is considered as the light source, not just the portion of the glass which is not shaded by external objects, and the direct and diffuse radiation are geometrically distributed to the inner glazed area and treated in the same manner as the exterior window (the two windows are modelled with two identical components). This could represent a limitation in the case of a window with a high frame ratio because the radiation entering the zone is then reduced by a geometrical factor. Once inside the zone, diffuse light is scattered uniformly while the exact target location of the direct light beam is computed.

Previous analyses have shown that the "Double Glass Façade"

Table 1
Performances of the 'Double Glass Façade' model in modelling a single-story DSF: mechanically [21] and naturally ventilated [41] – see Eq. (2) and Eq. 3

	Mechanical Ventilation		Natural Ventilation					
	Exhaust Air		Thermal Buffer		Outdoor Air Curtain		Supply Air	
	MBE	RMSE	MBE	RMSE	MBE	RMSE	MBE	RMSE
Transmitted irradiance [W/m^2]	0.2	21	−0.4	14	−0.6	9.1	−2.0	15.7
Airgap Temperature [°C]	−0.3	2.6	1.4	3.7	−1.7	2.8	0.1	1.7
Surface Temperature [°C]	0.4	1.5	−0.8	1.8	0.5	1.8	0.4	1.1
Heat Flux [W/m^2]	2.6	15	N/A	N/A	−2.1	5.0	N/A	N/A

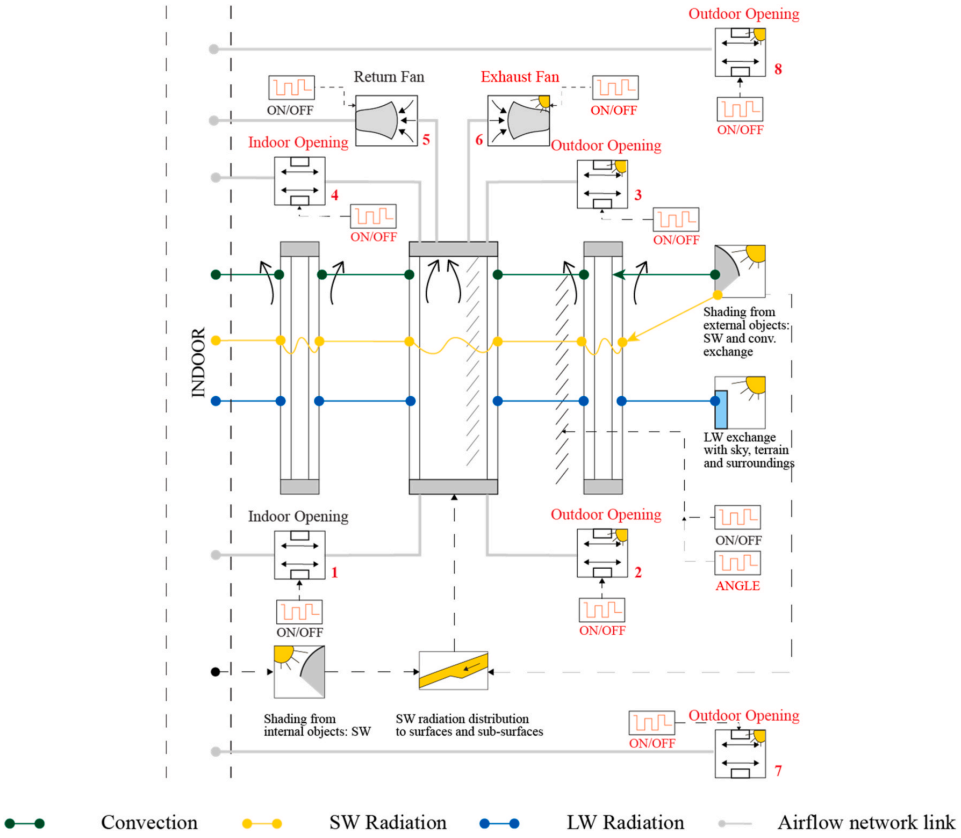

Fig. 4. Schematic view of the adaptive façade model implemented in IDA ICE based on the fully flexible DSF architecture (the model can switch among all the configurations presented in Fig. 1 within the same simulation) – in red, the newly added elements. (For interpretation of the references to colour in this figure legend, the reader is referred to the Web version of this article.)

component, in combination with the *"Detail Window Model"*, is more sensitive to the parameters describing the glazing thermal and optical properties and shading optical properties than the geometrical and frame properties [40]. The performances of this component have been tested under different conditions (winter and summer) and, with different ventilation strategies (mechanical [21] and natural) in previous studies. The validation results showed good agreement with the experimental results (Table 1) for a validation covering OAC, SA, and TB configurations. The naturally ventilated cases have a similar level of error as the mechanically ventilated ones, even though the level of uncertainty is usually higher (being the buoyancy effect, the primary driver whilst in the mechanically ventilated façade, the airflow is known). In the mechanically ventilated case, the airgap temperature better agrees with the experimental data during the days when the shading was not deployed in the cavity, while the model underestimates the peaks with the shading activated, showing a limitation of the tool in modelling the heat transfer between the shading device and the air in the cavity. The natural ventilated façade models do not show this difference. In both cases, the peaks during the daytime are underestimated. This could be linked to the uncertainty connected to the airflow estimation (size of the leaks to represent the opening, pressure loss at the level of the openings, etc.). In the thermal buffer case, the beaviour differs greatly between when the shading is drawn and when it is not. Without the shading, the model shows a slight overestimation in modelling the night-time, while the day peaks are usually well predicted; nce the higher errors occur in the part of the day where only the external and internal temperatures play a crucial role, it is possible to identify the weak link in the two-dimensionality of the component. When the shading device is

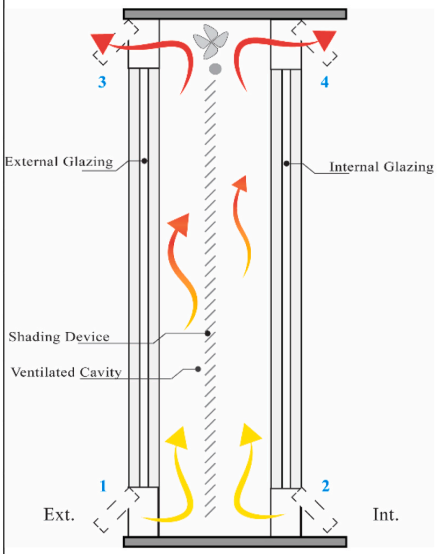

	Ext.Glazing	Shading	Cavity	Int. Glazing
Type	Double glazing – lowE inner glass	Venetian blind	Ventilated	Double glazing – lowE inner glass
s [mm]	29	10	250	29
τ_{sol} [-]	0.55	-	-	0.55
ρ_{out} [-]	0.20	0.15	-	0.20
ρ_{in} [-]	0.07	0.15	-	0.07
U [W/m^{2}K]	1.21	-	-	1.21
g [-]	0.58	-	-	0.58
U_f [W/m^{2}K]	1.50	-	-	1.50

1 Outdoor inlet **2** Indoor inlet **3** Outdoor outlet **4** Indoor outlet			
1→3	Outdoor Air Curtain - **OAC**	1→4	Supply Air - **SA**
2→3	Exhaust Air - **EA**	2→4	Indoor Air Curtain - **IAC**
All openings closed		Thermal Buffer - **TB**	
FAN **ON**	**Mechanically** Ventilated	FAN **OFF**	**Naturally** Ventilated

Fig. 5. Schematic section and glazing configuration of the DSF.

present in the cavity, the prediction of the air gap temperature worsens, leading to quite high errors.

2.3.2. Enhanced flexibility of the double glass façade model

In order to be able to control the façade in different operation modes, with full control over the different openings and maximum freedom to combine the façade with the HVAC (as schematised in Fig. 2), the air links of the *"Double Glass Façade"* component were modified (Fig. 4). First of all, to be able to control the ventilation path, operable elements were needed. This modification allows dynamic control of the connection between the cavity and the indoor and outdoor environment during the simulation runtime. A conventional model for a DSF, which is based on a concept where the airflow has a fixed path, does not require this flexibility, and therefore the link between the cavity and the two surrounding environments is defined with simple representations (leakage or free cross areas) that are not to be controlled during the simulation. To meet the operational requirements connected to the concept of the flexible DSF concept, the outside and inside connections, modelled as leaks, were replaced with operable openings (*2 and 3* - Outdoor Opening and *4* - Indoor Opening - Fig. 4). The Indoor Opening (*1*) was retained from the previously described model. Once the ventilation path is controllable, to be able to alternate between the ventilation mode (natural or mechanical), it is necessary to have a mechanical fan that extracts the air from the cavity and directs it either towards the outdoor (exhaust fan) or indoor environment (return fan). In reality, this switch could be achieved using the same fan placed at upstream of the outlet section of the DSF; however, implementing this function in BES requires the presence of two fans (due to how the elements in an airflow network are connected). The existing model presented only the Return Fan - Fig. 3-a. Therefore, an Exhaust Fan (*6* - Fig. 4) connected directly to the outdoor was added to ensure that the EA and OAC ventilation strategies were possible under a mechanical regime. Finally, to ventilate the room while by-passing the cavity (ventilated thermal buffer – TB-V), it is necessary to exclude the cavity from the ventilation path and open all the operable openings simultaneously. As for the fan, it is impossible to change the node connection of an airflow network element (to set, for example, that the outdoor windows open towards the indoor environment rather than towards the cavity). The only way to model this configuration is to have two openings not connected to the DSF air node. Therefore, two Outdoor openings (*7 and 8*- Fig. 4) were added on the same surface hosting the flexible DSF.

The openings, fans, and shading devices were connected to a controller (*[ON/OFF]* - Fig. 4). In order to be able to control the angle of the slats of the shading device, a controller (*[ANGLE]* - Fig. 4) was connected to the shading device of the external window. The fans work as an idealised exhaust terminal, which works as an ON/OFF fan controlled by a schedule. If the fan is set to OFF, the fan behaves as a leak and adopts the nominal minimum airflow rate (this value cannot be set to zero, but since the field accepts rational numbers, it was possible to set this variable to a value very close to zero). The infiltrations were modelled in the opening components, which, when closed, are still modelled as a two-way flow opening with a reduced width.

Compared to the standard component described in 2.2.1, the modifications implemented in the new model have introduced the possibility of controlling the façade with the five different air paths available (including switching between naturally and mechanically ventilated mode) and, therefore, enhanced the DSF model's flexibility. The controllers can be connected to a schedule or implemented with an external control logic that accounts for the ambient conditions (radiation, temperature, etc.).

Nevertheless, some of the limitations of the original model persist. The unique value of the airgap temperature and the modelling of the shading device as part of the external window are not easily addressable without changing the equations inside of the component. On the other hand, the geometrical distribution of the solar radiation and the two-dimensional heat exchange can be addressed, if the dedicated case

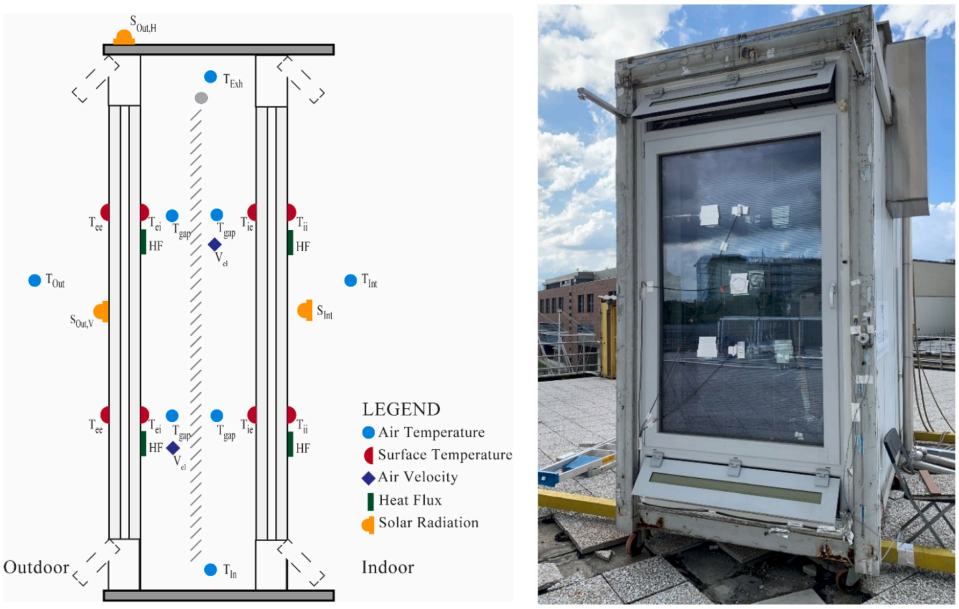

Fig. 6. Sensor a) scheme and b) instalment on the experiment facility.

requires so, with some work-around within the IDA ICE model, as explained in section 4.1, where the application of this model to model an existing DSF mock-up will be later presented.

3. Experimental set-up and data collection for model validation

The validation of the performance of the modified "Double Glass Façade" component to address the simulation needs of the flexible DSF concept was carried out by comparing simulation results with experimental data. Experimental data were collected using a single-storey DSF mock-up that was run in a fully dynamic way (i.e., changing the operational configuration of the façade), as explained in the following sections. The experimental set-up is described in 3.1. The control strategies adopted during the experimental campaign to collect data under very different operational modes are presented in 3.2, whilst the boundary conditions for those selected weeks are in 3.3.

3.1. Experimental set-up

The DSF mock-up was installed in an outdoor test-cell facility in a temperate sub-continental climate in Torino, Italy (45° N latitude). The test-cell was located on a flat roof of a building on the campus of Politecnico di Torino, not shaded by the surrounding buildings and had a (nearly perfect) South exposure. The test cell room had internal dimensions of 1.60 m (façade test rig) x 3.6 m (depth) and 3.0 m (height). These dimensions are derived from the IEA-SHC TASK 27 specifications for typical dimensions of spaces behind façade modules used in office buildings. The test cell's indoor air conditions were controlled with a full-air system that can maintain the room's indoor air temperature between 20 °C and 26 °C with a single set-point or the test cell can be left uncontrolled for free-floating tests.

The façade used for the validation of the flexible model had dimensions of 1.60 m (width) and 2.90 m (height, including the opaque bottom/top inlet/exhaust section), and a ventilated cavity of 0.25 m (depth) and hosted a highly reflective venetian blind as a shading device located at the centre of the cavity (Fig. 5). The airflow entered the ventilated cavity from the pivoting openings at the bottom of the façade and exited it from the cavity top openings. The openings towards the inside or outside are chosen depending on the operational mode. If the façade was mechanically ventilated, four fans were activated at the top of the glazed cavity, upstream of the outlet section, and their total nominal volumetric airflow was 15 l/s. Both skins of the DSF were made of an insulated glazed unit with two glass panes with a low-e coating. Details of the thermal and optical properties of the components of the DSF mock-up are given in Fig. 5.

The test cell and the DSF mock-up (Fig. 6) were equipped with a wide range of sensors (resistance temperature detectors for air temperatures, thermocouples for surface temperature measurements, heat flux meter sensors, anemometers for the airspeed, and pyranometers both inside and outside) to record the thermophysical and optical processes occurring in the DSF. Temperature and heat flux sensors were placed at two height levels, both inside and outside of the façade, measuring: the surface temperature of the interior glazing and the exterior glazing (both towards the indoor and the cavity); the temperature of the air in the cavity both in front and behind the shading (when present); the inlet and outlet cavity-air temperature; the frame temperature; the heat flux exchanged at the indoor surface of the glazing. Thermocouples and heat flux meters directly exposed to solar radiation were shielded with highly reflecting aluminium foils to reduce the influence of solar irradiance on the measured physical quantity, following best practices established in the literature [42]. Though the mock-up's cavity also hosted hot-wire anemometers, air speed readings in the cavity are not always reliable, as values can fall below the lower threshold of the sensors. Generally speaking, a continuous characterisation of the air velocity in the cavity is a challenging task [36], so we decided not to employ the air speed values measured by the hot-wire anemometers in the validation process.

The outdoor solar irradiance was measured horizontally and vertically, employing two pyranometers. The solar irradiance transmitted through the DSF was measured, on the vertical plane, with an additional pyranometer installed right next to the inner skin of the DSF. The wind

a)

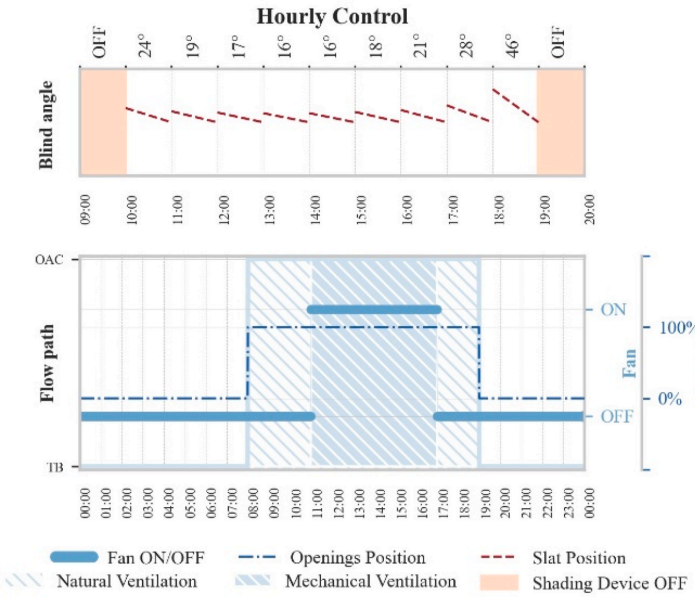

b)

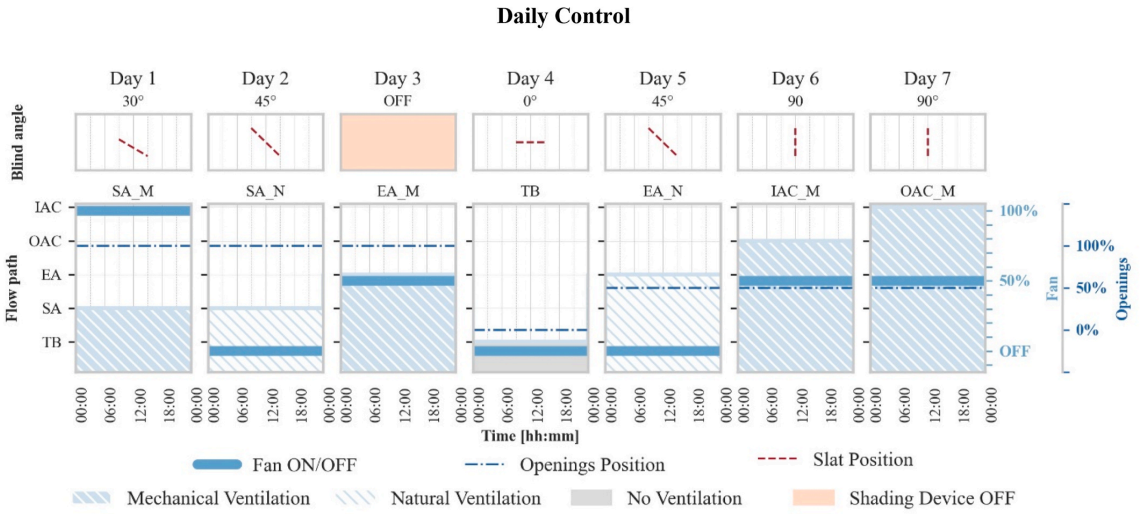

Fig. 7. Control strategies applied in the two analysed periods a) Hourly Control – applied for every day of the week and b) Daily Control.

speed and wind direction were also recorded. The test cell was also equipped with RTD (PT100) sensors to record the indoor air temperature values. The cell surfaces' temperatures were measured by thermocouples in parallel, so only the mean value for the whole set of surfaces (other than the DSF mock-up) surrounding the indoor air volume was registered.

All the data were acquired with a 1 min resolution. The measurement accuracies for the entire measurement chain, after calibration and verification, were: ±0.3 °C for the resistance temperature detectors, ±0.5 °C for thermocouples and ±5% for the flux meters and pyranometers.

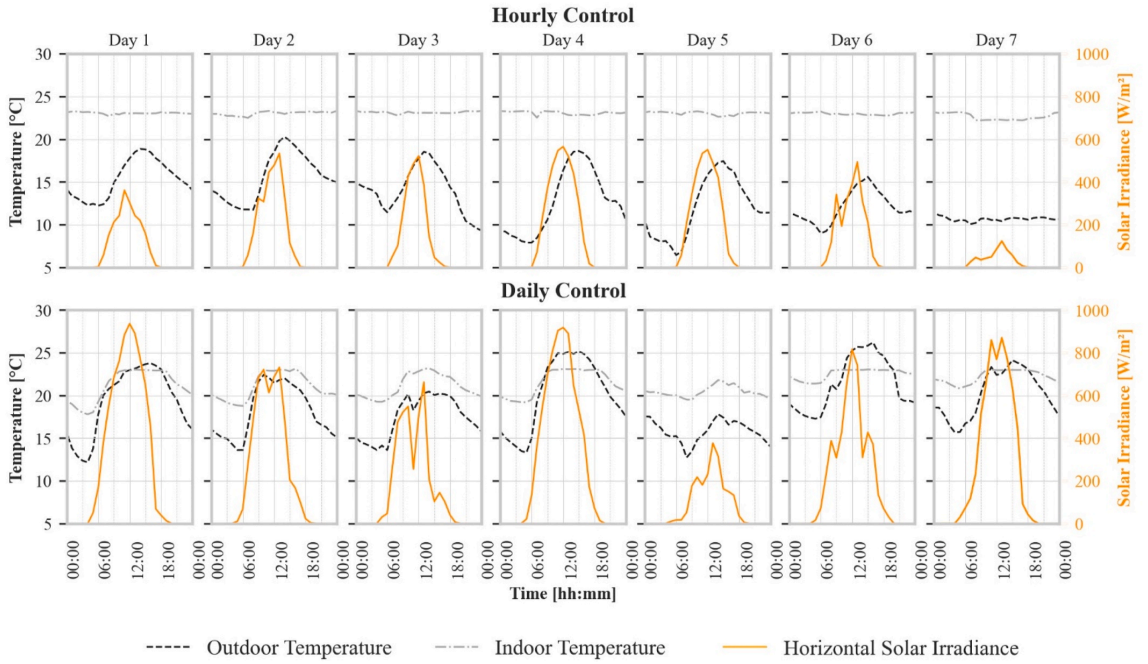

Fig. 8. Time profile of the outdoor and indoor air temperature [°C] and horizontal global solar irradiance [W/m2] for the two modelling periods: a) Hourly Control and b) Daily Control.

3.2. DSF's control under experiments for model validation

The data set chosen for the validation is relative to two different periods of measurement when the operational modes of the façade, managed by its onboard controller, were as follows: in the first period (called *Hourly Control*), the façade configuration was changed every hour using a pre-defined, scheduled-based, control; in the second period (*Daily Control*), the configuration of the façade was changed every day by exploring a wider range of combinations of all the possible configurations that the façade can assume, but the configuration of the façade was fixed for 24 h. By designing the validation process to include these two periods, we aimed to assess the numerical model's ability to replicate both fast-time processes and more long-term dynamics and simulate an extensive range of operational conditions. Overall, both mechanical and natural ventilation were employed, the shading device was deployed or retracted, and the slats of the venetian blinds were changed every hour by a few degrees to direct solar radiation cut-off (for the Hourly Control only), and different ventilation paths were employed (see Fig. 5). Fig. 7 shows the details of the operational conditions of the façade applied in each period.

3.3. Boundary conditions for validation

Fig. 8 shows the main boundary conditions (outdoor and indoor air temperature and global irradiance on the horizontal plane) for two selected periods, equivalent to two weeks. In the first period, the indoor temperature was controlled and set to 23 °C, while in the second one, the indoor air temperature of the room was left free to float between 18 °C and 23 °C to increase the range of boundary conditions employed in the validation process.

The experimental data of the boundary conditions during the experiments were used to construct a customised 10 min-resolution weather data file. The measurements available to create the customised weather data files included the global solar irradiance data on the horizontal plane, the outdoor air temperature and the wind direction and velocity. The required weather data are, in addition to the outdoor dry bulb temperature, the direct beam and diffuse horizontal solar irradiance, the cloud cover fraction of the sky, and the relative humidity of the air. The beam and diffuse components of the solar radiation were calculated using the ENGERER2 separation model [43] with a 1-min parametrisation. The source of the relative humidity was the official weather station of Politecnico di Torino, installed on campus, relatively near the testing site, and the source of the cloudiness factors was the climate reanalysis ERA5 [44]. The different time resolution of each dataset was set to 10 min to create a unique weather file.

A sensitivity analysis was carried out to verify that the uncertainty in the decomposition of the solar irradiance in the direct and diffuse components (which were not directly measured) showed little impact on the validation process results. Furthermore, since the measurement of the global irradiance on the vertical (façade) plane was available from the experimental dataset, the goodness of the decomposition procedure adopted was verified by comparing the numerically calculated global solar irradiance on the vertical (façade) plane with the measured value for the same quantity.

The measured indoor air temperature and the test cell's opaque surfaces' temperatures were adopted in the simulation to ensure identical boundary conditions to the experiments as shown in Fig. 8, and better described in Section 4.2.

4. Numerical model validation: methods, results, and discussion

4.1. Implementation of the façade prototype in IDA-ICE for simulation of the experimental campaign

The numerical representation of the DSF mock-up was developed, modelling the cavity as a ventilated wall because of the geometry of the

façade, characterised by a high frame ratio. This choice had other implications on how the inner face had to be modelled, which are discussed later in this section.

To replicate the operational strategies of the façade used during the experimental campaign, each leak was replaced with a two-way flow vertical opening, and an exhaust fan was added. Each opening was a 1.4 m wide and 0.30 m high top-hinged window. The maximum opening angle was 45%. In order to reflect this geometry, the opening width was calculated using Equation 14 of the TRNFLOW manual [45]. A schedule controlled the openings, the fans and the shading device. The fans worked as an idealised exhaust terminal, which worked as an ON/OFF fan controlled by a schedule. If the fan was set to OFF, the fan behaved as a leak and adopted the nominal minimum airflow rate. This value cannot be set to zero, but it was set to a value close to it (10^{-4} l/s). The effect of infiltration was included in the openings' representation. When closed, openings are still modelled as a two-way flow section with a reduced width. A leakage coefficient of 10^{-4} was considered for each opening to represent the air infiltration from the closed openings.

As mentioned earlier, the ventilated cavity was modelled as a *"ventilated wall"*. This choice was made because such an approach allows the modeller to modify the solar radiation distribution onto the inner glazing once it goes through the outer one. By default, the total transmitted solar irradiance is evenly distributed to the inner glazing and frame area, independently from the incident angle or the view factor between the two glazing. The frame ratio of the case study was around 60%; thus, only 40% of the solar radiation entering the cavity was transmitted to the inner glazing, resulting in a much lower irradiance transmitted towards the inside room.

To overcome this limitation, the internal facade was modelled as a smaller window –of the same dimension as the glazed area of the internal glazing – with a 0.1% of frame; the wall to which the window belongs was modelled with the same U-value of the aluminium frame, and the external skin was modelled as a ventilated wall, occupying the whole exposed façade. In the external window, no changes to the geometry were made. When adopting this modelling strategy, the ratio of solar radiation hitting the inner glazing was changed to 70% - and 30% distributed to the wall frame; in this way, a more realistic transmitted solar irradiance was calculated, and the solar heat absorbed by the inner frame was accounted for, as well as the heat loss through the external frame.

No enclosing elements around the cavity were considered in the calculation, except for the façade elements (glazing, frames, shading) parallel to the façade [46]. To consider the heat transfer through the sides of the ventilated cavity, the U-value of the external frame was set to an equivalent U-value (3 W/(m^2K)) which accounted for the external frame itself, the thermal bridges, and the side surfaces of the cavity.

The shading layer was set as part of the exterior window, and it was modelled as an interior venetian blind. Its distance was defined as measured from the external skin and set as in the experimental set-up. A schedule controlled the shading's presence inside the cavity and the angle of the blinds.

4.2. Methods and procedure for experimental validation

The goal of the validation procedure was to check to what extent the modified *"Double Glass Façade"* model could replicate the thermophysical and optical behaviour of the façade mock-up. For this reason, the focus of the validation was placed on the DSF modelling alone and not on the combination DSF and room (or test cell). This means that each surface of the virtual room and the indoor air node temperature of the virtual room were given values through schedules created using the available experimental data. The geometry of the virtual room replicated the geometry of the test cell where experiments were carried out and used the same dimensions as the physical room. This strategy allowed us to replicate the indoor and outdoor boundary conditions surrounding the DSF, thus focusing the validation on the DSF models' performance since all the other possible uncertainties in the simulation tools linked to the environments surrounding the DSF were removed. Alternative approaches such as a validation using room-level quantities (e.g. indoor air temperature or energy/power required to climatise the test cell) would likely lead to much higher uncertainty because more unknowns and more simulation routines are involved, and to the impossibility of assigning potential discrepancies to the different routines of the tool (e.g. whether a discrepancy is due to insufficient performance of the routine under test or is due to other routines used to model other components in the room, or due to unknown in the modelling of the other components of the room).

This validation approach adopted in this study, which is commonly exploited for validating individual simulation routines of building envelope systems, has however a disadvantage in the impossibility of finding literature reference values to define when the simulation output is "well enough" to consider the model validated. For example, the ASHRAE Guideline 14 [47] defines model calibration criteria that can be used to check the reliability of a simulation model to replicate the energy use in the whole building. However, when the parameters used in the validation are "detailed" physical quantities (as explained in the following paragraphs), there are no reference literature values that can be used for this purpose; it is left to the sensitivity of the researcher to decide if the level of accuracy reached by the numerical simulation is deemed sufficient.

Simulations were then run using the custom built weather data file and all the experimental data that could represent the boundary conditions around the DSF mock-up. The maximum simulation time step (IDA ICE adopts a dynamic simulation time-step) was set to 10 min, which means that if the simulation converged sooner, the time step was lower. The numerical outputs were extracted and sampled with a time-step of 10 min. The following (simulated) physical quantities were obtained:

- the transmitted solar irradiance through the innermost windowpane of the DSF [W/m^2];
- the air temperature of the cavity [°C];
- the surface temperature of the interior surface of the interior glazing [°C];
- the heat flux on the interior surface of the interior glazing [W/m^2];

These quantities were compared with the following experimental data:

- the transmitted solar irradiance through the entire DSF structure, measured on the vertical plane [W/m^2].
- the averaged air temperature of the cavity (average value of 4 sensors) [°C];
- the averaged surface temperature of the interior surface of the interior glazing (2 sensors) [°C];
- the (average) specific heat flux (i.e., the sum of the convective heat flux exchanged between the surface of the inner skin and the indoor air and the radiative heat flux in the longwave infrared region exchanged between the surface of the inner skin and the surfaces of the room behind the DSF) (2 sensors) [W/m^2];

Moreover, an indicator called "total transmitted energy", which gives the energy crossing the façade (normalised for per square meter of façade), expressed in [Wh/m^2], was derived using the heat flux exchanged at the indoor-facing surface of the DSF and the transmitted solar radiation as shown in Eq. (1). The total transmitted energy can be calculated for a single hour, a period of 24 h (total daily energy) or for a longer period (e.g., one week). The aim of this performance metric, in a validation perspective, is to assess how well the entire room load due to the façade is replicated by the simulation environment, regardless of the more or less perfect match between individual physical quantities. These values were calculated both for the experimental and the simulated data

for both periods analysed for both the overall period (7 days for the Hourly Control period and 7 days for the Daily Control period) and for each day.

$$E_{tot} = \sum_{i=1}^{t} \left(Q_{HF}^{+} - Q_{HF}^{-} + Q_{SOL}\right) \quad (1)$$

where.

E_{tot} is the total energy for the t interval
Q_{HF}^{+} is the positive flux entering the room for a single hour;
Q_{HF}^{-} is the negative flux entering the room for a single hour;
Q_{SOL} is the solar flux entering the room for a single hour;
t number of hours for the analysed period.

The model validation was carried out through combined qualitative and quantitative analyses. This approach allows quantifying the performance and understanding the different observed behaviours. The time profiles of the thermophysical quantities identified in the previous section were helpful in supporting the qualitative (and explanatory) assessment. The quantification of the mismatch between the experimental data and the numerical data was assessed through the calculation of two commonly used statistical indicators, as described in the following equations: the Root Mean Square Error (RMSE) (Eq. (2)) and the Mean Bias Error MBE (Eq. (4)). The normalised values of these indicators were calculated for evaluating the fitness of the models in predicting the total energy crossing the DSF: Coefficient of Variation of the Root Mean Square Error [CV(RMSE)] (Eq. (3)) and the Normalised Mean Bias Error (NMBE) (Eq. (5)).

$$RMSE = \sqrt{\frac{\sum_{i=1}^{n} (P_i - M_i)^2}{n}} \quad (2)$$

$$CV(RMSE) = \frac{RMSE}{\bar{y}} \bullet 100 \quad (3)$$

$$MBE = \frac{\sum_{i=1}^{n} (P_i - M_i)}{n} \quad (4)$$

$$NMBE = \frac{MBE}{\bar{y}} \bullet 100 \quad (5)$$

where.

P_i – predicted value by the simulation;
M_i – measured value at one point;
n – total number of measurements;
$\bar{y}$ – mean value of the measured values.

When it comes to the calculation of CV(RMSE) for the total energy indicator, this statistical indicator can be performed using different integration time to calculate the total energy, i.e. $CV(RMSE)_{1H}$ if the total energy is calculated hour by hour and then the experimental value is compared to the simulated value; $CV(RMSE)_{24H}$ if the total energy is calculated for an entire day and then this experimental datum is compared with the simulated one. Clearly, because of how NMBE is defined, there is no difference in the value of this indicator for different integration periods of the total energy quantity.

The set of statistical indicators adopted in this study had been used in previous model validation dealing with some specific configurations of DSF [41] activities that can be used for benchmarking the performance of the flexible model – i.e., to assess whether the performance of the developed numerical model that replicates the flexible DSF is at least equal to that of the "basic" DSF model of IDA ICE. For this purpose, both the experimental and the simulated data were averaged to hourly values.

4.3. Model performance analysis

4.3.1. Overview and prediction of total transmitted energy

This section gives an overview of the flexible model's performance for the physical quantities employed in the validation process. As previously mentioned, the transmitted solar irradiance, airgap and surface temperature, and heat flux transmitted were chosen for this comparison to assess the model reliability for detailed thermophysical process simulation, while the total energy indicator was used to assess the accuracy of the simulation to replicate the overall impact of the façade system on the room thermal load. As mentioned, the simulated data were collected for seven days for both the hourly and daily controlled periods. The statistical indicators were calculated for the entire simulation periods of the Hourly Control and Daily Control (Table 2) and in detail (Table 3) for each day of the Daily Control.

The distribution of the errors for the different ventilation modes and the different variables shown in Fig. 9-a highlights how, for most of the configurations, the predictions are very similar to the measured values, with the supply air configurations having the biggest overestimation of the airgap temperature and heat flux, while the thermal buffer underestimates the heat flux. As shown in Fig. 9-b, the surface temperature has the lowest error (RMSE) for all the configurations, while the heat flux has the highest one. The simulation error of the airgap temperature value is highest during the mechanical supply configuration. A more detailed analysis of each of the four thermophysical variables is given in the following sections.

When comparing the total energy crossing the façade, which includes the energy gained and lost by the DSF due to all the heat transfer mechanisms, the values predicted during the Daily Control showed a better agreement with the measured data than the Hourly Control period (Table 4) when the analysis is done comparing total energy values hour by hour using the $CV(RMSE)_{1H}$. The cause of this is linked to the dynamicity of the façade (in terms of ventilation strategy and shading position) which is likely more emphasised during the hourly controlled period. This difference disappeared when comparing experimental and simulated daily total energy values ($CV(RMSE)_{24H}$). By using this metric, the daily variations seen when analysing the dynamic parameters are no longer distinguishable and this shows that the influence of the discrepancy on an hourly basis has very little influence on the overall energy balance. When the focus is placed on each day of the Daily Control the prediction of the total energy values for the façade configurations operated under naturally driven ventilation had a higher error compared to the cases when the ventilation in the cavity was mechanically driven. Nonetheless, the overall assessment demonstrated that when used to assess the overall performance in terms of total energy crossing the façade for a long enough period of time (as typically done through BES tools), the flexible DSF model gives estimations that are close to the measured values, with MBE in the range of 5–15%.

In summary, the general assessment covering the four detailed thermophysical quantities and the total energy parameter demonstrated the model's ability to predict the behaviour of the flexible DSF that is characterised by fast changes in the schedule for both the ventilation

Table 2
MBE and RMSE values calculated for the model run adopting the Hourly Control and the Daily Control.

	Hourly Control		Daily Control	
	MBE	RMSE	MBE	RMSE
Airgap Temperature [°C]	1.5	2.2	1.3	2.4
Surface Temperature [°C]	−0.2	0.3	0.5	0.9
Transmitted solar irradiance [W/m^2]	2.0	4.8	−0.6	2.5
Surface Heat flux [W/m^2]	3.9	4.7	0.7	3.7

Table 3
Detail of the MBE and RMSE calculated for each ventilation strategy adopted in the Daily Control.

Ventilation path	*Day 1*		*Day 2*		*Day 3*		*Day 4*		*Day 5*		*Day 6*		*Day 7*	
	SA_M		**SA_N**		**EA_M**		**TB**		**EA_N**		**IAC_M**		**OAC_M**	
Opening %	100		100		100		0		50		50		50	
Fan %	100		OFF		50		OFF		OFF		50		50	
Shading device	30°		45°		OFF		0°		45°		90°		90°	
	MBE	RMSE	MBE	RMSE	MBE	RMSE	MBE	RMSE	MBE	RMSE	MBE	RMSE	MBE	RMSE
Airgap Temperature [°C]	3.2	3.8	2.1	2.3	2.3	2.5	−0.2	2.7	2.0	2.1	−0.2	1.1	−0.1	0.7
Surface Temperature [°C]	0.9	0.9	1.0	1.1	0.8	0.9	−0.1	1.2	1.1	1.1	−0.3	0.5	−0.1	0.2
Transmitted solar irradiance [W/m^2]	−1.3	2.0	0.9	1.6	−2.9	4.8	−0.9	2	1.5	2.2	−0.4	1.1	−0.9	1.9
Surface Heat flux [W/m^2]	3.5	4.9	2.6	3.4	0.6	2.5	−2.5	5.7	1.2	2.4	−0.5	2.4	0.3	2.7

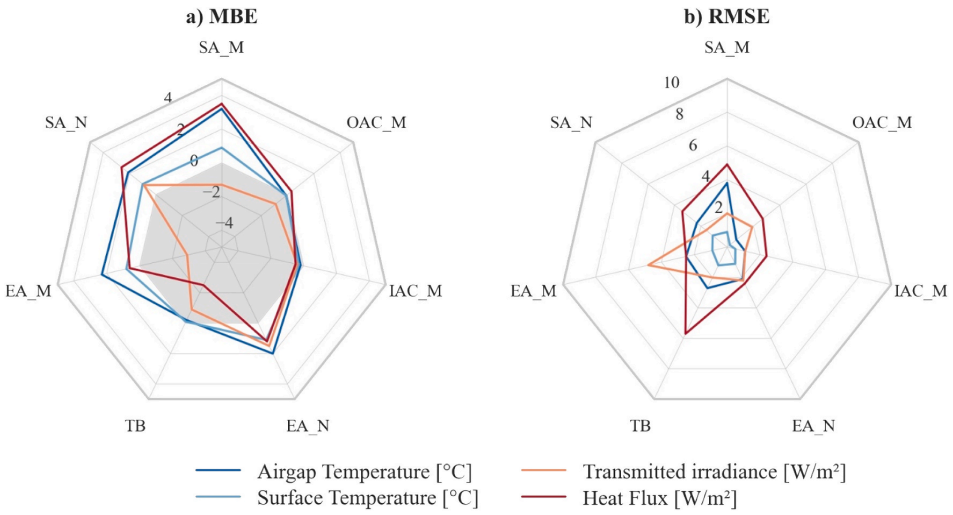

Fig. 9. Statistical indicators a) MBE and b) RMSE distribution for each configuration tested during the Daily Control.

strategy and the solar control. The flexible model shows similar results compared to the base model runs (Table 1); the statistical values show lower or similar results for most variables. More details on the prediction of the four thermophysical quantities are presented in the following sections.

4.3.2. Prediction of transmitted solar irradiance

During the Hourly Control (Fig. 10), the control on the shading device and the actuator on the blind angle replicated the profiles the schedule gave. The simulation slightly overpredicted the transmitted solar, particularly during the first hours of mostly sunny days. The error during the sunny days was circa 10 W/m^2, and it was mainly linked to the uncertainty of the exact position that the blind acquired during the selected week. The angle settings were recorded from the blind controller, but the exact angle adopted was not measured. With just a little adjustment of 5°, the errors were reduced by half, in line with the error magnitude of the Daily Control. During these days (Fig. 11), the time profile showed a good agreement with the measurements, both with the shading device activated and without it. It is also not fully possible to exclude that, for particular angles, due to the geometrical relationship between the sun position, the blinds, and the pyranometer, the sensor was partially shaded, and thus the reading obtained by this device might not have been fully representative of the average value across the whole glazed area (which is instead the value obtained by the simulation). This effect could explain why, in cases where no shading devices were deployed (Fig. 11 - Day 3), i.e., when the sensor's reading

Table 4
Daily total transmitted energy performances and statistical values (NMBE and CV(RMSE)) calculated for the Hourly Control and Daily Control (7 days period) and for each day of the Daily Control (24H period).

	Hourly Control	Daily Control	*Day 1*	*Day 2*	*Day 3*	*Day 4*	*Day 5*	*Day 6*	*Day 7*
			SA_M	SA_N	EA_M	TB	EA_N	IAC_M	OAC_M
Measured total energy [Wh/m^2]	1766	1766	253	181	466	461	64	167	184
Predicted total energy [Wh/m^2]	1858	1524	253	198	360	343	90	134	146
NMBE [%]	5	−14	−0	9	−23	−26	41	−20	−21
CV(RMSE)$_{1H}$ [%]	75	42	35	53	31	37	110	32	36
CV(RMSE)$_{24H}$ [%]	26	25	N/A	N/A	N/A	N/A	N/A	N/A	N/A

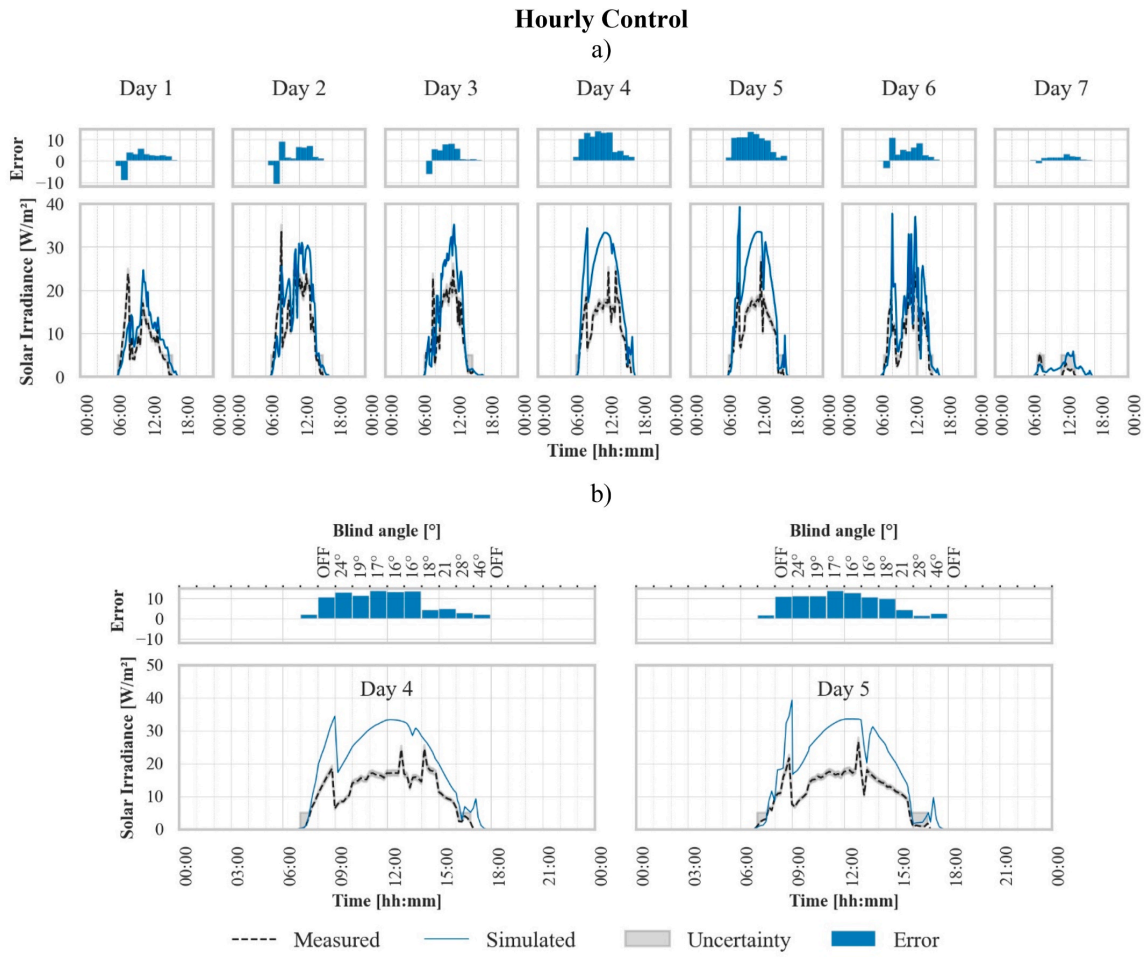

Fig. 10. a) Time profile of the transmitted solar irradiance for the hourly controlled days; b) detailed view of Day 4 and 5. The error is expressed in [W/m^2]. The uncertainty band is calculated as ±5% of the measured values.

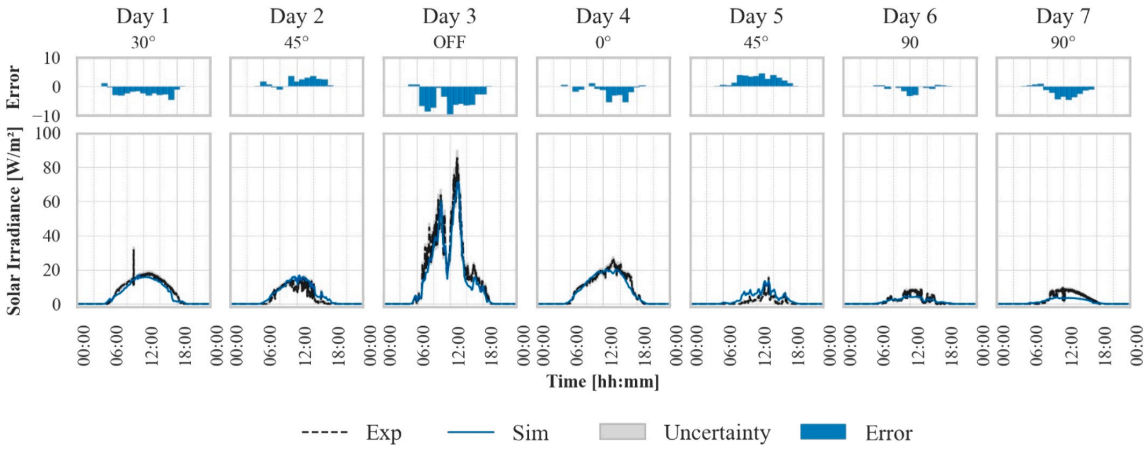

Fig. 11. Time profile of the transmitted solar irradiance for the daily controlled days. The error is expressed in [W/m^2]. The uncertainty band is calculated as ±5% of the measured values.

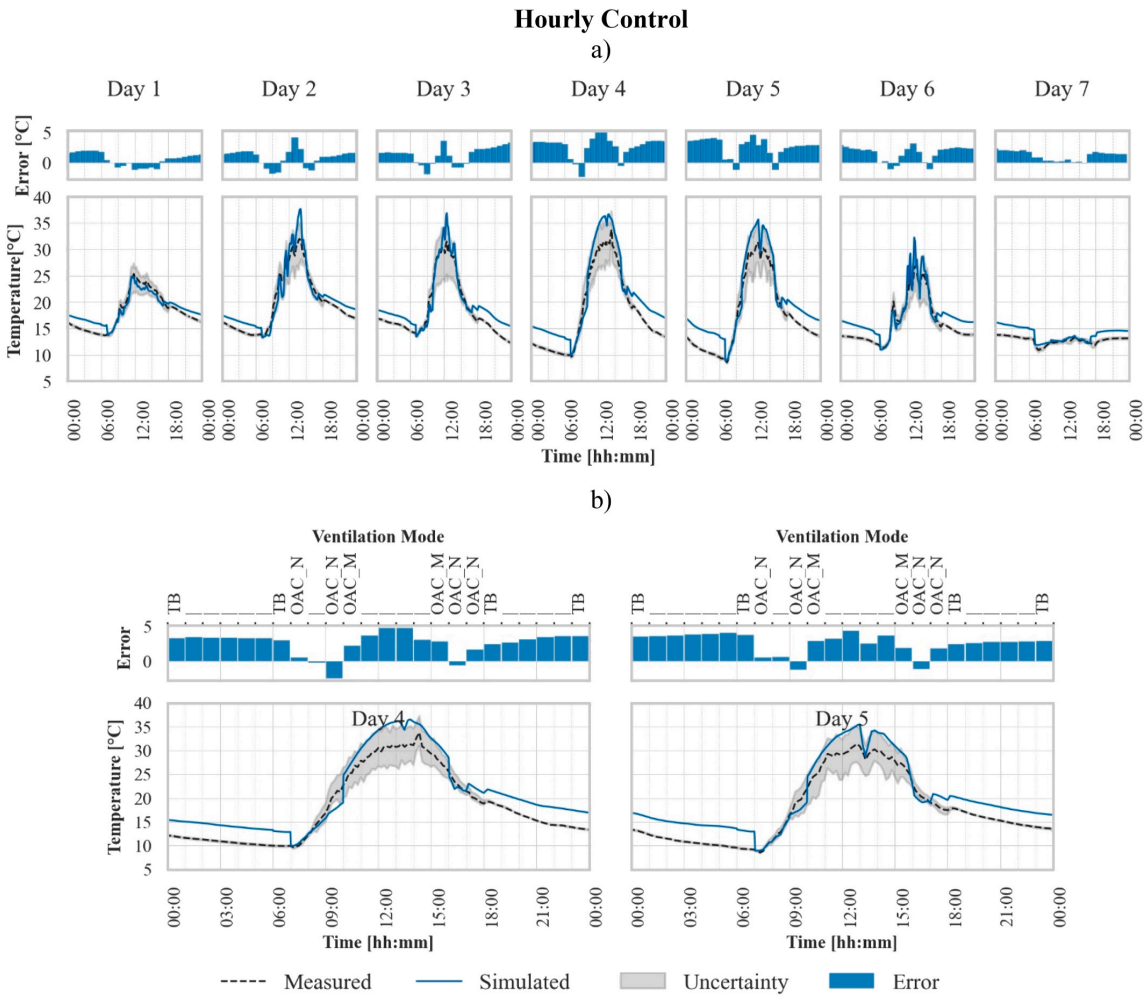

Fig. 12. a) Time profile of the air gap temperature for the hourly controlled days; b) detailed view of Day 4 and 5. The error is expressed in [°C]. The uncertainty band shows the experimental values measured by the sensors in the cavity placed at two different heights in the cavity.

cannot be affected by unwanted local shading phenomena due to the blind structure, the match between the experiment and simulation was very high (considering the higher value of transmitted irradiance).

4.3.3. Prediction of air gap temperature

The airgap temperature prediction varied according to the ventilation strategy adopted. During the Hourly Control (Fig. 12), the façade adopted the thermal buffer mode, the naturally ventilated outdoor air curtain mode and the mechanically ventilated outdoor air curtain mode. Among these, it is possible to notice that when the façade was naturally ventilated, the model's predictions were lower than the measured values. On the other end, the model overestimated the temperature inside the cavity when the ventilation switched to the mechanical mode and during the night-time when all the openings were closed. This latter effect could be connected to the two-dimensional approximation done in the component; the heat losses through the external frame of the cavity might not be high enough to replicate the actual heat losses through the sidewalls of the cavity.

This trend was confirmed during the daily controlled period (Fig. 13). Generally, there was an overestimation of the air gap temperature during the days when the façade was mechanically ventilated, and this overestimation was reduced when the façade was run with natural ventilation. Looking at the trends, we can see that the model well depicted this quantity's dynamics and variation, with the highest error being around 5 °C. The thermal buffer mode showed a slight underprediction during the day and, as during the hourly controlled period, a slight overprediction during the night-time. The tool was able to replicate the high temperature reached in the gap (around 50 °C) during the

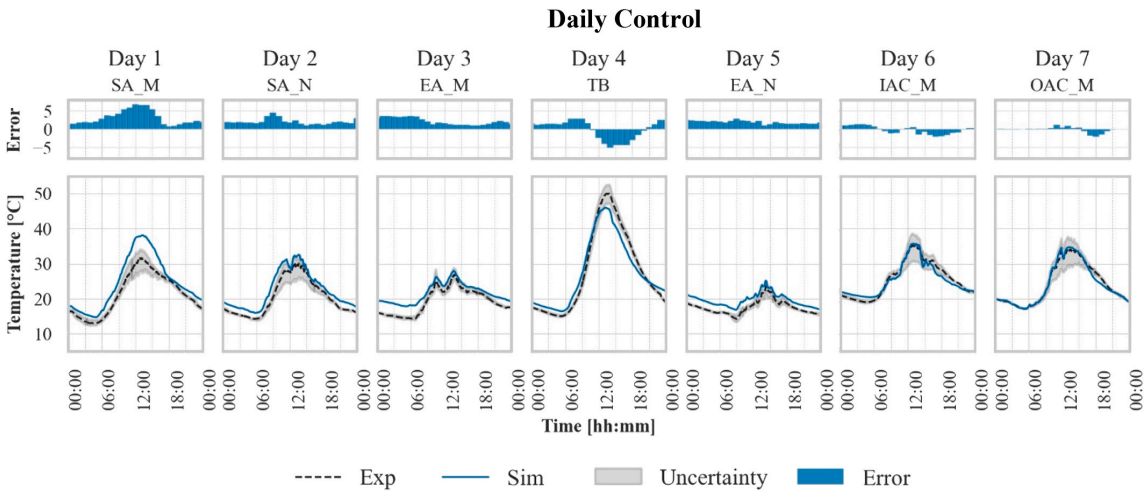

Fig. 13. Time profile of the air gap temperature for the daily controlled days. The error is expressed in [°C]. The uncertainty band shows the experimental values measured by the sensors in the cavity placed at two different heights in the cavity.

experiment: the shading device played a crucial role in absorbing the solar irradiance and transferring this energy quantity to the air via convection. During the night-time, the temperature was slightly over-predicted (around 1 °C), but it performed better than the night-time of the hourly controlled days due to the more negligible difference between the cavity and outdoor temperature. Similarl to what happens in the night-time of the hourly controlled period, this effect can probably be linked to the approximation of modelling the gap in two dimensions (the sides of the cavity are not modelled, and are thus not exposed to outdoor air). During Day 4 and 5, in particular, the outdoor temperature fell below 10 °C (see Fig. 8), and from the experimental data, it was possible to see that there was a heat loss from the cavity towards the outside, which the simulation cannot depict.

When the façade was run in supply air mode with the fan ON, the predicted airgap temperature values were higher than the measured data. This phenomenon could be due to an underestimation of the supplied airflow in the experimental data; as also visible in the Hourly Control data, when the openings were at 100% of their open area, the gap temperature was underestimated by around 5 °C. It could be that, due to how the experiment was run, the natural airflow was higher than the flow generated by the fan alone (which is used as input data), therefore reducing the cavity temperature more than predicted.

4.3.4. Prediction of surface temperature (of the inner skin)

The prediction of the indoor surface temperature was generally accurate in all the configurations, except for the thermal buffer mode. The surface temperature is affected by the room conditions and less affected by the cavity temperature, especially considering the insulated glazed unit of the inner skin. Therefore, if the simulated temperature of the air gap was a few degrees lower than the actual one, this led to a less significant (or none) impact on the inner face of the DSF. Most of the time, the predicted values were within the range of measure values from the experimental set-up. As shown in [21], the possibility given by IDA ICE of modelling the capacitive node in the glass led to no shifting in the surface temperature of the inner glass, an effect that is sometimes seen in other BES tools. The time profiles of the hourly controlled period (Fig. 14) showed simulated values with an error smaller than 1 °C, and the highest errors were only seen when there was a peak in the experimental data (corresponding to the peak of transmitted solar radiation in the morning).

The results of this parameter showed a very good approximation of the trend for each day, also during the daily controlled period (Fig. 15). In general, there was a slight overestimation of the results, with the only exception being the daytime of the thermal buffer (Day 4 in Fig. 14 - a). The local peak in the experimental data profile of the temperature values around 09:00 (see Fig. 14 - b) was likely due to direct irradiation of the temperature sensor, whose solar shield was possibly not perfect for ensuring all-day-long protection from the influence of the solar irradiance. At this time of the day, the shading device was off, and it was turned on at 10 a.m. The smaller peak in the simulation is likely to be a more realistic value that would have been recorded if the measuring device was not hit by solar irradiance impinging on the measurement point.

4.4. Prediction of surface heat flux (exchanged at the indoor-facing interface of the inner skin)

The readings from the surface heat flux meter included the longwave radiative and convective exchange between the indoor-facing surface of the inner glazing and the other surfaces and air of the room. The heat flux is probably the most complicated physical quantity to measure among those used in this validation process due to how the measurement is carried out and how the presence of the sensor modifies the physical phenomena locally. Even with all the precautions taken during the measurements, inaccuracy in the measurement is unavoidable due to the technology adopted. Inaccuracies are usually further amplified when the sensor is under solar irradiation. The sensors applied on the glazing surface increase the local absorptance of the glass in a way that cannot be represented in the simulation. Moreover, simplifying by averaging all the surface temperatures in one value may lead to errors connected to

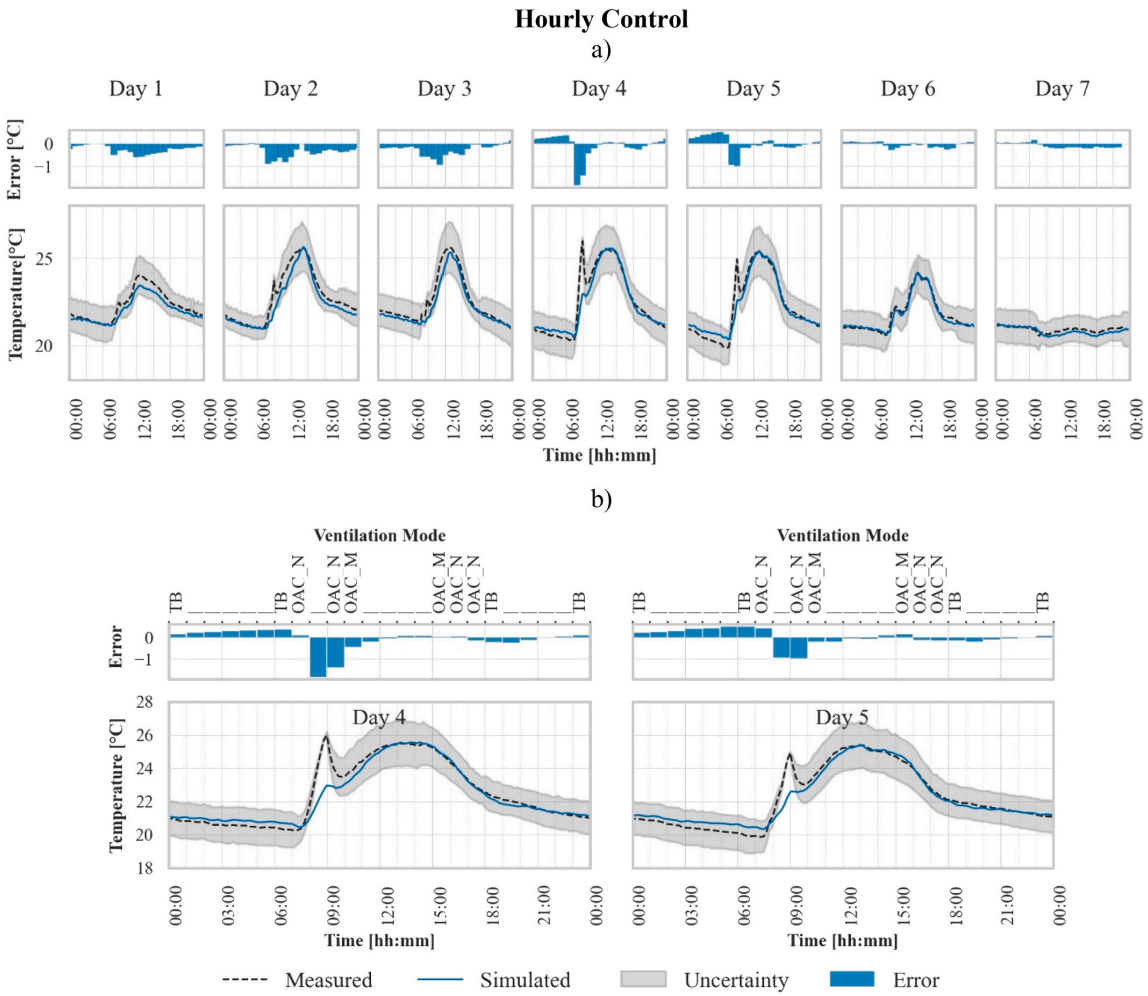

Fig. 14. a) Time profile of the surface temperature for the hourly controlled days; b) detailed view of Day 4 and 5. The error is expressed in [°C]. The uncertainty band shows the two experimental values measured by the sensors on the surface.

the radiative exchange between surfaces. Considering the very good prediction of the inner glazing temperature and that the general trend of the heat flux was followed (with the maximum difference being ±10 W/m^2), it seems that the model can reasonably predict the values of the surface heat flux (Figs. 16 and 17). The differences in magnitude between the heat flux under different configurations were well visible, and the peaks were aligned with the measured data.

5. Conclusion

The simulation work presented in this paper underlined the complexity of modelling a highly adaptive façade element, such as a fully flexible DSF concept, using a BES tool. The need to adopt BES tools in predicting the short-term dynamic of a DSF is linked to the necessity of having an integrated environment to replicate the interactions between airflow in the façade, the HVAC system, and the building energy management system. The challenges are not only connected to the accuracy with which such tools can predict the performance of the DSF but also to the limitations that these tools present when it comes to adapting an existing element.

In this work we have: *i) demonstrated how to modify an existing routing (Double Glass Facade")* available in a BES tool (IDA ice) to tackle that multi-path ventilation strategies in a DSF, enabling a flexible model to represent dynamic DSF systems that can switch between different

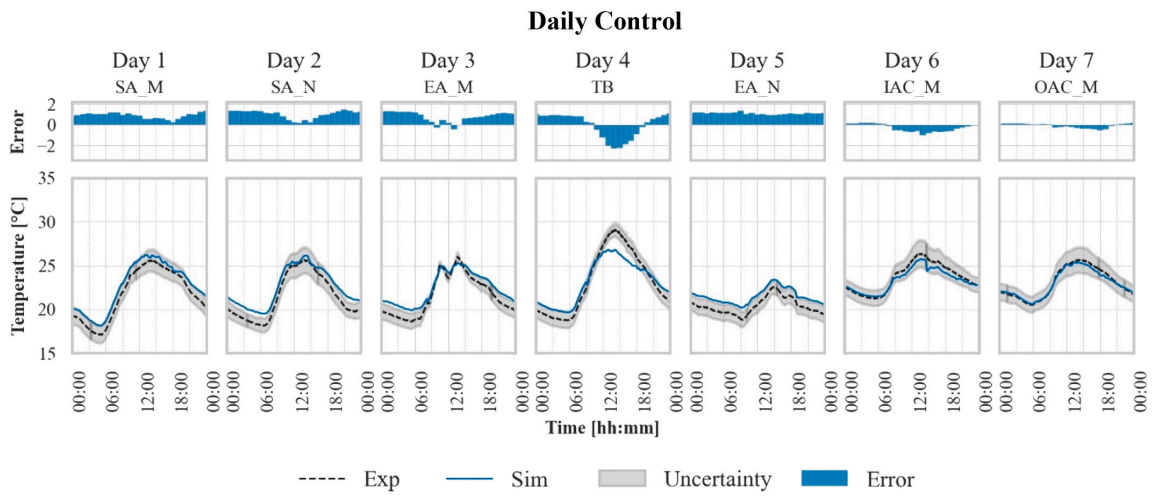

Fig. 15. Time profile of the surface temperature for the daily controlled days. The error is expressed in [°C]. The uncertainty band shows the two experimental values measured by the sensors on the surface.

ventilation modes (five flow paths – mechanically or naturally driven – and by-pass of the cavity) and driving force (natural and mechanical ventilation; *ii) compared the simulation results with experimental data from a dedicated measurement campaign* that covered a large range of operational modes, to assess and quantify the performance of the upgrade routine; *iii) verified that the model can replicate trends and dynamic profiles* of four main thermophysical quantities with mean bias errors lower than 1.5 °C and 4 W/m^2, for air and surface temperature values and for transmitted long-wave or short-wave heat flux values, respectively; *iv) quantified the simulation error for long-term* (e.g. 7 days) *energy simulations* that compute the thermal load on the room behind the façade, and this is, depending on the exact configuration and tested period, within the range of 5%–15%, which is considered suitable for energy simulations of buildings.

The enhanced model accurately depicts and approximates the switch from one configuration to the other. In terms of predictions, the airgap temperature is slightly overpredicted but much in line with the value measured in the higher portion of the cavity and is, therefore, more similar to what will be used from the outlets of the façade (i.e., a good approximation of the temperature used to climatise the indoor space). The surface temperature is in line with the mean measured value, which assures a good approximation for local discomfort analysis. The transmitted solar radiation is relatively well predicted, too, particularly if the position of the blinds is changed by a significant number of degrees. The heat flux estimation adequately depicts the daily profile of the incoming and exiting flux from the inner glazing, leading to a reasonable assessment of the overall energy calculation.

The limitations of the model we have developed in this study regarding simulation reliability are primarily linked to the limitations of the in-built DSF model of IDA ICE and not the alterations to match the functional features of the flexible DSF concept. By using an existing component within a BES tool, there is no possibility to intervene on the numerical assumptions of the component – unless further changes at the level of the source code are implemented. For example, there is only one air gap node, so the temperature stratification inside of the cavity is not represented. Even if the openings are modelled with controllable elements, choosing the right values to use in order to model hinged openings is not straightforward; the definition of the leakage values for these openings when closed is of similar complexity.

Despite these limitations, the model presented in this work appeared to be a good trade-off for modelling a dynamic envelope like a DSF in terms of accuracy and model complexity. The enhanced model enables a vast range of variability in the façade, responding to the need for a flexible model that allows switching flow paths, controlling the degrees of openings and intertwining the room's active systems. In closing this article, in an effort to make our research freely accessible and to allow easy replication of our results, we make available, in an open-access repository, both the flexible DSF model developed in this research (Fig. 4) and the experimental dataset employed to validate the model. These can be found at and referenced using the following links: http://doi.org/10.5281/zenodo.7090264 [23] and http://doi.org/10.5281/zenodo.7090274 [48], for the model and the experimental dataset, respectively.

CRediT authorship contribution statement

Elena Catto Lucchino: Writing – original draft, Visualization, Validation, Software, Methodology, Investigation, Formal analysis, Data curation, Conceptualization. **Giovanni Gennaro:** Validation, Methodology, Investigation, Data curation, Writing – review & editing. **Fabio Favoino:** Writing – review & editing, Project administration, Methodology, Resources. **Francesco Goia:** Writing – review & editing, Supervision, Resources, Project administration, Methodology, Conceptualization, Formal analysis, Funding acquisition.

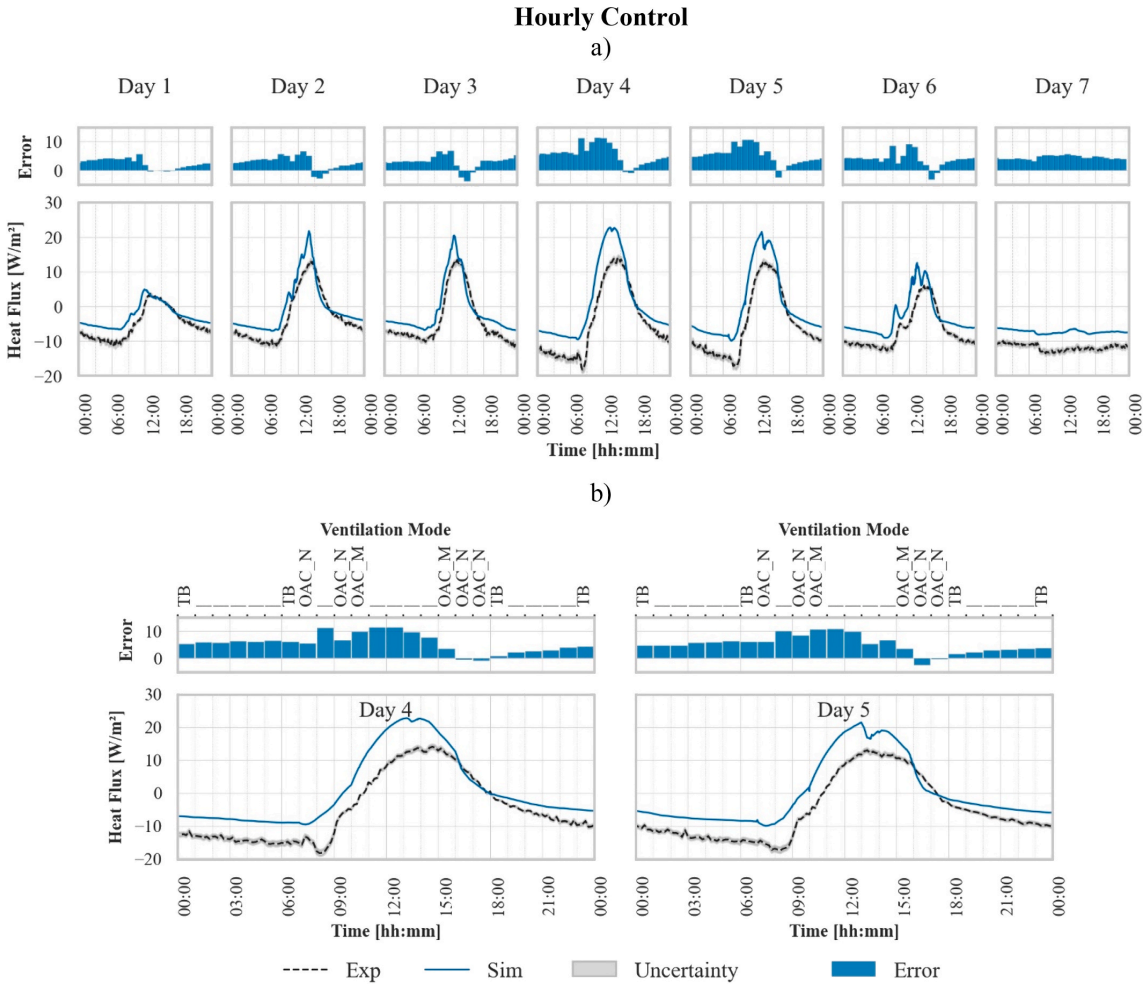

Fig. 16. a) Time profile of the transmitted heat flux for the hourly controlled days; b) detailed view of Day 4 and 5. The error is expressed in [W/m^2]. The uncertainty band shows the two experimental values measured by the heat flux meters.

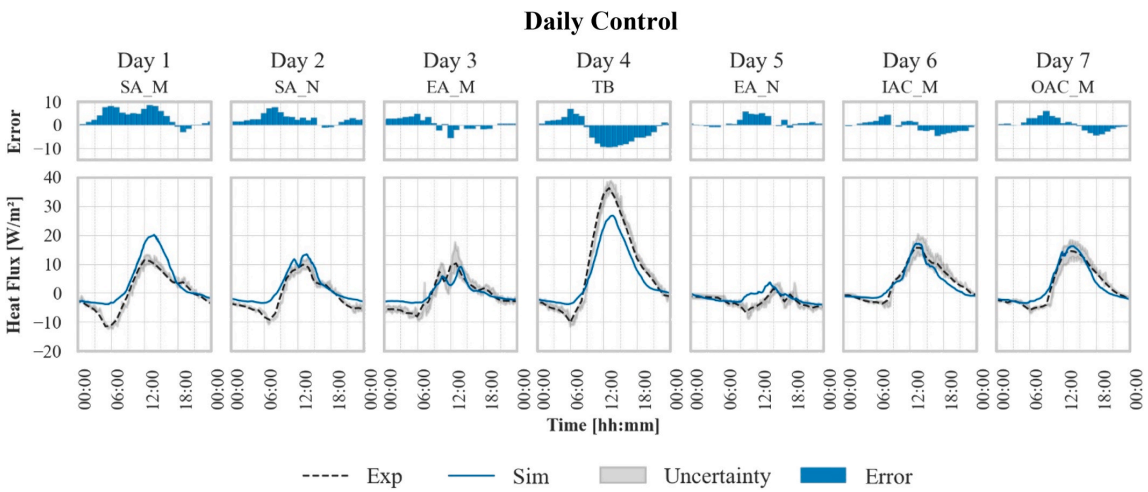

Fig. 17. Time profile of the transmitted heat flux for the daily controlled days. The error is expressed in [W/m^2]. The uncertainty band shows the two experimental values measured by the sensors on the surface.

Declaration of competing interest

The authors declare that they have no known competing financial interests or personal relationships that could have appeared to influence the work reported in this paper.

Data availability

The numerical model in IDA ICE and the experimental data for model validation are made available in an online repository as described in the article

Acknowledgement

The research activities presented in this paper were carried out within the research project "REsponsive, INtegrated, VENTilated - REINVENT – windows", supported by the Research Council of Norway through the research grant 262198, and partners SINTEF, Hydro Extruded Solutions, Politecnico di Torino, Aalto University. The authors would like to thank Mika Vuolle from Equa Simulation Finland Oy for his input and consulting on the IDA ICE software tool during the development of the flexible DSF model.

References

[1] V. Huckemann, E. Kuchen, M. Leão, É.F.T.B. Leão, Empirical thermal comfort evaluation of single and double skin façades, Build. Environ. 45 (2010) 976–982, https://doi.org/10.1016/j.buildenv.2009.10.006.
[2] F. Pomponi, P.A.E. Piroozfar, R. Southall, P. Ashton, E.R.P. Farr, Energy performance of Double-Skin Façades in temperate climates: a systematic review and meta-analysis, Renew. Sustain. Energy Rev. 54 (2016) 1525–1536, https://doi.org/10.1016/j.rser.2015.10.075.
[3] M. Haase, F. Marques da Silva, A. Amato, Simulation of ventilated facades in hot and humid climates, Energy Build. 41 (2009) 361–373, https://doi.org/10.1016/j.enbuild.2008.11.008.
[4] A.S. Anđelković, I. Mujan, S. Dakić, Experimental validation of a EnergyPlus model: application of a multi-storey naturally ventilated double skin façade, Energy Build. 118 (2016) 27–36, https://doi.org/10.1016/j.enbuild.2016.02.045.
[5] U. Eicker, V. Fux, U. Bauer, L. Mei, D. Infield, Facades and summer performance of buildings, Energy Build. 40 (2008) 600–611, https://doi.org/10.1016/j.enbuild.2007.04.018.
[6] I. Khalifa, L.G. Ernez, E. Znouda, C. Bouden, Coupling TRNSYS 17 and CONTAM: simulation of a naturally ventilated double-skin facade, Adv. Build. Energy Res. 9 (2015) 293–304, https://doi.org/10.1080/17512549.2015.1050694.
[7] N.M. Mateus, A. Pinto, G.C. Da Graça, Validation of EnergyPlus thermal simulation of a double skin naturally and mechanically ventilated test cell, Energy Build. 75 (2014) 511–522, https://doi.org/10.1016/j.enbuild.2014.02.043.
[8] F. Pomponi, S. Barbosa, P.A.E. Piroozfar, On the intrinsic flexibility of the double skin façade: a comparative thermal comfort investigation in tropical and temperate climates, Energy Proc. 111 (2017) 530–539, https://doi.org/10.1016/j.egypro.2017.03.215.
[9] J.-S. Yu, J.-H. Kim, S.-M. Kim, J.-T. Kim, Thermal and energy performance of a building with PV-Applied double-skin façade, Proc. Inst. Civ. Eng. Eng. Sustain. 170 (2017), https://doi.org/10.1680/jensu.16.00017.
[10] R. Høseggen, B.J. Wachenfeldt, S.O. Hanssen, R. Hoseggen, B.J. Wachenfeldt, S. O. Hanssen, Building simulation as an assisting tool in decision making. Case study: with or without a double-skin facade? Energy Build. 40 (2008) 821–827, https://doi.org/10.1016/j.enbuild.2007.05.015.
[11] H. Elarga, A. Zarrella, M. De Carli, Dynamic energy evaluation and glazing layers optimization of façade building with innovative integration of PV modules, Energy Build. 111 (2016) 468–478, https://doi.org/10.1016/j.enbuild.2015.11.060.
[12] V. Leal, E. Erell, E. Maldonado, Y. Etzion, Modelling the SOLVENT ventilated window for whole building simulation, Build. Serv. Eng. Technol. 25 (2004) 183–195, https://doi.org/10.1191/0143624404bt103oa.
[13] A. Gelesz, A. Reith, Climate-based Performance Evaluation of Double Skin Facades by Building Energy Modelling in Central Europe, Energy Procedia, 2015, pp. 555–560, https://doi.org/10.1016/j.egypro.2015.11.735.
[14] N. Papadaki, S. Papantoniou, D. Kolokotsa, A parametric study of the energy performance of double-skin façades in climatic conditions of Crete, Greece, Int. J. Low Carbon Technol. 9 (2013) 296–304, https://doi.org/10.1093/ijlct/cts078.
[15] W. Choi, J. Joe, Y. Kwak, J.H. Huh, Operation and control strategies for multi-storey double skin facades during the heating season, Energy Build. 49 (2012) 454–465, https://doi.org/10.1016/j.enbuild.2012.02.047.
[16] C.S. Park, G. Augenbroe, Local vs. integrated control strategies for double-skin systems, Autom. ConStruct. 30 (2013) 50–56, https://doi.org/10.1016/j.autcon.2012.11.030.
[17] C.S. Park, G. Augenbroe, T. Messadi, M. Thitisawat, N. Sadegh, Calibration of a lumped simulation model for double-skin façade systems, Energy Build. 36 (2004) 1117–1130, https://doi.org/10.1016/j.enbuild.2004.04.003.
[18] C.S. Park, G. Augenbroe, N. Sadegh, M. Thitisawat, T. Messadi, Real-time optimization of a double-skin façade based on lumped modeling and occupant preference, Build. Environ. 39 (2004) 939–948, https://doi.org/10.1016/j.buildenv.2004.01.018.
[19] S.H. Yoon, C.S. Park, G. Augenbroe, On-line parameter estimation and optimal control strategy of a double-skin system, Build. Environ. 46 (2011) 1141–1150, https://doi.org/10.1016/j.buildenv.2010.12.001.
[20] D. Kim, C.-S. Park, A Heterogeneous System Simulation of a Double-Skin Façade, 12th Int. IBPSA Conf, Sydney, 2011, pp. 14–16, in: http://ibpsa.org/proceedings/BS2011/P_1281.pdf.
[21] E. Catto Lucchino, A. Gelesz, K. Skeie, G. Gennaro, A. Reith, V. Serra, F. Goia, Modelling double skin façades (DSFs) in whole-building energy simulation tools: validation and inter-software comparison of a mechanically ventilated single-story DSF, Build. Environ. 199 (2021), https://doi.org/10.1016/j.buildenv.2021.107906.
[22] E. Catto Lucchino, F. Goia, G. Lobaccaro, G. Chaudhary, Modelling of double skin facades in whole-building energy simulation tools: a review of current practices and possibilities for future developments, Build. Simulat. 12 (2019) 3–27, https://doi.org/10.1007/s12273-019-0511-y.

[23] E. Catto Lucchino, G. Gennaro, F. Favoino, F. Goia, Model for a Single-Storey Flexible Double-Skin Façade System in IDA ICE, 2022, https://doi.org/10.5281/zenodo.7090264.
[24] S. Kropf, G. Zweifel, Validation of the building simulation program IDA-ICE according to CEN 13791 "thermal performance of buildings - calculation of internal temperatures of a room in summer without mechanical cooling - general criteria and validation procedures, Adv. HVAC Nat. Gas Technol. 24 (2001). http://www.equaonline.com/iceuser/validation/ICE_vs_prEN 13791.pdf.
[25] EQUA, Validation of IDA indoor climate and energy 4 . 0 with respect to CEN standards EN 15255-2007 and EN 15265-2007, Http://Www.Equaonline.Com/Iceuser/Validation/. (2010) 19, http://www.equaonline.com/iceuser/validation/CEN_VALIDATION_EN_15255_AND_15265.pdf.
[26] A.B. EQUA Simulation, Validation of IDA Indoor Climate and Energy 4.0 Build 4 with Respect to ANSI/ASHRAE Standard 140-2004, ASHRAE Stand., 2010, p. 44.
[27] M. Vuolle, A. Bring, P. Sahlin, An NMF based model library for building thermal simulation, in: Proc. 6, Th IBPSA Conf., Kyoto, Japan, 1999, pp. 1–8.
[28] P. Sahlin, L. Eriksson, P. Grozman, H. Johnsson, A. Shapovalov, M. Vuolle, Whole-building simulation with symbolic DAE equations and general purpose solvers, Build. Environ. 39 (2004) 949–958, https://doi.org/10.1016/j.buildenv.2004.01.019.
[29] E. Taveres-Cachat, F. Favoino, R. Loonen, F. Goia, Ten questions concerning co-simulation for performance prediction of advanced building envelopes, Build. Environ. 191 (2021), https://doi.org/10.1016/j.buildenv.2020.107570.
[30] R.C.G.M. Loonen, F. Favoino, J.L.M. Hensen, M. Overend, Review of current status, requirements and opportunities for building performance simulation of adaptive facades, J. Build. Perform. Simul. 10 (2017) 205–223, https://doi.org/10.1080/19401493.2016.1152303.
[31] Y. Wang, Y. Chen, J. Zhou, Dynamic modeling of the ventilated double skin façade in hot summer and cold winter zone in China, Build, Environ. Times 106 (2016) 365–377, https://doi.org/10.1016/j.buildenv.2016.07.012.
[32] Y. Li, J. Darkwa, G. Kokogiannakis, Heat transfer analysis of an integrated double skin façade and phase change material blind system, Build. Environ. 125 (2017) 111–121, https://doi.org/10.1016/j.buildenv.2017.08.034.
[33] A. Dama, D. Angeli, O. Kalianova Larsen, Naturally ventilated double-skin façade in modeling and experiments, Energy Build. 144 (2017) 17–29, https://doi.org/10.1016/j.enbuild.2017.03.038.
[34] R.C.G.M. Loonen, F. Favoino, J.L.M. Hensen, M. Overend, Review of current status , requirements and opportunities for building performance simulation of adaptive facades, J. Build. Perform. Simul. (2016) 1–19, https://doi.org/10.1080/19401493.2016.1152303.
[35] A. Gelesz, E. Catto Lucchino, F. Goia, V. Serra, A. Reith, Characteristics that matter in a climate façade: a sensitivity analysis with building energy simulation tools, Energy Build. 229 (2020), https://doi.org/10.1016/j.enbuild.2020.110467.
[36] E. Catto Lucchino, F. Goia, G. Lobaccaro, G. Chaudhary, Modelling of double skin facades in whole-building energy simulation tools: a review of current practices and possibilities for future developments, Build. Simulat. 12 (2019), https://doi.org/10.1007/s12273-019-0511-y.
[37] ISO 15099, Thermal Performance of Windows, Doors and Shading Devices: Detailed Calculations, 2003.
[38] ISO 52022-3:20, ISO 52022-3, Energy Performance of Buildings - Thermal, Solar and Daylight Properties of Building Components and Elements - Part 3: Detailed Calculation Method of the Solar and Daylight Characteristics for Solar Protection Devices Combined with Glazing, 2017.
[39] A.B. EQUA Simulation, User Manual IDA Indoor Climate and Energy 4.8 (2018).
[40] A. Gelesz, E. Catto Lucchino, F. Goia, A. Reith, V. Serra, Reliability and sensitivity of building performance simulation tools in simulating mechanically ventilated double skin facades, in: V. Corrado, A. Gasparella (Eds.), Proc. Build. Simul. 2019 16th Conf, IBPSA, Rome, 2019.
[41] G. Gennaro, E. Catto Lucchino, F. Goia, F. Favoino, Modelling double skin façades (DSFs) in whole-building energy simulation tools: validation and inter-software comparison of naturally ventilated single-story DSFs, Submitt. to Build. Environ. (2022) (Submission Nr. BAE-D-22-03720).
[42] F. Goia, V. Serra, Analysis of a non-calorimetric method for assessment of in-situ thermal transmittance and solar factor of glazed systems, Sol. Energy 166 (2018) 458–471, https://doi.org/10.1016/j.solener.2018.03.058.
[43] J.M. Bright, N.A. Engerer, Engerer2: global re-parameterisation, update, and validation of an irradiance separation model at different temporal resolutions, J. Renew. Sustain. Energy 11 (2019), https://doi.org/10.1063/1.5097014.
[44] J.-N. Hersbach H, B. Bell, P. Berrisford, G. Biavati, A. Horányi, J. Muñoz Sabater, J. Nicolas, C. Peubey, R. Radu, I. Rozum, D. Schepers, A. Simmons, C. Soci, D. Dee, Thépaut, ERA5 hourly data on single levels from 1979 to present, in: Copernicus Climate Change Service (C3S) Climate Data Store (CDS), 2018, https://doi.org/10.24381/cds.adbb2d47. (Accessed 26 April 2021). Accessed on.
[45] TRNFLOW, 56, in: A Module of an Air Flow Network for Coupled Simulation with TYPE 56 (Multi-zone Building of TRNSYS), 2009, pp. 1–58.
[46] EQUA Simulation AB, IDA –Indoor Climate and Energy Ver 3.0 NMF-Model Documentation, ((n.d.)).
[47] ASHRAE, ASHRAE Guideline 14 - Measurement of Energy, Demand, and Water Savings, 2014.
[48] E. Catto Lucchino, G. Gennaro, F. Favoino, F. Goia, Experimental Data for Validation of a Single-Storey Flexible Double-Skin Façade System Model, 2022, https://doi.org/10.5281/zenodo.7090274.

7 Multi-domain model-based control of a flexible double skin façade system

P6 *E. Catto Lucchino, F. Goia. Multi-domain model-based control of an adaptive façade based on a flexible double skin system. Energy and Buildings – under revision*

Adaptive envelopes have the potential to significantly reduce energy use in buildings while ensuring high performance. These envelopes interact with multiple interconnected domains, such as daylight, indoor air quality, thermal comfort, and energy use, which can often conflict with one another. Identifying and developing suitable control strategies that can optimally manage the envelope's impact on many domains and avoid sub-optimal operations is an open challenge. Conventional approaches commonly adopted in buildings and building envelope control based on schedules or relatively simple decision trees may be unable to tackle the dynamic behaviour of adaptive envelopes. Due to their complexity, more advanced control approaches based on simulation-informed decision-making are scarce in both research and practice. In this work, we propose a multi-domain model-based control (MBC) algorithm for an adaptive façade concept based on a flexible Double Skin Façade (DSF). The proposed method, which aims for a balanced performance over different comfort domains and energy use, employs a co-simulation approach where the DSF is modelled in a Building Energy Simulation (BES) tool and the control algorithm to manage the simulation and optimize the control of the façade is developed in a generic programming language. To the best of our knowledge, this is one of the first attempts to design and demonstrate the effectiveness of a simulation-informed control strategy that can handle and optimise the behaviour of a complex façade by considering multiple performance objectives. The innovation of this approach lies in the MBC algorithm that selects the optimal façade state among over seventy possible states at each timestep, the practical demonstration of the feasibility in a BES tool, and the complexity of the controlled

façade system. To verify the effectiveness of the proposed control approach, we compared the innovative MBC to more traditional control strategies, such as schedule and rule-based controls, revealing how it enabled the façade to achieve a better performance in all the analysed domains. By applying the MBC to three different year periods, we showed that the energy and environmental performance was within the selected comfort criteria for all the domains for more than 80% of the occupied hours, and an energy reduction of up to 70% was simultaneously obtained if compared to more traditional approaches. The control approach presented in this study and the simulation method employed can be used not only to improve the performance of advanced adaptive façades by providing an effective solution to the challenge of balancing multiple conflicting performance domains but also for more conventional building envelope systems that exhibit a certain degree of dynamic behaviour.

Energy & Buildings 285 (2023) 112881

Contents lists available at ScienceDirect

Energy & Buildings

journal homepage: www.elsevier.com/locate/enb

Multi-domain model-based control of an adaptive façade based on a flexible double skin system

Elena Catto Lucchino, Francesco Goia *

Department of Architecture and Technology, Norwegian University of Science and Technology, NTNU, Trondheim, Norway

ARTICLE INFO

Article history:
Received 20 November 2022
Revised 25 January 2023
Accepted 6 February 2023
Available online 10 February 2023

Keywords:
Model based control (MBC)
Multi-domain optimisation
Adaptive facades
Double Skin Façade (DSF)
Building energy simulation
IDA ICE

ABSTRACT

Adaptive envelopes have the potential to significantly reduce energy use in buildings while ensuring high performance. These envelopes interact with multiple interconnected domains, such as daylight, indoor air quality, thermal comfort, and energy use, which can often conflict with one another. Identifying and developing suitable control strategies that can optimally manage the envelope's impact on many domains and avoid sub-optimal operations is an open challenge. Conventional approaches commonly adopted in buildings and building envelope control based on schedules or relatively simple decision trees may be unable to tackle the dynamic behaviour of adaptive envelopes. Due to their complexity, more advanced control approaches based on simulation-informed decision-making are scarce in both research and practice. In this work, we propose a multi-domain model-based control (MBC) algorithm for an adaptive façade concept based on a flexible Double Skin Façade (DSF). The proposed method, which aims for a balanced performance over different comfort domains and energy use, employs a co-simulation approach where the DSF is modelled in a Building Energy Simulation (BES) tool and the control algorithm to manage the simulation and optimize the control of the façade is developed in a generic programming language. To the best of our knowledge, this is one of the first attempts to design and demonstrate the effectiveness of a simulation-informed control strategy that can handle and optimise the behaviour of a complex façade by considering multiple performance objectives. The innovation of this approach lies in the MBC algorithm that selects the optimal façade state among over seventy possible states at each timestep, the practical demonstration of the feasibility in a BES tool, and the complexity of the controlled façade system. To verify the effectiveness of the proposed control approach, we compared the innovative MBC to more traditional control strategies, such as schedule and rule-based controls, revealing how it enabled the façade to achieve a better performance in all the analysed domains. By applying the MBC to three different year periods, we showed that the energy and environmental performance was within the selected comfort criteria for all the domains for>80% of the occupied hours, and an energy reduction of up to 70% was simultaneously obtained if compared to more traditional approaches. The control approach presented in this study and the simulation method employed can be used not only to improve the performance of advanced adaptive façades by providing an effective solution to the challenge of balancing multiple conflicting performance domains but also for more conventional building envelope systems that exhibit a certain degree of dynamic behaviour.

1. Introduction

1.1. Background

Adaptive façades are envelope systems that dynamically adjust their physical properties in response to transient boundary conditions [1]. Adaptive facades can exploit a large range of possibilities enabled by different technologies; among them, double skin façades (DSFs) are highly transparent façades that can exhibit adaptive capabilities thanks to the cavity ventilation flow [2] and shading systems in the cavity. These adaptive properties may be

Abbreviations: ***API***, Application Programming Interface; ***BES***, Building Energy Simulation; ***DSF***, Double Skin Facade; ***EA***, Exhaust Air; ***IAC***, Indoor Air Curtain; ***MBC***, Model-Based Control; ***MPC***, Model-Predictive Control; ***OAC***, Outdoor Air Curtain; ***RBC***, Rule-based control; ***SA***, Supply Air; ***SBC***, Schedule-Based Control; ***SK***, Single Skin facade; ***TB***, Thermal Buffer; $\boldsymbol{TB_v}$, Ventilated Thermal Buffer.

* Corresponding author.
E-mail address: francesco.goia@ntnu.no (F. Goia).

https://doi.org/10.1016/j.enbuild.2023.112881
0378-7788/

Nomenclature

AFP	Airflow paths
$\Delta CO2$	difference between the outdoor and room CO2 concentration level [ppm]
$\bar{E}_{plane}$	illuminance on the working plane [lux]
φ	angle of the slats [°]
F	Fan settings
Q_{heat}	Heating deand [W]
Q_{cool}	Cooling demand [W]
Q_{SOL}	Solar radiation on the façade [W/m^2]
SH	shading position
T_{op}	operative temperature in the room [°C]
Tmr	Running medium temperature [°C]
T_{GAP}	Airgap temperature [°C]
V_{min}	Minimum airflow [l/s]
V_{mid}	Medium airflow [l/s]
V_{max}	Maximum airflow [l/s]

benifitial for reducing energy use for building climatisation [3] and improving thermal and visual comfort conditions compared to a traditional single-skin façade [4].

The mere presence of adaptive capabilities in a building envelope does not directly guarantee its successful operation. The adaptive behaviour has to simultaneously satisfy multiple interdependent performance requirements, which often conflict with one another. Therefore, the correct operation of an adaptive façade is as crucial as the chosen materials and technologies that enable a dynamic behaviour, but this aspect is quite often neglected. For example, in most cases, DSFs are run using simple, rule-based controls (e.g. *"if this, do that*" under certain circumstances) focusing on a single criterion. This control structure intrinsically limits the optimal performance of a DSF since it is pre-set (hence cannot fully adapt to what really happens) and is by necessity linked to a limited number of output states. As a result, it is not unusual that the potential performance of DSFs is not met [5].

More advanced forms of control for adaptive envelopes that can foster a better and more balanced performance across different domains can be based on the exploitation of (real-time) simulation to identify the most effective state for the façade at each timestep. An example of such an approach for a DSF is present in Park et al.'s work, where the optimal control is the solution of a cost function that optimises energy use [6,7]. However, the development and application of advanced control strategies is relatively little explored in research and practice, where RBC are still largely employed.

1.2. Research aims and questions

In the research activity presented in this paper, we aimed to develop a model-based control method able to fully exploit an adaptive facade's abilities across several different performance domains–indoor lighting, air quality, thermal comfort, and energy consumption (not just minimising the energy consumption). The dynamic facade concept linked to the control approach in this study is a flexible DSF module capable of switching between different cavity ventilation flow paths, driving force and interplaying with the HVAC plant of the building. However, the control approach developed in this research is generally valid for any adaptive façade tackling a balanced behaviour across different domains and can be scaled and expanded further to meet performances that were not selected in this specific case.

We developed this innovative control approach, which goes beyond the current practice in control of building envelope systems, using a building energy simulation (BES) tool, as we believe that this class of tools best ensures an integrated simulation between the envelope system and the building energy and environmental systems. By doing this, we also demonstrated how recent developments in building performance simulations (e.g. the increasing availability of APIs or software interfaces for external control of BES tools) greatly enhance the possibility of developing more advanced control architectures.

In a nutshell, the research presented in this paper addresses a gap in the current knowledge and practice for control of (advanced) building envelopes, and tackles the the research question of *how adaptive envelopes can be controlled effectively by exploiting the flexibility that these building enclosure systems have.* The element of novelty in this research covers both *i) a new approach to multi-domain optimal control* of adaptive facades by exploiting a model-based control and *ii) a demonstration of the feasibility of such an approach by leveraging the latest developments in co-simulation schemes for BES*. At the best of our knowledge, this study is the first of its kind demonstrating the use of model-based control for an adaptive façade system characterised by a very large range of possible states, which is a system that clearly cannot be efficiently controlled using common control strategies conventionally adopted for building envelopes.

1.3. Article structure and readership

The article is structured as follows: in *Section 2–Control structures and control simulation for adaptive building envelopes,* we provide the reader with an overview of the current control possibilities for adaptive facades, highlighting the challenges and limitations and building the case for a more sophisticated approach in the case of a façade system with many degrees of freedom; in *Section 3–Adaptive façade concept and its numerical model in a BES tool,* the concept of flexible DSF is explained in detail, together with the simple case-study building used in this study; *Section 4–Control strategy definition* presents the multi-domain model-based control strategy developed for this work and the more conventional control approaches used as a baseline. Section 5–*Implementation of MBC in a BES tool via co-simulation* presents the workflow for implementing the model-based control in co-simulation with IDA ICE. The interaction between IDA ICE and the optimal control algorithm in Python is described together with the process automation. In *Section 6–Results,* the results for all the control strategies used in three different analysed periods are presented and compared. This is followed by *Section 7–Discussion,* where we reflected on the results and expanded the assessment of the outcomes of the work. Finally, the conclusive summary of the article is presented in *Section 8–Conclusion*.

2. Control structures and control simulation for adaptive building envelopes

2.1. Current possibilities for control structures for building envelope systems

The automation of actively controllable dynamic envelope systems is, in principle, based on two alternative approaches [10]: rule-based control (RBC) and model-based control (MBC). RBCs

represent the majority of control decision-making currently adopted in building automation [11]. A set of pre-determined rules with time schedule could also be considered a very simple form of RBC. MBC is a relatively novel way emerging in building control, especially for the control of envelope systems. Nevertheless, it still requires a lot of development before reaching a mature state and achieving widespread implementation. Henceforth in this workwe refer to schedule RBC as Schedule Based Control (SBC), while we use the term RBC to refer to threshold-base control.

Defining time schedules to control active elements of a façade is straightforward and easy to implement, but they may not be as flexible or responsive to changes in the system as more advanced control methods. This type of control is often used in systems where the desired outcome is known, and the timing of the various elements is critical to achieving that outcome. Schedule-based control is based on the assumed performance of a system given "average" or "common" conditions. While this approach can be suitable for systems with binary values (e.g. deployed/not deployed, open/-closed) in domains with high predictability, it cannot truly exploit the potential of an adaptable system. Simple control strategies for shading devices, deployed or tuned following the progression of time during the day, are a good example of this type of control.

Taking the complexity to a slightly higher level, embedded or building-level sensors can be used to include environmental parameters in the decision process. RBC consists of a set of *if-then* rules where input data derived from sensors are compared against specific threshold values to determine the state of one or more actuators. Controlling the position of solar devices based on the amount of solar irradiance on the façade is a common application of this approach. If the reading from the irradiance sensor is combined with other input data, such as outdoor temperature, occupancy sensor, or a schedule, more complex decision trees can be created [12].

RBCs can use signals from environmental monitoring in combination with a more or less complex decision tree to realise the so-called *open-loop* or *closed-loop* controls. In open-loop RBCs, the control action does not affect the control input signal. For example, when using an outdoor irradiance sensor to control the state of a shading device, the controller has no information on the effect of shading on the indoor environment [13]. Conversely, in a closed loop the input sensor signal depends on the control action. For example, when a shading system is deployed due to the indoor illuminance exceeding a certain threshold value, the closed-loop control is based on the effect of the control action [14]. Open-loops are usually simpler to realise and are hence widely adopted in controlling adaptive facades [15], but closed-loops could provide more effective management as the control is done on the final effect of the system [16–18].

Even if rule-based control can easily be made more complex, for example, by combining sensor-based input with schedule-based rules or using variable threshold values depending on the season or the room occupancy level [19], they still suffer from several limitations. Any rule-based control (scheduled, open- and closed-loop) only allows a limited number of alternative states, as making a decision tree with many output states is neither trivial nor too functional. Particularly for those control strategies that tackle multiple domains (e.g. thermal environment and light environment) and have contrasting objectives, a rigid structure makes it challenging to provide the right answer for any combination of conditions and objectives. Moreover, understanding meaningful threshold values might be challenging [20], especially in open-loop algorithms.

MBC strategies generally employ a linear and differentiable system model to describe the behaviour of the system and choose the best strategy to reach predefined goals. This provides higher flexibility than RBC as an indirect logic approach is employed [21]. They exploit the prediction (through simulation) of the impact of the control action on the indoor environment to perform decision-making, aiming to maximise one or more building-level performances [22], thereby improving upon the performance of closed-loop controls. This usually requires a high-level optimal objective definition (e.g. minimisation or maximisation of a particular performance) combined with suitable optimal search algorithms to ensure that the computational load remains within a suitable range [20]. In the case of a limited number of states, a full-factorial search might still be an option. In contrast, if the number of states is high and/or a prediction functionality is included in this control strategy (with a certain future prediction horizon, as for model predictive control), the need for a more intelligent search of the desired performance in a given solution space is a must [23].

Implementing MBCs to improve the operational performance of a building by integrating adaptive building envelopes is complex (and expensive), not only in real-life but even in the context of a simulation study. Different examples of implementations of MBCs (and model predictive control, MPC) to control adaptive building envelope systems are available in literature. Nevertheless, these are limited to research applications [24] and, most of the time, only to simulation studies [25–28]. This is mainly due to the high cost and effort in designing and implementing MBC strategies linked to the modelling and automation requirements [10]. Models (of the façade element, of the building in which it is integrated to evaluate its impact, and for forecasting the system disturbances, i.e. weather and occupancy) are required to be accurate and fast at the same time (enabling the possibility to perform extensive exploration in a time compatible with the control action). Only very few studies have analysed the influence of control on multi-comfort domains [29,30]; most works focus on daylight and visual comfort performance and energy minimisation by controlling the position of blind slats [31–33] or the properties of electrochromic glazing [21,34,35]. Only a few studies have applied MBC on DSFs [8,36], where the interaction of multiple domains plays a key role.

2.2. Current state and limitations of advanced control of adaptive facades in BES tools

Simple control approaches and routines are commonly implemented in BES tools. For example, schedule controls or controllers based on threshold values for shadings systems are available in the most commonly adopted tools (EnergyPlus [37], Trnsys [38], IES VE [39], IDA ICE [40], etc.). The implementation of open-loop controls over a certain element is often restricted to a particular domain without taking into consideration the effect that it could have on other domains (e.g. the threshold for controlling the shading device is often set in terms of radiation hitting the facade and not linked to the thermal domain). EnergyPlus allows users to control shading, openings, HVAC and other active systems via the implementation of diverse pre-set controls, with the option of accounting for more than one variable (commonly the presence of occupants, incident solar radiation and temperature of the room). IES VE provides basic controls for most of the building components (like time schedule or threshold values to apply basic open-loop algorithms), and some more developed controllers for the HVAC system. Trnsys has quite an extensive control library that allows implementing complex open and closed-loop controls without having to recur to co-simulation. Similarly, IDA ICE offers highly customizable control strategies when using the "Advance level", providing diverse elements (NMF library) to create advanced strategies and allowing access to most of the models' inputs and outputs [41]. These features are indispensable when more advanced control routines are required. However, when there are many levels for the states of the actuators/functions, the number of possible permutations can quickly reach hundreds. Even without considering how suitable

this control strategy is, implementing very complicated decision trees in BES tools is challenging. Tools like IDA ICE or Trnsys are more suitable for this use as they provide greater flexibility in creating complex control structures without the need to use advanced functions, such as the Energy Management System (EMS) module in EnergyPlus.

Moreover, given the current level of development of BES tools, no simulation environment allows straightforward implementation of model-based control routines [42,43]. To have a simulation that includes MBC, it is necessary to have a model that represents the physical system and a control-oriented model that is used to take decisions on the best operations of the system. While the former model can be easily made in a BES tool, control-oriented models often take the form of a reduced-order model [44], and the control performance is determined using a forecasting horizon [6,45,46]. Calibrated reduced-order models are commonly used to achieve a good balance between speed and accuracy. Implementing a MBC algorithm with BES tools thus requires two simulations to proceed in parallel and exchange information within the simulation runtime (co-simulation). The primary simulation replicates the system's performance given the selected operational mode and computes the evolution of the energy and mass balances in the building. A secondary simulation explores at each time step the ranges of performance that can be achieved in a particular time-window, given a set of boundary conditions, and the past states (this is usually relevant only for some domains, i.e. thermal and mass balance, while it might be neglected for others that are not affected by the previous history). Co-simulating the two models relies on the possibilities of a specific BES tool to be integrated into a co-simulation framework either directly or using middleware software. While co-simulation for BES has been in the field for a while, co-simulation targeting control for building envelope systems is relatively new.

Co-simulation infrastructures can be realised between a BES tool and other external scripts in different ways that depend on the individual features of the simulation environment. In Energy Plus, for example, this can be achieved with a high-level control method, the Energy Management System (EMS). Using the EMS, it is possible to access a wide variety of "sensor" data and use this data to direct various types of control actions with co-simulation [47]. Moreover, using the software *EnergyPlusToFMU* it is possible to perform co-simulation with all tools that support an FMI (Functional Mock-Interface), e.g. Modelica [48]. Similarly, Trnsys allows co-simulation control using a dedicated FMI via Python [49,50] or other programming languages. Similar integrated access to the software APIs is provided by IES VE, where an in-built Python interface allows the extraction of the simulation data and access to some of the variables of the model [51]. Finally, IDA ICE also allows interaction over socket communication, providing a library with API functions accessible with general-purpose programming languages, e.g. Python, Matlab, Excel, C++, Java or similar [52]. A commonly adopted environment for co-simulations is the BCTVB Toolbox, where BES tools like Energy Plus or Trnsys can be coupled with MATLAB/Simulink control sequences [53].

This study tackles the challenge of setting up a multi-domain control for an adaptive façade concept characterised by a large variety of possible states. The investigated façade concept can modify its performance by changing the state of three actuators, each of which can assume multiple states. In a reduced version of the façade concept, this equals 69 possible different states to be explored when the best control sequence needs to be found.

Examining different options for controlling such a system revealed that advanced control strategies such as model-based control architecture are needed to fully utilize the potential of flexible façade concepts, as opposed to traditional RBC structures, which can currently be directly implemented in BES [54,55].

Therefore, in the following sections, we will demonstrate the coupling between the adaptive façade model and a multi-domain optimisation control algorithm thanks to the co-simulation features accessible in a BES tool. A suitable simulation workflow was developed for this purpose in IDA ICE to enable the MBC of the adaptive façade concept, leveraging the possibilities to automate the workflow process, the start/stop of simulation runs and co-simulation functionality. Moreover, more traditional rule-based controls described in the previous sections (schedule-based and open-loop control) are also applied to the same model for a more comprehensive comparison.

3. Adaptive façade concept and its numerical model in a BES tool

3.1. Adaptive façade concept

The adaptive façade concept exploited in this research has been presented in detail in a previous study [9], which focused on the challenge of building a suitable physical–mathematical representation of the façade concept and its validation using comparison with experimental data. It is a façade based on the architecture of a double-skin façade, with different cavity ventilation paths achievable thanks to a dedicated inlet and outlet section. The cavity can have an airflow driven by mechanical devices (fans) and naturally-induced phenomena (natural ventilation). The façade concept also allows one to close the cavity fully and either decouple the indoor from the outdoor in terms of mass exchange or bypass the ventilated cavity and allow air exchange between indoor and outdoor through openings at the bottom and the top of the façade element. The facade manages the direct solar and luminous gains through an integrated shading system in coordination with the building energy management system.

In the framework of such an integrated façade concept that needs to interact dynamically with the building services, the coupled simulation of the whole building and the specific building components is an essential prerequisite to correctly assessing the overall energy and comfort performance and replicate the complex interaction between airflow in the façade, the HVAC system, and the building energy management system.

The physical–mathematical representation of the façade concept was developed using the BES tool IDA ICE, employing the in-built model '*Double Glass Façade*', which was modified to switch between all the air path configurations. This in-built module, described more in detail in [9], is already integrated into the thermal and airflow network of the BES tool and allows the combined simulation between the façade component and the indoor space (and the HVAC). The existing model was further developed to model all the natural and mechanical airflow paths and to control the facade within the same simulation.

The presented model (Fig. 1) allows the modeller to change the configuration of the façade by controlling the actuators of each opening and fan and integrate this control with the building HVAC system. Each controlled element receives different input from the controller: a) the openings' actuators allow the setting of the opening percentage (from 0–closed to 1–fully open); b) the fans' actuators receive two inputs: a *centralMode* control that sets the fan ON or OFF and a flow *control* that controls the amount of mechanical flow (max*(centralMode*(m_max*control + m_min*(1-control)), c_low*m_min)*) with c_low detailing the behaviour of the fan as crack when it is off; c) the shading device' actuator receives two input: a 1/0 control that sets the shading ON/OFF and an *ANGLE* input that sets the position of the slats in case a blind is used.

As explained in more detail in the next section, the model of the adaptive façade was combined with three different types of control

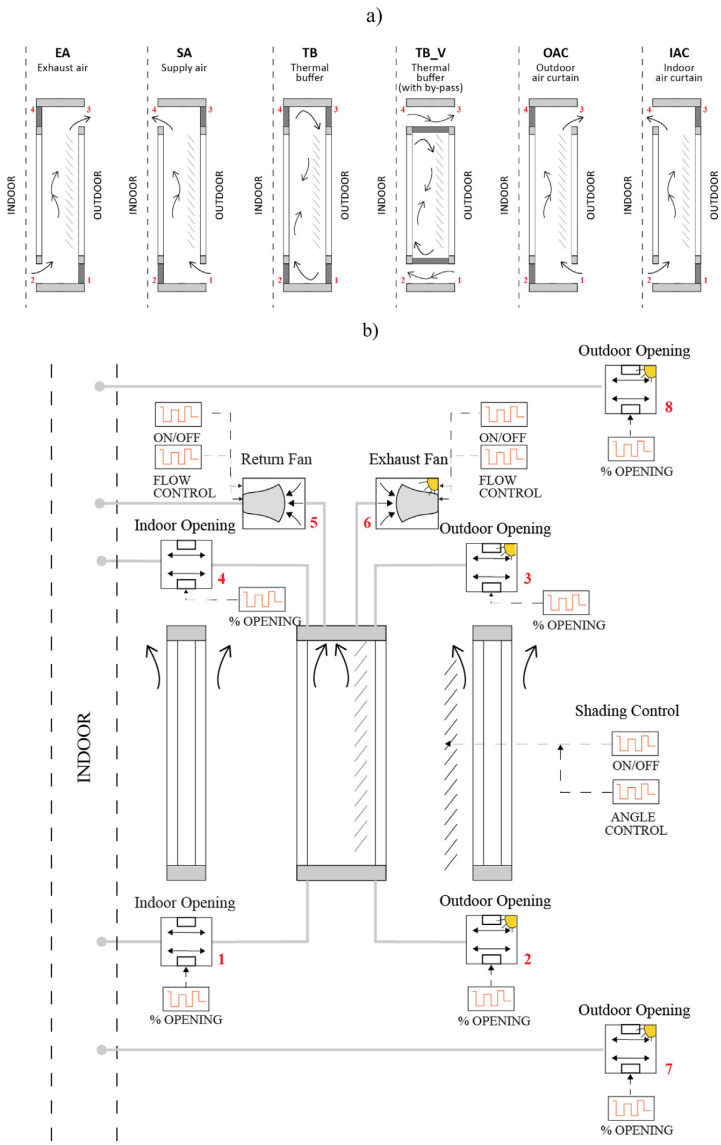

Fig. 1. A) Ventilation strategies implementable in a fully flexible DSF module; b) Schematic view of the fully flexible DSF model implemented in IDA ICE [9].

architectures: i) a MBC, ii) a RBC, iii) a SBC. While the first approach represents the key theoretical contribution of this research, the other two approaches were chosen to perform as a reference baseline to compare the functioning (and potential advantage) of the more advanced control approach to managing the façade.

In order to apply the MBC, a specific routine involving running a script from an external programming language tool was necessary, and the procedure is described in detail in Section 5. When using the last two types of controls (scheduled and RBC control), the control happened within the BES tool. While applying schedules to each actuator is straightforward, the definition of the rules to control each element was possible by employing a component in IDA ICE called '*Macro*'. In this area of the simulation environment, the modeller can use predefined controls or create new ones. By using different logical operators, it was possible to define the control logic that established a connection between the boundary conditions (indoor, cavity, outdoor, solar radiation, CO2, etc.) and the configuration to choose from.

3.2. Case study definition

We tested and demonstrated the working of the advanced control approach developed in this study by using a case study building equipped with the adaptive façade concept and alternative control routines. The simple building used in this research was adapted from the BESTEST Building–Base Case 600 [56]. The base building is a single-story 48 m^2, low-mass building with a rectangular prism geometry and two south-facing windows of 12 m^2. The

opaque walls, floor and roof were set to reach a U of 0.28 W/m^{2}K–corresponding to the required U-value for the German building reference building [57] -. The two regular windows of the BESTEST were modelled using the adaptive façade model developed in the previous study [9], where the transparent part was made of two low-e double glazing units (one on each of the two skins of the double façade structure), leading to an overall window system with the reference building values (U = 1.4 W/m^{2}K, g = 0.48, τ = 0.72). The geometry was kept as in the Base Case 600 (2 m wide and 3 m high), and the frame ratio was set to 10 %. The ventilated gap of the adaptive façade concept based on a flexible DSF architecture was set to 25 cm, and a venetian blind in the ventilated gap was added. The size of the openings was set to 5 % of the total glazed area, one at the bottom and one at the top of each ventilated window. The extraction fans connected to the ventilated cavity were set to have the same flow, which is calculated according to the conditions of class II as described in Table B.8 of EN 16798–1 [58] for occupied hours and set to the minimum value of 0.15 l/s m^2 when the room is empty [58]. When using MBC, the fans were allowed to also work with a higher setting, which was circa twice the airflow for the occupied hours.

The building was located in Frankfurt, and the weather file used was the default one for the location. The reason for this location was to select a climate characterised by both cooling and heating load in order to test the performance of the control over a large range of boundary conditions and not only for one or the other case (heating or cooling). The heating and cooling system was modelled as an ideal heater and cooler of 10 kW, with an ON/OFF thermostat control that would control the temperature according to the heating or cooling season as described in Table B.5 of EN 16798-1 [58] for naturally ventilated buildings (Table 1).

The occupancy was set ON during working days with schedules 8-18. The calculation for the occupancy was carried out according to the CEN/TR 16798–2 [59] for a landscape office. The artificial lighting was set to 12 W/m^2 [60] and set ON during the occupied hours only if the outdoor conditions allowed maximum illuminance values lower than 300 lx on the plane. The equipment loads were set to 300 W and set to 100 % during occupied hours and 25 % during unoccupied ones.

4. Control strategy definition

In this section, the multi-domain trade-off algorithm that is at the core of the model-based control (MBC) is presented (Section 4.1). The objectives and procedures of this innovative approach are explained, while its implementation in IDA ICE is described in the following chapter, Section 5. Adopting a MBC requires the modeller to control the tool from an external script via its API.

In the rest of the chapter, the other two control strategies applied are presented: first, the RBC–Section 4.2 - defined to adopt a set of rules that accounted for the outdoor conditions and the cavity temperature only, as would be recorded by an onboard control; and last the SBC–Section 4.3 - defined to reflect the common usage of DSF. Applying these two approaches requires the development of more or less complicated construction to be compatible with the BES tool, but no co-simulation is needed.

Table 1
A) indoor temperatures range as a function of the running mean temperature [58]; b) Internal Loads; c) Airflows values for fans (for each window) calculated according to the conditions of Class II [58].

a)

	T_{mr}	Indoor Temperature
Heating Season	<10 °C	20–24 °C
Cooling Season	>15 °C	23–26 °C
Mid - Season	10° C < Tmr < 15 °C	20–26 °C

b)

	Loads	Schedule
Occupants	3 persons	Weekdays 8–18
Lighting	48 W	Weekdays 8–18–if $E_{plane\_achievable}$ < 300
Equipment	300 W	Weekdays 8–18 *100 %* - Rest of the time *25 %*

c)

	$V_{unoccupied}$	$V_{occupied}$
Mechanical Airflow	3.6 l/s	27.3 l/s

4.1. Multi-domain model-based control–multi-objective trade-off algorithm

The principle behind control-based modelling is that the behaviour of a controlled element is stirred by the prediction, through a model, of the desired performance. Ideally, the strength of this type of control is that after evaluating all possible performances over a certain time range as a result of the degree of freedom of the system, the chosen configuration is the one that fulfils a specific range of requirements, and/or optimises an objective function. The control applied in the MBC proposed in this work covers four different domains. For this reason, an overarching control tree was developed to set priorities among the different domains as we preferred not to formulate the optimisation problem as a single objective by weighting the different domains. Because of considerations about how the adaptive façade works and its possible interaction with the surroundings, the following priorities were developed: indoor lighting, indoor air quality, thermal comfort, and minimum energy consumption (see Fig. 2).

The first step in the MBC is to run parametric simulations over the entire domain of possibilities for the given timestep and to calculate the selected KPIs: i) illuminance on the working plane - $\bar{E}_{plane}$; ii) CO2 concentration in the room - $\Delta CO2$; iii) operative temperature in the room - T_{op}; and iv) the heating and cooling demand - ($|Q_{heat}| + |Q_{cool}|$). The presence of occupants in the room affected which domains were further analysed utilizing the control tree. In the case of an occupied room, the first domain that filtered the results was the *'natural light domain'*; all the configurations that fulfilled the minimum requirements set for the values on the illuminance plane were used to check the following domain requirements '*air quality domain*'. In case none of the simulated cases gave results within the criteria, the filter was disregarded and all the configurations were used for the next step. This happens because there is no minimisation (maximation function) in any of the filtering domains (except for the last one) to avoid the risk of selecting a solution at the beginning that only satisfies (or partially satisfies) the requirements of one domain. After the '*air quality domain*', the '*thermal domain*' filtered the results; here, the operative temperature in the room was checked with the tolerance levels. Finally, the configurations that respected all these domains were filtered by the last condition:˝"*minimum energy consumption*". This last condition imposed a minimisation function to end up with a unique set of configurations to apply to the analysed timestep. Once the optimal multi-domain solution was found for the specific timestep, the values were stored to build the history of the simulation period; this process was followed to find the optimal configuration for each time step (1 h) of the analysed period.

The described algorithm can be applied to any controlled element (a window, HVAC system, heating and cooling device, etc.). For the presented case, a flexible DSF coupled with the HVAC system, a wide range of parameters for the control was available. The proposed adaptive façade can work by adopting six different ventilation strategies (Fig. 1a), and four (EA, IAC, OAC, SA) can work either mechanically or naturally. The openings of the operable win-

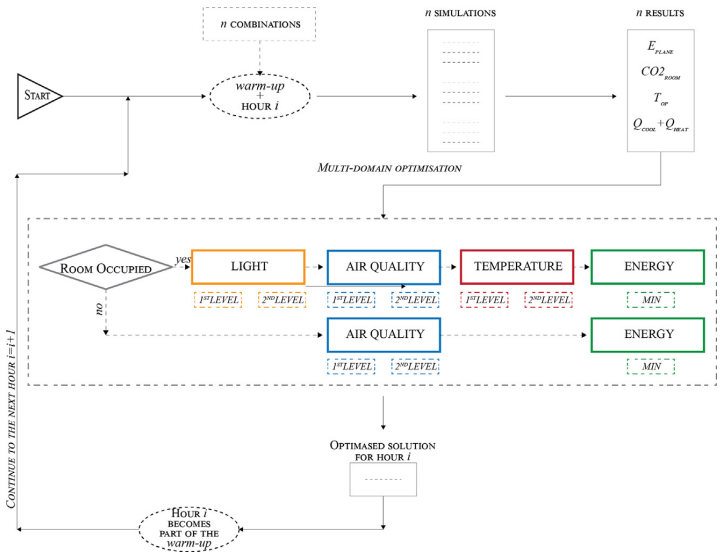

Fig. 2. MBC scheme: the simulated cases are filtered by the multi-domain trade-off algorithm to obtain the optimised solution for the ith timestep.

dow were controlled to three different positions: 0 % - CLOSED, 50 % OPEN, and 100 % OPEN. This *'opening'* input was used to control the flow path by closing the openings not used in that specific flow path and adjusting the degree of openness. The fan received two inputs: i) ON–if the façade was run mechanically, or OFF–naturally ventilated. ii) if the fan was ON, the flow was set as: V*min, Vmid* or *Vmax. Vmin* corresponded to the minimum airflow necessary to ventilate the room if not occupied, as described in Table 1-c, while *Vmid* to the value during occupation; *Vmax* was set to 2* *Vmid* + V*min.* Finally, the shading device was controlled with an ON/OFF control and by choosing 3 different angle positions: 0° - *cut*-off – 90° angle. The cut-off angle is calculated from eq. 10 and 11 of [61] taken from the work of [62].

The control optimisation problem can be formulated as the combination of Eqs. (1) and (2):

$$\min\left(|Q_{heat}| + |Q_{cool}|\right)[Occ, AFP, OP, F, SH, \varphi] \tag{1}$$

With $|Q_{heat}| + |Q_{cool}|$ - the sum of heating and cooling demand; Occ–the presence of the occupants; AFP–the possible airflow paths; OP–openings position; F–fan settings (operation and flow); SH–shading position; φ–angle of the slats.

Moreover, the KPIs were subject to the following constraints:

$$\begin{cases} \bar{E}_{plane} > 1^{st}LEVEL_{limit} else \bar{E}_{plane} > 2^{nd}LEVEL_{limit}; \\ \Delta CO2 < 1^{st}LEVEL_{limit} else \Delta CO2 > 2^{nd}LEVEL_{limit}; \\ 1^{st}LEVEL_{low-limit} < T_{op} < 1^{st}LEVEL_{high-limit} \\ \qquad\qquad else \\ 2^{nd}LEVEL_{low-limit} < T_{op} < 2^{nd}LEVEL_{high-limit}; \end{cases} \tag{2}$$

Being $\bar{E}_{plane}$–illuminance on the working plane [lux]; $\Delta CO2$–difference between the outdoor and room CO2 concentration level [ppm]; T_{op}–operative temperature in the room [°C]. The threshold values for the 1st and 2nd LEVEL are presented in Table 3.

This set of parameters led to 69 different combinations that had to be simulated for each time step (1 h). To reduce the computational effort required by this control approach, a reduced number of cases was simulated for the nighttime. In particular, the position of the shading was kept ON and fixed at 90° when there was no radiation hitting the façade or if there was not enough natural light to guarantee 300 lx (indoor lights were ON). Moreover, when the room was empty (but with solar radiation hitting the facade), the shading position could vary between OFF and ON and fixed at 90° (Table 2).

Once all the simulations were run, their results were filtered according to the hierarchy shown in Fig. 2 and Eq. (2). The multi-domain filters were applied with two fulfilment levels: for the indoor lighting, the thresholds were set according to the ISO 8995 [63] for office space; for the indoor air quality and thermal comfort, the thresholds were set according to the EN 16798-1 [58]; finally, the energy consumption for cooling and heating was minimised.

4.2. Rule-based control

The definition of the rules for the RBC strategy is based on a previous work [64], where a similar concept of façade was controlled to reduce the room's heating and cooling gains. This work further detailed the strategy to include the air quality domain in the algorithm. Figs. 3 and 4 show which thresholds and conditions choose the state of the façade. The proposed algorithm in Fig. 3 is a closed-loop algorithm that has two independent variables (the TMR–mean running temperature - and the Q_SOL–the solar radiation hitting the vertical south facade) and two dependent variables (T_GAP–the airgap temperature of the DSF–and the CO2 in the room). The algorithm shown in Fig. 4 is an open-loop control based only on the external radiation on the façade (Q_Sol). For each time step of the simulation, the independent variables are checked and fed into the algorithms, while, in order to reduce the instability of the control, the dependent variables have a time delay element that takes the average value over the previous hour. The two algorithms are executed independently. The algorithm that controls the shading device's solar absorption affects the temperature of the cavity (T_GAP), which is one of the control variables used by the algorithm that controls the openings. However, this latter algorithm does not influence the decision-making process to deploy and tilt the blades of the venetian blinds at a given angle.

These algorithms allowed us to explore all the available ventilation paths that the flexible DSF described in section 3.1 allows, both

Table 2
Possible combinations of all the controlled parameters in the model-based controlled DSF.

Conditions	Parameters	Combinations
OCC: ON $SOL_{facade} > 0$	$\{SA, IAC, OAC, EA\} \times \{N \times \{50\%, 100\%\}, M \times \{Vmin, Vmid, Vmax\}\} \times \{ON \times \{OFF, 0^{\circ}, cut-off, 90^{\circ}\}\}$ $TB \quad TB_V \times \{50\%, 100\%\}$	69
OCC: OFF $SOL_{facade} > 0$	$\{SA, IAC, OAC, EA\} \times \{N \times \{50\%, 100\%\}, M \times \{Vmin, Vmid, Vmax\}\} \times \{ON \times \{OFF, 90^{\circ}\}\}$ $TB \quad TB_V \times \{50\%, 100\%\}$	46
OCC: OFF $SOL_{facade} < 0$	$\{SA, IAC, OAC, EA\} \times \{N \times \{50\%, 100\%\}, M \times \{Vmin, Vmid, Vmax\}\} \times \{ON - 90^{\circ}\}$ $TB \quad TB_V \times \{50\%, 100\%\}$	23

Table 3
KPI selected for each set of simulations and their thresholds values.

$\bar{E}_{plane}$ [lux]		ΔCO2[PPM]		T_{op} °C	
1st level	2nd level	1st level	2nd level	1st level	2nd level
Office space [63]	Circulation [63]	II Class [58]	III Class [58]	II Class [58]	III Class [58]
500	300 lx	800	1350	20–24	19–25
				23–26	22–27
				20–26	19–27

*The thresholds of the operative temperature differ according to the season.

with mechanical and natural ventilation, as well as the control of the shading device in the cavity. The openings were controlled as open/closed (0 % - CLOSED and 100 % - OPEN), similarly to how the fan was controlled (0 % - OFF and 100 % - ON). When the fan was on, the airflow was set as the flow required to ventilate the room when it was occupied or unoccupied (Table 1-c). The cut-off angle is calculated as described in the model-based case.

4.3. Scheduled-based control

The SBC of the DSF was applied on two elements: i) the ventilation strategy adopted and ii) the operation of the shading device. The schedules shown in Table 4 to be applied to the façade were decided according to the following principles: the DSF should reduce the heating load in winter and the cooling load in summer. At the same time, it should also provide fresh air during the hours of occupation. Since the facade conditions are usually unknown at the time of the schedule definition, the DSF was run only with mechanical ventilation to ensure sufficient airflow on every occasion. During the occupied hours, the fans were working with the *Voccupied* airflow (Table 1-c), while the value for non-occupied hours was used for the rest of the time. The angle of the shading device was always varied throughout the day and the seasons, aiming to maximize the indoor lighting in the first and last hours of the day and reduce glare during the rest of the time.

5. Implementation of MBC in a BES tool via co-simulation

The challenges of implementing a MBC with a whole building model developed in a BES tool are connected to the structure and interoperability of these simulation environments. This type of control is a one-step at-a-time model predictive control, i.e. where the prediction horizon is set equal to the timestep under assessment and does not include optimising a given performance over a longer time horizon. This approach requires both parallel runs to explore the impact of each controllable parameter and a time-dependent correlation. The crucial aspect of implementing this type of control is being able to run simulations to explore a domain of possibilities and keep the thermal memory of the previous runs for the following timestep. Moreover, ensuring that the initial conditions are kept the same for each simulation for the exploration domain is essential. To establish the optimal length of the preconditioning horizon, a parametric study was carried out to quantify the influence of the length of preconditioning. A 10-daypreconditioning horizon was sufficient to ensure convergence of the energy balance of the room.

Considering the high degree of freedom that a DSF allows and the relatively low time step usually adopted in simulations, the number of simulations necessary for just a few days was in the order of hundreds. By limiting the prediction horizon to the present timestep, the size of the exploitation domain can still be kept to a number that, though requiring a certain computational effort, makes it possible to perform a full-factorial search of the domain. This allowed us to avoid using an optimal search algorithm to reduce the exploration domain, a non-trivial procedure that might lead to very different results. The relatively high number of runs necessarily requires automation of the process that is not available within the structure of the BES tool. Therefore, the use of co-simulation is needed. In this case study, the physical model was run in IDA ICE 5.0 and the optimisation engine in Python 3.8.

MBC can only be implemented if the process of setting up, running, and analysing multiple simulations is automatised. To do

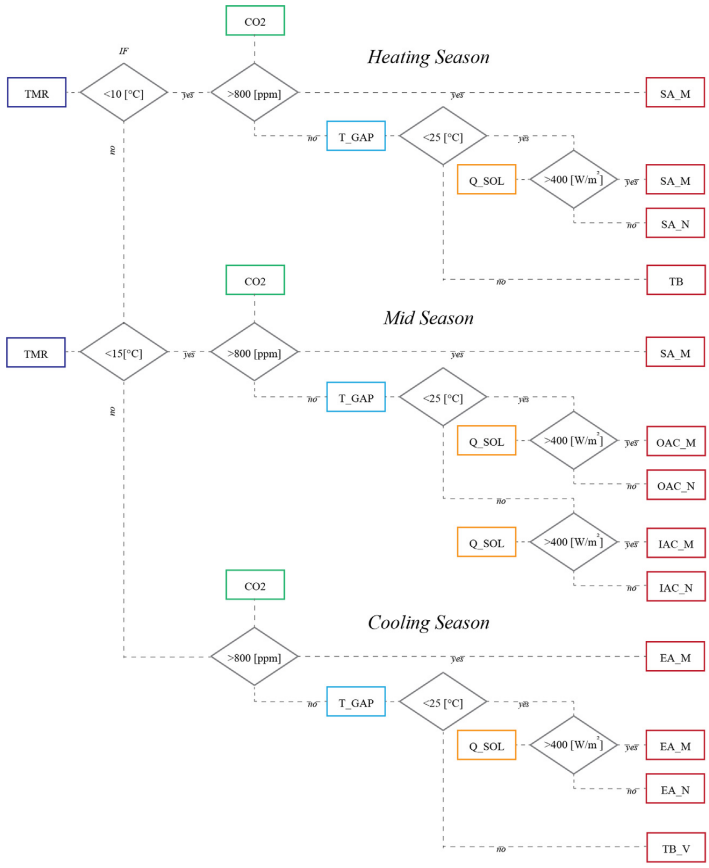

Heating Season: set point 20-24 °C *Mid Season:* set point 20-26 °C *Cooling Season:* set point 23-26 °C

Fig. 3. RBC strategy for the thermal and air quality domain. TMR–Running medium temperature [°C]; T_GAP–Temperature inside of the DSF airgap [°C]; Q_SOL–Solar radiation hitting the façade on which the DFS is installed [W/m^2]; CO2-Amount of CO2 in the occupied room [PPM].

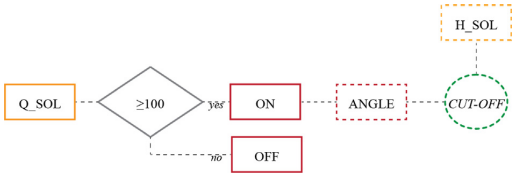

Fig. 4. RBC strategy for the visual domain; Q_SOL–Solar radiation hitting the façade on which the DFS is installed [W/m^2]; H_SOL–Solar altitude [°].

this, the model in IDA ICE was run via the IDA ICE API (Application Programming Interface). IDA ICE provides API functions in C programming language through a dynamic-link library *idaapi2.dll*. With direct calls to API functions, it is possible to load a previously developed model into IDA ICE and perform operations using Python scripts. The IDA Message Broker Service communicates with IDA ICE and the external program. The functions available in the API allowed both to connect to IDA ICE (opening the model, saving the model, etc.) and to manage the model objects.

It was necessary to adopt a programming language to automate the process and to carry out the data analysis of the obtained results. The version of Python 3.8 64bit was used. The Python library *win32process* and *ctypes* enabled the IDA ICE process in Windows environment and interacted with the API, calling API functions.

The data structure of an IDA ICE model (IDM) is represented as a hierarchical tree, where branches have subtrees of children with parent nodes. The tree of an IDM starts from the building object and then goes down to the level of the building body, zones, HVAC components, etc. It is possible to access each branch of the tree by calling the children of nodes. Objects of each node have attributes made up of names and values. These values can be accessed, read, and manipulated by using the LISP language [65].

The workflow used to apply the MBC is illustrated in Fig. 5, and the functions used in the Python code are collected in Table 5. The baseline IDM was created manually, as described in Section 3.2, and then accessed by the algorithm implemented in Python.

Manipulating the values of a node via the LISP language, as also underlined by Chenglong [52], requires a high computational time. For this reason, this method was limited to modifying the simulat-

Table 4
Schedule definition for the SBC of the DSF flow path and shading position.

Winter				
	Flow path	Airflow	Blind ON/OFF	Slat Angle
00:00–08:00	TB	–	ON	90°
08:00–10:00	IAC_M	*Voccupied*		0°
10:00–12:00				Seasonal average cut-off angle
12:00–16:00	SA_M			
16:00–18:00	TB	–		0°
18:00–24:00				90°
Summer				
	Flow path	Airflow	Blind ON/OFF	Slat Angle
00:00–05:00	EA	*Vunoccupied*	ON	90°
05:00–08:00	SA_M			
08:00–10:00		*Voccupied*		0°
10:00–16:00	OAC_M			Seasonal average cut-off angle
16:00–18:00				0°
18:00–24:00	EA	*Vunoccupied*		90°
Mid-Season				
	Flow path	Airflow	Blind ON/OFF	Slat Angle
00:00–06:00	TB	–	ON	90°
06:00–08:00	SA_M	*Vunoccupied*		
08:00–10:00		*Voccupied*		0°
10:00–12:00				Seasonal average cut-off angle
12:00–15:00	OAC_M			
15:00–16:00	SA_M			
16:00–18:00				0°
18:00–24:00	TB	–		90°

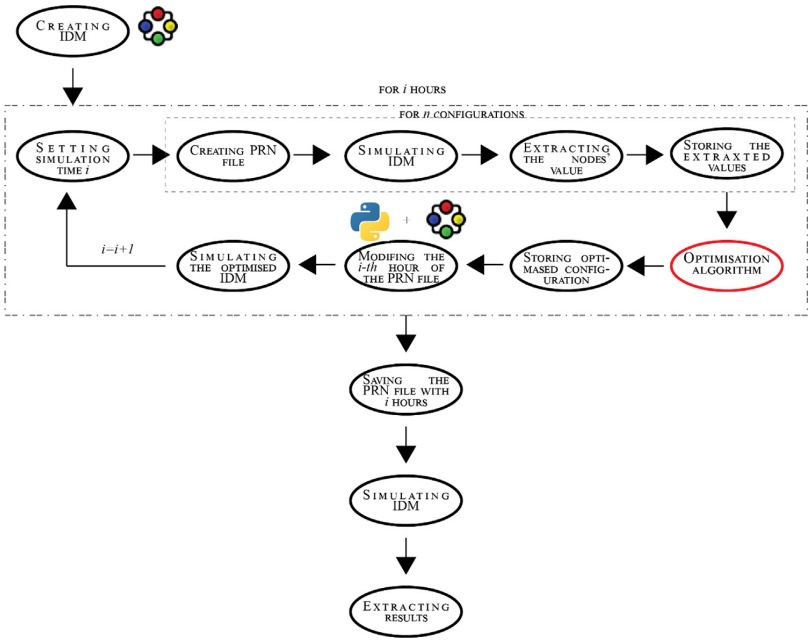

Fig. 5. Workflow of the automated process to adopt the MBC. The interaction between IDA ICE and Python is carried out by the API's functions called directly via Python.

ing time. The controlled parameters were modified by using an external *PRN* file. This approach was also necessary to replicate the same preconditioning time for each parametric run since the previous facade state can be stored in the PRN file. IDA ICE uses these formatted text (space delimited) files to read external data such as weather files and write the simulation results. To be read by the software, these files require time-stamped columns with the hours of the year (it is possible to define the fraction of the hour if necessary). Creating PRN files in Python was more efficient and allowed the automation of the process to simulate all the necessary configurations. In fact, the different state of the opening, fan, shading etc., was defined as a number in the PRN file. Once loaded in

Table 5
List of API functions used in the Python workflow.

Function	Description
connect_to_ida	Perform the connection to the IDA message broker.
call_ida_api_function	Call any IDA function with given parameter values in json format.
ida_disconnect	Terminate the connection to IDA message broker.
openDocument	Open the building specified in path. Return the building object
saveDocument	Save the building object to a path.
runSimulation	Run simulation for the building object.
runIDAscript	Execute a general IDA script with node as base object.
getZones	Return a list of the node's zones.
findNamedChild	Return the object of the child that has a particular name.
getAttribute	Return the value of the attribute of node.

IDA ICE, this number was interpreted by a function defined in a *Macro*, and the correct signal was sent to the actuator of the opening, fan, shading, etc.

The simulation was run using the *"Advanced level"* simulation, and the results of the simulation at the end of each parametric run are accessed directly from the model by reading the node value of the analysed element (room temperature, CO2 level, etc.). This action reduces the computational time compared to saving the file and reading the PRN result file but has the drawback of only giving the instantaneous value at the last moment of the simulation (not averaged over the hour). This operation is done automatically for each hour of the analysed period (two weeks per season). The use of hourly timesteps is connected to the computational time, but it could be either lowered or increased. Once the script had run for the whole simulation period, the script's output was a PRN file with the optimal configuration for the selected period, which was then used to run a continuous simulation for each period and obtain the results shown in the next section.

6. Results

6.1. Model-based control

The MBC was applied for two weeks in three different seasons. In this study, we first want to focus on whether or not the controller enabled the full exploitation of the flexibility that the adaptive façade concept offered (i.e. up to 69 different functioning modes). As a second goal for this analysis, we wanted to assess whether or not the full complexity of the façade was necessary to offer the best performance or if a façade with a reduced domain of possibilities could have performed equally well–in other words, if there were sub-domains in the domain of possibilities that were either never used or hardly used. Fig. 6 shows how the adaptive facade was run during one week of the winter period. The analysis of the different configurations used during this period shows that the most recurring ventilation path was the thermal buffer (TB– 87 % of the not occupied hours and 40 % of the occupied ones - Table 6). During the occupation, IAC_M, IAC_N and OAC_N configurations were each used around 10 % of the time. During mechanical ventilation, the fan mainly used the minimum flow (42 %), while in natural ventilation, the openings were mostly fully open (60 % of the time). The shading device was rarely deployed during

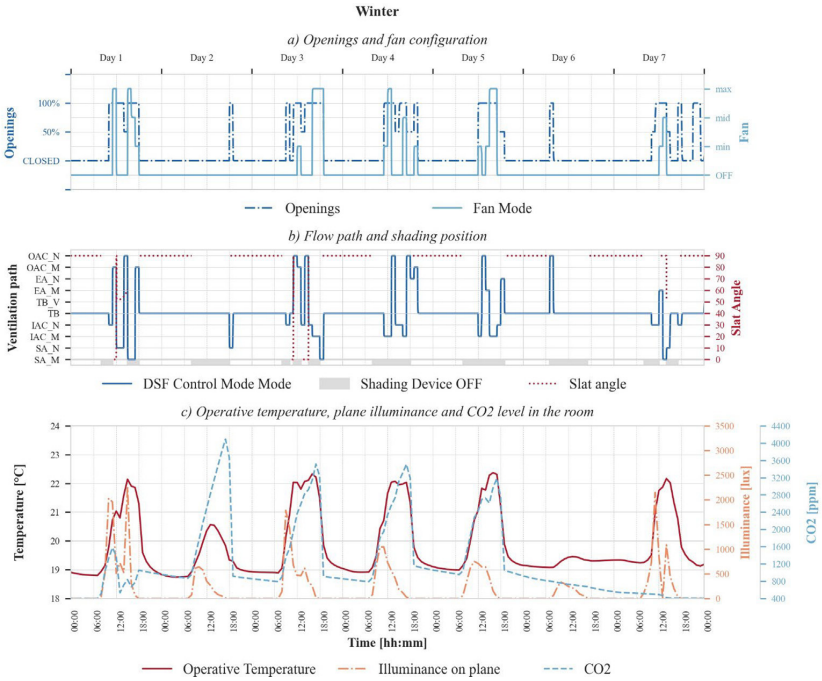

Fig. 6. MBC results for the winter period. a) The openings often shifted between CLOSED, 50 % and 100 % during the occupied hours, while both the fan and the openings were OFF/CLOSED since the façade mainly worked as a thermal buffer. When the façade was mechanically ventilated, all the airflow settings were used with equal frequency; b) the main flow path adopted in winter was TB, with few hours during the occupied period, run in SA or OAC mode. The shading device was mainly OFF during the day. c) the operative temperature was within the 2nd level range [19–25 °C] during most of the occupied hours, while the CO_2 level in the room reached very high values (above 1350 ppm) during the occupied hours. The level of illuminance on the working plane was above 300 lx for most of the occupied hours, remaining under the 3000 lx threshold set for avoiding glare.

Table 6
Ventilation strategies adopted during the different simulated periods.

Mode	Winter [%]		Summer [%]		Mid-Season [%]	
Occupation	ON	OFF	ON	OFF	ON	OFF
SA_M	6	3	3	4	4	2
SA_N	6	2	2	5	5	4
IAC_M	*10*	2	3	6	*10*	5
IAC_N	***12***	2	1	2	3	3
TB	**40**	**87**	4	**54**	***19***	**63**
TB_V	1	0	**45**	8	**37**	***12***
EA_M	7	1	***24***	8	*10*	*9*
EA_N	1	1	*11*	5	9	3
OAC_M	6	1	1	2	1	0
OAC_N	10	1	6	6	2	1

the daytime (20 %), and during these few hours, the slats angle was set to 0° for most of the time (60 %); during the rest of the time, the cut-off angle was used. The results for the multi-domain optimisation showed that while the lighting and thermal requirements were met (Eq. (3)–winter season), the CO_2 levels grew relatively high (always above 1350 ppm when the room was occupied), and the control algorithm was not able to choose the right configuration to reduce the CO_2 to under 800 ppm during the nighttime. This resulted in a high baseline for the following day without the possibility of reducing it further once the room was occupied again.

During the summer period (Fig. 7), the operational modes adopted varied more, even though approximately 40 % of the simulated time used the thermal buffer configuration. This is because, during the unoccupied hours (which correspond to 54 % of the time), the facade was run in TB. During occupation, the most recurring configurations were the ventilated thermal buffer (45 %), the mechanical (24 %) and natural exhaust-air facade (11 %). All the other configurations were used, but for very short periods. When the facade was run mechanically, the fan setting was mainly on the mid-flow (60 %), followed by the maximum flow (25 %). In natural ventilation, the openings were mostly fully open (80 %). During the summer, the shading device was ON half of the occupied time (49 %) with the slat position set at 0° (94 %). The indoor conditions showed a better fulfilment of the multi-domain criteria than the winter case did. Besides the temperature being controlled within the set point of the 2nd level as indicated by Eq. (3). for the summer season, the CO_2 level was within the 1st level threshold most of the occupied time. It is interesting to notice that the temperature inside of the room was mainly controlled by the façade ventilation since the shading

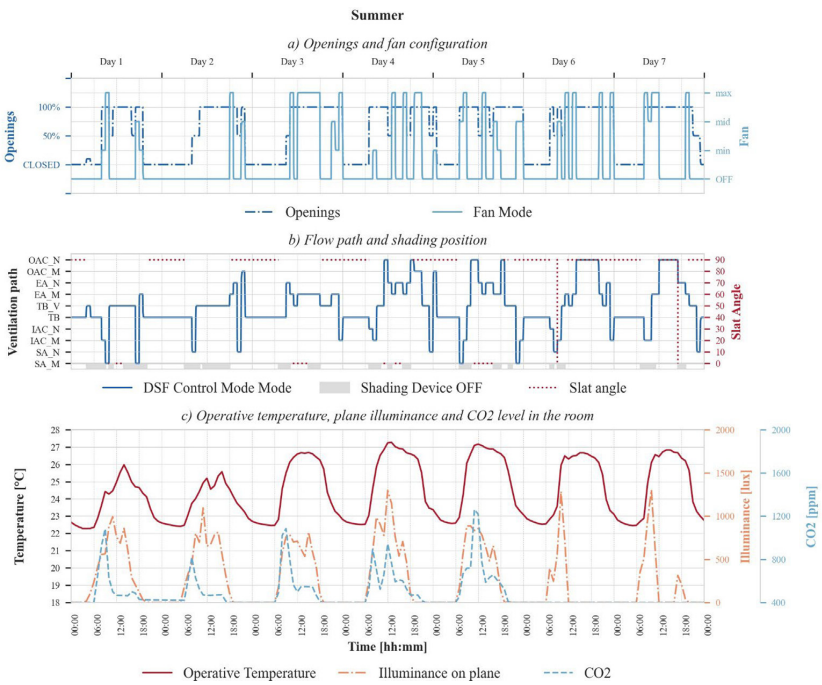

Fig. 7. MBC results for the summer period. a) During occupied hours, the openings were modulating the flow, often shifting between 50 % and 100 %. When the façade was run with mechanical ventilation, the fan mostly worked with the maximum flow setting. B)during the night the optimal configuration was the thermal buffer, while during occupation the flowpath switched among many different configurations, mainly EA, SA and OAC. The shading device was mostly OFF during the daytime c) the operative temperature was within 22–27 °C for most of the time. The CO_2 levels were always under 1350 ppm and the illuminance on the work plane was above 300 lx during most of the occupied hours.

device was mostly OFF during the occupied hours. Consequently, the illuminance values on the workplane were within the requirements.

Similar to the summer season, during the mid-season weeks (Fig. 8), the most adopted configuration strategies were the thermal buffer (50 %), the ventilated thermal buffer (19 %) and the mechanical exhaust air (9 %). Looking at the difference between occupied and unoccupied times, the distribution shifts a bit. The most adopted configuration during occupied hours was the TB_V (37 %), followed by the TB (19 %), while during the unoccupied time it was the TB (63 %). Other configurations were evenly used during occupation: IAC_M, EA_M and EA_N were used around 10 % of the time. Compared to the winter season, the mild outdoor temperatures guaranteed an exchange of fresh air to control the CO2 level without affecting thermal comfort; in this way, the CO2 levels were mainly under the acceptable threshold for most occupied hours (2nd level = 1350 ppm). When the fans were used, the airflow chosen was mostly the mid-flow (48 %), and the rest of the time was equally split between the minimum and maximum settings. Similar to the other simulated periods, the openings were fully open during naturally ventilated modes (69 %). The shading device was mostly unused during the occupied time (63 %), but when ON, the slats were always set to 0°(99 %). Similar to the summer case, the comfort requirements were also met during the mid-season weeks. The CO2 and the illuminance level were within the boundaries identified by Eq. (3)., as was the operative temperature. Also, during this period, the shading device did not play a crucial role in controlling the room conditions, as it was activated only for a few hours per day to allow daylight to enter the room.

6.2. Comparison of the performance with different control strategies

The results shown in this section are compared the three controlled strategies presented in Section 4. The criteria for the comparison are defined as the percentage of the occupied hours that fulfil the requirements for natural lighting, indoor air quality and operative temperature presented in Eq. (3). Moreover, the energy necessary for cooling and heating when the air temperature did not meet the dual set points defined in Table 1-a was considered (Eq. (4)).

$$\%ofoccupiedhours \begin{cases} \bar{E}_{plane} > \begin{cases} 500lux & 1^{st}level \\ 300lux & 2^{nd}level \end{cases} \\ \Delta CO2 < \begin{cases} 800ppm & 1^{st}level \\ 1350ppm & 2^{nd}level \end{cases} \\ \begin{cases} 20^{\circ}C \\ 19^{\circ}C \end{cases} < T_{op_{winter}} < \begin{cases} 24^{\circ}C & 1^{st}level \\ 25^{\circ}C & 2^{nd}level \end{cases} \\ \begin{cases} 23^{\circ}C \\ 22^{\circ}C \end{cases} < T_{op_{summer}} < \begin{cases} 26^{\circ}C & 1^{st}level \\ 27^{\circ}C & 2^{nd}level \end{cases} \\ \begin{cases} 20^{\circ}C \\ 19^{\circ}C \end{cases} < T_{op_{mid-season}} < \begin{cases} 26^{\circ}C & 1^{st}level \\ 27^{\circ}C & 2^{nd}level \end{cases} \end{cases} \quad (3)$$

$$\sum Q_{heating} and \sum Q_{cooling} \quad (4)$$

The results of Table 7 show that the control strategies used impacted the different domains differently; the illuminance on the working plane ($\bar{E}_{plane}$) was highly under reached with a tradi-

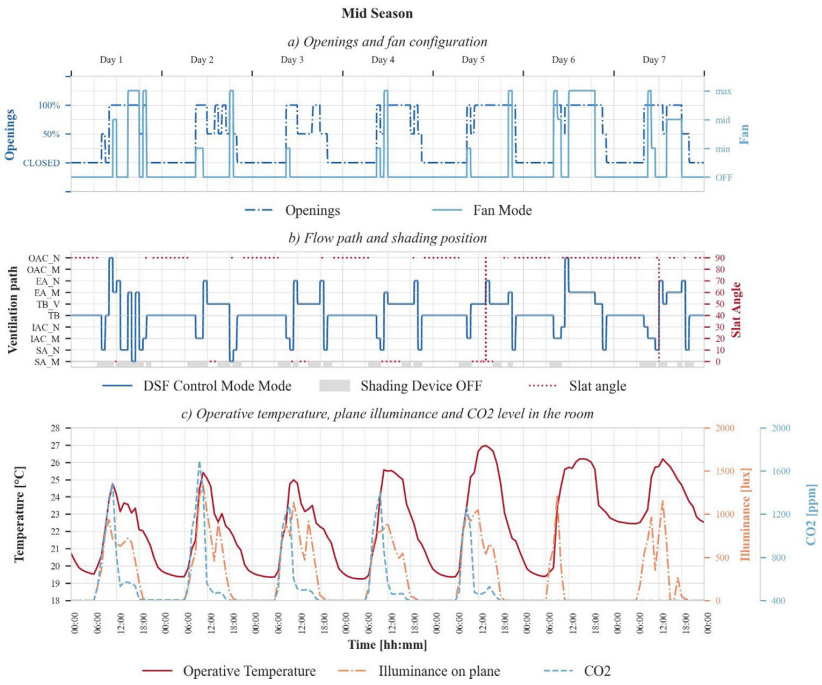

Fig. 8. MBC results for the mid-season. a) When the façade was not in thermal buffer (CLOSED), the openings were mostly open 100 %, and the fan worked with maximum flow settings; b) the thermal buffer was predominant during night hours, while during the day the flow often switched to TB_V, holding the settings for a few hours. Other paths frequently adopted are IAC, EA and SA. c) The operative temperature fluctuated between the thresholds 20–26. The CO2 levels were under 1350 ppm, and the illuminance on the plane was above 300 lx during most of the occupied hours.

Table 7
Fulfilment criteria for the different control strategies adopted during the combined three simulation periods. The KPIs $\bar{E}_{plane}$, ΔCO2 and T_{op} are calculated only during the occupied hours. Q is calculated for the whole simulation hours.

Control	$\bar{E}_{plane}$		ΔCO2		T_{op}		Q	
	1st level $\%_{occ\_hours}$	2nd level $\%_{occ\_hours}$	1st level $\%_{occ\_hours}$	2nd level $\%_{occ\_hours}$	1st level $\%_{occ\_hour}$	2nd level $\%_{occ\_hour}$	Heating *kWh*	Cooling *kWh*
SBC	30	73	38	65	46	90	206	143
RBC	47	91	100	100	35	94	711	163
MBC	81	96	68	81	68	91	210	69

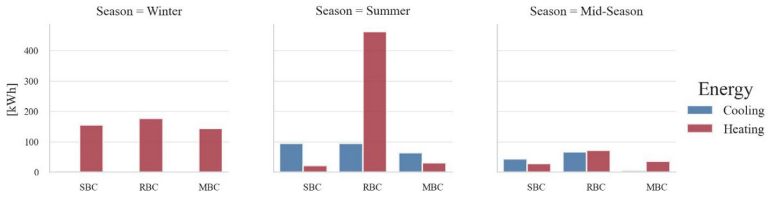

Fig. 9. Energy uses from the different control strategies in the three simulated periods. SBC, RBC and MBC control.

tional SBC. Better results were obtained when a rule-based control was adopted, even though the values were below 500 lx>50 % of the occupied time. Conversely, adopting the MBC yielded satisfactory results (80 % of the occupied hours meet the 1st-level requirements).

As for the indoor air quality domain, the results of the SBC show a very low percentage of compliance with the CO^2 values in the room. Even considering the 2nd level criteria (1350 ppm), only 66 % of the occupied hours satisfied this requirement. For the case of the RBC, this 100 % value is explainable with the rigid control in the algorithm tree (Fig. 3); in fact, whenever the CO2 level reached a value above 800 ppm, the DSF would run with mechanical ventilation to bring fresh air inside the room at the expense of the room temperature, and consequently of the energy use. Conversely, the MBC worked towards a solution that was a trade-off of all three domains; the results for the air quality were lower than the other two strategies but still satisfactory (above 65 % for the 1st level and 80 % for the 2nd level).

For both the SBC and RBC the thermal domain values were<50 % of occupied hours within the boundaries defined for the 1st level of the operative temperature, while the model-based control results approached 70 %. When checking the 2nd level, the values became much more similar due to the ideal heating and cooling action; this good achievement resulted in much higher energy consumption for the RBC case to maintain the set point temperatures. Remarkably, the RBC results showed an extremely high heating demand during summer (more than twice that in winter - Fig. 9). This is probably connected to the rule definition for the cooling season (Fig. 3), which would run the façade in exhaust mode–thus extracting heat from the room whenever the TMR was above 15 °C. Most likely, for the weather conditions of Frankfurt, this was not the optimal ventilation strategy - as Table 7 shows, the thermal buffer was the most adopted configuration, even in summer. During winter, all three control strategies performed similarly (with the MBC consuming less energy), while during summer and the mid-season, the MBC outperformed the other two control strategies in terms of cooling loads.

7. Discussion

This work originates from the challenge and limitation of using traditional control strategies to properly manage an adaptive façade with high degrees of freedom. We defined a simple SBC for the façade that aimed at reducing the room heating load in winter and the cooling load in summer while providing fresh air during occupation hours and guaranteeing indoor natural light without glare. It was already obvious from the development of the algorithm that this would not take full advantage of the flexibility of the façade; the DSF was only run in mechanical mode with a fixed flow and fixed openings. We also developed an RBC algorithm for this work that only used the airgap temperature and the CO_2 level in the room as dependent variables and external air temperature and the solar irradiance on the facade as the independent variables of the. The assumptions made related to the model, and the RBC control, were based on the authors' experience with the main aim of demonstrating the functionality of the developed model and based on previous work [64]; with this decision tree, all the available flow paths were explored, and the control of the shading device in the cavity was also controlled with a more advanced strategy than the scheduled case. Nevertheless, not even this algorithm allowed the fully exploitation of the flexibility that this model offered since it could only account for a limited number of states. Not even rather advanced RBC approaches could effectively exploit the full potential of a complex adaptive façade.

The analysis of the results also highlighted the importance of defining the correct thresholds for RBCs; the proposed algorithm led to sub-optimal thermal and indoor comfort performance, despite having been developed with this goal in mind. Choosing the most appropriate control strategy as a function of the climate condition is critical. Indeed, RBC solutions not optimised for the climate can lead to worse results than the classical use of the DSF, as clearly shown by this work's results.

The developed model, adopting a full factorial MBC, demonstrated instead how it it possible to fully exploit the flexibility of the façade while aiming at a multi-domain optimisation that was not reached with the other control strategies. The approach presented in this paper shows how MBC and multi-domain control can be combined. It is, of course, an open question of how different domains should be prioritised. In addition to great flexibility, the proposed control algorithm showed that the optimal configuration of the façade varies a lot within the same period. The strength of this type of control is that it does not require prior knowledge of the performance of the controlled element to be defined. It differs from the other types of control because it only sets the target

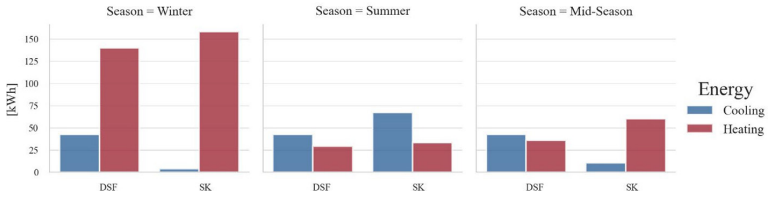

Fig. 10. Comparison of the energy requirements for cooling and heating between the DSF and SK models.

Table 8
KPIs of the MBC applied to the flexible DSF and to a simpler single skin (SK). $\bar{E}_{plane}$, ΔCO2 and T_{op} were calculated only during the occupied hours. Q was calculated for the whole simulation hours.

Control	$\bar{E}_{plane}$		ΔCO2		T_{op}		Q	
	1st level $\%_{occ\_hours}$	2nd level $\%_{occ\_hours}$	1st level $\%_{occ\_hours}$	2nd level $\%_{occ\_hours}$	1st level $\%_{occ\_hours}$	2nd level $\%_{occ\_hours}$	Heating *kWh*	Cooling *kWh*
DSF	81	96	68	81	68	91	210	69
SK	84	100	65	79	71	95	274	81

rather than defining the ways to reach it, leaving open the exploitation of the façade's flexible behaviour as the means to reach the desired target. All the results showed that, in all analysed domains, the MBC performed better than the more traditional control strategies.

Due to its nature, this multi-domain, MBC strategy is suitable for controlling every type of façade that exhibits some degree of adaptability–hence requiring control. To exemplify the possibility of using the presented control approach with a wider range of façade systems, we applied the same MBC strategy to a more conventional façade system. Fig. 10 shows the application of the MBC for a single skin façade (SK) with equivalent glass properties to the DSF, two operable openings and a between-glass shading device. Compared to the DSF model proposed, this type of façade has much less degree of freedom, yet it can be beneficial to control the way this façade is operated using a multi-domain MBC. The single skin façade simulated to demonstrate the wider applicability of our method had similar features to the adaptive façade in terms of optical and thermophysical properties. The energy need results and indoor comfort performance (Table 8) show similar results to the adaptive façade when controlled with the MBC proposed in this study. When the single skin was controlled with an advanced type of control, and its performance was compared to that of the adaptive façade controlled with more traditional control strategies (e.g. schedules and RBCs), the single skin outperformed the more complex adaptive façade, not only in terms of comfort performances but also in terms of energy. This demonstrates that adaptive facades can only perform better than more traditional envelopes if properly controlled and that an advanced façade characterised by a large degree of freedom requires more advanced control methods.

One of the main drawbacks of the MBC approach, as formulated in this study, is the computational time required to run an explicit physical model for a full-factorial exploration. The full factorial exploration adopted was already a reduced from of a more exhaustive analysis where, ideally, the openings of the façade or the position of the shadings could have even more intermediate settings. Due to the heavy computational load, the analysis had to be limited only to a few weeks of the year. In order to overcome these limitations, a solution could be the use of this approach to identify the most adopted configurations over a limited period (like the one in this study) and then run the model over an extended period or in real applications, with a reduced amount of states. For example, from the simulated weeks, it could be deducted that at night, no matter the season, the predefined configuration is the thermal buffer, reducing the exploration domain to only the hours with considerable solar gains. The number of simulation runs (hence the total simulation time) could also be reduced by adopting an algorithm for optimal search (e.g. a genetic algorithm) instead of performing a full-factorial exploration. .

Combining a MBC and RBC could also lead to suitable performance. Particularly in real building applications, a development of the presented MBC control could be combined with the more traditional control, like hierarchical rule-based control to reduce the search domain based on a series of pre-set rules. Developing a control-oriented model of the flexible double skin system with significantly shorter simulation time is however a prerequisite to take this approach to in-field, real-time applications. Alternatively, MBC-enhanced RBC strategies, which are proved of being a cost-effective solution, can allow to reach the optimal control with a decrease in operational time [35,66] by means of rule extraction from an MBC simulation dataset [10].

8. Conclusion

Thanks to the increasing capabilities to interface BES tools with external simulation environments, we developed in this study an innovative model-based control (MBC) for adaptive facades that can adjust their physical properties to satisfy multiple interdependent performance requirements (across multiple domains–i.e. energy, thermal comfort, natural lighting, indoor air quality). To the best of our knowledge, this is one of the first attempts to conceive and demonstrate how an adaptive facade characterised by a large variation in its operational model can be effectively managed by exploiting a simulation-informed control. The multi-domain MBC was applied to a double skin façade highly capable of switching between different ventilation flow paths and interconnecting with the HVAC plant of the building. The specific case presented a very large number of possible states for the operation of the façade (in the order of one hundred), thus making this system unsuitable for conventional control approaches adopted for building envelopes. This approach takes advantage of the capabilities of BES tools to replicate the behaviour of adaptive envelopes and to explore the full potential of an optimal management of their dynamic features. In this work, we have not only demonstrated

how traditional control strategies are inappropriate for achieving high performance goals in facades characterised by a large freedom in their operation, but we addressed a knowledge gap by proposing a method that can outperform the current approaches and contribute to the know-how for advanced building envelope controls. Furthermore, it has been shown that this approach is not only suitable for complex facades; it can be easily transferred to more conventional facade configurations, characterised by a lower degree of freedom, but targeting multiple performance domains. Applying this MBC to a less complex (with a minimum of automatization) envelope showed how a good control strategy plays an equal role as the technology chosen. Overall, the proposed method can be applied to various typologies of adaptive facades, allowing optimal integration with the HVAC system of the building.

The proposed approach control has only been tested through simulations thus far. Only parallel tests in identical (laboratory or in-field) environments would be suitable to give an empirical demonstration of the effectiveness of one control approach against another. Though we have access to such experimental facilities that allow this type of investigation (i.e. [67]), such tests are expensive and very time consuming. Simulation-based studies are normally carried out in the first stages of a research activity to investigate a new approach or technology, while experimental assessments and demonstrations are carried out once the new technology has been numerically verified. In the next steps of the research, we will apply the method proposed in this study, pending suitable modifications to make it possible run in real-time, to control a mock-up of a flexible DSF system. Furthermore, we will keep developing the proposed method to optimise the performance of the façade considering future states too (so-called model-prediction control).

Data availability

Data will be made available on request.

Declaration of Competing Interest

The authors declare that they have no known competing financial interests or personal relationships that could have appeared to influence the work reported in this paper.

Acknowledgements

The authors would like to thank Mika Vuolle and Federica Marongiu from Equa Simulation Finland Oy for their input and consulting on the IDA ICE API implementation, and Equa Simulation AB for granting access to the IDA ICE API.

The activities presented in this paper were carried out within the research project “REsponsive, INtegrated, VENTilated - REINVENT–windows,” supported by the Research Council of Norway through the research grant 262198, and the partners SINTEF, Hydro Extruded Solutions, Politecnico di Torino and Aalto University.

References

[1] R.C.G.M. Loonen, M. Trčka, D. Cóstola, J.L.M. Hensen, Climate adaptive building shells: state-of-the-art and future challenges, Renew. Sustain. Energy Rev. 25 (2013) 483–493, https://doi.org/10.1016/j.rser.2013.04.016.

[2] M. Haase, F. Marques da Silva, A. Amato, Simulation of ventilated facades in hot and humid climates, Energy Build. 41 (2009) 361–373, https://doi.org/10.1016/j.enbuild.2008.11.008.

[3] V. Huckemann, E. Kuchen, M. Leão, É.F.T.B. Leão, Empirical thermal comfort evaluation of single and double skin façades, Build. Environ. 45 (2010) 976–982, https://doi.org/10.1016/j.buildenv.2009.10.006.

[4] F. Pomponi, P.A.E. Piroozfar, R. Southall, P. Ashton, E.R.P. Farr, Energy performance of Double-Skin Façades in temperate climates: a systematic review and meta-analysis, Renew. Sustain. Energy Rev. 54 (2016) 1525–1536, https://doi.org/10.1016/j.rser.2015.10.075.

[5] Y. Kim, C. Park, W. Suh, Comparison of different optimal control strategies of a double-skin facade DOUBLE-SKIN FACADE, (2011).

[6] S.H. Yoon, C.S. Park, G. Augenbroe, On-line parameter estimation and optimal control strategy of a double-skin system, Build. Environ. 46 (2011) 1141–1150, https://doi.org/10.1016/j.buildenv.2010.12.001.

[7] C.S. Park, G. Augenbroe, T. Messadi, M. Thitisawat, N. Sadegh, Calibration of a lumped simulation model for double-skin façade systems, Energy Build. 36 (2004) 1117–1130, https://doi.org/10.1016/j.enbuild.2004.04.003.

[8] C.S. Park, G. Augenbroe, Local vs. integrated control strategies for double-skin systems, Autom. Constr. 30 (2013) 50–56, https://doi.org/10.1016/j.autcon.2012.11.030.

[9] E. Catto Lucchino, G. Gennaro, F. Favoino, F. Goia, Modelling and validation of a single-storey flexible double-skin façade system with a building energy simulation tool, Build. Environ. 226 (2022), https://doi.org/10.1016/j.buildenv.2022.109704.

[10] F. Favoino, M. Baracani, L. Giovannini, G. Gennaro, F. Goia, Embedding intelligence to control adaptive building envelopes, in: Rethink. Build. Ski., 2022: pp. 155–179. 10.1016/b978-0-12-822477-9.00007-3.

[11] F. Oldewurtel, A. Parisio, C.N. Jones, D. Gyalistras, M. Gwerder, V. Stauch, B. Lehmann, M. Morari, Use of model predictive control and weather forecasts for energy efficient building climate control, Energy Build. 45 (2012) 15–27, https://doi.org/10.1016/j.enbuild.2011.09.022.

[12] X. Hong, J. Lin, X. Yang, S. Wang, F. Shi, Comparative analysis of the daylight and building-energy performance of a double-skin facade system with multisectional shading devices of different control strategies, J. Energy Eng. 148 (2022) 1–15, https://doi.org/10.1061/(asce)ey.1943-7897.0000828.

[13] S. Zhang, D. Birru, An open-loop venetian blind control to avoid direct sunlight and enhance daylight utilization, Sol. Energy. 86 (2012) 860–866, https://doi.org/10.1016/j.solener.2011.12.015.

[14] T. Iwata, T. Taniguchi, R. Sakuma, Automated blind control based on glare prevention with dimmable light in open-plan offices, Build. Environ. 113 (2017) 232–246, https://doi.org/10.1016/j.buildenv.2016.08.034.

[15] A. Tabadkani, A. Roetzel, H.X. Li, A. Tsangrassoulis, A review of automatic control strategies based on simulations for adaptive facades, Build. Environ. 175 (2020), https://doi.org/10.1016/j.buildenv.2020.106801.

[16] P. Chaiwiwatworakul, S. Chirarattananon, P. Rakkwamsuk, Application of automated blind for daylighting in tropical region, Energy Convers. Manag. 50 (2009) 2927–2943, https://doi.org/10.1016/j.enconman.2009.07.008.

[17] R. Delvaeye, W. Ryckaert, L. Stroobant, P. Hanselaer, R. Klein, H. Breesch, Analysis of energy savings of three daylight control systems in a school building by means of monitoring, Energy Build. 127 (2016) 969–979, https://doi.org/10.1016/j.enbuild.2016.06.033.

[18] E. Shen, J. Hu, M. Patel, Energy and visual comfort analysis of lighting and daylight control strategies, Build. Environ. 78 (2014) 155–170, https://doi.org/10.1016/j.buildenv.2014.04.028.

[19] L. Karlsen, P. Heiselberg, I. Bryn, H. Johra, Solar shading control strategy for office buildings in cold climate, Energy Build. 118 (2016) 316–328, https://doi.org/10.1016/j.enbuild.2016.03.014.

[20] Y. Peng, Y. Lei, Z.D. Tekler, N. Antanuri, S.K. Lau, A. Chong, Hybrid system controls of natural ventilation and HVAC in mixed-mode buildings: a comprehensive review, Energy Build. 276 (2022), https://doi.org/10.1016/j.enbuild.2022.112509.

[21] F. Isaia, M. Fiorentini, V. Serra, A. Capozzoli, Enhancing energy efficiency and comfort in buildings through model predictive control for dynamic façades with electrochromic glazing, J. Build. Eng. 43 (2021), https://doi.org/10.1016/j.jobe.2021.102535.

[22] D. Lee, Y.H. Cho, J.H. Jo, Assessment of control strategy of adaptive façades for heating, cooling, lighting energy conservation and glare prevention, Energy Build. 235 (2021), https://doi.org/10.1016/j.enbuild.2021.110739.

[23] L. Shen, Y. Han, Optimizing the modular adaptive façade control strategy in open office space using integer programming and surrogate modelling, Energy Build. 254 (2022), https://doi.org/10.1016/j.enbuild.2021.111546.

[24] C.S. Park, G. Augenbroe, N. Sadegh, M. Thitisawat, T. Messadi, Real-time optimization of a double-skin façade based on lumped modeling and occupant preference, Build. Environ. 39 (2004) 939–948, https://doi.org/10.1016/j.buildenv.2004.01.018.

[25] A. Ganji Kheybari, T. Steiner, S. Liu, S. Hoffmann, Controlling Switchable Electrochromic Glazing for Energy Savings, Visual Comfort and Thermal Comfort: A Model Predictive Control, CivilEng. 2 (2021) 1019–1053. 10.3390/civileng2040055.

[26] C. Gehbauer, D.H. Blum, T. Wang, E.S. Lee, An assessment of the load modifying potential of model predictive controlled dynamic facades within the California context, Energy Build. 210 (2020), https://doi.org/10.1016/j.enbuild.2020.109762.

[27] F. Favoino, Q. Jin, M. Overend, Design and control optimisation of adaptive insulation systems for office buildings. Part 1: adaptive technologies and simulation framework, Energy 127 (2017) 301–309, https://doi.org/10.1016/j.energy.2017.03.083.

[28] J.M. Dussault, L. Gosselin, Office buildings with electrochromic windows: a sensitivity analysis of design parameters on energy performance, and thermal

and visual comfort, Energy Build. 153 (2017) 50–62, https://doi.org/10.1016/j.enbuild.2017.07.046.
[29] A.G. Kheybari, S. Hoffmann, Exploring the potential of the dynamic facade: simulating daylight and energy performance of complex fenestration systems (Venetian blinds), BauSIM2018, 7th Ger. IBPSA Conf. (2018) 286–294.
[30] A. Tabadkani, A. Roetzel, H.X. Li, A. Tsangrassoulis, Simulation-based personalized real-time control of adaptive facades in shared office spaces, Autom. Constr. 138 (2022), https://doi.org/10.1016/j.autcon.2022.104246.
[31] M. Valitabar, A. GhaffarianHoseini, A. GhaffarianHoseini, S. Attia, Advanced control strategy to maximize view and control discomforting glare: a complex adaptive façade, Archit. Eng. Des. Manag. (2022) 1–21, https://doi.org/10.1080/17452007.2022.2032576.
[32] A. Katsifaraki, B. Bueno, T.E. Kuhn, A daylight optimized simulation-based shading controller for venetian blinds, Build. Environ. 126 (2017) 207–220, https://doi.org/10.1016/j.buildenv.2017.10.003.
[33] A. Eltaweel, Y. Su, Controlling venetian blinds based on parametric design; via implementing Grasshopper's plugins: a case study of an office building in Cairo, Energy Build. 139 (2017) 31–43, https://doi.org/10.1016/j.enbuild.2016.12.075.
[34] R.C.G.M. Loonen, S. Singaravel, M. Trčka, D. Cóstola, J.L.M. Hensen, Simulation-based support for product development of innovative building envelope components, Autom. Constr. 45 (2014) 86–95, https://doi.org/10.1016/j.autcon.2014.05.008.
[35] M.S. Piscitelli, S. Brandi, G. Gennaro, A. Capozzoli, F. Favoino, V. Serra, Advanced control strategies for the modulation of solar radiation in buildings: MPC-enhanced rule-based control, Build. Simul. Conf. Proc. 2 (2019) 869–876, https://doi.org/10.26868/25222708.2019.210609.
[36] X. Xu, X. Chen, Elite bias generic algorithm for optimal control of Double-skin Facade, IEEE Congr. Evol. Comput. (2015), https://doi.org/10.1109/CEC.2015.7257310.
[37] Energy Plus, EnergyPlus 9.1 Engineering Reference: The Reference to EnergyPlus Calculations, (2019) 1–847.
[38] TRNSYS 17, Multizone Building modeling with Type56 and TRNBuild, 5 (2013) 1–79.
[39] IES VE, ApacheSim User Guide, IES VE User Guid. (2014).
[40] EQUA Simulation AB, User Manual IDA Indoor Climate and Energy 4.8, (2018).
[41] P. Sahlin, L. Eriksson, P. Grozman, H. Johnsson, A. Shapovalov, M. Vuolle, Whole-building simulation with symbolic DAE equations and general purpose solvers, Build. Environ. 39 (2004) 949–958, https://doi.org/10.1016/j.buildenv.2004.01.019.
[42] E. Atam, Current software barriers to advanced model-based control design for energy-efficient buildings, Renew. Sustain. Energy Rev. 73 (2017) 1031–1040, https://doi.org/10.1016/j.rser.2017.02.015.
[43] E. Atam, L. Helsen, Control-oriented thermal modeling of multizone buildings: methods and issues, IEEE Control Syst. 36 (2016) 86–111.
[44] S. Zhan, A. Chong, Data requirements and performance evaluation of model predictive control in buildings: a modeling perspective, Renew. Sustain. Energy Rev. 142 (2021), https://doi.org/10.1016/j.rser.2021.110835.
[45] Z. Zeng, G. Augenbroe, J. Chen, Realization of bi-level optimization of adaptive building envelope with a finite-difference model featuring short execution time and versatility, Energy. 243 (2022), https://doi.org/10.1016/j.energy.2021.122778.
[46] B. Coffey, Integrated control of operable fenestration systems and themally massive HVAC systems, 2012.
[47] G. Chaudhary, F. Goia, S. Grynning, Simulation and control of shading systems for glazed facades, IOP Conf. Ser. Earth Environ. Sci. 352 (2019), https://doi.org/10.1088/1755-1315/352/1/012069.
[48] Lawrence Berkeley National Laboratory, EnergyPlusToFMU, (n.d.). https://simulationresearch.lbl.gov/fmu/EnergyPlus/export/.
[49] E. Widl, W. Müller, Generic FMI-compliant Simulation Tool Coupling, Proc. 12th Int. Model. Conf. Prague, Czech Republic, May 15-17, 2017. 132 (2017) 321–327. 10.3384/ecp17132321.
[50] TRNSYS, The FMI++ TRNSYS FMU Export Utility, (n.d.). https://github.com/fmipp/trnsys-fmu.
[51] IES VE, Python API Guidance, (n.d.). https://help.iesve.com/ve2021/python_api_guidance.htm.
[52] F.u. Chenglong, Automation of Building Energy Performance Simulation with IDA ICE, KTH, 2020.
[53] M. Wetter, Co-simulation of building energy and control systems with the Building Controls Virtual Test Bed, J. Build. Perform. Simul. 4 (2011) 185–203, https://doi.org/10.1080/19401493.2010.518631.
[54] R.C.G.M. Loonen, F. Favoino, J.L.M. Hensen, M. Overend, Review of current status, requirements and opportunities for building performance simulation of adaptive facades, J. Build. Perform. Simul. 10 (2017) 205–223, https://doi.org/10.1080/19401493.2016.1152303.
[55] E. Taveres-Cachat, F. Favoino, R. Loonen, F. Goia, Ten questions concerning co-simulation for performance prediction of advanced building envelopes, Build. Environ. 191 (2021), https://doi.org/10.1016/j.buildenv.2020.107570.
[56] J. Neymark, R. Judkoff, M. Kummert, R. Muehleisen, A. Johannsen, N. Kruis, J. Glazer, R. Henninger, M. Witte, E. Ono, H. Yoshida, Y. Jiang, X. Zhou, T. McDowell, M. Hiller, J. An, D. Yan, J. Allison, P. Strachan, Update of ASHRAE Standard 140 Section 5.2 and Related Sections (BESTEST Building Thermal Fabric Test Cases), (2020) 211. https://www.osti.gov/biblio/1643690-update-ashrae-standard-section-related-sections-bestest-building-thermal-fabric-test-cases%0Ahttps://www.osti.gov/servlets/purl/1643690/.
[57] Gebäudeenergiegesetz - GEG, Gesetz zur Einsparung von Energie und zur Nutzung erneuerbarer Energien zur Wärme-und Kälteerzeugung in Gebäuden*, 2020. www.gesetze-im-internet.de.
[58] EN 16798 -1, EN 16798 -1 Energy performance of buildings - Ventilation for buildings - Part 1: Indoor environmental input parameters for design and assessment of energy performance of buildings addressing indoor air quality, thermal environment, lighting and acoustics, 2019.
[59] DS/CEN/TR 16798-2:2019, DS/CEN/TR 16798-2:2019 - Energy performance of buildings - Ventilation for buildings - Part 2: Interpretation of the requirements in EN 16798-1 - Indoor environmental input parameters for design and assessment of energy performance of buildings addressing, 2019. www.ds.dk.
[60] ISO 23045:2008(E), ISO 23054:Building environment design — Guidelines to assess energy efficiency of new buildings, 2008.
[61] J.A. Roberts, G. De Michele, G. Pernigotto, A. Gasparella, S. Avesani, Impact of active façade control parameters and sensor network complexity on comfort and efficiency: a residential Italian case-study, Energy Build. 255 (2022), https://doi.org/10.1016/j.enbuild.2021.111650.
[62] B. O'Neill, Model-based control of venetian blinds, 2008.
[63] ISO 8995, ISO 8995 - Lighting of indoor work places, 2002.
[64] G. Gennaro, F. Goia, G. De Michele, M. Perino, F. Favoino, Embedded single-board controller by dynamic transparent facades: a co-simulation virtual testbed, Proceeding BS2021 Conf, Sept, Bruges, Belgium, 2021, pp. 1–3.
[65] J. McCarthy, Recursive functions of symbolic expressions and their computation by machine, Commun. ACM (1960) 213–224, https://doi.org/10.7551/mitpress/12274.003.0023.
[66] P. May-Ostendorp, G.P. Henze, C.D. Corbin, B. Rajagopalan, C. Felsmann, Model-predictive control of mixed-mode buildings with rule extraction, Build. Environ. 46 (2011) 428–437, https://doi.org/10.1016/j.buildenv.2010.08.004.
[67] G. Cattarin, L. Pagliano, F. Causone, A. Kindinis, F. Goia, S. Carlucci, C. Schlemminger, Empirical validation and local sensitivity analysis of a lumped-parameter thermal model of an outdoor test cell, Build. Environ. 130 (2018) 151–161, https://doi.org/10.1016/j.buildenv.2017.12.029.

8 Conclusions

8.1 Research Outputs

The presented work examined how building energy simulation tools (BES) can assist in designing and optimising adaptive building envelopes, with a specific focus on DSFs (Double Skin Façades). DSFs are a type of adaptive envelope that offers a high degree of adaptability as they can impact the thermal, daylight, and air quality domains and can be integrated with the active systems of the building. The study aimed to investigate the reliability and capabilities of these BES tools in simulating the performance of DSFs and to identify the challenges designers may face when using these tools. To fully utilise the operational capability of a fully flexible double-skin façade, the abilities of the building energy simulation tools had to be improved, and a new model was presented. Additionally, the interconnection that this type of façade has with other building systems requires careful consideration of how they are operated. Several approaches for their control were evaluated, and a novel multi-domain optimal control was developed. This control approach allows for any type of adaptive façade to be optimally controlled with the use of building energy simulation tools. The proposed control approach can be a valuable tool for optimising the building envelope's performance and achieving the desired thermal, daylighting, and air quality conditions.

In the previously presented chapters, the main research question: "*How can an adaptive façade based on a flexible DSF concept be modelled, simulated, and controlled*?" was answered by addressing four specific sub-questions. These sub-questions were related to the modelling, simulation, and control of adaptive façades and were pursued to achieve a comprehensive understanding of the topic.

RQ1. *"What are the current possibilities to model a DSF with the existing BES tools?"*

This research question is mainly answered by the literature review presented in *P1* (Chapter 1) and by showing their application to case studies in *P2, P3* and *P4* (Chapters 3, 4 and 5). The modelling possibilities of DSFs were investigated in four main BES tools: EnergyPlus, IDA ICE, IES-VE and TRNSYS. The features of the tools employed in this research were thoroughly investigated and described in the previously

mentioned chapters. In particular, the different approaches to address the heat transfer problems (conduction, convection, radiation, airflow mass transportation, etc.) were listed and compared to understand similarities or differences in the models employed. In P1, this was investigated through a literature review, while in *P2, P3* and *P4*, the information obtained from the user manuals, combined with the modeller's experience, helped in describing the modelling assumptions present in each of the tools using the different modelling approaches available. This analysis provided a comprehensive understanding of the capabilities and limitations of each tool regarding modelling and simulating DSFs, thereby allowing for a critical evaluation of their performance and suitability for different applications.

DSFs can be modelled in building energy simulation tools by adopting a zonal approach or an in-built model already existing within the chosen tool. The second approach is limited to only certain tools that implement such a model, while the first can be applied to all analysed tools. Among the tools analysed, EnergyPlus, IDA-ICE, and TRNSYS made in-built models available. As *P1* shows, the zonal approach is the most commonly used in the literature. One of the main reasons for this is that existing in-built models often offer limited flexibility in terms of the type of ventilated DSF that can be modelled. One of the major challenges in modelling DSF systems using BES tools is the inability to model a flexible system using the existing models. This limitation arises from the fact that most in-built BES models are designed for a specific type of DSF, such as mechanically ventilated or naturally ventilated, and do not provide the flexibility to model different types or configurations of DSF systems within the same simulation. As demonstrated in the case studies of *P3* and *P4*, the in-built DSF models of EnergyPlus and TRNSYS are limited to only mechanically ventilated cavities (i.e. when the airflow crossing the cavity is known). Furthermore, the in-built model of TRNSYS presents a major limitation that further restricts its applicability. The inlet temperature has to be assigned, either as a fixed value or a schedule, and cannot be connected to the node of the thermal zone to which it belongs. Conversely, IDA-ICE implements a model that also allows for natural ventilation cases.

Starting from the challenges identified in *P1*, the sensitivity analyses conducted in *P2* and 5 highlighted the most critical aspects to focus on when modelling DSFs with BES tools. The analysis presented in *P2* identified i) the optical (solar transmittance) and ii) thermal properties (thermal transmittance) of the glazing and iii) the optical properties (solar reflectance) of the shading systems as the most influential parameters when modelling a mechanically ventilated DSF using the in-built models. Similarly, as seen in *P4*, when modelling naturally ventilated DSFs, the most challenging aspect is correctly modelling the inlet opening. The literature review already supported this finding as the need for more realistic discharge coefficients to correctly represent operable windows was found to be one of the main challenges faced.

Another key element in modelling a DSF was found to be the presence of the heat capacity node in the glass. Among all the software used, only IDA-ICE implements window models with the possibility to assign a capacity to the glass layer. As highlighted in *P2*, *P3* and *P4*, this can produce quite significant discrepancies in estimating the surface temperature since the inertia of a rather large glass system (50 mm of glass when both the exterior and the interior skin are considered) is not negligible. The heat capacity

node, which allows the simulation of the thermal mass of the glass, can provide more accurate predictions of the temperature changes and thus improve the overall performance of the simulation. The presented work highlighted the importance of including this feature in building energy simulation tools to ensure the accurate simulation of DSFs.

Finally, the presence of the shading device and, in particular, the models available in the tools to represent the convective heat exchange between the shading layer and the cavity air proved to be a critical aspect when predicting the cavity air temperature. This might not have a large effect in the particular case of mechanically ventilated cavities, as seen in *P3*. The shading device's presence does not dramatically affect the tools' performance as the heat released to the airflow does not determine the actual air mass rate. Conversely, as shown in *P4*, in the case of the naturally ventilated cavity, particularly with very low flow rates like the thermal buffer case, the influence of the convection coefficient adopted for the shading device can influence the predicted air gap temperature by up to 5°C, thereby influencing the entire system performance.

RQ2. *What is the performance of the available models in the BES tools?*

Defining the performance of the existing models in modelling DSFs is not a trivial task. From the literature review *P1* (Chapter 1), it was found that among the many studies that presented a validation of the model employed, a clear evaluation of the tool's performance was not reached. One reason for this is that the examples found in literature often addressed different typologies of DSF, and no commonly agreed method of evaluating their performance was available. This insight highlighted the need for a standardised method of evaluating the performance of BES tools in modelling DSFs to ensure accurate and consistent results.

On this premise, the work presented in *P2*, *P3* and *P4* was structured to fill this gap. Using an experimental rig of a box window DSF, different ventilation strategies were assessed using the BES tools mentioned before: EnergyPlus, IDA ICE, IES-VE and TRNSYS. In *P2*, the performances of two of the three available in-built models (EnergyPlus and IDA ICE) were compared in modelling a mechanically ventilated exhaust (EA) façade. From this comparison, IDA ICE stood out as the better tool for predicting the indoor surface temperature and the energy transmitted through the DSF. The RMSE values for surface temperature in case of the shading down (0.7 °C – Winter and 0.6°C – Summer) were circa one-third of the prediction of Energy Plus and a half when the shading device was not in use (1.1 °C – Winter and 0.9°C – Summer).

This comparison was later extended in *P3 (*Chapter 4) to also include the in-built model in TRNSYS, and the results showed that its performance was worse than the zonal approach modelled with the same tool. This, together with the limitations that this model presents (the need for angular properties of the glass, the need for a known inlet temperature value, and the possibility to only model EA façades), led to the exclusion of this model for the comparison with the other tools. Nevertheless, from the numerical results, it is clear that IDA ICE outperforms the other in-built models, not only due to its flexibility but also to its capabilities in accurately modelling the indoor surface temperature of the glass (RMSE - IDA ICE - 1.5 °C,

Energy Plus – 2.4 °C, TRNSYS – 2.5 °C) and the air gap temperature of the cavity (RMSE - IDA ICE - 2.6 °C, Energy Plus – 3.9 °C, TRNSYS – 3.7 °C). In terms of heat flux and solar irradiance transmitted through the façade, the three in-built models obtained comparable results, but the model of Energy Plus performed slightly better in terms of transmitted solar irradiance.

When the comparison was extended to include the other modelling approach (zonal approach), it was evident that determining which software performed better was not a straightforward task. The findings of this comprehensive investigation indicate that no single BES tool outperforms the others for the different DSF configurations examined, and this finding is valid for both mechanically and naturally ventilated cavities. Regarding surface temperatures, heat flux and transmitted solar radiation, TRNSYS appears to perform slightly better than the other tools. However, there is no consistency of more accurate or inferior predictions related to a specific period; as a general trend, the winter conditions are not predicted more accurately than the summer conditions. The same type of conclusion is valid for the presence of the shading device in the cavity.

The use of periodic data is interesting, for example, when the focus is not on the DSF itself but on the influence that installing a DSF has on the energy balance. When comparing the energy gained and lost by the DSF over a period of time, the performance of the tools was very similar, particularly in those periods when the shading was present in the cavity. All tools, except for IES VE, allowed this information to be obtained, and among the evaluated ones, all tended to overpredict the total transmitted energy, but TRNSYS had the best overall performance. Using this metric, the tools' behaviour appears to be more in line with the experimental data, and the daily variations seen when analysing the dynamic parameters are no longer distinguishable. Furthermore, it was observed that the tools have their own strengths and weaknesses, and the choice of a tool should be based on the specific application and the level of detail required in the simulation. For this reason, even if the results did not point to IDA ICE as the best performance tool, its acceptable results for all the analysed variables, together with the flexibility already provided by the tool in improving the connections of the in-built model to implement the concept of a flexible DSF, made IDA ICE the preferred tool to carry out the work, as shown in Chapter 6.

RQ3. *What improvements are needed to model an adaptive façade based on the concept of a flexible DSF?*

P5 (Chapter 6) presented a comprehensive answer to the research question. Starting from the existing in-built model available in IDA ICE, we developed a new model for a flexible DSF module that was able to accurately replicate the thermophysical behaviours of such a dynamic system. This was achieved by leveraging the "Double Glass Façade" component available in IDA ICE and conducting a dedicated experimental activity to collect relevant data for comparison.

The ventilation strategies natively available (*P5* - Fig. 3 b) in this component could cover all the needs in terms of flow path: 1) OAC naturally ventilated; 2) EA naturally ventilated; 3) IAC naturally and 4) mechanically ventilated; 5) SA naturally and 6) mechanically ventilated; 7) TB. In order to model the thermal buffer mode, at least one small leak (either toward the inside or outside) had to be modelled.

However, these strategies could only be modelled as fixed-configuration, thus limiting the model's versatility because of two main constraints: the inability to control some opening/connection types and the inability to model all the connections at the same time (i.e., within a single simulation run it is not possible to alternate flow paths and ventilation strategies). A conventional DSF model, which is based on a concept where the airflow has a fixed path, does not require this flexibility, and therefore the link between the cavity and the two surrounding environments can be defined with simple representations (leakage or free cross areas) and controlled during the simulation.

In order to be able to control the façade in different operation modes, with full control over the different openings and maximum freedom to combine the façade with the HVAC (as schematised in Figure 2), the air links of the "Double Glass Façade" component were modified (*P5*- Fig. 4). First, to be able to control the ventilation path, operable elements replaced the openings modelled as leaks. This modification allowed dynamic control of the connection between the cavity and the indoor and outdoor environment during the simulation runtime. To alternate between the ventilation mode (natural or mechanical), a mechanical fan extracting air from the cavity and directing it towards the outdoor (exhaust fan) was added. Finally, to model the case in which the room's ventilation occurs by bypassing the cavity altogether (ventilated thermal buffer – TB-V), it was necessary to exclude the cavity from the ventilation path and add two more operable windows that directly linked the room to the outdoors.

Compared to the standard component available by default, the modifications implemented in the new model introduced the possibility of controlling the façade with the five different air paths (including switching between naturally and mechanically ventilated modes) and, therefore, enhanced the DSF model's flexibility. The controllers, added to each of the operable elements, the fans and the shading device, can be linked to a schedule or implemented with an external control logic that accounts for the ambient conditions (radiation, temperature, etc.), therefore allowing for full control of the DFS model.

The performance of the new model was then rigorously assessed by comparing the simulation results with the experimental data, and this analysis provided valuable insights into the capabilities and limitations of the model in replicating the thermophysical behaviour of a flexible DSF. This model included blinds with a controllable angle to maximise the degree of freedom that this adaptive façade could offer.

The model was compared with two different measurement periods in which the operational modes of the façade were changed i) every hour using a pre-defined, scheduled-based control; and ii) every day by exploring a wider range of combinations of all the possible configurations that the façade could assume, but the configuration of the façade was fixed for 24 h. By designing the validation process to include these two periods, the aim was to assess the numerical model's ability to replicate both fast-time processes and more long-term dynamics and simulate an extensive range of operational conditions. Overall, both mechanical and natural ventilation were employed, the shading device was deployed or retracted, and the slats of the venetian blinds were changed every hour by a few degrees.

The enhanced model could accurately depict and approximate the switch from one configuration to another. In terms of predictions, the airgap temperature was slightly overpredicted but much in line with the value measured in the higher portion of the cavity and was, therefore, more similar to what will be found from the outlets of the façade (i.e., a good approximation of the temperature used to climatise the indoor space). The surface temperature was in line with the mean measured value, which assures a good approximation for local discomfort analysis. The transmitted solar radiation was also relatively well predicted, particularly if the blinds' position was significantly changed. The heat flux estimation adequately depicts the daily profile of the incoming and exiting flux from the inner glazing, leading to a reasonable assessment of the overall energy calculation. Finally, when analysing the energy balance, the configurations operated under naturally driven ventilation had a higher error compared to the cases when the ventilation in the cavity was mechanically driven. Furthermore, the week with more frequent configuration changes had lower accuracy than the week when the configurations were changed once a day. Nonetheless, the overall assessment demonstrated that when used to assess the overall performance in terms of total energy crossing the façade for a long enough period of time (as is typically done with BES tools), the flexible DSF model gives estimations that are close to the measured values, with NMBE in the range of 5–15% and a $CV(RMSE)_{24H}$ of 25%.

RQ4. *What is a suitable approach to control adaptive façades to fully exploit their potential?*

Generally speaking, it is possible to control an adaptive façade with rule- and model-based control. In *P6* (Chapter 7), I investigated how these two alternative approaches perform by employing the flexible DSF model developed in *P5 (*Chapter 6).

As demonstrated through the literature review, while rule-based controls can be made more complex through the integration of sensor-based input and variable threshold values that vary depending on factors such as season or room occupancy level (Karlsen et al. 2016), they still pose several limitations. Rule-based control methods, whether scheduled, open-loop, or closed-loop, are limited in the number of alternative states they can provide, and the decision tree structure is fixed once established, making it difficult to adapt to more complex control objectives, particularly those that involve multiple domains such as thermal and light environments, with contrasting objectives. Additionally, determining meaningful threshold values can be difficult, particularly when adopting open-loop algorithms (Peng et al. 2022).

Conversely, model-based control exploits the prediction (through simulation) of the impact of the control action on the indoor environment to perform its decision-making, aiming to maximise one or more building-level performances (Lee, Cho, and Jo 2021), thus providing more flexibility than RBC controls. This usually requires a high-level optimal objective definition (e.g. minimisation or maximisation of a particular performance) combined with suitable optimal search algorithms to ensure that the computational load remains within a suitable range (Peng et al. 2022). The high computational demand is the main reason this type of control is not often used together with explicit models, like the ones

available in BES tools, and is rather applied to control-oriented models in the form of a reduced-order model (Zhan and Chong 2021).

With this in mind, an advanced model-based control was developed for adaptive façades that can adapt their physical properties to meet multiple interdependent performance requirements across various domains, including thermal comfort, daylighting, indoor air quality, and energy efficiency. This approach utilises a co-simulation method between a BES tool, IDA ICE, and a multi-objective optimisation algorithm written in Python to achieve optimal performance.

The developed algorithm was tested using a model of the flexible DSF in three different seasons (winter, summer, and mid-season), and the results demonstrated that the model is able to handle a façade with a high degree of freedom (up to 70 different configurations). Furthermore, this approach takes advantage of the capabilities of BES tools to accurately replicate the behaviour of adaptive façades and offers the possibility, already at the design stage, to fully explore the potential of passive strategies such as natural ventilation, solar gains, and night cooling. Additionally, it allows for the optimisation of the integration with active building systems such as HVAC and indoor lighting. The results in terms of comfort requirements showed how this control allows satisfying simultaneously multiple domains, guaranteeing higher comfort levels for 80% (daylight), 70% (air quality) and 70% (temperature) of the occupied hours.

Moreover, the comparison with more traditional control strategies confirmed the literature review's findings. Traditional controls are incapable of handling the complexity of an adaptive façade such as a DSF. When using a scheduled-based control, the flexibility of the façade was not at all taken advantage of, and while the energy results were not the worst (comparable to the results of the MBC), the performance over the other investigated domains was quite low: only around 30% (daylight), 40% (air-quality) and 45% (temperature) of the occupied time were the higher comfort requirements satisfied. Conversely, adopting a non-optimised rule-based control with thresholds not adjusted to the climate led to extremely poor energy performance, thus confirming that this approach is not the most suitable when dealing with an adaptive façade of high complexity.

The presented control method with multi-domain optimisation proved to be applicable to any type of adaptive façade, and that even a single skin façade with the right type of control can outperform a poorly controlled DSF.

8.2 Discussion and limitations

The study found a lack of a standardised method for evaluating the performance of BES tools in modelling DSFs and tried to fill this gap by carrying out a multi-tool comparison by using a box window double skin façade and different ventilation strategies. The findings of this research indicate that there is no clear winner among the analysed BES tools as the performance in predicting different thermophysical parameters and the system's energy efficiency were not always consistent or flawless. Moreover, these tools presented several limitations in the implemented models, including numerical assumptions in their

correlations, limitations in the user interface, lack of adaptability to less standard building elements, and limited capabilities for advanced control integration. However, when considering the need for integration with the whole building system and the ultimate goal of efficient building management, the use of BES tools is still the best available approach.

While using detailed simulation models, such as on-purpose built models (Park, Augenbroe, Messadi, et al. 2004; Park, Augenbroe, Sadegh, et al. 2004; Wang, Chen, and Zhou 2016) or dedicated CFD simulations (Li, Darkwa, and Kokogiannakis 2017; Dama, Angeli, and Kalianova Larsen 2017) can lead to more accurate results in predicting thermophysical parameters. Using these models alone without integrating them into the building can limit the ability to fully understand the performance of the adaptive façade in relation to the rest of the building. Without considering the complexity involved in developing an on-purpose or CFD model, to truly assess the overall energy and comfort performance, it is essential to couple the simulation of the whole building and specific building components. This allows for replicating the complex interactions between airflow in the façade, the HVAC system, and the building energy management system. This is particularly needed when it is evident that the key aspect of an adaptive façade lies in its operation more than the technology itself, and therefore the control of the system is a key aspect that cannot be overlooked.

As said, the most critical aspects when modelling a DSF in BES tools are the accuracy of the numerical assumptions and correlations used in the physical models as they can greatly affect the results of the simulation and the overall performance of the DSF. For example, an inaccurate numerical assumption in the thermal model can lead not only to an overestimation or underestimation of the energy performance of the DSF, which may not be so relevant in the long run, but if that model is using outputs from the cavity as feedback sensors for the control strategy, to an improper control output that can have a greater effect on the total energy of the system. For this reason, the need to have an accurate physical model that describes the inlet and outlet openings is essential for estimating the correct value of the air gap temperature. Similarly, adopting more accurate convective correlations that describe the heat exchange between the shading system and the cavity air is important. Finally, implementing models that account for the overall thermal inertia, including the glass panes, can improve the prediction of the discomfort parameters, which in the case of a high glass-ratio envelope like DSF is greatly influenced by the surface glass temperature (radiative exchange, local drafts, etc.).

The validation process that led to these results was closely tied to the experimental activity, both for providing input and boundary conditions and for having meaningful parameters to compare the models with. The experimental design and its execution were carried out thoroughly to minimize measurement errors as much as possible. However, some of the inaccuracies that inevitably affect any experimental campaign did have some impact on the final evaluations of the tools' performances. In particular, the fact that the heat-flux meters were not working when the façade was run with natural ventilation made it impossible to have a consistent validation over all of the analysed parameters in the mechanical ventilation case. This resulted in the overall tool evaluation lacking data on a rather important aspect, the

energy behaviour of the naturally ventilated system. This limitation was partially overcome during the validation of the flexible DSF model, where the experimental data also contained naturally ventilated days. Thus, the model in IDA ICE was compared with the measured heat-flux and the derived energy passing through the façade, but it was not possible to evaluate this performance for the other tools.

Another critical aspect was the measuring of solar radiation. In both experiments, the total solar radiation on the vertical and horizontal planes were measured. That meant that, as explained in the methodology section (Chapter 1.5), the direct and diffuse components had to be derived using a decomposition model, which adds uncertainties to the process as with any numerical model. The availability of both horizontal and vertical values allowed the cross-control of the outputs, thus giving assurance for the model's fitness. Surely, though, during the experimental campaign for the mechanically ventilated DSF, the quality of the solar data impacted the final results, showing an excessive shift in the transmitted solar irradiance that is not seen when using other experimental data. In this case, the data processing had to be carried out from solar data with a high time resolution (hourly) since the experiment was previously carried out and the raw data was unavailable. Not being fully able to offer quality assurance on the modality of how the data were sampled introduced some inaccuracies in the validation process not addressable to the tools themselves.

One of the challenges when validating the performance of adaptive envelopes was selecting the appropriate evaluation methods. The research conducted for this thesis highlighted that using traditional metrics is not always the most effective approach for assessing the behaviour of rapidly changing parameters. In order to provide a comprehensive understanding of the prediction of a given variable, it is necessary to consider not only numeric results from statistical indicators such as RMSE or MBE, but also qualitative methods to aid in interpreting results that may be misleading when considered alone. For example, if a temperature prediction follows the peaks and lows accurately but is shifted by one or more hours (like in the case of indoor surface temperature), the error shown by the statistical indicator will be high even though the prediction of the variable's dynamics is meaningful and can be used to correctly inform the design or a control strategy. This shift may not have a significant impact when considering the total energy over a longer period of time. Conversely, if the predictions of the peaks are highly inaccurate (or overpredicted), these unmet predictions would not have a major impact on the error prediction of that particular performance when using an averaged error value. By only evaluating the goodness of a model based on its error distribution, a model that produces errors with a significant impact on the overall system may be adopted.

Moreover, as already addressed in the presented papers, thresholds for defining a validated model are available only when referring to the system's total energy. The ASHRAE guideline 14 (ASHRAE 2014) and IPMVP (EVO 2012) provide ranges into which models must fit to be considered validated. No such indication is given when other thermal properties are considered, therefore the researcher it must rely on their own experience of or t on similar studies in the literature (if present) to decide if the results are

acceptable or not. With the comprehensive validation of case studies presented in the thesis, future modellers can hopefully use this work to benchmark their models.

In real practice, the performance of adaptive façades is still a very difficult task to assess during the design stage due to time-varying dynamic behaviour. Dealing with a multi-domain problem makes it difficult to choose which performances are acceptable and which not in accordance with all the domains involved. It is not an easy task to identify a trade-off of the façade's performances so that an optimal behaviour is achieved. In many cases, this requires costly experimental validation using mock-up scales, which can hinder their practical application. The detailed analysis BES tools provide when designing this type of technology is key, particularly in evaluating their operation. By implementing controls within BES tools, and specifically using a model-based control approach, it is possible to explore advanced control techniques that would otherwise only be applied to simplified models or single elements without taking into account the interaction of the controlled element with the rest of the building's active systems. In practice, "active" elements are often only controlled using threshold values, and their impact on other domains is ignored. As this thesis demonstrates, using non-optimized control can lead to suboptimal results, making it more likely that a less advanced solution is chosen because the benefits of installing a more expensive technology are not realized due to a failure to fully exploit the adaptive façade's potential. Additionally, the presented approach is not limited to adaptive façades and can be applied to any type of controllable element. This can increase the use of simple technologies already available on the market, such as automated operable openings and shading elements, to improve indoor comfort and energy efficiency.

Even if the application of this approach looks promising from the results perspective, the computational costs required to apply to a real case study are still very high, which is one of this work's main drawbacks. Moreover, the need for a co-simulation approach in order to carry out MBC makes it less appealing for those with limited time and little programming experience, like most of the users of BES tools. As a general concept, applying a control algorithm to a system with many possible states, like the DSF case, leads to an extremely high number of combinations that need to be considered. MBCs are often applied to simplified models (space-state, grey or black-box models) for this exact reason. As explained before, adopting these models leads to losing essential information about the whole building system. Moreover, optimisation algorithms are often adopted to try to reduce the possible number of combinations that need to be simulated, but the presence of mostly discrete states (airflow path, ventilation mode, etc.) makes it more challenging.

8.3 Original contribution and impact of the work

My work aims to be considered the state of the art of how to model DSFs using BES tools. The element of novelty in this research can be summarised in the following points:

- This work offers a comprehensive review of the current practices of modelling DSFs, with a deep focus on the available models in the most commonly used tools for evaluating the whole

building's performance; this analysis highlights the critical aspects of modelling DSFs and it gives directions on how the existing tools can be improved, and benchmarks the accuracy that the existing models can provide under different conditions;

- This work provides a detailed description of the assumptions employed in each analysed BES tool. This information is typically found in user manuals but can be difficult for other software users to access. By presenting the mathematical models and available settings (specific to DSF modelling) for each tool, this work aims to compare the tools comprehensively. This will provide a better understanding of each tool's underlying assumptions and limitations, which can aid in selecting the appropriate tool for a specific project or application. Additionally, it will help in understanding the results obtained from each tool and allow for a more accurate interpretation of the results. The models developed in this work have been made available on online repositories so that researchers or other users interested in using the models or the experimental data used for the validation can access them.
- This work systematically evaluates DSF models in various BES tools using different ventilation strategies. The last similar inter-software validation that adopted the same dataset to verify the performance of different BES tools was conducted over ten years ago (Kalyanova et al. 2009) and only addressed two types of ventilation strategies: thermal buffer and naturally ventilated outdoor curtain. By evaluating both mechanically and ventilated DSFs, and using the most commonly employed ventilation strategies, this work aims to provide a benchmark for future model evaluations.
- This work presents model developed and validated with experimental data that is able to replicate more than six ventilation strategies and integrate them with the HVAC system of the building. This is the first attempt to replicate the concept of a flexible DSF within a BES tool and to compare its performance with a full-scale experimental set-up run using different control strategies. This model has also been made available on an online repository. This model can be seen as an archetype of DSF model, as it can be used not only to model the fully flexible DSF but also the other configurations not available in the in-built component of IDA ICE.
- This work introduces an original approach to multi-domain optimal control of adaptive façades by exploiting a model-based control and a demonstration of the feasibility of such an approach by leveraging the latest developments in co-simulation schemes for BES. To this day, this study is the first of its kind to demonstrate the use of model-based control for an adaptive façade system characterised by a very large range of possible states, which is a system that clearly cannot be efficiently controlled using common control strategies conventionally adopted for building envelopes.
- The presented control approach is not limited to the application to DSFs, but it can be used to control any adaptive envelope with controllable elements, as shown in the application of a natural ventilation strategy with a simple window.

The work presented in this research targets both the R&D and professional communities. The presented validated models, the concept of the highly flexible adaptive façade and its numerical model, and the multi-domain advanced control are relevant for the first group, which can further investigate the performance of this concept and expand the knowledge about the challenges and possibilities in modelling (and controlling) advanced façade systems in BES. Furthermore, the experimental dataset used in this process is also openly shared in a repository for any researcher to use for model validation or performance analysis purposes.

This thesis allows the professional community to better understand the correlations and assumptions in the different tools. Moreover, the work outlined in this thesis is useful as a demonstration of how to exploit existing BES tools to model advanced functionalities for building envelope systems that are not found in the modules embedded in the release of a BES. It also offers the possibility to investigate the adoption of advanced control strategies during the design stage. This could expand the adoption of more advanced technologies in the building sector, giving the envelope a whole new role.

Finally, this work addresses the tool developers. In the presented research, many limitations to the existing models have been highlighted, and the key elements that play crucial roles in obtaining more accurate predictions have been identified. Moreover, the need for more seamless integration of advanced control strategies can only be addressed by the software houses. The possibility to access the tools through API interfaces needs to be further developed, and their integration with the software itself needs improvements to become accessible to all users without requiring co-simulation approaches that are time demanding to develop and run.

8.4 Future outlook

The presented work focused on the existing models in BES tools, and from that an enhanced model was developed, but no improvements were made to the physical correlations inside the model. Therefore, the limitations of the existing models (convective correlations used in the cavity, openings definitions, one temperature representative for the entire cavity, etc.) were not addressed. One way of approaching this problem would be to develop a dedicated model to test different correlations. Software with a modular architecture (like IDA ICE, TRNSYS, or Modelica) is more appropriate for this task as this approach would require the coupling of the dedicated model with one of the BES tools, which, as we have seen, is not a trivial task.

Another future development of this work would be the improvement of the control integration in the model. The presented approach requires a high level of knowledge of the BES tool and a programming language. Developing a solution that is more integrated into the software and with fewer workarounds could be beneficial for applying advanced control to more conventional projects.

Moreover, this work laid the basis for future applications for advanced control in real buildings. Indeed, the presented MBC control could be combined with the more traditional control, like hierarchical rule-

based control and extrapolating behaviour paths, to define optimal control rules. MBC-enhanced RBC strategies can provide a cost-effective solution by reaching the optimal control with a decrease in operational time [35,66] using rule extraction from an MBC simulation dataset [10].

Finally, developing the presented MBC into a predictive one is a natural continuation of this work. Coupling the façade performance and its effect on the indoor environment could be interestingly addressed by an MPC – because the inertial characteristics of the system will play a larger role. For example, an MPC strategy with minimisation of energy use and maximisation of (cumulated) comfort conditions over a certain time horizon might lead to better exploitation of the dynamic features of the façade.

Bibliography

ASHRAE. 2014. *ASHRAE Guideline 14 - Measurement of Energy, Demand, and Water Savings*.

Bright, Jamie M., and Nicholas A. Engerer. 2019. "Engerer2: Global Re-Parameterisation, Update, and Validation of an Irradiance Separation Model at Different Temporal Resolutions." *Journal of Renewable and Sustainable Energy* 11 (3). https://doi.org/10.1063/1.5097014.

Catto Lucchino, Elena, Adrienn Gelesz, Kristian Skeie, Giovanni Gennaro, András Reith, Valentina Serra, and Francesco Goia. 2021. "Modelling Double Skin Façades (DSFs) in Whole-Building Energy Simulation Tools: Validation and Inter-Software Comparison of a Mechanically Ventilated Single-Story DSF." *Building and Environment* 199 (April). https://doi.org/10.1016/j.buildenv.2021.107906.

Catto Lucchino, Elena, Giovanni Gennaro, Fabio Favoino, and Francesco Goia. 2022. "Modelling and Validation of a Single-Storey Flexible Double-Skin Façade System with a Building Energy Simulation Tool." *Building and Environment* 226 (109704). https://doi.org/10.1016/j.buildenv.2022.109704.

Catto Lucchino, Elena, and Francesco Goia. 2023. "Multi-Domain Model-Based Control of an Adaptive Façade Based on a Flexible Double Skin System." *Energy and Buildings* 285: 112881. https://doi.org/10.1016/j.enbuild.2023.112881.

Catto Lucchino, Elena, Francesco Goia, Gabriele Lobaccaro, and Gaurav Chaudhary. 2019. "Modelling of Double Skin Facades in Whole-Building Energy Simulation Tools: A Review of Current Practices and Possibilities for Future Developments." *Building Simulation* 12 (1): 3–27. https://doi.org/10.1007/s12273-019-0511-y.

Chan, ALS. 2011. "Energy and Environmental Performance of Building Façades Integrated with Phase Change Material in Subtropical Hong Kong." *Energy and Buildings* 43 (10): 2947–55. https://doi.org/10.1016/j.enbuild.2011.07.021.

D. M. Hamby. 1994. "A Review of Techniques for Parameter Sensitivity Analysis of Environmental Models." *Environmental Monitoring and Assessment* 32 (c): 135–54.

Dama, Alessandro, Diego Angeli, and Olena Kalianova Larsen. 2017. "Naturally Ventilated Double-Skin Façade in Modeling and Experiments." *Energy and Buildings* 144: 17–29. https://doi.org/0.1016/j.enbuild.2017.03.038.

EN 16798 -1. 2019. *EN 16798 -1 Energy Performance of Buildings - Ventilation for Buildings - Part 1: Indoor Environmental Input Parameters for Design and Assessment of Energy Performance of Buildings Addressing Indoor Air Quality, Thermal Environment, Lighting and Acoustics*.

Energy Plus. 2019. "EnergyPlus 9.1 Engineering Reference: The Reference to EnergyPlus Calculations."

EQUA AB. 2009. "IDA Indoor Climate and Energy 4.0 EQUA Simulation AB.," no. February.

Eskinja, Z., L. Miljanic, and O. Kuljaca. 2018. "Modelling Thermal Transients in Controlled Double Skin Façade Building by Using Renowned Energy Simulation Engines." In *2018 41st International Convention on Information and Communication Technology, Electronics and Microelectronics, MIPRO 2018 - Proceedings*, 897–901. https://doi.org/10.23919/MIPRO.2018.8400166.

Gelesz, Adrienn. 2019. "Sensitivity of Exhaust-Air Façade Performance Prediction to Modelling Approaches in IDA ICE." *International Review of Applied Sciences and Engineering* 10 (3): 241–52.

Gelesz, Adrienn, Ádám Bognár, and András Reith. 2018. "Effect of Shading Control on the Energy Savings of an Adaptable Ventilation Mode Double Skin Facade." In *13th Conference on Advanced Building Skins, 1-2 October 2018, Bern, Switzerland - in Progress*.

Gelesz, Adrienn, Elena Catto Lucchino, Francesco Goia, Valentina Serra, and András Reith. 2020. "Characteristics That Matter in a Climate Façade: A Sensitivity Analysis with Building Energy Simulation Tools." *Energy and Buildings* 229. https://doi.org/10.1016/j.enbuild.2020.110467.

Gennaro, Giovanni, Elena Catto Lucchino, Francesco Goia, and Fabio Favoino. 2023. "Modelling Double Skin Façades (DSFs) in Whole-Building Energy Simulation Tools: Validation and Inter-Software Comparison of Naturally Ventilated Single-Story DSFs." *Building and Environment*, January, 110002. https://doi.org/10.1016/j.buildenv.2023.110002.

Gratia, Elisabeth, and André De Herde. 2004. "Optimal Operation of a South Double-Skin Facade." *Energy and Buildings* 36 (1): 41–60. https://doi.org/10.1016/j.enbuild.2003.06.001.

Haase, M., F. Marques da Silva, and A. Amato. 2009. "Simulation of Ventilated Facades in Hot and Humid Climates." *Energy and Buildings* 41 (4): 361–73. https://doi.org/10.1016/j.enbuild.2008.11.008.

Heiselberg, Per. 2012. "Integrating Environmentally Responsive Elements in Buildings." *ECBCS Annex 44*. http://files/21975/Heiselberg et al. - Integrating Environmentally Responsive Elements in.pdf.

Hersbach, H., Bell, B., Berrisford, P., Biavati, G., Horányi, A., Muñoz Sabater, J., Nicolas, J., Peubey, C., Radu, R., Rozum, I., Schepers, D., Simmons, A., Soci, C., Dee, D., Thépaut, J-N. 2018. "ERA5 Hourly Data on Single Levels from 1979 to Present. Copernicus Climate Change Service (C3S) Climate Data

Store (CDS)." https://doi.org/10.24381/cds.adbb2d47.

Huckemann, Volker, Ernesto Kuchen, Marlon Leão, and Érika F.T.B. Leão. 2010. "Empirical Thermal Comfort Evaluation of Single and Double Skin Façades." *Building and Environment* 45 (4): 976–82. https://doi.org/10.1016/j.buildenv.2009.10.006.

Hyndman, Rob J., and Anne B. Koehler. 2006. "Another Look at Measures of Forecast Accuracy." *International Journal of Forecasting* 22 (4): 679–88. https://doi.org/10.1016/j.ijforecast.2006.03.001.

IES VE. 2014. "ApacheSim User Guide." *IES VE User Guide*.

ISO 8995. 2002. *ISO 8995 - Lighting of Indoor Work Places*.

Jankovic, Aleksandar, and Francesco Goia. 2021. "Impact of Double Skin Facade Constructional Features on Heat Transfer and Fluid Dynamic Behaviour." *Building and Environment* 196 (March): 107796. https://doi.org/10.1016/j.buildenv.2021.107796.

Kalyanova, Olena, Per Heiselberg, Clemens Felsmann, Harris Poirazis, Paul Strachan, and Aad Wijsman. 2009. "An Empirical Validation of Building Simulation Software for Modelling of Doubleskin Facade (DSF)." In *Eleventh International IBPSA Conference*. Glasgow, Scotland.

Karlsen, Line, Per Heiselberg, Ida Bryn, and Hicham Johra. 2016. "Solar Shading Control Strategy for Office Buildings in Cold Climate." *Energy and Buildings* 118 (0130): 316–28. https://doi.org/10.1016/j.enbuild.2016.03.014.

Kim, Dongsu, Sam J. Cox, Heejin Cho, and Jongho Yoon. 2018. "Comparative Investigation on Building Energy Performance of Double Skin Façade (DSF) with Interior or Exterior Slat Blinds." *Journal of Building Engineering* 20 (January): 411–23. https://doi.org/10.1016/j.jobe.2018.08.012.

Kim, Young-jin, Cheol-soo Park, and Wonjun Suh. 2011. "Comparison of Different Optimal Control Strategies of a Double-Skin Facade DOUBLE-SKIN FACADE," no. January 2015.

Kristensen, Martin Heine, and Steffen Petersen. 2016. "Choosing the Appropriate Sensitivity Analysis Method for Building Energy Model-Based Investigations." *Energy and Buildings* 130: 166–76. https://doi.org/10.1016/j.enbuild.2016.08.038.

Leal, V., E. Erell, E. Maldonado, and Y. Etzion. 2004. "Modelling the SOLVENT Ventilated Window for Whole Building Simulation." *Building Services Engineering Research and Technology* 25 (3): 183–95. https://doi.org/10.1191/0143624404bt1030a.

Lee, Dongseok, Young Hum Cho, and Jae Hun Jo. 2021. "Assessment of Control Strategy of Adaptive Façades for Heating, Cooling, Lighting Energy Conservation and Glare Prevention." *Energy and Buildings* 235: 110739. https://doi.org/10.1016/j.enbuild.2021.110739.

Li, Yilin, Jo Darkwa, and Georgios Kokogiannakis. 2017. "Heat Transfer Analysis of an Integrated Double

Skin Façade and Phase Change Material Blind System." *Building and Environment* 125: 111–21. https://doi.org/10.1016/j.buildenv.2017.08.034.

Loonen, R., M. Trčka, D. Cóstola, and J. L.M. Hensen. 2013. "Climate Adaptive Building Shells: State-of-the-Art and Future Challenges." *Renewable and Sustainable Energy Reviews* 25: 483–93. https://doi.org/10.1016/j.rser.2013.04.016.

Loonen, Roel C.G.M., Fabio Favoino, Jan L.M. Hensen, and Mauro Overend. 2016. "Review of Current Status , Requirements and Opportunities for Building Performance Simulation of Adaptive Facades." *Journal of Building Performance Simulation*, 1–19. https://doi.org/10.1080/19401493.2016.1152303.

Mateus, Nuno M., Armando Pinto, and Guilherme Carrilho Da Graça. 2014. "Validation of EnergyPlus Thermal Simulation of a Double Skin Naturally and Mechanically Ventilated Test Cell." *Energy and Buildings* 75: 511–22. https://doi.org/10.1016/j.enbuild.2014.02.043.

Oesterle, E, R D Leib, G Lutz, and B Heusler. 2001. *Double Skin Facades: Integrated Planning: Building Physics. Construction, Aerophysics, Air-Conditioning, Economic Viability*. Munich: Prestel.

Park, Cheol Soo, and Godfried Augenbroe. 2013. "Local vs. Integrated Control Strategies for Double-Skin Systems." *Automation in Construction* 30: 50–56. https://doi.org/10.1016/j.autcon.2012.11.030.

Park, Cheol Soo, Godfried Augenbroe, Tahar Messadi, Mate Thitisawat, and Nader Sadegh. 2004. "Calibration of a Lumped Simulation Model for Double-Skin Façade Systems." *Energy and Buildings* 36 (11): 1117–30. https://doi.org/10.1016/j.enbuild.2004.04.003.

Park, Cheol Soo, Godfried Augenbroe, Nader Sadegh, Mate Thitisawat, and Tahar Messadi. 2004. "Real-Time Optimization of a Double-Skin Façade Based on Lumped Modeling and Occupant Preference." *Building and Environment* 39 (8 SPEC. ISS.): 939–48. https://doi.org/10.1016/j.buildenv.2004.01.018.

Peng, Yuzhen, Yue Lei, Zeynep Duygu Tekler, Nogista Antanuri, Siu Kit Lau, and Adrian Chong. 2022. "Hybrid System Controls of Natural Ventilation and HVAC in Mixed-Mode Buildings: A Comprehensive Review." *Energy and Buildings* 276: 112509. https://doi.org/10.1016/j.enbuild.2022.112509.

Perino M. et al. 2008. "Annex 44 - Responsive Building Elements: State of the Art Review. Vol. 2A." *IEA SHC/ECBS*, 197.

Pomponi, Francesco, Sabrina Barbosa, and Poorang A.E. Piroozfar. 2017. "On the Intrinsic Flexibility of the Double Skin Façade: A Comparative Thermal Comfort Investigation in Tropical and Temperate Climates." *Energy Procedia* 111: 530–39. https://doi.org/10.1016/j.egypro.2017.03.215.

Pomponi, Francesco, Poorang A.E. Piroozfar, Ryan Southall, Philip Ashton, and Eric R.P. Farr. 2016. "Energy Performance of Double-Skin Façades in Temperate Climates: A Systematic Review and Meta-Analysis." *Renewable and Sustainable Energy Reviews* 54: 1525–36.

https://doi.org/10.1016/j.rser.2015.10.075.

Ruiz, Germán Ramos, and Carlos Fernández Bandera. 2017. "Validation of Calibrated Energy Models: Common Errors." *Energies* 10 (10). https://doi.org/10.3390/en10101587.

Saelens, Dirk, Staf Roels, and Hugo Hens. 2008. "Strategies to Improve the Energy Performance of Multiple-Skin Facades." *Building and Environment* 43 (4): 638–50. https://doi.org/10.1016/j.buildenv.2006.06.024.

Singh, M.C., S.N. Garg, and Ranjna Jha. 2008. "Different Glazing Systems and Their Impact on Human Thermal Comfort—Indian Scenario." *Building and Environment* 43 (10): 1596–1602. https://doi.org/10.1016/j.buildenv.2007.10.004.

Taveres-Cachat, Ellika, Fabio Favoino, Roel Loonen, and Francesco Goia. 2021. "Ten Questions Concerning Co-Simulation for Performance Prediction of Advanced Building Envelopes." *Building and Environment* 191. https://doi.org/10.1016/j.buildenv.2020.107570.

Taveres-Cachat, Ellika, Steinar Grynning, Judith Thomsen, and Stephen Selkowitz. 2019. "Responsive Building Envelope Concepts in Zero Emission Neighborhoods and Smart Cities - A Roadmap to Implementation." *Building and Environment* 149 (December 2018): 446–57. https://doi.org/10.1016/j.buildenv.2018.12.045.

TRNSYS 17. 2013. "Multizone Building Modeling with Type56 and TRNBuild."

Wang, Yanjin, Youming Chen, and Juan Zhou. 2016. "Dynamic Modeling of the Ventilated Double Skin Façade in Hot Summer and Cold Winter Zone in China." *Building and Environment* 106: 365–77. https://doi.org/10.1016/j.buildenv.2016.07.012.

Zhan, Sicheng, and Adrian Chong. 2021. "Data Requirements and Performance Evaluation of Model Predictive Control in Buildings: A Modeling Perspective." *Renewable and Sustainable Energy Reviews* 142 (February): 110835. https://doi.org/10.1016/j.rser.2021.110835.